Garbacz

CONTRACT NO. NAS5-3173

DESIGN REPORT FOR THE TIROS OPERATIONAL SATELLITE (TOS) SYSTEM

Prepared for the

GODDARD SPACE FLIGHT CENTER
NATIONAL AERONAUTICS AND
SPACE ADMINISTRATION
WASHINGTON, D.C.

By the

ASTRO-ELECTRONICS DIVISION
DEFENSE ELECTRONIC PRODUCTS
RADIO CORPORATION OF AMERICA
PRINCETON, NEW JERSEY

AED R-2489

Issued: December 30, 1964

CONTRACT NO. NAS5-3173

DESIGN REPORT FOR THE TIROS OPERATIONAL SATELLITE (TOS) SYSTEM

Prepared for the

GODDARD SPACE FLIGHT CENTER
NATIONAL AERONAUTICS AND
SPACE ADMINISTRATION
WASHINGTON, D.C.

By the

ASTRO-ELECTRONICS DIVISION
DEFENSE ELECTRONIC PRODUCTS
RADIO CORPORATION OF AMERICA
PRINCETON, NEW JERSEY

AED R-2489

Issued: December 30, 1964

PREFACE

This document is the design report for converting the TIROS OT-2 spacecraft from the standard axial camera configuration to a "Wheel" mode configuration, for use in the first TIROS Operational Satellite (TOS) system. In this report, two "Wheel" mode configurations are covered: one involving two fully redundant Automatic Picture Transmission (APT) systems, and the other, two fully redundant Advanced Vidicon Camera Systems (AVCS). The design was produced for the Goddard Space Flight Center of the National Aeronautics and Space Administration by the Astro-Electronics Division of the Radio Corporation of America under NASA Contract No. NAS5-3173.

TABLE OF CONTENTS

TABLE OF CONTENTS (CONTINUED)

TABLE OF CONTENTS (CONTINUED)

TABLE OF CONTENTS (CONTINUED)

TABLE OF CONTENTS (CONTINUED)

LIST OF ILLUSTRATIONS

LIST OF ILLUSTRATIONS (CONTINUED)

LIST OF ILLUSTRATIONS (CONTINUED)

LIST OF ILLUSTRATIONS (CONTINUED)

LIST OF ILLUSTRATIONS (CONTINUED)

LIST OF ILLUSTRATIONS (CONTINUED)

LIST OF ILLUSTRATIONS (CONTINUED)

LIST OF TABLES

LIST OF TABLES (CONTINUED)

LIST OF TABLES (CONTINUED)

PART 1. INTRODUCTION

SECTION I. GENERAL

RCA, under NASA contract No. NAS 5-3173, has produced a system design for a TIROS OT-2 spacecraft that will operate in a "Wheel" mode in a sun-synchronous orbit at an altitude of 750 nautical miles. The spacecraft is being designed in two configurations: one utilizing two fully redundant Automatic Picture Transmission (APT) systems; the other, two fully redundant Advanced Vidicon Camera Systems (AVCS). In either configuration, the spacecraft will be capable of meeting its primary mission objective of providing daily observations of the complete global cloud cover by means of TV pictures.

The OT-2/APT spacecraft would meet the primary mission objective by providing direct-readout real-time TV pictures to a world-wide network of APT ground stations equipped with facsimile printers. The OT-2/AVCS spacecraft would meet the primary mission objective by means of a "remote-record" mode of operation, in which the spacecraft would take pictures while orbiting over the sunlit portion of the earth and record these pictures for later playback to special Command and Data Acquisition stations. With either configuration, only one of the two redundant camera systems aboard each spacecraft need operate for the spacecraft to meet the mission objective; the second subsystem will be used as back-up to provide enhanced reliability and increased system operational lifetime.

The design of both systems is based on space-proven techniques as applied to the design of TIROS "I", the first "Wheel" spacecraft, which is scheduled for launch in the first quarter of 1965. It is anticipated that experience gained through orbital operation of TIROS "I" will provide additional design confirmation and aid in selection of the most effective programming and data-utilization techniques for the OT-2 spacecraft.

Although the system designs have been established with unit-interchangeability as a design goal, the differences in size and weight of the two camera systems dictate two discrete spacecraft layouts and harness designs; and the differences in operational concept dictate various additional modifications to the subsystems which support and control the camera systems.

The radiation environment at the design orbital altitude of 750 nautical miles will be much more severe than the radiation environments encountered in the previous TIROS missions. However, experience with orbital operations of the Relay satellite has shown that spacecraft can survive similar environments for long periods and, with implementation of the precautionary measures outlined elsewhere in this report, radiation damage will not prevent the OT-2 spacecraft from meeting its design objectives.

SECTION II. MISSION REQUIREMENTS

A. OT-2/APT SPACECRAFT

The basic purpose of the OT-2/APT spacecraft is to provide APT field stations with slow-readout facsimile photographs of the existing daytime cloud cover in their locale. Cloud coverage must be provided once per day to each of a network of field stations. The individual stations may be located anywhere in the world. Each picture is to be taken while the camera optical axis is pointing toward the center of the earth. Pictures from successive orbits should leave no areas of the earth uncovered between the orbits. Successive pictures along the orbital path must provide greater than 30-percent overlap. To provide consistent illumination conditions, the orbit is to be sun synchronous.

The Nimbus APT camera subsystem is to be adapted to perform this mission at an orbital altitude of 750 nautical miles. The start of an APT picture-taking sequence is to be programmed from a Command and Data Acquisition (CDA) station. Two different sequence lengths are required and the selected sequence is to repeat itself each orbit, starting at the parallel of latitude originally programmed, until a change in the sequence is commanded.

The design of the spacecraft will permit a mission life of six months of orbital operation.

B. OT-/AVCS SPACECRAFT

The purpose of the OT-2/AVCS spacecraft is to provide to meteorological centers complete daytime cloud-cover pictures every day. The cloud-cover pictures taken by the spacecraft are to be stored by means of a magnetic-tape recorder. When the spacecraft is within communications range of either of two CDA stations, one located on the East Cost of the United States and one located in Alaska, the tape recorder is played back and the pictures are transmitted during the spacecraft-to-ground station contact, with a minimum of delay. The pictures are to be taken when the camera optical axis is either collinear with the local vertical or displaced 15 degrees from the local vertical in the orbital plane. A 50-percent overlap is required between successive pictures along the orbit track. The orbit is to be sun synchronous at an altitude of 750 nautical miles.

The Nimbus AVCS camera and tape recorder are to be adapted to perform the mission. The picture-taking sequences are to be programmable by the CDA stations as in the OT-2/APT spacecraft.

The design of the spacecraft will permit a mission life of six months of orbital operation.

PART 2. SYSTEM DESCRIPTION

SECTION I. BASIC SPACECRAFT

A. FUNCTIONAL DESCRIPTION

The OT-2 spacecraft is a polyhedron which approximates a right-circular cylinder, 42 inches in diameter and 22.5 inches in height. Solar cells are mounted on the top and sides of the polyhedron to generate electrical power for the spacecraft. The spin axis is defined as the cylinder's axis of revolution. The cameras are mounted on the base-plate and are perpendicular to the spin axis. In the normal operating mode, the spin axis is maintained perpendicular to the orbit plane. Therefore, as the spacecraft rotates on its axis, each camera alternately looks toward and away from the earth.

1. Spacecraft Dynamics

Immediately after the spacecraft has been launched and has separated from the final stage of the booster rocket, the spacecraft spin-axis lies approximately in the plane of the orbit and its spin rate is the same as that of the final-stage rocket. Before the spacecraft can begin to perform its mission, the spin rate must be reduced to 10.9 rpm for the OT-2/APT spacecraft and 9.2 rpm for the OT-2/AVCS spacecraft, and, for both spacecraft, the spin axis must be perpendicular to the plane of the orbit.

The sequence of events following spacecraft separation from the third-stage rocket constitutes the orientation maneuver, and results in the proper spacecraft attitude and spin rate. This sequence is as follows:

(1) The precession dampers are released to reduce spin-axis nutation to a very small value.

(2) The Yo-Yo de-spin devices are released to reduce the spin rate to within a few rpm of the desired rate.

(3) A spin-axis torquing (Quarter-Orbit Magnetic Attitude or QOMAC) program is initiated to start the attitude maneuver which will move the spin axis until it is perpendicular to the orbital plane.

(4) After the orientation of the spin-axis is partially completed, "real-time" control of the spacecraft's spin is initiated to achieve the desired spin-rate (Magnetic Spin Control or MASC program).

Since the spacecraft utilizes a passive thermal-control system, the orientation maneuver is initiated within the first several orbits to preclude the occurrence, depending on the launch time, of abnormally low temperatures. The orientation maneuver is to be accomplished within two days after launch.

Operation of the camera shutter is synchronized with satellite spin by means of an orthogonal horizon sensor that is mounted perpendicular to the spin axis and radially located so as to produce a horizon-crossing pulse at the time when the camera is pointing at the earth along the local vertical. On the OT-2/AVCS spacecraft, an alternate set of horizon-crossing sensors (one for each camera) may be selected by programming, to provide a camera-pointing angle which is 15 degrees off-set from the local vertical in the plane of the orbit.

In addition to requiring a signal to trigger the camera shutter at the proper time, both OT-2 systems also require that the spin axis be maintained perpendicular to the orbit plane. Because the orbit is sun synchronous, it precesses eastward at 0.986 degree per solar day. Correspondingly, the spin axis must be precessed a like amount in order to maintain perpendicularity.

Two methods will be provided for changing the spin-axis orientation by ground command. The primary method utilizes the QOMAC coil and the spacecraft programmer that is not in use for picture-taking. The programmer properly phases and cycles current through the torquing coil in response to instructions sent by ground command. The instructions include orbit-period data which permit the programmer to use the actual orbit period rather than a nominal period.

The secondary method utilizes the magnetic-bias coil which, in normal operation, is used to null the spacecraft residual magnetic moment in order to eliminate any undesired spin-axis drift. If it becomes necessary to use this device as the sole means of attitude control, the associated multi-position switch will be "stepped" by ground command and attitude control will be effected in much the same manner as on previous TIROS spacecraft.

2. Spin-Rate Control

In order to make the measurement of the spacecraft spin-rate a useful means of timing picture-taking functions with acceptable accuracy, precision control of the spin rate is necessary. In addition, internal camera timing must be synchronized with the shutter. This is conveniently done by making the spacecraft spin-period conform to the desired camera timing interval. For the OT-2/APT camera, the timing interval is 5.5 ± 0.025 seconds, and this parameter governs the accuracy with which the spin rate must be controlled.

In the OT-2/AVCS system the spin period is 6.5 seconds, which simplifies the synchronization of camera-shutter timing with the 6.5-second frame time required for camera timing.

"Real-time" commands from the CDA stations are used to control the spin rate with the required precision by regulating the period of operation of the magnetic spin-control coil.

3. APT Picture Programming

The OT-2/APT spacecraft can be programmed by a CDA ground station to take either 8-picture, or 4-picture sequences. In either sequence, the interval between successive pictures is 352 seconds. Once programmed, a sequence is automatically repeated every orbit period until a new program is transmitted to the spacecraft. The time for an orbit period is included in the program data and nominally is 113.5 minutes. The start of a picture-taking sequence is controlled by the interrogating CDA ground station and can be delayed by a maximum period of approximately 188 minutes.

An 8-picture sequence permits full daytime global coverage with approximately 35-percent overlap of successive pictures. The sequence of eight pictures can be positioned such that the "terminator" (day/night line on the earth) appears in the corner of the first and eighth picture. The distance covered along the orbit track during a remote sequence is approximately 9,500 nautical-miles. The adjacent pictures of successive orbits are contiguous.

The design of the spacecraft also provides for the 4-picture sequence even though (1) additional components are required to permit the capability of choosing the desired sequence length, and (2) the spacecraft mission plan, itself, does not include the requirement for varying sequence lengths. The capability for a 4-picture sequence was added to the design because of several factors. First, the length of the operating life of an APT camera is directly dependent on the total operating time. Since APT ground stations are not distributed uniformly over the earth, on some occasions an 8-picture sequence would not be completely utilized, entailing an unnecessary use of power and camera operating time. Consequently, the availability of the shorter, 4-picture sequence, allows lengthening of the system life while still accomplishing the mission of supplying APT ground stations with pictures of local weather systems. A second consideration leading to the incorporation of the additional sequence is radiation damage to the solar-cell array. After the spacecraft has been operating in space for six months, the reduced amount of available power could limit full programming under certain conditions. Therefore, the additional programming flexibility also permits operation after six months under reduced power conditions without seriously jeopardizing the spacecraft mission of providing weather information.

4. AVCS Picture Programming

Picture programming is the same for the AVCS system as for the APT, except that the two picture sequences available are 6- and 12-picture sequences rather than 4- and 8-picture sequences. After the initial programmed delay, the sequences are repeated each orbit until commanded off.

For the AVCS system, 6.5 seconds has been chosen for the spacecraft spin period. This corresponds to the AVCS camera frame time and is the basic increment of picture-sequence timing.

The length of the picture sequence is determined by the required picture overlap. Ultimately, the pictures will be processed automatically and, because a sun-glint in a picture would make such processing difficult, sufficient overlap is necessary to ensure that areas obscured by a sun-glint in one picture will be visible in the next picture of the sequence. In the prescribed 12-picture sequence, pictures will be separated by 40 spins of the spacecraft (260 seconds). This separation will provide greater than 50 percent overlap and will ensure complete coverage. The adjacent pictures of successive orbits will be contiguous.

The required tape recorder storage is a function of the number of "blind" orbits. If a minimum radio horizon of 10 degrees is assumed for the Alaska station and a minimum radio horizon of 5 degrees for the East Coast station, it is possible to have two consecutive orbits during which a ground station will not contact the spacecraft. Because it is necessary to receive the data from the satellite as soon as possible, and because the CDA ground stations are both located in the northern hemisphere, a daytime ascending orbit was selected for the OT-2/AVCS spacecraft. This orbit causes the first contact following the two "out-of-view" passes to occur on a descending nighttime pass at the East Coast station. At the time of this contact, the tape recorder will have stored 36 pictures, which can be read out within 4.8 minutes.

All other readouts will contain data from only one orbit and will be read out within 1.6 minutes. Since the readout time is less than the time between pictures, readout of the tape recorder can be accomplished between picture-taking cycles without losing a picture or interrupting a sequence. The system is also provided with the capability for taking direct pictures, i.e., individual pictures taken and immediately transmitted to a ground station in response to individual commands, but this is primarily for spacecraft evaluation purposes.

5. OT-2/APT Spacecraft Orbital Operation

Figure 2-I-1 is the block diagram of the OT-2/APT spacecraft. As in the previous TIROS spacecraft, the command receivers demodulate the RF carrier and present the resulting audio tones to the inputs of the decoders. Receiver I supplies tones to decoder I only, and receiver II supplies decoder II only. Prior to receipt of any FSK digital commands, an appropriate decoder "Enable" tone (separate frequencies are provided for side I and side II) must be received for a period of time sufficient to overcome an initial delay. The enable tone must be followed by the FSK tone associated with the enabled decoder. Reception of this command sequence provides decoder selection, and, simultaneously, causes power to be supplied to that decoder and to its directly associated equipment. Either decoder has the capability of operating, upon command, with either programmer. The selected decoder, in conjunction with the command matrix logic, decodes the address and the commands. The commands select the programmer, the camera, the orthogonal horizon-sensor pair, the transmitter, etc., to be used in the operating sequence, and apply the command data to the appropriate programmer.

For programs such as QOMAC or MASC operations, beacon selection, solar-aspect telemetry, magnetic-bias amplitude and polarity, or back-up commands for the separation functions, a similar technique is followed. The command storage and associated power switching is accomplished in the command distribution unit (CDU). The command distribution unit also gates power to the selected transmitter and activates the coaxial relay to couple the transmitter output to the single-dipole antenna located on the spacecraft hat.

Prior to remote camera sequencing, the selected programmer counts out the initial time delay (T_0) that precedes the picture-taking sequence and, upon alarm, generates the commands required to cycle the selected camera through its programmed sequence of operation. When the sequence has been completed, the programmer returns the camera system to "standby". Until commanded otherwise, the programmer causes the same sequence to be repeated on each successive orbit.

During picture data transmission, the input to the transmitter is the amplitude-modulated video subcarrier. The scanned video generated by the active camera is processed in the camera electronics and applied to the video modulator. The output from this modulator is applied to a video combiner which permits the modulation to be applied to either transmitter.

Synchronization of the timing signals for camera operation is obtained from orthogonal horizon-sensors which are positioned to view the horizon at the same instant that the camera is aligned with the local vertical. Either pair of orthogonal horizon-sensors can supply the required signals to either camera/programmer combination. Logic circuits within the command control subsystem and reference the camera shutter command to the proper horizon pulse, so that the active camera is looking down at the local vertical when its vidicon is exposed.

The MASC program (which controls the spin rate) is designed for short-duration operation under direct control of ground command. The QOMAC program (for maintaining the spacecraft spin-axis orientation) is controlled by the programmer in response to commands received from the ground and stored within the programmer. System redundancy and versatility permits operation of one camera by one programmer while the other programmer controls QOMAC operation.

Beacon transmitters are used for transmitting telemetry and for tracking purposes. Both beacon transmitters operate on the same frequency; however, only one is active at any time. Each beacon is provided with three sub-carrier oscillators which are continuously active. Two of the three in each set are modulated with the outputs from the two channels of the V-head (attitude) horizon-sensor. The third is modulated by selected, time-shared telemetry consisting of the commutated "housekeeping" telemetry, command-data verification, orthogonal horizon-sensor outputs (including a shutter-time marker), and solar-aspect telemetry. "Housekeeping" telemetry is processed for application to the commutators in the telemetry conditioner. The lift-off signal (third-stage separation) is applied to one of the continuously active sub-carrier oscillators. The spacecraft is equipped with timers to remove the beacon power after 18 months.

The solar-cell array provides power directly to the spacecraft and to the battery charging regulators. Spacecraft power is routed to both the unregulated bus and the load voltage regulators. Appropriate power distribution and high-current failure-mode protection circuits are provided at the outputs of the regulators and of the unregulated bus.

6. OT-2/AVCS Spacecraft Orbital Operation

Figure 2-I-2 is the block diagram of the OT-2/AVCS spacecraft. The operation of this spacecraft is very similar to that of the OT-2/APT spacecraft described previously.

The two AVCS cameras are completely redundant and their output video can be recorded on either one of the two AVCS tape recorders. A flutter and wow carrier is recorded on a separate track of the tape recorder while the picture data is being recorded, and is transmitted to the CDA station to provide for ground correction of spacecraft tape-recorder fluctuations. Satellite reference time and a frame of telemetry is also recorded on the fourth track of the tape recorder for transmission on the beacon link during playback.

The camera, tape recorder, and transmitter to be used for a particular picture-taking sequence are selected by FSK cross-coupling commands. Picture taking is controlled by the operating programmer. This unit provides commands which are processed by the CDU to supply power, synchronizing signals, and sequencing signals to the AVCS camera and tape recorder. Picture playback is commanded by the CDA station when the spacecraft is within communication range.

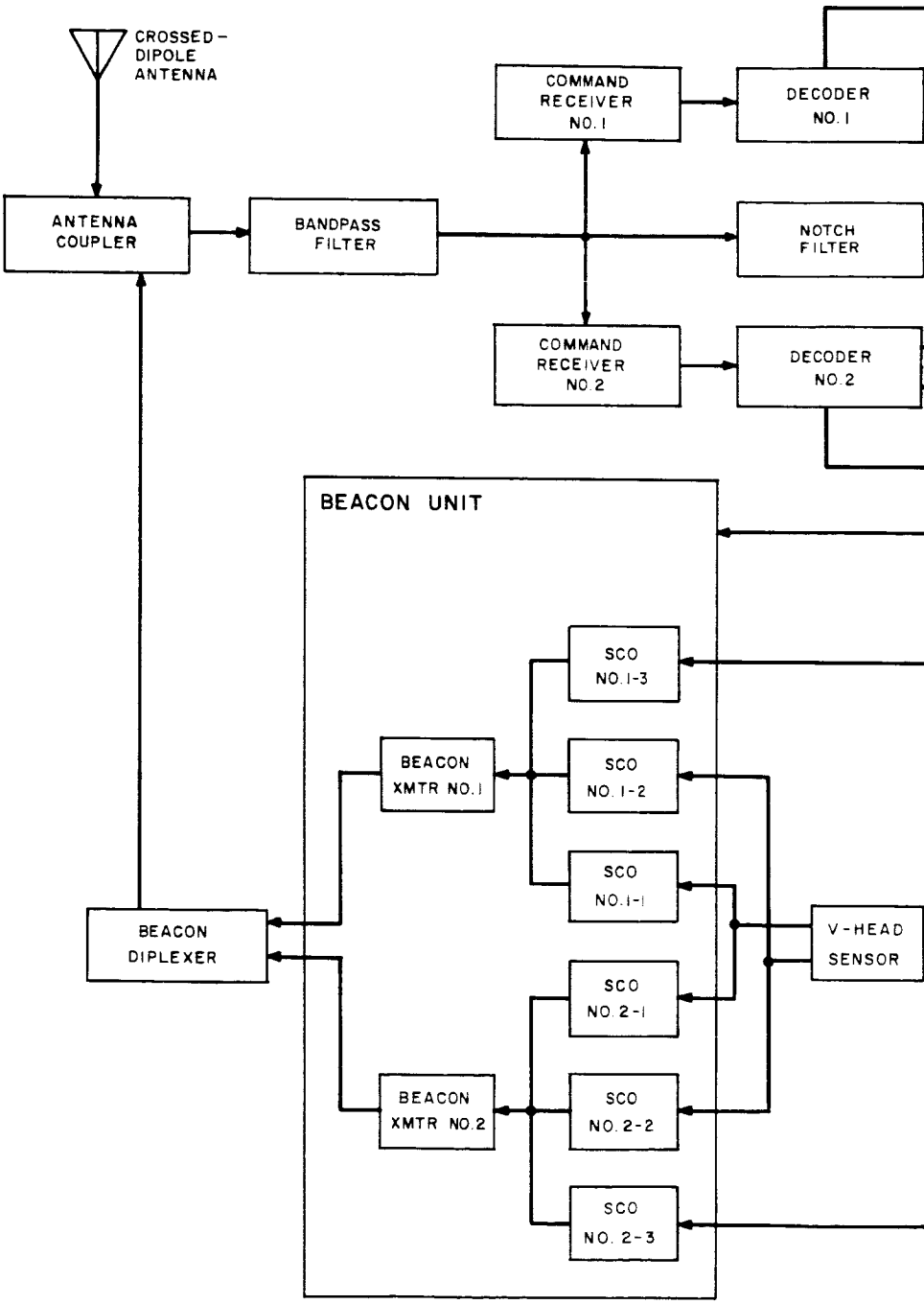
CROSSED-
DIPOLE
ANTENNA
ANTENNA
COUPLER
BANDPASS
FILTER
COMMAND
RECEIVER
NO. 1
DECODER
NO. 1
NOTCH
FILTER
COMMAND
RECEIVER
NO. 2
DECODER
NO. 2
BEACON UNIT
SCO
NO. 1-3
BEACON
XMTR NO. 1
SCO
NO. 1-2
SCO
NO. 1-1
BEACON
DIPLEXER
V-HEAD
SENSOR
SCO
NO. 2-1
BEACON
XMTR NO. 2
SCO
NO. 2-2
SCO
NO. 2-3

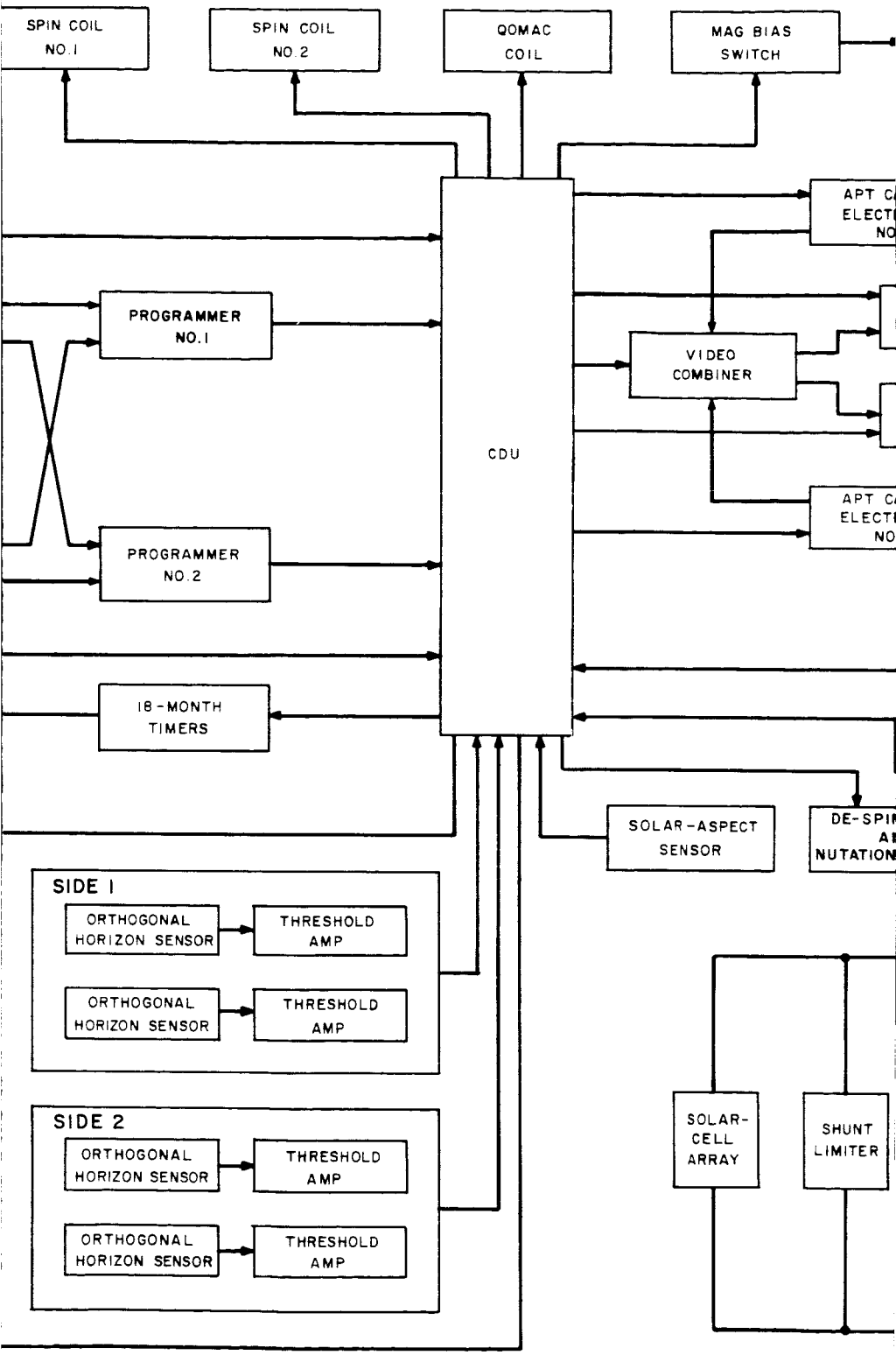
SPIN COIL NO.1
SPIN COIL NO.2
QOMAC COIL
MAG BIAS SWITCH
APT C
ELECT
NO
PROGRAMMER NO.1
VIDEO COMBINER
CDU
APT C
ELECT
NO
PROGRAMMER NO.2
18-MONTH TIMERS
SOLAR-ASPECT SENSOR
DE-SPIN
A
NUTATION
SIDE 1
ORTHOGONAL HORIZON SENSOR
THRESHOLD AMP
ORTHOGONAL HORIZON SENSOR
THRESHOLD AMP
SIDE 2
ORTHOGONAL HORIZON SENSOR
THRESHOLD AMP
ORTHOGONAL HORIZON SENSOR
THRESHOLD AMP
SOLAR-CELL ARRAY
SHUNT LIMITER

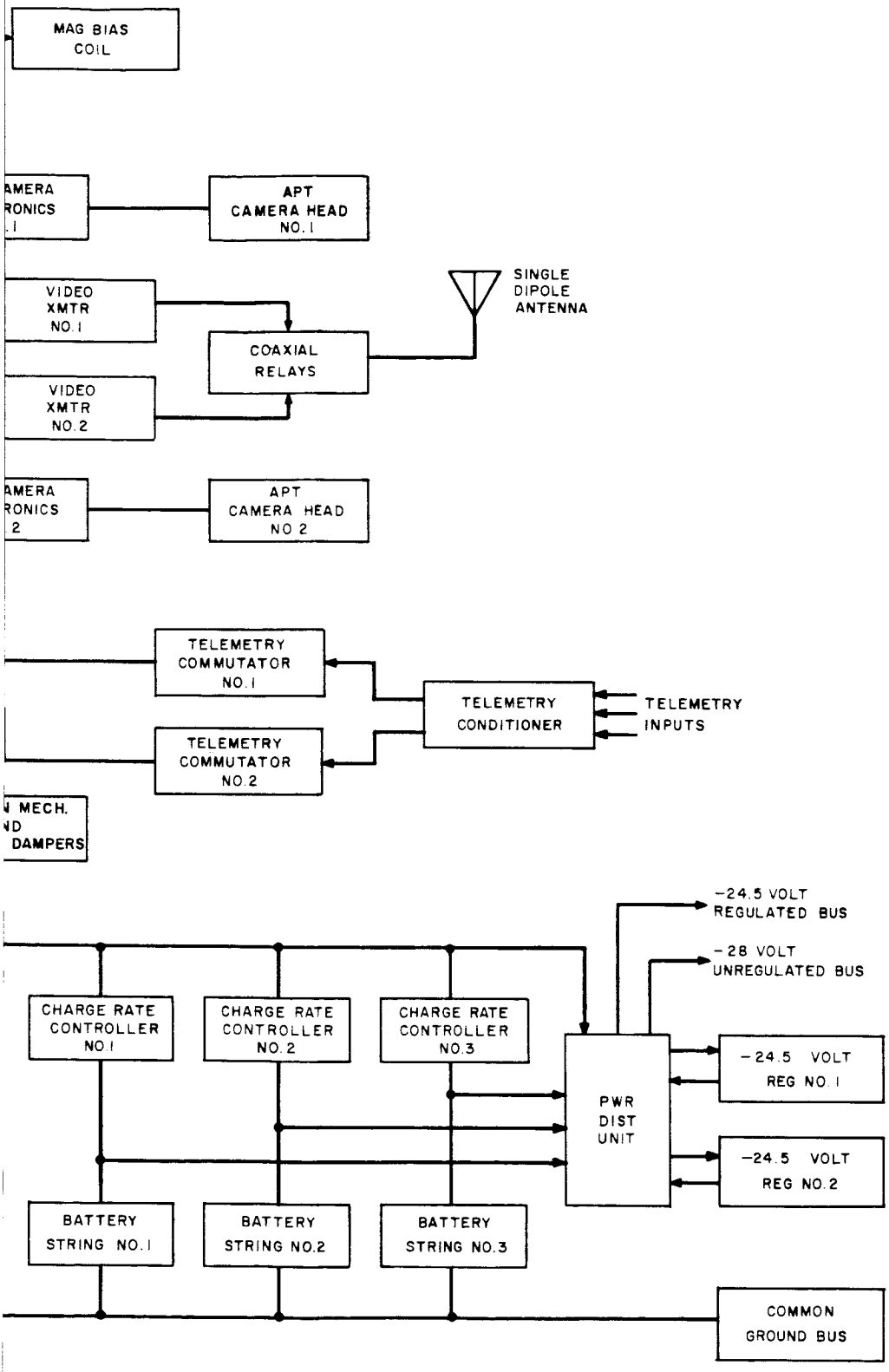

Figure 2-I-1. OT-2/APT Spacecraft, Block Diagram

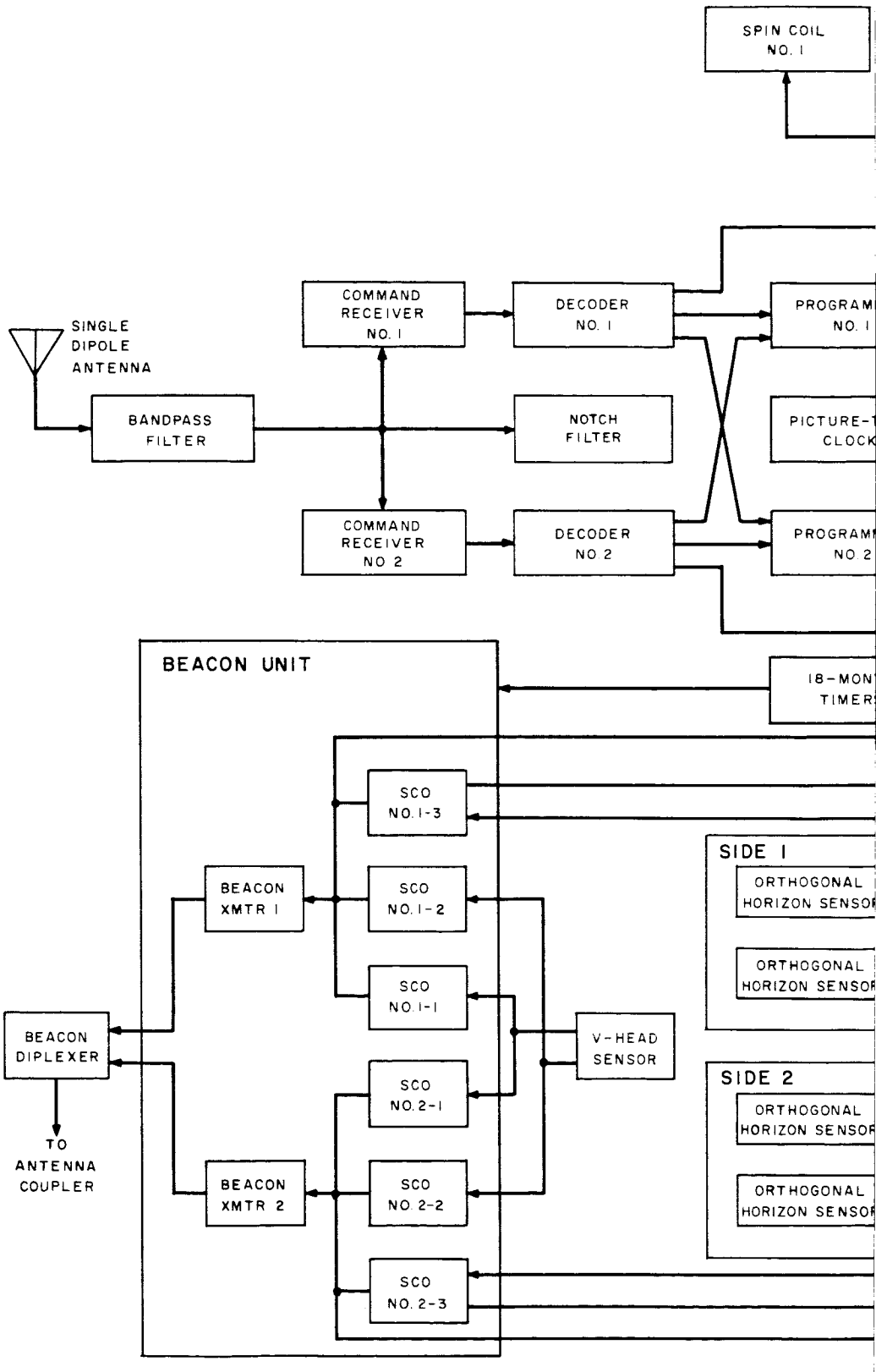
SPIN COIL NO. 1
SINGLE DIPOLE ANTENNA
BANDPASS FILTER
COMMAND RECEIVER NO. 1
COMMAND RECEIVER NO 2
NOTCH FILTER
DECODER NO. 1
DECODER NO 2
PROGRAM NO. 1
PICTURE-T CLOCK
PROGRAM NO. 2
BEACON UNIT
18-MON TIMER
SCO NO. 1-3
SCO NO. 1-2
SCO NO. 1-1
SCO NO. 2-1
SCO NO. 2-2
SCO NO. 2-3
BEACON XMTR 1
BEACON XMTR 2
BEACON DIPLEXER
TO ANTENNA COUPLER
V-HEAD SENSOR
SIDE 1
ORTHOGONAL HORIZON SENSOR
ORTHOGONAL HORIZON SENSOR
SIDE 2
ORTHOGONAL HORIZON SENSOR
ORTHOGONAL HORIZON SENSOR

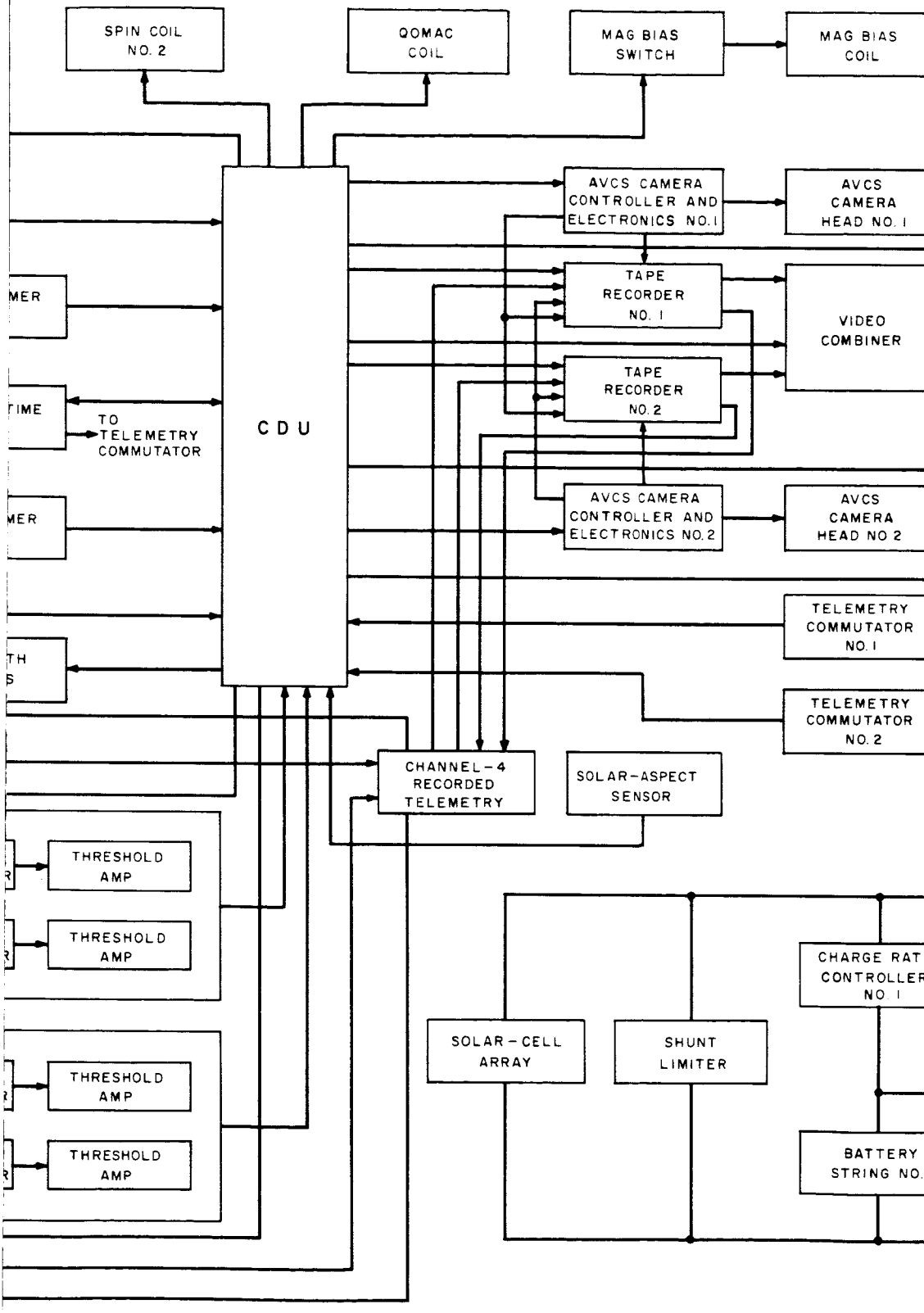
SPIN COIL NO. 2
QOMAC COIL
MAG BIAS SWITCH
MAG BIAS COIL
AVCS CAMERA CONTROLLER AND ELECTRONICS NO. 1
AVCS CAMERA HEAD NO. 1
TAPE RECORDER NO. 1
VIDEO COMBINER
TAPE RECORDER NO. 2
CDU
TO TELEMETRY COMMUTATOR
AVCS CAMERA CONTROLLER AND ELECTRONICS NO. 2
AVCS CAMERA HEAD NO 2
TELEMETRY COMMUTATOR NO. 1
TELEMETRY COMMUTATOR NO. 2
CHANNEL-4 RECORDED TELEMETRY
SOLAR-ASPECT SENSOR
THRESHOLD AMP
THRESHOLD AMP
THRESHOLD AMP
THRESHOLD AMP
SOLAR-CELL ARRAY
SHUNT LIMITER
CHARGE RAT
CONTROLLER NO. 1
BATTERY STRING NO.

(2)

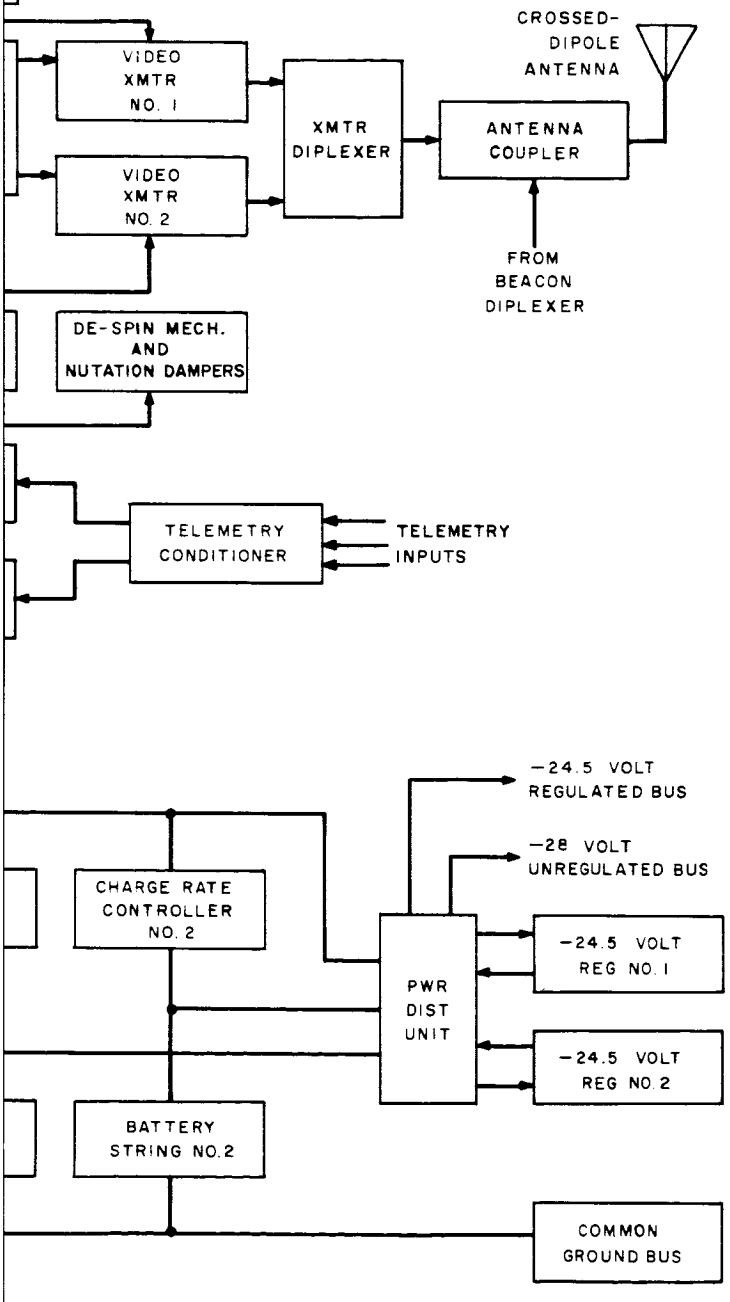

Figure 2-I-2. OT-2/AVCS Spacecraft, Block Diagram

Only one of the TV transmitters is in operation at any time. The transmitter to be operated is selected by ground command and is turned on whenever playback of stored data or readout of direct pictures is required. The TV transmitters operate at 235 Mc, the standard TIROS frequency.

The use of tape recorders to store video for subsequent playback to a CDA station results in a significant reduction in TV-transmitter operation time as compared with the transmitter operating time in the direct-readout APT system. This results in a considerable reduction in the average power consumption of the spacecraft. Because of the lower power consumption, only two strings of storage cells are required to support the AVCS mission. Individual storage cells are, however, identical to the cells used for the APT mission.

B. REDUNDANCY CONSIDERATIONS

The OT-2 spacecraft subsystems are fully redundant in both configurations except for portions of the power supply subsystem. In addition, within the subsystems, some of the units are also redundant. These units may be selected independently by ground command to form an operating system. As a result, only failures of identical redundant units could prevent the spacecraft from performing its mission. Throughout the design, every effort has been made to eliminate the possibility of a single component failure causing a system failure.

The following is a listing, grouped according to subsystem, of the redundant units:

(1) Command and Control Subsystem

- (a) Receiver and decoder,
- (b) Programmer,
- (c) MASC coil, and
- (d) Orthogonal horizon-sensors.

(2) Beacon and Telemetry Subsystem

- (a) Beacon and subcarrier oscillators, and
- (b) Telemetry commutator.

(3) Power Supply

Minus 24.5-volt voltage regulators.

(4) Camera Subsystem

(a) APT Configuration

1. Camera, and

2. Transmitter.

(b) AVCS Configuration

1. Camera,

2. Transmitter, and

3. Tape recorder.

The loss of one programmer could cause a slight reduction in system performance capability, because a picture-taking and a QOMAC program could no longer take place simultaneously. However, a QOMAC program need only be used three or four times a week, and this relatively small number of QOMAC operations could be scheduled to have a minimum effect on the mission of obtaining global, daily, cloud-cover.

The non-redundant units are as follows:

(1) Command and Control Subsystem

(a) Attitude control coil (QOMAC),

(b) Magnetic bias coil, and

(c) Picture-time clock (AVCS).

(2) Power Supply Subsystem

(a) Solar-cell array,

(b) Batteries and charge limiters, and

(c) Shunt limiter.

(3) Beacon and Telemetry Subsystem

(a) V-head attitude horizon-sensor, and

(b) Solar-aspect sensor.

In most cases, single failures of non-redundant units would not be catastrophic. The failure of the attitude control coil after initial orientation of the spacecraft spin-axis would reduce the precision of spin-axis control, but would not mean loss of control.

The spin-axis attitude can be maintained by switching current in the magnetic bias coil. Loss of the magnetic bias coil, or of its associated switch, would necessitate an increase in the frequency of QOMAC programming to obtain the same degree of spin-axis control.

The picture-time clock can be backed up by using knowledge of the spacecraft spin-period and of the spin number at camera shutter operation to compute the time of the picture.

The solar-cell array, though not redundant, cannot be disabled by individual solar-cell failure. Failure of individual solar cells would not be catastrophic, although it would cause performance degradation which, if extreme, would result in reduced picture-taking capability. Single failures in the batteries and charge limiters would result in reduced system performance. The size of the batteries was determined not by required storage capacity but by continuous overcharge capability; hence the recharge rate limits the system capability. The failure of a battery string would reduce the picture-taking capability of the spacecraft. If a failure were to result in an open battery circuit, some of the picture-taking capability could be regained by judiciously commanding the charge limiters to provide a high charge rate. The shunt limiter is internally redundant and protected against single component failures.

The V-head attitude scanner is redundant in the sense that if one of the two horizon sensors in the scanner should fail, spacecraft attitude could still be determined from the data supplied by the other, operating, sensor; however, the precision of the attitude measurement would be reduced. In addition, the data from one channel of the V-head scanner can be used with the data from the solar-aspect sensor to determine spacecraft attitude.

C. CDA/SPACECRAFT INTERFACE

1. General

The three channels of communication between the spacecraft and the ground are as follows: (1) a command link from the CDA stations to the spacecraft; (2) a beacon-telemetry link from the spacecraft to the CDA station; and (3) a video link from the spacecraft to the ground stations.

2. Command Transmission

Commands to the OT-2/APT spacecraft are received on the crossed-dipole antenna mounted below the spacecraft baseplate. The commands are fed to an antenna coupling network, which provides outputs to the two independent and redundant command receivers. An RF notch filter, tuned to 137.5 Mc, and a band-pass filter tuned to the command frequency, are inserted in the coupling cables between this network and the receivers to provide isolation from the beacon and APT transmitter frequencies.

Commands to the OT-2/AVCS spacecraft are received on the single dipole and are processed in much the same way.

Four audio tones are used in commanding the spacecraft. A pair of tones is provided for each of the two receiver-decoder combinations in the spacecraft. One tone is used to enable one of the receiver-decoders; the other is modulated by frequency-shift-keying to convey digital command data to the control and programming equipment on board the spacecraft. The transmission of the enable tone to either receiver-decoder for a specified period will initiate the transmission of "housekeeping" telemetry from the spacecraft. The digital data transmitted to the spacecraft includes a 12-bit address, a 12-bit command, and, if required, 28 bits of picture-taking or QOMAC data for the programmer.

3. Beacon-Signal and Telemetry Transmission

The beacon signal is used by the CDA station for tracking purposes and as a means of obtaining telemetry data from the spacecraft. The spacecraft contains two beacon transmitters; either transmitter can be selected for continuous operation. Both transmitters are equipped with the capability for temporary and permanent (after 18 months of operation) turn-off. The beacon transmitters drive a crossed-dipole antenna in phase quadrature to transmit circularly polarized waves.

Telemetry and attitude data are transmitted to the ground by modulation of the beacon transmissions. A system of frequency-division multiplexing is used. This system is implemented with three subcarrier oscillators for each of the two redundant beacon transmitters. The data from the V-head attitude horizon-sensor continuously modulates two of the subcarrier oscillators, each oscillator handling the output from one "head" of the horizon sensor. The third subcarrier oscillator is used in sequence for the transmission of (1) the normal "housekeeping" telemetry data, (2) data from the solar-aspect sensor, (3) command-verification signals, and (4) the camera-trigger pulse, with the camera-shutter signal superimposed.

The "housekeeping" telemetry yields information on the equipment status, component temperatures, the power status of the spacecraft, and satellite reference time. The solar-aspect sensor provides a direct measure of the sun angle with respect to the spacecraft. This measurement is particularly useful during the initial spin-axis orientation maneuver.

4. APT Video Transmission

The transmission of APT video signals to a ground station is preceded by the transmission of 3 seconds of the 300-cps "start" tone, followed by 5 seconds of the phasing pulses, which are modulated on the 2400-cps subcarrier. The video readout for each picture comprises 800 lines of data and lasts for 200 seconds. In the spacecraft, the video data amplitude-modulates a 2400-cps carrier which is then frequency-modulated on the 137.5-Mc TV carrier.

There are two video transmitters, only one of which is used at a time. The signals are transmitted from the single dipole antenna.

5. AVCS Video Transmission

The AVCS video data contains 833-1/3 active lines plus sync for each 6.5-second picture frame. The 60-kc video baseband is frequency-modulated on a 96-kc subcarrier. A 9.6-kc, tape-recorder wow and flutter signal is added to the video baseband and the combined signal frequency-modulates the 235-Mc carrier of the TV transmitter. There are two TV transmitters, only one of which operates at a time. The transmission of AVCS picture data on a 235-Mc carrier through the crossed-dipole antenna allows the standard TIROS antenna-coupling system and transmitting antenna to be used. No relays or RF switching are required.

6. CDA and APT Ground Stations

On the ground there are two primary CDA stations, one at Fairbanks, Alaska, and one on the East Coast of the United States. These stations will be completely independent of the TIROS ground stations already in existence at those locations.

The design of these stations is based on existing ground stations and makes use of much of the ground equipment currently comprising the AVCS operational station at Fairbanks, Alaska. The equipment used for generating the commands transmitted to the spacecraft is completely digital. Punched-tape readers are employed to minimize the possibility of operator errors in programming.

The OT-2/APT spacecraft has been designed for compatibility with the existing APT ground stations. These stations will, therefore, be capable of receiving APT video data directly from the spacecraft, and no modifications are required.

Table 2-I-1 is a summary of communication margins.

TABLE 2-I-1. SUMMARY OF COMMUNICATION MARGINS

System	Frequency	Threshold	C/N (5^{o} Above Horizon)	Margin Above Threshold
Command Receiver (1000-watt transmitter)	148 Mc	-107 dbm	28.2 db	16.2 db
Beacon (85-foot dish, 250-mw transmitter)	136.77 Mc	-119.7 dbm	17.3 db	14.5 db
APT Video (12.5-db antenna gain, 5-watt transmitter)	137.5 Mc	-111.3 dbm	14.8 db	5.8 db
AVCS Video (85-foot dish, 5-watt transmitter)	235 Mc	-103.2 dbm	20.8 db	11.8 db

SECTION II. AVCS/APT COMPARISON

A. INTRODUCTION

This section presents comparisons between the equipment on the OT-2/APT and OT-2/AVCS spacecraft. Many of the units are the same for both spacecraft; where there are extensive differences, they are discussed under separate headings for the APT and AVCS configurations. Where appropriate, comparisons are made with previous TIROS spacecraft equipment.

B. COMMAND AND CONTROL SUBSYSTEM

1. General

Operation of the spacecraft will be controlled by programs transmitted from Command and Data Acquisition (CDA) stations and stored and implemented by the command and control subsystem of the spacecraft. Programming transmissions from the CDA stations can command the spacecraft to do the following:

(1) Perform the "Wheel"-orientation maneuver so that the spacecraft spin-axis is normal to the orbital plane and its cameras alternately view space and the earth with each revolution.

(2) Maintain the "Wheel" attitude within the limits specified for the desired photocoverage.

(3) Activate the selected camera system.

(4) Store and count out the delay time to the start of a picture-taking sequence, complete the sequence, and repeat that sequence on each orbit until such time as a different program is transmitted to the spacecraft.

(5) Provide a beacon signal for spacecraft tracking.

(6) Transmit telemetry and attitude data to CDA stations.

In addition to the above, the CDA station can command the OT-2/AVCS spacecraft to play back the tape recorder and transmit the video data.

2. Dynamics Control

The ability of the OT-2 spacecraft to meet its mission requirements is highly dependent upon maintaining the proper spin-axis attitude and the proper spin-rate. These parameters will be maintained at the required values by means of the attitude and spin-control components consisting of a nutation damper, a de-spin mechanism, a Quarter-Orbit Magnetic Attitude Control (QOMAC) device, a Magnetic Bias Control (MBC), a Magnetic Spin Control (MASC), horizon sensors, and a solar-aspect sensor.

The nutation damper dissipates, as heat, any energy tending to cause the spacecraft to wobble. Two types of dampers will be used; a tuned-energy-absorption mass (TEAM) damper and a liquid damper. The purpose of the TEAM dampers, which were used in previous TIROS spacecraft, is to reduce rapidly the nutation angle to approximately 0.6 degree, the inherent threshold of the dampers. At this point the liquid damper, which has an extremely small threshold, will continue, at a slower rate, to reduce the nutation angle toward 10^{-2} degree.

The de-spin device is designed to reduce the orbit-injection spin rate of 125 rpm (nominal) to the operational spin-rate prescribed for the spacecraft. This device is of the same design used on all previous TIROS spacecraft. However, as in the case of TIROS "I", the device will be relocated so that the de-spin cables wrap about the spacecraft approximately halfway between the baseplate and the top of the hat assembly.

The MASC device is used to acquire and maintain the required operational spin period of 5.50 ± 0.025 seconds for the APT configuration, or 6.5 ± 0.025 seconds for the AVCS configuration. Although the design of this device is based on the device used for TIROS "I", two coils rather than one are used, and both coils are installed on the inside of the spacecraft hat (refer to Section 4-II-B). During spin-rate acquisition, these coils can be used simultaneously to provide a high-level magnetic torque and thus shorten the acquisition period. However, during normal orbital operation these coils are operated individually by means of completely redundant control circuits. It is anticipated that the use of only two to three MASC cycles per week will be sufficient to maintain the spin rate within the prescribed limits.

The QOMAC device is designed to maintain the "Wheel" attitude to within ± 1 degree. In order to limit the number of QOMAC cycles required to keep the OT-2 spacecraft "on station", the MBC will be used to eliminate any unwanted spin-axis drift due to the residual dipole moment of the spacecraft after injection into orbit. The MBC will be similar to the Magnetic-Attitude Control employed successfully on previous TIROS spacecraft and should allow the spacecraft to be maintained on station with only three or four QOMAC cycles per week.

Two types of horizon sensors are included on the OT-2 spacecraft: orthogonal horizon sensors for camera triggering and a V-head horizon-sensor for attitude and spin-rate measurements. The orthogonal horizon-sensors are similar to their counterparts on

TIROS "I", having a field-of-view of 1.3 degrees ±20 percent, and sensitivity to infrared radiation in the 1.8- to 23-micron region. The included angle of the V-head scanner will be modified to suit the higher altitude of the OT-2 spacecraft, and the range of infrared sensitivity changed to the 13- to 23-micron region. This is to provide better definition at the earth-to-sky horizon crossing and to reduce the interference from the sun in the up-looking sensor. The solar-aspect sensor is identical to its counterpart on TIROS "I". Information supplied by this sensor will be used to establish spacecraft attitude during the Wheel-orientation maneuver and during passes with short satellite-to-earth contact times, when insufficient V-head horizon-sensor data is received from the spacecraft.

3. Command Receiver, Decoder, and Command Distribution Unit

a. General

The design principles employed in adding some digital command functions to the TIROS "I" spacecraft have been extended to equip the OT-2 spacecraft with a fully digital command and control subsystem. Although many of the command functions are similar to those of TIROS "I", the camera triggering system has been simplified since spin-controlled operation of the spacecraft obviates the need for a computing trigger. Other changes in command functions have been made because of the differences between the requirements of the TIROS, APT, and AVCS camera systems.

Finally, the circuits that perform the command functions have been repackaged to include two command receivers, two decoders, and one command distribution unit (CDU).

b. Command Receivers

The command receivers are of the same design as those used on all TIROS spacecraft since TIROS IV. The antenna filter, which isolates the command receivers and beacon transmitters, is of the same basic design as that employed on TIROS VIII.

c. Decoders

The two decoders are completely redundant. Each consists of circuits for decoding the digital commands. Although all spacecraft commands are digital, an analog "enable" signal must be received by the command and control equipment before the communications channel is opened. Once enabled, the decoder accepts the frequency shift keyed (FSK) command signals from the CDA station and, provided the correct spacecraft address code is included, supplies the commands to the CDU.

d. Command Distribution Unit

The CDU includes two fully redundant sets of circuits. This unit distributes commands to the designated unit or subsystem, provides impedance matching between subsystems, and contains the switching circuits necessary for cross-coupling the various elements within each picture-taking system. As in the TIROS "I" cross-coupling circuits, latching-type circuits are employed in the OT-2 spacecraft. Thus, once a cross-coupled mode is slected (i.e., camera No. 1, transmitter No. 2, Programmer No. 1, etc.), the mode will be maintained until a different command is received by the spacecraft.

4. APT Programmer

The two programmers are fully redundant. The operating programmer receives, stores, and counts out the delay time specified for the start of either a picture-taking or QOMAC sequence, and controls the operation of the spacecraft during the sequence. In the case of QOMAC operation, the programmed sequence can be repeated up to eight times in response to one ground command. For the picture-taking sequences, the programmer starts the sequence, counts out the number of pictures programmed (4 or 8), turns off the picture-taking equipment, and repeats the entire sequence one orbit later. The programmer continues to repeat the sequence each orbit until such time as a different picture-taking command is received from the ground station.

The programmer turns on power to the camera, provides a signal to start the prepare, expose, and develop cycle, and one spacecraft spin later provides a signal for activating the camera shutters.

5. AVCS Programmer

The AVCS programmer is essentially the same as that for the OT-2/APT spacecraft. The differences result from the different basic-timing rate of the AVCS camera, the different sync rate required by the camera, and the difference in operational concept (i.e., remote-storage versus real-time operation). Also, in the OT-2/AVCS spacecraft, the command and control subsystem provides the flutter-and-wow carrier and tape-recorder ON/OFF controls. In addition, a non-redundant picture-time clock is operated from programmer power. Data from the picture-time clock will precede each frame of "housekeeping " telemetry.

C. POWER SUPPLY SUBSYSTEM

1. General

The power supply subsystem consists of N-on-P solar cells mounted on the top and sides of the spacecraft hat, nickel-cadmium storage cells, a shunt current-limiter, and voltage and charge-rate regulators. The solar cells are identical to those employed on TIROS "I". However, the interconnection wiring has been altered to provide the slightly higher output voltage required to compensate for the gradual degradation of the cells due to radiation damage.

2. Batteries

The storage cells will each have the same ampere-hour capacity as those on TIROS "I", but will be rectangular rather than cylindrical. This change in cell type was made on the basis of studies and tests which showed that the rectangular cells possess greater inherent reliability than cylindrical cells.

Because the power requirements for the OT-2/AVCS spacecraft are lower then those for the OT-2/APT spacecraft, only two battery strings and, thus, only two charge-rate limiters will be employed in the AVCS system instead of three.

3. Shunt Voltage Limiter

Because the power dissipation requirements during the initial months of OT-2 operation will be greater than for TIROS "I", a shunt current-limiter has been used in place of the previously employed by-pass regulator. This limiter, used in conjunction with a blocking diode, will limit the output voltage and dissipate the excess energy supplied by the solar array.

4. Charge Rate Regulator

The bi-level charge-current regulators are essentially the same as those used for TIROS "I". However, several component changes have been made to ensure satisfactory performance despite the high radiation levels that will be encountered at the OT-2 spacecraft orbital altitude. One regulator is installed in series with each battery string to limit the charge rate. The low charge rate is 400 milliamperes per battery string while the high charge rate is 600 milliamperes per string.

5. Voltage Regulator

The voltage regulator is identical to the -24.5-volt regulator employed on TIROS "I".

D. BEACON AND TELEMETRY SUBSYSTEM

Because the OT-2 spacecraft will be at a greater altitude than TIROS "I", the TIROS beacon power of 50 milliwatts does not provide a sufficient communication margin. As a result, a beacon with an output power of 250 milliwatts and a design similar to the beacon used on the Relay Satellite will be used.

Only one beacon will be operated at a time and the beacon RF carrier will be phase-modulated with the outputs of three frequency-modulated subcarrier oscillators (SCO). The SCO's are frequency-modulated with telemetry, attitude, and command verification data.

Attitude data from the V-head horizon sensors will be continuously telemetered to the ground via two of the SCO's associated with the active beacon. The third SCO will be used to transmit the data from the telemetry commutator, command verification circuit, orthogonal horizon-sensor and the solar-aspect sensor on a time-shared basis.

The telemetry commutator used for "housekeeping" telemetry is similar to that used for the TIROS "I" spacecraft.

E. APT CAMERA SUBSYSTEM

The APT spacecraft includes two TV cameras and two transmitters that are similar to the APT camera and transmitter employed on TIROS VIII; however, only one of these cameras and transmitters is active at any given time. The TV transmitters are coupled to the single dipole antenna located on the top of the hat. Each camera is equipped with a Kinoptik Tegea 5.7-mm lens and a 1-inch polystyrene storage vidicon. The active camera is sequenced by the command and control subsystem to privide, in normal operation, a sequence of eight APT pictures. Each picture is approximately 1700 nautical-miles square; in a picture-taking sequence, each picture overlaps the preceding picture by 35 percent. The pictures are taken at 64-spin intervals and a 200-second readout period is used. This long readout enables picture reception and reproduction by means of the relatively simple APT ground stations which are situated throughout the world.

F. AVCS CAMERA SUBSYSTEM

The two AVCS cameras are essentially the same as those employed on the Nimbus satellite. However, the lens has been changed to the 5.7 mm Tegea, and the shutter has been changed to a TIROS shutter, modified for a one-inch vidicon. Some simplification has been possible insofar as the electronics unit is concerned, because many of the functions originally performed by this unit are performed on the OT-2 spacecraft by the command and control subsystem.

Each AVCS picture cycle lasts 39.25 seconds. The vidicon exposure period is 1.5 milliseconds; with the traveling slit shutter, it takes 10 milliseconds to completely expose the vidicon. Vidicon readout requires 6.5 seconds.

The two tape recorders are similar to the AVCS/Nimbus tape recorders. The four available channels on each tape recorder are used in the OT-2 application; one for camera No. 1 video, one for camera No. 2 video, one for the flutter-and-wow carrier, and one for spacecraft reference time and "housekeeping" telemetry. However, since only one of the two cameras will operate at any given time, only one of the two video channels will be used at any given time.

The frequency of the TV transmission is 235 Mc. The transmitter output is coupled to the crossed-dipole antenna. The two transmitters are identical to the 5-watt units used on TIROS "I".

PART 3. ORBITAL CHARACTERISTICS

SECTION I. GENERAL

The orbit for the OT-2 spacecraft is sun synchronous and circular at an altitude of 750 nautical miles. This orbit provides excellent utilization of the spacecraft's capabilities for obtaining total earth coverage (1) on a regular, recurring basis, (2) in a minimum time, and (3) with consistent illumination. The mechanics of the sun-synchronous orbit are the same as those of any circular earth orbit, with the unique exception that the precession of the orbital plane around the earth's polar axis is in the same direction and at the same rate as the earth's annual movement around the sun. This nodal precession of approximately one degree per day results in a nearly constant angle between the orbital plane and the sun vector, so that the spacecraft's subtrack on the surface of the earth receives nearly the same solar illumination throughout the mission period.

SECTION II. ORBITAL PARAMETERS

A. SUN-SYNCHRONOUS ORBIT

The unique mechanics of a sun-synchronous orbit derive from the spheroidal (rather than spherical) shape of the earth and the consequent non-symmetry of the earth's gravitational field. As a result of these factors, there is a gradual precession of the orbit nodes, westward if the orbital inclination is less than 90 degrees, and eastward if the inclination is greater than 90 degrees.

The orbital precession rate is a function of both altitude and inclination. The earth revolves eastward about the sun at the rate of 0.986 degree per solar day; therefore, the orbital precession about the earth must be at the same rate to maintain a fixed position relative to the sun. Figure 3-II-1 shows the geometry of a sun-synchronous orbit. For an orbital altitude of 750 nautical miles and a precession rate of 0.986 degree per solar day, the required inclination is 101.4 degrees.

The angle between the line of nodes and the projection of the earth-sun line in the equatorial plane is defined as the "o'clock angle". For the sun-synchronous orbit, the "o'clock angle" is nearly constant. The angle between the sun vector and vehicle spin axis is defined as the gamma angle (sun angle). For a sun-synchronous orbit, this angle will vary depending upon vehicle orientation and seasonal variations ("apparent" motion of sun above and below the equator). Since vehicle orientation is maintained constant in the wheel mode, only the seasonal variation in sun position with respect to the earth's equator will appreciably affect the gamma angle. Figure 3-II-2 illustrates the gamma angle and the other angles used to describe camera coverage. Figure 3-II-3 shows the seasonal variation in gamma angle for different nodal crossings.

B. EFFECT OF INJECTION ERROR

Since the nodal precession rate is a function of altitude and inclination, an injection error will cause a variation from the desired rate of precession. Figures 3-II-4 and 3-II-5, respectively, show the effect on precession of altitude and inclination variations (around the nominal values of 750 nautical miles and 101.4 degrees, respectively). The nodal drift shown is the difference between the actual precession and the desired rate. The total error in the desired rate of precession is the sum of the effects of the altitude error and the inclination error. For both altitude and inclination errors, any resultant positive "drift" in precession is in the eastward direction.

Since data on the performance of the booster rocket is not available at this time, precession errors cannot be predicted. However, the booster rocket performance must ensure that the angle between the orbit normal and the earth sun-line is maintained between 30 and 60 degrees for the six-month operational life of the spacecraft.

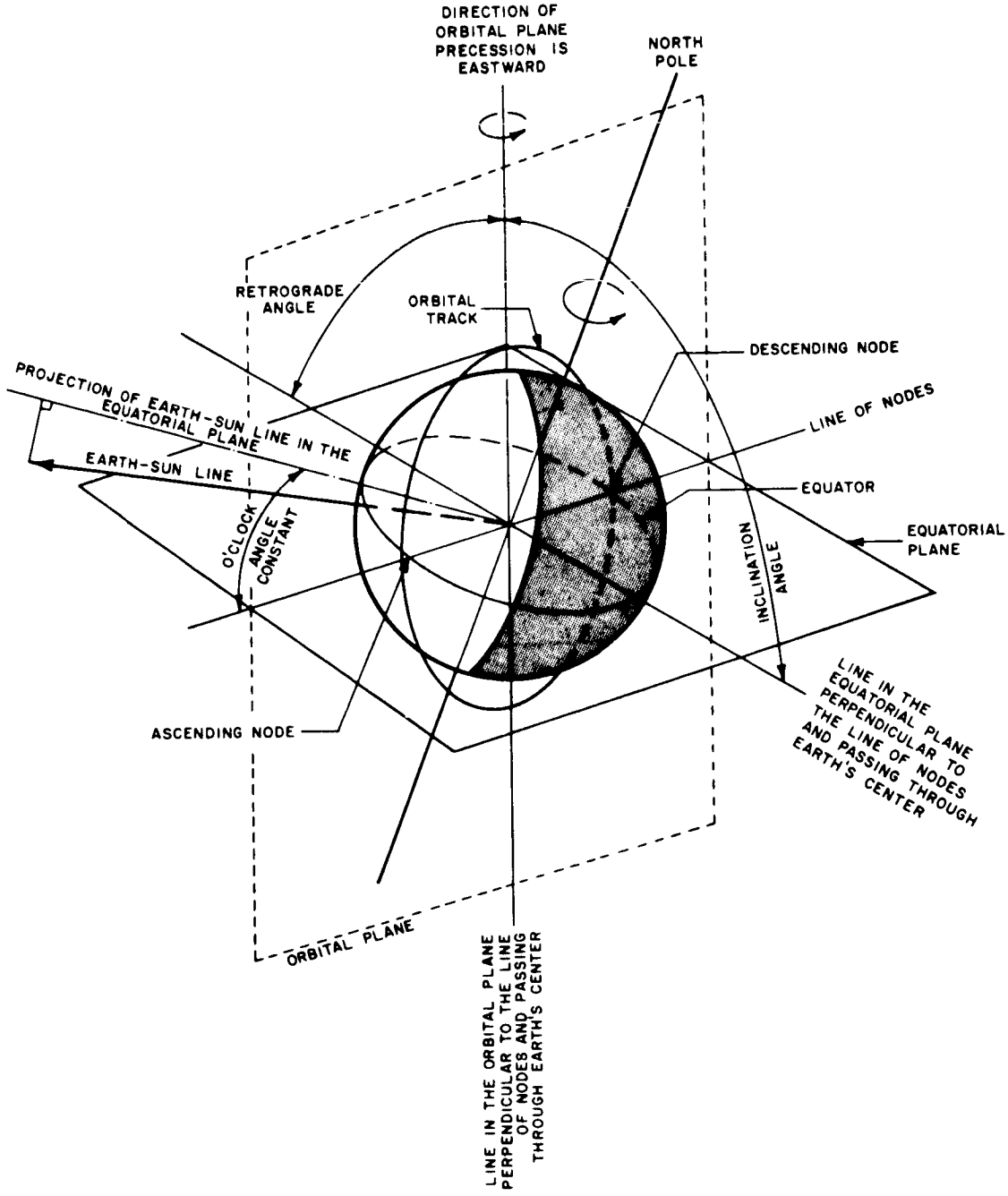

Figure 3-II-1. Geometry of a Sun-Synchronous Orbit

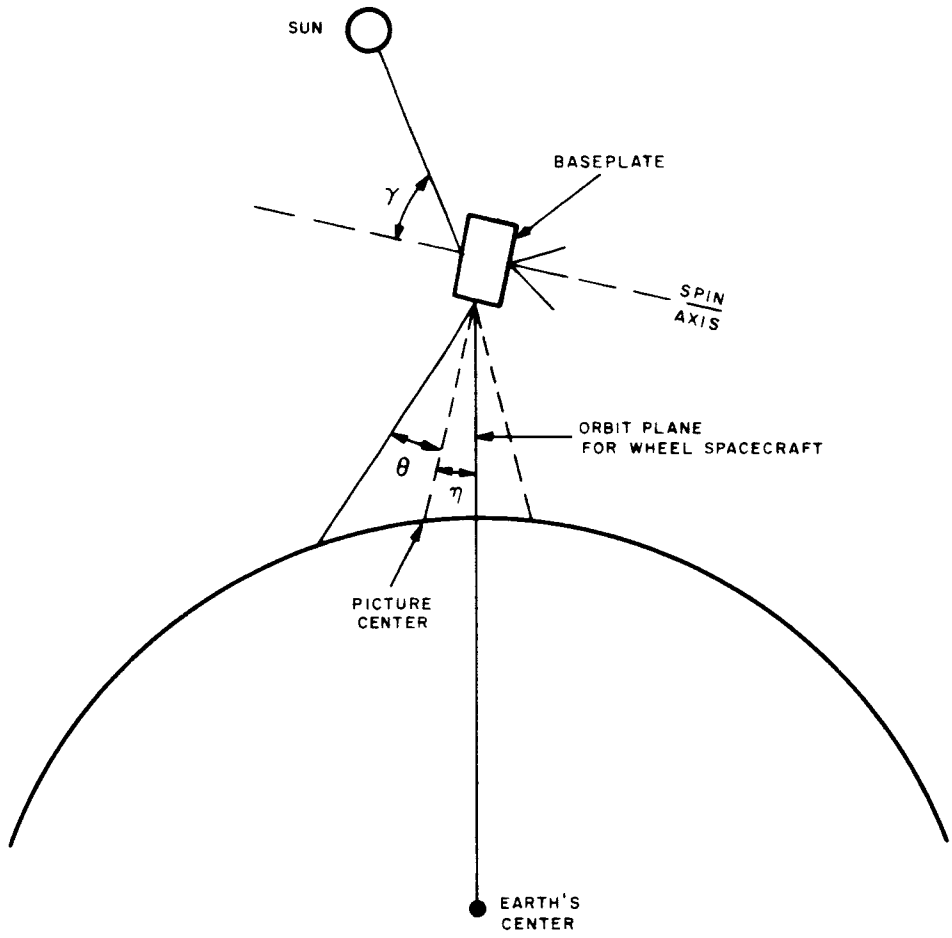

NOTE: THIS ILLUSTRATION IS FOR REFERENCE ONLY TO SHOW THE VARIOUS ANGLES INVOLVED IN SPACECRAFT OPERATION. IN WHEEL-MODE OPERATION, THE PICTURE CENTER WILL BE COINCIDENT WITH THE ORBIT PLANE.

η: NADIR ANGLE – ANGLE BETWEEN SPACECRAFT SUBPOINT AND PICTURE CENTER.

θ: CAMERA HALF-FIELD OF VIEW.

γ: GAMMA ANGLE (SUN ANGLE) – ANGLE BETWEEN SPIN AXIS AND SPACECRAFT SUNLINE.

Figure 3-II-2. Definitions of Gamma Angle (Sun Angle) and Angles Used to Describe Camera Coverage

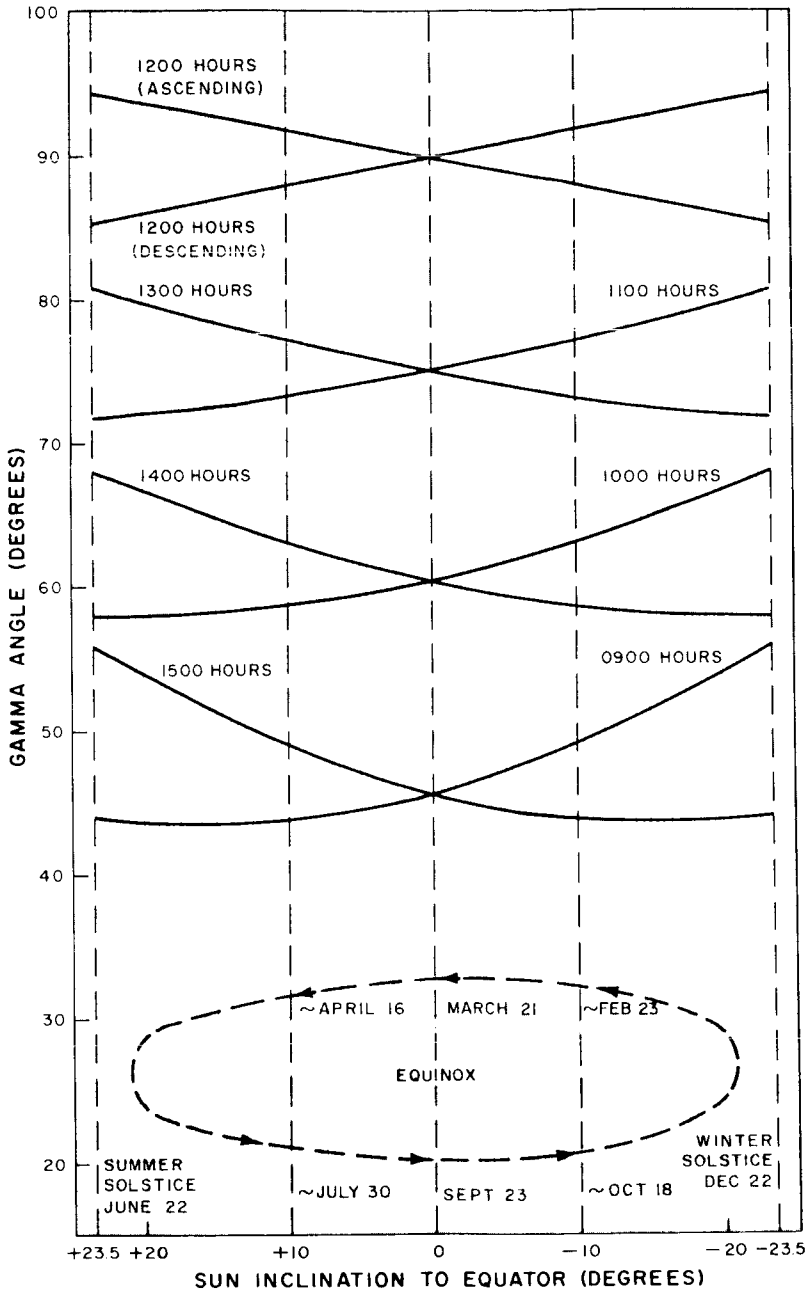

NOTE:
ALL AFTERNOON TIMES ARE FOR ASCENDING NODAL CROSSINGS.
ALL PRE-NOON TIMES ARE FOR DESCENDING NODAL CROSSINGS.

Figure 3-II-3. Seasonal Variation in Gamma Angle (Sun Angle) for Different Nodal Crossings

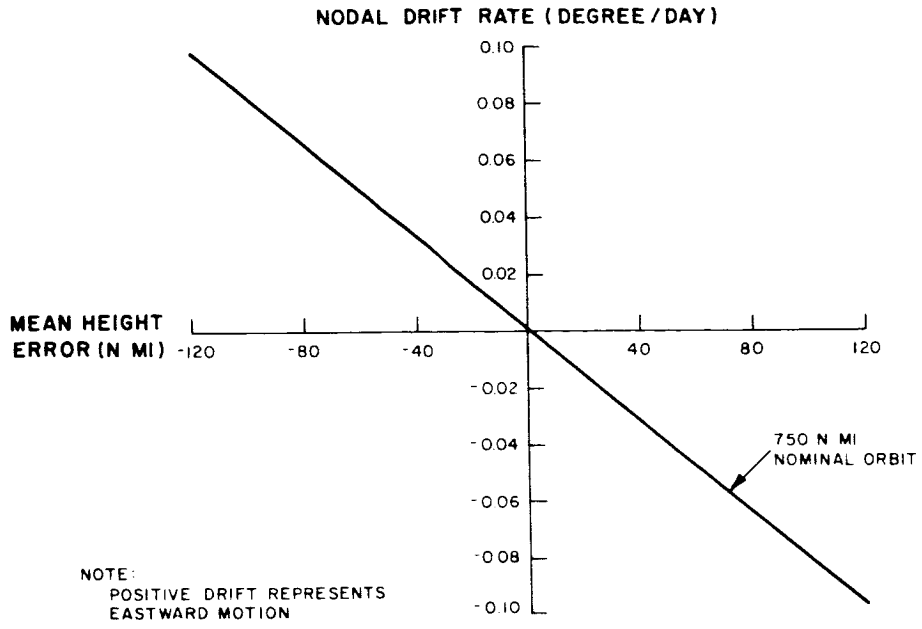

Figure 3-II-4. Mean-Height Error Versus Nodal Drift Rate

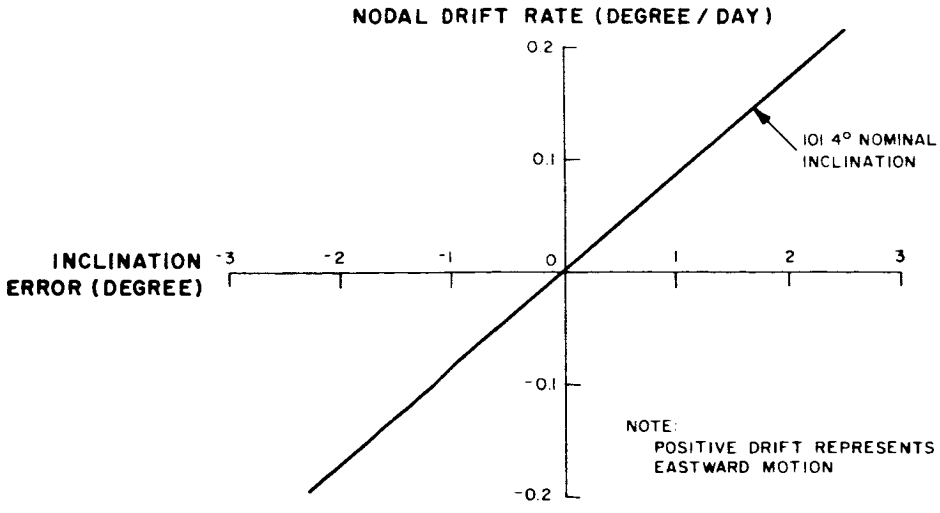

Figure 3-II-5. Inclination Error Versus Nodal Drift Rate

SECTION III. RADIATION ENVIRONMENT

A preliminary analysis of the effects of radiation on the OT-2 mission was performed. This investigation covered the effects of naturally occuring radiation (Van Allen, cosmic, and solar-flare radiation) and artifically produced radiation (Starfish belt). Appendix C presents the radiation profile expected for the six-month mission period. In Appendix C, curves are also given showing ionization damage and crystal lattice damage (over the six-month period) versus shielding thickness. The effective shielding provided by the spacecraft and the theoretical effects of radiation on various components, such as transistors, lenses, and vidicons, are also presented in Appendix C.

The practical experience gained from operation in orbit of the Relay Communication Satellite, built for NASA by RCA, has also been examined in relation to the OT-2 mission. The survival of the Relay Communication Satellite is relevant to an analysis for the OT-2 mission because of the similarity between the radiation environments of the two spacecraft and the similarity between some of the spacecraft hardware. During one year of exposure, the Relay Communications Satellite experienced the same total dosage as would the OT-2 spacecraft in six months. The successful operation of the Relay Satellite indicates a discrepancy between actual flight experience and what might be predicted with pessimistic estimates. At the present time, sufficient information is not available on radiation effects to evaluate these discrepancies.

The most serious radiation effect appears to be lens "browning". Theoretical computations indicate that the transmission of an undoped Tegea lens would decrease approximately 15 to 30 percent during the six-month OT-2 mission (assuming 250 mils of equivalent shielding). While the spacecraft is operating in space, an annealing process will take place which will reduce total damage.

During the subsystem design phase, radiation damage will be examined in greater detail and tests will be conducted to evaluate specific effects, particularly lens degradation. Based on previous experience, it is felt that the spacecraft subsystems can be designed to survive the radiation environment without significantly limiting mission objectives.

SECTION IV. CAMERA COVERAGE

A. ILLUMINATION

The ground illumination pattern "seen" by the camera depends on the orientation of the orbit relative to the sun, which is specified by the time of the nodal crossing and the time of the year. Since the orbit is sun synchronous, its orientation with respect to the sun, once established, will remain essentially constant. On the bottom "spinner" of Figure 3-IV-1, contours of constant ground illumination (constant solar-elevation angles) are plotted for the equinoxes. This pattern is based on a cosine variation of illumination from the sub-solar point (100 percent) to the terminator (zero percent). By setting the ascending node of the coverage diagram to the appropriate time on the illumination pattern, the illumination of successive pictures can be seen. The pattern changes with time of year, but the equinoctial pattern gives a sufficient indication of the variation of illumination across the pictures to permit a discussion of orbit selection.

Power-supply limitations prohibit an afternoon ascending node earlier than 1400 hours. In addition, the ground illumination is not adequate for a crossing later than 1600 hours (see Figure 3-IV-1). Because of the inclination of the orbit, a longer period of ground illumination in the northern hemisphere is obtained from an afternoon ascending node than from a forenoon ascending node. Consequently, an ascending node between 1400 and 1600 hours is indicated. A similar illumination pattern is obtained with a descending node between 0800 and 1000 hours; therefore, with respect to illumination, either of these orbits is acceptable.

An ascending node between 1400 and 1600 hours will provide optimum coverage of the Northern Hemisphere as well as the earliest recovery of data by the CDA station at Fairbanks; therefore this afternoon orbit is recommended for the AVCS system. The APT system, since it uses field stations, does not have any apparent preference for nodal crossings other than stated in the preceding paragraph.

The top spinners in Figure 3-IV-1 shows an APT picture sequence. By using both spinners, it is possible to see both the coverage and, for a given crossing time, the illumination variation in any picture.

In using the illumination spinner in Figure 3-IV-1, it is necessary to take account of the earth's rotation. For example, for an ascending-node orbit at 1500 hours, the illumination pattern for the first picture ("A" on the coverage chart) is obtained by setting 1500 hours on the illumination pattern to the ascending node of the coverage

chart. For the second picture ("B" on the coverage chart), the 1500-hour mark is moved to the second graduation ("B" on the coverage chart), and so on. In this case, it is found that, for picture "A" with the sub-point at the equator, the left-hand edge is in the 85- to 90-percent range of illumination, whereas the right-hand edge is reduced to 50 percent. For the fifth picture (not shown on the coverage chart), the sub-point and one diagonal lie approximately on the 30-percent contour, but the illumination of the other diagonal varies from total darkness to 52 percent.

B. FIELD-OF-VIEW PROJECTION

The cameras on the OT-2 spacecraft use the Tegea lens with a focal length of 5.7 mm. This lens, with a picture side length of 11.2 mm, gives a field-of-view of 89 degrees on a side and 107.8 degrees across the diagonals. As shown in Figure 3-IV-2, the area covered by this field of view from a height of 750 nautical miles is approximately 1700 nautical miles on a side and 3180 nautical miles across the diagonals. Figure 3-IV-2 also shows the satellite elevation angle (the angle formed between the local horizontal and a line to the spacecraft) for varying distances from the spacecraft sub-point.

The principal result of the large-area coverage obtained from the wide field-of-view and high altitude is that there is no gap between pictures taken at the equator on successive orbits so that complete coverage of the earth can be obtained in 24 hours of operation. There is, in fact, a small lateral overlap at the equator due to the projecting picture corners, and the degree of overlap increases as the latitude increases and the successive orbit tracks converge. Along the orbit track, the overlap of successive pictures is a function of the camera sequencer (APT or AVCS).

The top spinner of Figure 3-IV-1 shows a typical sequence of APT pictures, starting from the equator and proceeding in a northerly direction. The coverage obtained with this sequence for any orbit can be determined by rotating the spinner to the appropriate position over the map of the earth. Figures 3-IV-3 and 3-IV-4 shows picture coverage for two consecutive orbits for the APT and AVCS system, respectively.

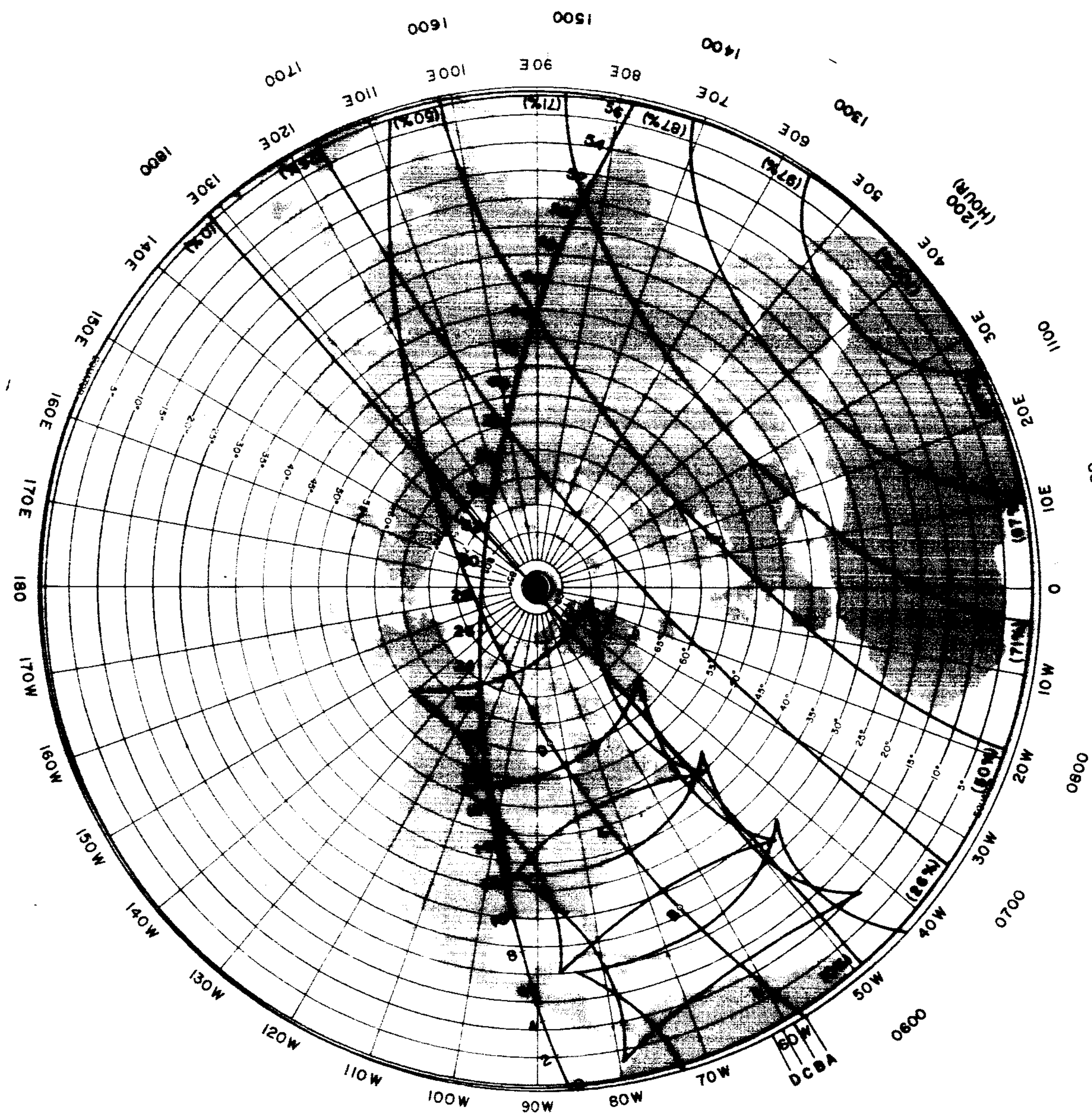

Figure 3-IV-1. Polar Stereographic Projection of Northern Hemisphere Showing Camera Coverage and Illumination for the OT-2 Spacecraft

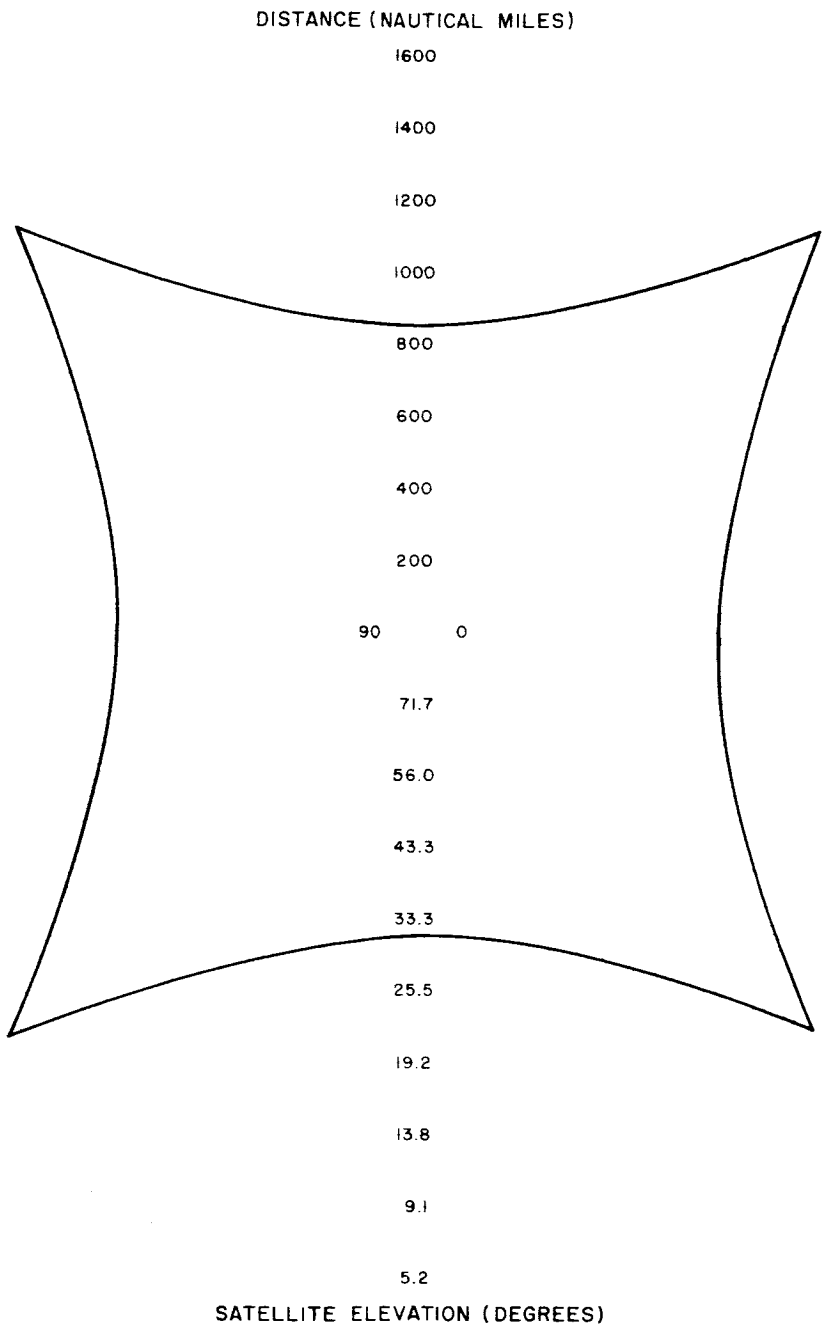

Figure 3-IV-2. Camera Field-of-View for Orbit at 750-Nautical-Mile Altitude

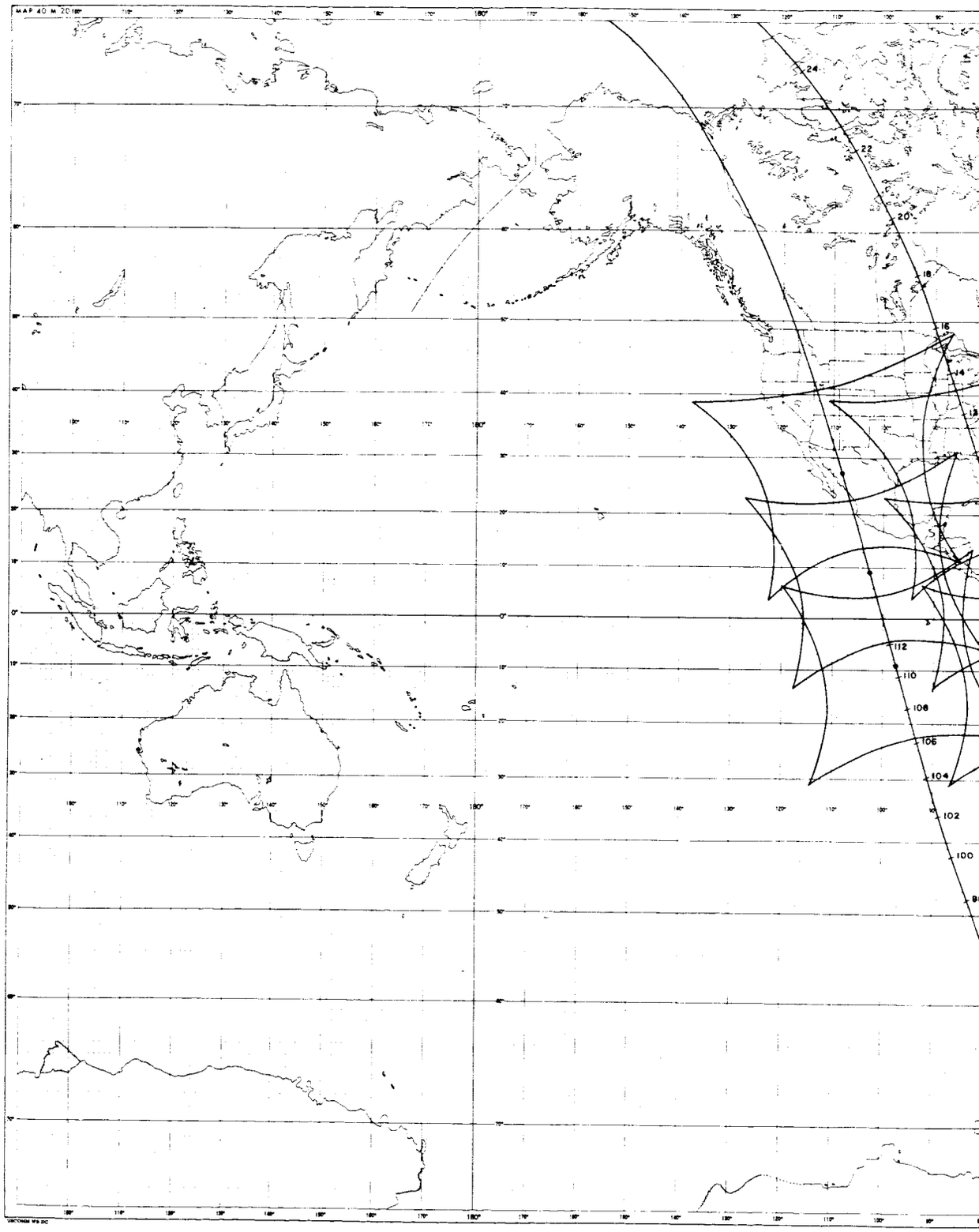
MAP 40 M 2D 180°
24
22
20
18
16
14
112
110
108
106
104
102
100

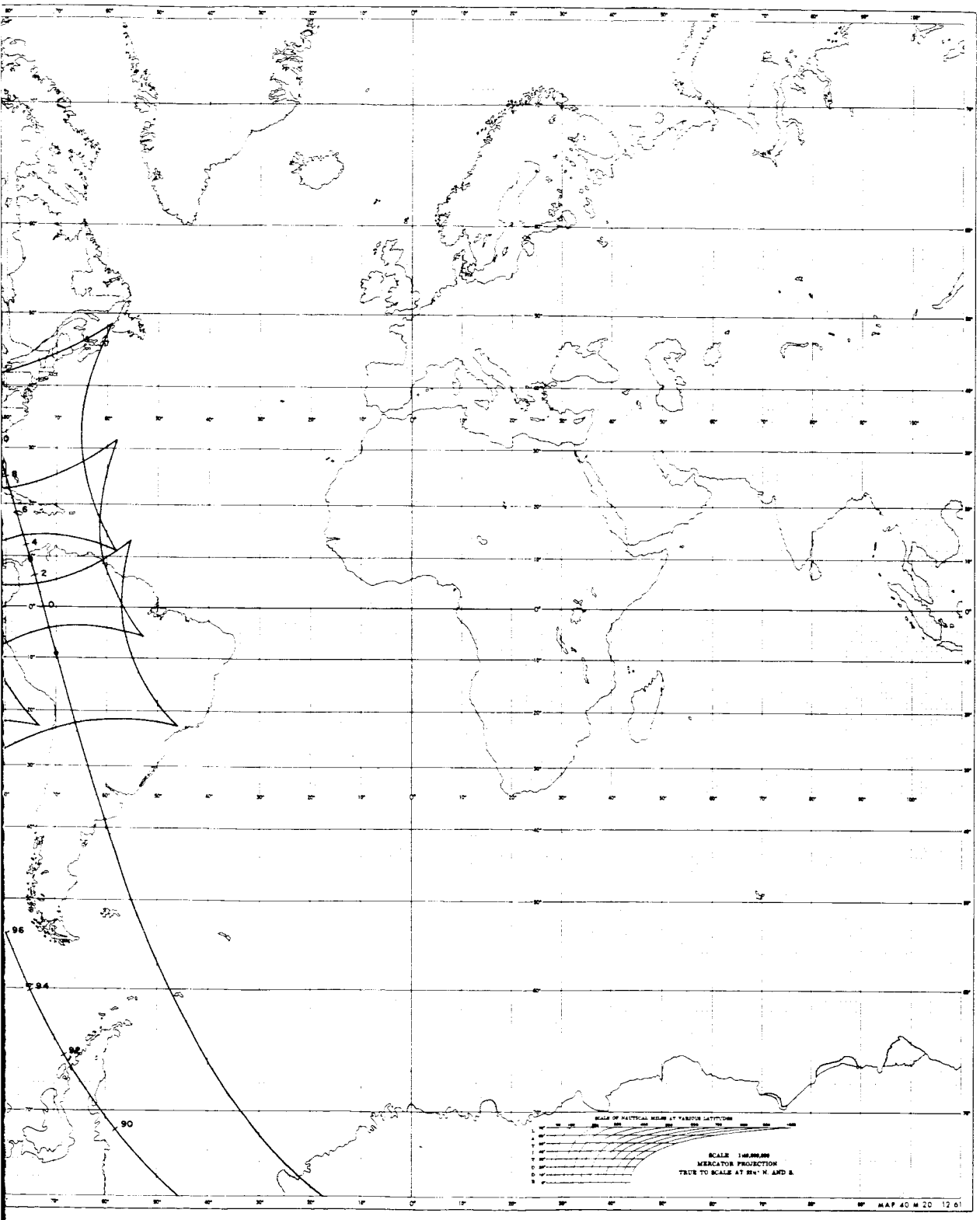

Figure 3-IV-3. APT Picture Coverage for Two Consecutive Orbits

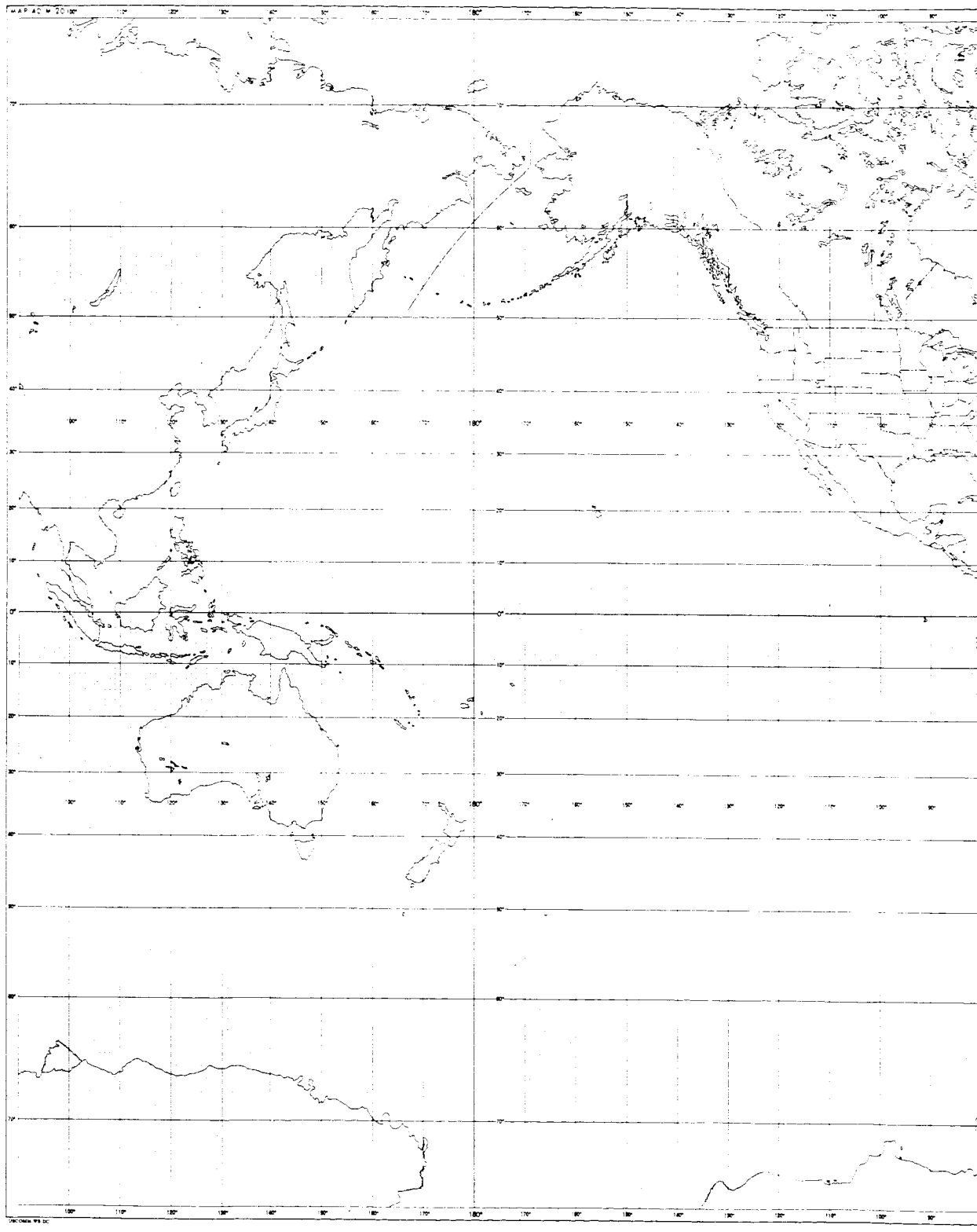

9 1

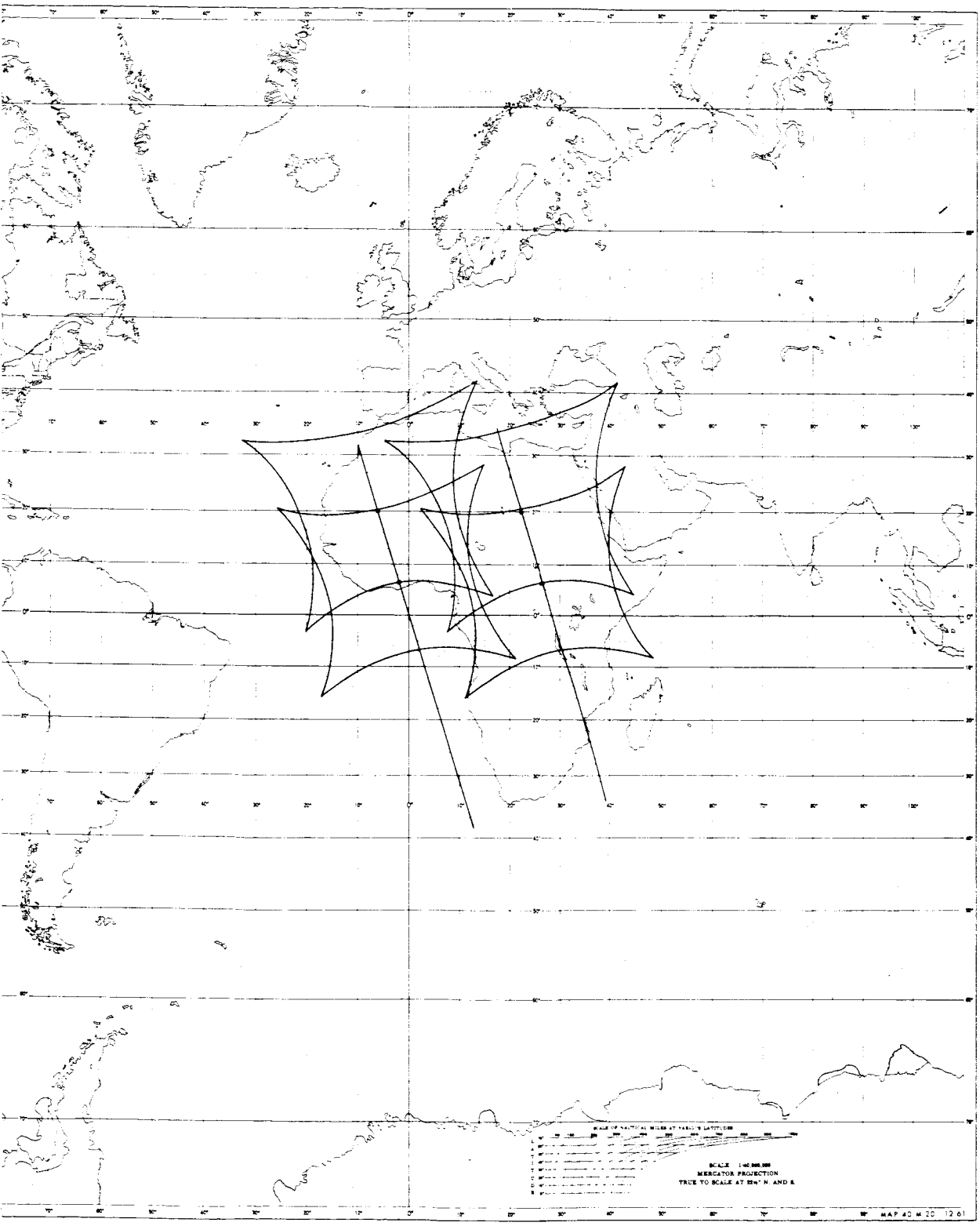

Figure 3-IV-4. AVCS Picture Coverage for Two Consecutive Orbits

SECTION V. GROUND STATION CONTACT TIME

A. ALASKA CDA STATION

Due to the high latitude of the Alaska CDA ground station located at Fairbanks, Alaska, the spacecraft will be in view more frequently at that station. As an illustrative example, one specific set of conditions for this station was selected, beginning with a pass in which the spacecraft ground track was tangent to a 5-degree elevation-angle contact circle. The next nine consecutive passes were within acquisition range of the Fairbanks station, and the contact time varied from 10 to 17 minutes, allowing more than adequate time to obtain video information as well as to program the vehicle for succeeding orbits.

However, it is also recognized that the assumption of a 5-degree minimum elevation angle for the Fairbanks antenna might be optimistic due to practical constraints at the antenna site. Therefore, further performance data on the antenna characteristics will be required for a more specific assessment of the contact time characteristics for the Fairbanks station.

B. EAST COAST CDA STATION

An analysis of station contact time was also performed for the East Coast CDA station. Using a 5-degree contact circle, two consecutive passes were within acquisition range. The contact time varied from 13 to 17 minutes.

C. APT FIELD STATIONS

Due to the existence of a great many APT field stations at varied locations, the question of contact time with the spacecraft is considered in a general sense. Studies utilizing simulated OT-2 orbits have indicated a nominal 10- to 15-minute contact time for approximately 50 to 75 percent of the orbits during which the spacecraft is in view of the ground station.

The location at which contact time is a minimum is the equator. For this "worst-case" condition, assuming a 10-degree antenna elevation angle, and an orbit altitude of 750 nautical miles the radius of the ground-station contact ring would be 26 great-circle degrees. For the same altitude, but with a 5-degree antenna elevation angle, the radius of the ground-station contact ring would be 28.5 great-circle degrees. The variation in

contact time will then be from zero minutes, for a missed pass, to 15.7 minutes for the 10-degree elevation angle, or to 17.1 minutes for the 5-degree elevation angle.

At the equator, a ground station will acquire the spacecraft on two to three consecutive passes. If acquisition occurs on an overhead pass, the duration of the contact will be near the maximum of 17 minutes. However, as previously indicated, a contact time of from 10 to 15 minutes should be considered a more typical value. This contact time will permit a readout of from two to three pictures per pass at each field station.

SECTION VI. PICTURE RECTIFICATION

A. COMPONENT ERRORS

Orientation of pictures received from the OT-2 spacecraft can be readily accomplished because the camera optical axis lies nominally in the orbit plane and points at the sub-satellite point. Picture-center location can be determined from the time of shutter triggering and the spacecraft emphemeris.

Attitude errors will cause the picture center to deviate from the nominal position. In addition, spin-rate variations will cause uncertainties in determining the picture time. Other errors not discussed here are lens distortion and rhombic picture distortion due to the travelling-slit shutter.

The following paragraphs describe the various deviations or errors that can occur and the effect of each upon picture rectification. Although the deviations possible are the same for each spacecraft (APT or AVCS), the effect on picture rectification will depend upon the particular system. The APT and AVCS considerations are described in Paragraphs C and D, respectively, of this section.

B. COMPOSITE CAMERA-POINTING ACCURACY

Assuming no attitude error, the location of the picture center is given by the satellite sub-point at the time of picture taking. The time at which the picture is taken can be determined from a knowledge of the spacecraft spin-rate and the particular spin on which the shutter was triggered. The satellite sub-point can be obtained from the ephemeris data. The camera shutter is triggered by the orthogonal horizon-sensor "sky-earth" pulse. The orthogonal horizon sensor is geometrically positioned relative to the camera so that this pulse will occur when the camera is pointing at the satellite sub-point. The angle between the camera optical axis and the orthogonal horizon-sensor optical axis is pre-set and is a function of altitude. For an orbital altitude of 750 nautical miles, this angle is approximately 55 degrees.

The picture principal-point will deviate from the sub-point as a function of the spacecraft orientation (roll, pitch, and yaw variation). The roll angle is defined as 90 degrees minus the angle between the spin vector and the local vertical. The pitch angle is the angle between the optical axis and local vertical, measured in the orbital plane. The yaw angle is the angle between the spin vector and the plane defined by the orbit normal and the local vertical.

The roll or yaw deviation between QOMAC operations will be ± 1 degree. Part 4, Section VIII, Paragraph B describes the various errors that can occur in roll and yaw determinations due to earth radiance, horizon gradients, factors attendant on data reduction, and nutation. The uncertainty in roll and yaw is ± 0.5 degree.

Pitch errors which affect camera triggering can be caused by orthogonal horizon-sensor errors and by injection errors. Orthogonal horizon-sensor errors are the result of variations in earth radiance and in horizon temperature gradients. Paragraph 4-VIII-B shows the total error from these causes to be a maximum of ±0.52 degree. Pitch deviations due to injection errors occur because the angle between the camera optical axis and the orthogonal horizon-sensor optical axis is pre-set to obtain properly timed camera triggering at the design altitude of 750 nautical miles. Figure 3-VI-1 shows the variation of pitch error with orbital altitude. Table 3-VI-1 summarizes the attitude errors that can occur.

Determination of the satellite sub-point at the moment of picture taking depends upon accurate knowledge of the spin rate and of the spacecraft ephemeris. Therefore, the primary method of picture location is dependent upon the accuracy of spin-rate measurements. For the AVCS system, there is a secondary method for determining the time of picture taking, using a picture-time clock.

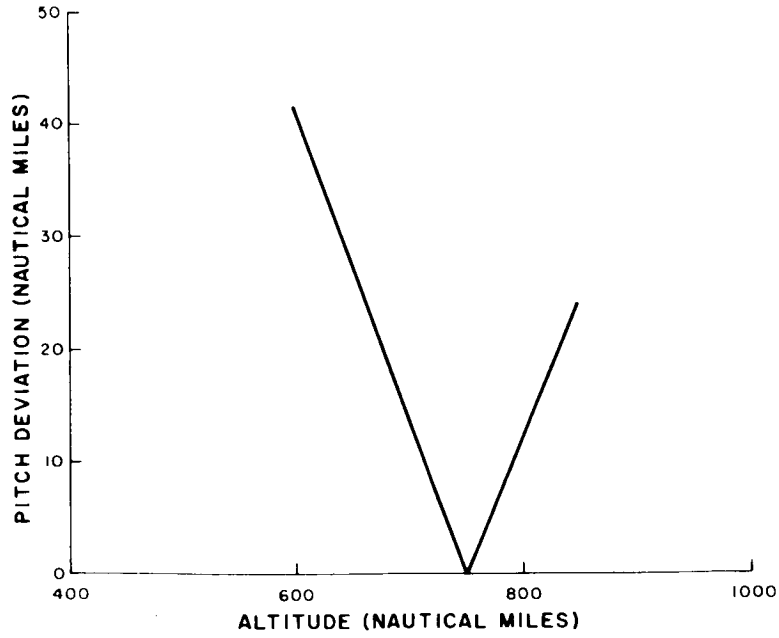

Figure 3-VI-1. Pitch Deviation Due to Injection Error

TABLE 3-VI-1. SUMMATION OF POINTING ERRORS

Item	Angular Displacement (degrees)	Equivalent Ground Distance (nautical miles)
1. Roll deviations between QOMAC operations	±1	±13.1
2. Roll measurement accuracy	±0.5	±6.5
3. Pitch deviation due to orthogonal horizon sensor	±0.52	±6.86
4. Pitch deviation due to injection	See Figure 3-VI-1	See Figure 3-VI-1
5. Yaw deviation between QOMAC operations	±1	Rotation about principal point
6. Yaw measurement accuracy	±0.5	Rotation about principal point

The accuracy of any sub-point determination is a function of the duration of the spin-measuring period, the number of spins between T_o, (time at which the first picture in a sequence is taken) and the time for which the subpoint is being determined, and the accuracy of determining spacecraft location at T_o. Paragraph 4-VIII-C discusses in detail the technique by which spin rate is determined and the various errors that can occur in spin-rate measurement. Figure 3-VI-2 presents a curve of sub-point error (nautical miles) versus spins from T_o. This curve is the same as the curve for an 8-minute measuring period in Figure 4-VIII-26 with the ordinate scale changed from seconds to nautical miles on the ground.

Since the maximum number of orbits for which the spacecraft is out of contact with a ground station is two, and since the spin can be counted backward or forward from T_o, the maximum error in sub-point measurement will occur for 1240 spins (approximately one orbit). This could result in a worst-case error of 1.95 nautical miles in spacecraft sub-point determination.

C. APT SPECIAL CONSIDERATIONS

Because the APT field stations will not be equipped to obtain attitude data from the spacecraft, this information will have to be supplied in advance or attitude deviation will have to be neglected (as in the Nimbus-APT procedure). Assuming the latter approach and a flat earth, the rectangle of uncertainty of picture principal point around the

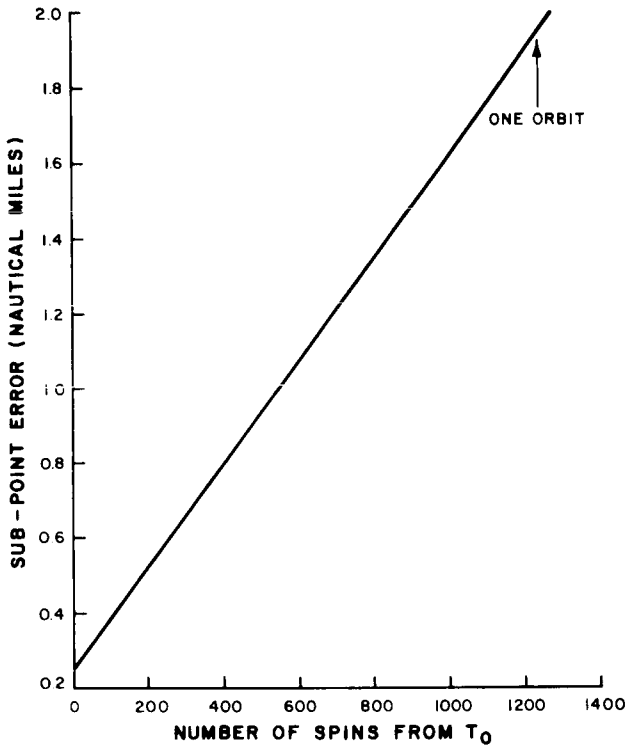

Figure 3-VI-2. Sub-Point Error Versus Number of Spins from T_0

spacecraft sub-point is given in Figure 3-VI-3. This figure is based upon Items 1 and 3 in Table 3-VI-1.

Yaw errors are not shown in this figure because the maximum yaw error would only rotate the rectangle 1 degree about the sub-point. Pitch deviation due to injection error (Item 4, Table 3-VI-1) is not an uncertainty but rather a fixed known deviation.

The spacecraft sub-point can be determined at APT field stations from spacecraft ephemeris and time of picture receipt. APT field stations, in general, will not have the capability for using the spin-counting method.

D. AVCS SPECIAL CONSIDERATIONS

The CDA stations where AVCS pictures will be received have the capability for determining spacecraft attitude. The accuracy of locating the picture principal point will therefore be greater than for the APT system. The error in principal point will be composed of roll measurement error and pitch error (Items 2 and 3 in Table 3-VI-1). The rectangle of uncertainty for the AVCS configuration is given in Figure 3-VI-4. The

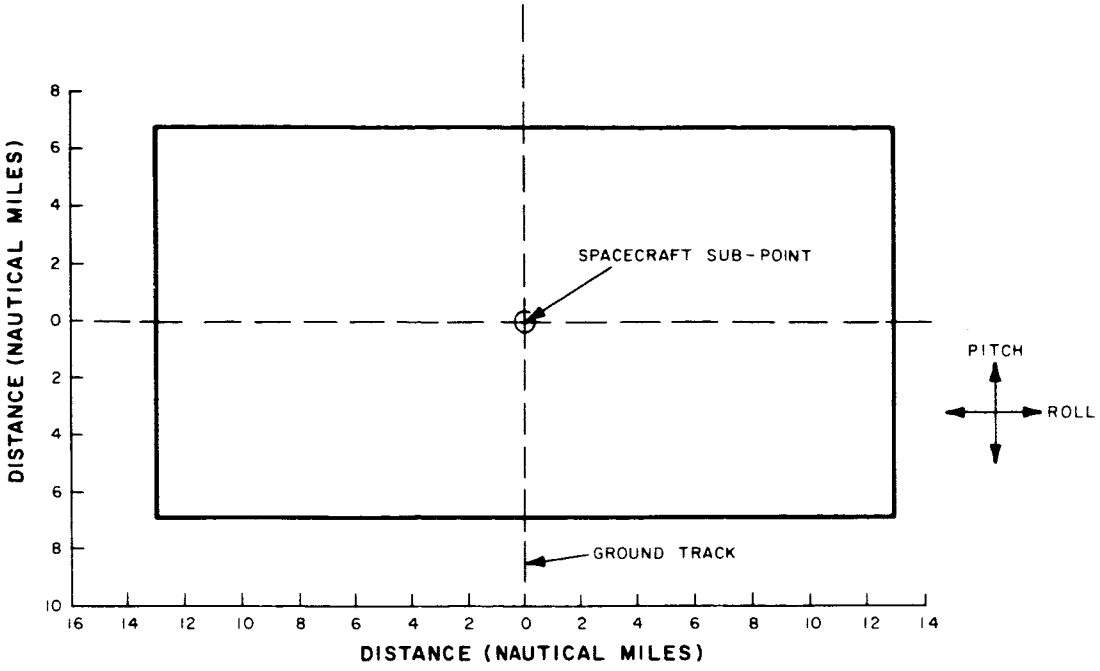

Figure 3-VI-3. APT Rectangle of Uncertainty

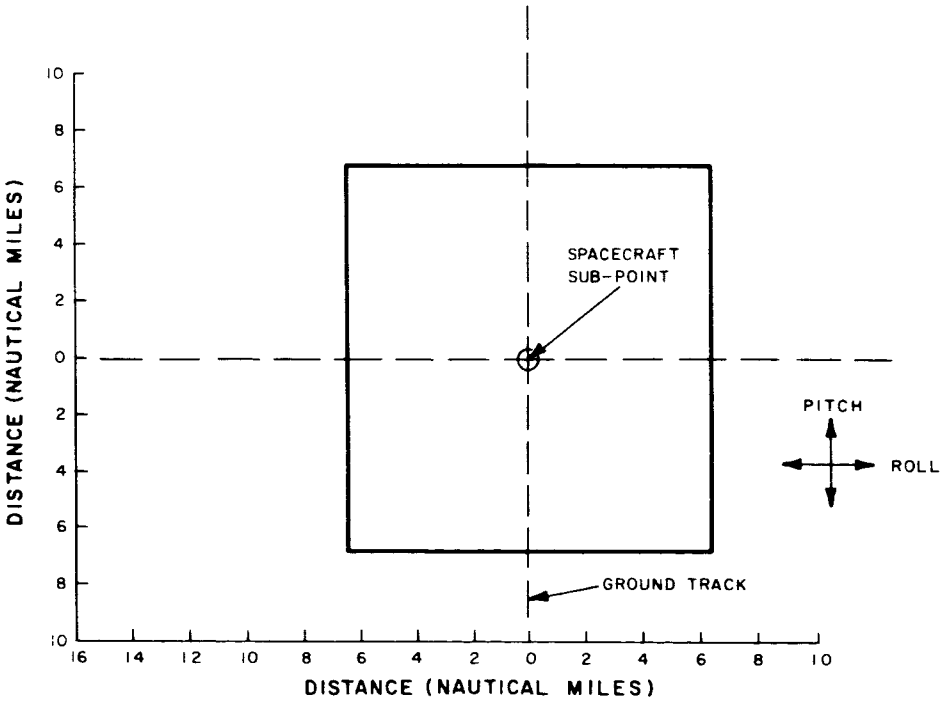

Figure 3-VI-4. AVCS Rectangle of Uncertainty

rectangle is shown for zero roll error. Roll deviations would simply move the rectangle perpendicular to the ground track. Yaw is again not shown because of its negligible effect. Pitch deviations due to injection are again not included because they do not represent an uncertainty.

Sub-point location for the AVCS configuration will be obtained using the spin-counting method with the accuracy described in Paragraph 3-VI-B. A secondary locating technique is also available using the picture time clock on board the OT-2/AVCS spacecraft. This clock has an accuracy of 0.5 second, which corresponds to a 1.6-nautical mile ground distance.

PART 4. OT-2 SPACECRAFT DESIGN

SECTION I. INTRODUCTION

The OT-2 spacecraft will consist of components comprising the basic functional subsystems shown on the block diagrams in Figures 2-I-1 and 2-I-2. These components will be mounted within a conventional TIROS structure which will be modified to accommodate the radially oriented cameras. The spacecraft structure and the design and operation of each of the functional subsystems are described in separate sections of this Part of the report.

The general structural configuration and the locations and orientation of components are described and illustrated in Section 4-II. The results of the thermal analyses performed on the spacecraft are presented in Appendix D.

A discussion of the OT-2/APT and OT-2/AVCS camera subsystems is presented in Section 4-III. This section contains descriptions of the operation of the subsystems and their relation to the overall system, as well as descriptions of the spacecraft operating modes and command-signal characteristics.

The command and control subsystem is described in Section 4-IV. This section discusses the function and operation of the components in the subsystem and, also, the interfaces between this subsystem and the other subsystems.

A description of the spacecraft power-supply subsystem is presented in Section 4-V. This section describes configurations of the solar-cell array and the storage-battery pack and their capabilities and capacities under various orbital conditions and spacecraft operating loads. The functions and characteristics of the power-supply protection units and voltage regulators, and the characteristics of the solar cells and storage batteries are also described.

The beacon and telemetry subsystem is described in Section 4-VI. This section describes the subsystem analysis of the beacon and telemetry subsystem, including the beacon modulation techniques used for the OT-2 spacecraft. This section also contains specifications for the telemetry switches, and a list of spacecraft telemetry points and parameters.

The system margins, path losses, and data links for the communication interface are discussed in Section 4-VII. This section describes the design parameters for command, beacon, and TV reception that are associated with the spacecraft. The link analysis is based on spacecraft operation in conjunction with standard CDA-station equipment.

Section 4-VIII presents a discussion of the theory and operation of the components utilized for attitude and spin-control techniques. This section compares the techniques required for the OT-2 system with the techniques used in the TIROS "I" system and indicates where functions of the TIROS "I" system can be utilized or modified for use in the OT-2 system.

SECTION II. MECHANICAL AND THERMAL DESIGN

A. GENERAL

The basic structure that will be used for the OT-2 spacecraft is similar to the conventional TIROS structure. Certain modifications have been made either to optimize the structure or to accommodate the "Wheel" mode of operation. The OT-2 spacecraft structure can be divided into two major components, (1) the baseplate and (2) the hat assembly. The function of the baseplate is to support the electronic subsystems mounted directly to it and the hat assembly. The hat assembly encloses the spacecraft and supports the solar-cell array. In addition, certain attitude and spin-control components are mounted on the hat assembly.

The baseplate modifications include simplification of the radial-rib arrangement and increasing the material gage. On early TIROS spacecraft, the rib arrangement provided space for a NASA infrared (IR) experiment (Figure 4-II-1). Since this particular experiment will not be used on the OT-2 spacecraft, the rib arrangement has been changed to provide a symmetrical configuration as shown in Figure 4-II-2. Because of the more severe vibration environment to be imposed on the OT-2 spacecraft and to provide additional margin in the structure for future growth, the following material thickness changes were made to the baseplate:

	From (inch)	To (inch)
radial ribs	0.040	0.051
intercostals	0.025	0.032
gussets	0.040	0.051
reinforcing channels	0.040	0.051

The hat assembly has been modified to a configuration that is similar to the TIROS "I" spacecraft. These changes include cutouts to accommodate the cameras, the V-head horizon sensor, and the orthogonal horizon-sensors. The de-spin mechanism will be relocated to approximately midway up the side of the hat assembly (same as TIROS "I").

The vertical posts in the hat assembly were simplified by the elimination of the north-indicator brackets.

A preliminary stress analysis based on the environment established in Table 4-II-1 has been performed. This analysis showed that the OT-2 spacecraft structure is satisfactory.

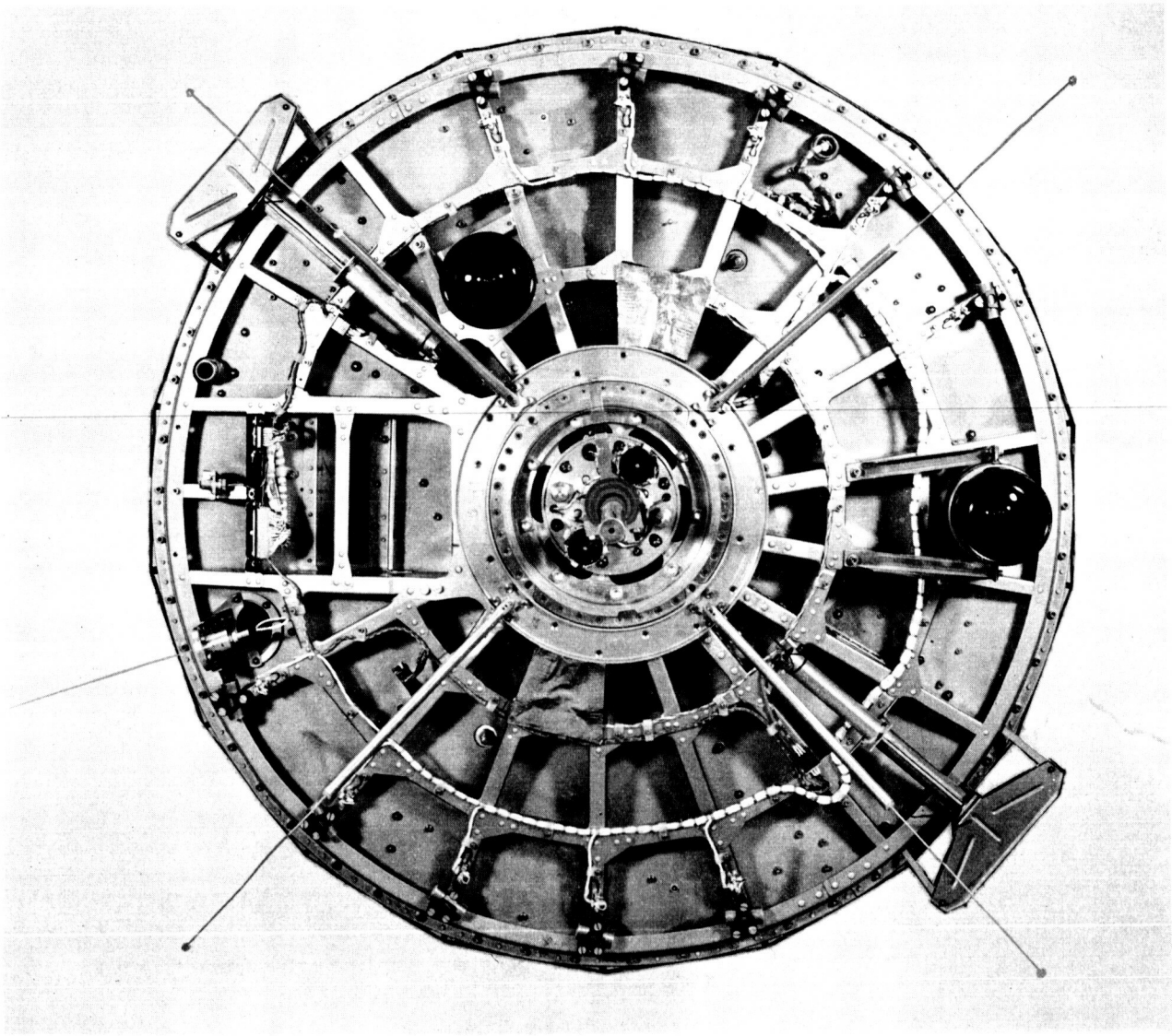

Figure 4-II-1. TIROS VII Spacecraft, Bottom of Baseplate

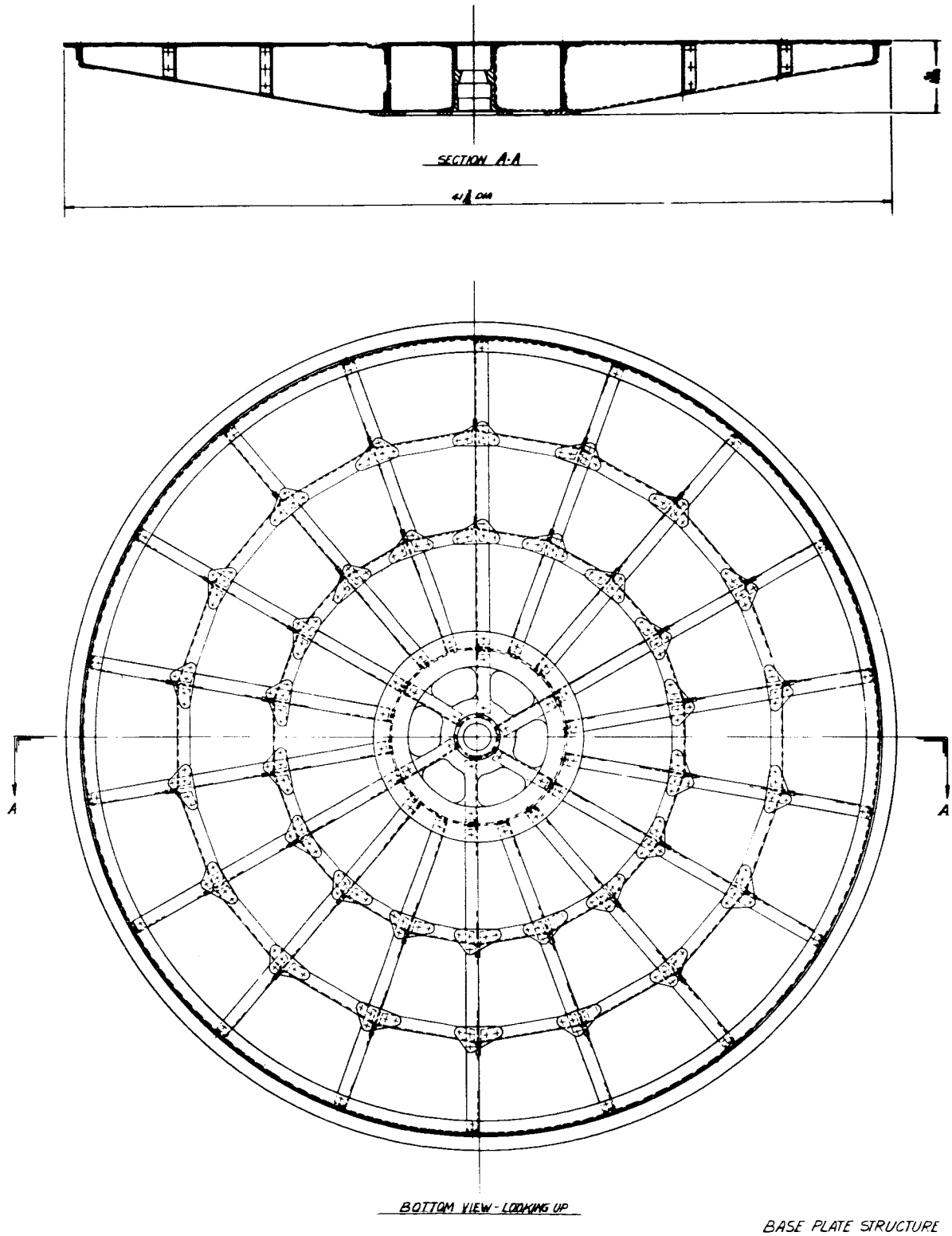

Figure 4-II-2. Modified Radial-Rib Arrangement of the Baseplate

TABLE 4-II-1. OT-2 SPACECRAFT ENVIRONMENTAL SPECIFICATIONS, PROTOTYPE LEVELS

Sinusoidal Input			
Frequency Range (cps)	Thrust Axis ("g" zero-to-peak)	Transverse Axes ("g" zero-to-peak)	Sweep Rate (octave/minute)
10 - 500	3.75	2.25	2
500 - 2000	21.00	3.75	2
Random Noise Input			
Frequency Range (cps)	Thrust Axis ("g" rms)	Transverse Axis ("g" rms)	Time/Axis (minutes)
20 - 2000	11.5	11.5	4

B. ATTITUDE AND SPIN-RATE CONTROL COMPONENT LOCATION

Figure 4-II-3 shows the location of the various components used for attitude and spin-rate control.

C. APT BASEPLATE LAYOUT

Figure 4-II-4 shows the equipment layout on the baseplate for the APT configuration. Table 4-II-2 presents the weight breakdown for the OT-2/APT spacecraft. The center of gravity is located on the spin (thrust) axis. This balancing is achieved by carefully locating equipment on the baseplate, with a final balancing operation accomplished with balance weights. The moment-of-inertia about the spin-axis, I_{zz}, is predicted to be 57,900 lb-in^2. The ratio of the moment-of-inertia, $I_{transverse}/I_{spin}$, is equal to 0.75.

D. AVCS BASEPLATE LAYOUT

Figure 4-II-5 shows the equipment layout on the baseplate for the AVCS configuration. As in the APT configuration, the camera is raised off the baseplate to provide line-of-sight clearance for the lens. The camera is mounted on a bracket assembly which allows space for positioning the camera electronics beneath the camera (AVCS only). This arrangement is shown in Figure 4-II-6. Table 4-II-3 presents the weight breakdown for the spacecraft. The center of gravity is located on the spin (thrust) axis. Component layout and balance weights are used to achieve this location. The spacecraft moment-of-inertia about the spin axis, I_{zz} is 59,800 lb-in^2. The moment-of-inertia ratio, $I_{transverse}/I_{spin}$, is 0.752.

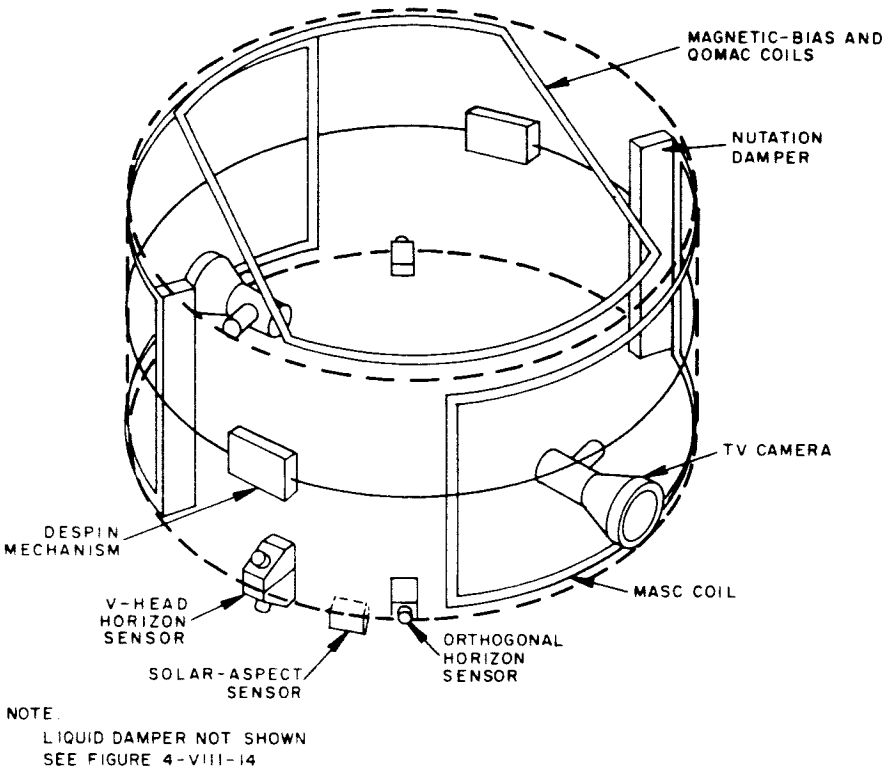

Figure 4-II-3. Location of Attitude and Spin-Rate Control Components

TABLE 4-II-2. ESTIMATED WEIGHT OF OT-2/APT SPACECRAFT

Component	Estimated Weight (pounds)
Assembly, Baseplate	
1. Structural Assembly - Lower Plate	26.7
2. APT Cameras	23.0
3. Magnetic Shield	8.4
4. Camera Mounting Bracket	4.0
5. Command Distribution Unit	8.1
6. Orthogonal Horizon-Sensor	3.0
7. Threshold Amplifier	0.7
8. Command Programmer, Decoder	13.03

TABLE 4-II-2. ESTIMATED WEIGHT OF OT-2/APT SPACECRAFT (Continued)

Components	Estimated Weight (pounds)
Assembly, Baseplate (Continued)	
9. V-Head Sensor	1.0
10. Magnetic Bias Switch	0.8
11. Battery	42.0
12. Shunt Limiter	3.0
13. Charge Rate Controller	3.5
14. Voltage Regulator	3.1
15. Power Distribution Unit	1.0
16. Solar-Aspect Sensor and Electronics	1.5
17. Precession Damper	2.4
18. Camera Electronics	21.2
19. Beacon Transmitter	2.5
20. Video Transmitter	5.0
21. Commutator	4.2
22. Signal Conditioner	2.0
23. Command Receiver	2.5
24. Antenna Coupler	2.1
25. SCO	1.7
26. Beacon Timer	0.8
27. Video Coupler	0.46
28. Lift-Off and Separation Switch	1.0
29. Ground Plate	0.5
30. Balance Weight	2.0
31. Bracketry and Hardware	5.0
32. Harness (upper)	11.7
33. Harness (lower)	1.0

TABLE 4-II-2. ESTIMATED WEIGHT OF OT-2/APT SPACECRAFT (Continued)

Components	Estimated Weight (pounds)
Assembly, Baseplate (Continued)	
34. RF Cabling	2.0
35. Coaxial Relay	0.5
Assembly, Hat	
1. Hat Structure	42.2
2. Solar Cells	22.7
3. Masc Coil	1.5
4. QOMAC Coil	0.5
5. Bias Coil	2.25
6. Yo-Yo Despin Mechanism	2.8
7. Filter	0.5
8. Temperature Sensors	0.2
9. Damper (liquid)	3.2
10. Notch Filter	0.25
Antennas	2.2
Total	289.7

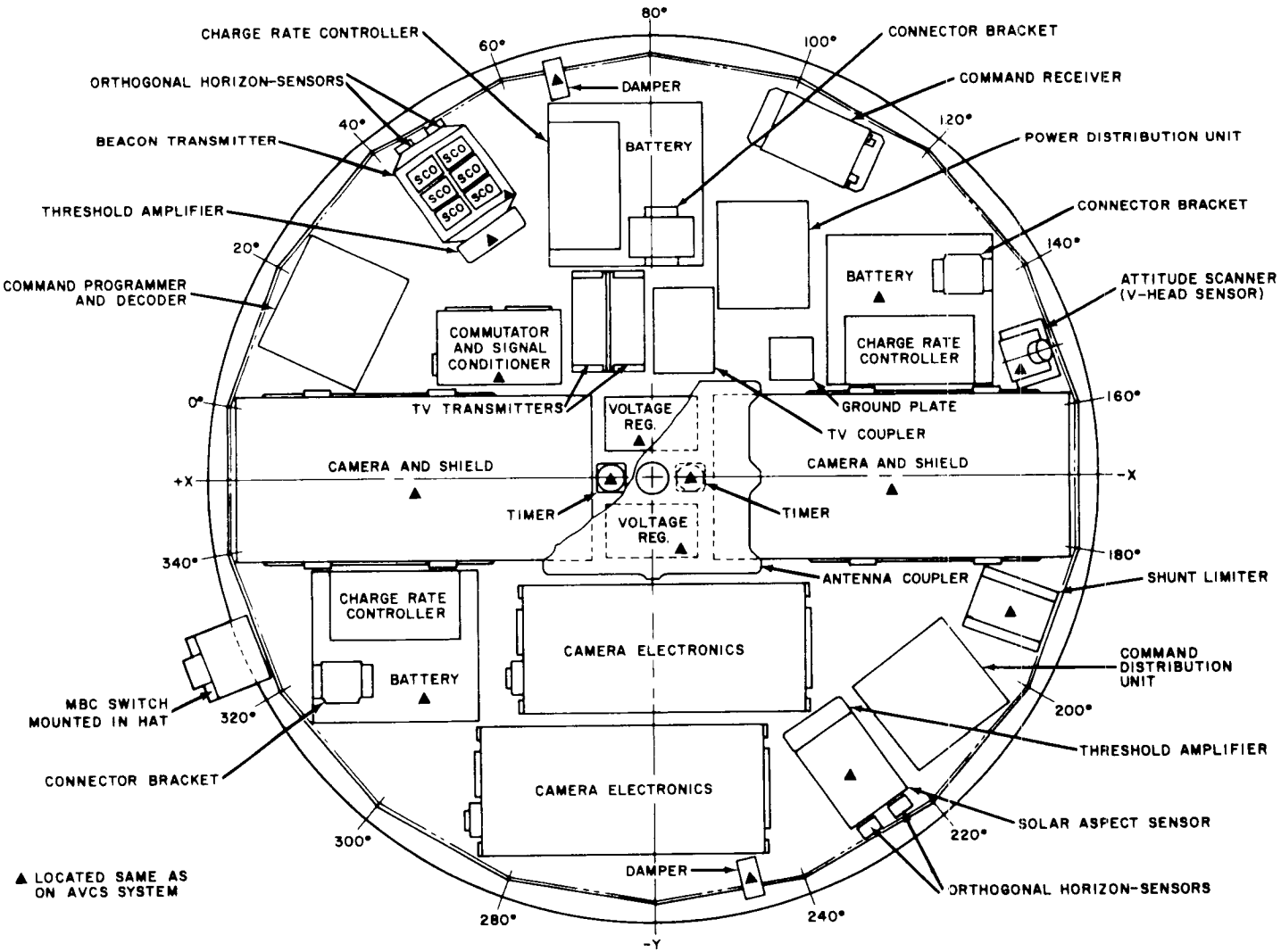

Figure 4-II-4. APT Baseplate Layout

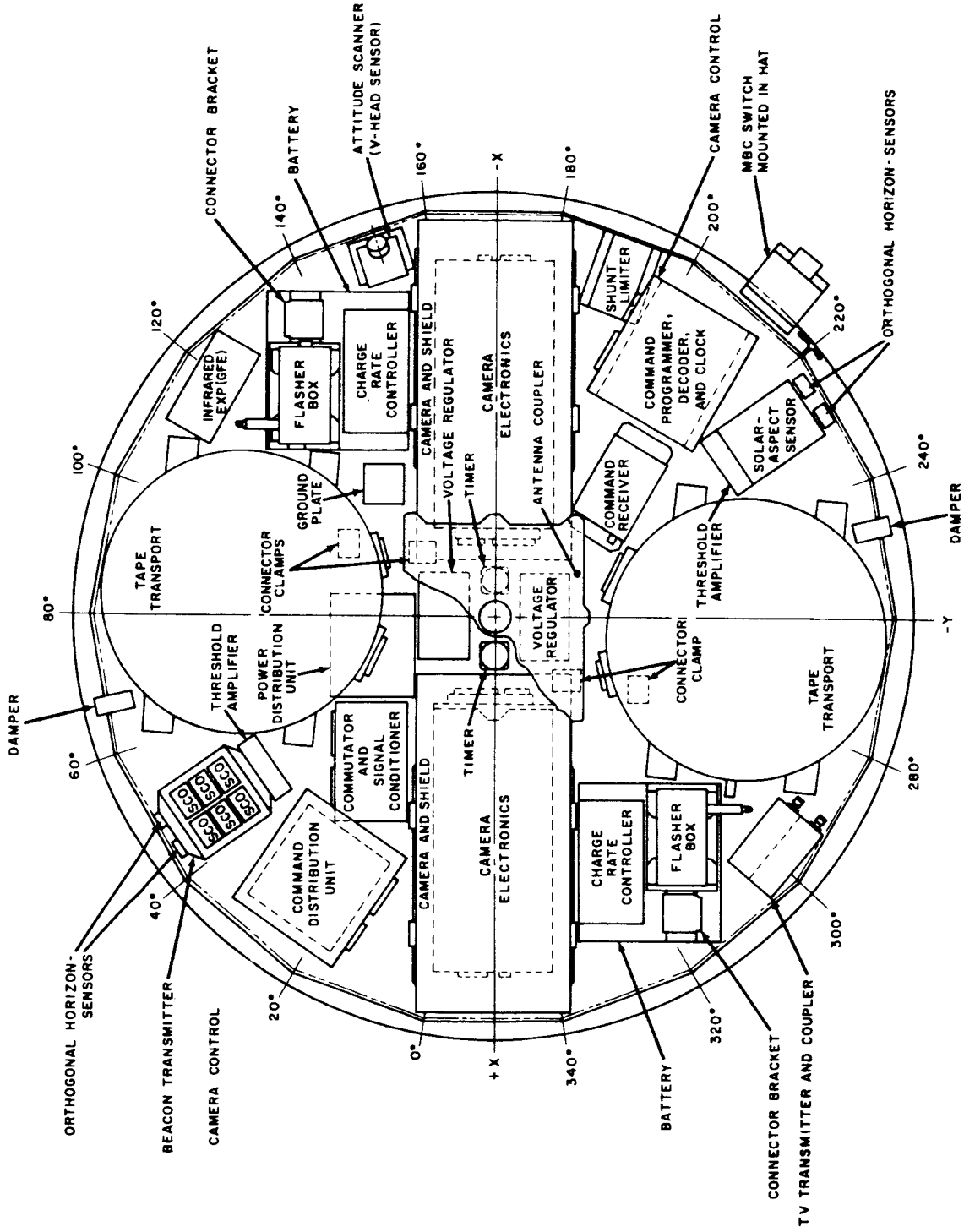

Figure 4-II-5. AVCS Baseplate Layout

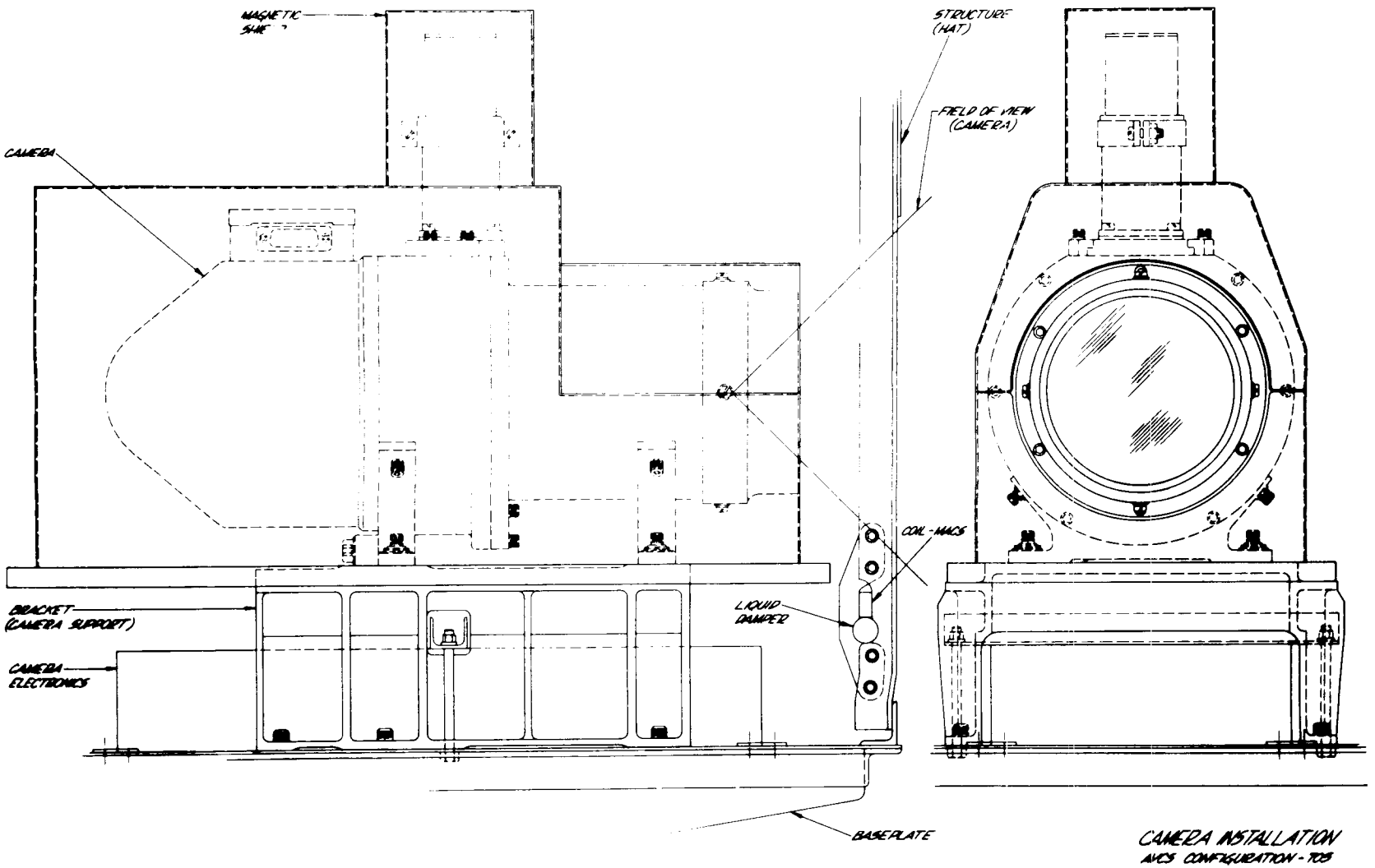

Figure 4-II-6. Camera Mounted on Bracket Assembly

TABLE 4-II-3. ESTIMATED WEIGHT OF OT-2/AVCS SPACECRAFT

Component	Estimated Weight (pounds)
Assembly, Baseplate	
1. Structural Assembly - Lower Plate	26.7
2. AVCS Cameras	23.4
3. Magnetic Shield	8.4
4. Camera Mounting Bracket	4.0
5. Command Distribution Unit	9.2
6. Orthogonal Horizon-Sensor	3.0
7. Threshold Amplifier	0.7
8. Command Programmer, Decoder, and Clock	14.31
9. V-Head Sensor	1.0
10. Magnetic Bias Switch	0.8
11. Battery	28.0
12. Shunt Limiter	3.0
13. Charge Rate Controller	2.3
14. Voltage Regulator	3.1
15. Power Distribution Unit	1.0
16. Solar-Aspect Sensor and Electronics	1.5
17. Precession Damper	2.4
18. Camera Electronics	13.6
19. Beacon Transmitter	2.5
20. Video Transmitter	4.0
21. Commutator	4.2
22. Signal Conditioner	2.0
23. Command Receiver	2.5
24. Antenna Coupler	2.1

TABLE 4-II-3. ESTIMATED WEIGHT OF OT-2/AVCS SPACECRAFT (Continued)

Components	Estimated Weight (pounds)
Assembly, Baseplate (Continued)	
25. SCO	1.7
26. Beacon Timer	0.8
27. Video Coupler	3.2
28. Lift-Off and Separation Switch	1.0
29. Ground Plate	0.5
30. Tape Recorder	34.6
31. Flasher	2.2
32. Camera Controller	4.2
33. Infrared Experiment	4.0
34. Balance Weight	2.5
35. Bracketry and Hardware	5.0
36. Harness (upper)	11.7
37. Harness (lower)	1.0
38. RF Cabling	2.0
Assembly, Hat	
1. Hat Structure	42.2
2. Solar Cells	22.7
3. Masc Coil	1.5
4. QOMAC Coil	0.5
5. Bias Coil	2.25
6. Yo-Yo Despin Mechanism	2.8
7. Filter	0.5
8. Temperature Sensors	0.2
9. Damper (liquid)	3.2
10. Notch Filter	0.25
Antennas	2.2
Total	316.4

E. EXPECTED SPACECRAFT TEMPERATURES

A preliminary thermal analysis of the OT-2 spacecraft has been conducted. Appendix D gives a detailed mathematical description of this analysis. Briefly, the analysis consisted of a study of thermal transients in which the spacecraft was divided into three isothermal bodies. The effect of power dissipation and sun angle on spacecraft temperatures was examined. Figure 4-II-7 presents the temperature response of baseplate and components, and solar-cells versus sun angle for various sections of the spacecraft. From this figure, it can be seen that at a sun angle of 45 degrees the temperature of the baseplate and components, and side solar cells will be approximately 17°C, and the solar cells on the top of the hat assembly will be 65°C. The required component temperature limits are 0°C and 30°C.

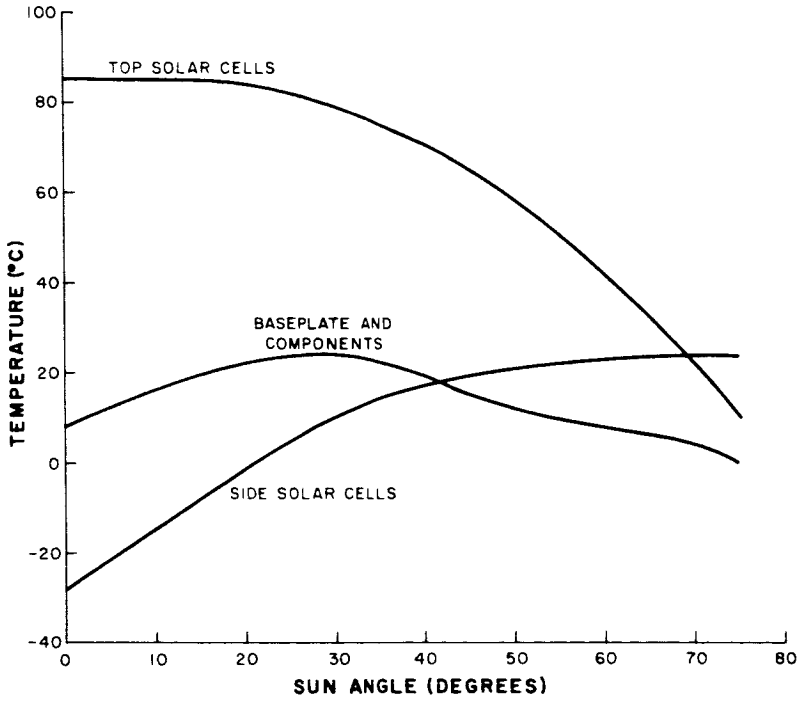

Figure 4-II-7. Variations in Spacecraft Temperatures with Sun Angle

The effect of the initial orientation maneuver has also been examined. Figure 4-II-8 shows the temperature response for the worst case orientation versus time from launch. The effect of QOMAC is also shown in this figure.

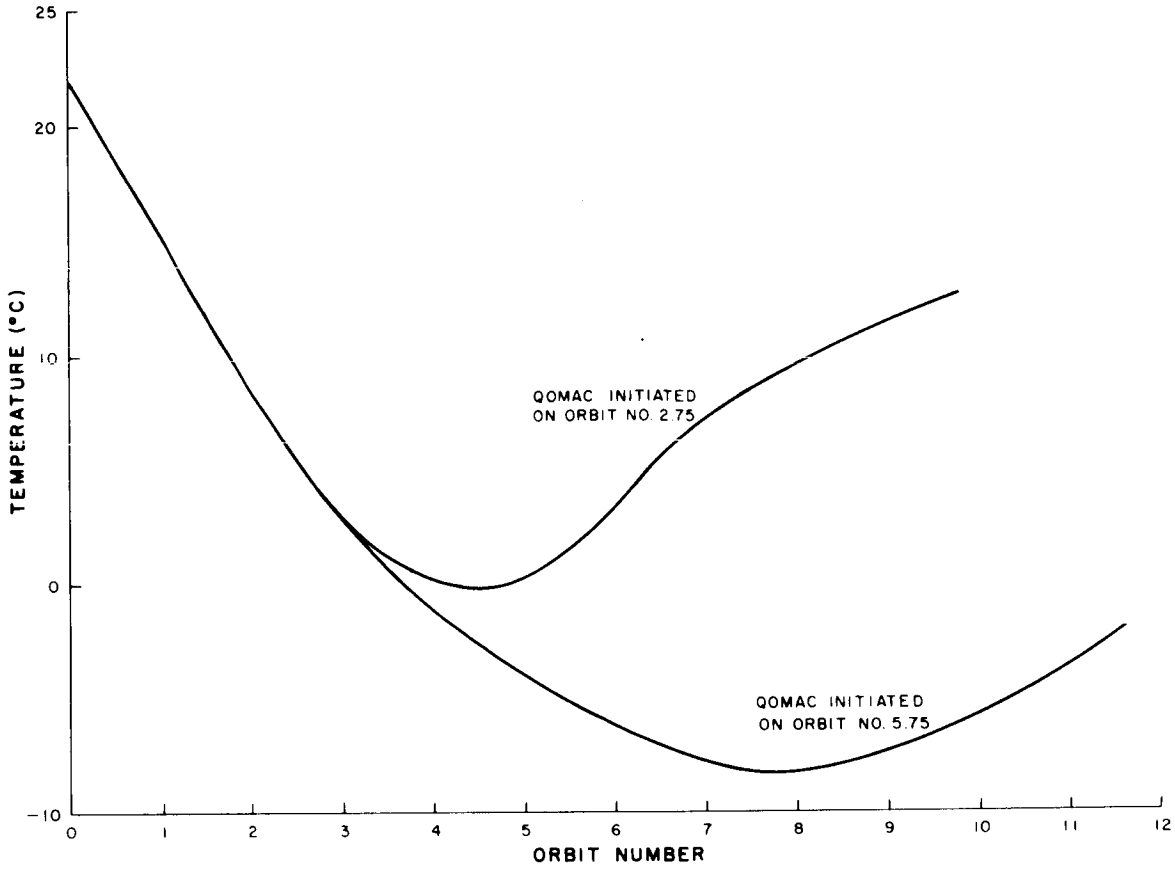

Figure 4-II-8. Component Temperature Response for the Worst-Case Orientation Versus Time from Launch

SECTION III. CAMERA SUBSYSTEM

A. APT CAMERA SUBSYSTEM

1. Functional Description

The major components of the APT camera subsystem are shown in the block diagram in Figure 4-III-1; the components are (1) a camera assembly that converts the optical image into an electrical signal, (2) a camera-electronics module that includes timing, control, amplification, modulation, and power-supply equipment for the subsystem, (3) a video combiner that couples the camera to the FM transmitter, (4) an FM transmitter that supplies the narrow-band RF carrier for the video data, and (5) an antenna coupling network that couples the FM transmitter to the single dipole antenna. When the spacecraft is within communication range of an APT field station, the radiation from the spacecraft TV antenna is received by the helical antenna of the station. The received signal is amplified by the pre-amplifier, demodulated by the FM receiver, and fed to the facsimile recorder to produce a "hard" copy of the TV picture.

The OT-2 spacecraft is programmed by the CDA ground stations to start a picture-taking sequence at a predetermined point in the orbit. Once the sequence is initiated, the APT subsystem will continue to take pictures under spacecraft control and will transmit these pictures to the APT ground stations. The process will then be repeated automatically each orbit until commanded otherwise by a CDA station. The ground station will automatically receive a picture sequence from the beginning of a 208-second picture frame. During the first 8 seconds of each 208-second period, the camera operates as follows:

(1) the vidicon tube is prepared to receive the optical image;

(2) the shutter of the camera assembly is triggered, and the image is projected onto the photoconductive face of the vidicon; and

(3) the image is transferred electrostatically from the photoconductive face to a polystyrene storage layer.

This sequence of operations is known as the PED (prepare-expose-develop) cycle. The polystyrene layer stores the image as a charge pattern until the electron scanning beam sweeps the surface, reading out the image information in a 200-second readout cycle. All sequencing is controlled by the sequence-timing circuits of the subsystem. These circuits are, in turn, controlled by the command programmer.

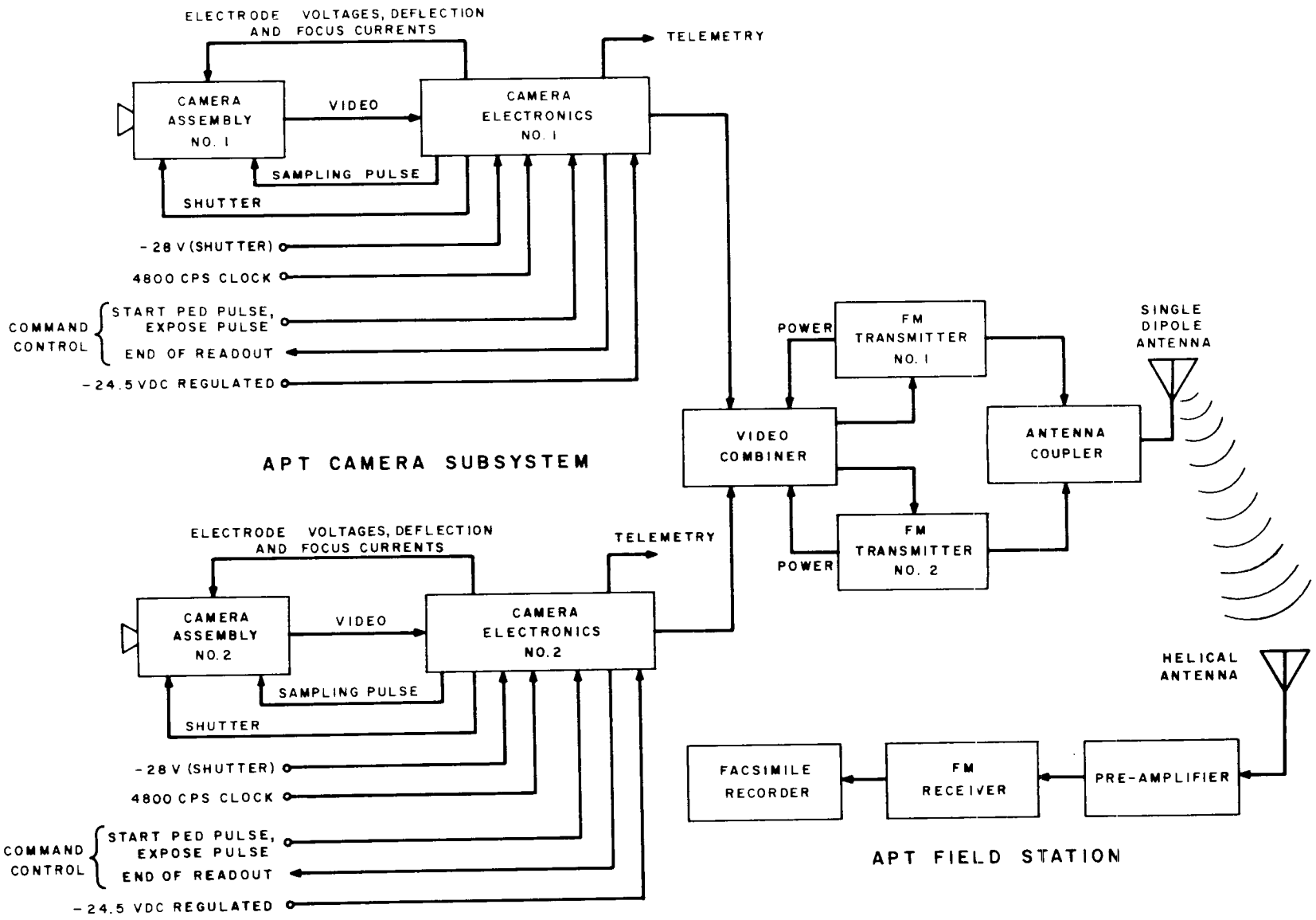

Figure 4-III-1. APT Camera Subsystem, Block Diagram

Camera operation begins with a "Start PED" pulse from the command and control subsystem. This pulse initiates the 208-second PED and readout cycles. The "Expose" pulse, which triggers the camera shutter, normally occurs 5.500 seconds $\pm$25 milliseconds after initiation of the PED cycle. This time interval is imposed by the camera to ensure that optical "Expose" occurs (1) within the electrical expose interval and (2) at the optimum time to provide maximum camera sensitivity. If the camera subsystem fails to receive the "Expose" pulse, the shutter is triggered automatically by the camera logic circuits 5.5625 seconds after the start of PED.

If control of the spin rate is lost and the spin period increases, the picture quality will degrade slightly until the period is equal to 5.5625 seconds, at which time the APT back-up shutter command will take over control of shutter operation. Picture quality will then remain constant; however, as the spin period increases further, the camera will develop a pointing error. The pointing error in degrees will be:

$$360^{o} - 5.5625\ (f),$$

where f is the spacecraft spin rate in degrees per second.

If the spin rate increases, the picture rate-of-degradation will gradually increase until at 12 rpm, there will be no video data.

Data readout of the stored image is accomplished using a pulse technique. During readout, the vidicon scanning-beam is pulse-modulated, resulting in a PAM (pulse-amplitude-modulated) video signal. The video information is then detected, producing a continuous analog readout which is used to amplitude-modulate a 2400-cps subcarrier. This modulation produces a double-sideband-modulated subcarrier having sidebands extending 1600 cycles above and below the subcarrier frequency. This amplitude-modulated subcarrier, in turn, frequency-modulates the 137.5-Mc carrier, which is then applied to the transmitting antenna system.

Figure 4-III-2 shows a detailed timing diagram indicating the operations required for picture taking with the APT camera. A detailed description of the theory of operation of the APT camera is presented in the "Nimbus Instruction Manual for the Automatic Picture Transmission Subsystem (APTS), Flight Models F2, and F4, Satellite Equipment for TIROS Meteorological Satellite". The sequence, as shown, differs from the operation of the APT camera used in TIROS VIII in one respect. The logic sequence originally provided for an indeterminate hold period between the "Prepare" and "Expose" portions of the PED cycle. This has been found to be unsatisfactory because the post-optical-expose time varies as a result of the synchronous operation of the APT horizontal scan and the spacecraft triggering signals. If the original logic were to be maintained, this variation in expose time would result in a black bar in the video readout.

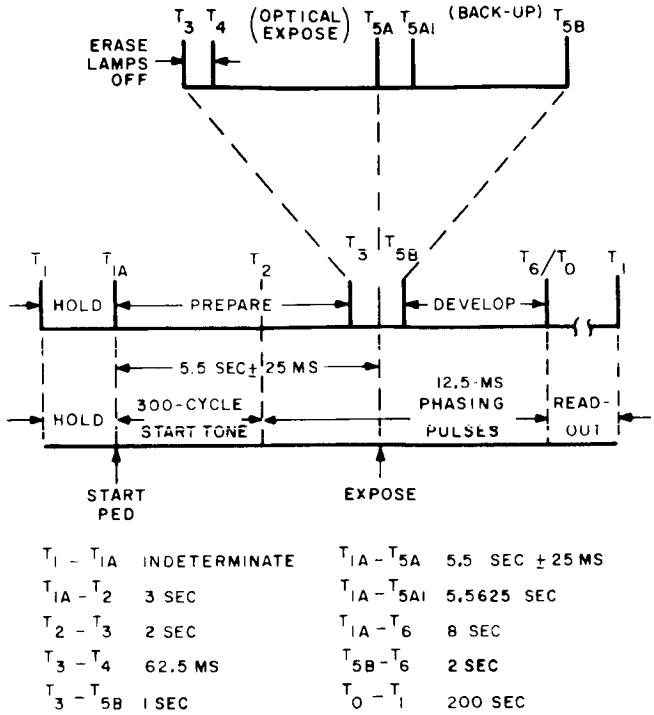

Figure 4-III-2. APT Camera, Picture-Taking Sequence

The revised logic sequence, as shown in Figure 4-III-2, is as follows:

(1) The logic sequence is interrupted at the end of readout cycle, and the camera goes into an indefinite "hold" period.

(2) The "hold" period is ended by a "Start PED" signal from the command and control equipment. This signal occurs 5.5 seconds ±25 milliseconds before optical exposure.

(3) The command and control subsystem supplies a second, or "Expose", signal to initiate optical exposure in the APT camera. If this signal is not received, the APT camera generates its own "Expose" signal 62.5 milliseconds after the expected primary signal.

2. Camera Assembly

The camera assembly, as shown in Figure 4-III-3, contains the following major components:

(1) a 1-inch, electrostatic-storage vidicon tube,

(2) a wide-angle, 107.8-degree, Tegea-Kinoptic, f/1.8 objective lens with a focal length of 5.7 mm,

(3) a video amplifier,

(4) a focal-plane shutter mechanism, (TIROS shutter modified for a 1-inch vidicon)

(5) a deflection-yoke assembly,

(6) a camera housing,

(7) a magnetic shield, and

(8) a focus coil.

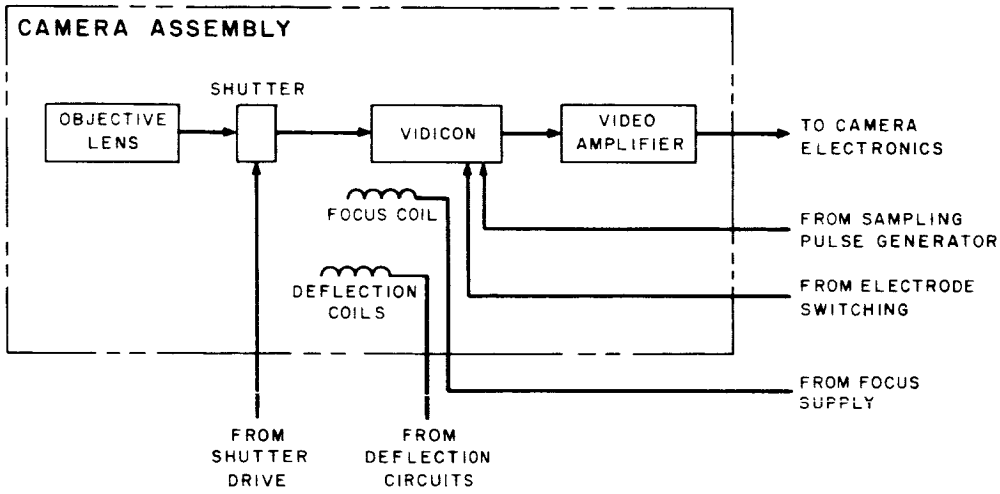

Figure 4-III-3. APT Camera Assembly, Block Diagram

The cylindrical magnesium camera housing comprises the main body of the camera, to which the other components are mounted. The magnetic shield is incorporated to protect the camera assembly against the adverse effects of the combined earth magnetic field and the local spacecraft magnetic field. The faceplate of the vidicon has reticle marks to aid in determining cloud position during picture-taking operations. The reticle marks are transmitted as a part of the video information and are reproduced as part of the composite facsimile picture. If the transmitted picture is distorted because of improper operation of the APT-camera deflection circuits, the reticle marks can be used to determine the nature and amount of distortion when the picture information is interpreted. The configuration of the reticle pattern within the scanned area is shown in Figure 4-III-4; this pattern consists of 25 cross-marks evenly spaced over the raster area. The line width of each mark is 1 mil, twice the width of a scanning line. The reticle marks are also used to help check the system linearity during pre-launch calibration and testing.

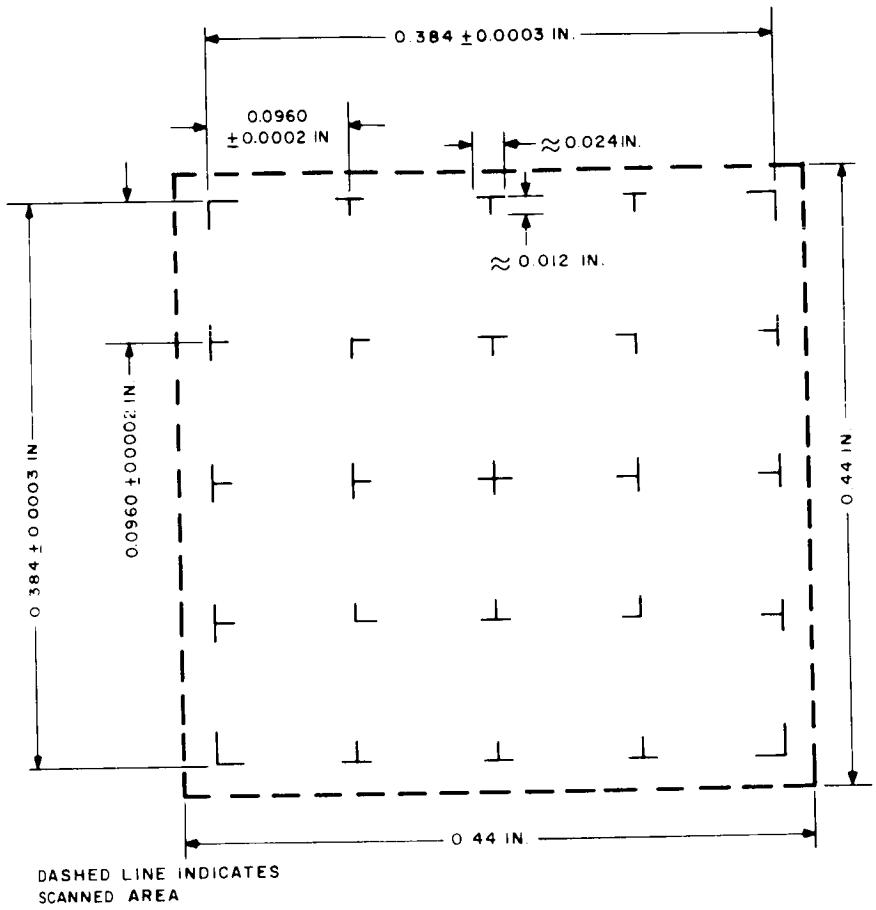

Figure 4-III-4. Vidicon Reticle Pattern

3. Camera Electronics

The camera electronics module, as shown in Figure 4-III-5, contains the following components:

(1) dc-to-dc converters,

(2) electrode switching and beam-current regulator,

(3) shutter drive (same as used in APT camera on TIROS VIII),

(4) focus supply,

(5) sampling pulse generator,

(6) sequence timer,

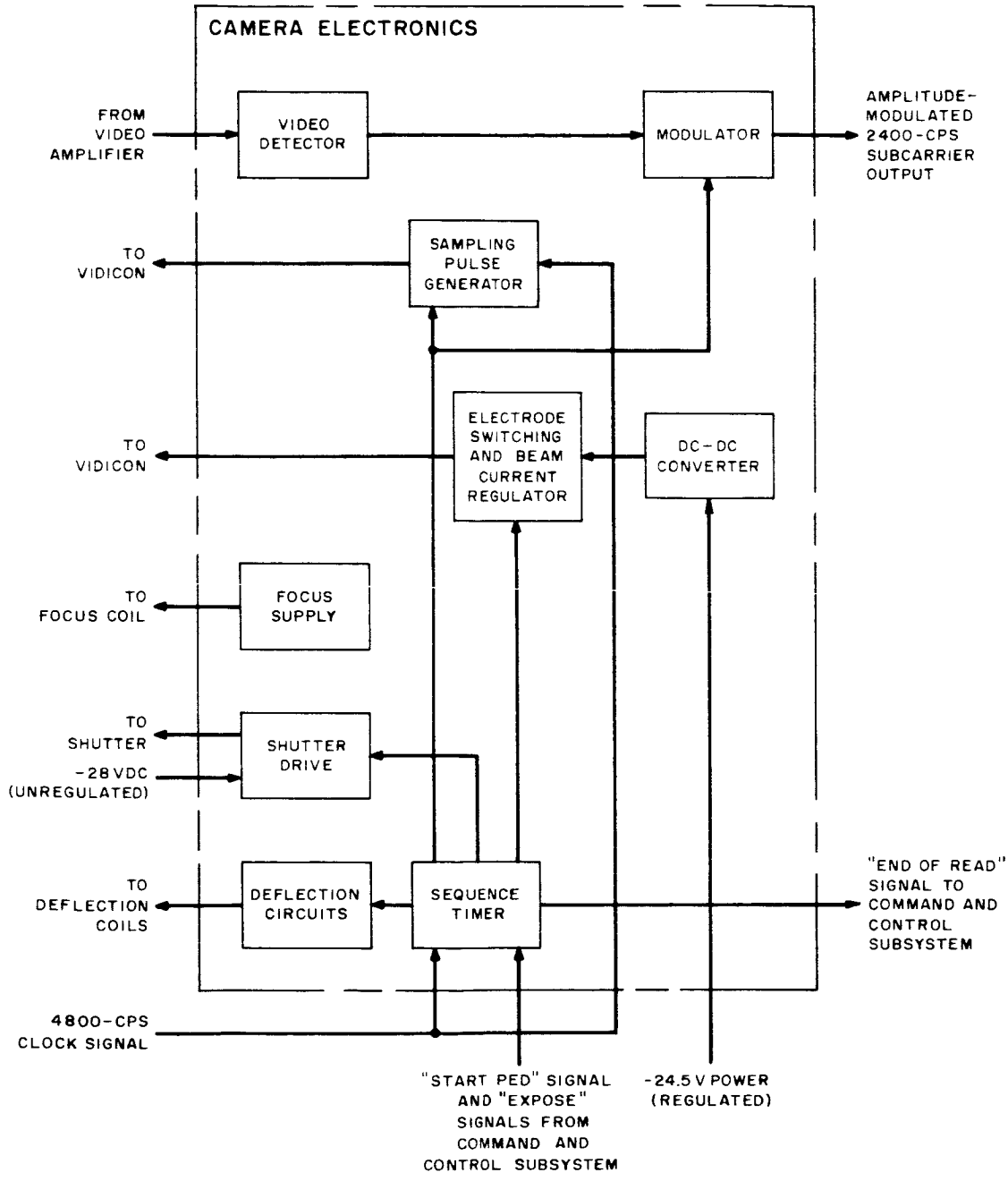

Figure 4-III-5. APT Camera Electronics, Block Diagram

(7) video detector,

(8) modulator, and

(9) deflection circuits

4. APT Video Combiner

The APT video combiner couples the output of either APT camera system to the operating APT transmitter. It is shown in the block diagram of Figure 4-III-6. Combining is accomplished by cross-coupled summing amplifiers which are powered by the supply to the operating transmitter.

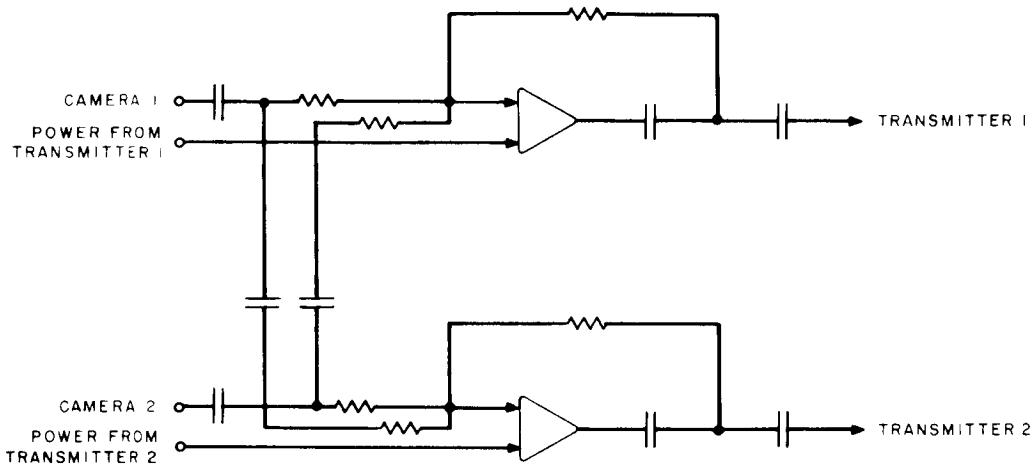

Figure 4-III-6. APT Video Combiner, Block Diagram

5. FM Transmitter

The FM transmitter is a United Electro-Dynamics Inc., Model TR-17 (or equivalent) frequency-modulated telemetry transmitter operating at a center frequency of 137.5 Mc. The unit is capable of delivering at least 5 watts of RF power to the antenna system. The amplitude-modulator used in the APT link has been previously designed and employs balanced-modulation techniques. A 2.4-kc subcarrier is amplitude-modulated by the video baseband and frequency modulates the TV transmitter to provide the input signal required by the APT field-station facsimile receiver. The FM-TV transmitter is specified by the Nimbus APT system and is, therefore, incorporated in the TIROS-wheel design. Specifications for the unit are tabulated below:

Manufacturer:	UED or equivalent
Model:	TR-17, Solid state

Modulation:	FM
Carrier:	137.5 Mc
Carrier Stability:	±0.005 percent
Baseband:	0 to 1.6 kc
Subcarrier:	2.4 kc
Peak Deviation:	+10.0 kc
Maximum Deviation Rate:	4.0 kc
Power Output:	5.0 watts, minimum (37 dbm)
Power Input (total):	23 watts
Supply Voltage:	-24.5 vdc ±5 percent
Weight:	40 ounces
Size:	4.7 x 3.5 x 1.6 inches

6. Antenna Coupling

Figure 4-III-7 shows a quarter-wave coupler for coupling the TV transmitters to the single dipole antenna. The technique of isolating the OFF transmitter from the ON transmitter by using a quarter-wave short-circuit stub has been successful on all TIROS satellites that carried an IR transmitter. The ON transmitter "sees" a quarter-wave short-circuit stub at the junction of the antenna port and the transmitters. This stub appears as an open circuit at the "T"; therefore, all energy is coupled to the antenna. The latching coaxial relays are connected in opposite senses; thus, as power is applied to one transmitter, the coaxial relay nearest the opposite transmitter is latched. This design approach is seen to be a simple solution to the problem of coupling the TV transmitters to the single dipole antenna.

7. APT Field Station (See Figure 4-III-1)

a. Antenna

A bifilar helix over ground plane is used for the APT field station antenna. The minimum gain is 12.5 db over a circular isotropic source. Half-power beam width is 35 degrees. Polarization of this antenna is right-hand circular.

b. Receiver

The APT-TV signal from the helical antenna is fed to a NEMS-Clarke preamplifier, Model PR-204, which has a maximum noise figure of 4.5 db.

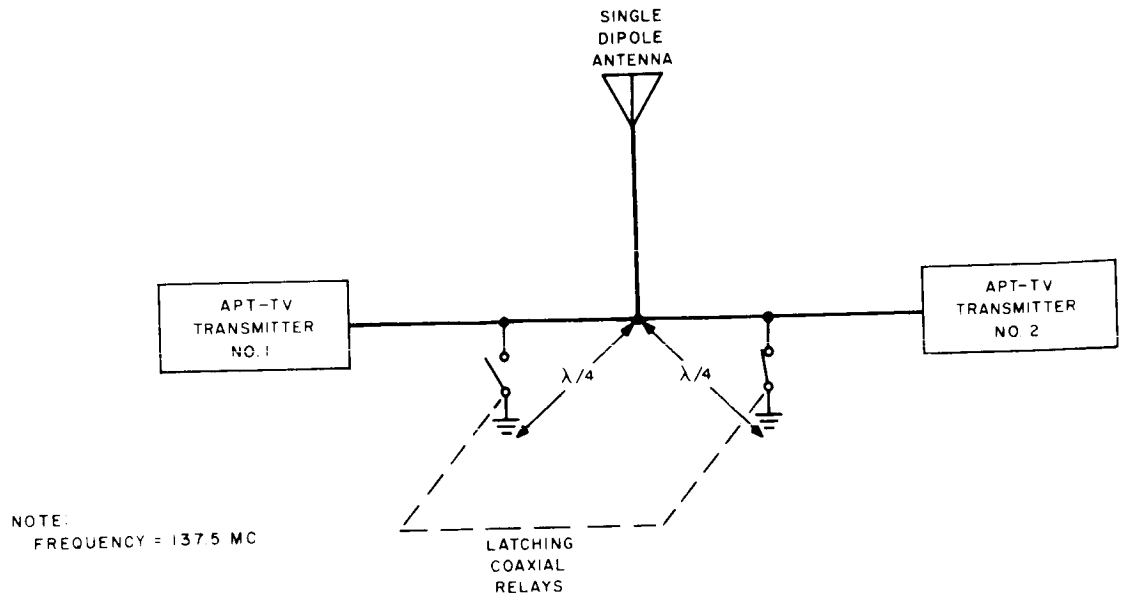

Figure 4-III-7. Antenna Coupler for APT-TV Transmitter

A Nems-Clarke FM receiver, type 1440, is employed. This receiver utilizes phase-lock detection which has a threshold carrier-to-noise ratio of about 9db. IF-bandwidth selection for the APT receiver is 50 kc and 100 kc.

c. Facsimile Recorder

The facsimile receiver requires a 2.4-kc subcarrier which is amplitude-modulated with picture information. This requirement necessitates the inclusion of a 2.4-kc modulator in the APT-camera electronics. A "hard" copy of the TV picture is produced by the facsimile recorder.

B. AVCS CAMERA SUBSYSTEM

1. Introduction

The purpose of the OT-2/AVCS system is to provide daytime cloud-cover pictures from remote locations to a Command and Data Acquisition (CDA) station. As a means of accomplishing this, the system has a magnetic tape recorder for picture storage. The camera and tape recorder used in the OT-2/AVCS spacecraft are essentially the same equipment as employed in the Nimbus AVCS subsystem, with some modifications made to adapt them to the "Wheel" mode of operation. The OT-2/AVCS system functionally differs from the OT-2/APT system described in Paragraph 4-III-A only insofar as the differences inherent in the operation of the camera subsystems are

concerned. This section outlines those camera requirements peculiar to the OT-2/AVCS system. Reference should be made to the "Nimbus Instruction Manual for the AVCS Satellite Equipment" for a detailed description of the Nimbus AVCS design.

2. Functional Description

A block diagram of the camera subsystem is shown in Figure 4-III-8. The AVCS camera assembly and its associated electronics provide a composite video signal which has a bandwidth of approximately 0 to 60 kc. This signal frequency-modulates a 96-kc subcarrier (peak deviation of 24 kc), and the resulting signal is stored by the magnetic tape recorder. Upon command, the tape recorder reads out the modulated 96-kc subcarrier along with a 9.6-kc flutter-and-wow correction tone, which in turn, frequency-modulates the TV transmitter carrier. The output of the TV transmitter is applied to a crossed-dipole antenna that radiates a circularly polarized signal.

A block diagram of the camera assembly and camera electronics is shown in Figure 4-III-9. Figure 4-III-10 shows a diagram of the camera timing cycle. When the camera power is turned on at time T_0 by means of an internally generated signal from the command and control subsystem, the following operational sequence occurs in the camera: At time T_0, -24.5-volt power is applied to the DC/DC converters, thereby applying high voltage to the vidicon and low voltage to the camera circuits. The horizontal and vertical deflection amplifiers are energized, causing the vidicon beam to scan at a 133.3-cps horizontal rate and a 6.5-second vertical period. Also at time T_0, the erase-light switch is triggered, flooding the vidicon faceplate with light for 250 milliseconds, discharging the vidicon photoconductor, and eliminating any stored or residual image.

For the first four frame periods, or 25 seconds, the photoconductor is scanned at the normal AVCS horizontal and vertical rates. During the same period of time, the vidicon cathode is switched to a low negative potential in order to recharge the vidicon photoconductor to cathode potential in preparation for exposure.

At time T_0 +26 seconds, scanning is disabled and the flash tube is ignited for the first time, impressing a calibrated gray-scale image along the edge of the vidicon faceplate. The camera is held in this state for the next 6.5 seconds, to time T_0 +31.5 seconds, when the cathode is switched to ground potential.

At time T_0 +32.5 seconds, the flash tube is ignited for a second time and the shutter is triggered, exposing the vidicon.

At time T_0 +32.75 seconds, the deflection is again enabled and vidicon readout occurs. The video signal is amplified and aperture-corrected by the video pre-amp and amplifier. The video processing amplifier then inserts sync pulses into the video signal, sets both the black and white video level, and provides a low impedance output signal to the frequency-modulator in the tape recorder.

At time T_0 +39.25 seconds, the readout process is complete and power to the camera is switched OFF.

As shown in Figure 4-III-10, turn-on of the tape recorder by the command and control subsystem occurs 1 second before exposure (T_0 +31.5 seconds) and turn-off of the recorder occurs at T_0 +39.25 seconds.

Since the AVCS camera time is derived from the spacecraft spin rate, some discussion is necessary to describe what happens if the spin rate is other than nominal. The horizontal sweep rate is controlled by the spacecraft high-frequency generator and is not affected by spin rate; however, the rest of the signals are spin-rate dependent.

If the spin period increases, the picture quality remains essentially constant, but there will be extra non-data-carrying horizontal scan lines in a picture frame. This will increase the tape recorder record and playback time. If the spin period is greater than 6.6 seconds, the pointing error in degrees will be:

$$360° - 6.6(f),$$

where f is the spacecraft spin-rate in degrees per second. Reliable programmer operation ceases below 7.95 rpm.

If the spin period decreases, the shutter is triggered at the proper time; the picture quality remains the same except the picture contains fewer horizontal scan lines and some data is lost. If the spin period becomes less than 5.9 seconds, the tape recorder will not start in time to record all the data.

3. Camera Assembly

The camera assembly contains a ruggedized, 1-inch vidicon, a Kinoptic-Tegea f/1.8, 5.7-millimeter lens with an iris which will be operated at a fixed setting, a TIROS shutter, modified for the 1-inch vidicon, to provide 1.5-millisecond exposure, and a gray-scale prism and flash tube for impressing a gray-scale pattern on each picture. In addition, the assembly contains a deflecting and focusing yoke and a video preamplifier. The mounting position of the deflection yoke will be different from that used in the present AVCS Nimbus design; the yoke will be rotated 90 degrees counterclockwise (looking into camera lens) so that the vidicon scanning lines will be perpendicular to the orbit track. The camera assembly is completely encased in a magnetic shield. All of the components of the camera assembly are identical to the present AVCS Nimbus design with the exception of the lens, shutter, and magnetic shield.

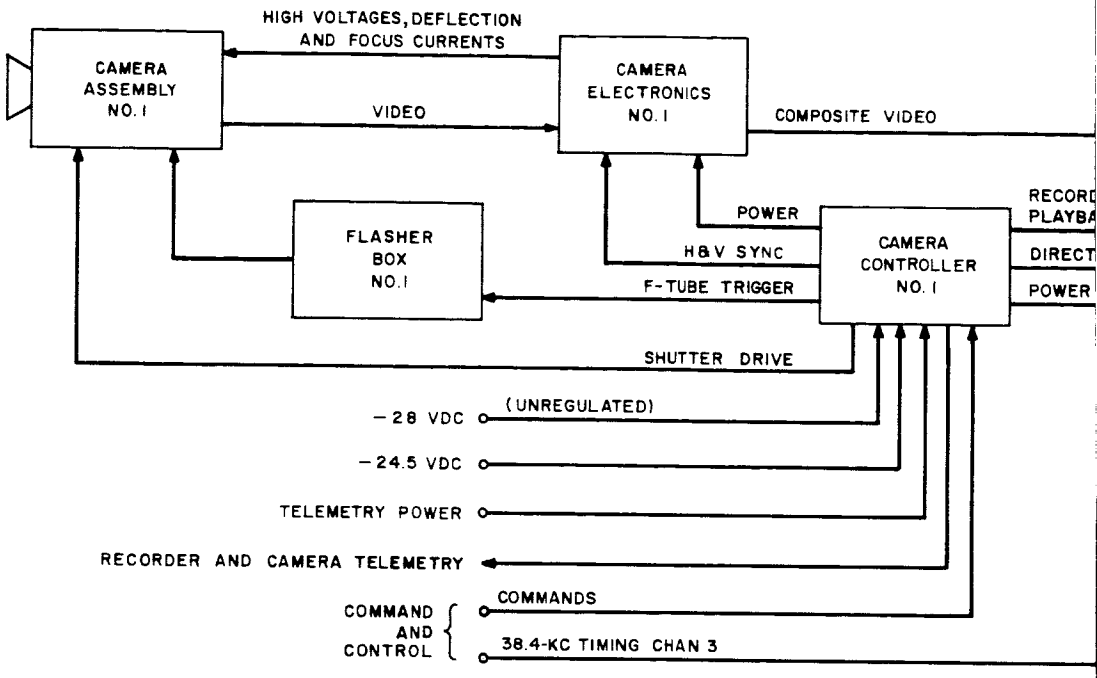

PICTURE TIME CLO
TELEMETRY FRO

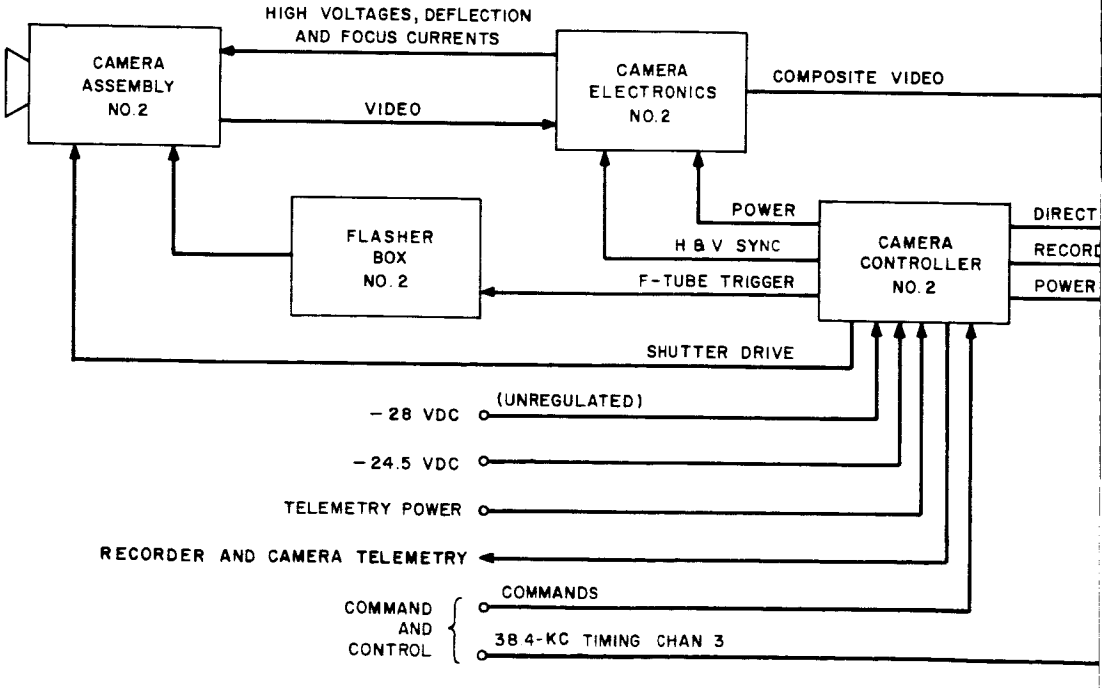

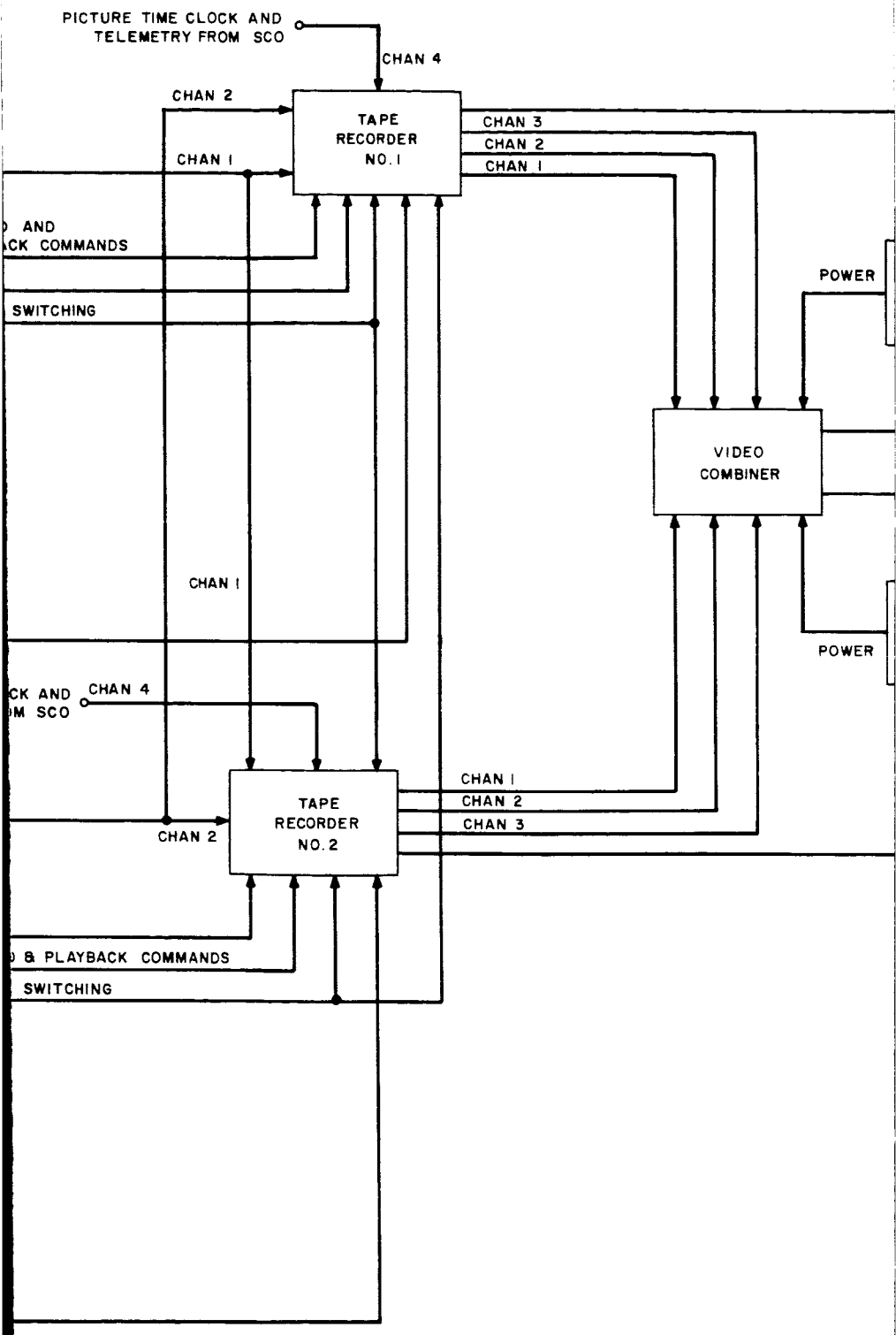
PICTURE TIME CLOCK AND
TELEMETRY FROM SCO
CHAN 4
CHAN 2
CHAN 1
TAPE
RECORDER
NO. 1
CHAN 3
CHAN 2
CHAN 1
AND
ACK COMMANDS
SWITCHING
POWER
VIDEO
COMBINER
CHAN 1
POWER
CK AND
M SCO
CHAN 4
TAPE
RECORDER
NO. 2
CHAN 1
CHAN 2
CHAN 3
CHAN 2
& PLAYBACK COMMANDS
SWITCHING

14

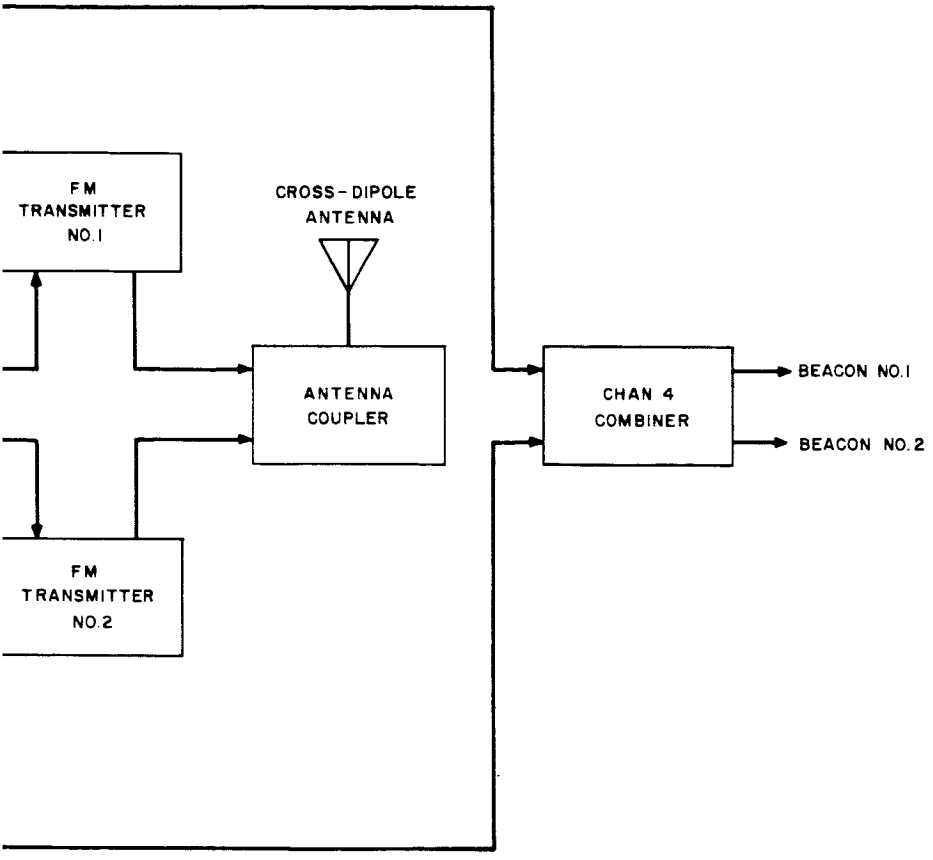

Figure 4-III-8. AVCS Camera Subsystem, Block Diagram

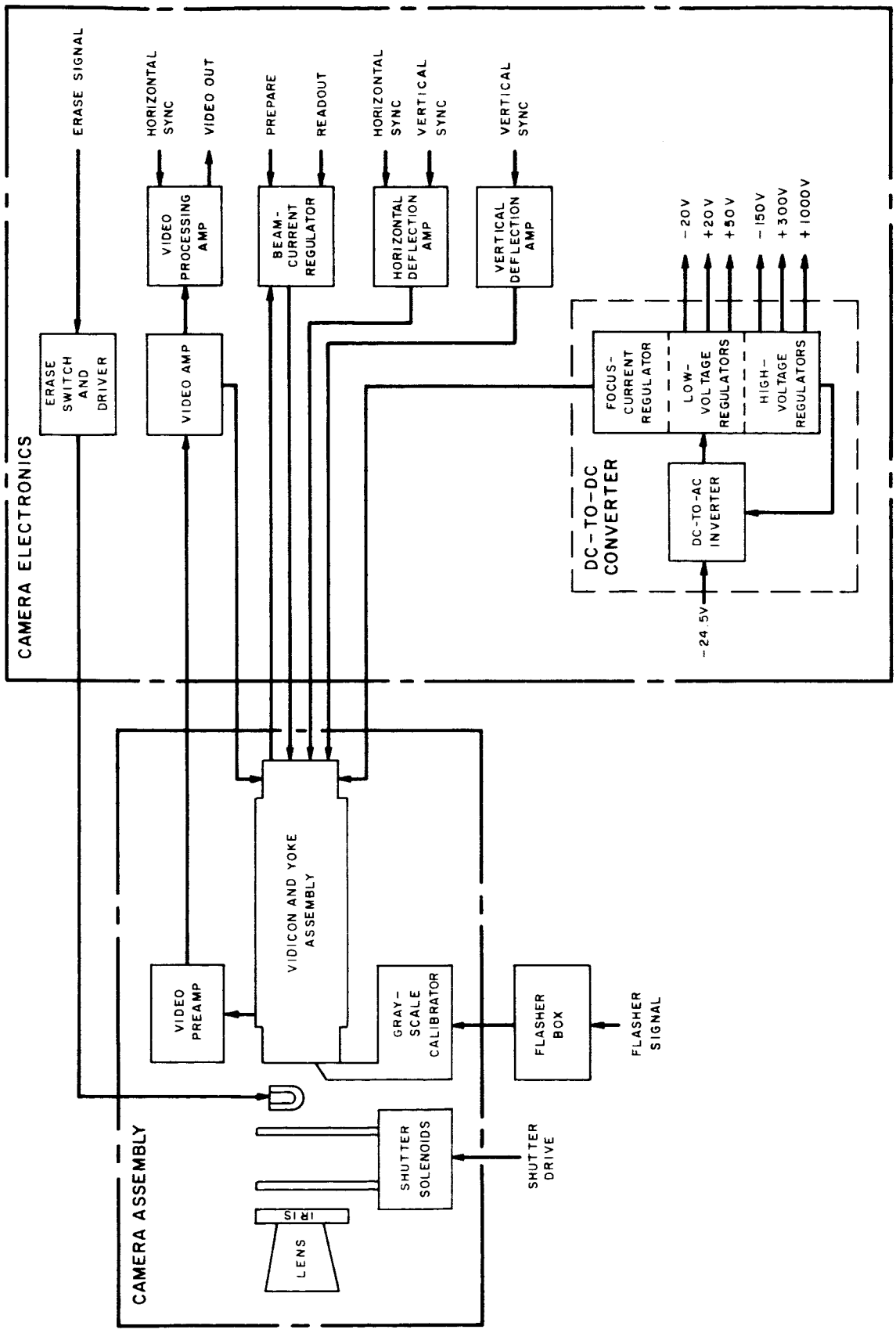

Figure 4-III-9. Camera Assembly and Camera Electronics, Block Diagram

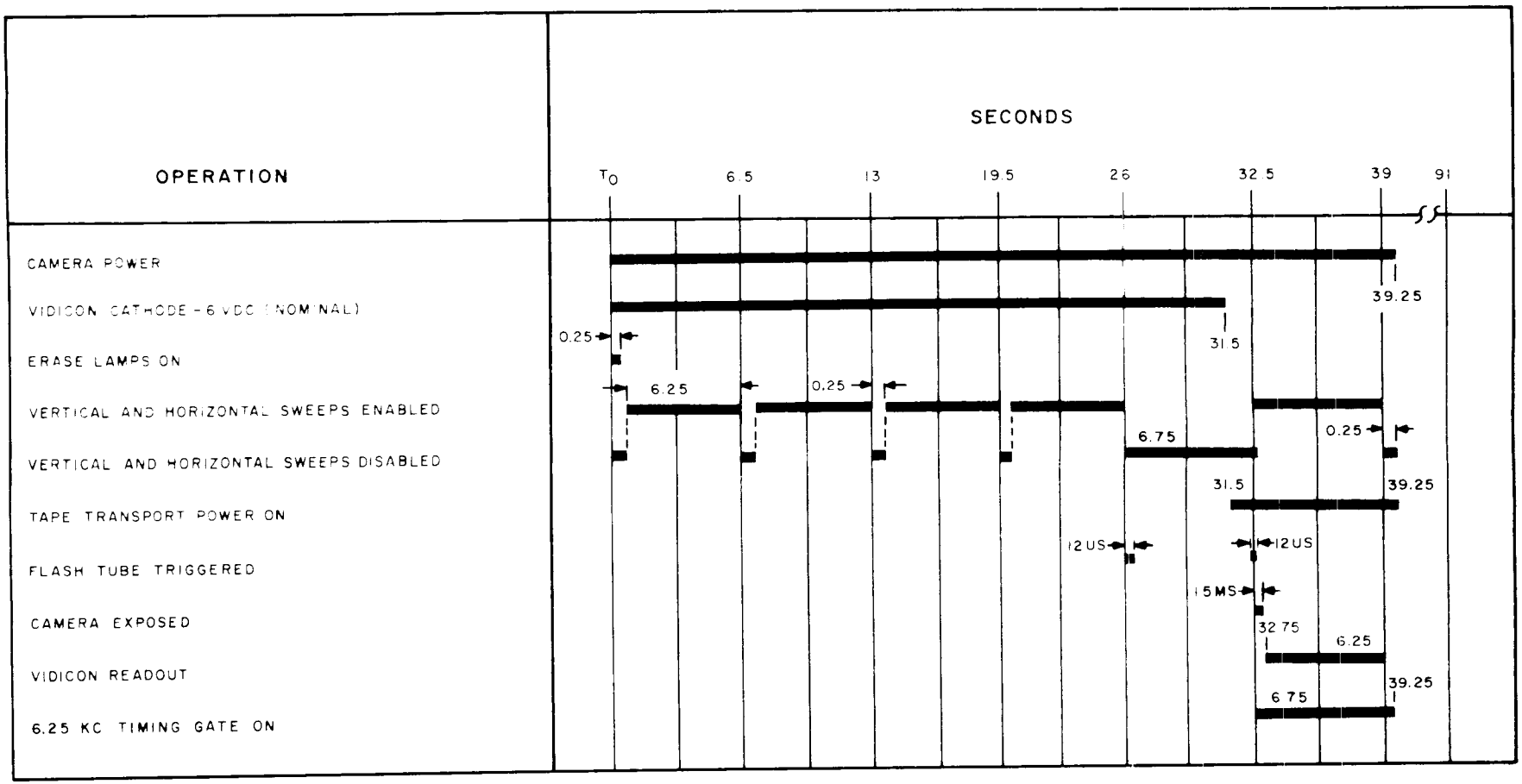

Figure 4-III-10. AVCS Camera Timing Cycle

4. Flasher Box

The flasher box is a 2- x 3- x 5-1/2 inch module which weighs 1.0 pound. The unit contains decoupling circuits for all the vidicon electrode voltages in addition to the circuits necessary to ignite the flash tube of the gray-scale calibrator.

5. Camera Electronics

The camera electronics is a 2- x 6- x 13-inch module weighing 6.8 pounds. The module contains the following circuits, all of which are identical in design to present Nimbus AVCS circuits:

(1) video amplifier and blanking generator,

(2) dc-to-ac high-voltage inverter,

(3) high-voltage regulator,

(4) low-voltage regulator,

(5) focus-current regulator,

(6) video-processing amplifier,

(7) beam-current regulator,

(8) horizontal-deflection amplifier,

(9) vertical-deflection amplifier, and

(10) erase-light switch.

6. Camera Controller

In the AVCS/Nimbus application, the camera controls consisted of a sequence timer and a power-control module. However, a study of the functions which will be performed by the OT-2 command and control subsystem has indicated that the sequence-timer functions, i.e., generating sync pulses and various timing signals for the camera, can be performed more efficiently by the spacecraft command programmer.

The only function that must be completely carried over from the sequence timer, and that does not have its counterpart in the TIROS "I" command and control subsystem is the flutter-and-wow carrier-transmission gate that is used to provide flutter-and-wow correction for the tape recorder and vertical sync information to the ground stations. However, this circuit will be included in the OT-2 command and control subsystem.

The use of the spacecraft command and control subsystem to provide all timing functions will result in greater system simplicity with accompanying weight reduction and improved reliability.

Since very little of the Nimbus power-control switch will be applicable to the OT-2 mission, only elements of this unit that are specifically associated with the AVCS camera will be maintained and the unit will be repackaged and designated as the camera controller to distinguish it from the more complex power-control switch employed in Nimbus. The camera controller shown in Figure 4-III-11 will be housed in a container measuring 2 x 6 x 6 inches and will weigh approximately 2.0 pounds. One camera controller will be provided for each AVCS camera.

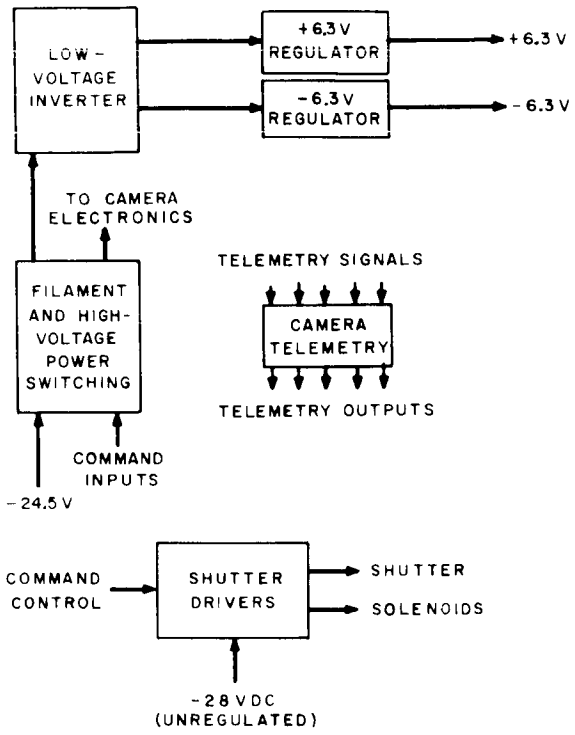

Figure 4-III-11. Camera Controller, Block Diagram

The AVCS shutter-drive circuit will be replaced by the same circuit as that used in the APT camera on TIROS VIII.

The camera controller package will continue to provide the following telemetry outputs:

(1) positive high voltage,

(2) focus current,

(3) horizontal sync,

(4) vertical sync,

(5) vidicon-filament current,

(6) camera-electronics temperature,

(7) camera-housing temperature,

(8) video output, and

(9) 6-volt power.

However, because the OT-2 telemetry subsystem will differ from the Nimbus subsystem, some redesign of the telemetry output circuits will be required. Although the alternate method of adding conditioning circuits to satisfy the OT-2 interface requirements does exist, the need for repackaging the power-control switch has already been established and implementation of this alternate approach would serve only to increase the complexity and reduce the reliability of the system.

7. System Interface Requirements

The camera requires the following inputs:

(1) -24.5 vdc ±1% at 0.3 ampere standby power,

(2) -24.5 vdc +1% at 0.86 ampere prepare and readout power,

(3) -28 vdc, unregulated, at 4.0 amperes shutter power,

(4) "Camera Power ON" command,

(5) "Direct Picture" command,

(6) horizontal sync,

(7) vertical sync,

(8) shutter trigger,

(9) pulse at time T_o,

(10) pulse T_o +26 sec,

(11) pulse T_o +31.5 sec,

(12) pulse T_o +32.5 sec, and

(13) pulse T_o +39.5 sec.

In addition to the telemetry outputs, the video output from the camera will be provided from a source impedance of 200 ohms, and will have the following characteristics:

(1) tip of sync: -6.4 to -6.5 v,

(2) black level: -7.75 ±0.25 v, and

(3) peak white: -11.25 ±0.1 v for 0.6 foot-candle-seconds faceplate illumination.

8. Design Considerations and Specifications

The performance characteristics for the AVCS camera is given in the following listing:

Frame Time:	6.5 sec
Video Bandwidth:	60 kc
Signal-to-Noise Ratio:	32 db, min
Horizontal Centering:	±2%
Vertical Centering:	±2%
Response, 750 to 800 lines:	7%
Vertical and Horizontal Non-Linearity:	±0.5%
Residual Image:	5%
Vidicon Yoke Alignment:	±0.5%
Dynamic Range:	50:1, min
Vertical Shading:	30%, max
Horizontal Shading:	30%, max
Skew:	1%, max
Optical Alignment:	±0.1 degree

9. Tape Recorder

a. General

The proposed magnetic tape recorder is based on the Nimbus AVCS recorder, appropriately modified to satisfy the mission requirements of the OT-2 spacecraft. A functional block diagram of the recommended tape recorder is shown in Figure 4-III-12. The four tape-recorder tracks will be utilized for this mission. Two tracks will be available for recording camera video information, the third track will record the flutter-and-wow compensation carrier, and the fourth track will record a spacecraft picture-time code at the time of picture-record cycle. However, only one video track will be used at any one time.

The tape recorder will be capable of operating in a record, playback, or direct-picture mode upon command from the ground station. The mode of operation will be controlled by the command distribution unit (CDU) of the command and control subsystem.

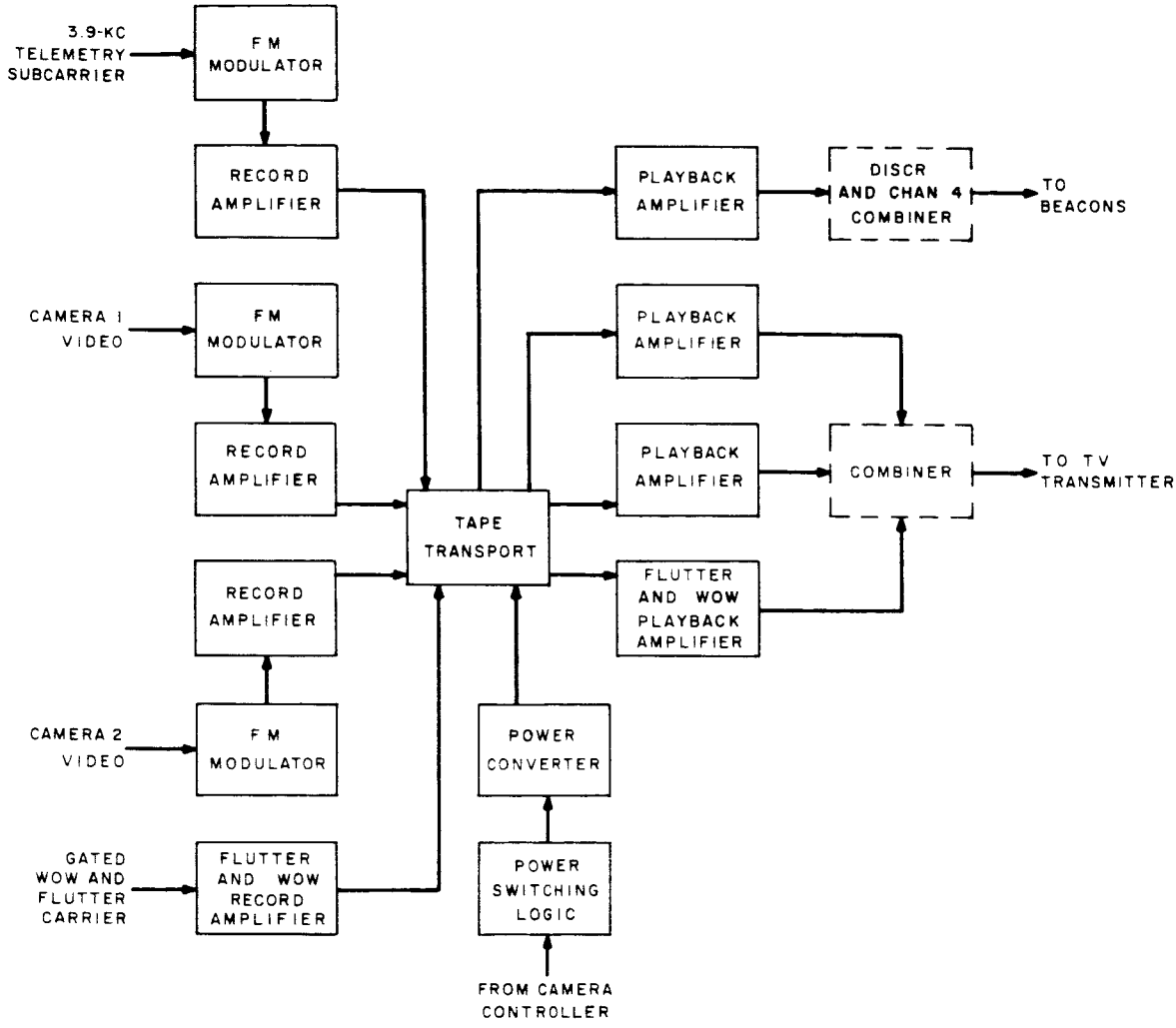

NOTE:

EQUIPMENT ENCLOSED BY DOTTED LINE IS NOT PART OF TAPE RECORDER

Figure 4-III-12. Tape Recorder, Block Diagram

As shown in Figure 4-III-12, the baseband video signal from the selected AVCS camera is applied to a frequency-modulator that produces a 96-kc, FM, video-subcarrier signal. An FM video signal varying between 72 kc for sync to 120 kc for a peak-white signal is generated from the baseband video and is recorded on either of the two video tracks. (One video track is associated with each camera; selection of the desired camera and tape recorder enables the record and playback electronics associated with that camera.)

During the playback mode, the recorder video signal is read from the tape, amplified, and limited to remove undesired amplitude variations. Normally at this point in the operation of the standard Nimbus system, the signal would be frequency-doubled to provide the desired deviation to the Nimbus transmitter. However, for the OT-2 system, doubling of the frequency before transmission will be eliminated in the spacecraft, and instead performed after reception at the ground station. Reasons to substantiate this approach are given in detail in Section 4-III-D, paragraph 1b.

During the direct mode of operation, the FM video signal from the frequency-modulator is applied directly to the playback amplifier. If desired, the tape recorder may be inhibited at this time by ground command.

The frequency of the flutter-and-wow correction tone recorded on the third track will be 38.4 kc instead of 50 kc as used in Nimbus. The 38.4-kc frequency is used because it already exists in the command and control subsystem, and this lower frequency is still within the frequency range of the tape recorder. However the 38.4-kc signal cannot be used for transmission because it extends into the spectrum of the FM video signal which contains frequency components down to 24 kc. Therefore, after playback the 38.4-kc signal is frequency-divided by four in the video combiner to produce a 9.6-kc signal, which is well below the spectrum of the FM video signal.

Table 4-III-1 lists the basic specifications of the tape recorder.

b. Operation

(1) Tape Transport

The recorder tape transport consists of a base casting on which are mounted two coaxial reels, a capstan, three magnetic recording heads (record, playback, and erase), three tape rollers, a flywheel, and a negator-spring assembly. The two tape reels are torqued in opposing directions of rotation by the negator springs to provide constant tape tension. A minimum of 36 pictures can be provided at a video frame rate of 6.5 seconds by 1200 feet of 3M-591 magnetic tape. The extra tape length should be maintained to minimize design changes on the present negator spring and end-of-tape micro-switch support assembly. The additional tape weight of 2 to 3 ounces is not considered to be a design problem.

TABLE 4-III-1. BASIC SPECIFICATIONS OF THE MODIFIED AVCS TAPE RECORDER

Physical Requirements	
Diameter:	13.5 inches
Height:	7.5 inches
Weight:	16.0 pounds
Tape Speed:	30 inches per second
Tape Speed Drift:	±0.5 percent
Tape Capacity:	1200 feet
Tape Type:	3M-591 Magnetic
Tape Thickness:	1.1 mils
Tape Width:	0.5 inch
Uncompensated Momentum:	±0.015 lb-in. sec

Electrical Interface Requirements

Inputs

1. Camera Video 1: 6.5 to -11.5 v, 0- to 60-kc baseband
2. Camera Video 2: -6.5 to -11.5 v, 0- to 60-kc baseband
3. Flutter-and-Wow: 1 v p-p, 38.4 kc
4. Picture Time Code and Telemetry: 3.9-kc FM subcarrier, deviation ±7.5%, -5.3 to 7.3 volts.
5. Record Command Power: -24.5 vdc (20 watts)
6. Record Power (delayed 1 second): -24.5 vdc (4 watts)
7. Direct Command Power: -24.5 vdc (4 watts)
8. Playback Power: -24.5 vdc (20 watts)
9. Motor Signal Input: 18-v p-p, 400-cps squarewave, 2K-ohm load

TABLE 4-III-1. BASIC SPECIFICATIONS OF THE MODIFIED AVCS TAPE RECORDER (Continued)

Electrical Interface Requirements (Continued)
Outputs
1. Video 1: 5-v p-p limited output, source impedance 1 K-ohm, 72- to 120-kc deviation
2. Video 2: 5-v p-p limited output, source impedance 1 K-ohm, 72- to 120-kc deviation
3. Flutter-and-Wow: 5-v p-p limited output, source impedance 1 K-ohm, 38.4-kc center frequency, deviating at the flutter-and-wow rate
4. Picture Time Code: 5-v p-p limited output, source impedance 1K-ohm, 70-kc center frequency, ±10% deviation

The capstan will be driven by a single-speed, 400-cps hysteresis motor.

Separate four-track record- and-playback heads will be employed to optimize sensitivity and frequency response. A single permanent-magnet saturated erase head will be employed. Playback will be in the reverse direction of recording so that the tape travels over the erase head after playback and again before recording.

When the tape becomes completely wound during the record operation, end-of-tape microswitches are actuated by tape buildup, which closes the microswitch points of contact. Upon reaching the end of tape, the microswitch powers a latching relay which will interrupt power to the motor power amplifier, stopping the transport.

The sequencer in the command system initiates each record cycle, which is selectable at either 6 or 12 video frames per orbit. Upon receipt of a playback command, power is applied to two relays which reverse the direction of the transport motor rotation and latch playback power to the motor power amplifier. Playback takes place until the playback end-of-tape microswitch is actuated, stopping the motor. Removal of the playback power command automatically reverses the direction of the transport motor rotation in preparation for the next record cycle.

(2) Motor-Power Amplifier

The solid-state motor-power amplifier functions as the tape transport motor drive. It receives an 18-volt (peak-to-peak), 400-cps, square-wave input signal and minus 24.5-volt d-c power from the CDU power switching circuits. To conserve

power, start and run taps are provided on the output transformer and are switched by a latching relay. The start tap provides rated voltage to the motor during the motor acceleration period. After the motor has reached synchronous speed, the voltage input is reduced to two-thirds of its start value by switching to the run taps, reducing the power consumption to one-half the value required to start the transport.

(3) Video FM Modulator

Each baseband video signal is applied to an FM modulator to provide an FM carrier signal for recording on magnetic tape. The incoming video baseband signal is amplified and fed into a voltage-controlled oscillator whose frequency changes linearly with the video-signal amplitude. The oscillator center frequency is 192 kc, and the video signal produces deviation from 144 to 240 kc. The oscillator output is fed into a bistable multivibrator which produces a symmetrical square-wave output which deviates between 72 and 120 kc. The signal is then applied to a record amplifier and to a single channel of the record head.

(4) Video Playback Amplifier and Limiter

During readout, the recorded FM video signals are played back in the reverse direction of recording. The FM output from the playback head is amplified and limited. The resultant output is a constant-amplitude FM signal deviating from 72 to 120 kc.

(5) Flutter-and-Wow Channel

A stable 38.4-kc signal from the decoder in the command and control subsystem is gated into a limited-bandwidth record amplifier and then to one track of the four-track record head. During readout, this signal will be amplified, limited-divided by four, and filtered to provide a constant-amplitude FM signal having a center frequency of 9.6 kc and frequency deviations proportional to the flutter-and-wow characteristics of the recorder.

c. Command Requirements

The recorder system requires three -24.5-volt power commands, i.e., record, direct, and playback. The appropriate electronics will be enabled for the particular mode. Since the recorder requires a finite time to reach synchronous speed (less than one second), record power will have to be applied at least one second before vidicon information is fed to the recorder.

10. AVCS Video Combiner

The video combiner includes both command or selection functions, and coupling functions. It provides a means of selecting which of the two video channels of the tape recorders shall be coupled to a TV transmitter, and a means of combining the output of the selected video channel with the output of the flutter-and-wow channel of the selected tape recorder. It includes circuits for coupling the signals to either TV transmitter.

A block diagram of the combiner is shown in Figure 4-III-13. Channel selection is made by a latching relay, and signal combining is accomplished in summing amplifiers. Two summing amplifiers, which receive their power from the operating TV transmitter, are included for redundancy.

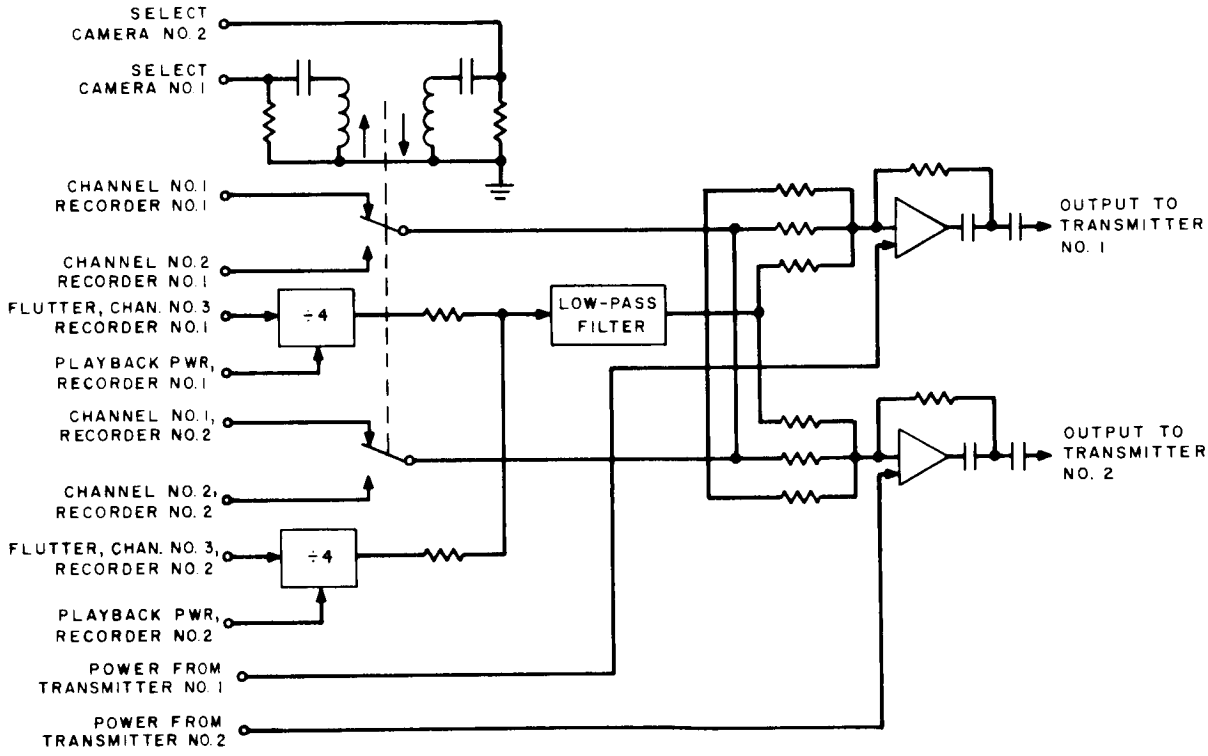

Figure 4-III-13. AVCS Video Combiner, Block Diagram

The command which selects camera 1 or camera 2 operates the latching relay. This connects the outputs of channel 1 or channel 2 of both tape recorders to both summing amplifiers. Whichever tape recorder is played back provides both a video signal and a flutter-and-wow signal (at 38.4 kc). The frequency of the flutter-and-wow signal is divided by four and filtered before the sync is applied to the summing amplifiers. The output is then coupled to the operating TV transmitter.

11. Antenna Coupling

The standard TIROS antenna and coupling circuits will be employed in the OT-2/AVCS system. All associated circuitry has been used on previous TIROS programs and no difficulty is anticipated in obtaining similar performance from this flight-proven equipment in the AVCS application. The antenna-coupling arrangement shown in Figure 4-III-14 is the standard TIROS arrangement. The antenna coupling network will couple both beacon transmitters and the AVCS TV transmitters to the crossed-dipole antenna, match the transmitters to the antenna, isolate the transmitters from one another, and affect circular polarization by exciting the antenna elements in phase quadrature.

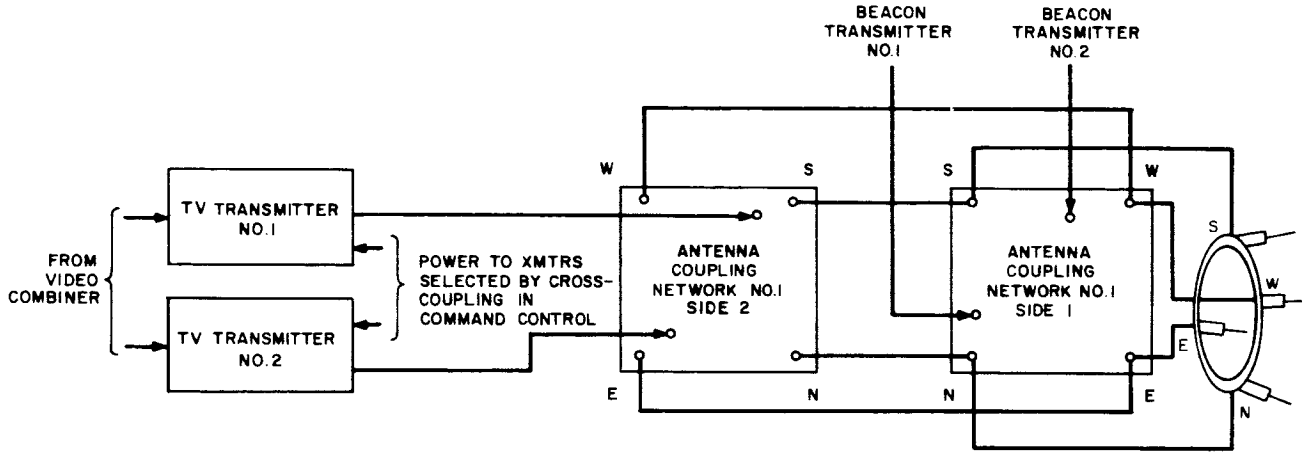

Figure 4-III-14. AVCS Antenna Coupling Network

12. TV Transmitter

The TV transmitter will transmit television pictures at a carrier frequency of 235 Mc to the CDA stations. The frequency deviations in the TV transmitter due to the subcarrier and correction signals are summarized in Table 4-III-2. The upper limit of the frequency spectrum for the TV subcarrier is set at 120 kc by a filter in the tape recorder which attenuates the upper sideband of the video subcarrier signal. The output of the TV transmitter (5 watts) is radiated with circular polarization by means of the crossed-dipole antenna.

TABLE 4-III-2. TV TRANSMITTER FREQUENCY DEVIATION DUE TO MODULATION

Signal	Frequency Spectrum	Corresponding Deviation of Transmitter
Flutter-and-Wow Correction	9.6 ±1 kc	10 kc
Modulated Video	20 to 120 kc	115 kc

The AVCS-TV transmitter is a higher powered version of the present TIROS-TV transmitter which is now being built by the Leach Corporation. Tentative specifications are as follows:

Manufacturer:	Leach, Inc.
Modulation:	FM
Deviation:	125 kc
Power Output:	5.0 watts, minimum
Power Input:	23.0 watts
Size:	5 x 4 x 2 inches
Weight:	40 ounces
Stability:	±0.005 percent
Carrier:	235 Mc
Supply Voltage:	-24.5 vdc

SECTION IV. COMMAND AND CONTROL SUBSYSTEM

A. FUNCTIONAL DESCRIPTION

1. General

The command and control subsystem on the OT-2 spacecraft performs the following functions:

(1) Enables the spacecraft to receive commands from CDA stations while ensuring against the receipt of spurious commands.

(2) Decodes commands from the CDA stations and either processes them for "real-time" operation or stores them for remote operation of the spacecraft.

(3) Retransmits commands received from the ground for the purpose of command verification.

(4) Provides for selective commanding of an individual spacecraft to permit operation of a multiple-spacecraft system.

(5) Initiates remote picture-taking cycles and remote attitude-correction cycles in response to commands from the CDA stations.

(6) Provides the master timing signals required for synchronization of spacecraft operation.

(7) Provides synchronization of the spacecraft operations with the spacecraft spin-rate and rephases these operations if the synchronism is disturbed.

(8) Provides back-up horizon-sensor pulses to maintain spin synchronization if the actual horizon-sensor pulses are interrupted.

(9) Provides real-time switching of power to the Magnetic Spin-Control (MASC) System.

(10) Controls the number of pictures to be taken on each orbit.

(11) Routes commands and internally sequenced signals to the various electronic systems of the spacecraft.

(12) Provides appropriate cross-strapping and redundancy to prevent single failures from disabling the entire spacecraft.

(13) Allows telemetry to be requested, by other than CDA ground stations, by means of a special tone signal.

Functionally, the command and control subsystem consists of three major units: the command receiver and decoder, the programmer, and the command distribution unit (CDU). Ancillary to these major functional units are the orthogonal horizon-sensors, the magnetic-bias control switch, and, in the AVCS configuration of the spacecraft, the picture-time clock. Figure 4-IV-1 is a block diagram of the command and control subsystem.

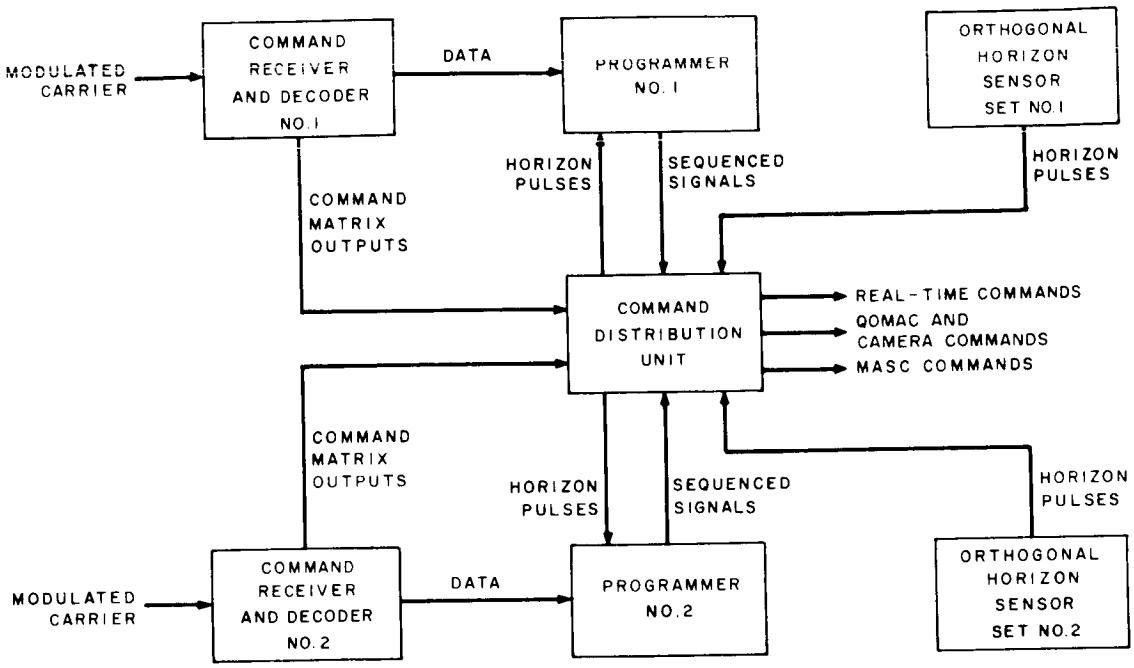

Figure 4-IV-1. Command and Control Subsystem, Block Diagram

2. Command Receiver and Decoder

The functions of the command receiver and decoder are to receive and demodulate the modulated command carrier, to demodulate the frequency-shift-keyed (FSK'd) audio tones, and to supply the CDU with a digital-command matrix input. This unit also supplies digital, remote-programming data to the programmer.

3. Programmer

The programmer receives demodulated command data from the command receiver and decoder. These data are stored for control of either (1) spacecraft attitude by the QOMAC components or (2) picture taking by the cameras. The programmer uses input signals from the orthogonal horizon-sensors to synchronize operation with spin rate.

4. Command Distribution Unit

The CDU converts the 12-line decode matrix signals received from the decoder into actual commands, and routes these commands to the various spacecraft subsystems. It also routes programmer-sequenced signals to the camera subsystem, and performs the logical real-time current switching for the MASC system.

B. COMMAND RECEPTION AND DECODING

1. General

Each of the two channels of the command receiver and decoder consists of an a-m receiver and a tone-and-digital decoder. Both channels are normally "off", with power applied only to the receiver and tone detectors. Only one channel will normally receive commands when the spacecraft is in contact with a ground station. This channel will command all spacecraft equipment, with the second channel offering a back-up capability.

2. Command Receiver

Two identical command receivers, which were developed by RCA and have performed reliably on previous TIROS satellites, will be used in the OT-2 spacecraft. The receivers are solid-state units which are fixed-tuned to the command frequency. The specifications for the receivers are as follows:

Manufacturer:	RCA
Noise Figure:	8 db (maximum)
IF-Bandpass Characteristics	
6-db bandwidth:	40 kc (minimum)
50-db bandwidth:	100 kc (maximum)
bandpass variations:	± 1.5 db (maximum)
center frequency:	20.00 Mc ± 4 kc
Sensitivity:	0.7-vrms audio output (minimum) for 1-microvolt input, modulated 90 percent with 1-kc signal

AGC Control Range	
Input:	2 microvolts to 10 millivolts
Output:	0.9 volt to 1.4 volts rms
Signal-to-Noise at 1-Microvolt Input:	12 db in the IF bandpass
RF Input Source Impedance:	50 ohms
Audio Output Load Impedance:	5000 ohms
Spurious Responses	
20 Mc:	-60 db
image:	-50 db
Operating Temperature:	-15°C to +60°C
Power Supply	
voltage:	-22 to -30 vdc
current:	15 milliamperes (maximum)
Weight:	20 ounces
Size (Both receivers in one integral unit):	6.5 x 5.9 x 2.9 inches

3. Decoder

a. Functional Operation

A decoder channel (Figure 4-IV-2) is made up of a tone detection section, a digital data handling section, and a power supply. The tone detection section is continuously supplied with -23 volt power, while power is gated to the digital data handling section by the presence of a valid FSK tone. Power is also gated from the decoder to the CDU for the decoding and actuation of certain commands. Figure 4-IV-3 presents a logical flow chart for the complete decoding function, and Figure 4-IV-4 is a command timing diagram.

The decode operation starts when an audio "enable" tone is received from the command receiver. Receipt of the "enable" tone for a minimum of 5 seconds conditions the decoder so that a 4-second monitoring period will begin when the "enable" tone drops out. If, during the 4-second monitoring period, at least 1 second of FSK tone is detected,

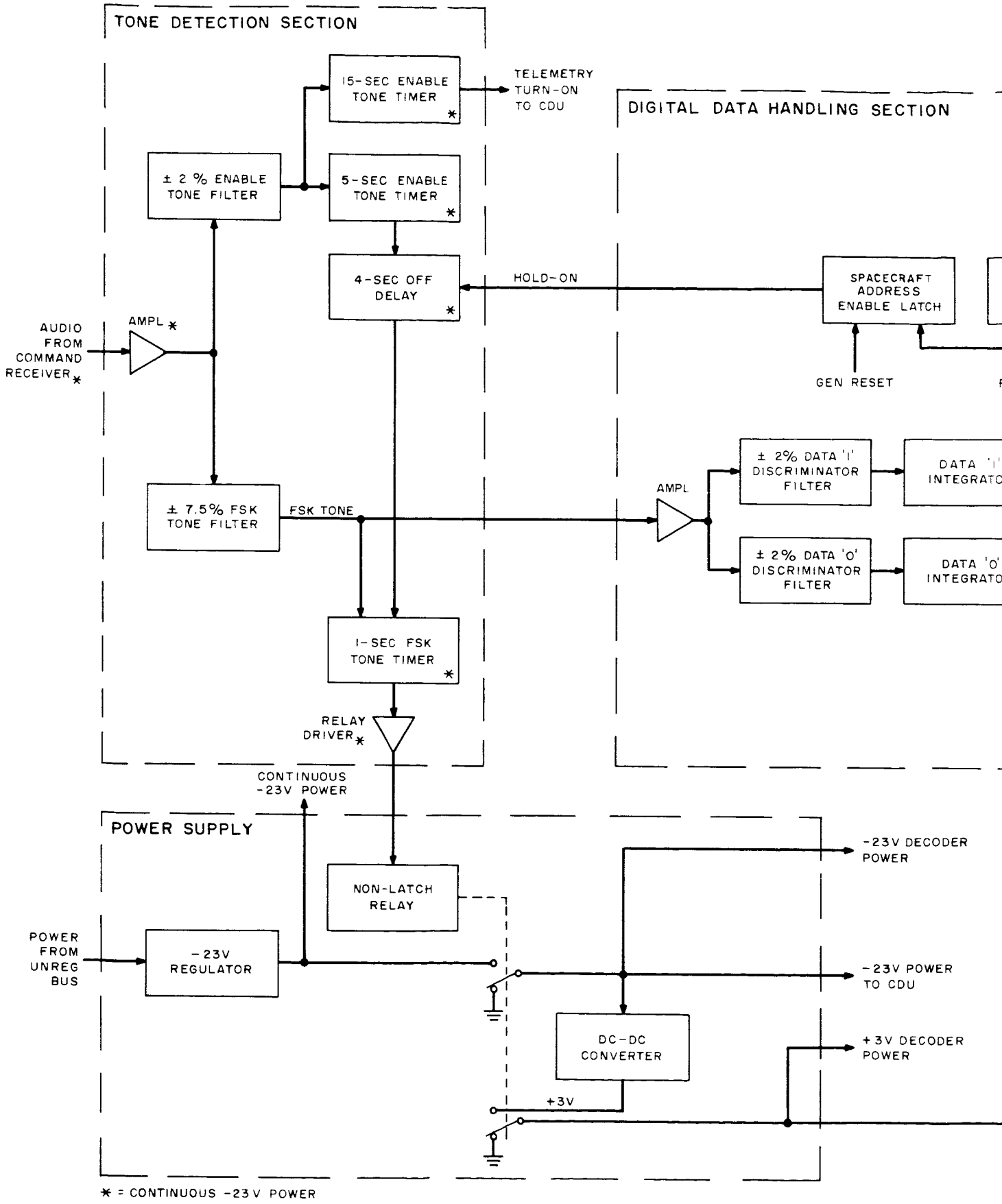
TONE DETECTION SECTION
15-SEC ENABLE TONE TIMER *
TELEMETRY TURN-ON TO CDU
DIGITAL DATA HANDLING SECTION
± 2 % ENABLE TONE FILTER
5-SEC ENABLE TONE TIMER *
4-SEC OFF DELAY *
HOLD-ON
SPACECRAFT ADDRESS ENABLE LATCH
GEN RESET
AUDIO FROM COMMAND RECEIVER *
AMPL *
± 7.5% FSK TONE FILTER
FSK TONE
AMPL
± 2% DATA '1' DISCRIMINATOR FILTER
DATA '1' INTEGRATO
± 2% DATA '0' DISCRIMINATOR FILTER
DATA '0' INTEGRATO
1-SEC FSK TONE TIMER *
RELAY DRIVER *
CONTINUOUS -23V POWER
POWER SUPPLY
NON-LATCH RELAY
-23V DECODER POWER
POWER FROM UNREG BUS
-23V REGULATOR
-23V POWER TO CDU
DC-DC CONVERTER
+3V DECODER POWER
+3V
* = CONTINUOUS -23 V POWER

5 (1)

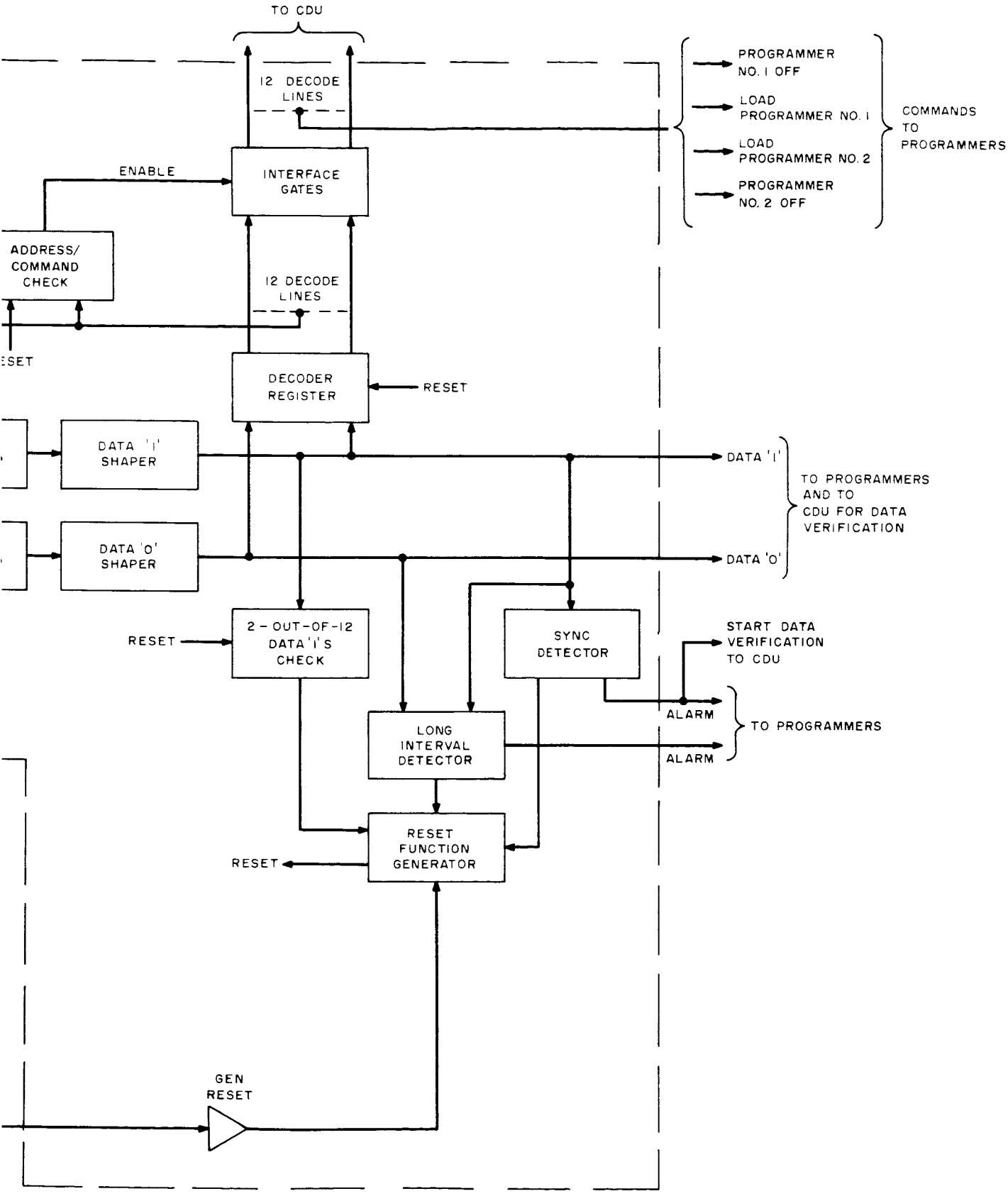

Figure 4-IV-2. Decoder Channel, Block Diagram

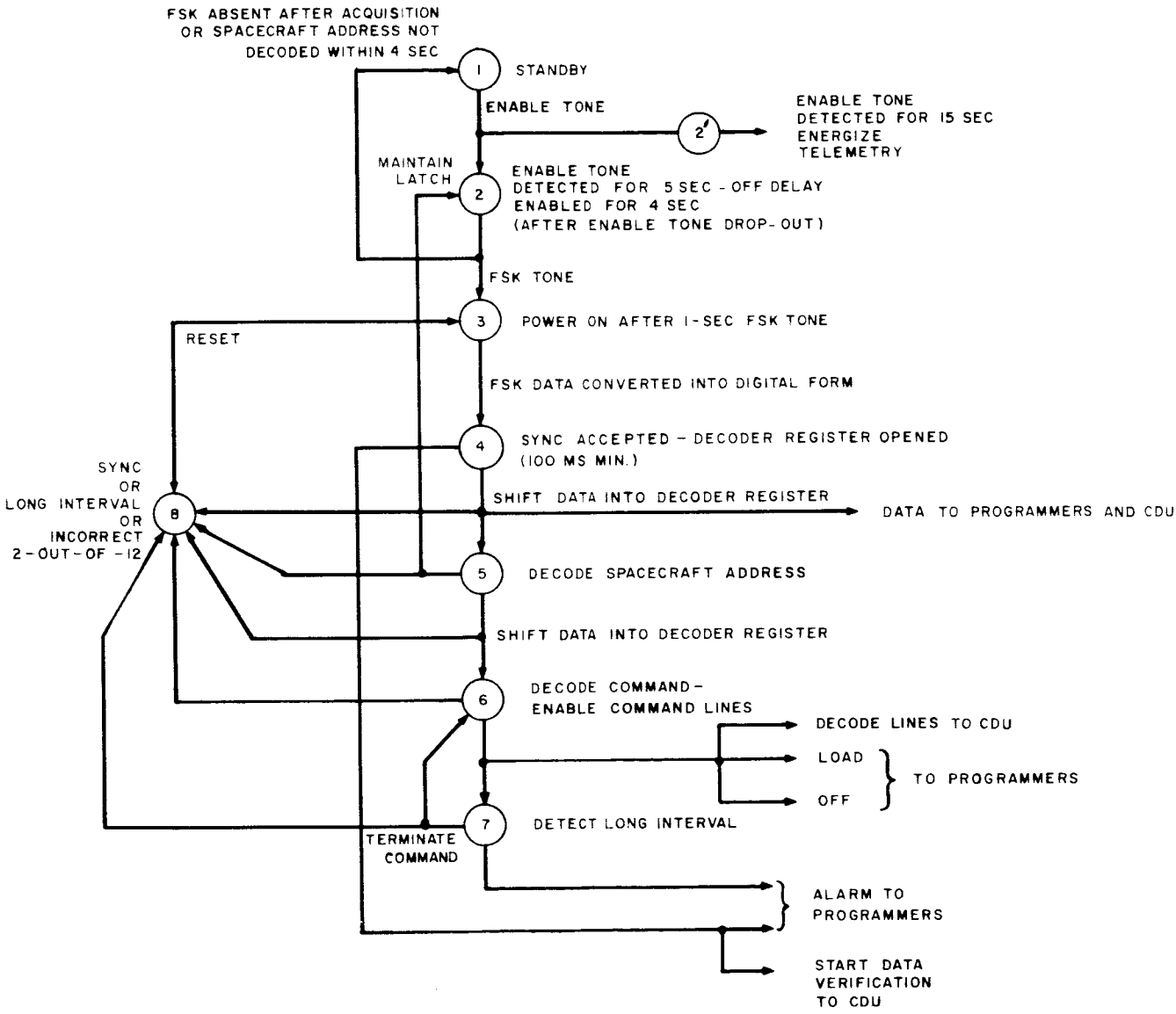

Figure 4-IV-3. Decoder Channel, Flow Chart

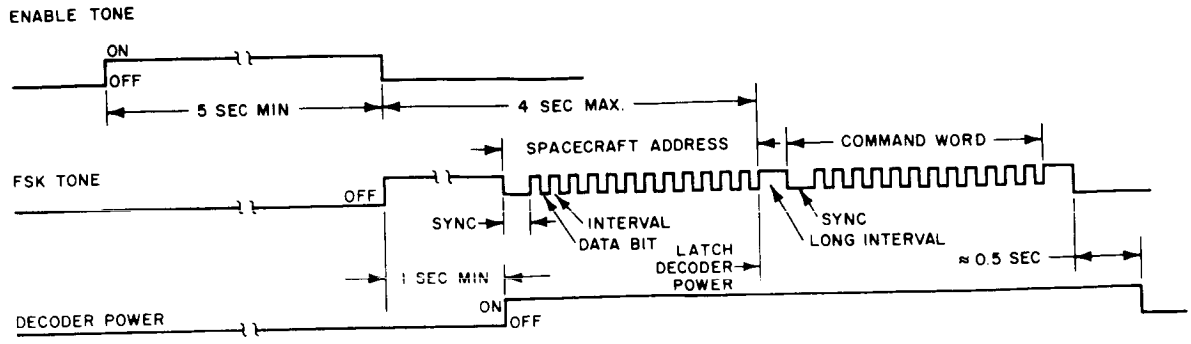

Figure 4-IV-4. Command Timing Diagram

power is switched "on" for the digital data handling section and the CDU. This allows the digital data bits to be extracted from the FSK transmission. The data are shifted into the decoder register upon detection of sync, where they are examined for the presence of a valid spacecraft address. If the spacecraft address is received before the end of the timed 4-second period, the power for the digital data-handling section is latched "on", and processing continues. The next sequence of data must correspond to a valid command word sequence. A valid command word sequence consists of a sync interval of at least 1 second duration followed by 12 bits, exactly 2 of which must be data "1"s. Commands to "load" or turn "off" a programmer are decoded and are sent directly to the appropriate programmer. All other valid commands are presented to the CDU for further decoding and implementation. All data bits received after recognition of a valid "load" command are sent to the programmers for program loading. All data bits that follow receipt of the first valid sync signal are re-transmitted to the CDA station in real time, by means of the data verification telemetry channel. Telemetry can be turned "on" by receipt of either a 15-second "enable" tone or the appropriate command message.

The decoder power supply receives input power from the unregulated bus. It consists of a -23 volt regulator and a +3 volt dc-to-dc converter.

b. Summary of Design Characteristics

The data code format for actuation of a command is as follows:

(1)	Sync:	2 baud
(2)	Spacecraft address:	12 baud
(3)	"Long" interval:	2 baud
(4)	Sync:	2 baud
(5)	Command word:	12 baud
(6)	"Long" interval:	2 baud
(7)	Data for programmer, if required:	28 baud

The information rate is about 10 bauds (code elements per second) i.e., the period of a single code element is 100 ± 10 milliseconds. Sync is noted by a shift to the "1" level for 150 ± 15 milliseconds, followed by a 50-millisecond return to the FSK center frequency. A data bit is noted by a shift to the "1" or "0" level for 50 ± 5 milliseconds, followed by a return to the center frequency for 50 ± 5 milliseconds. A "long" interval is noted by the lack of data for more than 100 milliseconds. It may be safely assumed that a return-to-center-frequency has been accomplished if no data are present and power is still "on" for the digital data handling section.

Commercial programming makes it advisable to select subcarrier frequencies as high in the audio spectrum as possible, while the receiver bandwidth limits the upper end of the spectrum to about 10 kc.

Four separate tones are utilized in the OT-2 spacecraft. The use of four separate tones increases the security of the system without increasing the number of components in the spacecraft. This arrangement provides maximum isolation between channels and guarantees that the opposite channel will not be enabled during commanding, which would be the case if a common "enable" tone were used.

The operation of the decoder is analogous to a "push-to-talk" system, with the advantage of automatically being turned "off" by any of the following conditions:

(1) If the spacecraft address is not received within 4 seconds of "enable" tone drop-out, power will turn "off". The "enable" tone must again be received for 5 seconds and the FSK tone for 1 second before power will again be applied to the digital data handling section.

(2) If the power has been latched "on", the "enable" tone dropped, and the FSK tone drops for 0.5 second (approximate), power will turn "off". The restart procedure is the same as described for condition (1).

(3) If the power has been latched "on", the "enable" tone is present, and the FSK tone drops for 0.5 second (approximate), the power will turn "off". The FSK tone must again be sent for 1 second before decoder power will again be applied.

c. Immunity to Spurious Operation

Before any command can be executed, access to the spacecraft must be gained through the two-tone entry system and coded digital data of the precise format must be received. The coding required for a command to be activated is that a 12-bit spacecraft address be received and followed by a 12-bit command word. To be a valid command, the command word must contain exactly 2 data "1"s out of the total 12 bits. There are a possible 66 valid commands. Each spacecraft has its own unique 12-bit address. There are a possible 66 unique spacecraft addresses. Those 2-out-of-12 codes not used for command words will be used for spacecraft addresses, as long as is practical in view of launch dates and spacecraft life.

Although immunity to spurious commands is mainly a function of digital data coding, the following basic restrictions are placed upon bit timing:

(1) Any shift to the data "1" level for more than 100 milliseconds will be interpreted as a sync signal, causing the decode register to reset.

(2) Any period lasting longer than 100 milliseconds during which decoder power is "on" and no data bit "1" or "0" is received will cause the decoder register to reset.

(3) In the case of data to the programmer register, a shift to the data "1" level or any static level for more than 100 milliseconds will cause the programmer register to reset if it has not already received its full program of data.

Decoding is essentially independent of internally generated spacecraft clocking pulses. The only synchronism between ground transmitted pulses and spacecraft signals exists as a result of ground station data coordination with orthogonal horizon-sensor telemetry.

To determine the probability of spurious latching of decoder power "on", the conservative assumptions are made that a random bit stream is being received, the maximum bit rate recognizable (as set by integrators following the demodulator filters) is 30 bits per second, sync receipt has been satisfied, and the "enable" tone has been present for longer than 5 seconds and dropped. Thus, the spacecraft address must be received within 4 seconds to latch power "on". The probability of such an event occurring within 4 seconds is

$$\frac{1 \text{ valid address}}{2^{12} \text{ addresses}} \times \frac{30 \text{ bits}}{\text{second}} \times \frac{1 \text{ address}}{12 \text{ bits}} \times \frac{4 \text{ seconds}}{} = 0.0025$$

In determining the probability of actuating a valid command word, with a random bit stream, it is assumed that the "enable" tone is continuously present, (so that tone integration need not occur), that the available access time is 20 minutes, and that the maximum bit rate is 24 bits per second (to modify the requirements for sync and interval as part of the 24-bit code word structure). The probability of receiving a valid command in 20 minutes is

$$\frac{66 \text{ valid commands}}{2^{12} \cdot 2^{12} \text{ cmds}} \times \frac{1 \text{ command}}{\text{second}} \times \frac{20 \text{ minutes}}{} \times \frac{60 \text{ seconds}}{1 \text{ minute}} = 0.00474$$

The probable time between such commands is

$$\frac{2^{24}}{66} \times \frac{1 \text{ second}}{\text{command}} \times \frac{1 \text{ hour}}{3600 \text{sec}} \times \frac{1 \text{ day}}{24 \text{ hrs.}} = 2.94 \text{ days.}$$

4. Command Distribution Unit

The CDU contains circuitry to decode and store digital command information received from the decoder on the 12-bit data lines. Table 4-IV-1 lists the available commands for control of the spacecraft.

TABLE 4-IV-1. COMMANDS FOR THE OT-2 SPACECRAFT

Command	Function
APT and AVCS	
Regulator No. 1 On, Regulator No. 2 Off Regulator No. 2 On, Regulator No. 1 Off Both Regulators Off	To select the voltage regulator for the -24.5-volt regulated bus or to remove all power from the bus.
Load Programmer No. 1 Load Programmer No. 2 Programmer No. 1 Off Programmer No. 2 Off	To switch "on" or "off" the selected programmer.
Select Camera No. 1 Select Camera No. 2 Select Transmitter No. 1 Select Transmitter No. 2	To select the principal components of the camera subsystem.
Select Orthogonal Horizon-Sensor 1A Select Orthogonal Horizon-Sensor 1B Select Orthogonal Horizon-Sensor 2A Select Orthogonal Horizon-Sensor 2B	To select one of the redundant sensors on each side of the spacecraft.
QOMAC Power Off QOMAC Power On	To turn QOMAC power "on" and "off".
Magnetic Bias Positive Magnetic Bias Negative Magnetic Bias Off Step Magnetic Bias Switch	To select proper magnitude and polarity of magnetic bias current.

TABLE 4-IV-1. COMMANDS FOR THE OT-2 SPACECRAFT (Continued)

Command	Function
APT and AVCS (Continued)	
Beacon No. 1 On Beacon No. 2 On Beacons Off	To select either one of the redundant beacons and its three associated subcarrier oscillators. Only one beacon can be "on" at a time.
Commutators Normal Commutators Crossed Request housekeeping Telemetry	To enable one frame of telemetry from the commutator and to permit either comutator to be used with either beacon.
Request Solar Aspect Telemetry Solar Aspect Telemetry Off	To select solar aspect data for transmission on the third SCO of the selected beacon.
Spin-Up Spin-Down Select MASC Coil No. 1 Select MASC Coil No. 2 MASC Coils Off	To select either one of the spin-control coils, and to select polarity of MASC coil current so that either a spin-up or a spin-down is obtained.
Release Yo-Yo's Release Dampers	To provide a back-up command to ensure the release of the de-spin mechanism and the TEAM nutation dampers.
High Level Charge Mode On High Level Charge Mode Off	To permit a more rapid charging of the batteries in the event of an open-circuit loss of a battery string.
ADDITIONAL FOR AVCS ONLY	
Select Tape Recorder No. 1 Select Tape Recorder No. 2	To select tape recorder.
Inhibit Tape Recorder Enable Tape Recorder	To permit direct picture tests without running the tape recorder.
Playback	Turns "on" transmitter and enables playback of tape recorded video.

TABLE 4-IV-1. COMMANDS FOR THE OT-2 SPACECRAFT (Continued)

Command	Function
ADDITIONAL FOR AVCS ONLY (Continued)	
Transmitter On Transmitter Off	Used to request direct picture transmission.
Record Mode	A back-up to put tape recorder in record mode.
Picture Time Clock Programmer No. 1 Programmer No. 2	Selects programmer which will supply power to the picture time clock.
IR Spare IR Spare IR Spare	Operates latching relay for possible use on IR package.

The configuration of the circuitry used to perform the decode and storage function is shown in Figure 4-IV-5. Each of the 12 data lines from both decoders is connected to a buffer amplifier (BA) which drives a number of "and" gates. Each "and" gate is a 2-input type, assigned to decode one of the specific commands listed in Table 4-IV-1. When both inputs to an "and" gate are simultaneously activated for a period between 50 and 100 milliseconds, its associated relay is energized and latched "on". Contacts of the operated relay complete the connections to implement the received command.

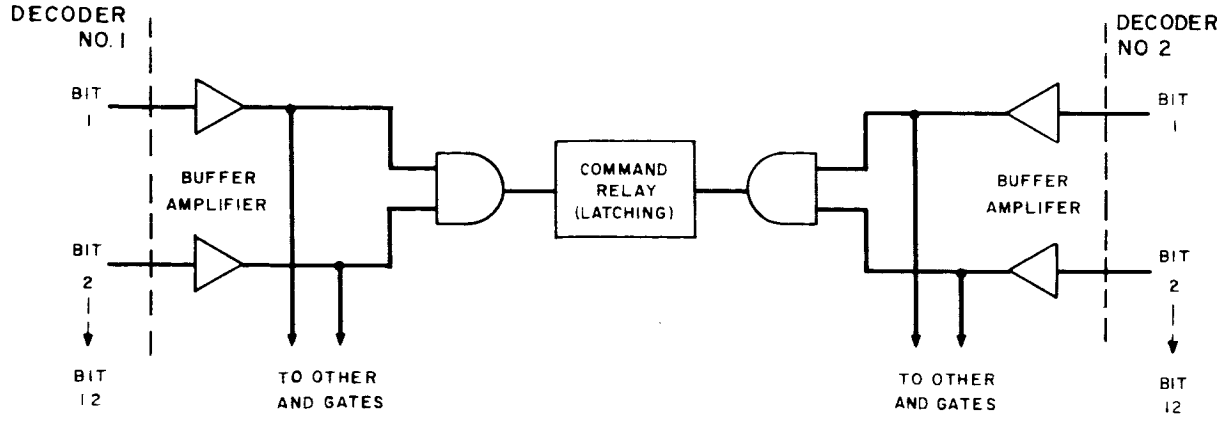

Figure 4-IV-5. Command Decoding Circuit, Logic Diagram

Since the "and" gates are powered by the decoder which supplies the data inputs, failures in these circuits can be bypassed by using the alternate decoder. Interaction effects on the latching relay are prevented through the insertion of isolation diodes, between the "and" gates and their associated relays.

C. CAMERA CONTROL

1. General

The camera-sequencing program is decoded and implemented by circuits located in the programmer and CDU. Upon receipt of a "load" programmer command, the programmer circuits store the camera information contained in the 28-bit digital data received from the decoder. Then, the programmer generates the camera-sequencing signals required to implement the requested program. These signals are routed to components of the camera subsystem through paths established in the CDU by previously processed 12-bit commands.

Since the spin rate of the spacecraft is nearly constant, the generation of the camera-sequencing program is synchronized with horizon pulses received from the orthogonal horizon-sensors. Figures 4-IV-6 and 4-IV-7 show the relative orientations between cameras and horizon sensors required for proper synchronization of the APT and AVCS systems, respectively. In both systems, the lines of sight of the two cameras are parallel, with their actual viewing directions 180 degrees apart. Each camera, also, is capable of being controlled by either of the two assigned horizon sensors mounted on the camera's side of the spacecraft. The horizon-sensor selections are made through ground-station commands (Table 4-IV-1).

All of the APT horizon sensors and two of the AVCS horizon sensors are positioned so that their lines of sight form an angle α with respect to a camera's line of sight. Angle α is chosen so that when the sensor's line of sight crosses a sky-earth intersection, the camera's line of sight is at the midpoint of its earth-viewing time. The two remaining AVCS horizon sensors are located at angle β so that their lines of sight cross the sky-earth intersection when the associated camera's line of sight is looking at an angle offset 15 degrees from the local vertical.

Since a time period between 5.355 seconds (minimum) and 6.545 seconds (maximum) is required to receive and process a complete request for a picture-sequence program and since the APT and AVCS spin periods, nominally 5.5 and 6.5 seconds, respectively-fall within this required time period, precautions must be taken to prevent the receipt of a request which might end during "earth" time. This undesirable type of request, which produces a 1-spin ambiguity in the start of a picture-sequence program, would be produced if the CDA station were to start its transmission at the time of a sky-earth pulse from a horizon sensor associated with the energized camera. To prevent this

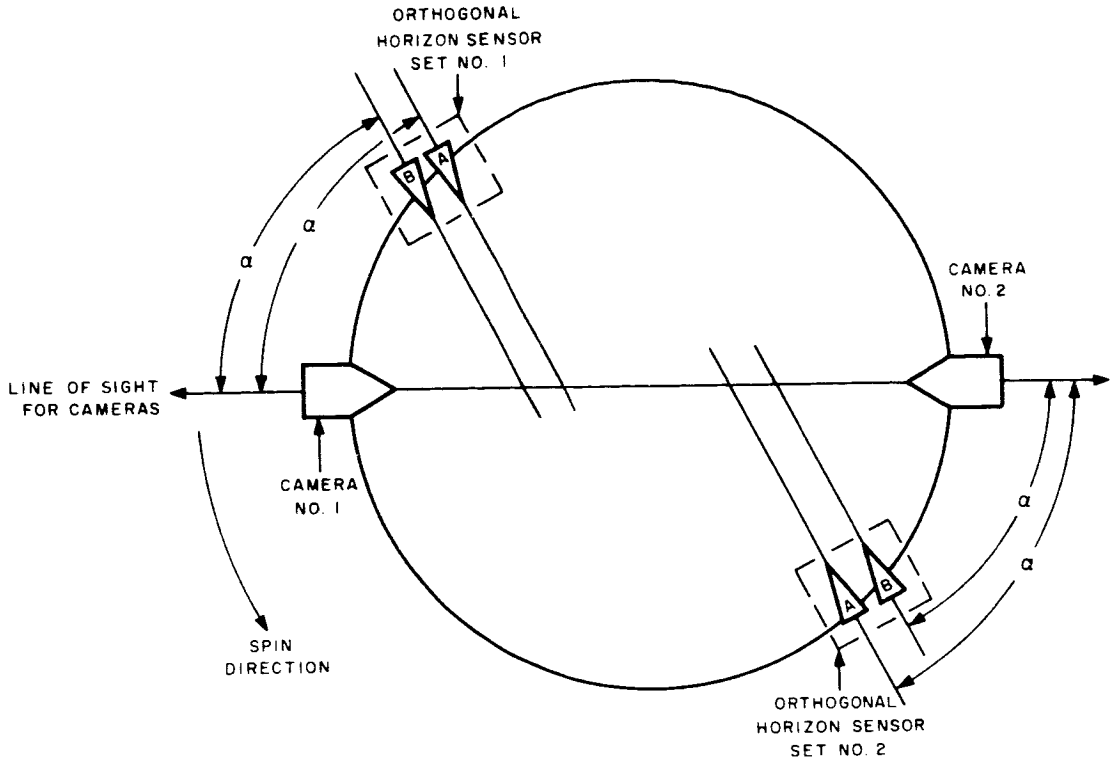

Figure 4-IV-6. Orientation of APT Orthogonal Horizon-Sensors

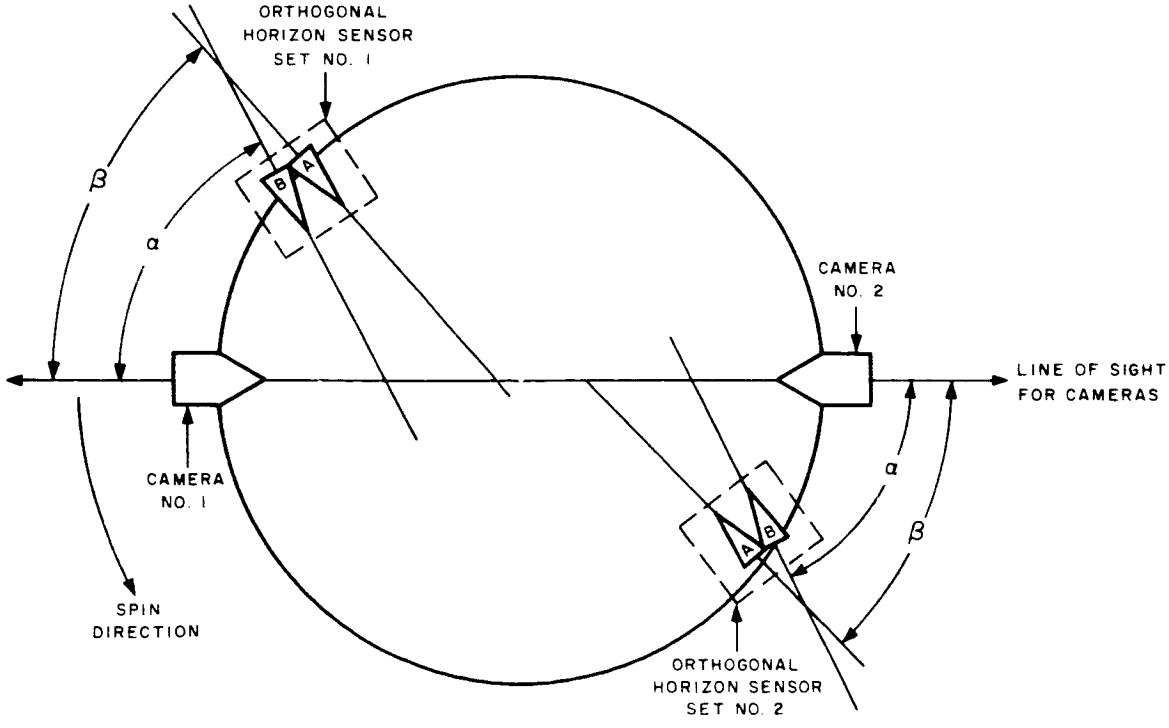

Figure 4-IV-7. Orientation of AVCS Orthogonal Horizon-Sensors

type of request generation, the CDA station is synchronized so that it starts its transmission within a specified tolerance of the time of a sky-earth pulse from a horizon sensor associated with the de-energized camera. For an APT request, transmission must begin within 1.6 seconds after receipt of the appropriate sky-earth pulse. (See Figure 4-IV-8.) For an AVCS request, transmission must begin between 0.4 seconds (minimum) and 2.8 seconds (maximum) after receipt of the appropriate sky-earth pulse. (See Figure 4-IV-9.)

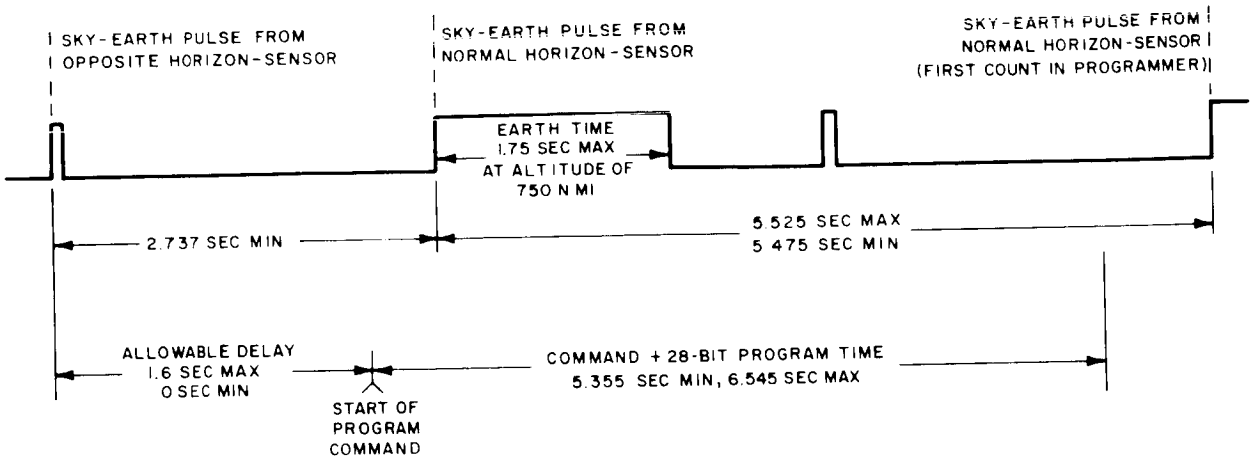

Figure 4-IV-8. APT Command-Transmission Timing Diagram

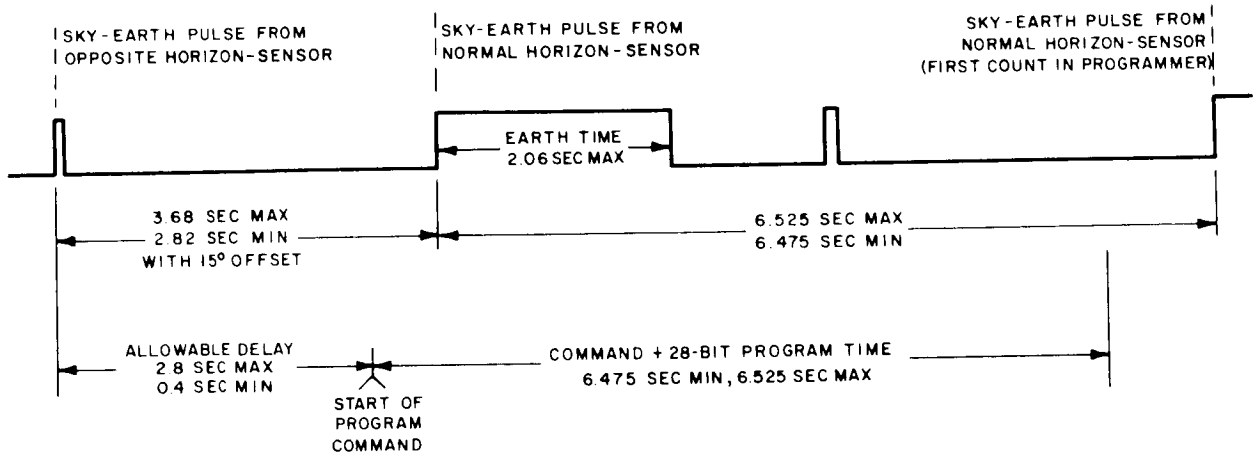

Figure 4-IV-9. AVCS Command-Transmission Timing Diagram

2. Programmer Signal Inputs and Outputs

Inputs for both the APT and AVCS programmers consist of the following:

(1) A "load" command, which resets the programmer and enables it to be loaded with 28-bit digital data. (If power is "off", the "load" command will turn power "on".)

(2) An "off" command, which turns power "off".

(3) Program information, which consists of 28-bits of digital data. (Table 4-IV-2 lists the information assignments for each bit.)

(4) Horizon pulses used to synchronize the free-running operation of the programmer to the spin rate.

The APT programmer receives an additional signal, known as "end-of-readout", from the energized camera.

The output signals from the APT and AVCS programmers are listed in Table 4-IV-3.

TABLE 4-IV-2. BIT ASSIGNMENTS OF PROGRAMMING DATA

Bit No.	Camera Information	QOMAC Information
1 thru 3	NA	2's complement of the desired number of cycles
4 thru 14	2's complement of the number of spins between the end of programming and time T_0.	NA
15	Selects a picture sequence or QOMAC	
16	Controls the number of pictures	NA
17 and 18	NA	NA
19 thru 28	2's complement of the difference between the number of spins in an orbit and 1024 (APT) or 640 (AVCS) spins.	2's complement of the difference between the number of spins in an orbit and 256 spins.

TABLE 4-IV-3. PROGRAMMER OUTPUTS

AVCS Output	APT Output	Subsystem
Camera filament "on/off"	Camera "on/off"	Camera
Camera high-voltage "on/off"	Transmitter "on/off"	
Camera vertical sync	Camera "prepare/expose"	
Gated 38.4-kc timing	Gated 4800-cps timing	
Camera shutter trigger	Not applicable	
Five-percent horizontal sync		
Ten-percent horizontal sync		
Tape recorder "run"		
Camera flash-tube trigger		
400-cps timing	Not applicable	Tape recorder and picture time clock
Power (3-volt and -24.5 volt)	Not applicable	Picture time clock
133-1/3-cps timing	Same as AVCS	Telemetry
Data verification "hold-on"		
Quarter-orbit switching	Same as AVCS	QOMAC

3. Functional Operation of Programmer (See Figure 4-IV-10)

a. General

The general processing functions are performed by both the APT and AVCS programmers as follows. A "load" command received from the decoder turns power "on" (if it was "off") and resets the picture sequencer, shift register, count register, and program-sequence controller. (In the AVCS programmer, power is also supplied to the picture time clock.) This allows the 28-bit digital data to be shifted into the shift register, and the data verification hold-on level to be generated. After the first 14 bits of data have been shifted into the shift register, an overflow signal causes the parallel-transfer of these bits into the count register. After the remaining 14 bits of data are shifted into the shift register, the camera-sequence program starts. The program is clocked by pulses received from the horizon-pulse synchronized counter, which receives inputs from the free-running high-frequency generator and the energized orthogonal horizon-sensor.

b. Detailed Camera-Sequencing Program for APT System (See Figure 4-IV-11.)

The camera-sequencing program generated by the APT programmer, after complete programming data are received, proceeds as follows:

(1) Time T_0 is counted out at the spin rate (about 5.5 seconds per count). This time interval, the programmed delay, can last between 41 and 2048 spins of the spacecraft. Thus, the maximum delay is approximately 188 minutes.

(2) At time T_0-40 spins, the APT camera is turned"on". At "turn-on", the camera starts its 200-second readout, which takes approximately 36 spins. At the "end-of-readout" the camera returns a signal to the programmer, and goes into a "hold" state.

(3) At time T_0-5 spins, the transmitter power is turned "on".

(4) At time T_0, the programmer signals the camera to "prepare", and the next clock pulse is sent to the camera as an "expose" signal.

(5) After receiving the "expose" signal, the camera goes through a develop-readout cycle. The "hold" signal is dropped at the end-of-the-develop time, and raised again at the end-of-readout. The transmitter is turned "off" upon receipt of each "hold" signal following time T_0.

(6) At 64 spins after time T_0, the programmer again sends a "prepare" signal, followed on the next spin by an "expose" signal. The transmitter is turned "on" 5 spins before the "prepare" signal is sent. This process continues at 64-spin intervals.

(7) When the programmer counts the time for the appropriate number of pictures (4 or 8) to have been fully read out and a "hold" signal is received from the camera, the camera is turned "off".

(8) At time T_0 plus 1024 spins, the contents of the first 10 stages of the shift register are transferred into the count register. Overflow from the first 11 stages of the count register indicates a one-orbit displacement from time T_0. Forty spins before this overflow the camera is again turned "on" for a picture-taking sequence. (The minimum orbit time at a nominal 5.5 seconds per spin is approximately 94 minutes, and the maximum orbit time is 188 minutes.)

(9) The programmer will continue to repeat its picture-taking operations until an "off" command is received from a CDA station.

The APT system provides direct readout of the video information. Therefore, if a readout is required when the spacecraft is over a CDA station, it can only be accomplished by loading the programmer with a minimum time delay (41 spins). Unless the programmer is reprogrammed for a revised sequence after the overhead readout is accomplished, or commanded "off", it will continue to perform the originally programmed sequence.

c. Detailed Camera - Sequencing Program for AVCS System (See Figure 4-IV-12.)

The camera-sequencing program generated by the AVCS programmer, after complete programming data are received, proceeds as follows:

(1) Time T_o is counted out at the spin rate (about 6.5 seconds per count). This time interval, the programmed delay, can last between 1 and 2048 spins of the spacecraft. Thus, the maximum delay is approximately 222 minutes.

(2) At time T_o, the first 6 flip-flops of the count register are changed into a 40-count counter. The AVCS filament power and high-voltage power are turned "on", and vertical-and horizontal-sync signals are supplied to the camera. On appropriate successive spins the flashtube and shutter are actuated. The tape recorder is turned on approximately 1 second before the shutter is actuated. The 38.4-kc flutter-and-wow signal is gated to the tape recorder during the interval which starts at the beginning of the shutter pulse and ends on the trailing edge of the vertical-sync pulse that follows the video signal. The start of the shutter pulse is used to start telemetry and picture-time clock readouts.

(3) The camera high voltage is turned "off" at the trailing edge of the vertical-sync pulse, ending picture readout. When the count register reaches time T_o + 40 spins, the camera electronics are again turned "on", and the appropriate picture-taking signals are again supplied.

(4) A picture is commanded every 40 spins, until the end-of-the-picture-taking cycle is reached by the count register. Then the camera is turned "off" completely. Either 6 or 12 picture may be taken during each sequence, as determined by the ground-commanded program data.

(5) At time T_o + 640 spins, the contents of the first 10 stages of the shift register are transferred into the count register. The count register then counts in straight binary fashion. An overflow from the first 11 stages of the count register indicates a one-orbit displacement from time T_o, at which time the AVCS camera is turned "on" for another series of pictures. (The minimum orbit time for a nominal spin period of 6.5 seconds is 641 spins or 69.4 minutes. The maximum orbit time is 640 + 1024 spins, or 180 minutes.)

b. Detailed Camera-Sequencing Program for APT System (See Figure 4-IV-11.)

The camera-sequencing program generated by the APT programmer, after complete programming data are received, proceeds as follows:

(1) Time T_0 is counted out at the spin rate (about 5.5 seconds per count). This time interval, the programmed delay, can last between 41 and 2048 spins of the spacecraft. Thus, the maximum delay is approximately 188 minutes.

(2) At time T_0-40 spins, the APT camera is turned"on". At "turn-on", the camera starts its 200-second readout, which takes approximately 36 spins. At the "end-of-readout" the camera returns a signal to the programmer, and goes into a "hold" state.

(3) At time T_0-5 spins, the transmitter power is turned "on".

(4) At time T_0, the programmer signals the camera to "prepare", and the next clock pulse is sent to the camera as an "expose" signal.

(5) After receiving the "expose" signal, the camera goes through a develop-readout cycle. The "hold" signal is dropped at the end-of-the-develop time, and raised again at the end-of-readout. The transmitter is turned "off" upon receipt of each "hold" signal following time T_0.

(6) At 64 spins after time T_0, the programmer again sends a "prepare" signal, followed on the next spin by an "expose" signal. The transmitter is turned "on" 5 spins before the "prepare" signal is sent. This process continues at 64-spin intervals.

(7) When the programmer counts the time for the appropriate number of pictures (4 or 8) to have been fully read out and a "hold" signal is received from the camera, the camera is turned "off".

(8) At time T_0 plus 1024 spins, the contents of the first 10 stages of the shift register are transferred into the count register. Overflow from the first 11 stages of the count register indicates a one-orbit displacement from time T_0. Forty spins before this overflow the camera is again turned "on" for a picture-taking sequence. (The minimum orbit time at a nominal 5.5 seconds per spin is approximately 94 minutes, and the maximum orbit time is 188 minutes.)

(9) The programmer will continue to repeat its picture-taking operations until an "off" command is received from a CDA station.

The APT system provides direct readout of the video information. Therefore, if a readout is required when the spacecraft is over a CDA station, it can only be accomplished by loading the programmer with a minimum time delay (41 spins). Unless the programmer is reprogrammed for a revised sequence after the overhead readout is accomplished, or commanded "off", it will continue to perform the originally programmed sequence.

c. Detailed Camera - Sequencing Program for AVCS System (See Figure 4-IV-12.)

The camera-sequencing program generated by the AVCS programmer, after complete programming data are received, proceeds as follows:

(1) Time T_o is counted out at the spin rate (about 6.5 seconds per count). This time interval, the programmed delay, can last between 1 and 2048 spins of the spacecraft. Thus, the maximum delay is approximately 222 minutes.

(2) At time T_o, the first 6 flip-flops of the count register are changed into a 40-count counter. The AVCS filament power and high-voltage power are turned "on", and vertical-and horizontal-sync signals are supplied to the camera. On appropriate successive spins the flash-tube and shutter are actuated. The tape recorder is turned on approximately 1 second before the shutter is actuated. The 38.4-kc flutter-and-wow signal is gated to the tape recorder during the interval which starts at the beginning of the shutter pulse and ends on the trailing edge of the vertical-sync pulse that follows the video signal. The start of the shutter pulse is used to start telemetry and picture-time clock readouts.

(3) The camera high voltage is turned "off" at the trailing edge of the vertical-sync pulse, ending picture readout. When the count register reaches time T_o + 40 spins, the camera electronics are again turned "on", and the appropriate picture-taking signals are again supplied.

(4) A picture is commanded every 40 spins, until the end-of-the-picture-taking cycle is reached by the count register. Then the camera is turned "off" completely. Either 6 or 12 picture may be taken during each sequence, as determined by the ground-commanded program data.

(5) At time T_o + 640 spins, the contents of the first 10 stages of the shift register are transferred into the count register. The count register then counts in straight binary fashion. An overflow from the first 11 stages of the count register indicates a one-orbit displacement from time T_o, at which time the AVCS camera is turned "on" for another series of pictures. (The minimum orbit time for a nominal spin period of 6.5 seconds is 641 spins or 69.4 minutes. The maximum orbit time is 640 + 1024 spins, or 180 minutes.)

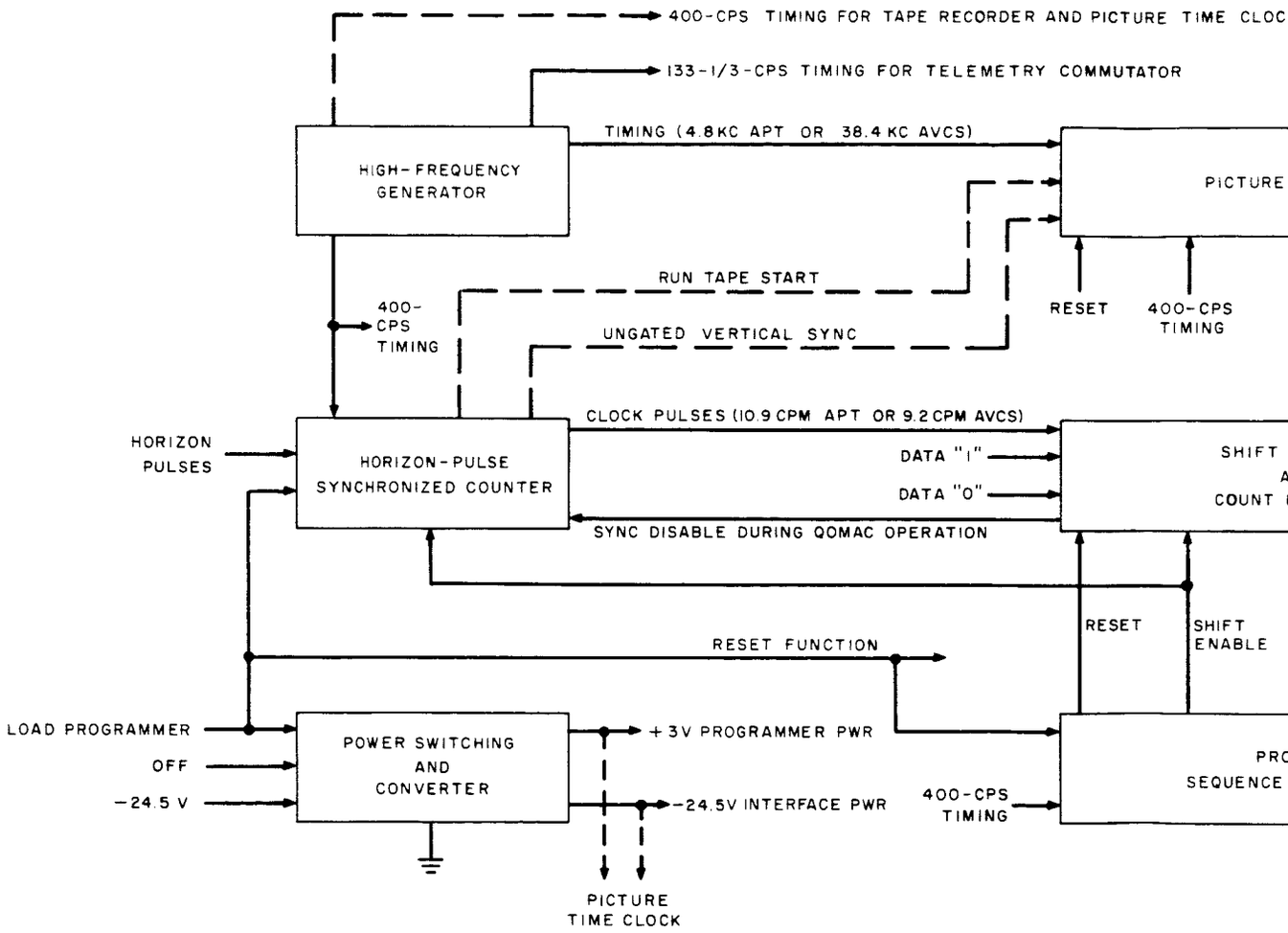
400-CPS TIMING FOR TAPE RECORDER AND PICTURE TIME CLOC
133-1/3-CPS TIMING FOR TELEMETRY COMMUTATOR
HIGH-FREQUENCY GENERATOR
TIMING (4.8KC APT OR 38.4 KC AVCS)
PICTURE
RUN TAPE START
400-CPS TIMING
UNGATED VERTICAL SYNC
RESET
400-CPS TIMING
CLOCK PULSES (10.9 CPM APT OR 9.2 CPM AVCS)
HORIZON PULSES
HORIZON-PULSE SYNCHRONIZED COUNTER
DATA "1"
DATA "0"
SHIFT
COUNT
SYNC DISABLE DURING QOMAC OPERATION
RESET
SHIFT ENABLE
RESET FUNCTION
LOAD PROGRAMMER
OFF
-24.5 V
POWER SWITCHING AND CONVERTER
+3V PROGRAMMER PWR
-24.5V INTERFACE PWR
400-CPS TIMING
PRO
SEQUENCE
PICTURE TIME CLOCK

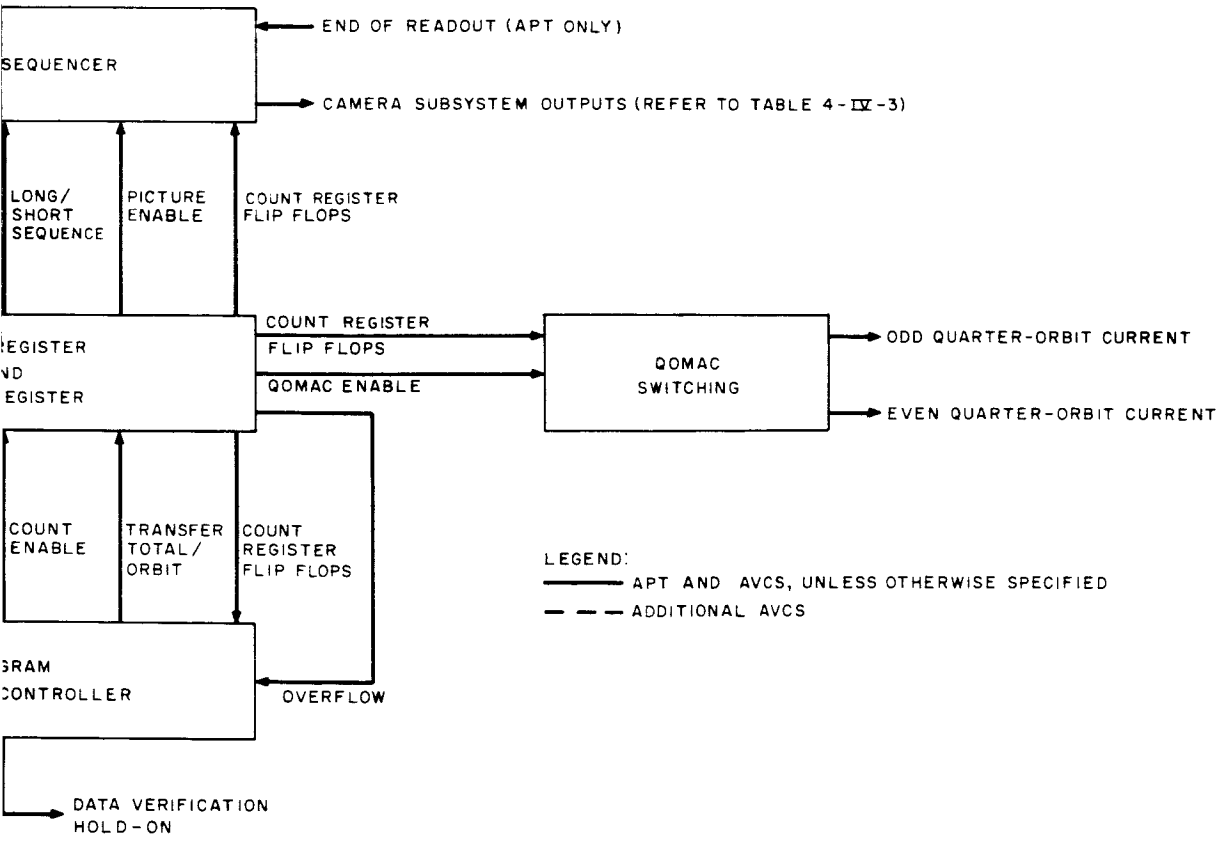

Figure 4-IV-10. Programmer, Block Diagram

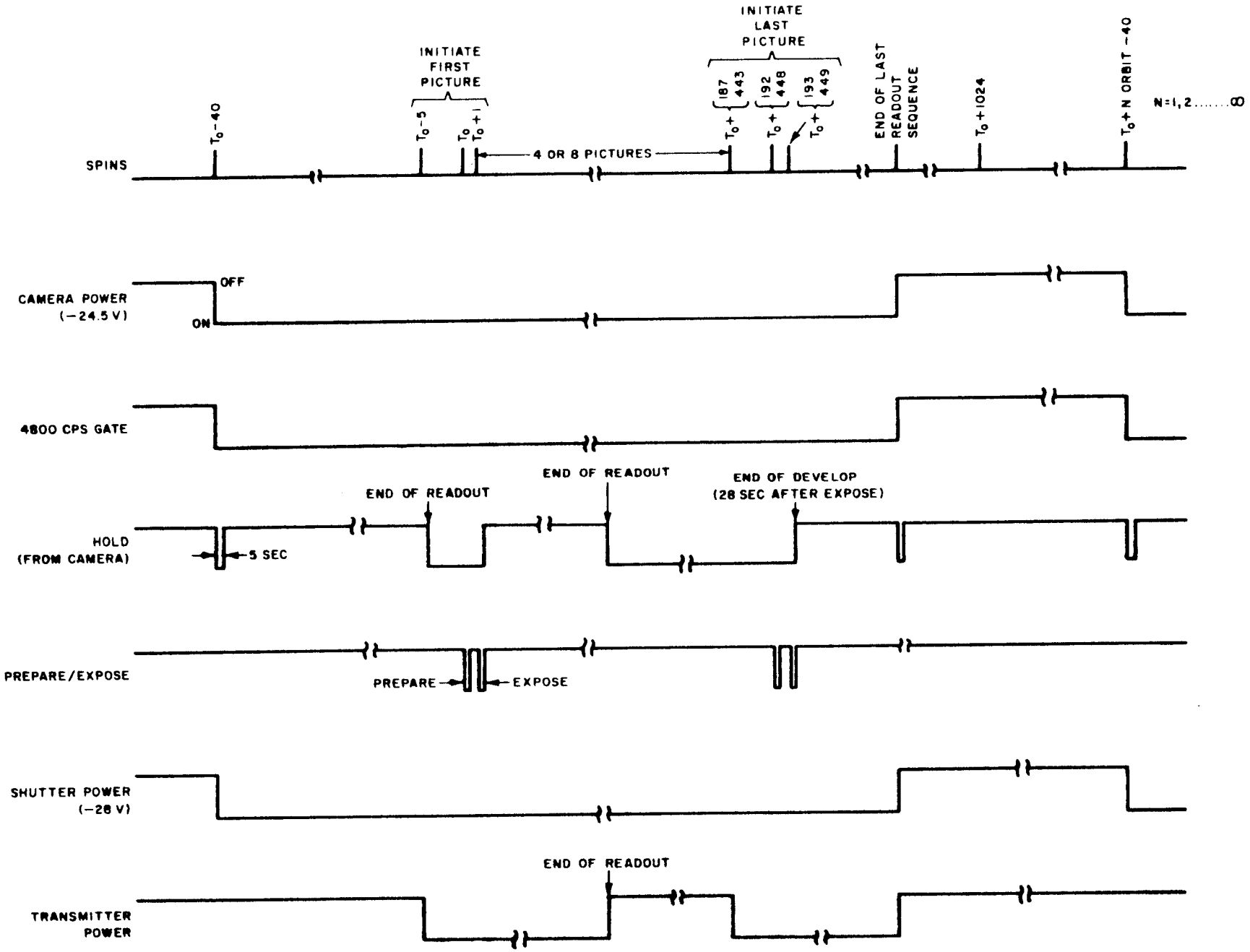

Figure 4-IV-11. APT Picture-Sequencing Timing Diagram

(6) The programmer will continue its picture-taking operations, repeating the programmed sequence on each orbit, until an "off" command is received from a ground station.

There are two ways of observing real-time picture readouts; one is with the tape recorder running and the other is with the tape recorder not running. These "direct picture" modes are achieved through the following ground commands:

(1) Video transmitter "on": This command causes power to be applied to the video transmitter previously selected. A signal is sent also to the AVCS camera controller "direct picture" input, which causes power to be applied to the video modulator output stage of the tape recorder amplifier. Using this command, the signal being recorded on the tape recorder can also be transmitted to the ground. The function is disabled if decoder power drops out.

(2) "Inhibit tape recorder": This command causes the "run-tape" signal to the tape recorder to be inhibited. This permits the real-time readout of the camera without recording the data. The function is disabled if decoder power drops out.

(3) "Enable tape recorder": This command allows the programmer to send tape-run signals.

If a sequence of pictures in a program are being taken over the ground station, a video transmitter "on " command is sufficient to obtain a real-time direct readout. Otherwise, a "load" programmer command is also required, and a minimum (1-spin) delay is loaded into the programmer. After the picture is received, a programmer "off" command must be sent to the spacecraft; otherwise, the programmer will continue to perform the programmed picture sequence.

4. Operation of Programmer Circuits

a. General

Unless otherwise specified the following descriptions of operation for the programmer circuits are applicable to both the APT and AVCS systems. All of the programmer circuits shown in Figure 4-IV-10 are not described; only the circuits of unusual or special design are covered.

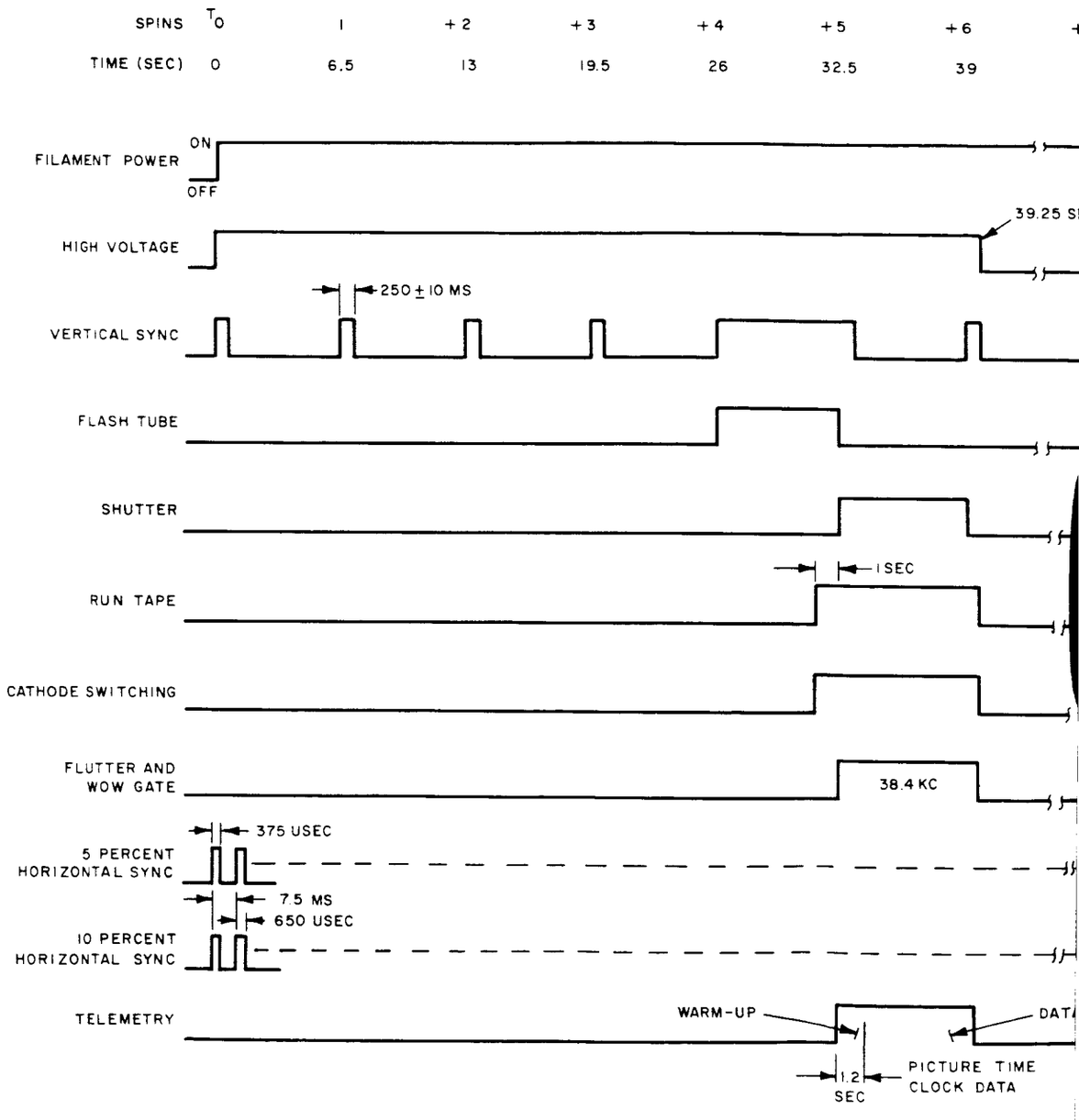
SPINS
T_0
1
+2
+3
+4
+5
+6
TIME (SEC)
0
6.5
13
19.5
26
32.5
39
FILAMENT POWER
ON
OFF
HIGH VOLTAGE
39.25 S
250 ± 10 MS
VERTICAL SYNC
FLASH TUBE
SHUTTER
1 SEC
RUN TAPE
CATHODE SWITCHING
FLUTTER AND
WOW GATE
38.4 KC
375 USEC
5 PERCENT
HORIZONTAL SYNC
7.5 MS
650 USEC
10 PERCENT
HORIZONTAL SYNC
TELEMETRY
WARM-UP
DAT
1.2
SEC
PICTURE TIME
CLOCK DATA

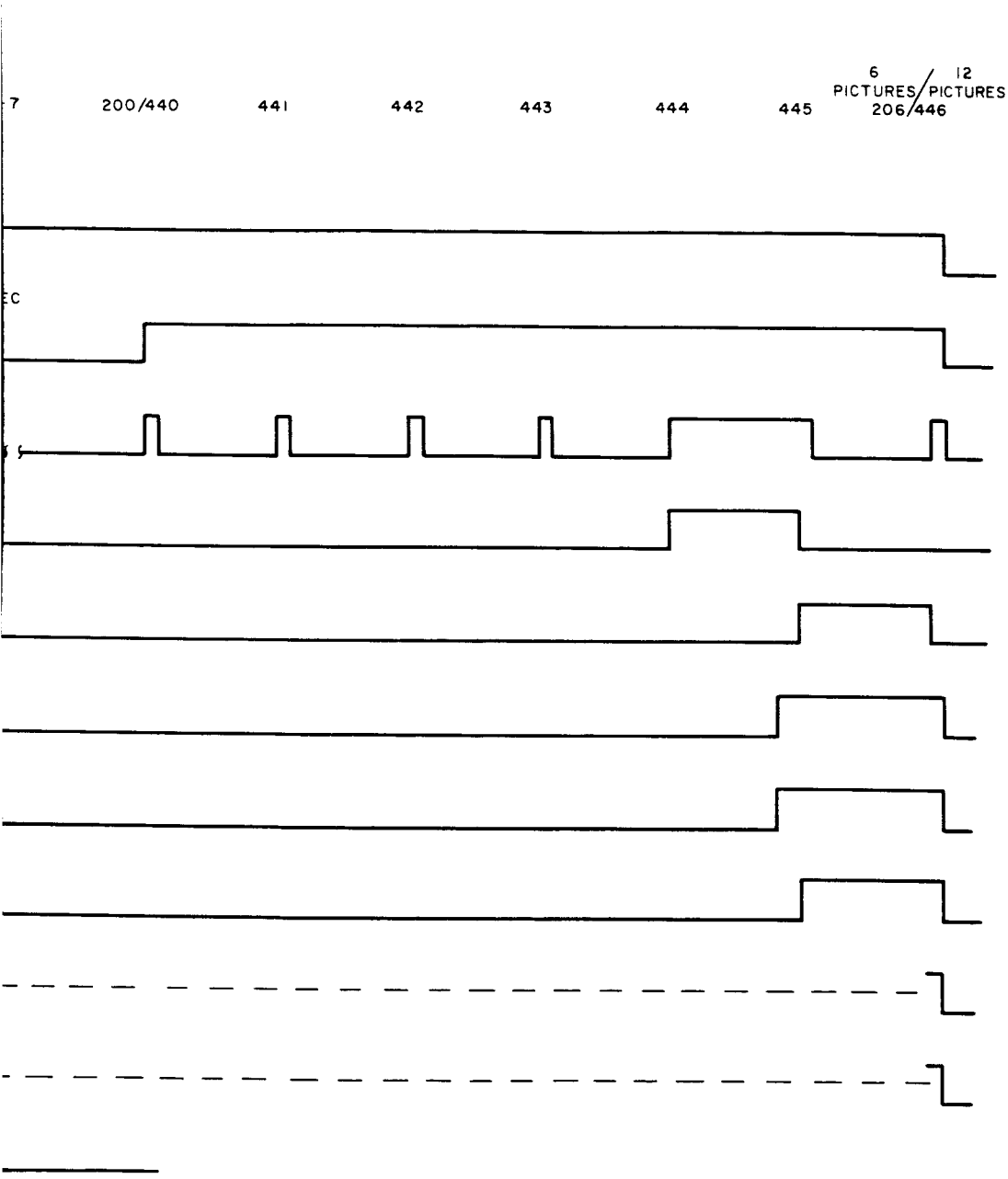

Figure 4-IV-12. AVCS Picture-Sequencing Timing Diagram

b. High-Frequency Generator

The high-frequency generator consists of 2.4576-Mc crystal oscillator and a flip-flop countdown chain. The frequency of the crystal-oscillator signal is divided down to provide signals with the frequencies required to operate the programmer. (These output signals are shown in Figure 4-IV-10.) The frequency division above 153.6 kc is performed by Fairchild MWuL 913 D integrated circuits. Division below 153.6 kc is performed by Texas Instruments Series 51 integrated circuits.

c. Horizon-Pulse Synchronized Counter

(1) Function

The function of the horizon-pulse synchronized counter is to provide clock pulses suitable for sequencing programmer operation. During a camera-sequencing operation, the clock pulses are generated in synchronization with sky-earth pulses received from the normal horizon sensor (the sensor associated with the energized camera), as long as these pulses indicate that the spin rate of the spacecraft is within acceptable limits. When horizon pulses are missing, the counter generates clock pulses at a free-running rate near the nominal spin rate. In addition, the counter resynchronizes itself upon the receipt of a horizon pulse, following a period during which an excessive number of horizon pulses were missing in a row, or during which horizon pulses indicated too fast or slow a spin rate. During a QOMAC-sequencing operation, the generated clock pulses are not synchronized.

(2) Scheme of Operation

The horizon-pulse synchronized counter continuously evaluates the time-of-receipt of horizon pulses with respect to an internally generated "window". The width and free-running rate of the window are established so that normal horizon pulses which occur within the limits of the allowed spin-period will fall within this "window". If horizon pulses are received during the "window", as expected, the output clock pulses are sunchronized with the horizon-pulse inputs. If one horizon pulse is received before or after the "window", this indicates that the spin period might be incorrect, and an intermediate fill-in clock pulse is produced. The receipt of the first incorrect horizon pulse is noted, and, if three more successive incorrect pulses indicate the same type of error as the first pulse, the operation of the horizon-pulse synchronized counter is rephased and started again. The circuit never skips the generation of a clock pulse, and is always attempting to establish synchronization with correct-period horizon pulses. Clock pulses will continue to be generated at a rate close to the nominal spin rate even if horizon pulses are missing.

(3) Major Components (See Figure 4-IV-13)

The horizon-pulse synchronized counter consists of acquisition reset logic, earth blanking and horizon recognition logic, a 12-stage counter, error logic, and synchronization logic. The acquisition reset logic allows operation to start only after the programmer has been fully loaded with the 28 bits of digital data, upon receipt of the next sky-earth pulse from the normal horizon sensor. The earth blanking and horizon recognition logic generates one horizon pulse output (which is synchronized to the 400-cps timing input) each time a sky-earth pulse is received, and inhibits all extraneous pulse inputs received during "earth" time. This is accomplished by the setting and resetting of a flip-flop with the outputs from the orthogonal horizon sensors located on opposite sides of the spacecraft. The 12-stage counter times (at the 400-cps rate) and produces the "window" used for evaluating horizon pulse outputs from the earth blanking and horizon recognition logic. The "window" and horizon pulse comparison is performed in the synchronizing logic and the error logic. The synchronizing logic controls the generation of the clock pulse output and "reset" of the 12-stage counter. The error logic registers the receipt of improper horizon pulses from the earth blanking and horizon recognition logic, and controls the rephasing function.

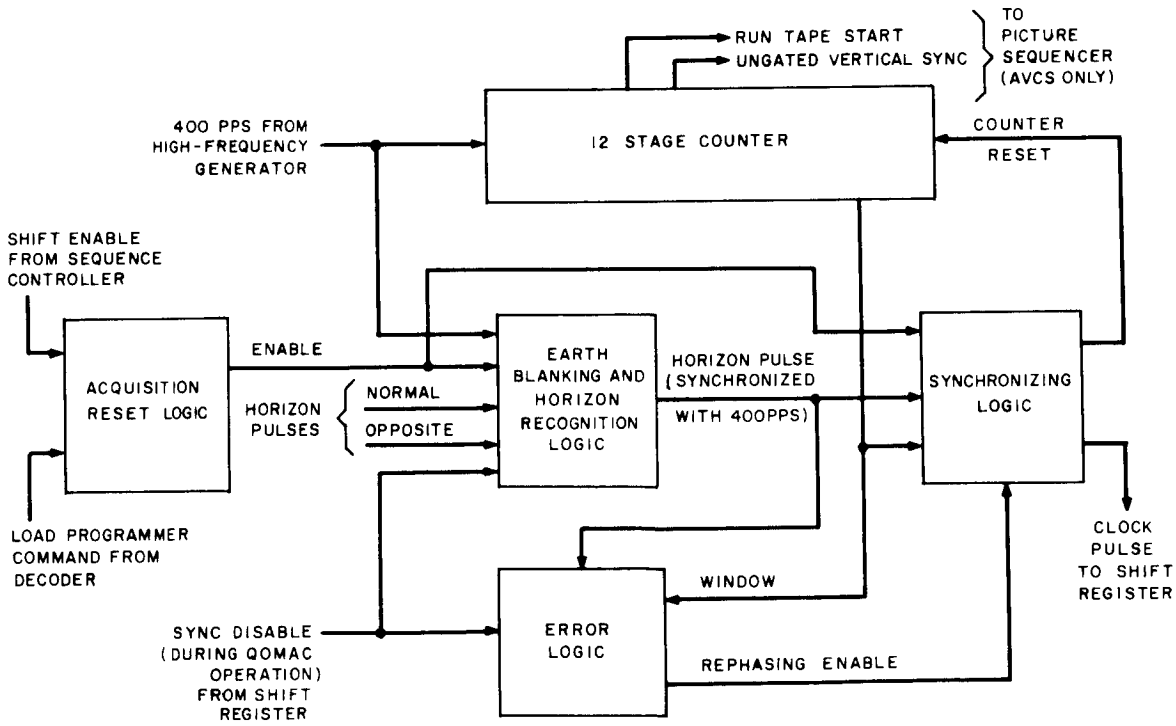

Figure 4-IV-13. Horizon-Pulse Synchronized Counter, Block Diagram

(4) Modes of Operation

(a) APT and AVCS Timing Periods

The 5.5-, 5.6-, and 5.525-second periods referenced in the following description are for the APT configuration only. The comparable periods for the AVCS configuration are 6.5- 6.6-, and 6.525-seconds, respectively.

Figure 4-IV-14 is a flow chart illustrating the overall inter-relationship between the operations described separately in the following paragraphs.

(b) Normal Operation

Immediately upon receipt of the first sky-earth pulse which follows the completion of the programmer loading operation, the synchronizing logic generates the first clock pulse output, and the 12-stage counter begins counting from the reset state, t_o, at the 400-cps input rate. At time t_o + 5.12 seconds (count 2048), the counter opens the "window". If the next horizon pulse is a proper one, it will be received before the normal free-run closing time of the "window", t_o + 5.6 seconds (2240). Assuming that a proper horizon pulse appears, its receipt will trigger the generation of the second clock pulse, and terminate the "window" by recycling the counter to its reset (starting) condition. The interruption of counter operation is momentary, and no counts are lost. Thus, if proper horizon pulses continue to be received, the clock-pulse generation remains in synchronization with the horizon pulses.

(c) Operation With Spin Rate Too Fast

Operation starts as described for the normal mode, but the next (second) horizon pulse will be received before the "window" opens if the spin rate is too fast. This causes the following actions: (1) the receipt of the first early pulse is noted by the error logic; and (2) the second clock pulse is triggered and the counter is reset at the time of free-run close of the "window" (t_o + 5.6 seconds).

The counter immediately starts counting again, without missing a count. If the next immediately following horizon pulse again appears too soon, a second error is noted, and actions (1) and (2) repeat. This sequence of operation continues until receipt of the fourth incorrect pulse, whereupon the counter reset is resynced to the time of occurrence of the received horizon pulse, and not to the time of the free-run close of the "window" as previously performed. Normal operation is not resumed until a horizon pulse appears in the window, at which time the error counter will reset to zero.

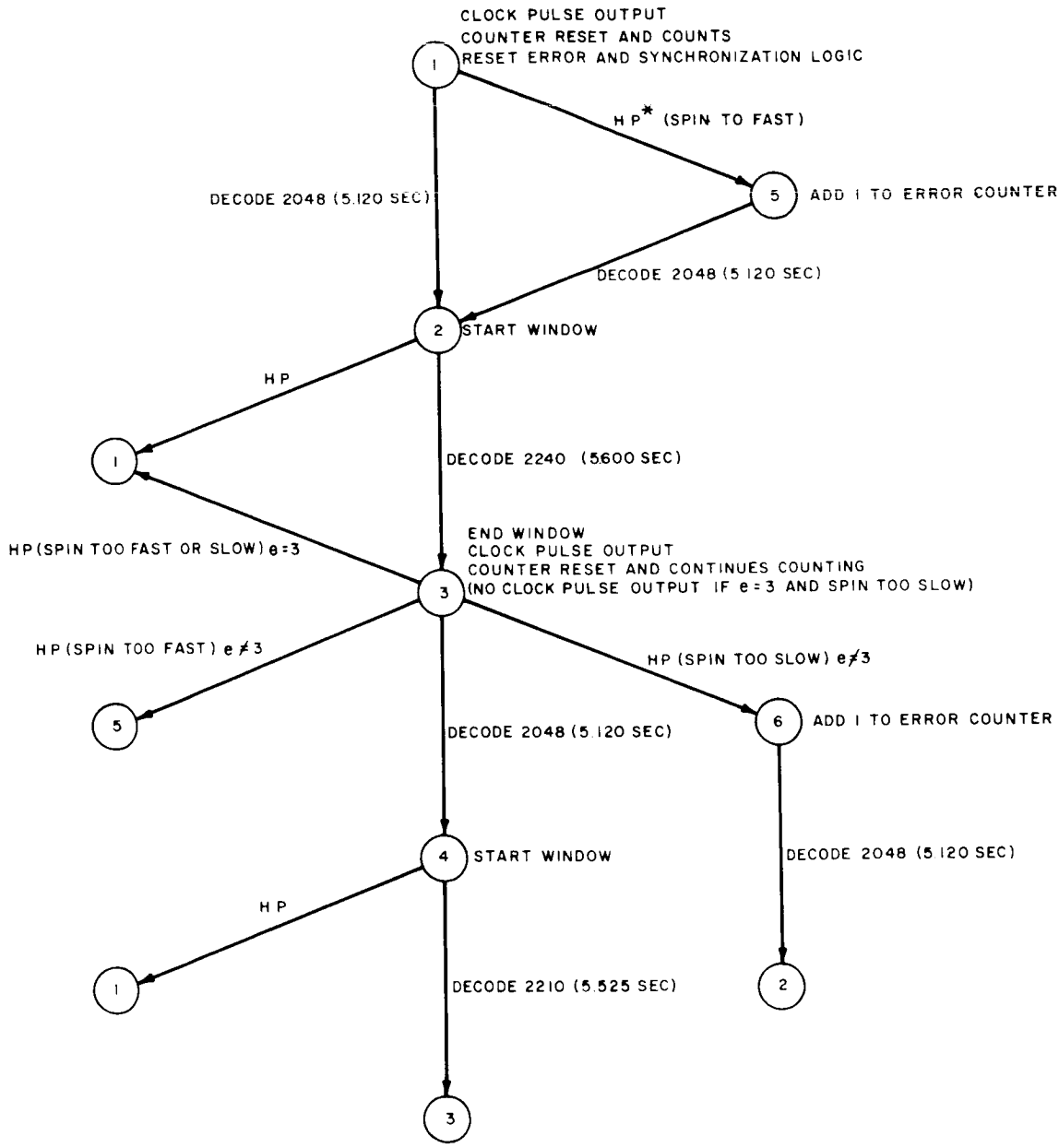

Figure 4-IV-14. Horizon-Pulse Synchronized Counter, Flow Chart

(d) Operation with Spin Rate too Slow

The operation when the spin rate is too slow is identical with that described for a too-fast spin rate, with one exception. In this case, horizon pulses will be received after the free-run close of the "window", and a clock pulse is not generated during rephasing on the fourth pulse. The horizon pulse synchronized counter will continue to produce clock pulses at the expiration of the window and will be reset by horizon pulses. Normal operation will not be resumed until a horizon pulse is received in the window, at which time the error counter will reset to zero.

(e) Operation with Missing Horizon Pulses

Operation starts as described for the normal mode. However, if a second horizon pulse is never received, the free-run ending time of the "window" will be shortened from 5.6 seconds to 5.525 seconds (2210 counts). (This time is closer to the nominal spin period of 5.5 seconds). The unsynchronized clock pulses will continue to be generated at this 5.525-second rate until a horizon pulse is received. When a horizon pulse is received, the counter reset will be rephased to the time of occurrence of the pulse.

5. Operational Restraints

The following three restrictions are imposed on the operation of both the APT and AVCS configurations.

(1) The number of missing horizon pulses (N) tolerable before a half-spin slip in phase is encountered can be computed from

$$N = \frac{T_S - 2(T_2 - T_1)}{2(T_1 - T_S)} - 4 \qquad (1)$$

where

T_S is the nominal spin period,

T_2 is the normal (unshortened) end-of-gate time counted by the counter, and

T_1 is the shortened end-of-gate time counted by the counter.

Note that is a slip of more than a half-spin occurs, it is not known whether the spacecraft is spinning too fast or too slow. Therefore, an output of 1 clock pulse may be erroneously added or subtracted.

Using equation (1), the computed numbers (N) for three different spin periods for the APT and AVCS spacecrafts are listed below:

APT		AVCS	
T_s	N	T_s	N
5.475 sec	49	6.475 sec	59
5.500 sec	103	6.500 sec	123
5.525 sec	∞	6.525 sec	∞

(2) The number of missing horizon pulses (N) tolerable before a horizon pulse occurs outside of the "window" can be computed from

$$N = \frac{T_s - T_w - (T_2 - T_1)}{T_1 - T_s}, \tag{2}$$

where T_w, is the start-of-"window" time, and all other symbols are defined as in equation (1).

The numbers computed using equation (2) and theee different spin periods for the APT and AVCS spacecrafts are listed below:

APT		AVCS	
T_s	N	T_s	N
5.475 sec	5	6.475 sec	25
5.500 sec	12	6.500 sec	52
5.525 sec	∞	6.525 sec	∞

(3) In order not to add or subtract an erroneous count, the spin period must obey the following inequality:

$$\frac{8}{9} T_1 \leq T_s \leq \frac{8}{7} T_2 . \tag{3}$$

Using values for the APT configuration, we compute

4.98 sec $\leq$ spin period $\leq$ 6.40 sec, or

9.38 rpm $\leq$ spin rate $\leq$ 12.05 rpm.

Similarly, for the AVCS configuration,

5.87 sec $\leq$ spin period $\leq$ 7.55 sec, or

7.95 rpm $\leq$ spin rate $\leq$ 10.2 rpm.

D. ATTITUDE AND SPIN CONTROL

1. APT and AVCS Applicability

Unless otherwise specified, the following descriptions are applicable to both the APT and AVCS systems.

2. Attitude Control (QOMAC)

a. General

For attitude control, current must be switched each quarter orbit in a coil mounted in a plane perpendicular to the spacecraft spin axis. There are two sets of center tapped coils which lie in the correct plane for attitude control. They are the QOMAC coil and the magnetic-bias coil. The QOMAC coil is used for the quarter orbit torquing of the spin axis, while the magnetic-bias coil is normally used to null the spacecraft residual magnetic dipole. However, during initial orientation of the spin axis, when high torque is needed, both coils are driven in the QOMAC mode. After the initial orientation, the magnetic-bias coil is operated to null the residual magnetic dipole and only the QOMAC coil is used for attitude control. The generation of the sequencing signals required to implement the QOMAC program is performed by the programmer.

b. Functional Operation of Programmer

The programmer will generate a QOMAC program after it has received the appropriate 28-bits of digital data which define this request. Table 4-IV-2 lists the information contained in a QOMAC request.

The major difference in the operation of the programmer circuits during the generation of a QOMAC program as compared with operation during a picture-sequencing program, is that the horizon-pulse synchronized counter is not synchronized by horizon-pulse inputs. Instead, this counter is free-running and generates clock pulses at a

rate approximately equal to the spin rate of the spacecraft (i.e., a rate equivalent to the nominal 5.5-second APT period or the 6.5-second AVCS period). The detailed operations which are performed by the programmer to implement a QOMAC program (see Figure 4-IV-15) are as follows:

(1) Time T_0 is counted out at the clock pulse rate. This time interval, the requested program delay, can last between 1 and 2048 spins. Thus, the maximum delay can be about 188 minutes for the APT system or 222 minutes for the AVCS system

(2) At time T_0, current is allowed to flow through one half of the center-tapped QOMAC coil. This is denoted "odd quarter-orbit current". When the count register reaches a value equal to time T_0 + 256 counts, the contents of 10 flip-flops of the shift register are transferred into the count register. Counting continues, and overflow of the 9th flip-flop indicates the end-of-a-quarter-orbit.

(3) Current is now directed through the other half of the center-tapped QOMAC coil. This is denoted "even quarter-orbit current". When the count register reaches a value equal to a quarter orbit + 256 counts, the contents of the shift register are again transferred into the count register. Overflow of the 10th flip-flop indicates the completion of half an orbit of torquing (or 1 complete cycle). The number of elapsed cycles are counted by flip-flops.

(4) The half-cycle sequence continues until the programmed number of cycles have been completed, at which time current is no longer applied to the coils.

The maximum quarter-orbit time for the APT configuration at 5.5 seconds per spin for 512 spins is about 47 minutes; for the AVCS configuration at 6.5 seconds per spin, the maximum quarter-orbit time is about 56 minutes. The minimum quarter-orbit times for APT and AVCS configurations are about 24 and 28 minutes, respectively.

c. QOMAC and Magnetic-Bias-Coil Circuit (See Figure 4-IV-16)

The magnetic-bias-coil stepping switch has two decks. One deck is used to develop a telemetry signal to indicate the switch position. The second deck is used to select the magnitude of the current in the magnetic-bias coil, or, when in position 11, to switch the magnetic-bias coil in parallel with the QOMAC coil. A relay is used to make this parallel connection of coils that is required to implement the high-torque QOMAC mode for initial spin-axis orientation.

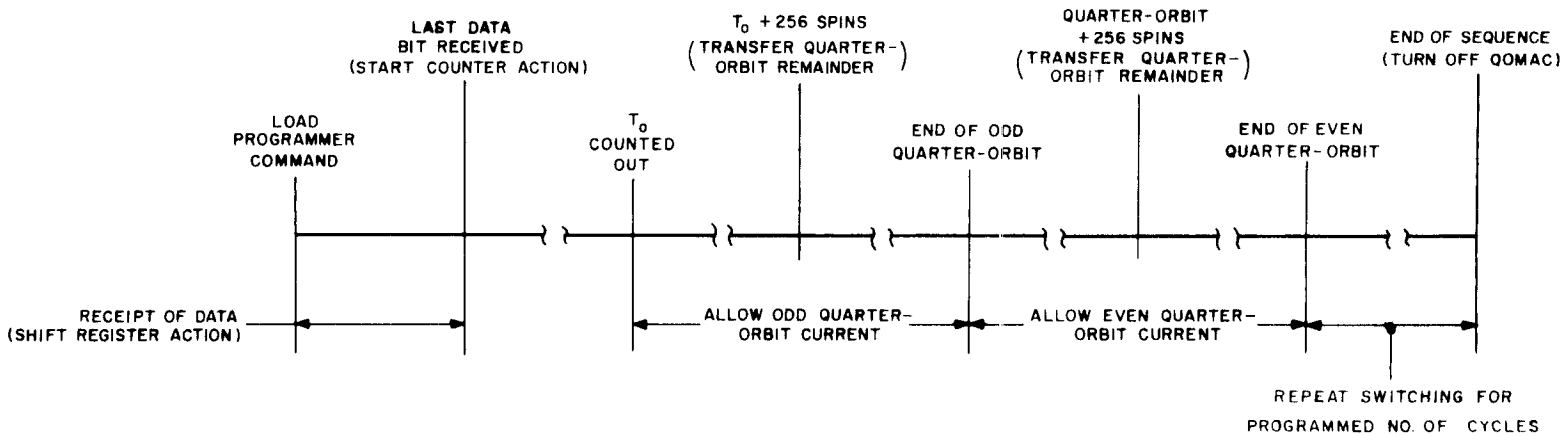

Figure 4-IV-15. QOMAC Timing Diagram

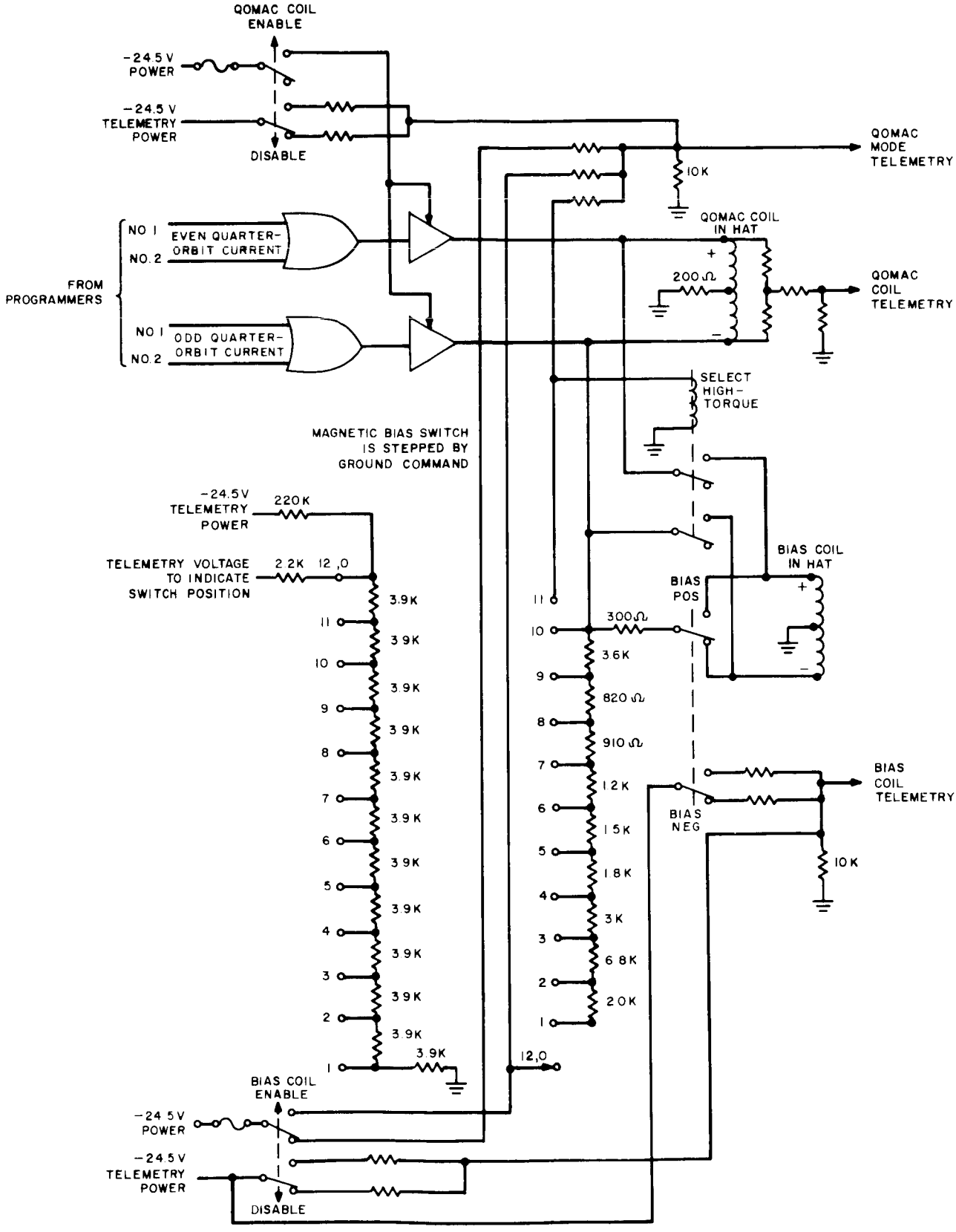

Figure 4-IV-16. QOMAC and Magnetic-Bias Coil Circuit, Logic Diagram

The magnetic-bias-coil switch is stepped by ground command. There are two commands to operate the latching relay which controls the polarity of the magnetic dipole moment generated by the magnetic-bias-coil current. Also, to permit the isolation of coil failures, two relays which are operated by a ground command are used to control the complete removal of power from either coil.

The currents are driven through alternate halves of the QOMAC coil as sequenced by the odd and even quarter-orbit signals provided by the programmer.

3. Spin Control (MASC)

The purpose of the MASC system is to keep the spin rate of the spacecraft constant. The MASC circuits (Figure 4-IV-17) are located in the CDU and the spacecraft "hat". The two redundant center-tapped coils are each powered separately through fused lines from the -24.5-volt regulated bus. The commands for control circuits No. 1 and No. 2 are received from the decoders. The orthogonal horizon-sensors provide the pulses which sequence the required coil-switching operations.

Five commands provide complete control of the MASC system. (Refer to Table 4-IV-1.) And, although a MASC operation is normally stopped by receipt of the MASC coils "off" command, a drop-out of decoder power produces the same result.

The MASC cycle is performed in real time. The operation consists of driving currents through alternate halves of the selected center-tapped coil every half-spin of the spacecraft to set up magnetic fields which will interact with the magnetic field of the earth to produce a torque which increases or decreases the spin rate, as desired. The triggers for controlling the half-spin switching are obtained alternately from a selected pair of oppositely mounted orthogonal horizon-sensors.

An example of current switching for performing a spin-up and spin-down operation is illustrated in Figure 4-IV-18. In this example, horizon pulses are being provided by a pair of oppositely mounted horizon sensors (No. 1 and 2), one each from side 1 and side 2 of the spacecraft. The halves of the MASC coil are arbitrarily designated a and b. The example illustrates that the switching of currents through the coils halves a and b are 180 degrees out-of-phase when the spin-up and spin-down operations are compared.

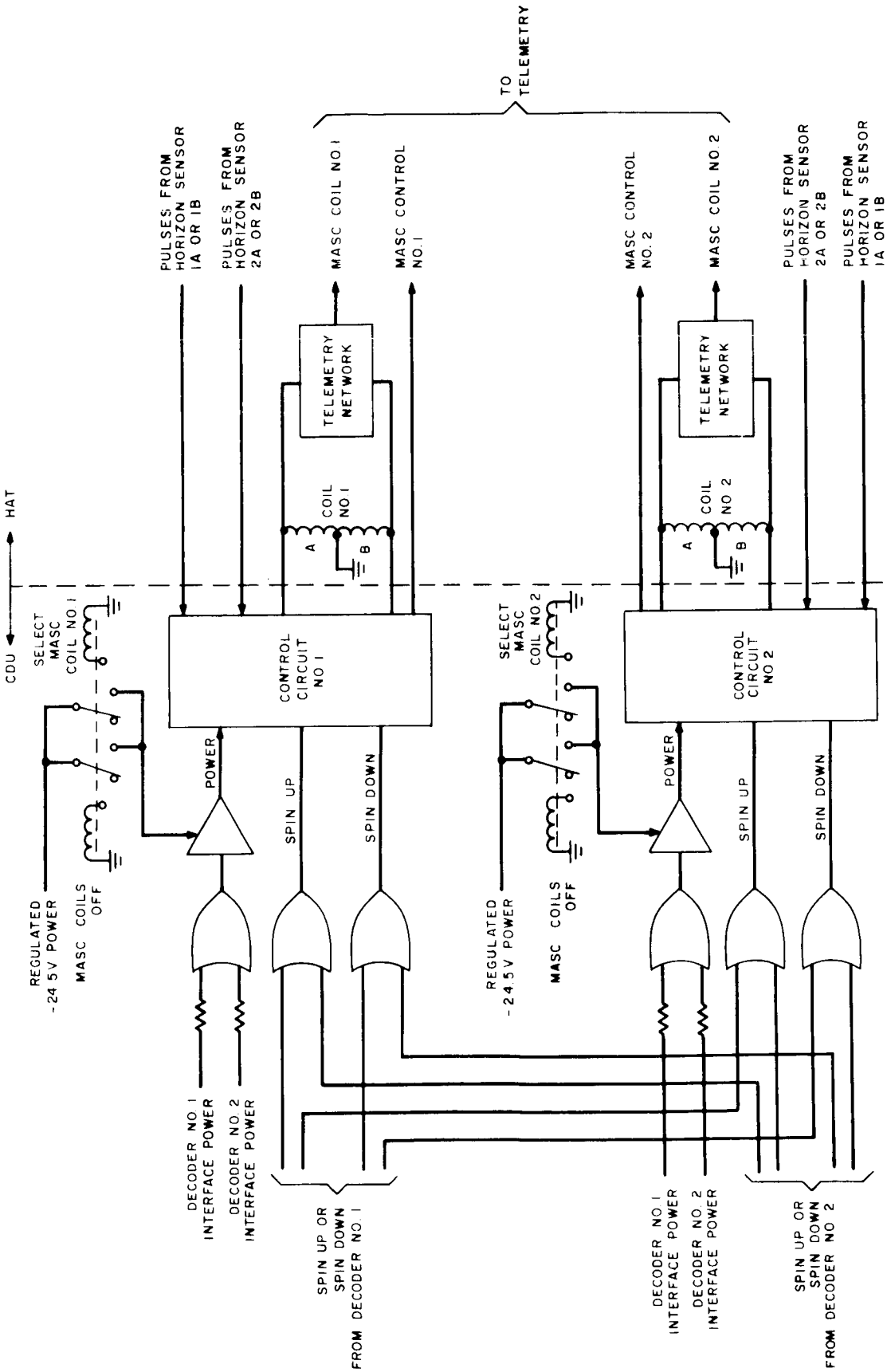

Figure 4-IV-17. MASC Circuit, Logic Diagram

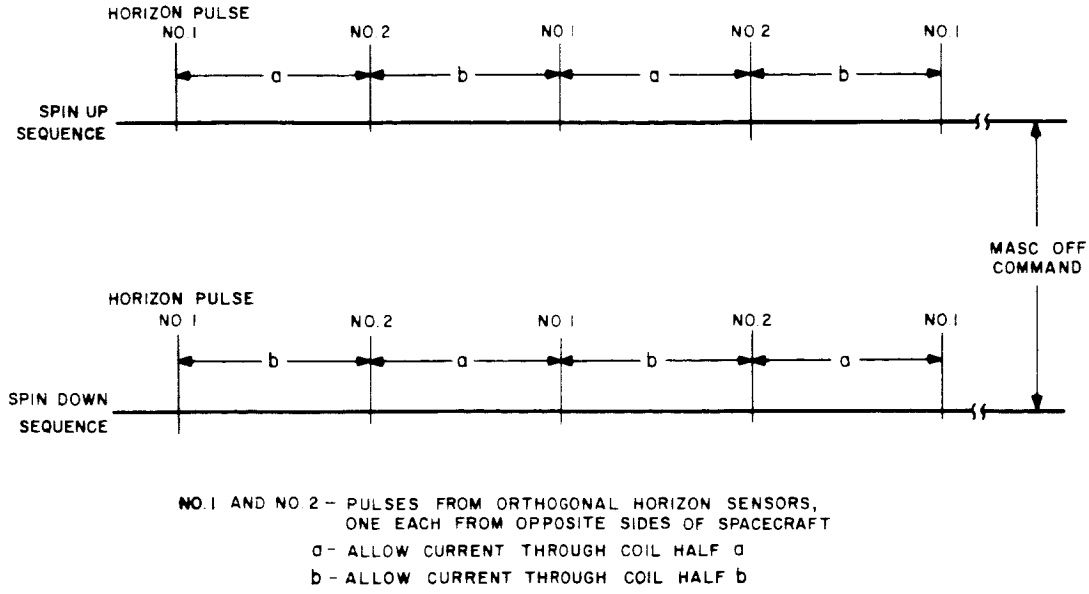

Figure 4-IV-18. MASC Timing Diagram

E. AUXILIARY COMMAND FUNCTIONS

1. AVCS Picture Time

a. General

In the AVCS configuration, each telemetry frame is preceded by a serial digital readout generated by the picture-time clock. This readout provides a binary count (in Gray code) of the number of half-second increments which have elapsed since programmer power was turned "on". The maximum accumulative capacity is limited to a count of 2^{20} half-second intervals, or 6 days, 1 hour, 38 minutes and eight seconds.

b. Input and Output Signals

The input signals are capable of being provided by either of the two programmers. The input signals consist of the following:

(1) -24.5-volt power

(2) 3-volt power

(3) 400-cps clock pulses

The output signal is a series of 20-bit Gray-code words which are provided once during each half-second period. Figure 4-IV-19 shows the form of these digital data. The zero-volt level signifies a binary "1" and the -5-volt level signifies a binary "0".

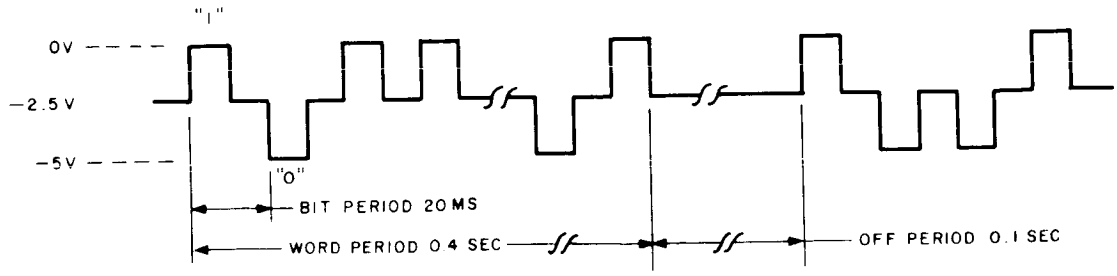

Figure 4-IV-19. Digital Data Output of Picture-Time Clock

c. Picture-Time Clock Operation (See Figure 4-IV-20.)

When the 3-volt power is received, the counter register, burst register, and mode flip-flop are reset and held in that state for approximately 150 milliseconds.

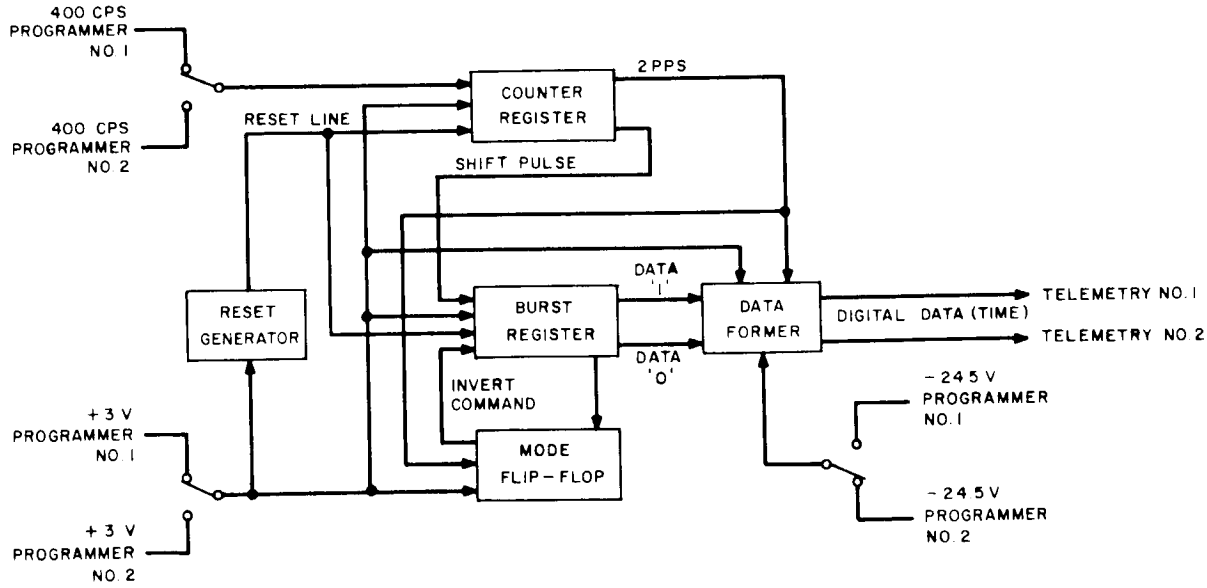

Figure 4-IV-20. Picture-Time Clock, Block Diagram

Upon release from the reset state, the counter register divides the 400-cps input to develop a 2-cps gate with a duty cycle of 80 percent, and generates 50-cps pulses.

The 2-cps gate is supplied to the data former, and is also used to gate the 50-cps pulses to the burst register for shifting. Twenty 50-cps shift pulses are supplied in a 400-millisecond envelope every half-second.

Upon receipt of a burst of shift pulses, the burst register, in conjunction with the mode flip-flop, counts the time and shifts out the picture time information. The burst register contains 20 stages.

The scheme of operation for the 20-stage register may be better understood by describing, as an example, a 3-stage register as follows: The example register receives a burst of 3 shift pulses every half second (instead of twenty shift pulses each half second). Each burst of pulses represents 1 count. If when the burst of shift pulses is received stage C is a logical "0", the content of stage C is inverted and shifted into stage A. The other two shifts, A into B and B into C, are accomplished without inversion. If stage C is a logical "1", C is inverted and shifted into A, and each subsequent shift is inverted until stage C receives a logical "0". This operation is illustrated below:

	A	B	C	
Reset	0	0	0	
Shift and invert and then stop inverting	1	0	0	
Shift	0	1	0	
Shift	0	0	1	Count 1
Shift and invert	0	0	0	
Shift and invert, then stop inverting	1	0	0	
Shift	0	1	0	Count 2
Shift and invert, then stop inverting	1	0	1	
Shift	1	1	0	
Shift	0	1	1	Count 3

The mode flip-flop controls the inversion shifting in the burst register. If a logical "0" is in stage 1, the flip-flop is set and the "enable" invert level is generated. If a logical "0" is in stage 9, the flip-flop is reset and the "inhibit" invert level is generated.

The data former converts the non-return-to-zero data output of the burst register into the return-to-zero form shown in Figure 4-IV-19.

2. Despin and Damping Backup

Since it is possible for both of the redundant Yo-Yo timers to fail to release the spacecraft despin mechanism, a backup circuit has been incorporated for this function. The backup circuit will be operated upon receipt of the "release Yo-Yo's" command from a CDA station.

A similar circuit for backup of the release of the precession dampers has also been included in the spacecraft. This circuit operates upon receipt of the "release dampers" command from a CDA station.

F. ORTHOGONAL HORIZON-SENSORS

1. Component Design and Operation

Each orthogonal horizon-sensor is composed of a bolometer, amplifier, and threshold circuit; and is similar in design to the sensor used in the TIROS "I" spacecraft. The unit has a field of view of 1.3 ± 0.26 degrees. The bolometer is comprised of a lens assembly and two infrared-sensitive resistive flakes. Both flakes are sensitive to radiation in the 1.8-to 23-micron spectral range. One flake is subjected to radiation gathered by the lens; the other is shielded from this radiation to provide a reference. The amplifier is a-c coupled to the bolometer. The amplifier output is processed by a threshold circuit. The outputs of the threshold circuit indicate the following: "Zero" output indicates that the amplifier output is below a preset threshold; and the "One" output indicates that the amplifier output is above this threshold. This signal is used by the horizon-pulse synchronized counter and MASC commutation circuit. An output from the amplifier (taken ahead of the threshold circuit) of each orthogonal horizon sensor is "OR"ed for telemetering on the 3.9-kc subcarrier oscillator. The possibility of telemetering the output of the threshold amplifier, during the "V" - head horizon sensor sky-time, on one of the two lower-frequency SCOs is being investigated.

In producing the signals for camera triggering and spin control, only the sky-to-earth horizon transition is used, and horizon detection is based on exceeding a fixed threshold. The signal-to-noise ratio is the most important parameter for this first requirement. The better the signal-to-noise ratio at the "cold" horizon temperatures, the lower the threshold can be set; and the lower the threshold, the smaller the time variation in the horizon detection caused by "hot" and "cold" horizons. Data provided by the TIROS-Wheel spacecraft will be used to ensure selection of the optimum amplifier gain and threshold for the OT-2 spacecraft.

The spectral region in which the horizon is being detected has a wide energy range. These variations in energy can cause errors in detecting the horizon-location when a fixed-level threshold is used. Using the presently contemplated signal-to-noise margin and threshold level, this error can be as much as +0.5 degree in pointing accuracy. Since operational experience could show that greater accuracy is required, studies are being made of other spectral regions. Also, equipment that operates in the same spectral region, but obtained from other vendors, is being examined for better signal-to-noise characteristics.

The amplifier will be designed so that the threshold is exceeded for all horizon temperatures above 220°K in the spin-rate range of ±50 percent of nominal and above 200°K in the spin-rate range of ±10 percent of nominal.

2. Control of Sensor Selection (See Figure 4-IV-21)

Selections between the four orthogonal horizon-sensors are controlled through the use of four ground commands. For example, receipt of the "select horizon-sensor 1A" command will energize its corresponding relay. Contacts of the relay will complete connections which apply power to horizon sensor 1A, and route its horizon pulses to the logic gating circuit. The gate which is receiving power from the energized camera will couple the horizon pulses to the appropriate input programmers No. 1 and No. 2.

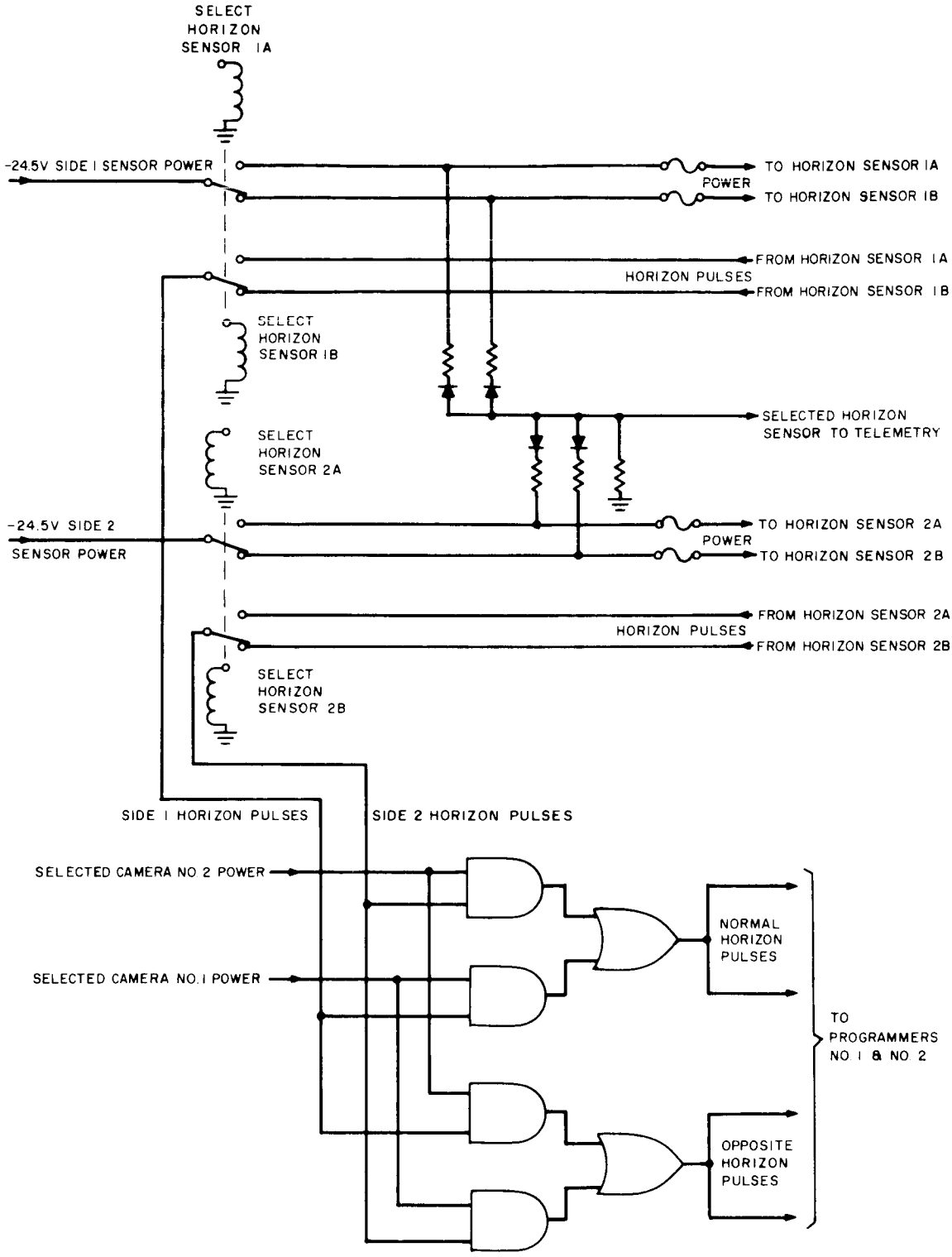

Figure 4-IV-21. Orthogonal Horizon-Sensor Selection Circuit, Logic Circuit

SECTION V. POWER SUPPLY SUBSYSTEM

A. INTRODUCTION

This section describes the analysis used to determine the design and final configuration for the APT and AVCS power supply subsystems which will operate at an orbital altitude of 750 nautical miles. The power supply subsystem will convert solar energy to electrical energy to power other operational subsystems. This electrical energy is also used to replace energy removed from the nickel-cadmium storage cells during orbit nighttime and when peak loads exceed the solar-cell array capabilities.

The current generated by the solar-cell array is a function of variables such as sun angle, solar-cell temperature, and array operating voltage. In order to permit a six-month period of operation, it is necessary to reduce the APT system power requirement. This can be achieved by turning off the APT transmitter between pictures, resulting in a decrease in the load requirement. Operation of the APT transmitter in this manner does not appear to have an adverse effect on its reliability. As discussed later in this section, the cross-over between available and required power occurs during a period of from five to seven months after launch and at a sun angle of 60 degrees. This, then, sets the upper limit on the sun angle at 60 degrees (an approximate nodal crossing at 1400 hours or 1000 hours). Because of camera illumination requirements, an approximate lower limit on the sun angle is 30 degrees (an approximate nodal crossing at 1600 hours or 1800 hours). The charge balance between the required and available loads could also be attained by means of reduced camera programming. Since this approach would not permit global coverage, the decision was made to reduce the power requirement by interrupting the transmitter between pictures.

B. FUNCTIONAL DESCRIPTION

1. Power Supply Subsystem

Figure 4-V-1 shows the major components that comprise the power supply subsystem. Functionally, the subsystem is composed of the solar-cell array, shunt limiter circuitry, battery charge-rate regulators, battery strings, unregulated load bus, -24.5-volt d-c regulators, regulated load bus, and the required fusing.

As shown in Figure 4-V-1, the solar-cell array supplies, through diode coupling, electrical power to the solar-cell bus. This bus supplies the three parallel charge-rate controllers which, in turn, provide the proper charging rate to the three battery

strings. (In the OT-2/AVCS spacecraft, only two battery strings and, consequently, only two charge-rate regulators are employed.) In addition the solar-cell array bus supplies power to the spacecraft unregulated load bus. When the array bus voltage is more negative than the voltage level of the batteries, the array bus is the power source to the unregulated bus. During orbit nighttime and high-current loads, the batteries supply power to the unregulated bus. The unregulated shutter bus is supplied entirely from the batteries, in parallel with the spacecraft unregulated bus. Circuits for the shutters, magnetic-bias switching, and third-stage separation-event circuitry are supplied from this bus. This setup provides some isolation of these short duration, high-current transient loads from the unregulated bus.

For the OT-2 spacecraft, a common, -24.5-volt d-c, regulated bus will be generated by the exclusive selection of the two main regulators as shown in Figure 4-V-1. The following discussion of shortcomings detail why this technique was selected in favor of either (1) coupling two continuously "on" regulators to a common bus, or (2) supplying two separate buses, each from its own regulator.

(1) If two regulators are continuously "on" and OR'ed through diodes to a common bus, the power system source impedance is appreciably increased. Also, should either regulator short through from input to output and thereby attempt to follow the unregulated bus voltage excursions, that regulator would become the dominant source through the OR gate. In addition, should a high-current mode failure be generated in the regulator, which is insufficient to blow the regulator power fuse, the regulator becomes a continuous drain on the power system.

(2) If two regulated buses are generated on the spacecraft, additional interface problems arise in the desired redundancy of the spacecraft. Since either programmer can control either camera (and tape recorder in the OT-2/AVCS spacecraft), problems arise in coupling signals generated in reference to one regulator, to circuitry referenced to the other regulator. Power must be OR'ed from both buses for the non-redundant equipment with the shortcomings of OR'ing power described above. Operating power must be supplied to two regulators instead of one.

The switched regulators and single-bus concept for the OT-2 spacecraft also has the advantage of permitting partial recovery of radiation-induced surface-leakage on the transistors in the regulators from which power has been removed.

An expanded fusing technique, as compared to previous TIROS satellites, will be employed on the OT-2 spacecraft. Individual load fusing, as shown in Figure 4-V-1, will permit the removal, from the operable equipment on the spacecraft, of an individual subsystem or unit if it fails in a high-current mode. For example, should a camera fail in a high-current mode, only that camera would be removed from the regulated bus. The second camera could still be operated from either programmer, and transmit through either video transmitter. Thus the similar

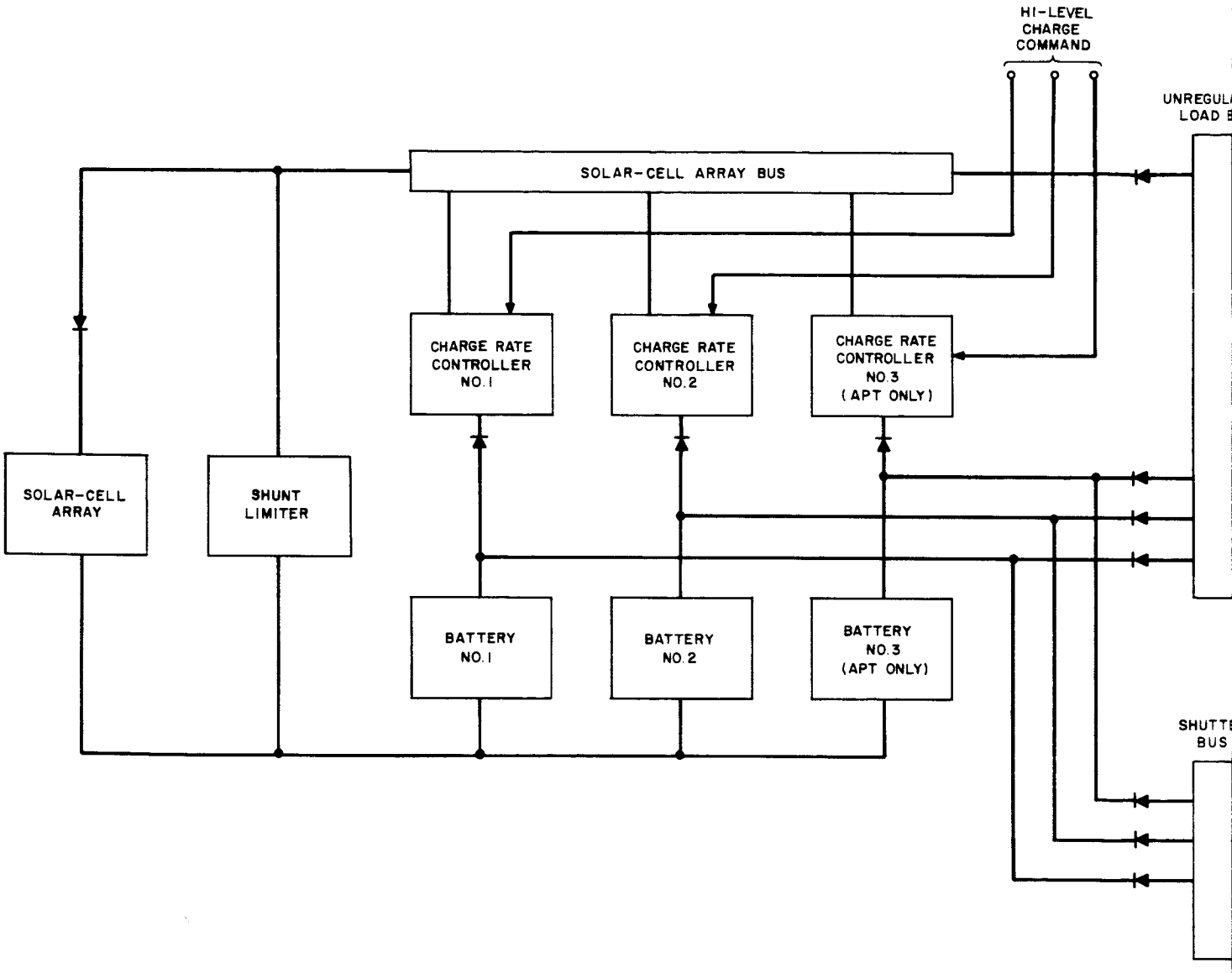
HI-LEVEL
CHARGE
COMMAND
UNREGULA
LOAD B
SOLAR-CELL ARRAY BUS
CHARGE RATE
CONTROLLER
NO. 1
CHARGE RATE
CONTROLLER
NO. 2
CHARGE RATE
CONTROLLER
NO. 3
(APT ONLY)
SOLAR-CELL
ARRAY
SHUNT
LIMITER
BATTERY
NO. 1
BATTERY
NO. 2
BATTERY
NO. 3
(APT ONLY)
SHUTTE
BUS

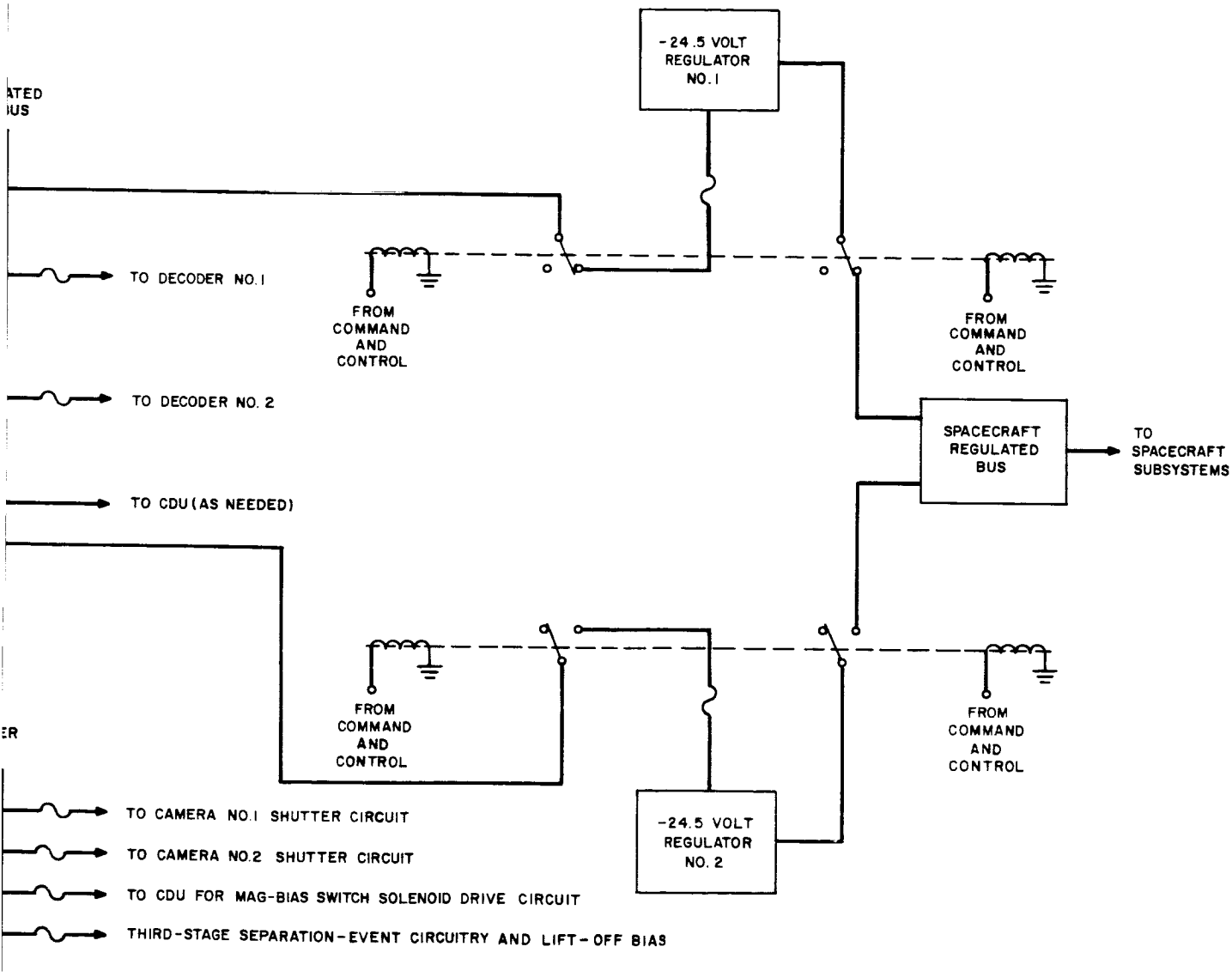

Figure 4-V-1. Power Supply Subsystem, Block Diagram

units, i.e., both cameras, both decoders, both programmers, both transmitters, both recorders (OT-2/AVCS spacecraft only) must independently fail before the spacecraft would be prevented from fulfilling its mission requirements.

During orbit nighttime, energy will be supplied by the batteries to the loads by way of the series voltage regulator and unregulated bus. As the spacecraft comes out of orbit night, array temperatures are such that a high voltage would normally be generated by the array. The shunt limiter, however, clamps the maximum voltage output of the array to a value of approximately 34 volts. Under these conditions, the voltage drops across the charge rate regulators exceed 1.0 volt and each battery will charge at a constant 400-milliampere rate. The array will be capable of supporting continuous loads estimated at 350 milliamperes (see Figure 4-V-2). All excess array energy will be shunted by the limiter. As the picture-taking load is programmed, energy shunted through the limiter is reduced. Should the load exceed the available array current, the extra energy will be supplied by the batteries. This condition will occasionally occur during the picture-taking portion of orbit daytime, as depicted in Figure 4-V-2.

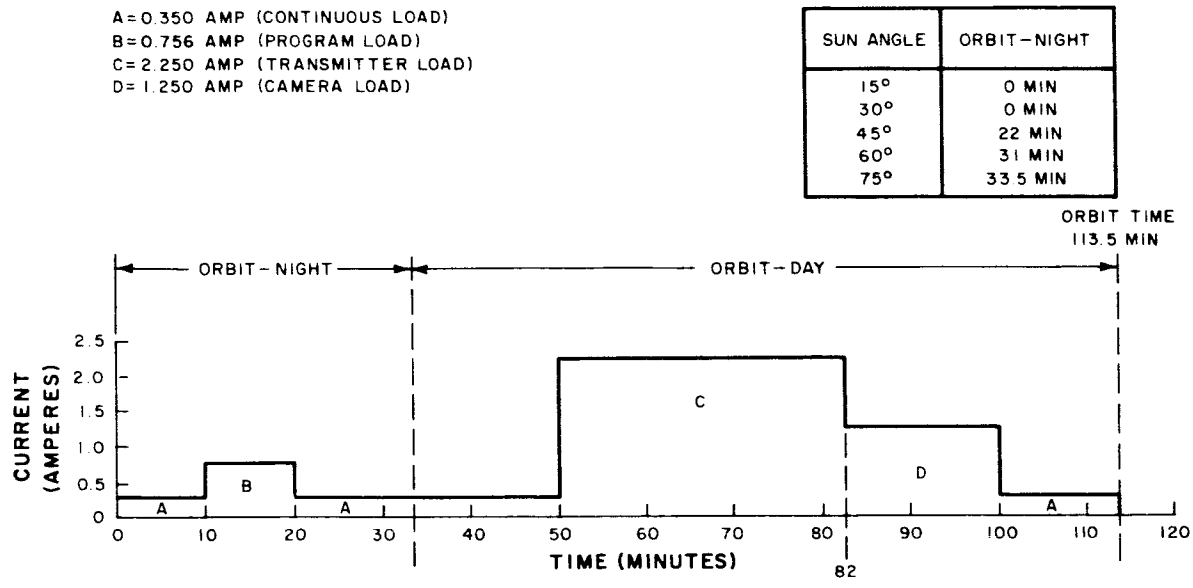

Figure 4-V-2. Composite Load Profile (APT System)

The composite APT load profile as shown in Figure 4-V-2 depicts the major load requirements placed on the power-supply subsystem discussed in this report. Level "A", which runs throughout the full orbit, represents the continuous loads required in the spacecraft. Level "B" represents those loads turned on during nighttime programming of the spacecraft. Levels "C" and "D" represent the APT

picture-taking load. The difference between levels "C" and "D" multiplied by the duration of level "D" (i.e., 18 minutes) represents the power saved by switching the transmitter "off" at specified intervals during the picture-taking cycle.

Thus, by switching the transmitter "off" when not needed, 18 ampere-minutes of energy are saved. For one picture the APT camera is "on" 352 seconds and the transmitter is "on" 236 seconds. Using values of 0.9 ampere for camera current and 1.0 ampere for transmitter current, a single picture therefore uses 9.2 ampere-minutes. Thus, turning the transmitter "off" saves the energy equivalent to almost two pictures; more important the reduced energy requirements for a picture sequence will allow maintenance of full mission capability for a longer period of time.

As degradation of the array continues during mission life, the shunt limiter will shunt less and less excess array-power until the available array power becomes less than that required by the load and batteries. However, during the estimated six months of mission life, predicted degradation will not be this excessive. The subsystem is designed so the batteries will be at full charge at the end of orbital daytime, in order to maintain energy balance and support the nighttime loads.

Initially, the present TIROS system was examined to determine the feasibility of using as much of the existing power-supply hardware as possible. Because of the high orbital altitude (750 nautical miles) required for the OT-2 mission, particular attention was given to degradation of the solar-cell array due to radiation. To achieve the required energy balance for the 15- to 75-degree sun-angle range considered, the APT composite load profile shown in Figure 4-V-2 was used to determine the optimum electrical configuration of the present hardware. All circuits involved in the power-supply subsystem, including the shunt limiter, charge rate regulator, batteries, series voltage regulators, and telemetry circuits, were examined; from this examination, it appeared that modifications or redesigns were required.

2. Systems Interface Requirements (APT)

The power supply subsystem will sustain the full APT load profile shown in Figure 4-V-2 (peak currents are not indicated) for a period of five to seven months in orbit, and between sun angles of 15 to 60 degrees. The system is capable, during the first several months, of operation over sun angles from 15 to 75 degrees. After the five-to seven-month period, further radiation degradation could require operation on a reduced mission basis by employing load programming techniques. Provisions for the APT load will be made at the following voltages:

(1) a regulated bus voltage of -24.5 volts dc, and

(2) an unregulated bus voltage of -25.2 to -34 volts dc (nominal -28 volts).

Load distribution will be such that no more than 5 amperes steady-state load will be drawn from the regulated bus. Table 4-V-1 lists the spacecraft subsystems and their loads at this time. Any significant change in these values would require re-examination of energy balance conditions; considering the tolerances of known data at this time, no disruptive changes are anticipated. Figure 4-V-3 shows the typical APT picture-taking load profiles which are condensed into the composite load profile of Figure 4-V-2.

TABLE 4-V-1. ESTIMATED OPERATIONAL AND STANDBY POWER REQUIREMENTS FOR APT SYSTEM

Unit	Ground Command		Clock Timing		APT Remote Sequence	
	No. of Units	Current (ma)	No. of Units	Current (ma)	No. of Units	Current (ma)
Receiver	2	30	2	30	2	30
Orthogonal Horizon-Sensor	2	15	2	15	2	15
Controls (CDU)	1	100	1	10	1	50
Decoder	1	50	1	5	1	5
High-Frequency Generator	1	35	1	35	1	35
Programmer	1	50	1	50	1	50
V-Head Horizon-Sensor	2	15	2	15	2	15
APT Camera and Transmitter	-	-	-	-	1	1900
Subcarrier Oscillator	3	60	2	40	2	40
Telemetry Commutator	2	250	-	-	-	-
Beacon	1	80	1	80	1	80
Load Regulator (-24.5V)	1	50	2	40	2	70
Total		735		320		2290

3. Systems Interface Requirement (AVCS)

The power supply subsystem required for the AVCS configuration is essentially the same as the subsystem required for the APT configuration. However, because of the lower power requirements, the battery pack consists of only two strings

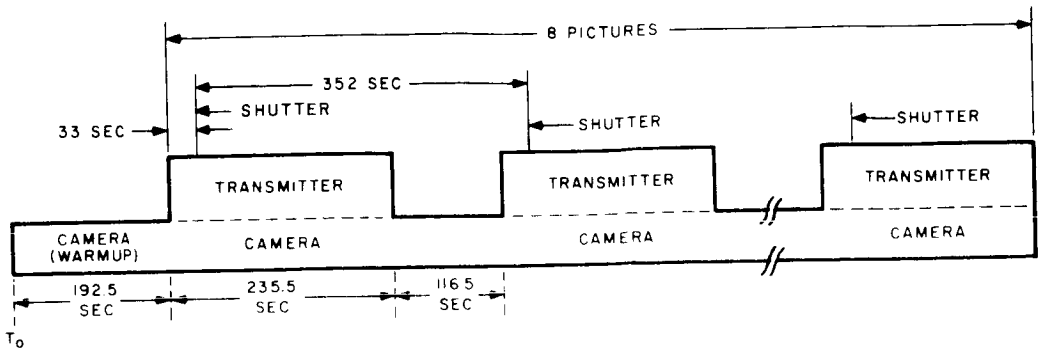

COMPONENT	POWER REQUIRED		
SHUTTER	57.2 WATTS	28.0 VDC	2.2 AMP
CAMERA	22.0 WATTS	24.5 VDC	0.9 AMP
TRANSMITTER	24.5 WATTS	24.5 VDC	1.0 AMP

Figure 4-V-3. Typical APT Picture-Taking Load Profile

(21 cells per string) of 4-ampere-hour cells as compared to the three strings required in the APT battery pack. The AVCS configuration also eliminates the need for the charge rate regulator and current telemetry circuit associated with the third string of cells. With these exceptions, all interface requirements and hardware for the AVCS subsystem are identical to the APT power supply subsystem.

As with the APT power supply, the AVCS power supply has been designed to meet the spacecraft power requirements even under the worst-case condition, i.e., the condition of a 75-degree sun angle. Because of this design approach, a failure in one battery string will not affect the ability of the spacecraft to meet the mission requirements, provided the desired 45-degree sun angle is achieved and maintained. Further, even if it should not be possible to maintain the sun angle at approximately 45 degrees, one battery string would provide sufficient power to enable partial fulfillment of the mission objective.

The bi-level charge-rate regulator of each battery string will be set for charge rates of 400 milliamperes (low rate) and 600 milliamperes (high rate). Although only the low-charge rate will be used during normal operation, the high rate will ensure adequate recharge in the event that one battery string fails, requiring that the other string be used to supply all of the power to the spacecraft.

Table 4-V-2 lists the spacecraft equipment and their loads. Figure 4-V-4 shows the AVCS power profile.

TABLE 4-V-2. ESTIMATED OPERATIONAL AND STANDBY POWER REQUIREMENTS FOR AVCS SYSTEM

Unit	No. of Units	Ground Command	Playback	Clock Timing	Picture Taking		
		Current (ma)	Current (ma)	Current (ma)	Current (ma)		
					A*	B*	C*
Receiver	2	30	30	30	30	30	30
Orthogonal Horizon-Sensor	2	15	15	15	15	15	15
Controls (CDU)	1	100	100	10	50	50	50
Decoder	1	50	50	5	5	5	5
Programmer	1	100	100	100	100	100	100
V-Head Horizon Sensor	2	15	15	15	15	15	15
AVCS Camera	1	-	-	-	680	650	150
AVCS Transmitter	1	-	1000	-	-	-	-
AVCS Tape Recorder	1	-	575	-	665	-	-
Subcarrier Oscillator	3	60	60	60	60	60	60
Beacon	1	80	80	80	80	80	80
Telemetry Commutator		260	-	-	260	-	-
Regulator		50	70	40	70	60	50
TOTAL		760	2095	355	2030	1065	555

*See Figure 4-V-4 for definition of A, B, and C.

C. SOLAR-CELL ARRAY

1. General

The previous TIROS power supply subsystem studies have shown that it is possible to compensate partially for temperature and degradation effects on a given array by reconfiguration of the solar-cell strings. This is accomplished by connecting the cells in a higher output-voltage arrangement, resulting in an operation that is closer to the maximum power point of the I-V curve.

Consideration of all pertinent variables, including temperature, sun angle, and degradation, resulted in an optimized modified array to support an APT load. Table 4-V-3 illustrates the relative magnitudes of current that can be expected with various quantities of shingles per string. The analysis shows that a modified assembly consisting of 20 shingles per string on top and 16 shingles per string on the side panels will best support the APT load.

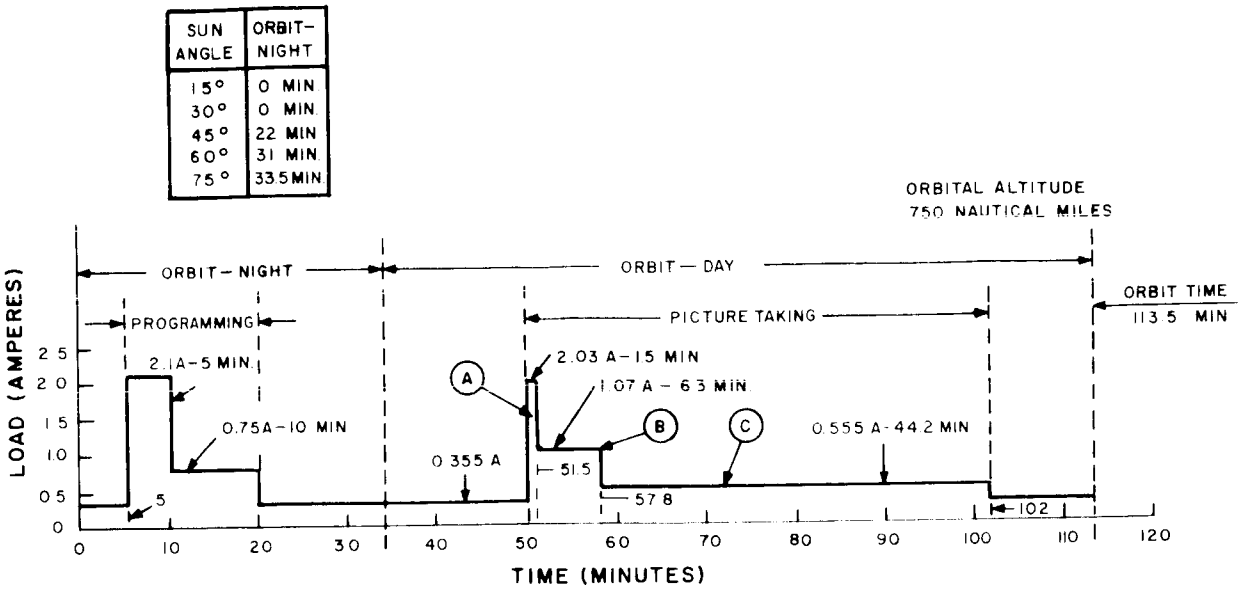

Figure 4-V-4. AVCS Load Profile

TABLE 4-V-3. RELATIONSHIP OF CURRENT MAGNITUDE OF VARIOUS SHINGLE QUANTITIES FOR MODIFIED ARRAY

Shingles/String		Current Magnitude (Sun Angle of 30 Degrees)	Current Magnitude (Sun Angle of 60 Degrees)
Top	Side		
18	16	0.506	1.0
20	16	0.765	0.990
22	16	0.851	0.972
24	16	0.852	0.940
18	18	0.490	0.940
20	18	0.749	0.930
22	18	0.831	0.902
24	18	0.832	0.881

NOTE: Magnitudes of current are relative values and not absolute.

An array layout study, preserving the use of the present solar-cell modules indicated that the number of shingles on top can also be increased from 704 to 740 and the average number of strings per side panel from 4 to 5. The modified configuration of the solar-cell array requires reworking of the top array into 37 strings of 20 shingles per string, and addition of more modules on available side area, allowing an average of 5 strings of 16 shingles per string per side panel. Modular construction of solar cells will be maintained. An array-degradation telemetry-patch function will be employed. This would consist of a four-shingle string (1/4 module) mounted in available area on the new array layout.

Increasing the cover glass on the solar cells from 6 to 60 mils was also considered for overcoming degradation; the indication was that this would result in a nominal increase in power of 9 percent. However, this would also result in an unacceptable increased weight of the array (approximately 10 pounds); therefore increasing cover-glass thickness was eliminated in favor of reconfiguration of the solar-cell strings. Figure 4-V-5 illustrates the available currents from such an array configuration with degradation effects included. The three solid curves represent the average array current available during the sunlit portion of the orbit for zero, three, and six months for sun angles from 15 to 75 degrees.

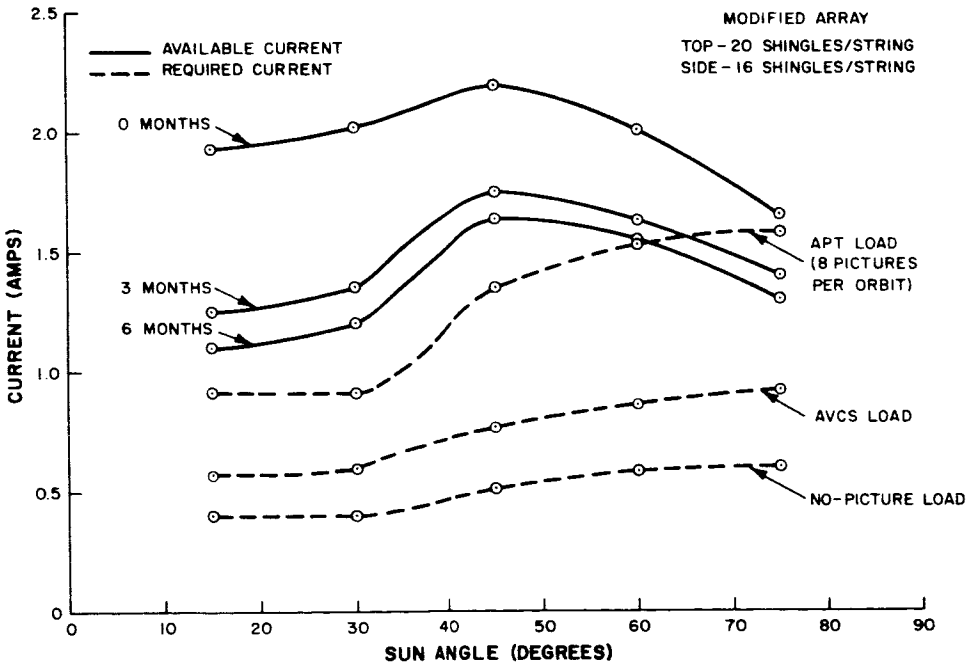

Figure 4-V-5. Available and Required Solar-Cell Array Current for Various Sun Angles

The upper dashed-curve represents the average required array current necessary to support the full APT load profile for the indicated sun angles; the middle dashed-curve represents the AVCS load. The lower dashed-curve represents the required current, assuming no picture load. This curve can be used to determine load programming requirements, which may become necessary as degradation increases. The reduction of sun-angle range (15 to 60 degrees) is evident at six-months degradation. It can be observed that the required current at higher sun-angles increases due to increased orbit nighttime. From Figure 4-V-6 it may be seen that the increase in orbit nighttime is a function of sun angle.

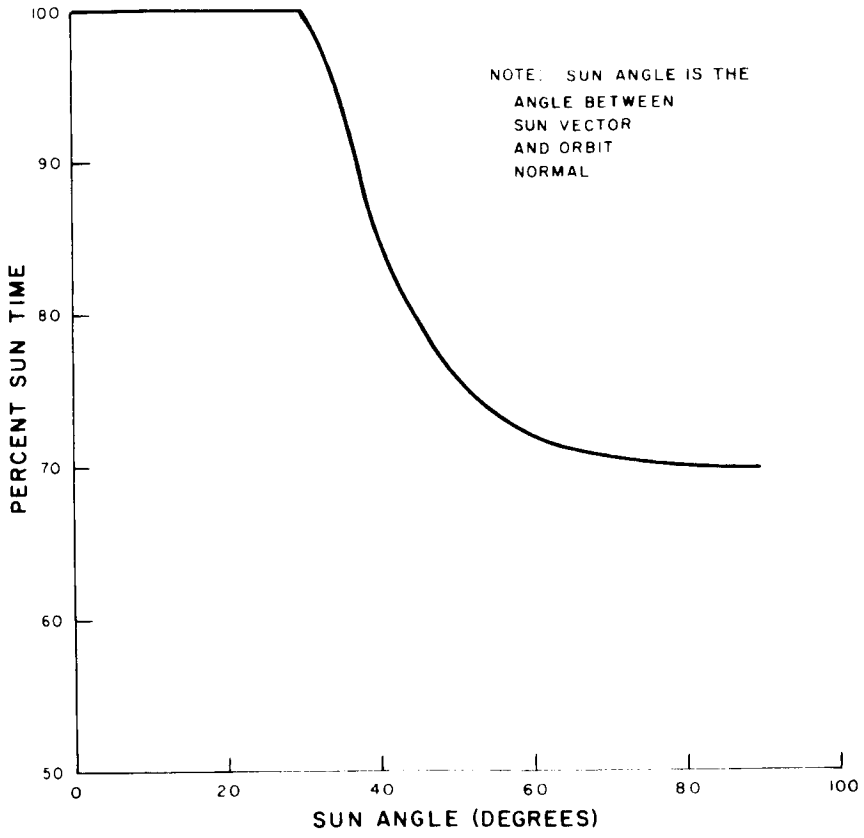

Figure 4-V-6. Percent Sun Time as a Function of Sun Angle

Figure 4-V-7 illustrates typical, array current profiles (at the end of 6 months) versus orbit time, for various loads and sun angles for the OT-2 spacecraft array configuration. Top and side temperature effects are included. *Curves 1, 2A, and 3 show the array current (I_A) at sun angles of 30, 45, and 60 degrees, respectively, with the APT load profile applied to the system and the shunt limiter set at 32.9 volts dc.

*Data for these curves was taken from the OT-2 energy-balance program (10/6/64), using six-month life I-V curves for the IRC 5-cell shingle (4 to 9 ohms per cm resistivity).

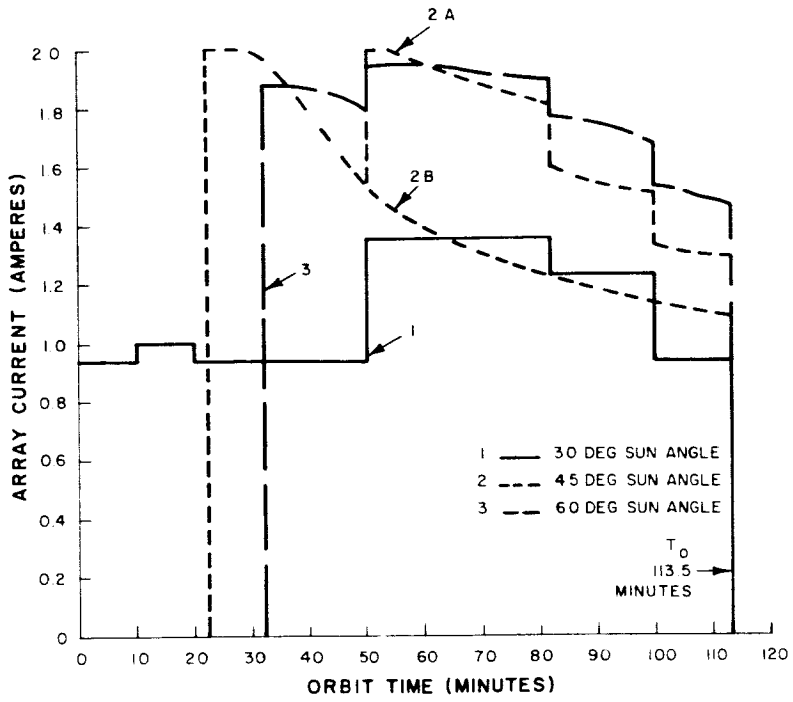

Figure 4-V-7. Array Current Versus Orbit Time at Various Sun Angles

At a sun angle of 30 degrees, assuming correct spin-axis orientation, there is no orbit night. The array top is at a constant temperature (80°) throughout the orbit. Under these conditions the system is just maintaining energy balance. The system is operating below the clamping level of the limiter and current is drawn from the array as required, so that array current follows a pattern very similar to the load profile as shown in Curve 1. Programming is evident at the 10-minute mark and picture load starts at the 50-minute mark.

Curve 2A shows 22 minutes of orbit night. Start of orbit day indicates that the array is operating on the constant current portion of its I-V curve and is at its coldest temperature. Increasing array temperature at low load is evidenced at the 30-minute mark, where I_A begins to decrease. Heavier loading at the 50-minute mark shifts operation back to the constant current portion of the I-V curve. The continuing increase in temperature causes I_A to begin a gradual decrease at the 54-minute mark and to continue to decrease throughout the remainder of the sunlit portion of the orbit.

Curve 2B is a projection of I_A showing temperature effects under a continuous low load. Array temperature increases rapidly initially, and then gradually levels off towards end of orbit. I_A acts inversely, rapidly decreasing initially, then leveling with temperatures. This curve is similar to the array current profile which would result with no load at a constant array voltage.

Curve 3 represents operation at a sun angle of 60 degrees. The curve is similar to curve 2A, with longer orbit night causing a slightly different temperature effects profile.

2. Array Modification

The modified array configuration requires modifications to the basic solar-cell mounting module, and a new wiring harness for the array. Although the basic substrate remains the same, new hole-locations for terminal penetration are required in the top plate and side panels.

In order to increase power while utilizing the existing module board assemblies, the following modifications can be effected:

(1) Side Panels. Eight solar-cell shingles per panel can be added to twelve of the eighteen side panels. Although this would result in an overhang of 0.055 inch at each end of the modified panels, this overhang can be reduced to 0.028 inch by removal of three of the ridges on the panel.

(2) Top. The number of shingles mounted on the top can be increased to 740, by making a total of 37 twenty-shingle circuits. To achieve this, seven modules would require modification to four-shingle circuits, two modules would require modification to 3 four-shingle circuits, and 3 individual four-shingle circuits would be required. The modifications can be performed on existing circuitry, but some losses should be anticipated during the rework cycle. The individual four-shingle circuits should be fabricated instead of cutting existing assembled module boards.

Should the mission requirements increase such that the required array power exceeds the capabilities of the array as modified above, modification of the assembly and bonding techniques could provide still more power with the existing area. This would, however, require the purchasing of new solar cells.

This second modification could be implemented as follows:

(1) Side Panels

(a) The maximum number shingles on a full side panel is 80.

(b) Side 13 will accept 73 shingles.

(c) Side 3 will accept 71 shingles.

(d) Side 18 will accept 38 shingles.

(e) Side 14 will accept 64 shingles.

(f) Side 5 will accept 64 shingles.

(2) Top

The top will accept a maximum of 820 shingles. This number of shingles would require revision of the shingle assembly and bonding process. The module board assembly would be eliminated, and insulating surface would be placed on the substrate, and shingle design modification of the connector tab configuration would be necessary.

Modification of the assembly and bonding process would increase the total array power output. Shingle circuits could be series/parallel connected and electrically tested prior to bonding to the substrate. Weight per watt of power would be decreased. A large portion of the array assembly would be completed prior to bonding to the substrate; thus, array repair (shingle replacement) would be simplified. Also it is expected that labor costs for assembly from shingle to array level would be reduced more than enough to compensate for the tooling required.

3. Irradiation

Previous experience with higher altitude spacecraft, namely, the Relay I satellite, has indicated that one of the problem areas in the power system is radiation degradation; in particular, degradation of the solar-cell array. Figures 4-V-8, -9, -10, -11, and -12 depict the predicted radiation damage to a typical IRC solar-cell shingle of the type presently employed on TIROS, starting with no degradation, and then after approximately 3, 6, 9, and 12 months of radiation exposure.

The development of the "irradiation-degraded" I-V curves of the TIROS n-on-p silicon solar-cell shingle considered the following five groups of basic parameters:

(1) The orbital electron and proton spectrums and flux rates for a 750-nautical mile, circular, polar orbit.

(2) The parameters of the unbombarded shingle.

(3) The backshielding materials.

(4) The electron and proton damage factors (Kd).

(5) The air-mass-zero, equivalent 1-mev electron damage rates; and the air-mass-zero, current and voltage temperature sensitivities.

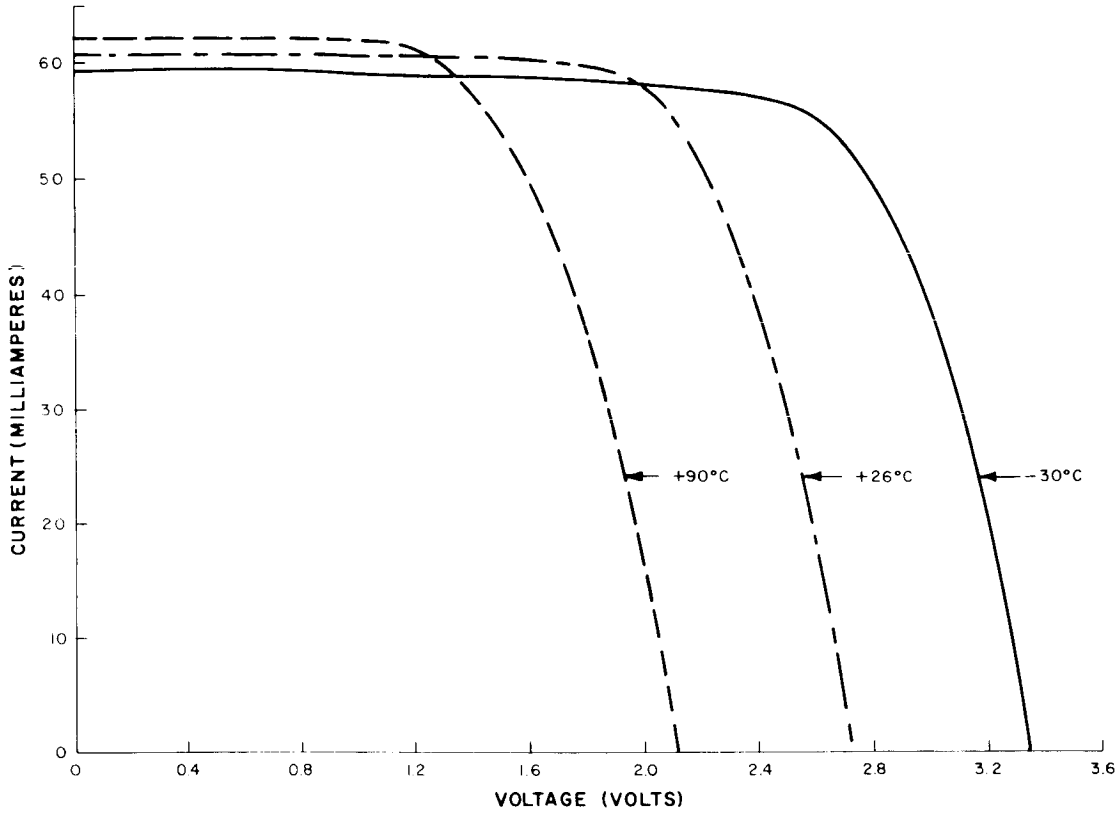

Figure 4-V-8. TIROS N-on-P Silicon Solar-Cell Shingle I-V Curve, No Degradation

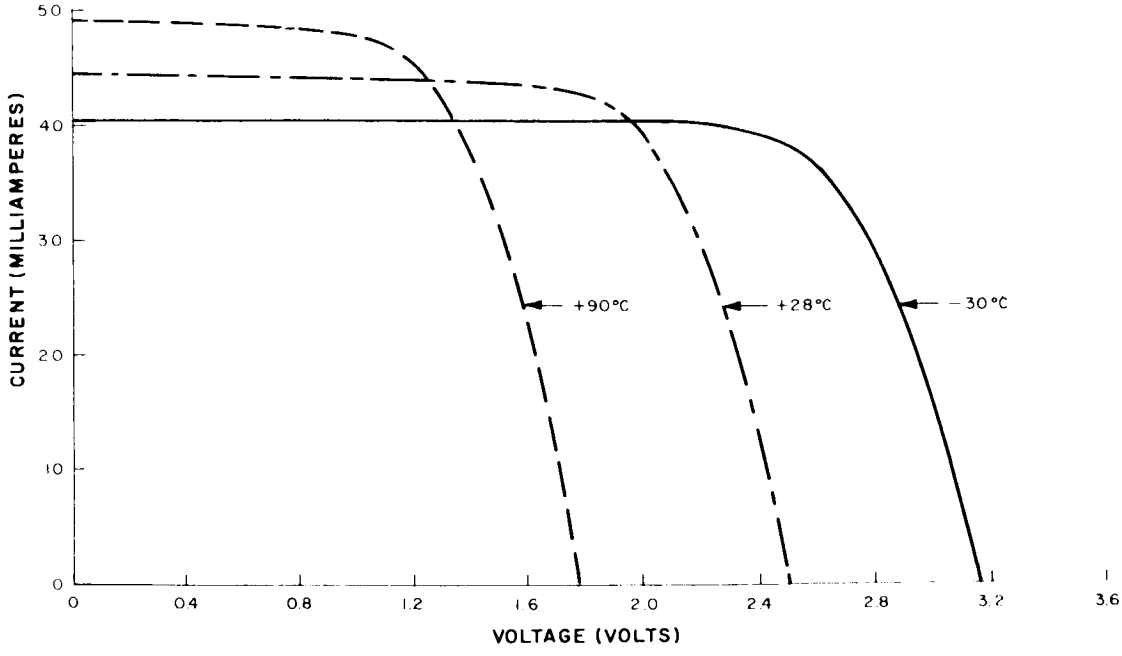

Figure 4-V-9. TIROS N-on-P Silicon Solar-Cell Shingle I-V Curve, 78- to 108-Day Degradation

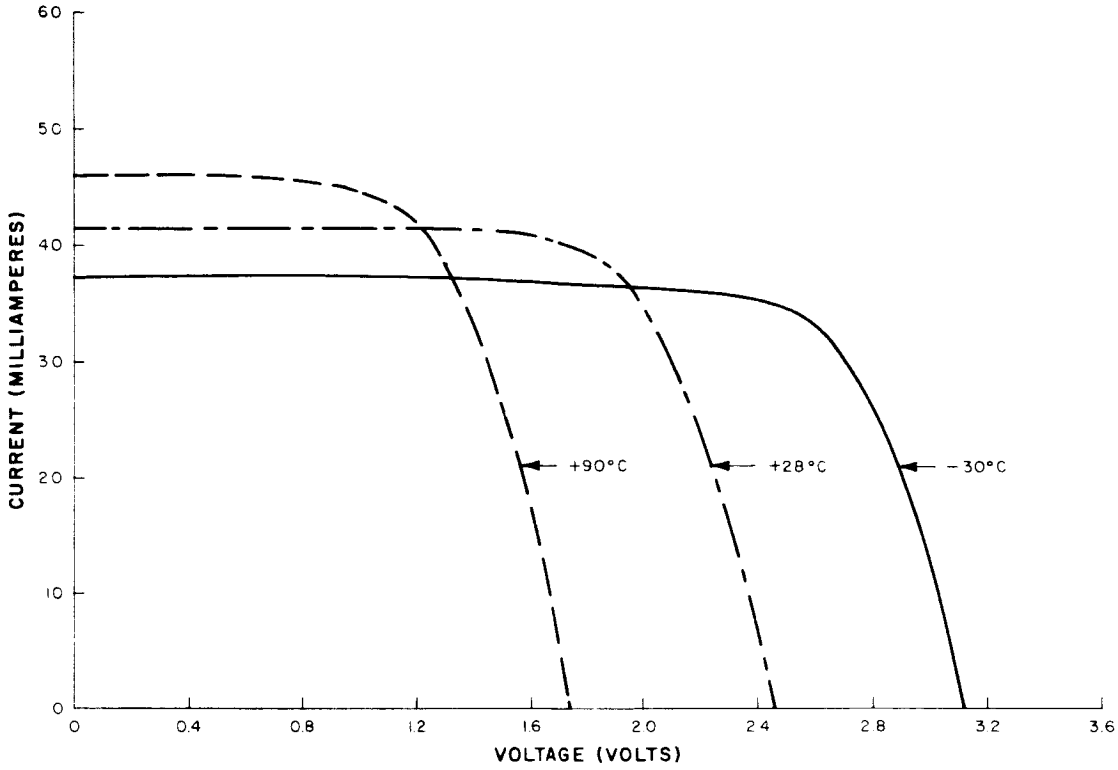

Figure 4-V-10. TIROS N-on-P Silicon Solar-Cell Shingle I-V Curve, 156- to 217-Day Degradation

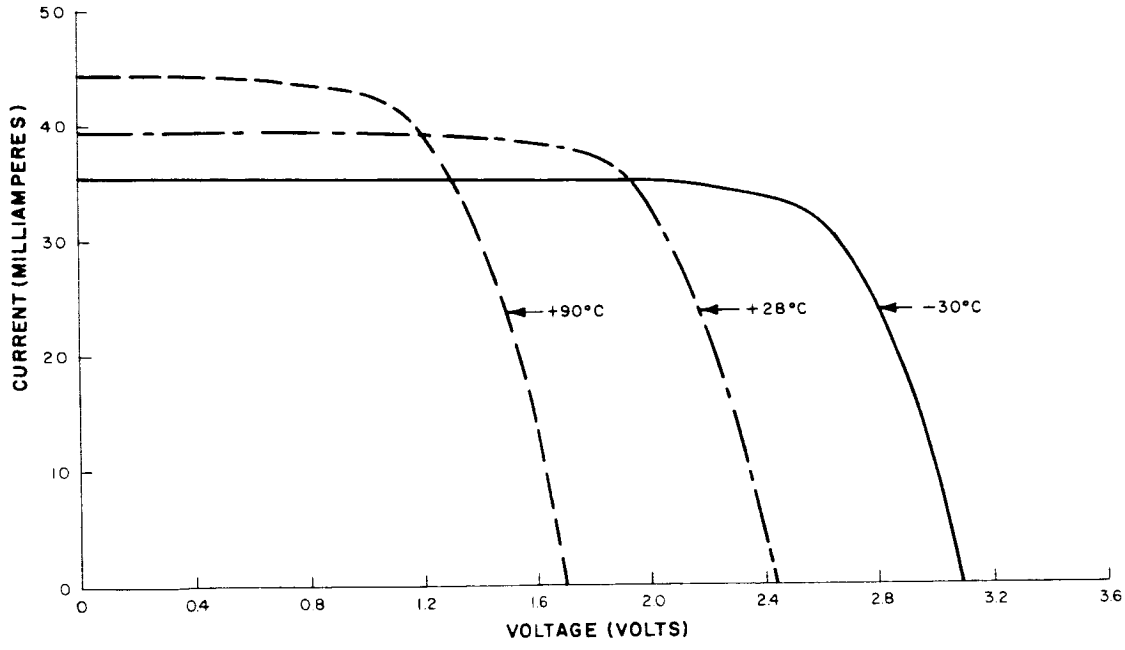

Figure 4-V-11. TIROS N-on-P Silicon Solar-Cell Shingle I-V Curve, 234- to 235-Day Degradation

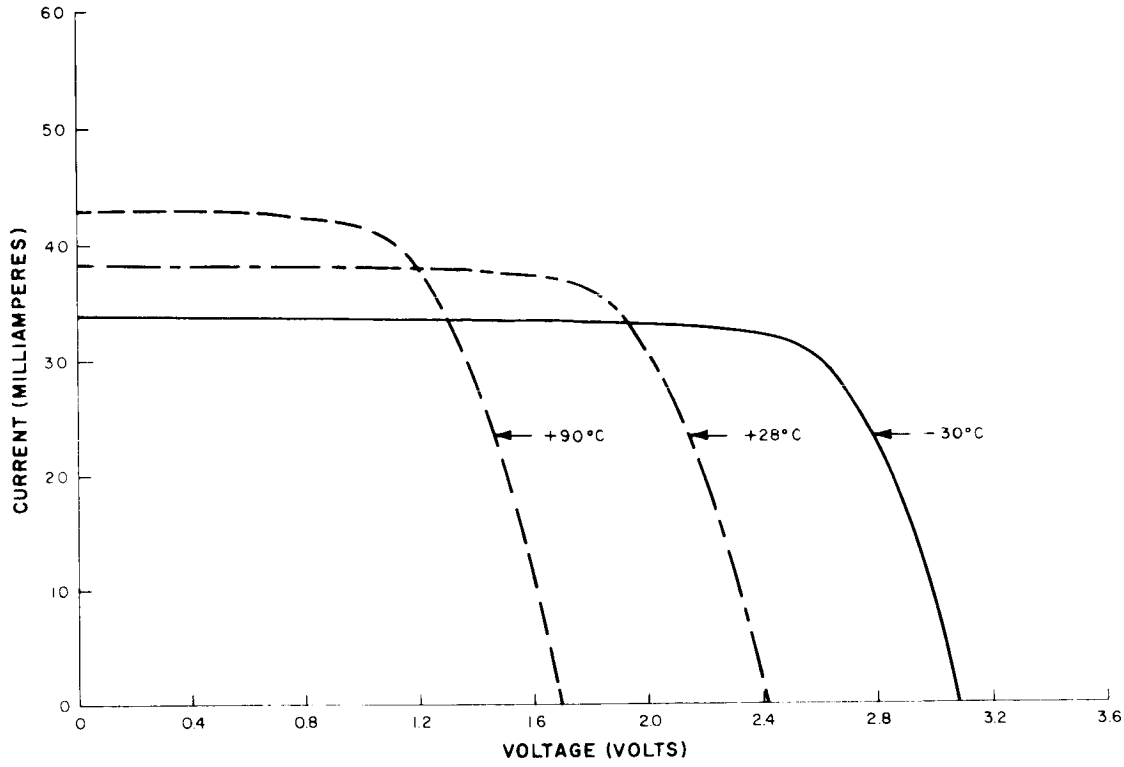

Figure 4-V-12. TIROS N-on-P Silicon Solar-Cell Shingle I-V Curve, 312- to 433-Day Degradation

RCA estimates of the orbital irradiation particle spectrums and flux rates were used; a NASA-computed grid was used for electron spectrums and flux rates; and NASA information was also used for the proton spectrums and flux rates. Both of these particle flux rates are omnidirectional and are for a 750-nautical mile, circular polar-orbit, which from a radiation standpoint is the same as a 750-nautical mile, 101.5-degree inclined, circular orbit.

The parameters of the unbombarded shingle were taken from RCA obtained data. The last two groups of parameters are irradiation parameters of the basic solar cell. There is no available irradiation data for the TIROS (IRC plated contact) solar-cell. As a result, the irradiation parameters of two solar cells which are, to some extent, similar in construction to the TIROS cell had to be used.

The electron and proton damage factors used are those* for the Western Electric solar cell, and they equate the damages of normally incident 1-mev electron flux to an uncovered solar-cell and omnidirectional particle flux to the cover-glassed solar cell with infinite backshielding. These damage factors are used because both solar cells are blue sensitive, n-on-p, silicon solar-cells and the Western Electric damage factor data is the only complete set of damage-factor data that is available.

*Brown, W. L., Gabbe, J. D., and Rosenweig, W., Results of the Telstar Radiation Experiments, The Bell System Technical Journal, July 1963, (Figures 32 and 33).

The 1-mev electron damage rate curves and the temperature sensitivities are basically the values used for the Nimbus solar cell, the only difference being that the values for the TIROS solar cell were modified in keeping with its active area, which is smaller than the area of the Nimbus solar cell.

The actual calculations with these parameters consisted of the following three major steps: (1) determining total equivalent 1-mev electron flux density for 3, 6, 9, and 12 months of operation; (2) determining shingle parameter values for each flux level at 28°C; and (3) shifting the 28°C parameter values to obtain values at +90°C and -30°C. The first step was carried out by multiplying the number of irradiation particles for each energy level by the damage factor for the level and totalling the results for the particles (electrons and protons) over their active energy ranges. In these calculations, contributions through the back-shielding were ignored because the internal flux level is believed to be very low and the 60-mil aluminum back-shield is a fairly effective particle barrier. In the second step, the total equivalent 1-mev electron flux densities were used to enter the damage rate curves and obtain the corresponding degraded parameter values for the solar cell at 28°C. These sets of solar-cell parameter values for each of the equivalent 1-mev electron flux densities were converted into sets of parameter values for the 5-solar-cell shingle at 28°C. In the third step, the 28°C values for the shingle were shifted to sets at +90°C and -30°C with the current and voltage temperature sensitivities. The three shifted points of the I-V curve, the short-circuit current, the maximum power, and the open-circuit voltage with the initial I-V curve shape as a master, were used to construct I-V curves at +90°C and -30°C for each flux density level.

The initial design philosophy was to use the present TIROS power supply subsystem as much as possible. Analysis has shown that the present TIROS solar-cell array, with 16 shingles per string on top and 16 shingles per string on the side, and with 44 strings on top and an average of 4 strings per side panel, would not be capable of supporting the APT mission beyond 3 months without employing load programming techniques. This analysis consisted of a mathematical determination of the array current available from the present array, compared to the current required by the APT load, at a sun angle of 45 degrees. The sun angle of 45 degrees was picked for the analysis because previously determined available current curves showed a peaking at this sun angle. If the system fails to supply energy balance at this sun angle, it would appear marginal or deficient at other sun angles. Calculations showed the available current to be just equal to the required current at 3 months. Considering the tolerances of parameters involved, this would be marginal operation at only half the mission life. Thus, the need for the previously described modifications is apparent.

D. BATTERIES

1. General

The determination of a battery to be used in an orbiting space vehicle is generally based on the following considerations:

(1) charge mode and rate,

(2) overcharge rate,

(3) discharge rate,

(4) depth of discharge,

(5) time for recharge,

(6) voltage regulation,

(7) battery temperature range, and

(8) required life and reliability.

Using a maximum charge current of 1.2 amperes, during a typical orbital power profile for the APT system (shown in Figure 4-V-2), 0.51 ampere-hour will be drawn from the battery, and the battery will be recharged 0.705 ampere-hours; thus, the ratio of charge to discharge capacity is 1.39/1. A charge-to-discharge capacity ratio of 1.39/1 is sufficient to recharge the batteries to full capacity. Available charge capacity is greatly dependent upon the sun angle, which is subject to deviations. The design is based on the "worst-case" (least sunlight) estimate.

Although proper discharge performance is the ultimate requirement of the battery, the required capacity is usually governed by the maximum allowable charge rate in low orbiting satellites with constant-current charging. In the absence of a voltage cut-off or tapered current charging, the overcharge capability of the battery is the limiting factor. (The battery is much more sensitive to overcharge current than it is to discharge current.) For example, a 10-ampere-hour battery should not be continuously charged at a current higher than 1.0 amperes. (This is limited by the overcharge characteristics.) However, the discharge current limit could be in the order of 10 times higher, if necessary.

Over the temperature range of approximately + 15°C to +50°C, C/10 is considered to be a safe charging rate for continuous overcharge, where "C" represents the room temperature capacity (ampere-hour) to the 1.0-volt end point when the cell is discharged at the 5-hour rate. (The charge rate could be higher, but the battery is limited by the overcharge capability, during which time there is internal generation of gas.) The C/10 factor has been empirically determined. Although it is subject to variation between cell types, C/10 represents a conservative cutoff point for continuous

overcharging. If the overcharge period is of relatively short duration, and punctuated by periods of discharge, the battery can accept higher overcharge currents, usually determined by specific experiment. A factor of C/8 has been used in previous TIROS spacecraft with cycled overcharge conditions.

Since the charge rate for the APT system is 1.2 amperes, initial calculations indicate that a 12-ampere-hour battery would be required. This will result in a depth of discharge which is less than 3 percent, and a maximum discharge rate of C/26. The charge rate was chosen such that at a 75-degree sun angle the charge-to-discharge ratio will be 1.25, the minimum desirable ratio.

In the expected orbital sun angle of 45 degrees, the recharge ratio will be above 2. Therefore, if one string of cells is removed from the circuit, the remaining string(s) can carry on the functioning of the system. The depth of discharge will be increased (and still remain below 10 percent), but the voltage level and general performance of the cells will not be significantly affected. If the sun-angle should actually be close to 75 degrees, the energy for a full mission will not be continually available during every orbit. However, the system has provision for programming a higher charge rate. This would put the system back into balanced operation. However, the C/6.7 rate is not recommended for continuous overcharge and hence greater care must be taken in programming the spacecraft to avoid overstressing the batteries. Should a cell short in any string, the terminal voltage of that string would be reduced and load sharing would be unevenly distributed between strings. However, since the depth of discharge is less than 3 percent, it is unlikely that such a failure would even be detectable.

The 4-ampere-hour, sealed rectangular-cell, as manufactured by the General Electric Company and Gulton Industries, is recommended for use in the OT-2 system. Three parallel strings of batteries will be used for the APT power-supply subsystem. Each string of cells will have an independent charge-current limiter. Therefore, loss of one string due to shorting, or development of an open circuit will not result in charging of the remaining strings at excessive currents.

A typical charge-discharge profile is illustrated in Figure 4-V-13. The solid profile represents the initial charge-discharge profile of an array, with no degradation and at a sun angle of 45 degrees, for one orbit of an APT mission. The dotted section illustrates the same profile after six months degradation of the array. It is evident that battery discharge has increased; however, at this time the power formerly shunted by the shunt limiter has decreased and the available array power is used to recharge the batteries.

2. Design Considerations

Based upon data from within RCA, and from manufacturers' information, it is recommended that the cells be of the rectangular configuration. Previous TIROS batteries were cylindrical and contained rolled plates.

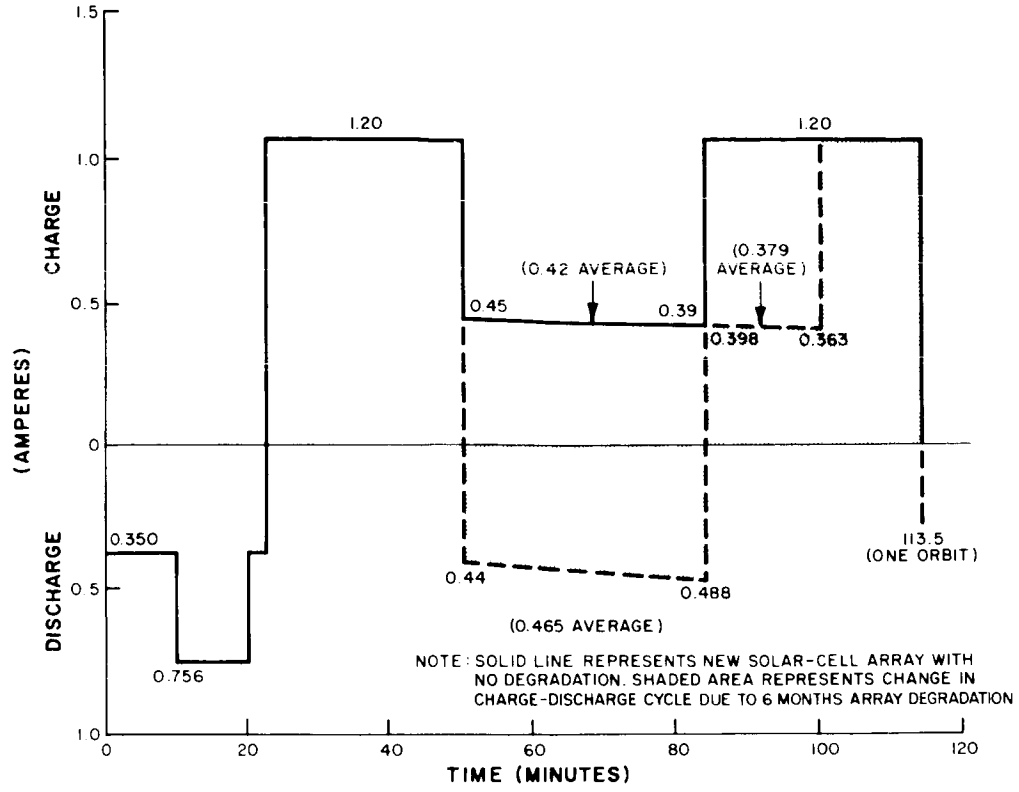

Figure 4-V-13. Array Charge-Discharge Profile for APT System (Typical)

One of the major reasons that most of the sealed-cell manufacturers prefer rectangular cells is that the battery plates in the rectangular cells are flat. In general, battery plates are fairly rigid and, thus, are susceptible to cracking and flaking when they are rolled for cylindrical cells. Rolling the plates also subjects the separator material to undue pressure in localized areas. Consequently, the reliability of the cylindrical cell is lower than that of the rectangular cell.

Experience at RCA shows an estimated rejection rate of cylindrical cells on the order of 50 percent, while the rejection rate of rectangular cells is 3 percent or less. Although the sampling quantities were not equal, the indications are most significant. In addition, all aerospace-cell manufacturers have had successful experience with rectangular cells, while only one manufacturer has had extensive experience with cylindrical cells.

The rectangular cell also has the advantage of containing many positive and negative plates, as opposed to the one or two of each type in the cylindrical cells. This factor permits blending of plates in order to achieve uniformity of capacity and negative-to-positive ratio.

The rectangular cell does not present the packaging problem which is usually involved with cylindrical cells. Potting the cells into position (a time-consuming, costly, and delicate operation which is performed with all cylindrical cells) can be eliminated. Battery retaining fixtures can be simple, four-sided, and relatively compact. (It should be noted that the Lunar Orbiter Project will use rectangular cells.)

3. Design Parameters

The major design parameters for the battery are (1) rectangular configuration and (2) approximately 12 ampere-hours required capacity. Since the system requires 25.5 volts, a 21-cell (1.21-volt per cell average) battery will be employed. The 4-ampere-hour cell will be packaged in groups of 11. Therefore, although two packages will be required to form one string, only 21 of the 22 cells will be electrically connected in the circuit. This alleviates the need for a 10-cell package design in addition to an 11-cell package design. As a result, one spare cell is included in each string, thus permitting "cell replacement" merely by rewiring the pack, rather than disassembling and replacing the cell. Furthermore, if system requirements should change, the 22-cell string could be employed without major repackaging. (For the 25.5-volt minimum requirement, 22 cells corresponds to 1.16 volts per cell average.)

Other RCA programs have recently completed an evaluation program on these cells, and qualified packs have been delivered. The concept of using a 4-ampere-hour battery as a building block to serve the needs of two systems merits some discussion: Three strings of 4-ampere-hour cells will be heavier than one string of 12 ampere-hour cells, due to the additional support members required. However, this system will permit the design, fabrication, and testing of one type of cell and battery pack to serve the requirements of both the APT and AVCS systems. The greatest value in this approach is the inherent redundancy which will allow continued operation, although with reduced programming, in the event of a battery failure.

E. PROTECTION

1. Shunt Limiter

a. General

A more desirable method of obtaining the voltage-limiting action provided by the bypass regulator used in the present TIROS power supply subsystem can be realized with a shunt limiter used in conjunction with a blocking diode as shown in Figure 4-V-1. The limiter is designed to dissipate only excess solar-cell array power. The 2-volt minimum drop across the bypass regulator located between the array and the unregulated bus in the present TIROS system is eliminated, resulting

in an overall increase in power-system efficiency. When load current is drawn from the array, the bypass regulator must dissipate power equal to the product of the load current and the bypass voltage-drop (2-volts minimum). Although the excess array-power dissipated by the shunt limiter is higher than the bypass dissipation at the beginning of the mission, the limiter power dissipation diminishes with mission life until it becomes negligible; the bypass regulator, on the other hand, is a continuous series load that would be experienced throughout mission life. Retaining the bypass regulator would require that the number of series shingles on top be increased still further to provide energy balance and satisfy the bypass regulator requirement. The present TIROS power supply subsystem allows the array output voltage to go as high as possible, the only restriction being a light, continuous load. Shunt limiter action clamps the array to a desirable operating level for the charge rate regulators and series voltage regulator, and restricts the end-of-charge voltage of the batteries to a desirable level.

The diode replacing the bypass regulator is redundant to reduce the probability of failure of the spacecraft due to an open diode. If the diode circuit opens completely, limited operation capabilities are still possible since the charge path to the batteries would still be maintained.

The shunt limiter circuit proposed is the same as that used successfully in Relay I and II. The mechanical and electrical designs would require those modifications necessary for the circuit to meet the different electrical and environmental conditions of the OT-2 mission.

b. Circuit Description

The shunt limiter is designed to load the solar-cell array when the solar-cell array bus voltage attempts to exceed a level of -33.3 volts. The circuit, as presently contemplated, would be designed for a "worst-case" condition in which as much as 90 watts of excess array power could be dissipated and the bus voltage still kept below the maximum allowable level of -34.6 volts. The worst case condition can occur during spacecraft integration with full array output through the limiter. The shunt limiter I-V characteristic can be thought of as similar to that of a zener diode with an extremely low dynamic resistance and a "knee" or threshold voltage of -33.3 ± 0.4 volts. The maximum shunt current at the 90-watt dissipation level is 2.6 amperes; therefore, the minimum allowable circuit transconductance is 2.6 amperes divided by -34.6 volts - (-33.7 volts), or 3.0 mhos. Stated another way, the maximum allowable "zener impedance" is 1/3.0 mhos or 0.333 ohm. The configuration necessary to produce the required characteristic is shown in Figure 4-V-14. The current gain of the three effective dc-coupled stages divided by the first-stage input resistance, results in a transconductance in excess of 3.0 mhos under all combined "worst-case" conditions.

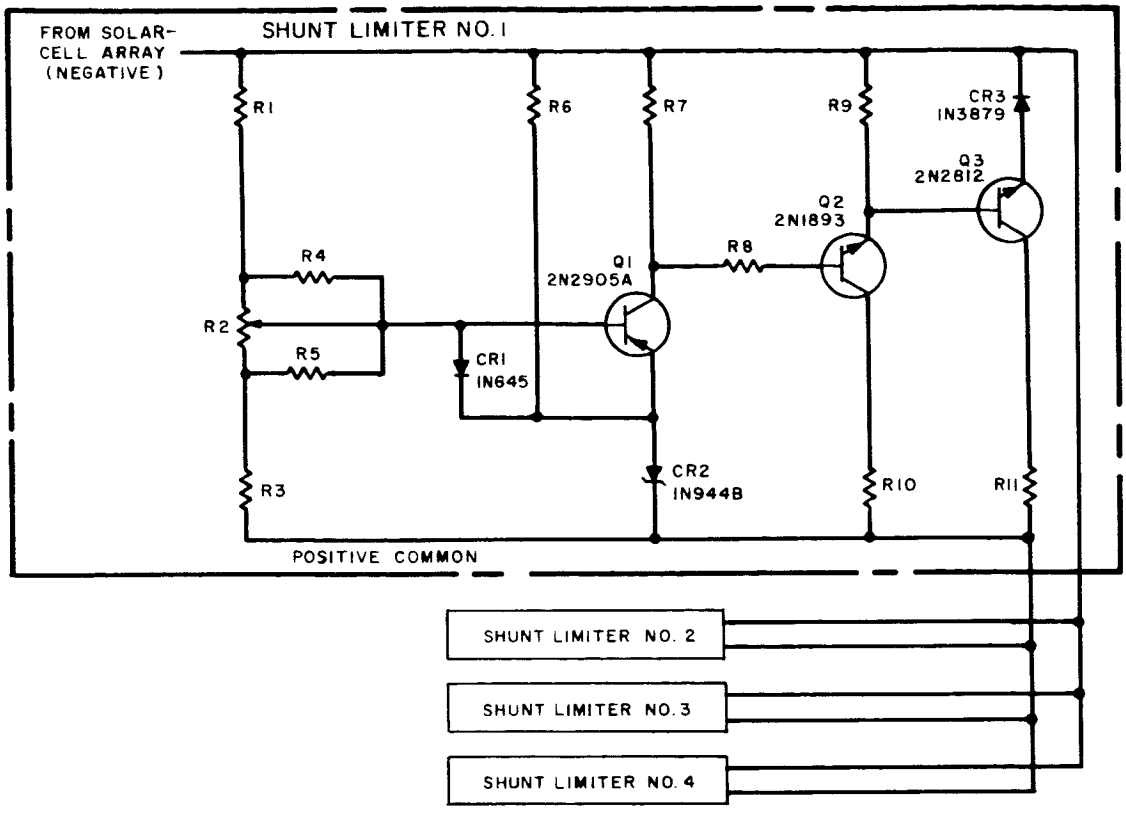

Figure 4-V-14. Shunt Limiter Circuit, Schematic Diagram

c. Circuit Operation

Referring again to Figure 4-V-14, the circuit operation is as described in the following: Below the minimum threshold voltage of -32.9 volts, the circuit appears as a high resistance across the solar-cell array bus, shunting only a small amount of current through the zener reference diode CR1, and the divider network made up of resistors R1 through R5.

The emitter of transistor Q1 is held at the fixed zener voltage of CR2 while the base is below the conduction point. For very low array voltages, the base would actually be positive with respect to the emitter and the transistor is, therefore, reverse-biased. With Q1 held in cut-off, Q2 and Q3 are also in the OFF state since their bias is derived from the Q1 collector current.

As the array-voltage bus rises more negatively, the base of transistor Q1 rises a proportionate amount due to the divider action of resistors R1 through R5. At the threshold conduction point, Q1 begins to deliver current to R7 and the base of Q2. As the bus voltage rises further and the forward bias of Q1 increases, the threshold conduction points of Q2 and Q3 are passed in turn and the circuit begins to shunt

heavy current through the Q3 power transistor stage. The same action occurs in all four of the parallel-connected circuits, causing the amount of shunt current drawn by the circuit to continually increase, as a function of increasing solar-cell array voltage, to the point where either the maximum output power capability of the array becomes limited, or the power transistors are driven into saturation. The circuit will be "worst-case" designed to ensure that the condition of saturation is not reached at a level below the 90-watt maximum power dissipation requirement. The complete limiting action is confined to a solar-cell array voltage differential, equal to, or less than 0.9 volt.

d. Design Details

Minimization of changes in electrical values, caused by temperature and time, of the R1 through R5 resistor divider and the CR1 reference diode is achieved through the use of highly stable, low temperature-coefficient devices. Diode CR1 protects the base-emitter junction of Q1 from high reverse voltages as the solar-cell array is turning on.

The use of high-gain, high-frequency silicon transistors in all stages provides the circuit with the necessary low dynamic resistance characteristic initially and throughout the mission, even when subjected to the radiation extremes of the high-altitude orbits. Silicon transistors, capable of operating safely at higher temperatures than equivalent germanium types, allow the use of a fewer number of components to meet the power handling requirements of the circuit. The inherently lower leakage currents give protection for both inadvertent "turn-on" of the circuit and lower shunt losses when the solar-cell array voltage is below the threshold level.

The four-circuit parallel combination shown in Figure 4-V-14 is recommended. This configuration allows a high measure of reliability by virtue of the multiple redundancy effected by four parallel shunting paths. This has been proven analytically by a failure mode and effects analysis on a similar limiting circuit developed for the Relay II satellite. In effect, if only one limiter is used and it fails in an open or shorted mode, catastrophic failure of the power system is imminent. Identical results occur with the present TIROS system if the bypass regulator fails by opening or shorting. If two parallel limiters are used, failures on one in a shorted mode will decrease available array power 33 watts. This is considered semi-catastrophic, causing immediate load profile reprogramming. Hence, four redundant units are used such that a failure of one in a shorted or open mode will not result in catastrophic failure of the power supply subsystem. The quadruple circuit has a probability of 0.9989 for 1 year of successful operation, as compared to 0.9508 for the single circuit. *

*Failure Mode and Effects Analysis - Voltage Regulator Circuit, Project Relay, Internal Memorandum, 25 March 1963.

2. Charge Rate Regulator

a. General

The basic TIROS charge rate regulator, a bi-level charge circuit will be retained. However, because of the higher radiation levels anticipated, substitutions for several of the electrical components must be made. Charge rate can be determined from Figure 4-V-5, which shows the required and available array current versus sun angle. The charge rate is equal to the maximum required current that the array can support minus the constant load current. The APT power supply subsystem contains three battery strings, and the AVCS power supply contains two battery strings, which are independently charged by the solar-cell array during the daylight portion of each orbit. Charge current to each battery passes through the charge rate regulator, which serves to limit the current to a 400-milliampere rate or a 600-milliampere rate per string, selectable by ground command.

b. Circuit Operation

A schematic diagram of the charge rate regulator is shown in Figure 4-V-15. Transistor Q1 serves as the main current-carrying element and Q2 serves to provide base drive current for Q1. As the solar-cell array bus voltage rises, Q2 begins to conduct. The collector current of Q2 is ultimately limited by the voltage across CR1 and the value of resistor R5 (or R5 in parallel with R6). As the array bus-voltage exceeds the battery voltage plus the threshold voltage of Q1 and CR2 in series, collector current flows in Q1 by virtue of Q2 collector current. As the array bus-voltage continues to increase, Q1 collector current becomes limited due to the fixed value of Q2 collector current (i.e., the base drive to Q1 is limited). When Q1 collector current reaches its maximum value and the array bus-voltage is still increasing, the excess voltage will appear from collector to emitter of Q1. Diode CR2 prevents the battery from discharging through any partial fault which might appear across the array bus and through Q1 in the reverse direction during dark portions of the orbit. Resistor R1 serves both to provide some current gain stabilization of Q1 and to provide a voltage proportional to battery charge current for the battery charge current telemetry.

c. Design Details

Although this circuit is basically the same as that employed in previous TIROS systems, there are slight differences. Transistors Q1 and Q2 are high-frequency silicon types selected for their relatively high radiation resistance. In addition, Q1 is a high-power (100 watts at 100°C case temperature), low saturation-voltage device. Because of the extremely low saturation voltages which can be expected from Q1 (typically 0.4 volt at 800 milliamperes with $h_{HE} = 50$, min), resistor R1 is included, with the advantages as mentioned above. The transistors proposed also have extremely low leakage-currents, thereby improving the margin of safety as regards thermal drift and thermal runaway.

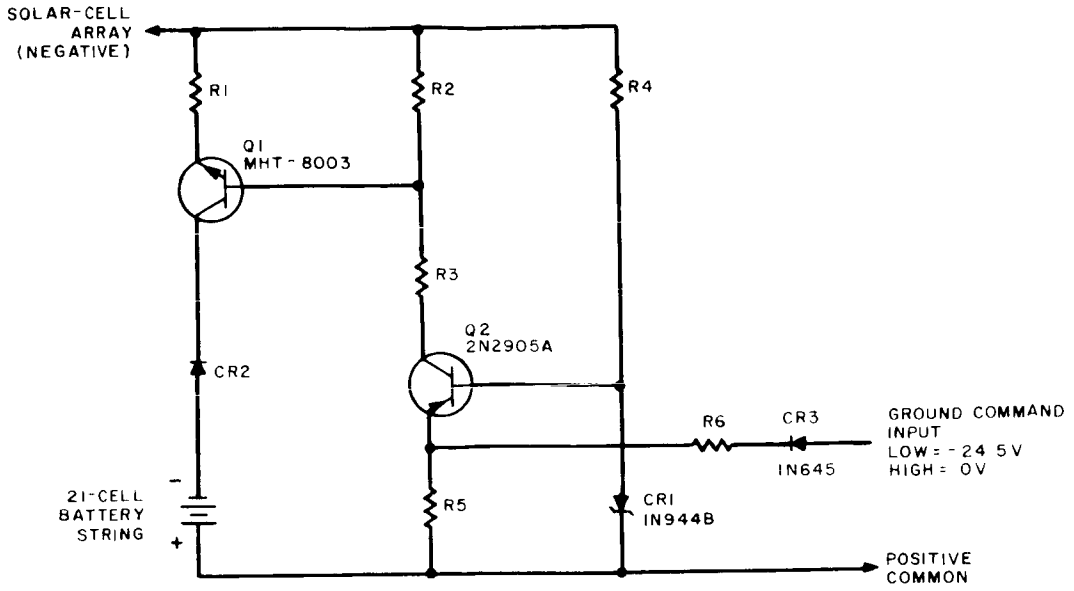

Figure 4-V-15. Charge Rate Regulator Circuit

3. Isolating Diodes

The power supply subsystem will contain isolating diodes as shown in Figure 4-V-1. The purpose of the diodes between the batteries and unregulated bus is to prevent the array from charging the batteries through this path rather than through the charge rate regulator. The purpose of the diode between the array and the unregulated bus is to prevent current flow from the battery to the array.

F. REGULATION

1. General

At the present, all of the subsystems on the OT-2 spacecraft will use voltage levels similar to previous TIROS spacecraft. The -24.5 series voltage regulator presently qualified for TIROS "I" will be retained. This particular unit is a recent design incorporating silicon transistors with increased dissipation capability and improved reliability. The unit's characteristics far exceed the former TIROS specifications and the components are inherently more radiation resistant. The voltage input requirements of 25.2 to 33 volts dc make it feasible for use with the OT-2 power supply subsystem concept using a shunt limiter. Initial investigation of loads and array profiles indicate that the voltage regulator will not exceed its internal dissipation limits.

2. Series Voltage Regulator

A redesign effort on the TIROS -24.5-volt regulator was started in January, 1964, and a post-breadboard design review held on March 31, 1964. This circuit has undergone complete "worst-case" analysis and design. Three assemblies (one prototype and two flight models) have successfully passed the environmental test phase. All component types in the circuit have been specially selected for their relatively high resistance to radiation. This is particularly true of the high-frequency, narrow-base silicon transistors used throughout.

Investigation will be made of the possible effects on performance by radiation at an altitude of 750 nautical miles, and adjustments will be made in the electrical design and packaging if necessary. This would probably involve only slight changes in a few resistor values and/or use of a thicker cover for increased shielding.

The series voltage regulator circuit will be subjected to slightly higher input voltages with the APT power supply subsystem configuration (-34.6 volts versus -33 volts in the previous TIROS subsystem). This should have no effect other than slightly increased power levels in certain components. A re-evaluation of the heat-sinks for these components will be made.

G. TELEMETRY CIRCUITS AND POWER SUPPLY PERFORMANCE EVALUATION

1. Telemetry Functions

The telemetry functions required by the power supply subsystem are compiled in Table 4-V-4. The telemetry information indicated will be useful in (1) assessing radiation degradation to the array and to other subsystem components, (2) monitoring operation of the total subsystem, and (3) assisting in determining when load programming is required. The top and side array temperatures, array current, unregulated bus voltage, and shunt-limiter current telemetry are necessary to confirm pre-launch predictions of array performance.

2. Array Current Telemetry Circuit

a. General

The addition of charge current telemetry will be accomplished by minor modifications to the array current telemetry circuit presently used on TIROS. The array current telemetry circuit to be described below provides a means for sensing a current flow and converting it to a signal voltage suitable for transmission by the telemetry subsystem. The basic circuit is applicable to both battery charge current and array current sensing.

TABLE 4-V-4. TELEMETRY FUNCTIONS

Monitored Function	Function Range
Array Top Temperature	-50°C to +100°C
Array Side Temperature	-50°C to +50°C
Array Current	0 Amp to 3 Amp
Shunt Limiter Current	0 Amp to 3 Amp
Battery Current	0 Amp to 0.5 Amp
Battery Voltage	-20 V to -35 V
Unregulated Bus Voltage	-20 V to -35 V
Regulated Bus Voltage	-20 V to -35 V
Battery Temperature	-10°C to +35°C
NOTE: All telemetry output signals will be conditioned to a range of 0 to -5 volts dc.	

b. Circuit Description

The circuit (see Figure 4-V-16) can be divided into four major sections as follows:

(1) Current sensing resistors R1 and R2.

(2) A dc amplifier consisting of Q1-A, R3, R9, CR2, and R7.

(3) A temperature-compensating bias source for the amplifier consisting of Q1-B, R4, R6, R5, and CR1.

(4) A combination switch and constant current source for the bias network consisting of Q2, R10, R12, C1, and CR3.

c. Circuit Operation

Current sensing resistors R1 and R2 (see Figure 4-V-16), connected in parallel, are inserted in series with the current to be measured. As the current varies

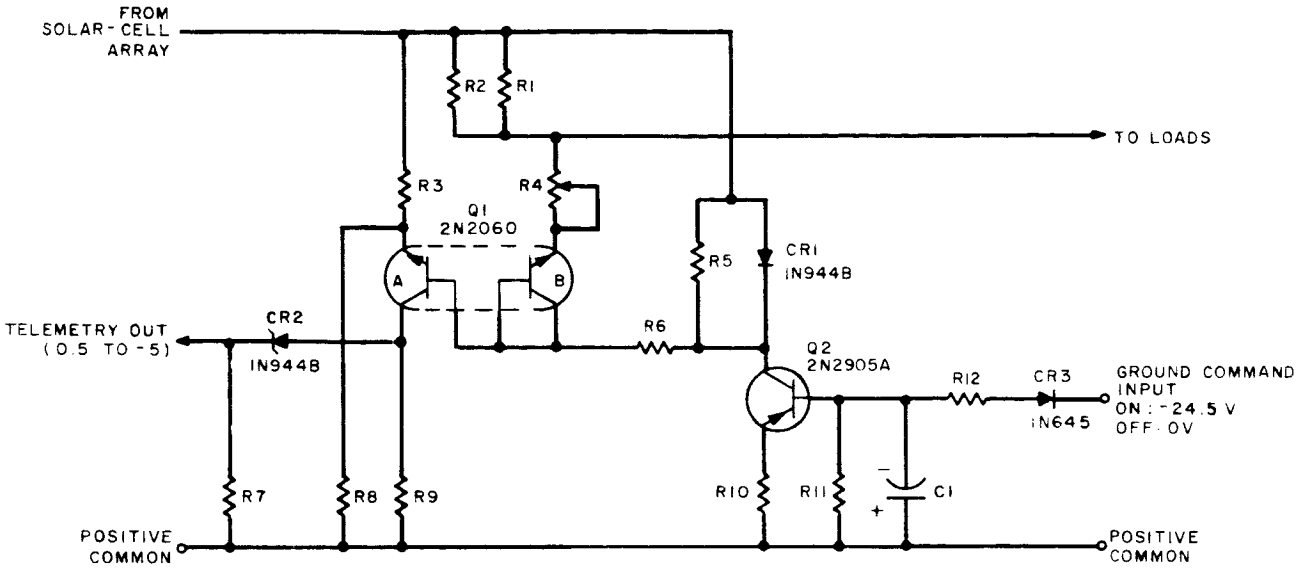

Figure 4-V-16. Array-Current Telemetry Circuit, Schematic Diagram

through its range, a voltage is developed across the sensing resistors. The use of two resistors in parallel reduces the risk of an open-circuited solar-cell array bus, in the event one resistor fails by opening.

Transistor Q1-A amplifies the voltage drop developed across the current-sensing resistors (R1, R2) to produce a telemetry signal ranging from a nominal 0.5 volt to 5.0 volts. Resistor R3 aids in stabilizing the voltage gain through degeneration. In order to achieve linear amplification, the transistor is operated in the central portion of the collector load line. Operation in the collector current cut-off region is obviated by the voltage off-set introduced by Zener diode CR2. Therefore, when signal current is zero, collector current will be minimum and the telemetry signal will be a nominal 0.5 volt. Resistor R8 is used to reduce the error in telemetry output voltage caused by supply-voltage variations. The collector current flowing in a transistor is not entirely independent of collector voltage and tends to increase slightly with an increase in applied voltage. This effect is compensated for by modifying the bias on the transistor in a manner that reduces the base current as voltage increases. Proper selection of resistor R8 when the circuit is calibrated will yield an output voltage error smaller than ± 1 percent through a large supply-voltage range.

Fixed bias is applied to the base of transistor Q1-A by a voltage divider connected across a constant voltage source (Zener diode CR1). The voltage divider consists

of resistor R6 as one leg, and resistor R4 plus the base-emitter junction of transistor Q1-B as the other leg. The temperature dependence of Q1-B V_{BE} is virtually identical to that of Q1-A V_{BE}; therefore, the bias voltage divider tends to follow or "track" variations in Q1-A V_{BE} due to changes in ambient temperature. The circuit configuration of Q1-B is arranged such that the majority of divider current flows in the collector with base current just sufficient to maintain the transistor at the verge of saturation. Resistor R6 is chosen to establish a collector current which is equal to the mean collector current flowing in Q1-A. Thus, it can be seen that the operating parameters for each section of Q1 are similar, resulting in improved temperature tracking. Furthermore, since both transistors are physically located in a common case, and are operated with similar parameters, the "warmup" time required for the circuit to stabilize can be minimized.

Transistor Q2 serves as a command-controlled switch and constant-current source for the bias network. During the time telemetry data is being taken, Q2 is turned on by a -24.5-volt signal from the telemetry subsystem. Resistors R11 and R12 form a voltage divider which determines the bias voltage at the base of Q2. Resistor R10 determines the collector current flowing in Q2 and is designed to produce a nominal 7.5-milliampere bias current in Zener diode CR1. This is the optimum bias current necessary to realize minimum voltage variation versus temperature. When the -24.5-volt command signal is removed, the bias voltage at the base of Q2 goes to zero, resulting in collector cut-off. This interrupts the circuit for the bias network causing Q1-A and Q1-B to cut off. Resistor R5 provides a path for collector leakage currents in order to maintain a cut-off condition at elevated temperatures. By virtue of cutting off the transistors, standby current drawn from the solar-cell array is reduced to the relatively small amount flowing in resistors R3 and R8. Transient voltages that might be present with the command signal are filtered out by capacitor C1. Diode CR3 prevents positive-going transients from appearing at the base of Q2 when the circuit is turned off.

3. Array-Voltage Telemetry

Voltage telemetry will be obtained by low-loss, high-precision, high-stability resistance dividers such as those presently used on TIROS.

SECTION VI. BEACON AND TELEMETRY SUBSYSTEM

A. FUNCTIONAL DESCRIPTION

1. General

The beacon and telemetry subsystem on the OT-2 spacecraft will provide for telemetering operating parameters, attitude data, solar-aspect data, picture-time data (AVCS), command data verification, and camera-triggering information to the CDA stations.

2. OT-2 Spacecraft Telemetry

a. Subcarrier Frequency Assignments

As shown in Figure 4-VI-1, two identical beacon transmitters, each with three subcarrier oscillators (SCO's) will be provided on the OT-2 spacecraft. The three subcarrier oscillators associated with beacon No. 1 (SCO 1-1, 1-2, and 1-3,) will have the same respective frequencies as the subcarrier oscillators associated with beacon No. 2 (SCO 2-1, 2-2, and 2-3). The lowest frequency subcarrier (2300 cps) will continuously carry the output of V-head sensor No. 1 (up-looking with respect to the baseplate), and the middle frequency subcarrier (3000 cps) will continuously carry the output of V-head sensor No. 2 (down-looking with respect to the baseplate). All other telemetry will be carried on the third SCO (3900 cps) on a time-shared basis.

In the OT-2 spacecraft, the subcarrier oscillator having the highest frequency (3900 cps) will be used for telemetering the following parameters in the indicated priority:

(1) Housekeeping telemetry (including picture-time clock on the OT-2/AVCS spacecraft).

(2) Command data verification.

(3) Solar-aspect sensor telemetry

(4) Orthogonal horizon-sensor telemetry (including shutter-actuation marker).

b. Housekeeping Telemetry

The telemetry commutator samples the 90 channels at a rate of 16-2/3 channels per second, when driven by a 133-1/3 cps signal from its associated

programmer. If the programmer is "off", the commutator operates at its internal rate of approximately 15 channels per second. When power is first applied to the commutator, a 1.2-second delay ensues before commutation begins. During this time, an input gate connected to the picture-time clock is enabled, permitting the output of the picture-time clock (OT-2/AVCS spacecraft only) to appear at the output of the telemetry commutator. In the OT-2/APT spacecraft the input to this gate is tied to -5 volts. All of the telemetry points monitored on the OT-2 spacecraft will be applied, through the telemetry conditioner, to both commutators. The output voltages from the telemetry conditioner will range tetween 0 and -5 volts. As shown in Figure 4-VI-1, a switching technique is provided that permits the output of either commutator to be transmitted through either beacon transmitter; this selection is accomplished by the ground command, "Commutators Normal/Commutators Crossed". The telemetry request and commutator power-steering circuitry is such that only the commutator telemetry request relay "on" beacon transmitter will be operated. This will also automatically steer the commutator output to the appropriate subcarrier oscillator. Telemetry may be requested by the standard digital command or by the reception, by the spacecraft, of a longer than normal enable tone. This added command capability is provided to permit the commanding of telemetry from a facility that does not possess the equipment required to generate the normal digital commands. However, if the beacons have been turned off, the emergency telemetry analog command has no facility to turn a beacon back on.

c. Command Data Verification

If housekeeping telemetry is not being requested, command data verification from the two decoders has priority. In this case, the data bits, as decoded, will be transmitted back to the ground station.

Each decoder has a data verification relay. On beacon system No. 1, only housekeeping telemetry has priority over decoder No. 1 data verification, which in turn has priority over decoder No. 2 data verification. On beacon system No. 2, the relative priorities of decoder No. 1 and decoder No. 2 data verification is reversed. The reason for interchanging priorities is to provide for data verification from the programmed decoders even if the other decoder generates an erroneous signal and energizes its data verification relay.

The data verification relays are non-latching devices that are energized by the associated decoder when sync is reduced and stay energized until the last bit of the twelve-bit word is received. In addition, if the Command is "Load Programmer", the associated relay will remain energized until the programmer indicates that it has received

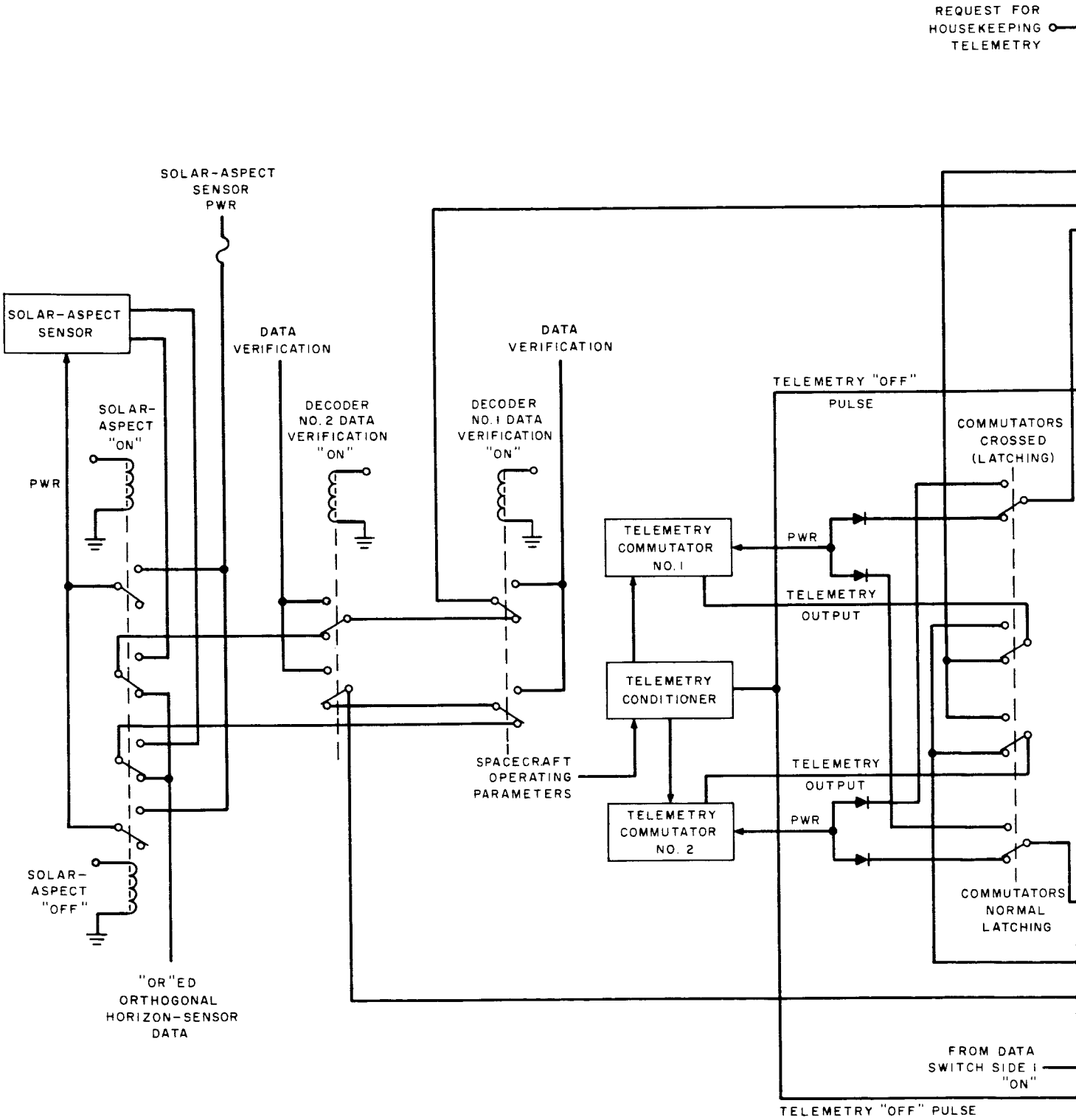
REQUEST FOR HOUSEKEEPING TELEMETRY
SOLAR-ASPECT SENSOR PWR
SOLAR-ASPECT SENSOR
DATA VERIFICATION
DATA VERIFICATION
TELEMETRY "OFF" PULSE
SOLAR-ASPECT "ON"
DECODER NO. 2 DATA VERIFICATION "ON"
DECODER NO. 1 DATA VERIFICATION "ON"
COMMUTATORS CROSSED (LATCHING)
PWR
TELEMETRY COMMUTATOR NO. 1
PWR
TELEMETRY OUTPUT
TELEMETRY CONDITIONER
SPACECRAFT OPERATING PARAMETERS
TELEMETRY OUTPUT
TELEMETRY COMMUTATOR NO. 2
PWR
SOLAR-ASPECT "OFF"
COMMUTATORS NORMAL LATCHING
"OR"ED ORTHOGONAL HORIZON-SENSOR DATA
FROM DATA SWITCH SIDE 1 "ON"
TELEMETRY "OFF" PULSE

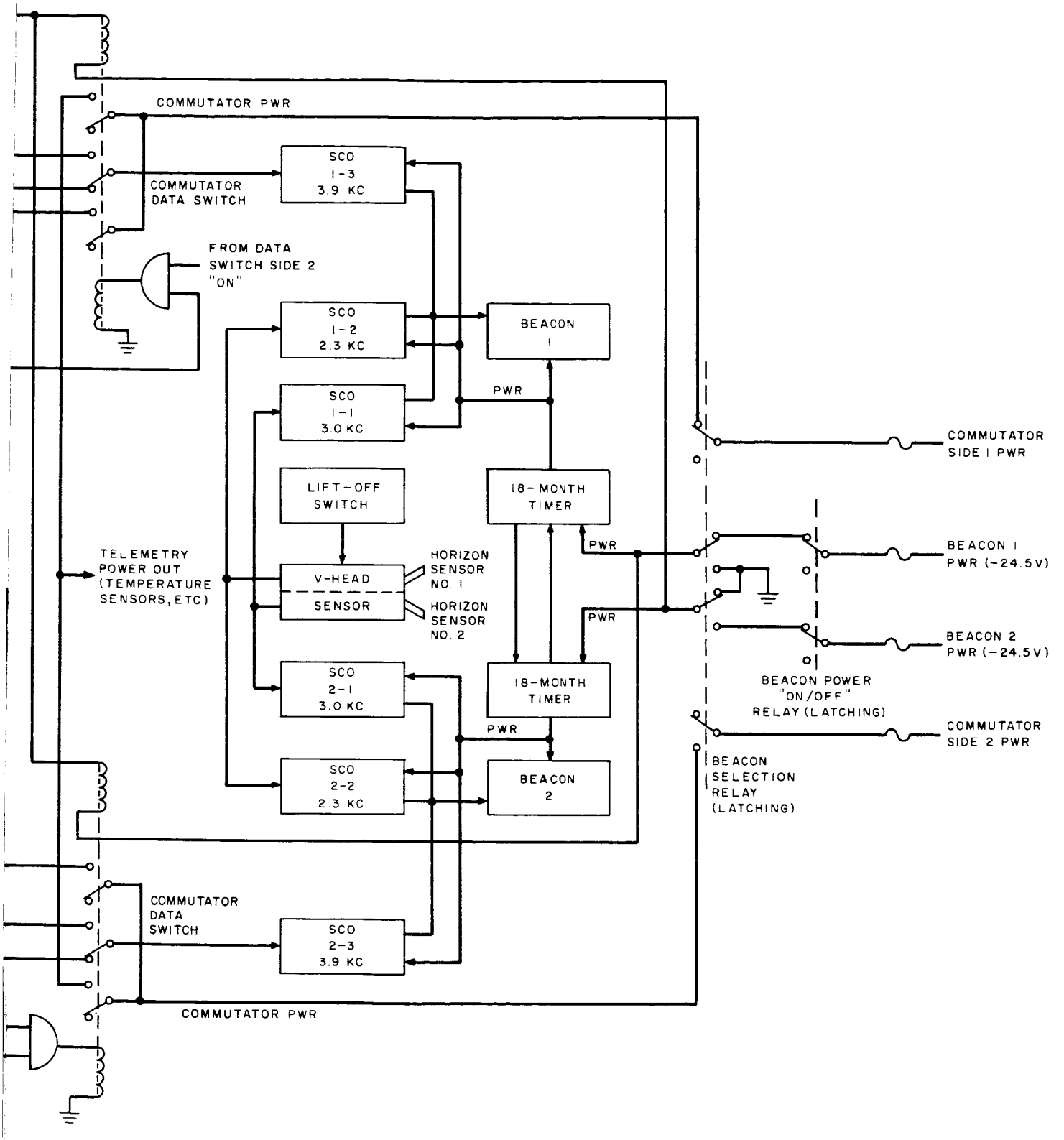

Figure 4-VI-1. Beacon and Telemetry Subsystem, Block Diagram

a full complement of bits. Hence should there be spurious bits generated in the equipment between their detection and re-transmission the programmer register will load too quickly and the data verification relay will be deenergized prematurely. Conversely, if a bit is lost between its generation and the programmers acceptance, the programmer will fail to deenergize the data verification relay, thereby indicating that erroneous data is stored in the programmer register.

d. Solar-Aspect Sensor Telemetry

The solar-aspect sensor is a separate telemetry device that can modulate either of the highest frequency subcarriers (SCO 1-3 or 2-3) associated with the beacons. The device is turned "on" and "off" by a ground command that actuates a latching relay in the spacecraft. This feature permits as many frames as desired of this telemetry to be read out sequentially.

e. Orthogonal Horizon-Sensor Telemetry

The orthogonal horizon-sensors are primarily used for picture-taking reference time. However, they also provide useful diagnostic information as a source of beacon modulation. If no other form of telemetry is requested and the beacon is on, the output of the sensors (horizon-crossing indications) will be transmitted. The outputs of the diametrically mounted sensors are OR'ed together for maximum use of this information. When a camera shutter actuates, a marker will be included on this channel, indicating where on the differentiated slope of the sensor output the shutter was actuated.

3. Channel 4 Telemetry on the OT-2/AVCS Spacecraft

a. General

The OT-2/AVCS spacecraft has a provision to record picture-time data and a frame of telemetry on channel 4 of the tape recorder. In the playback mode, the third SCO is disabled to permit the transmission, by means of the beacon, of the previously recorded subcarrier oscillator modulation. Figures 4-VI-2 and 4-VI-3 show the changes from the APT beacon and telemetry subsystem required to incorporate the channel 4 telemetry system.

b. Recording Channel 4 Telemetry

The output of the picture-time clock and housekeeping telemetry will be recorded on channel 4 of the tape recorders at the same time that video is recorded

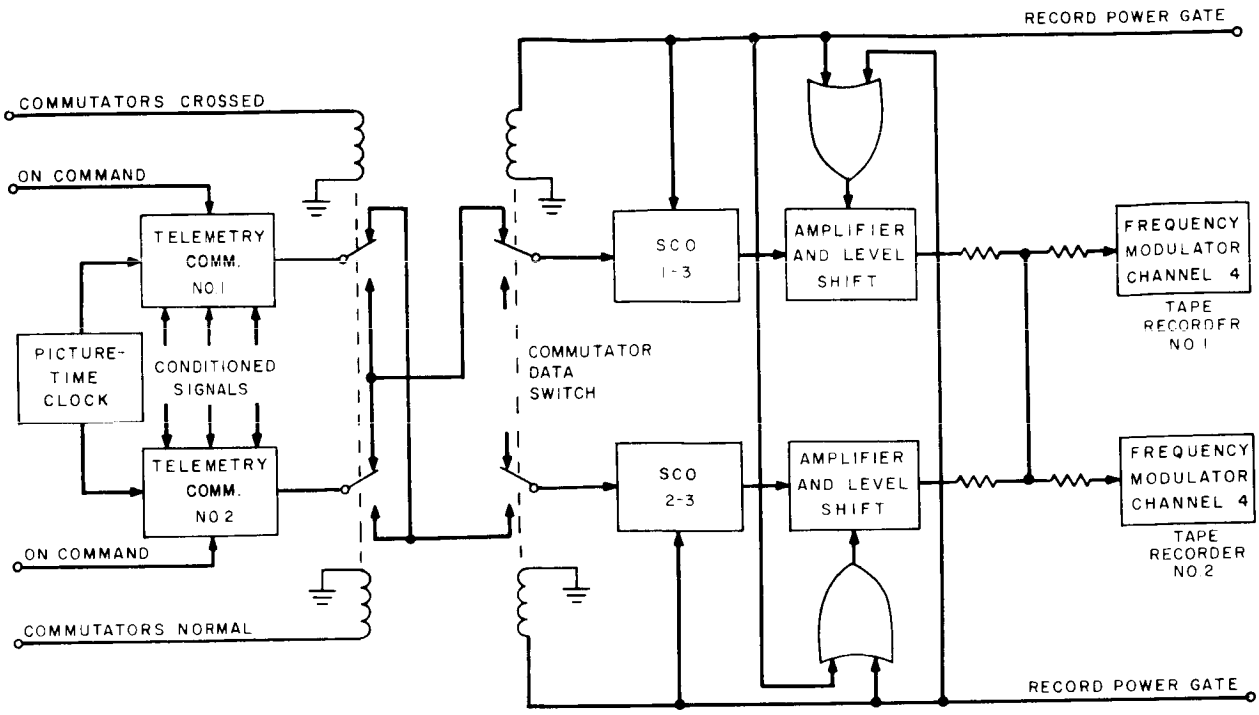

Figure 4-VI-2. Recording Channel 4 Telemetry and Picture-Time Clock on the OT-2/AVCS Spacecraft, Block Diagram

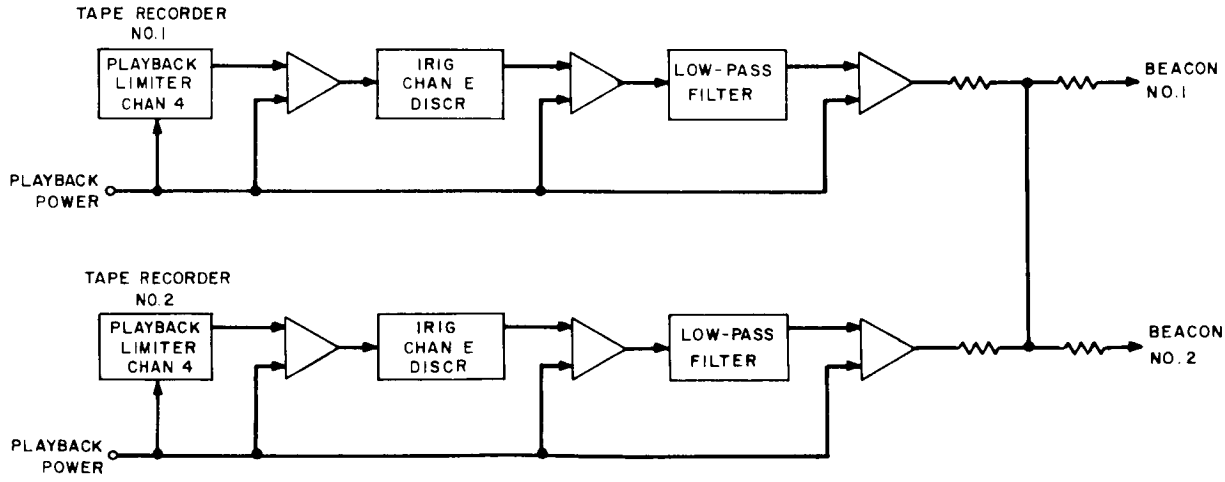

Figure 4-VI-3. Playback of Channel 4 Telemetry and Picture-Time Clock on the OT-2/AVCS Spacecraft, Block Diagram

on channel 1 or 2. Figure 4-VI-2 shows the switching used to accomplish the telemetry recording.

The shutter pulse from either programmer issues an "on" command to telemetry commutator No. 1 or No. 2. The output of the operating commutator is then coupled to SCO 1-3 or SCO 2-3, depending upon whether the commutators are normal or crossed. In either event, the commutated signals modulate an SCO whose output is then amplified, shifted in d-c level, and applied to the frequency-modulator in channel 4 of each tape recorder. The d-c level is shifted so that the SCO output will be centered around the voltage that produces the IRIG Channel E subcarrier in the frequency-modulators of channel 4 of the tape recorder.

During the initial delay period in the commutator, picture-time clock signals are directly coupled through the commutator; after the delay expires, the commutator becomes operational, selecting conditioned telemetry signals.

c. Playback of Channel 4 Telemetry

As shown in Figure 4-VI-3, when the tape recorder plays back, the output of its playback-limiter is demodulated by an IRIG Channel E discriminator and filtered, recovering the modulation which lies in IRIG Channel 9 (third SCO output). This output is then resistively coupled to both beacon transmitters. Circuitry which performs this function is provided for each tape recorder, and is operated by recorder playback power. During recorder playback, power is removed from the third SCO (1-3 and 2-3) of each beacon.

B. SUBSYSTEM ANALYSIS

1. Beacon Modulation

a. General

The beacon modulation system has been studied and the following conclusions have been reached:

(1) The 50-milliwatt AM beacons presently employed on TIROS satellites will not be adequate for reliable transmission of telemetry data. The orbital altitude of 750 nautical-miles and the requirement for a third SCO have necessitated investigation of a new beacon for the OT-2 mission.

(2) The use of a receiver with a narrow carrier-tracking filter and synchronous detection can permit a reduction in the threshold of the first demodulator. The significant threshold in the telemetry system should then become the threshold of the FM subcarrier demodulators rather than that of the receiving system.

(3) The modulation scheme compatible with the preferred receiving system and permitting the highest subcarrier "power-packing density" will be the optimum telemetry system. It is shown in Section VII that this can best be accomplished by phase-modulation of the beacon transmitter; therefore an FM-PM telemetry system will be used.

b. Selection of Beacon Subcarrier Frequencies

The beacon subcarrier frequencies to be used have been chosen so as to minimize harmonic and intermodulation distortion. The actual frequencies used are also chosen to match the desired information bandwidths; these frequencies comply with the recommended IRIG modulating signal bandwidths.

c. Modulating Bandwidths

(1) Attitude-Sensor Data

This data consists of positive and negative pulses, generated during horizon crossings. These pulses should have a "rise" time of the order of 20 milliseconds for accurate timing. This corresponds to a low-pass bandwidth of

$$B_{lp} = \frac{1}{2\,T_{rise}} = \frac{1}{2 \times 2 \times 10^{-2}} = 25 \text{ cps.}$$

The lowest IRIG channel number which is recommended for a 25-cps low-pass modulating bandwidth is Channel No. 6 (1700 cps ± 7.5 percent). Therefore, it is recommended that channels no lower than Channel No. 6 be utilized for transmitting horizon-sensor pulses.

(2) Commutated Telemetry Data

This data in the APT system places the most stringent requirement on the beacon and telemetry subsystem in terms of low-pass bandwidth requirements. This is due to the requirement for 70 percent of the ungated data to be flat, i.e., the data must become flat within the first 30 percent of the commutated pulse-period of 60 milliseconds if a 16-2/3 pps sampling rate is used. An 18-millisecond rise time will be assumed as the required "rise" time of the commutated signal. As in the analysis of the attitude-sensor data, the low-pass bandwidth required is

$$B_{lp} = \frac{1}{2\,T_{rise}} = \frac{1}{2 \times 18 \times 10^{-3}} = 27.7 \text{ cps.}$$

Thus, IRIG Channel 7 or higher would be completely suitable. However in the AVCS system, the commutated data is preceded by picture-time data. This data is digital at a 50-pps rate, and hence requires IRIG Channel 9 or a higher frequency Channel. The optimum selection of SCO's to correspond to each data input becomes a function of the intermodulation and harmonic distortion in each of the possible combinations of SCO's.

2. Channel Cross-Talk

Table 4-VI-1 shows the ranges of harmonics accompanying each SCO. It is desirable that the harmonics of one channel do not lie in the bandpass of any other channel. The table will be valuable in making a first-order estimate of the desirable combination of channels. It is also desirable to keep the highest channel number as low as possible so that the information bandwidth will be held as low as possible.

Table 4-VI-1 indicates that Channels 7, 8, and 9 can be used without fear of harmonic interference in the higher channels. Adjacent channel crosstalk will be down at least 20 db, if standard IRIG filters are used for separating the channels. Therefore, Channels 7, 8, and 9 will be employed in the OT-2 system.

3. Errors in V-Head Sensor Data

The basic construction of the V-head sensors is the same as that of the orthogonal horizon-sensor described in Section 4-IV, but without the threshold amplifier. However, since the function of this scanner is to provide signals for attitude determination, there are differences in the detailed design requirements. In this application the amplifier transient response is the more important parameter. This is because it is necessary to locate both the sky-to-earth transition and the earth-to-sky horizon crossings. "Hot" and "Cold" disturbances, at a point just before the sensor-view crosses from earth-to-sky, can cause uncertainties in locating the horizon. The transient response of the amplifier is optimized to reduce these uncertainties. In addition, the amplifier must have a short recovery time in the event that the sun's rays fall directly on the sensor and cause amplifier overload. (The range of sun angles that can cause overload can be greatly reduced by restricting the spectral response of the horizon sensor.)

The desirability of a more uniform response from the bolometer while viewing earth and of a reduced response to the sun has led to a change in the spectral response range of the V-head horizon sensors. A large amount of signal variation while viewing earth occurs in the 8 to 2 micron "window" from the wide temperature range in cloud tops. The energy received from the sun becomes greater at wavelengths less than 8 microns. For these reasons, filters to optimize the bolometer response in the spectral region from 13 to 23 microns are desirable.

TABLE 4-VI-1. HARMONIC INTERFERENCE BETWEEN IRIG CHANNELS

Channel	Lower Band Edge	Upper Band Edge	Range of Second Harmonics	Range of Third Harmonics	Range of Fourth Harmonics	Channels Affected by Harmonics
	(cps)	(cps)	(cps)	(cps)	(cps)	
5	1202	1398	2,404 - 2,796	3,606 - 4,194	4,808 - 5,592	2nd - 7 and 8 3rd - 9 4th - 10
6	1572	1828	3,144 - 3,656	4,716 - 5,484	6,288 - 7,312	2nd - 8 and 9 3rd - 10 4th - 11
7	2127	2473	4,254 - 4,946	6,381 - 7,419	8,508 - 9,892	2nd - none 3rd - 11 4th - 12
8	2775	3225	5,550 - 6,450	8,325 - 9,675	11,100 - 12,900	2nd - 10 3rd - none 4th - 12
9	3607	4193	7,214 - 8,386	10,821 - 12,579	14,428 - 16,772	2nd - 11 3rd - 12 4th - >12
10	4995	5805	9,900 - 11,610	14,985 - 17,415	19,980 - 23,220	2nd - 12 3rd - >12 4th - >12
11	6799	7901	13,598 - 15,802	20,397 - 23,703	27,196 - 31,604	2nd - >12 3rd - >12 4th - >12

4. Errors in Housekeeping Data

The estimated accuracy of this system is as follows:

	Maximum Error (% of Full Scale)
(1) Commutator linearity and scatter:	0.4
(2) SCO linearity and drift:	1.25
(3) FM demodulator linearity and drift:	0.7
(4) Telemetry conditioner:	1.0
(5) Chart reading error:	3.0
RMS Total:	3.5

The commutator calibration points provide a means for correcting for system nonlinearity and drift. However, since they are accurate to 1 percent, they do not significantly increase the system measuring accuracy unless the other components drift out of specification.

C. SUMMARY OF TELEMETRY POINTS

1. Housekeeping (Commutator Sampled) Telemetry

a. OT-2/APT Spacecraft Telemetry Sampling

Table 4-VI-2 lists the parameters that are to be monitored on the OT-2/APT spacecraft and the preliminary commutator channel assignments.

b. OT-2/AVCS Spacecraft Telemetry Sampling

Table 4-VI-3 lists the parameters that will be monitored on the OT-2/AVCS spacecraft and the preliminary commutator channel assignments.

TABLE 4-VI-2. TELEMETRY POINT ASSIGNMENTS FOR APT

Telemetry Commutator Channel	Assignment
1	Calibration; 0 volts
2	Calibration; -5 volts dc
3	Calibration; -3.5 volts dc
4	Calibration; -1.5 volts dc
5	Solar-cell array current
6	Shunt limiter current
7	Battery No. 1; charge current
8	Battery No. 2; charge current
9	Battery No. 3; charge current
10	Marker; -5 volts dc
11	Solar-cell array test patch
12	Solar-cell array voltage
13	Battery No. 1; voltage
14	Battery No. 2; voltage
15	Battery No. 3; voltage
16	Unregulated bus voltage
17	Regulated bus voltage
18	High-level charger ON/OFF
19	Spare
20	Marker; -5 volts dc
21	Horizon Sensors in use
22	Video transmitter No. 1 or No. 2
23	Decoder No. 1; internal power ON/OFF
24	Decoder No. 2; internal power ON/OFF
25	Spin Coil No. 1

TABLE 4-VI-2. TELEMETRY POINT ASSIGNMENTS FOR APT (Continued)

Telemetry Commutator Channel	Assignment
26	Spin Coil No. 2
27	Programmer No. 1; camera sequencing mode
28	Programmer No. 1; horizon-sync counter
29	MASC control No. 1;
30	Marker; -5 volts dc
31	Programmer No. 2; camera sequencing mode
32	Programmer No. 2; horizon-sync counter
33	MASC control No. 2
34	Coil enable telemetry
35	Camera No. 1 or No. 2
36	Programmer No. 1; internal power ON/OFF
37	Programmer No. 2; internal power ON/OFF
38	Programmer No. 1 or No. 2; shift enable ON
39	QOMAC coil
40	Marker; -5 volts dc
41	Programmer No. 1; T_0 counting
42	Programmer No. 1; true count enable
43	Programmer No. 2; T_0 counting
44	Programmer No. 2; true count enable
45	QOMAC mode
46	Magnetic-bias coil polarity
47	Magnetic-bias switch position
48	Spare
49	Spare
50	Marker; -5 volts dc

TABLE 4-VI-2. TELEMETRY POINT ASSIGNMENTS FOR APT (Continued)

Telemetry Commutator Channel	Assignment
51	Receiver No. 1: AGC
52	Receiver No. 2; AGC
53	Camera No. 1; G1 voltage
54	Camera No. 1; focus current
55	Camera No. 1; vidicon filament
56	Camera No. 1: horizontal and vertical deflection
57	Camera No. 1; -6.3 volt regulator
58	Camera No. 1; modulator
59	Camera No. 1; RF drive
60	Marker; -5 volts dc
61	Camera No. 1 or No. 2; 4800 cps
62	Camera No. 2; G1 voltage
63	Camera No. 2; focus current
64	Camera No. 2; vidicon filament
65	Camera No. 2; horizontal and vertical deflection
66	Camera No. 2; -6.3 volt regulator
67	Camera No. 2; modulator
68	Camera No. 2; RF drive
69	Spare
70	Marker; -5 volts dc
71	Spin coil No. 1
72	Spin coil No. 2
73	Battery No. 1; temperature
74	Battery No. 2; temperature
75	Battery No. 3; temperature

TABLE 4-VI-2. TELEMETRY POINT ASSIGNMENTS FOR APT (Continued)

Telemetry Commutator Channel	Assignment
76	Baseplate temperature No. 1
77	Video transmitter unit temperature
78	Solar-cell array top temperature
79	Solar-cell array side temperature
80	Marker; -5 volts dc
81	Camera No. 1; focus coil temperature
82	Camera No. 1; target temperature
83	Camera No. 1; power converter temperature
84	Camera No. 2; focus coil temperature
85	Camera No. 2; target temperature
86	Camera No. 2; power converter temperature
87	Baseplate temperature No. 2
88	Spare
89	Sync
90	Sync

TABLE 4-VI-3. TELEMETRY POINT ASSIGNMENTS FOR AVCS

Telemetry Commutator Channel	Assignment
1	Calibration; 0 volts dc
2	Calibration; -5 volts dc
3	Calibration; -3.5 volts dc
4	Calibration; -1.5 volts dc
5	Solar-cell array current

TABLE 4-VI-3. TELEMETRY POINT ASSIGNMENTS FOR AVCS (Continued)

Telemetry Commutator Channel	Assignment
6	Solar-cell array test patch
7	Shunt limiter current
8	Battery No. 1; charge current
9	Battery No. 2; charge current
10	Marker; -5 volts dc
11	Solar-cell array voltage
12	Battery No. 1; voltage
13	Battery No. 2; voltage
14	Unregulated bus voltage
15	Regulated bus voltage
16	High-level charger ON/OFF
17	Regulator selection
18	Spin coil No. 1
19	Spin coil No. 2
20	Marker; -5 volts dc
21	QOMAC coil
22	QOMAC mode
23	MASC control No. 1
24	MASC control No. 2
25	Magnetic-bias coil polarity
26	Magnetic-bias switch position
27	Horizon sensors in use
28	Decoder No. 1; internal power ON/OFF
29	Decoder No. 2; internal power ON/OFF
30	Marker; -5 volts

TABLE 4-VI-3. TELEMETRY POINT ASSIGNMENTS FOR AVCS (Continued)

Telemetry Commutator Channel	Assignment
31	Programmer No. 1; camera sequencing mode
32	Programmer No. 1; orbit counting
33	Programmer No. 1; true count enable ON/OFF
34	Programmer No. 1; internal power ON/OFF
35	Programmer No. 2; camera sequencing mode
36	Programmer No. 2; orbit counting
37	Programmer No. 2; true count enable ON/OFF
38	Programmer No. 2; internal power ON/OFF
39	Programmer No. 1 or No. 2; shift enable ON
40	Marker; -5 volts dc
41	Camera No. 1; positive high voltage
42	Camera No. 1; focus current
43	Camera No. 1; horizontal sync
44	Camera No. 1; vertical sync
45	Camera No. 1; vidicon filament current
46	Camera No. 1; video output
47	Camera No. 1; 6-volt power
48	Camera No. 1 or No. 2 selected
49	Spare
50	Marker; -5 volts dc
51	Camera No. 2; positive high voltage
52	Camera No. 2; focus current
53	Camera No. 2; horizontal sync
54	Camera No. 2; vertical sync
55	Camera No. 2; vidicon filament current

TABLE 4-VI-3. TELEMETRY POINT ASSIGNMENTS FOR AVCS (Continued)

Telemetry Commutator Channel	Assignment
56	Camera No. 2; video output
57	Camera No. 2; 6-volt power
58	Beacon Selection
59	Video transmitter selection
60	Marker; -5 volts dc
61	Recorder selection
62	Recorder No. 1; pressure
63	Recorder No. 1; channels 1 and 2 record drive
64	Recorder No. 1; channels 1 and 2 playback amplifier
65	Recorder No. 1; motor drive
66	Recorder No. 2; pressure
67	Recorder No. 2; channels 1 and 2 record drive
68	Recorder No. 2; channels 1 and 2 playback amplifier
69	Recorder No. 2; motor drive
70	Marker; -5 volts dc
71	Video transmitters; temperature
72	Spin coil No. 1
73	Spin coil No. 2
74	Recorder No. 1; temperature
75	Recorder No. 2; temperature
76	Camera No. 1 electronics; temperature
77	Camera No. 1 head; temperature
78	Camera No. 2 electronics; temperature

TABLE 4-VI-3. TELEMETRY POINT ASSIGNMENTS FOR AVCS (Continued)

Telemetry Commutator Channel	Assignment
79	Camera No. 2 head; temperature
80	Marker; -5 volts dc
81	Receiver No. 1; AGC
82	Receiver No. 2; AGC
83	Battery pack No. 1; temperature
84	Battery pack No. 2; temperature
85	Solar cell array; top temperature
86	Solar cell array; side temperature
87	Baseplate temperature No. 1
88	Baseplate temperature No. 2
89	Not available for telemetry
90	Not available for telemetry

D. BEACON AND TELEMETRY SUBSYSTEM COMPONENTS

1. Telemetry Commutators

Two telemetry commutators, one for each beacon, will sample the various telemetry channels in response to ground command. The commutators, which are similar to those used in TIROS "I", are solid-state and meet the following specifications:

Manufacturer:	Dynaplex
Power Requirement:	-24.5 vdc, 100 milliamperes
Channels:	90
Sampling Rate:	16-2/3 pps
Input Signal Level:	0 to -5.0 volts
Output Signal Level:	0 to -5 volts into 10 kilohm load (minimum)
PAM Ungated Output:	99% duty cycle

Frame Pulse:	60-ms pulse from 0 to -20 volts
Picture-time gate:	input gate enabled during 1.2-second delay
DC Power Output:	10 ma from 10-vdc supply
Weight:	2.0 lb
Size:	3-1/4 x 2-1/4 x 4-1/2 in.

2. Subcarrier Oscillators

Six subcarrier oscillators (SCO's) will be employed in the communications subsystem. Two will operate on IRIG Channel No. 7, two will operate on IRIG Channel No. 8, and two will operate on IRIG Channel No. 9. The redundant SCO's are used as backup units.

The IRIG Channel No. 7 SCO is currently planned for use on TIROS "I", and is being built by Sonex, Inc. No difficulty in obtaining a similar Channel No. 8 and a similar Channel No. 9 SCO is anticipated. The specifications for the SCO's are tabulated below:

Manufacturer:	Sonex, Phila.
Model:	Tex-3003, solid state
Frequency, F_c:	
Channel No. 7;	2.3 kc
Channel No. 8;	3.0 kc
Channel No. 9;	3.9 kc
Deviation:	±7.5 percent
Deviation Bandwidth, dbw:	15 percent of F_c
Input Impedance:	750 kilohms, (minimum)
Input Sensitivity:	0 to -5.0 vdc with -2.5 v producing F_c; less negative input decreases frequency
Output Impedance:	50 kilohms (maximum)
Linearity:	±0.25 percent (from best straight line)
Distortion:	Less than 1 percent
Amplitude Modulation:	1.0 db
Output Voltage:	Adjustable from 0 to 1.5 volts peak-to-peak into an 8 kilohm load; ac coupled

Supply Voltage:	-24.5 vdc (15 ma)
Supply Voltage Stability:	Internal regulator limits F_c deviation to less than 0.15 percent dbw-per-volt change in -24.5 v supply voltage
F_c Drift, Long Term:	Less than ±1 percent of dbw at 22°C
Temperature Stability:	F_c stable within ±1.5 percent dbw over temperature range of -20°C to +85°C (best straight-line measurement)
Weight:	3.0 ounces
Size:	1.5 x 1.6 x 1.0 in.

3. Beacon Transmitter

A phase-modulated transmitter similar to the one used on the RELAY satellite will be quite suitable for use on the OT-2 spacecraft. The worst-case of 250-milliwatt output power can be realized with a maximum input power of two watts. Tentative specifications for the transmitter are listed below:

Manufacturer:	RCA
Modulation:	Phase
Carrier:	136.77 Mc
Deviation:	2.4 radians peak
Carrier Stability:	±0.005 percent
Power Output:	250 milliwatts
Power Input:	2 watt (maximum)
Supply Voltage:	-24.5 vdc
Weight:	1 pound
Size:	4 x 4 x 1.25 in.

4. Crossed-Dipole Antenna and Coupling Network

a. Crossed-Dipole Antenna

The antenna to be used for beacon and telemetry transmission on the OT-2 spacecraft is essentially the same as has been used on all previous TIROS missions, where the antennas have proven to be satisfactory.

b. Coupling Network

The printed-circuit hybrid-coupler that was used with previous TIROS spacecraft beacon transmitters will be modified for the new beacon frequency.

E. REDUNDANCY

1. Component Data Chains

The beacon and telemetry subsystem is redundant except for the antennas, solar-aspect sensor, and V-head sensor. However, spacecraft attitude can be measured with solar-aspect sensor data and the output from a single channel of the V-head sensor. Attitude can be also determined, but less accurately, from the output of a single channel of the V-head sensor alone. Hence, although the equipment itself is not redundant, operational redundancy exists.

Table 4-VI-4 lists the components in the series data chains. A failure of any of the components within the chain will eliminate that path for data. For example, if SCO 1-1 fails, chain A will not be able to transmit data. If SCO 1-3 fails, chains E, H, J, K, N, and Q will not be able to transmit data. A single failure will not cause loss of data if the data source is redundant. The combinations and data loss resulting from failures can be determined from the list of data chains in Table 4-VI-4 and Figure 4-VI-1.

2. Data Switches

The relays that control commutators No. 1 and No. 2 (see Figure 4-VI-4) are of the latching type and can be set by digital command from either of the two decoders or by a long enable tone (15 seconds) from either of the two decoders. The relays can be reset either by the "End-of-Frame" pulse from the commutator by switching beacons and requesting telemetry.

The decoder No. 1 and No. 2 data switches are operated by decoder power, which is "on" only when the FSK tone is present. These switches are not latching; therefore a failure will leave the relay contacts in the de-energized position, permitting transmission of solar-aspect data and orthogonal horizon-sensor data.

The solar-aspect sensor data switch is controlled by a latching relay. The relay can be commanded "on" or "off" from either decoder. If it fails in the solar-aspect "on" position, the solar-aspect sensor will run continuously and orthogonal horizon-sensor data will be interrupted; however data verification, and telemetry commutator data are not interrupted. A failure in the "off" position, prohibits receipt of data from the solar-aspect sensor.

TABLE 4-VI-4. COMPONENTS IN VARIOUS SERIES DATA CHAINS

Chain	Components
A	V-head sensor, side A SCO 1-1 Beacon 1
B	V-head sensor, side B SCO 1-2 Beacon 1
C	V-head sensor, side A SCO 2-1 Beacon 2
D	V-head sensor, side B SCO 2-2 Beacon 2
E	Telemetry commutator No. 1 SCO 1-3 Beacon 1
F	Telemetry commutator No. 2 SCO 2-3 Beacon 2
G	Telemetry commutator No. 1 SCO 2-3 Beacon 2
H	Telemetry commutator No. 2 SCO 1-3 Beacon 1
J	Decoder No. 1 command verification Commutator data switch No. 1 SCO 1-3 Beacon 1
K	Decoder No. 2 command verification Decoder No. 1 data switch (non-latching) Commutator data switch No. 1 SCO 1-3 Beacon 1
L	Decoder No. 2 command verification Decoder No. 2 data switch (non-latching) Commutator data switch No. 2 SCO 2-3 Beacon 2
M	Decoder No. 2 command verification Commutator data switch No. 2 SCO 2-3 Beacon 2
N	Solar-aspect sensor Decoder No. 2 data switch Decoder No. 1 data switch Commutator data switch No. 1 SCO 1-3 Beacon 1
P	Solar-aspect sensor Decoder No. 1 data switch Decoder No. 2 data switch Commutator data switch No. 2 SCO 2-3 Beacon 2

TABLE 4-VI-4. COMPONENTS IN VARIOUS SERIES DATA CHAINS (Continued)

Chain	Components	Chain	Components
Q	Orthogonal horizon-sensor data Solar-aspect sensor data switch Decoder No. 2 data switch Commutator data switch No. 1 SCO 1-3 Beacon 1	R	Orthogonal horizon-sensor data Solar-aspect sensor data Decoder No. 1 data switch Decoder No. 2 data switch Commutator data switch No. 2 SCO 2-3 Beacon 2

SECTION VII. CDA/SPACECRAFT COMMUNICATION INTERFACE

A. COMMAND RECEPTION AND MARGINS

1. General

Programming commands will be transmitted to the OT-2 spacecraft only from the CDA stations. These programs will be composed of encoded command signals that frequency-shift-key (FSK) subcarriers in the CDA station. The subcarriers, in turn, amplitude-modulate the command transmitter which feeds the commands to the circularly polarized antenna for transmission to the spacecraft. On the OT-2/APT spacecraft, the command signals are received by the crossed-dipole baseplate antenna and coupled, in-phase, to the command receivers. The resulting command antenna pattern is almost identical to the dipole pattern now used with TIROS equipment. On the OT-2/AVCS spacecraft the normal TIROS receiving dipole feeds the command receivers. Verification of decoded FSK commands is provided by modulation of one of the spacecraft beacon subcarriers.

Although the command signals are received with linear polarization, the commands are transmitted from the ground with circular polarization. This method of coupling results in a 3-db polarization loss. Figures 4-VII-1 and 4-VII-2 are plots of the effective antenna patterns used in the calculation of system margins in this study report. Figure 4-VII-1 illustrates the crossed-dipole radiation pattern for the beacon transmission and 4-VII-2 the dipole pattern for command reception.

2. Link Geometry and Path Loss

Link geometry is fundamental in determining communication parameters such as look-angle and path loss. Look-angle, θ, is defined as the angle between the spacecraft's spin axis and a line from the ground antenna to the spacecraft. This angle is a minimum at conditions of maximum slant range when the spin-axis is in the plane formed by the ground-to-satellite line and the local vertical. For the 860-statute mile OT-2 orbit (750 nautical miles), the maximum slant range at a 5-degree antenna elevation angle can be shown to be 2400 statute miles. Correspondingly, the minimum spacecraft look-angles, θ, can be shown to be 35 degrees and 145 degrees. Table 4-VII-1 lists values of path loss for transmission in the 148-Mc band at various antenna elevation angles. Although the look-angles corresponding to these elevation angles are also given, the antenna pattern loss due to look-angle is not included in the path-loss figures.

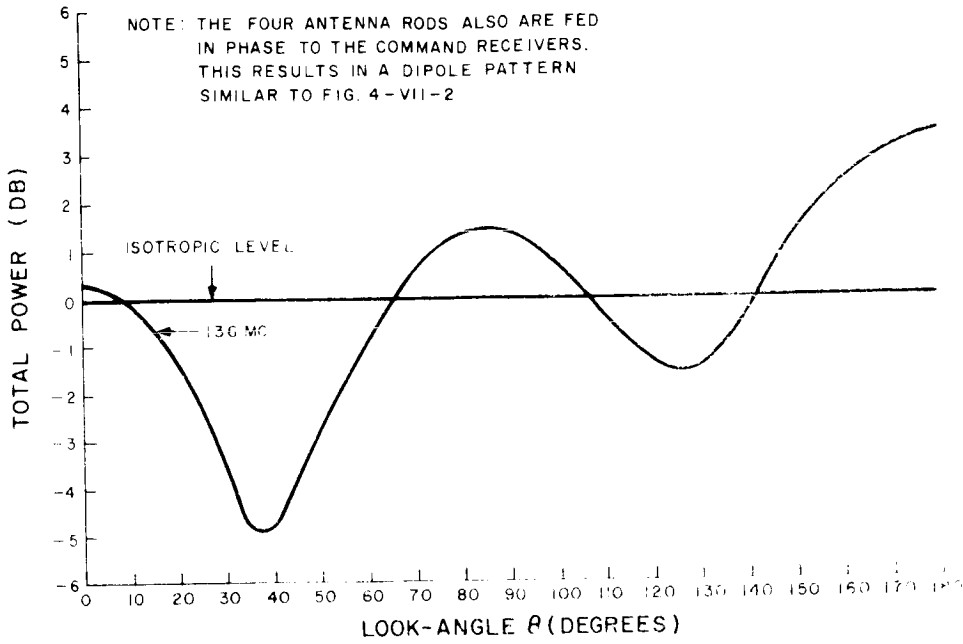

Figure 4-VII-1. Power Versus Look Angle for Circularly Polarized Beacon Transmission

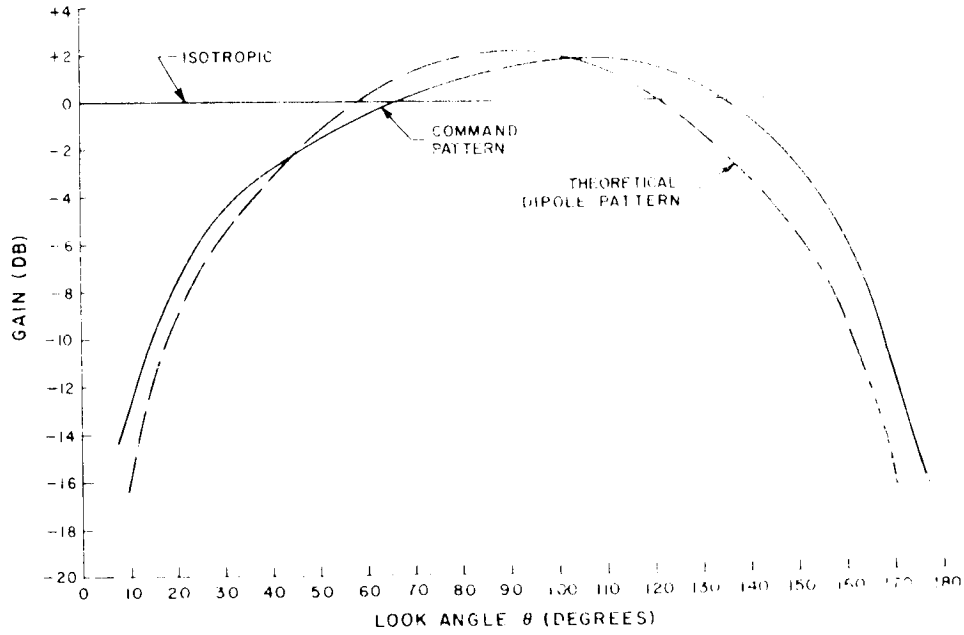

Figure 4-VII-2. OT-2/APT-TV Transmission Single Dipole-Antenna Radiation Pattern

TABLE 4-VII-1. PATH LOSS AND SPACECRAFT LOOK-ANGLE AT VARIOUS ANTENNA ELEVATION ANGLES FOR THE 148-MC COMMAND LINK

Ground Antenna Elevation Angle (degrees)	Path Loss (db)	Spacecraft Look-Angle, θ (degrees)
5	148.0	35
10	146.8	36
15	145.6	37
20	145.0	39
25	144.0	41

3. Doppler Shift and Stability

Doppler shift and frequency stability of equipment must be considered in determining RF bandwidth requirements. The shift is indicated by the following expression and is a maximum at the minimum elevation angle:

$$\Delta F = F \frac{V}{c} \cos B,$$

where V is spacecraft velocity, c is the velocity of light, and B is the angle between the ground station and the direction of the spacecraft's velocity vector. At the command link frequency of 148 Mc, the maximum Doppler shift is ± 2.88 kc or a total of 5.8 kc.

Frequency stability will be considered as $\pm$ 0.005 percent of the carrier frequency. This figure includes instabilities in the transmitter and the receiver local oscillator. At the command frequency of 148 Mc, the stability is $\pm$ 7.4 kc or a total of 14.8 kc.

4. Noise Temperature and Noise Power

External noise received by an antenna is a function of link frequency. Below one gigacycle, the major source of external noise is cosmic, and noise temperature varies approximately as $(\text{frequency})^{-2.7}$. Figure 4-VII-3 shows the maximum values of the galactic center, the maximum value of the coolest 95 percent and 99 percent of the radio sky, and the minimum value of cosmic or sky noise. The 700°K sky temperature for 148 Mc used in the calculations is taken from the "95 percent" curve.

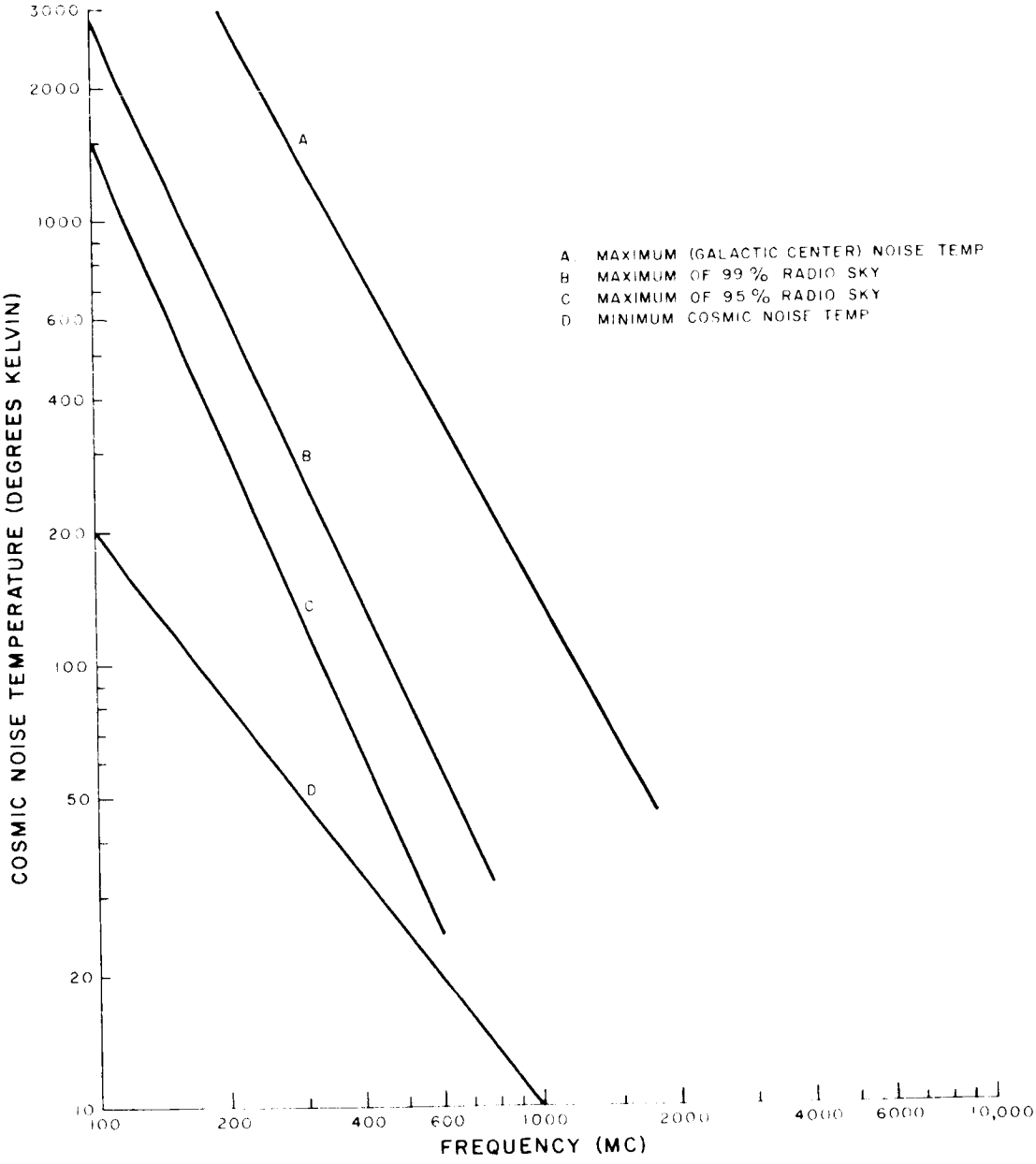

Figure 4-VII-3. Cosmic Noise Temperature Versus Frequency

The noise power at the receiving system input can be calculated as follows:

$$P_N = K T_{eff} B_{if} = -119 \text{ dbm},$$

where

K is Boltzman's constant $(1.38 \times 10)^{-23}$ joules/°K),

$T_{eff} = T_{sky} + T_{rec} = 2240°K$,

T_{rec} is receiver preamplifier noise $\left[290 \text{ (NF-1) } °K = 1540°K\right]$,

$T_{sky} = 700°K$,

NF = 8 db (maximum), and

B_{if} is receiver IF bandwidth (40 kc).

5. System Thresholds

a. General

With the noise power calculated above and acknowledge of the characteristics of the receiving system, a system threshold can be calculated. These figures will then be compared with the received signal power, and system margin predicted. System margin is defined as the difference between the calculated received power and the system threshold.

b. Command Link

The command receiver sensitivity is specified at -107 dbm. This is the level which provides 0.7 volt rms to the decoding subsystem, and is the level that will be considered as the command system threshold in the link calculations. This threshold level is chosen since the decoder interface requires a minimum level of 0.5 volt, whereas the receiver AGC characteristic specification provides a minimum signal output level of 0.7 volt for a -107 dbm signal input. The receiver input noise power for a 40-kc IF bandwidth is -119 dbm. Thus a -107 dbm signal power level provides a 12 db carrier-to-noise ratio in the 40-kc IF bandwidth. The command system is not limited by the 12-db signal-to-noise ratio in the IF bandwidth as it increases in the subcarrier filter as $\frac{B_{if}}{2_{fm}}$.

For the command system this is $\frac{40 \text{ kc}}{2 \times 30 \text{ cps}}$, or 28 db since the fastest bit rate acceptable by the receiver integrator is 30 cps. Thus the signal-to-noise ratio into the decoder Schmitt trigger is 12 + 28, or 40 db.

6. CDA Commands to Spacecraft

a. RF Bandwidth

The command encoder uses frequency-shift-keying (FSK) of IRIG tones to amplitude-modulate the command transmitter. "Ones" and "zeros" consist of +7.5 percent and -7.5 percent frequency deviations about the SCO center frequencies. The required RF bandwidth is determined by the highest tone frequency and the highest bit rate, which are 10.5 kc and 10 bps, respectively. Information bandwidth, B_i, can be estimated as follows:

$$B_i \approx 2 \left[f_t + f_m (\sigma + 1) \right] .$$

$$B_i \approx 2 \left[10.5 + \frac{50 \ (17)}{1000} \right] \text{kc}$$

$$B \approx 2 \ (11.35) \text{ or } 22.7 \text{ kc},$$

where

f_t, the highest tone frequency = 10.5 kc,

f_d, the maximum deviation = +0.79 kc,

f_m the 5th harmonic (for good rise-time characteristics) = 50 cps, and

σ, the deviation $= \frac{f_d}{f_m}$ = 16.

The total RF bandwidth for the command link to the spacecraft is as follows:

Information	22.7 kc
Doppler (750 n. mi)	5.8 kc
Stability (typical)	6.0 kc
Total RF Bandwidth	34.5 kc

The 6-db bandwidth of the recommended spacecraft command receiver is at least 40 kc and is adequate for command transmissions for tones no higher than IRIG Channel No. 12.

b. Received Power and Margin

For an orbital altitude of 750 nautical miles and an antenna elevation of 5 degrees, path loss in the command link is -148 db. Receiver threshold is -107 dbm, which is essentially a 1-microvolt signal. Since command reception by the OT-2/APT system is similar to a linearly polarized dipole pattern, a 3-db polarization loss is inherent in the link with a circularly polarized CDA station antenna. Received power and margin for both the OT-2/APT and OT-2/AVCS systems are determined as follows for an antenna elevation of 5 degrees:

Transmitter power (1000 watts)	+60.0 dbm
Spacecraft Antenna Gain (5°)	- 3.8 db (θ -35°)
CDA Station Antenna Gain	+10.0 db min
Line Losses	- 3.0 db
Polarization Loss	- 3.0 db
Path Loss	-148 db
Total Received Power	-87.8 dbm
Received Power for Each Receiver	-90.8 dbm
Receiver Threshold	-107.0 dbm
RF Margin	16.2 db

Table 4-VII-2 shows the variation of command link margin with antenna elevation angle. During launch phases, spacecraft attitude could be such that the command link involves small look-angles (θ). At these small θ values, dipole antenna gain is small since pattern nulls coincide with the spin-axis. Even at maximum slant range the received power does not decrease to receiver threshold except for θ values less than 5 degrees.

TABLE 4-VII-2. VARIATION OF OT-2 COMMAND LINK MARGIN WITH GROUND ANTENNA ELEVATION ANGLE

Ground Antenna Elevation Angle (degrees)	Received Signal Level (dbm)	Command System Margin (db)
5	90.8	16.2
10	89.7	17.3
15	88.2	18.8
20	87.0	20.0
25	85.0	21.2

B. BEACON RECEPTION AND MARGINS

1. Modulation System

a. General

The beacon system will use three IRIG FM subcarriers that modulate a transmitter. Three transmitter modulation schemes, PM, FM, and AM are considered with the following assumptions.

The use of a carrier-tracking "phase demodulator" is assumed for the FM-PM transmitter. The rms modulation index of all three subcarriers must be selected for an adequate ratio of P_c/P_{Total} to ensure carrier tracking. In addition, the modulation index must be low enough to avoid phase inversion of the carrier. An rms modulation index of one radian for the three multiplexed subcarriers is selected.*

The FM-PM ground receiver must use synchronous product detection of the incoming phase-modulated wave. The extremely narrow-band phase tracking loop, normally less than 100 cycles per second, permits the subcarrier demodulator to reach its threshold prior to the level at which the "carrier-tracking" loop fails.

The FM transmitter is assumed to have the same modulation index as the PM system. A conventional limiter-discriminator FM receiver will reach its threshold when the carrier-to-noise ratio in the IF bandwidth is 9 db.

---

*JPL Technical Report No. 32-215: "The Pioneer IV Lunar Probe; A Minimum Power FM-PM Design". Benn D. Martin, 15 March 1962.

When FM-AM is considered, the peak amplitude of the subcarriers will be chosen such that when they all reach their peak simultaneously, the modulation index will be 1.0. The ground receiver will use a carrier-tracking loop with synchronous AM detection.

Equal IF noise bandwidths (30 kc) can be assumed for all three systems.

b. FM-PM System

The use of synchronous product detection of the incoming phase-modulated wave permits the phase-demodulated output signal-to-noise ratio to decrease* linearly with input signal until the carrier-tracking loop loses "lock". This system will be designed to insure that the 12-db subcarrier demodulator signal-to-noise ratio is the significant threshold and that it will be reached simultaneously for all three subcarriers. The carrier power available at the level of subcarrier demodulator threshold will be well above the carrier-loop "in-lock" threshold.

The modulation index of the main carrier due to each subcarrier is selected in such a manner as to provide equal subcarrier-to-noise ratios at the output of the subcarrier filtering networks. The deviation on the main carrier is selected as being one radian (rms), a value which provides a nearly equal distribution of carrier power and subcarrier power, as will be shown. For the subcarrier-to-noise ratios to be equal at the output of the subcarrier bandpass filters, the peak deviation of each of the subcarriers must be proportional to the square root of the bandwidth of each subcarrier channel. The peak deviation is expressed as follows:

$$** \quad \frac{\Delta\theta_1}{\sqrt{B_1}} = \frac{\Delta\theta_2}{\sqrt{B_2}} = \frac{\Delta\theta_3}{\sqrt{B_3}},$$

where

$\Delta\theta_i$ is the peak deviation of the carrier due to the i^{th} subcarrier, and

B_i is the subcarrier filter bandwidth, and is equal to 15 percent of the IRIG subcarrier center frequency.

*This implies a receiver similar to the Electrac with no limiter preceding the PM detector and a proper AGC system.

**The three subcarriers chosen are IRIG Channels No. 7 through 9.

For an rms deviation of one radian:

$$\frac{\Delta\theta_1^2}{2} + \frac{\Delta\theta_2^2}{2} + \frac{\Delta\theta_3^2}{2} = (1)^2 .$$

Solving for the modulation index corresponding to each of the subcarriers.

$\Delta\theta_1$ = 0.707, the main carrier deviation due to the 2.3-kc subcarrier;

$\Delta\theta_2$ = 0.805, the main carrier deviation due to the 3.0-kc subcarrier; and

$\Delta\theta_3$ = 0.920, the main carrier deviation due to the 3.9-kc subcarrier.

The ratio of carrier power to total power is:

$$\frac{P_c}{P_{Total}} = \left[Jo(\Delta\theta_1) \cdot Jo(\Delta\theta_2) \cdot Jo(\Delta\theta_3) \right]^2 = 0.35,$$

or 35 percent of the total power is in the carrier. The available carrier level is then 4.6 db below total power.

Assuming a ground receiver similar to the Electrac in which the carrier tracking threshold is -166 dbm with a 1-cps bandwidth and -146 dbm with a 100-cps bandwidth, the required carrier power for "in-lock" threshold can be estimated at -146 dbm, the total power input required for tracking is:

-146 dbm + 4.6 db = -141.4 dbm.

The subcarrier system threshold occurs at a 12-db subcarrier signal-to-noise ratio and is calculated for one subcarrier as follows:

$$\frac{P_{sc_1}}{P_{Total}} = 2 \left[J_1(\Delta\theta_1) \cdot Jo(\Delta\theta_2) \cdot Jo(\Delta\theta_3) \right]^2$$

$$\frac{P_{sc_1}}{P_{Total}} = -10.1 \text{ db.}$$

$$\frac{B_{if}}{B_{sc_1}} = \frac{30 \text{ kc}}{0.35 \text{ kc}} = 86 = 19.3 \text{ db.}$$

Therefore,

$$P_{N_{sc}} = -122.5\text{*dbm} - 19.3 \text{ db} = -141.8 \text{ dbm.}$$

Total received power required at subcarrier demodulator threshold equals -141.8 dbm + 12 db + 10.1 db, or -119.7 dbm. Thus the input level required to reach subcarrier demodulator threshold of 12-db carrier-to-noise ratio is -119.7-(-141.4), or 21.7 db above that calculated for carrier tracking threshold. In this FM-PM system it is then evident that the system threshold is reached by the subcarrier demodulator before the PM carrier-locking threshold.

c. FM-FM System

Assuming the same modulation index as the FM-PM System, the conventional FM receiver threshold will occur at a carrier-to-noise ratio of 9 db. For the same receiver bandwidth and available noise power, the required signal input power is -122.5 dbm + 9 db, or -113.5 dbm. Note that the threshold of the first FM demodulator, rather than that of the second FM demodulator, is the controlling factor.

d. FM-AM System

The modulation index on the AM carrier is chosen to provide equal subcarrier signal-to-noise ratios at the receiver output and the peak modulation index is chosen not to exceed unity. The modulation index is expressed as follows:

$$\frac{M_1}{\sqrt{B_1}} + \frac{M_2}{\sqrt{B_2}} + \frac{M_3}{\sqrt{B_3}} ,$$

where

$$M_1 + M_2 + M_3 = 1.0,$$

$$M_1 = 0.29,$$

$$M_2 = 0.33, \text{ and}$$

$$M_3 = 0.38.$$

---

*Refer to Section 4-VII-B, Paragraph 4.

If synchronous detection of the carrier is used, similar to that with PM modulation, then system threshold will be due to the subcarrier demodulator input-signal threshold. This will be an improvement over the conventional AM receiver. For this case, it can be shown that the total power is 1.168 times the carrier power, and for the first subcarrier:

$$P_{Total} = P_c + \frac{P_c}{2} (M_1^2 + M_2^2 + M_3^2),$$

$$= (P_c + 0.5 P_c (0.29^2 + 0.33^2 + 0.38^2),$$

$$= 1.168 P_c.$$

$$P_{sc1} = \frac{P_c}{2} (M1)^2 = 0.042 P_c \text{ or } P_c = \frac{P_{sc1}}{0.042}.$$

$$P_{Total} = 1.168 \left(\frac{P_{sc1}}{0.042} \right) = 28 P_{sc1}.$$

$$\frac{P_{sc1}}{P_{Total}} = \frac{1}{28} = -14.5 \text{ db.}$$

It can be seen for the lowest subcarrier, the subcarrier power is down 14.5 - 10.1, or 4.4 db from the FM-PM system. This means 4.4 db of additional transmitter power is required in the FM-AM system (-119.7 + 4.4 = -115.3 dbm) to produce a threshold equivalent to that of the FM-PM system using synchronous detection techniques. The other subcarriers require the same level.

e. Comparison of FM Modulation Systems

A PM beacon based on the RELAY design should provide 250 milliwatts of RF power with a maximum of 2-watts input. An AM beacon supplying the same power must be capable of delivering one watt of peak power output at 100-percent modulation. A low order of modulation distortion is required and feedback circuits will have to be added to keep distortion to a reasonable level. This still does not include the efficiency of the modulator as considerable audio power must be developed for high-level modulation of the transmitter. It is anticipated that a practical design to provide rated power over the temperature environment will require 2.5-watts input power for the transmitter and 0.7 watts for the modulator, a total of 3.2 watts. To provide the same

threshold level as PM, 4.4 db additional AM power would be required. In terms of power-packing efficiency, it can be seen that the PM transmitter is superior to the AM transmitter.

Table 4-VII-3 gives a comparison of the three systems discussed for the OT-2 system and provides the justification of the selection of the FM-PM system.

TABLE 4-VII-3. THRESHOLDS AND SIGNAL-TO-NOISE RATIOS OF FM-AM, FM-FM, AND FM-PM SYSTEMS

System	Threshold	Signal-To-Noise Ratio of Subcarrier	Notes
FM-AM	-115.3 dbm	12 db	Carrier-Tracking Loop
FM-FM	-113.5 dbm	12 db	Conventional FM Receiver
FM-PM	-119.7 dbm	12 db	Phase demodulator and carrier tracking loop

Since the 12-db signal-to-noise ratio would be adequate at the inputs to the subcarrier demodulators, the FM-PM system requires lower transmitter power at system threshold than does either the FM-AM or FM-FM system.

2. Link Geometry and Path Loss

Link geometry is fundamental in determining communication parameters such as look-angle and path loss. Look-angle, θ, is defined as the angle between the spin axis and a line from the ground antenna to the spacecraft. This angle is a minimum at conditions of maximum slant range when the spin-axis is in the plane formed by the ground-to-satellite line and the local vertical. For the 860-statute mile OT-2 orbit (750 nautical miles), the maximum slant range at a 5-degree antenna elevation angle can be shown to be 2400 statute miles. Correspondingly, the minimum spacecraft look-angles, θ, can be shown to be 35 degrees and 145 degrees. Table 4-VII-4 lists values of path loss at 136 Mc for various antenna elevation angles. Although the look-angles corresponding to these elevation angles are also given the antenna pattern loss due to look angle is not included in the path-loss figures.

TABLE 4-VII-4. PATH LOSS AND SPACECRAFT LOOK-ANGLE AT VARIOUS GROUND ANTENNA ELEVATION ANGLES FOR THE 136-MC BEACON LINK

Ground Antenna Elevation Angle (degrees)	Path Loss (db)	Spacecraft Look-Angle, θ (degrees)
5	147.2	35
10	146.0	36
15	144.8	37
20	144.2	39
25	143.2	41

3. Doppler Shift and Stability

Doppler shift and frequency stability of equipment must be considered in determining RF bandwidth requirements. The shift is indicated by the following expression and is a maximum at the minimum elevation angle:

$$\Delta F = F\frac{V}{c} \cos B$$

where V is spacecraft velocity, c is the velocity of light, and B is the angle between the particular ground station and the direction of the spacecraft's velocity vector. At the beacon link frequency of 136 Mc, the maximum Doppler shift is ±2.65 kc or a total of 5.3 kc.

Frequency stability will be considered as ±0.005 percent of the carrier frequency. This figure includes instabilities in the transmitter and the receiver local oscillator. At the frequency of 136 Mc, the stability is ±6.8 kc or a total of 13.6 kc.

4. Noise Temperature and Noise Power

External noise received by an antenna is a function of link frequency. Below one gigacycle, the major source of external noise is cosmic, and noise temperature varies approximately as $(\text{frequency})^{-2.7}$ Figure 4-VII-3 shows the maximum values of the galactic center, the maximum value of the coolest 95 percent and 99 percent of the radio sky, and the minimum value of cosmic or sky noise. The 800°K sky temperature for 136 Mc used in the calculations is taken from the "95 percent" curve.

The noise power at the receiving system input can be calculated as follows:

$$P_N = K T_{eff} Bi f = -122.5 \text{ dbm},$$

where

K is Boltzman's constant ($1.38 (10)^{-2.3}$ joules/°K),

$T_{eff} = T_{sky} + T_{rec} = 1330.°K$,

T_{rec} is Receiver Preamplifier noise = 290 (F -1)°K = 530°K,

T_{sky} = 800°K,

NF = 4.5 db (maximum), and

B_{if} = Receiver IF Bandpass = 30 kc.

5. System Thresholds

a. General

With the noise power calculated above and a knowledge of the characteristics of the receiving system, a system threshold can be calculated. These figures will then be compared with the received signal power, and system margin predicted. System margin is defined as the difference between the calculated received power and the system threshold.

b. Beacon Link

The beacon receiver sensitivity using the FM-PM system is specified as -119.7 dbm as described in Paragraph 4-VII-B-1-a.

6. Beacon Telemetry to CDA Stations

a. RF Bandwidth

Three SCO's modulating the beacon results in an information bandwidth on the beacon carrier as follows: (Since the composite rms deviation is one radian, a $\Delta\theta$ of 1.4-radians peak will be used)

$$B_{fm} = 2\,fm\,(\Delta\theta + 1)$$

$$= 2\,fm\,(1.4 + 1) = 4.8\,fm,$$

$$fm = 4250\ cps$$

$$B_{fm} = 20,400\ cps$$

The total RF bandwidth for the beacon signal is

Information	20.4 kc
Doppler Shift	5.3 kc
Stability	6.8 kc
RF Bandwidth	32.8 kc

Since a carrier-tracking receiver will be used which is capable of tracking over a ±10-kc range, doppler shift and transmitter instabilities will be automatically compensated for, and a 30-kc IF bandwidth will be suitable.

b. Received Power, Margin, and Signal-to-Noise Ratio

The path loss at an antenna elevation angle of 5 degrees and an orbital altitude of 750 nautical miles is -147.2 db. The spacecraft antenna gain at a 35 degree look-angle, as determined from Figure 4-VII-1, is -5.0 db. Assuming diversity reception losses of 3.0 db, received power can be calculated as follows:

Transmitter Power (250 milliwatts)	+24.0 dbm
Spacecraft Antenna Gain (5°)	- 5.0 db
CDA Station Antenna Gain	+27.0 db
Line Losses	- 1.0 db
Polarization Loss (at Threshold)*	- 3.0 db
Path Loss	-147.2 db
Received Power Total	-105.2 dbm
System Threshold	-119.7 dbm
Margin	14.5 db
Noise Power	-122.5 dbm
Carrier-to-Noise Ratio	17.3 db

*This loss occurs when one of the signals may be below threshold. Above threshold the polarization loss should be a maximum of 1.0 db.

It has previously been shown that the system, performing at threshold, will provide subcarriers whose signal-to-noise ratios are each 12 db. The output of the subcarrier demodulator will have the baseband signal-to-noise ratios listed in Table 4-VII-5.

TABLE 4-VII-5. SIGNAL-TO-NOISE RATIOS OF SUBCARRIER DEMODULATOR OUTPUT

Channel No.	Low-Pass Output	Information	S/N (rms)
7	35 cps	V-head sensor	37.8 db
8	45 cps	V-head sensor	37.8 db
9	58 cps	Telemetry, command verify, and solar-aspect	37.8 db

Margin in the beacon link as a function of antenna elevation angle is given in Table 4-VII-6.

TABLE 4-VII-6. BEACON MARGIN AS A FUNCTION OF GROUND ANTENNA ELEVATION

Antenna Elevation (degrees)	Carrier-To-Noise Ratio (db)	Margin (db above System Threshold of -119.7 dbm)
5	17.3	14.5
10	18.7	15.9
15	20.2	17.6
20	21.2	18.4
25	22.8	20.0

C. APT-TV RECEPTION AND MARGINS

1. General

The APT transmission losses are similar to those of the 136-Mc beacon link. Since the frequencies are similar the Doppler shift and frequency stability are similar.

2. Link Geometry and Path Loss

The link geometry applicable to the beacon and command links, Paragraphs 4-VII-A-1 and 4-VII-B-1, also apply to the TV links. The path losses versus look angle for the APT-TV system (136 Mc) are the same as listed in Table 4-VII-3 for the 136 Mc beacon link.

3. Doppler Shift and Stability

Doppler shift and frequency stability of equipment must be considered in determining RF bandwidth requirements. The shift is indicated by the following expression and is a maximum at the minimum elevation angle:

$$\Delta F = F\frac{V}{c} \cos B,$$

where V is spacecraft velocity, c is the velocity of light, and B is the angle between the particular ground station and the direction of the spacecraft's velocity vector. At the APT-TV frequency of 136 Mc, the maximum Doppler shift is ±2.65 kc or a total of 5.3 kc. Frequency stability will be considered as ±0.005 percent of the carrier frequency. This figure includes instabilities in the transmitter and the receiver local oscillator. At the frequency of 136 Mc the stability is ±6.8 kc or a total of 13.6 kc.

4. Noise Temperature and Noise Power

External noise received by an antenna is a function of link frequency. Below one gigacycle, the major source of external noise is cosmic, and noise temperature varies approximately as (frequency) $^{-2.7}$. Figure 4-VII-3 shows the maximum values of the galactic center, the maximum value of the coolest 95 percent and 99 percent of the radio sky, and the minimum value of cosmic or sky noise. The 800°K sky temperature for 136 Mc used in the calculations is taken from the "95 percent" curve.

The noise power at the receiving system input can be calculated as follows:

$$P_N = k\, T_{eff}\, Bif,$$

where

k is Boltzmans constant $(1.38\ (10)^{-23}$ joules/°K),

$T_{eff} = T_{sky} + T_{rec} = 1330°K,$

T_{rec} is receiver preamplifier noise = 290 (NF-1)°K = 530°K,

T_{sky} = 800°K,

NF = 4.5 db (maximum), and

Bif = receiver IF bandpass = 50 kc.

5. System Thresholds

The threshold of a conventional FM receiver occurs when a abrupt degradation in performance is observed as the input carrier-to-noise ratio falls below a critical value. This threshold is more pronounced at a large modulation index. At a low index the break-point is not as sharp and the threshold occurs at lower carrier-to-noise (C/N) ratios (CNR's).

A 9 db C/N threshold will be considered for a modulation index of 1 and a 10.5 db C/N threshold will be considered for a modulation index of 2*. This data was obtained from Figure 1 of the referenced report where the input C/N is determined for an IF Bandwidth equal to $2f_b(m + 1)$, where (m) is the modulation index. It should be noted that a conventional FM receiver has its lowest threshold with an unmodulated carrier (m = 0) and tends to approach a constant threshold at large indices.

It is understood that the APT field stations use a phase lock demodulator (the Nems-Clarke Type 1440 receiver) and the APT-CDA stations use a conventional FM receiver. Threshold measurements on the Nems-Clarke 1440 receiver are not available. It is considered advisable to use the same threshold levels on both the APT field and CDA stations. At most, this will yield a conservative RF margin for the field stations, but this can be updated when the measurements are available.

For the APT system, a modulation index of 1 will be assumed for margin calculations. This corresponds to a level halfway between an all white and an all black signal and will result in a threshold of 9 db. Noise power in a 50-kc IF bandwidth is -120.3 dbm. Therefore, the APT-TV threshold for all stations will be 9 db higher or -111.3 dbm.

---

*These values were determined from MIT Lincoln Laboratory report "Thresholds for Several Analog Modulation Methods" by B. Reiffen, dated 6 May 1963.

6. APT-TV Data to Field Station

a. RF Bandwidth

A video signal with a baseband of 0 to 1.6 kc amplitude-modulates the 2.4 kc subcarrier. The frequency spectrum at the input of the FM transmitter is 0.8 to 4.0 kc, and the information bandwidth can be expressed as:

$$B = 2 F_m (\sigma + 1), \text{ or}$$

$$B = 2 (F_d + F_m).$$

Thus, for a peak deviation frequency of 8 kc, the information bandwidth is 24 kc which includes about 99% of the total power. The deviation ratio is expressed as:

$$R_d = \frac{F_m}{F_d} = 2.$$

The total RF bandwidth of the APT signal is as follows:

Information	24.0 kc
Doppler	5.3 kc
Stability	13.6 kc
Total RF Bandwidth	42.9 kc

The 50-kc IF bandwidth of the field station receiver is, therefore, adequate for APT reception.

b. Received Power and Margin

For an altitude of 750 nautical miles, the path loss at an antenna elevation angle of 5 degrees is 147.2 db, and the minimum look-angle, θ , is 35 degrees. As shown in Figure 4-VII-3, the available gain is minimum at θ equals 35 degrees and θ equals 145 degrees (180° -35°), and is -3.8 db below an isotropic source. The received power at the ground station will be as follows:

Transmitter Power	+37.0 dbm
Satellite Antenna Gain, (5°)	- 3.8 db
APT Field Station Antenna Gain	+12.5 db
Path Loss	-147.2 db
Polarization Loss	- 3.0 db
Line Loss	- 1.0 db
Total Received Power	-105.5 dbm

Noise power, N, in an IF bandwidth of 50 kc and for a receiving noise figure of 4.5 db is -120.3 dbm for this link. Therefore the carrier-to-noise ratio is 14.8 db and the margin is 5.8 db above the system threshold of -111.3 dbm when θ equals 5 degrees. Table 4-VII-7 shows the variation of RF margin with APT field station antenna elevation for a satellite altitude of 750 nautical miles.

TABLE 4-VII-7. APT-TV SYSTEM MARGIN VERSUS ANTENNA ELEVATION ANGLES

Antenna Elevation (degrees)	Carrier-to-Noise Ratio	System Margin (db Above System Threshold of -111.3 dbm)
5	14.8	5.8
10	16.2	7.2
15	17.7	8.7
20	18.7	9.7
25	20.3	11.3

c. Signal-to-Noise Ratio

S/N power ratio at the output of the APT field station receiver can be expressed as:

$$(S/N)_{fm} = \frac{C}{N} (3) \sigma^2 \left(\frac{B}{2F_m} \right),$$

$$(S/N)'_{fm} = 14.8 + 4.8 + 10 \log \frac{50(10)^3}{2(4)\ (10)^3},$$

$$(S/N)_{fm}\ (db) = 27.6\ db^*$$

where

σ = modulation index for subcarrier = 1.0*.

The signal-to-noise ratio at the output of the facsimile recorder can be expressed as:

$$(S/N)_{am} = (S/N)_{fm}\ M^2 \left(\frac{F_m}{2F_b}\right).$$

The modulation index on the AM subcarrier is approximately 95 percent, which corresponds to the CCIT standards for the peak-black to peak-white ratio for 10 gray levels. The values for F_m and F_b are 4000 cps and 1600 cps, respectively. Thus, the signal-to-noise ratio is

$$(S/N)_{am} = 27.6 + (-0.5) + 1\ db = 28.1\ db$$

Converting this expression to $\left(\frac{\text{peak-to-peak signal}}{\text{rms noise}}\right)$ increases the value by 9 db

and the ratio becomes

$$(S/N)\frac{\text{peak black-white}}{\text{rms noise}} = 37.1\ db$$

Since the facsimile-recorder picture requirement is of the order of 26 db, the system is sufficient for APT-TV picture transmission.

7. APT-TV to CDA Stations

Margins available at CDA stations are higher than those computed for the APT field station data link. Ground antenna gain will have a minimum gain of 27.0 db versus a field station gain of 12.5 db, therefore, the APT link margins will increase by a minimum value of 14.5 db (27.0 db -12.5 db)

---

*For an all white picture, the modulation index increases to 2, resulting in a 6 db increase in S/N out.

D. AVCS-TV RECEPTION AND MARGINS

1. General

a. AVCS Subcarrier Modulation

The AVCS camera and its associated electronics provide a baseband signal which has a bandwidth of approximately 0 to 60 kc. This signal frequency-modulates a 96-kc subcarrier (peak deviation of 24 kc) and the resulting signal is stored by the magnetic tape recorder.* Upon command the tape recorder reads out the modulated 96-kc subcarrier along with a 9.6-kc flutter-and-wow correction tone that, in turn, frequency-modulates the TV transmitter. Figure 4-VII-4 shows the crossed-dipole antenna power patterns for the TV data links.

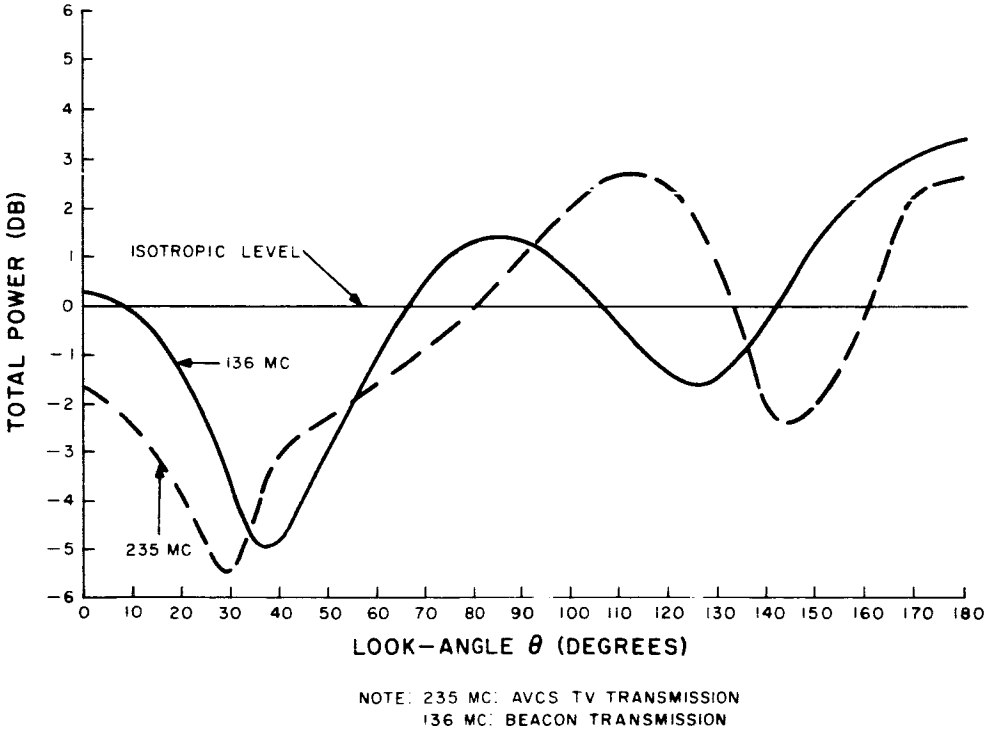

Figure 4-VII-4. Crossed-Dipole Antenna, Total Power Patterns

*Although the AVCS subsystem will have the capability for transmitting pictures directly to ground, it is anticipated that the primary operating mode will be that of taking pictures over remote areas and storing these pictures for later transmission to a CDA station.

The frequency deviations in the TV transmitter due to the subcarrier and correction signals are summarized in Table 4-VII-8. The upper limit of the frequency spectrum for the TV subcarrier is set by a filter which eliminates the upper sidebands of the video subcarrier signal above 120 kc. The output of the TV transmitter is radiated with circular polarization by means of the crossed dipole antenna.

TABLE 4-VII-8. TV TRANSMITTER FREQUENCY DEVIATIONS DUE TO MODULATION

Signal	Frequency Spectrum	Corresponding Deviation of Transmitter
Flutter-and-Wow Correction	9.6 $\pm$ 1 kc	10 kc
Modulated Video Subcarrier	36 kc to 120 kc	115 kc

b. Doubling of the Video Subcarrier Frequency

Because the frequency spectrum of the video-baseband is close to that of the video subcarrier, for a practable demodulation method, frequency doubling the subcarrier either before or after transmission is necessary.

In the present Nimbus System, a frequency-doubler is employed in the spacecraft.

Such an arrangement for the OT-2/AVCS system is not considered advisable for the following reasons:

(1) Doubling the subcarrier frequency before transmission results in a video signal-to-noise ratio which is 8.5 db lower than the undoubled subcarrier system. (This result is not intuitively obvious and is therefore shown in Appendix A.)

(2) The addition of the frequency-doubler to the spacecraft equipment adds unnecessary complexity, thereby degrading the reliability.

(3) The bandwidth of the existing TV transmitter would have to be increased to accommodate the increased information bandwidth of the signal.

2. Link Geometry and Path Loss

The link geometry considerations for the OT-2/APT system also apply to the OT-2/AVCS system. Path losses at various ground antenna elevation angles are given in Table 4-VII-9.

TABLE 4-VII-9. AVCS-TV DATA LINK PATH-LOSS AT VARIOUS GROUND ANTENNA ELEVATION ANGLES

Ground Antenna Elevation Angle (Degrees)	Path Loss at 235 Mc (db)
5	151.7
10	150.7
15	149.9
20	149.0
25	148.2

3. Doppler Shift and Stability

Doppler shift and frequency stability of equipment must be considered in determining RF bandwidth requirements. The shift is indicated by the following expression and is a maximum at the minimum elevation angle:

$$\Delta F = F\frac{V}{c} \cos B,$$

where V is spacecraft velocity, c is the velocity of light, and B is the angle between the particular ground station and the direction of the spacecraft's velocity vector. At the AVCS frequency of 235 Mc, the maximum Doppler shift is ±4.58 kc or a total of 9.16 kc.

Frequency stability will be considered as ±0.005 percent of the carrier frequency. This figure includes instabilities in the transmitter and the receiver local oscillator. At the frequency of 235 Mc, the stability is ±11.76 kc or a total of 23.5 kc.

4. Noise Temperature and Noise Power

External noise received by an antenna is a function of link frequency. Below one gigacycle, the major source of external noise is cosmic, and noise temperature varies approximately as $(\text{frequency})^{-2.7}$. Figure 4-VII-3 shows the maximum values of the galactic center, the maximum value of the coolest 95 percent 99 percent of the radio sky, and the minimum value of cosmic or sky noise. The 250°K sky temperature for 235 Mc used in the calculations is taken from the "95 percent" curve.

The noise power at the receiving system input can be calculated as follows:

$$P_N = k T_{eff} B_{if} = -112.2 \text{ dbm},$$

where

K is Boltzman's constant (1.38×10^{-23} joules/°K),

$T_{eff} = T_{sky} + T_{rec} = 876°K$,

T_{rec} is receiver preamplifier noise $\left[290\ (F-1)°K = 626°K\right]$,

$T_{sky} = 250°K$, and

B_{if} is receiver IF bandwidth (500 kc).

5. System Thresholds

a. General

With the noise power calculated above and a knowledge of the characteristics of the receiving system, a system threshold can be calculated. These figures will then be compared with the received signal power, and system margin predicted. System margin is defined as the difference between the calculated received power and the system threshold.

b. TV Data Link

If a 9-db carrier-to-noise ratio is assumed as the limiting factor in the receiving system, i.e., a conventional FM receiving system with a 500-kc intermediate frequency, the system threshold will be -103.2 dbm (-112.2 dbm + 9 db).

6. AVCS-TV Data to CDA Ground Station

a. RF Bandwidth

The RF bandwidth can be estimated by:

$$B_{if} = 2(F_d + F_m),$$

$$= 2\ (120 + 125) = 490 \text{ kc},$$

where

F_d is the transmitter peak deviation = 125 kc, and

F_m is the highest modulating frequency.

The RF bandwidth of the signal is comprised of

Information	490 kc
Doppler	9.2 kc
Transmitter Stability	11.8 kc
Total RF bandwidth	511.0 kc

The 500-kc IF bandwidth of the conventional Nems-Clarke FM receivers currently in use in CDA stations for TIROS TV reception would be quite suitable for AVCS TV reception, provided instabilities in the TV transmitter and receiver are compensated for by manual tuning of the receiver. The preamplifiers have a maximum noise figure of 5.0 db and a corresponding noise power at the input of -112.2 dbm.

b. Received Power and System Margin

The received power for the AVCS TV link is as follows:

Transmitter Power (5.0 watts)	+37 dbm
Satellite Antenna Gain, (5°)	- 4.2 db
CDA antenna Gain (Wallops)	+31.5 db
Path Loss (2430 statute miles)	-151.7 db
Polarization Loss (worst-case at receiver threshold)*	- 3.0 db
Line Loss	- 1.0 db
Net Received Power	-91.4 dbm
Input Noise Power	-112.2 dbm
Net Carrier-to-Noise Ratio	20.8 db

*This occurs when one of the signals may be below threshold. Above threshold the polarization loss should be a maximum of -1.0 db.

Assuming a threshold of the conventional FM receiving equipment of 9 db, i.e., a system threshold of -103.2 dbm, the resulting system margin would be 11.8 db. Table 4-VII-10 gives values of the system margin as a function of ground antenna elevation angle.

TABLE 4-VII-10. AVCS SYSTEM MARGINS FOR VARIOUS GROUND ANTENNA ELEVATION ANGLES

Ground Antenna Elevation Angle (Degrees)	Carrier-to-Noise Ratio (db)	System Margin (db)
5	20.8	11.8
10	22.1	13.1
15	23.5	14.5
20	24.7	15.7
25	25.7	16.7

c. Signal-to-Noise Ratio

The video rms signal-to-noise ratio, calculated with the Roth-Baumunk formula* is:

$$\left(\frac{S}{N}\right)_{rms} = \left(\frac{C}{N}\right)_{IF} \frac{F_1^2 F_2^2 B_{if}}{2\left[\frac{f_2^5}{5} - \frac{f_{sc} f_2^4}{2} + \frac{f_{sc}^2 f_2^3}{3} - \frac{f_1^5}{5} + \frac{f_{sc} f_1^4}{2} - \frac{f_{sc}^2 f_1^3}{3}\right]},$$

or

$$\left(\frac{S}{N}\right)_{rms} = 20.8 + 9.6 = 30.4 \text{ db.}$$

*Roth-Baumunk, Journal of the Society of Motion Picture and Television Engineers, Vol. 69, January 1960.

where

F_1 is the peak deviation of RF carrier due to the TV subcarrier,

F_2 is the peak deviation of the subcarrier,

f_{sc} is the center frequency of the subcarrier,

f_2 is the highest subcarrier frequency modulating the transmitter,

f_1 is the $f_{sc} - f_m$ = 96 kc - 60 kc = 36 kc, and

B_{if} = IF bandwidth = 500 kc.

In this computation the noise contribution is taken over a bandwidth of 36 kc to 120 kc, corresponding to the receiving bandpass filter. The signal spectrum is contained between 36 kc and 156 kc. However, due to the frequency characteristic of the tape recorder, frequencies above 120 kc are attenuated. The power spectrum of the video signal falls off rapidly at higher modulation frequencies and therefore, no significant error is introduced by neglecting the loss in higher frequency signal power in the signal-to-noise computation.

The calculated video signal-to-noise ratio is dependent upon the first and second demodulators being above threshold. In a well designed FM/FM system, the threshold carrier-to-noise level of the first demodulator occurs before the threshold level of the second demodulator.

In this case, the subcarrier power (S_c) to noise ratio is equal to:

$$\frac{S_c}{N} = \frac{3}{2}\,\frac{C}{N}\,\frac{B_{if}\,F_1}{f_2^{\,3} - f_1^{\,3}}\,,$$

$$= \frac{C}{N}\,\frac{3}{2}\,\frac{(500{,}000)\,(115{,}000)^2}{\left[(120{,}000)^3 - (36{,}000)^3\right]} = \frac{C}{N} \times 5.9,$$

$$= \frac{C}{N} + 7.7 \text{ db},$$

where

F_1 is the peak deviation of carrier by subcarrier,

f_2 is the upper sideband frequency,

f_1 is the lower sideband frequency, and

B_{if} is the receiver IF bandwidth.

It can be seen, therefore, that the second detector threshold will always be exceeded when the input signal is above receiver threshold.

Converting from rms signal-to-noise ratio to a black-to-white signal-to-rms-noise ratio, and allowing for a 30 percent sync tip, yields:

$$(S/N)_{B\text{-}W/rms} = (S/N)_{rms} + 20 \log \frac{(2\sqrt{2})}{(1.3)} ,$$

$$= 30.4 \text{ db} + 6.7 \text{ db} = 37.1 \text{ db.}$$

This value of signal-to-noise ratio indicates that high quality TV pictures will be obtainable from the AVCS subsystem. At system threshold, the signal-to-noise ratio would be 11.8 db lower than the above value, or

$$(S/N)_{B\text{-}W/rms} = 25.3 \text{ db.}$$

Because of the large system margin (11.8 db) it is doubtful that such a value for S/N would be experienced in practice.

E. ALASKA AND EAST COAST CDA STATIONS

1. General

The CDA stations will perform the following functions for OT-2/APT spacecraft and the OT-2/AVCS spacecraft:

(1) Command the spacecraft,

(2) Program the spacecraft dynamics control subsystem, and

(3) Receive beacon telemetry.

In addition, the CDA station will receive APT-TV pictures for engineering evaluation of APT system performance and receive AVCS-TV pictures for processing.

Two CDA stations will be used in the OT-2 program; one on the east coast, probably in Virginia, and the other at Fairbanks, Alaska. The Alaska (Fairbanks) station is superior to the present Wallops Island, Virginia station. An East Coast station will be built with performance similar to that of the Alaska station. The performance of the Alaska station was used in the link calculations.

2. Alaska Ground Station

The Alaska Ground Station uses an 85-foot parabolic-reflector for a receiving antenna with a gain of 27 db at 136 Mc. The antenna is equipped for polarization diversity reception.

The station uses a General Dynamics Diversity Receiver which can receive signals between 130 and 140 megacycles simultaneously on both diversity channels. The receiving system can demodulate AM or FM signals, has post-detection diversity-combining, and has a 3.25-Mc output suitable for the Electrac Model 215 pre-detection, diversity-combining system. The Electrac system can demodulate amplitude-modulated or phase-modulated signals and has a carrier-tracking phase-lock loop and combining.

The present receivers will have to be modified for a more suitable bandwidth for AVCS reception.

The output from the telemetry receiver will be fed to three subcarrier demodulators for separation and demodulation. These demodulators employ a limiter-discriminator demodulating scheme.

The command transmitter provides a 1000-watt amplitude-modulated command signal, and is modulated with FSK subcarrier tones. The highest frequency subcarrier tone will be 10.5 kc at center frequency and will be frequency shifted ±7.5 percent; corresponding to the binary signal input. The modulation rate will be 10 pulses per second.

SECTION VIII. ATTITUDE AND SPIN-RATE CONTROL TECHNIQUES

A. INTRODUCTION

1. General

This section describes the techniques to be used in controlling spacecraft attitude and spin rate, and discusses the factors which affect their employment. Detailed mathematical development of the basic theory underlying the control philosophy is presented, and factors influencing the design of various control components are discussed. In addition, the techniques to be used for measurement of spacecraft attitude and spin rate are described, and analyses of possible failure modes and redundancy considerations are included.

The attitude and spin-rate control techniques are based on experience acquired during the operational periods of the first eight standard TIROS satellites, and on the detailed design analyses performed for the TIROS "I" spacecraft. Although the techniques apply to both the APT and AVCS configurations of the OT-2 spacecraft, the performance of the two configurations may differ slightly, due to difference in nominal spin rates. These differences are explained in the text.

Symbols used throughout this section in mathematical and other discussions are defined in Table 4-VIII-1.

2. Brief Description of Attitude and Spin-Rate Control Operations

Prior to separation of the spacecraft from the third stage of the launch vehicle, the spacecraft and third stage will both be spinning at a nominal 125 rpm. (This spin is imparted to the third stage prior to its ignition in order to maintain stability during the final phase of the launch operation). After the spacecraft separates from the third stage, the nutation dampers will be actuated, reducing any nutation, or "wobble", imparted to the satellite to an acceptable level. Shortly thereafter, the despin mechanism (Yo-Yo) will be released, reducing the spacecraft spin rate to a value approximately equal to the required operational value.

Several orbits after orbit injection, a maneuver to orient the spacecraft's spin axis to a position normal to the orbital plane will be initiated. This orientation, or station-acquisition, maneuver will be effected through use of the high-torque mode of the Quarter Orbit Magnetic Attitude Control (QOMAC) system, a mode that will allow the

TABLE 4-VIII-1. SYMBOLS USED IN ATTITUDE AND SPIN-RATE CALCULATIONS

Symbol	Definition
A	Area of coil, in meters^2
$\bar{B}$	Earth's magnetic flux vector
B_b	Component of Earth's magnetic flux vector along $\hat{b}$
B_ℓ	Component of Earth's magnetic flux vector along $\hat{\ell}$
B_n	Component of Earth's magnetic flux vector along $\hat{n}$
$\bar{b}_f$	Earth's magnetic field unit vector
$\hat{b}$	Unit vector along an axis perpendicular to line of nodes in orbital plane
H	Angular momentum
i	Inclination of orbit normal with respect to geographic polar axis
i_m	Inclination of earth's magnetic dipole with respect to geographic polar axis
I_d	Inertia of liquid-damper fluid about the damper axis.
I_c	Coil current, in amperes.
I_s	Moment of inertia about the spin axis
I_T	Transverse moment of inertia
K	Constant of breakaway friction
$\hat{\ell}$	Unit vector along the nodal line toward the ascending node
M	Magnetic dipole moment
M_E	Geomagnetic dipole moment (8.1×10^{25} gauss-cm^3)
m	TEAM damper-cart mass
N	Number of sky-to-earth horizon pulses from reference
N_c	MASC coil normal
$\hat{n}$	Orbit normal
n_c	Number of turns in coil
R	Orbit radius

TABLE 4-VIII-1. SYMBOLS USED IN ATTITUDE AND SPIN-RATE CALCULATIONS (Continued)

Symbol	Definition
r	Radial distance of damper from spin axis
S	Roll-angle sensitivity constant
$\hat{s}$	Spin axis unit vector
T	Torque
T_A	Average spin period at beginning of prediction cycle
$T_{AVG/SPIN}$	Average MASC torque per spin period
$\frac{T_{AVG\ PREC}}{SPIN}$	Average precessional torque produced by MASC in one spin period
T_{HP}	Time of horizon pulse (sky-to-earth) of orthogonal sensor
T_{MAX}	Maximum earth temperature
T_{MIN}	Minimum earth temperature
T_n	Nutation-damping time constant
T_o	Time from ascending node to start of QUOMAC cycle
T_p	Time of one spin period
T_s	Torque vector along spin axis
t_{e_i} $i = 1$ $i = 2$	Earth scan time from sensor i of V-head horizon-sensor: 1 = positive spin vector side, 2 = negative spin vector side
t_o	Time of initial or reference V-head horizon-sensor (sky-to-earth) pulse
t_{sp}	Spin period
α	Angle between spin axis and optical axis of V-head sensor channel 1
β	Orbit angle measured counterclockwise around orbit normal from ascending node to satellite
β_i	Orbit angle when MASC torquing starts
β_f	Orbit angle when MASC torquing ends
β_o	Orbit-start angle for QOMAC cycling

TABLE 4-VIII-1. SYMBOLS USED IN ATTITUDE AND SPIN-RATE CALCULATIONS (Continued)

Symbol	Definition
γ	Angle between N_c and local vertical at commutation point
$\Delta N(T)$	Change in horizon-sensor input radiance from sky radiance as a function of temperature
$\Delta \omega_s$	Change in spin rate
θ	Orbit anomaly angle
θ_{1-2}	MASC commutation angle (or, angle between orthogonal horizon sensors 1 and 2)
θ_o	Nutation half-cone angle
θ_s	Line-of-sight lead angle of orthogonal horizon sensor with respect to V-head horizon sensor
λ	Argument of procession vector from ascending node
μ	Viscous friction coefficient
μ_o	Dynamic friction constant
μ_v	Fluid viscosity
ρ	Fluid density
ϕ	Roll angle
ϕ_{max}	Maximum value of attitude error
ψ	Yaw angle
ω_o	Orbital rate
ω_p	Precession rate
ω_{po}	Rate of orbital regression
ω_s	Spin rate of the spin axis about the pitch axis
Ω	Average angle between longitude of ascending node and line of nodes defined by magnetic equator and geographic equator.

spin axis to be precessed at a rate of 10 degrees per orbit. A maximum of eight torquing cycles (equivalent to 4 orbits) can be programmed from ground and stored in the spacecraft. This number is more than sufficient to ensure active attitude correction until the spacecraft comes within command range of another ground station. During the maneuver, the attitude of the spacecraft will be continuously computed by the ground stations in order to determine the changes required in the QOMAC program.

Once the spin axis has been precessed to within approximately 10 degrees of the orbit normal, the QOMAC device will be switched to the low-torque mode, a mode which provides a maximum precession of 2 degrees per orbit. At the same time, the Magnetic Spin Control (MASC) device will be activated to adjust the spin period to the required operational value (5.50 seconds for the OT-2/APT configuration and 6.50 seconds for the OT-2/AVCS configuration). If only a small correction in spin period is required, the low-torque (single-coil) MASC mode will be employed. Should a larger correction be required, the high-torque (two-coil) mode will be employed in order to shorten the time necessary to reach the operational spin rate.

After station and spin-rate acquisition, the QOMAC device will be deactivated and the spin axis will be permitted to drift for one day. During this period, the precessional direction and rate will be monitored in order to determine the residual magnetic bias of the spacecraft. The Magnetic Bias Control (MBC) coil will then be energized and the magnetic-bias switch positioned to compensate for the spacecraft's residual dipole moment and to establish a new dipole moment which will induce a 1-degree-per-day (approximate) precession rate. The QOMAC device will then be used, as necessary, to return the spin axis to station attitude.

Although the spin axis is expected to drift slowly with respect to the regression of the orbit normal, a maximum of two QOMAC cycles per week should be sufficient to maintain the spin-axis attitude within 1 degree of the orbit normal. Further, insofar as picture orientation and rectification is concerned, the actual attitude will be known to an accuracy of better than 1 degree.

For the anticipated spin-rate decay of 0.096 rpm per week, three MASC cycles per week should satisfy the accuracy requirements imposed by the camera controls.

B. REVIEW OF THEORY

1. General

Spacecraft attitude and spin-rate control is achieved by making use of the torque resulting from the interaction of controllable magnetic fields, internally generated in the spacecraft, with the earth's magnetic field. Three devices, built into the spacecraft and controllable from the ground stations, are used to generate the spacecraft's

magnetic fields: the Quarter Orbit Magnetic Attitude Control (QOMAC) and Magnetic Bias Control (MBC) coils, both of which generate magnetic fields used in attitude control operations; and the Magnetic Spin Control (MASC) coil, which generates magnetic fields used in spin-control operations.

Refer to Figure 4-VIII-1a. When an electrical current is passed through a coil, a dipolar magnetic field is set up about the coil in a manner such that the axis of the field lies at right angles to the plane of the coil and passes through its center. The coil is then said to have a magnetic dipole moment along this axis. When the coil is so energized and placed in the vicinity of a stationary magnetic field-namely, the earth's - its dipole moment attempts to align itself with the earth's field lines. From electromagnetic theory, the vector representation of the torque thereby produced will be normal to the plane determined by vectors representing the dipole moment of the coil and that portion of the earth's magnetic field in the vicinity of the coil, as shown in Figure 4-VIII-1b.

Depending upon the location of the coils in the spacecraft, the torque vector can be made to lie colinear or normal to the spacecraft's spin axis. Since a torque that either aids or opposes the spin momentum is required to effect spin rate control, the MASC coil is oriented such that its plane is parallel to the spin axis. Therefore, the torquing forces resulting from magnetic interaction will be applied about the spin axis, either aiding or opposing spin momentum, depending on dipole polarity. On the other hand, to effect a change in direction (or rotation) of the spin-axis itself — the type of motion required for effective attitude control — a torque which is applied about an axis normal to spin axis is required. Therefore, both the QOMAC and MBC coils are installed in the spacecraft such that their planes are perpendicular to the spin axis.

The placement of the attitude-control coils at right angles to the spin-axis causes the motion produced by the magnetic torquing to be precessional in nature, since the spacecraft, a spinning body, exhibits gyroscopic properties, and the applied torque is transverse to the direction of spin. The motion resulting in such a system will, therefore, be in conformance with the basic laws governing gyroscopic bodies: that is, the spin axis will move to a position colinear with the torque axis, rather than about it. A simplified vector diagram showing the direction of precession is shown in Figure 4-VIII-1c.

In order to utilize the motion of precession described above to acquire and maintain the wheel mode of operation in the most efficient manner, the current in the QOMAC coil is programmed in accordance with a technique that is characterized by two major parameters: (1) cycle variation of coil current direction (hence, magnetic dipole polarity reversals) every quarter orbit; and (2) phasing of these reversals with respect to the earth's magnetic field by delaying program initiation until the satellite reaches a specific point in orbit (orbit angle). A mathematical explanation of the QOMAC technique is given in Paragraph B-2 below. The MBC technique does not feature

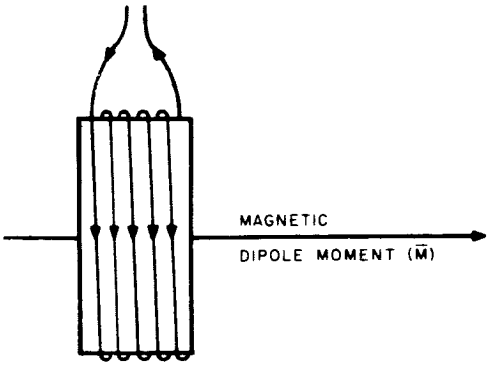

a. DIPOLE MOMENT OF CURRENT-CARRYING COIL.

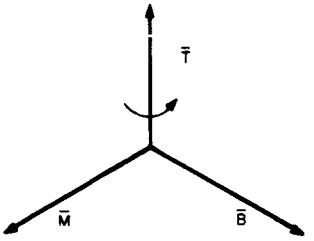

b. TORQUE ($\bar{T}$) DEVELOPED BY INTERACTION OF COILS DIPOLE MOMENT ($\bar{M}$) AND EARTH'S MAGNETIC FIELD ($\bar{B}$).

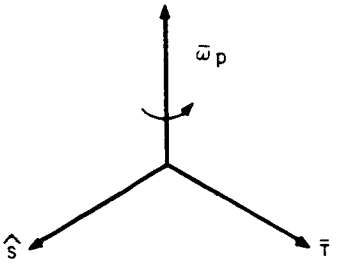

c. PRECESSION MOTION ($\bar{\omega}_p$) OF SPIN AXIS ($\bar{S}$) CAUSED BY TORQUE ($\bar{T}$).

Figure 4-VIII-1. Elements of Magnetic Attitude Control

coil-current reversals, but merely generates a dipole moment to both offset any inherent residual magnetism in the spacecraft and to compensate for orbital regression. The theory underlying the MBC technique is described in Paragraph B-3.

The MASC technique features MASC coil operation during alternate quarter-orbits and commutated coil-current reversals phased with spacecraft spin-rate during each operating period. A mathematical development of MASC theory is presented in Paragraph B-4.

2. Quarter Orbit Magnetic Attitude Control (QOMAC)

a. Analysis of Magnetic Torque and Precessional Motion

As noted in Paragraph B-1 above, the QOMAC coil is installed with its magnetic axis aligned with the spin axis of the spacecraft. Also, by convention, the positive dipole moment of the coil is taken in the positive direction of the spin vector. Therefore, the location of the spacecraft dipole moment can be expressed as:

$$\overline{M} = M\hat{s}. \tag{VIII-1}$$

The direction and magnitude of the control torque developed by the interaction of the dipole moment of the coil and the earth's magnetic field is given by the vector equation:

$$\overline{T} = \overline{M} \times \overline{B}. \tag{VIII-2}$$

This torque, acting on the spacecraft, will cause a time rate of change of its angular momentum. That is:

$$\overline{T} = \dot{\overline{H}} = \frac{d}{dt}(I_s \omega_s \hat{s}) = I_s \dot{\omega}_s \hat{s} + I_s \omega_s \frac{d\hat{s}}{dt}. \tag{VIII-3}$$

Assuming that $\overline{M}$ is parallel to $\hat{s}$, the developed torque which is normal to $\overline{M}$, must also be normal to $\hat{s}$. Such a torque cannot change the spacecraft spin rate; hence:

$$\dot{\omega}_s = 0. \tag{VIII-4}$$

The change in the unit vector, $\hat{s}$, expressed by $d\hat{s}/dt$, is, therefore, a change of direction only, which implies a rotation about an axis which is normal to $\hat{s}$. This is the precessional motion referred to above and having rate ω_p. It follows that:

$$\frac{ds}{dt} = \overline{\omega}_p \times \hat{s}, \tag{VIII-5}$$

and hence

$$\bar{M} \times \bar{B} = I_s \omega_s (\bar{\omega}_p \times \hat{s}). \qquad \text{(VIII-6)}$$

To evaluate the motion of the spin axis produced by this torque, it is necessary to include the effects of the earth's magnetic-field variations over the orbital path. Experience has shown that an excellent approximation of the earth's magnetic field at spacecraft altitude may be obtained by the assumption of a simple dipole source. In this approximation, the magnetic dipole is inclined from the earth's polar axis by 11.4 degrees, with the dipole axis intersecting the earth at Latitude 78.6°N, Longitude 70.1°W, and again at Latitude 78.65°S, Longitude 250.1°W. A further simplification of the earth's field characteristics may be made by assuming that the axis of the earth's field magnetic dipole is co-linear with the polar axis of the earth. This simpler model, which in practice has lead to excellent prediction, will be used in evaluating the following equations. The results for the more accurate assumptions are outlined in Paragraph 4-VIII-c.

Assuming a dipole representation of the earth's magnetic field, the magnetic field vector may be given as:

$$\bar{B} = \frac{M_E}{R_3} \bar{b}_f . \qquad \text{(VIII-7)}$$

Equation (VIII-6) then becomes:

$$\bar{\omega}_p \times \hat{s} = - \eta (\bar{b}_f \times \hat{s}), \qquad \text{(VIII-8)}$$

where

$$\eta = \frac{M_E M}{R^3 I_s \omega_s} .$$

From analyses of general gyroscopic motion, it can be shown that, for light-torque loading, the precession motion which satisfies equation (VIII-8) is given by:

$$\bar{\omega}_p = - \eta \bar{b}_f, \qquad \text{(VIII-9)}$$

indicating that for a positive dipole moment of the coil, the precessional motion of the spin axis at any instant will be negatively directed about the direction of the earth's magnetic field.

b. QOMAC Cycling and Phasing

The QOMAC technique utilizing cyclic reversals of spacecraft magnetic-dipole dipole polarity to effectively produce an average direction of the earth's magnetic field. By properly phasing these reversals, the magnetic torque (and resulting precession) caused by the interaction of the spacecraft dipole and the average earth's-field dipole can be made to lie in the properposition for the required attitude correction.

The following paragraphs present a detailed mathematical analysis of QOMAC cycling and phasing. The coordinate system used in the analysis, an orbit-axis system, is shown in Figure 4-VIII-2. The system is fixed in and rotates with, the plane of the orbit, with the $\hat{\ell}$ axis directed along the orbit line of modes (positive in the direction of the ascending mode), the $\bar{n}$ axis along the orbit normal, and the $\hat{b}$ axis defined by the vector relation: $\hat{b} = \hat{n} \times \hat{\ell}$. Negligible precession of the orbit is assumed to occur over the interval of a half-orbit, during which full torque averaging for a single QOMAC cycle takes place (i.e., a positive dipole polarity for one quarter orbit followed by a negative dipole polarity for the next quarter orbit).

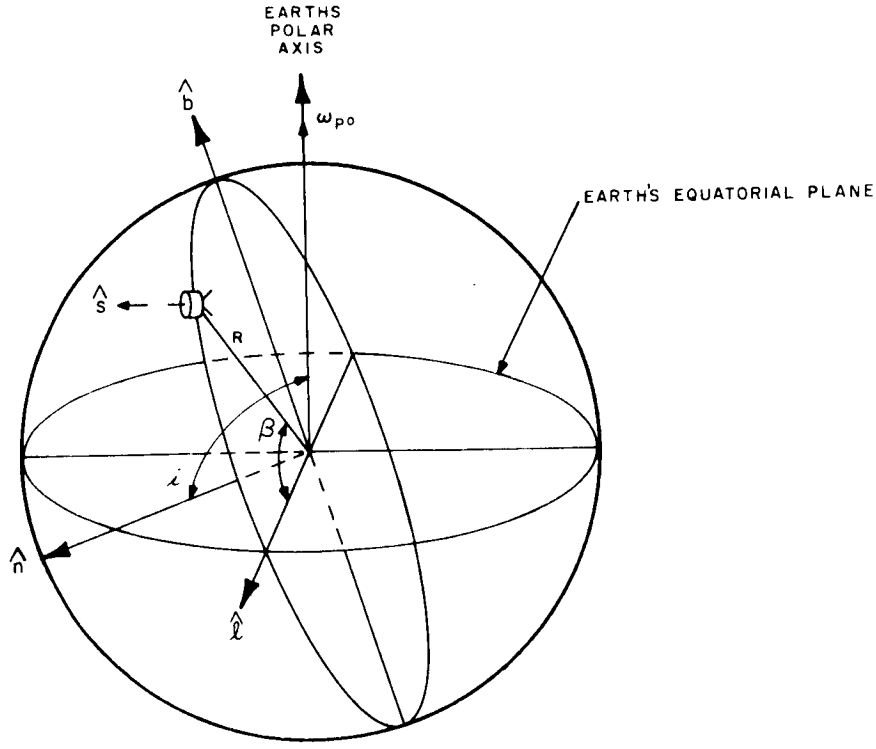

Figure 4-VIII-2. Coordinate System Used for Analyzing Attitude-Control Operations ($\hat{\ell}$, $\hat{b}$, $\hat{\omega}$ Axes)

Based upon the above assumptions, the earth's magnetic field at the spacecraft may be resolved into components of the orbit-axis coordinate system as follows:

$$B_\ell = -\frac{M_E}{R^3}\left(\frac{3}{2}\sin 2\beta \sin i\right),$$

$$B_b = +\frac{M_E}{R^3}\left(\frac{3}{2}\cos 2\beta \sin i - \frac{1}{2}\sin i\right), \text{ and} \qquad \text{(VIII-10)}$$

$$B_n = +\frac{M_E}{R^3}(\cos i).$$

If the components of the earth's magnetic field given in equation (VIII-10) are averaged over one cycle of quarter-orbit torquing, starting at an arbitrary delay angle, β_o (referenced to the ascending node) the average values for the earth's magnetic field become:

$$\tilde{B}_\ell = \frac{1}{\pi}\left[-\frac{M_E}{R_3}\left(\frac{3}{2}\sin i\right)\right]\left[\int_{\beta_o}^{\beta_o+\pi}\sin 2\beta\, d\beta - \int_{\beta_o+\frac{\pi}{2}}^{\beta_o+\pi}\sin 2\beta\, d\beta\right],$$

or, simply,

$$\tilde{B}_\ell = -\frac{3}{\pi}\sin i \cos 2\beta_o,$$

$$\tilde{B}_b = -\frac{3}{\pi}\sin i \sin 2\beta_o, \text{ and} \qquad \text{(VIII-11)}$$

$$\tilde{B}_n = 0.$$

If equation VIII-9 is expanded and the average values of the earth's magnetic field above are substituted, the following average values of the precession components are obtained:

$$(\tilde{\omega}_p)_{\ell} = \frac{3}{\pi}\ \eta \sin i \cos 2\beta_o,$$

$$(\tilde{\omega}_p)_b = \frac{3}{\pi}\eta \sin i \sin 2\beta_o, \text{ and} \qquad \text{(VIII-12)}$$

$$(\tilde{\omega}_p)_n = 0.$$

Since the $\hat{n}$ component of precession is zero, it follows that the precession axis is confined to the orbital plane. Further, since the $\hat{b}$ and $\hat{\ell}$ components of precession are functions, respectively, of the sine and cosine of the delay angle, β_o the average precession vector can be made to point in any direction in the orbital plane by suitable selection of the delay angle.

In order to move the spacecraft spin axis into coincidence with the orbit normal in the most efficient manner, the direction of the average precession vector is chosen to lie perpendicular to the spin axis. This is accomplished by delaying the initiation of QOMAC cycling to a point in orbit related to the existing attitude error. The nature of this relationship, and the criteria for selection of the QOMAC start angle, is discussed below.

Spacecraft attitude errors are normally expressed in terms of "roll" and "yaw" in relation to the instantaneous local earth radius vector, or local vertical. Roll error is defined as the complement of the angle between the spacecraft spin vector and the local vertical minus 90 degrees, while yaw angle is defined as the angle, ψ, between the spin vector and a plane determined by the orbit normal and the local vertical. Note, however, that the local vertical, referenced to the absolute attitude of the spacecraft, rotates 360 degrees each orbit. Since the roll and yaw errors are defined by the inertially rigid spin axis and the rotating local vertical, a cyclic interchange between roll and yaw will occur once an orbit. The nature of this interchange is expressed as:

$$\sin \phi = \sin \phi_{max} \sin (\beta - \lambda), \text{ and} \qquad \text{(VIII-13)}$$

$$\sin \psi = -\sin \phi_{max} \cos (\beta - \lambda). \qquad \text{(VIII-14)}$$

Notice, from the relationship above, that twice an orbit, the absolute value of ϕ reaches a maximum, and ψ falls to zero. At these points, the total attitude errro is in roll and can be expressed as $\pm \phi_{max}$. At points in orbit 90 degrees away from these $|\phi| = \phi_{max}$ points, the value of ϕ is zero, and the value of ψ equals $\pm \phi_{max}$.

Figure 4-VIII-3 shows the attitude-correction geometry in the $\hat{\ell}$, $\hat{b}$, $\hat{n}$ coordinate system. If the angle between $\hat{n}$ and $\hat{s}$ is defined to be ϕ_{max}, the point in orbit, e, where the orbit intersects the plane defined by $\hat{n}$ and $\hat{s}$ will be the point at which the instanteous roll error ϕ is equal to ϕ_{max}. For the average precession vector, $\tilde{\omega}_p$, to be perpendicular to $\hat{s}$, it must be normal to the plane containing $\hat{n}$ and $\hat{s}$. This means that the desired perpendicularity occurs at a point in orbit 90 degrees before e, the point corresponding to the conditions of $\phi = 0$, $\psi = \pm \phi_{max}$. From equations (VIII-13) and (VIII-14) this occurs when:

$$\beta = \lambda \text{ or } \lambda + \pi . \tag{VIII-15}$$

Since, from equation (VIII-12), the start angle is given by:

$$\tan \beta_o = \frac{(\tilde{\omega}_p)_b}{(\tilde{\omega}_p)_\ell} , \tag{VIII-16}$$

and the argument of the optimum average precession vector can be expressed as:

$$\tan \lambda = \frac{(\tilde{\omega}_p)_b}{(\tilde{\omega}_p)_\ell} \tag{VIII-17}$$

then the required start angle for proper QOMAC phasing is:

$$\beta_o = \frac{\lambda}{2} + m\pi , \tag{VIII-18}$$

or

$$\beta_o = \left(\frac{\lambda + \pi}{2}\right) + m\pi , \tag{VIII-19}$$

where m is either 0 or 1, depending on the required direction of precession.

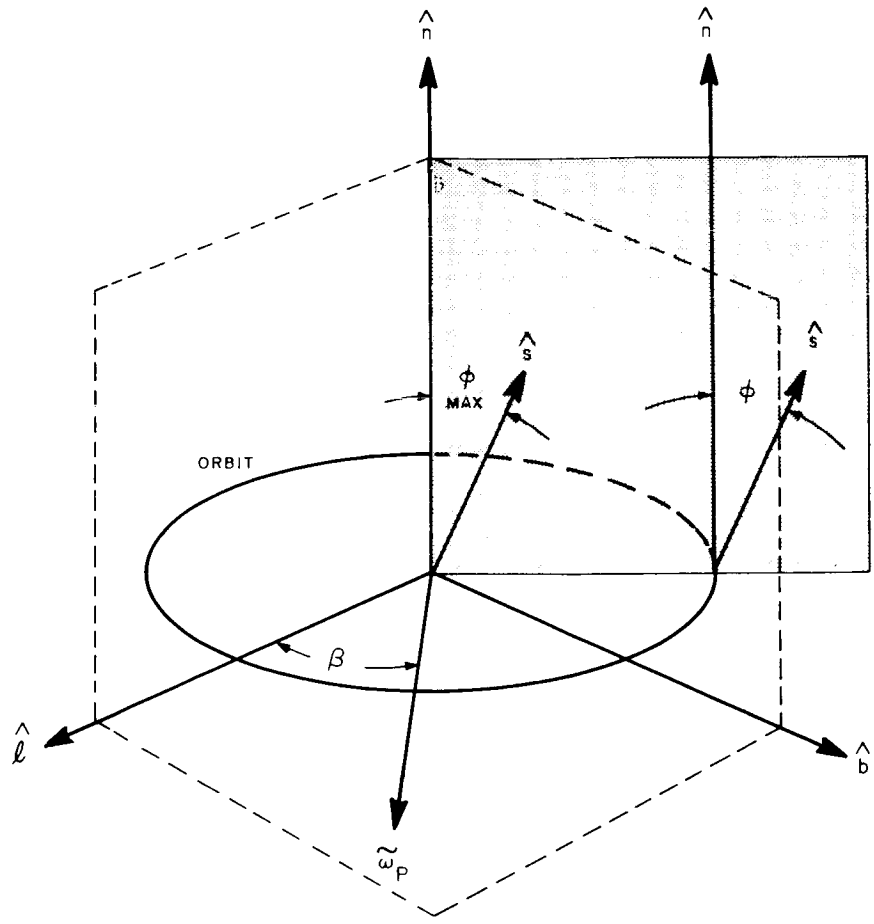

Figure 4-VIII-3. Optimum Location of Average Precession Vector, $\tilde{\omega}_p$

The average precession rate achieved after the completion of one QOMAC cycle is given by:

$$\left|\bar{\omega}_p\right| = \sqrt{(\omega_p)_\ell^2 + (\omega_p)_b^2} \quad , \tag{VIII-20}$$

$$= \frac{3}{\pi} \eta \sin i.$$

3. Magnetic Bias Control (MBC)

a. General

Several factors operate continuously to degenerate spacecraft attitude, causing the spin axis to move out of alignment with the orbit normal. The two most

significant of those are the magnetic torquing introduced by the interaction of the spacecraft's residual magnetic dipole with the earth's field, and the effects of the regressing sun-synchronous orbit on satellite attitude. The errors introduced by these two factors are kept to a minimum by the MBC technique, which utilizes a current-carrying coil to produce continuous torque that offsets the error-indicating factors.

b. Effects of Residual Magnetism

After final assembly, the inherent magnetism of the spacecraft is nulled to a small value, and an assessment is made of the magnetic dipoles generated in each spacecraft operating mode. However, experience with previous spacecraft has shown that the magnitude of the residual dipole moment undergoes significant changes after launch. Therefore, a sufficient range of programmable MBC dipole moments has been provided to compensate for these changes. The required dipole moment is determined analytically after launch.

c. Effects of Orbital Regression

The magnetic bias required to compensate for the 1-degree-per-day orbit regression is described in the following mathematical development.

The time derivative of a vector evaluation in a rotating system of coordinates may be expressed in terms of the Newtonian derivative by means of a transport term that adjusts for the rotation. Thus, the change of angular momentum produced by a torque can be written:

$$\left.\frac{d\bar{H}}{dt}\right)_F = \left.\frac{d\bar{H}}{dt}\right)_R + \bar{\omega}_{po} \times \bar{H}, \qquad \text{(VIII-21)}$$

where F and R refer to fixed and rotating systems respectively. Since the dipole moment, $\bar{M}$, of the MBC coil is coaxial with the spin axis, $\hat{s}$, the coil dipole moment can be expressed:

$$\bar{M} = M\hat{s} \; . \qquad \text{(VIII-22)}$$

It also follows that:

$$\bar{H} = I_s \; \omega_s \; \hat{s} \; . \qquad \text{(VIII-23)}$$

In addition, use will be made of the following relationships:

$$\overline{B} = \frac{M_E}{R}\overline{b}_f, \tag{VIII-24}$$

$$\overline{M} \times \overline{B} = \overline{T} = \left(\frac{d\overline{H}}{dt}\right)_F, \text{ and} \tag{VIII-25}$$

$$\eta = \frac{M M_E}{R^3 I_s \omega_s}. \tag{VIII-26}$$

If substitutions are made and rearrangement of terms effected, equation (VIII-21) may be solved for the derivative sought as follows:

$$\left(\frac{d\hat{s}}{dt}\right)_R = \eta (\hat{s} \times \overline{b}_f) - (\hat{s} \times \overline{\omega}_{po}). \tag{VIII-27}$$

This may be written in the form:

$$\left(\frac{d\hat{s}}{dt}\right)_R = \hat{s} \times \overline{a},$$

if

$$\overline{a} = \eta \overline{b}_f + \overline{\omega}_{po}. \tag{VIII-28}$$

If the orbit normal, $\hat{n}$, is to be continuously tracked, it follows that the spin axis, $\hat{s}$, must remain parallel to $\hat{n}$ at all times. This infers that the time rate of change of the spin vector, $\hat{s}$, in the rotating system of coordinates must be zero. That is:

$$\left(\frac{d\hat{s}}{dt}\right)_R = 0, \text{ or} \tag{VIII-29}$$

$$\hat{s} \times \hat{a} = 0, \text{ or}$$

$$\hat{n} \times \hat{a} = 0.$$

This means that for the spin axis to remain parallel to the orbit normal, the average value of the vector $\overline{a}$ must be parallel to $\hat{n}$. An evaluation of the average value of vector $\overline{a}$, denoted $\tilde{a}$, will now be made with this condition in mind.

The orbital precession vector, $\bar{\omega}_{po}$, is resolved into $\hat{\ell}$, $\hat{b}$, $\hat{n}$ components as follows:

$$\bar{\omega}_{po} = \omega_{po} (\hat{b} \sin i + \hat{n} \cos i). \tag{VIII-30}$$

Since the orbit inclination, i, is constant, these values also represent the average values of the precession components.

If the earth's magnetic-field components given in equation (VIII-10) are averaged over a full orbit, thus:

$$(\tilde{b}_f)\hat{\ell} = \frac{1}{2\pi}\left[-\frac{3}{2} \sin i \int_0^{2\pi} \sin 2\theta \, d\theta\right]\hat{\ell} = 0,$$

$$(\tilde{b}_f)\hat{b} = \frac{1}{2\pi}\left[\frac{1}{2} \sin i \left(\int_0^{2\pi} \{3 \cos 2\theta - 1\} \, d\theta\right)\right]\hat{b} = -\left(\frac{1}{2} \sin i\right)\hat{b}, \text{ and}$$

$$(\tilde{b}_f)\hat{n} = \frac{1}{2\pi}\left[\cos i \int_0^{2\pi} d\theta\right]\hat{n} = (\cos i)\hat{n}, \tag{VIII-31}$$

and if these values are substituted into equation (VIII-28), the average value of $\tilde{a}$ is obtained by:

$$\tilde{a} = \left(\omega_{po} - \frac{\eta}{2}\right) \sin i \, \hat{b} + \left(\eta + \omega_{po}\right) \cos i \, \hat{n}. \tag{VIII-32}$$

For $\tilde{a}$ to be parallel to $\hat{n}$, the $\hat{b}$-component of $\tilde{a}$ must be zero.

That is:

$$\omega_{po} - \frac{\eta}{2} = 0 \text{ , or} \tag{VIII-33}$$

$$M = \frac{2I_s \omega_s \omega_{po}}{M_E/R^3} . \tag{VIII-34}$$

For a spacecraft in which $I_S \omega_S$ is 160 inch-pound-seconds, and which is in a sun-synchronous orbit regressing at a rate of one degree per day, the magnetic-dipole moment required to maintain the spin axis in the orbit normal calculates to be 0.36 ampere-turns-meter ^{2}. (This figure is based upon the assumption of the uncanted dipole model of the earth's field discussed in Paragraph B-2a. Using the more accurate equations associated with the canted dipole model of the earth's magnetic field, evaluation by digital computer has shown, for comparable circumstances, that a drift error no greater than 0.5 degree in 10 days is introduced by assuming the simpler model of the earth's field.)

4. Magnetic Spin Control (MASC)

The magnetic-spin-control geometry is shown in Figure 4-VIII-4. Basically, magnetic spin control is accomplished by the placement of a current-carrying MASC coil in the spacecraft such that the coil axis, or normal, is perpendicular to the spacecraft spin axis (thereby causing torques to be generated about the spin axis) and by phasing half-spin-period current reversals through the coil (by means of the orthogonal horizon sensors) to maintain this torque in a constant direction. A mathematical discussion of the MASC concept is presented below.

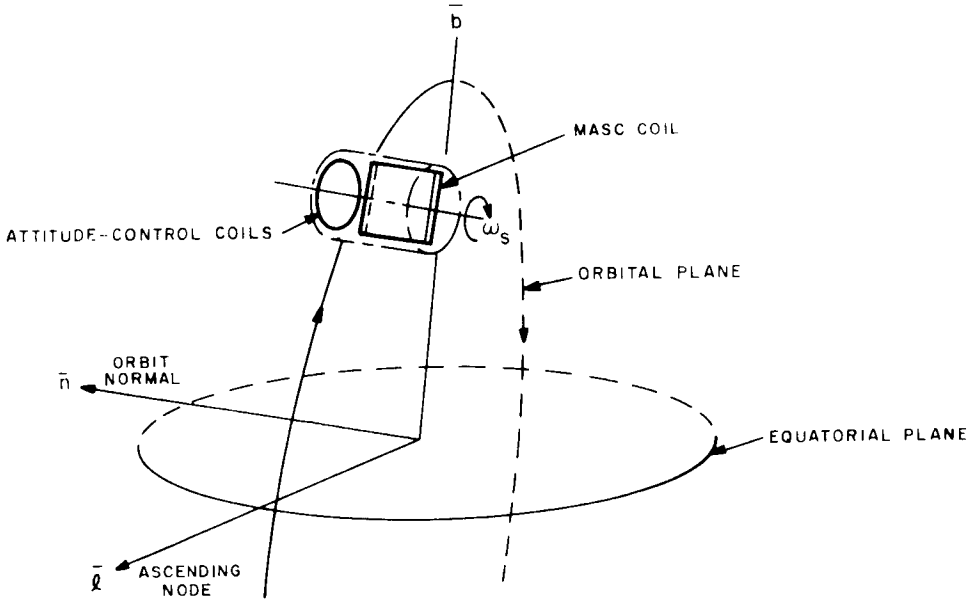

Figure 4-VIII-4. Magnetic Spin-Control Geometry

The instantaneous torque, T, acting upon the spacecraft due to the interaction of the magnetic dipole moment generated by the MASC coil, M, and the local earth's magnetic field, B, can be expressed as

$$\overline{T} = \overline{M} \times \overline{B}. \qquad \text{(VIII-35)}$$

(The local earth's magnetic field, in terms of the $\hat{\ell}$, $\hat{b}$, $\hat{n}$ coordinate system, is described in equation (VIII-10).)

If time, t, in one spin period is taken to be zero at the arbitrary position shown in Figure 4-VIII-5 (i.e., when orthogonal horizon sensor No. 1 senses a sky-to-earth transition), then the positive displacement of the coil normal, N_c, from the local vertical at the start of each spin period can be expressed by the angle γ. If a round earth is assumed, γ is a constant over any circular orbit of constant altitude. If the spin axis is normal to the orbital plane, then the unit vector in the direction of the positive coil normal is given by

$$N_c = \cos(\omega_s t + \gamma + \beta)\,\hat{\ell} + \sin(\omega_s t + \gamma + \beta)\,\hat{b}. \qquad \text{(VIII-36)}$$

The MASC concept requires that the magnetic moment of the coil, over one spin period be:

$$\overline{M} = M\,\overline{N}_c, \qquad \text{(VIII-37)}$$

when

$$0 \leq t \leq \frac{\theta_{1\text{-}2}}{\omega_s};$$

and

$$\overline{M} = -M\overline{N}_c, \qquad \text{(VIII-38)}$$

when

$$\frac{\theta_{1\text{-}2}}{\omega_s} \leq t \leq \frac{2\pi}{\omega_s}$$

where

$$M = n_c\, i_c\, A.$$

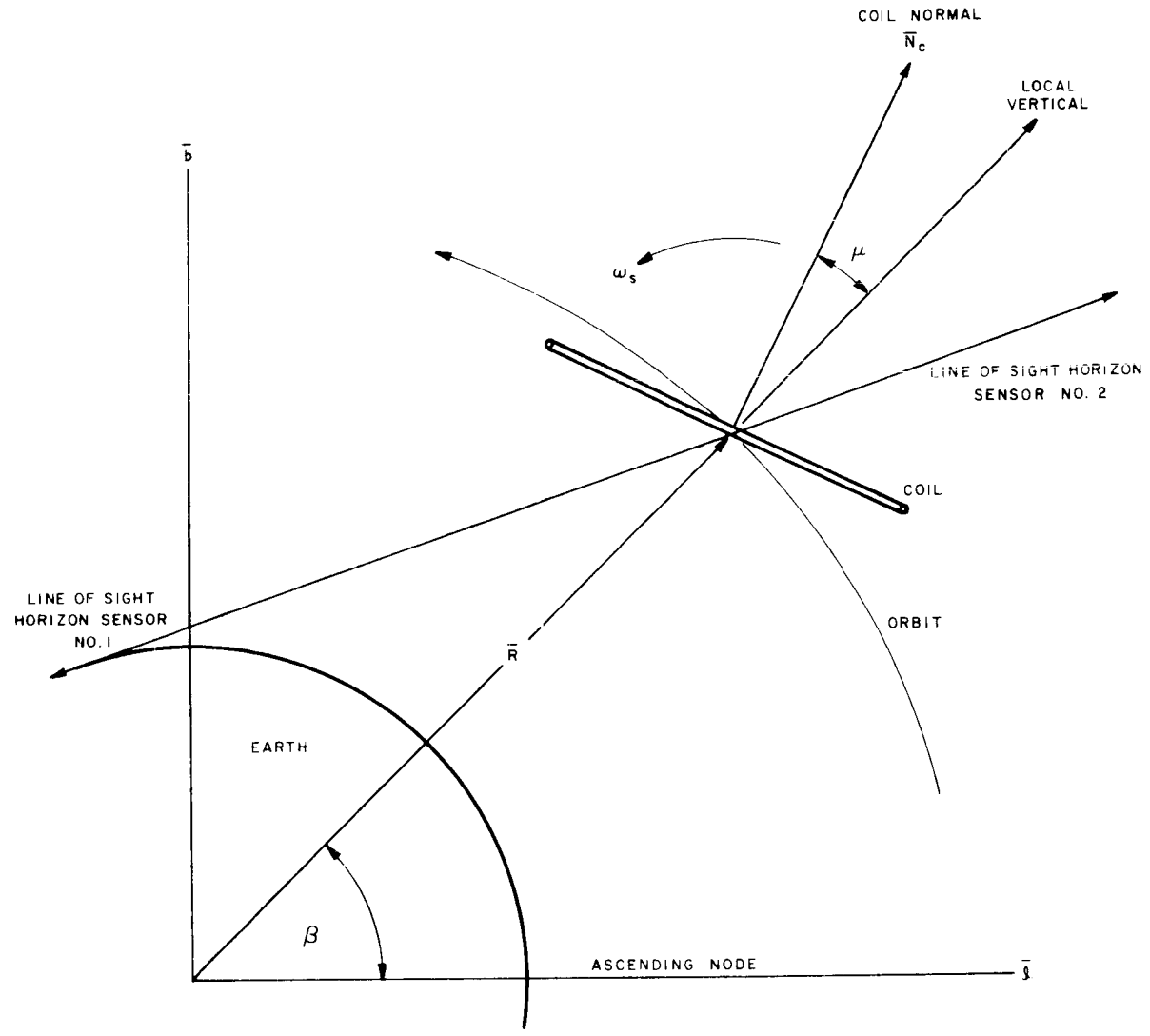

Figure 4-VIII-5. Angular Relationship of MASC Coil Normal to Local Vertical

Substituting in equation (VIII-35) produces the relationship:

$$\overline{T}(t) = \pm M \left\{ B_n \sin\left(\omega_s t + \gamma + \beta\right) \hat{\ell} - B_n \cos (CO\ t + \gamma + \beta)b \right.$$

$$\left. + \left[B_b \cos (\omega_s t + \gamma + \beta) - B_\ell \sin (\omega_s t + \gamma + \beta) \right] \hat{n} \right\}. \qquad \text{(VIII-40)}$$

The net average torque produced in one spin period is:

$$\overline{T}_{\frac{AVG}{SPIN}} = \frac{\omega_s}{2\pi} \int_0^{2\pi/\omega_s} \overline{T}\,(t)\, dt. \qquad \text{(VIII-41)}$$

Substituting equation (VIII-40) into equation (VIII-41) and simplifying:

$$\overline{T}_{\frac{AVG}{SPIN}} = \frac{2M}{\pi} \sin\frac{\theta_{1-2}}{2}\left\{ B_n \sin\left(\frac{\theta_{1-2}}{2} + \gamma + \beta\right)\hat{\ell} - B_n \cos\left(\frac{\theta_{1-2}}{2} + \gamma + \beta\right)\hat{b} \right.$$
$$\left. + \left[B_b \cos\left(\frac{\theta_{1-2}}{2} + \gamma + \beta\right) - B_\ell \sin\left(\frac{\theta_{1-2}}{2} + \gamma + \beta\right)\right]\hat{n} \right\}. \quad \text{(VIII-42)}$$

It can be demonstrated that optimum MASC operation occurs when θ_{1-2} is 180 degrees, and the angle γ is zero degrees. Since this is the case in the OT-2 spacecraft (acomplished by the mechanical orientation of the horizon sensors with respect to the MASC coil), equation (VIII-42) can be simplified to:

$$\overline{T}_{\frac{AVG}{SPIN}} = \frac{2M}{\pi}\left\{ B_n \cos\beta\,\hat{\ell} + B_n \sin\beta\,\hat{b} - \left[B_b \sin\beta + B_\ell \cos\beta\right]\hat{n} \right\}. \quad \text{(VIII-43)}$$

For spin-axis orientation perpendicular to the orbital plane, the $\hat{m}$ component of the T AVG/SPIN vector defined by equation (VIII-43) provides the spin-control torque, while the $\hat{\ell}$ and $\hat{b}$ components introduce some precession of the spin axis. The change in spin rate occuring over angular orbit sector $(\beta_f - \beta_i)$ can be obtained from the integration of the $\hat{n}$ component over that sector, thus:

$$\Delta\omega_s = \frac{2M}{\pi}\int_{B_i}^{\beta_f} \frac{-\left[B_b \sin\beta + B_\ell \cos\beta\right] d\beta}{I_s\,\omega_o}. \quad \text{(VIII-44)}$$

The torque components along the $\hat{\ell}$ and $\hat{b}$ axis that produce precession are both proportional to the $\hat{n}$ component of the earth's field, or B_n. From equation (VIII-43), the average precession producing torque for any one spin revolution is:

$$T_{\frac{AVG.\ PREC}{SPIN}} = \frac{2MB_n}{\pi}\left(\cos\beta\,\hat{\ell} + \sin\beta\,\hat{b}\right). \quad \text{(VIII-45)}$$

C. ATTITUDE CONTROL

1. General

The techiques employed for controlling attitude of the OT-2 spacecraft will be fundamentally identical to those employed on the TIROS "I" spacecraft. However, specific details of operational concepts and modifications to several operational units have been incorporated to reflect improved performance capabilities and to meet the requirements imposed by the 750-nautical-mile orbital altitude.

2. Quarter Orbit Magnetic Attitude Control (QOMAC)

a. Operational Considerations

The general mathematical theory underlying QOMAC philosophy is outlined in paragraph 4-VIII-B. Operationally, the control scheme utilizes the generation of a dipole moment of a positive polarity (where positive is taken as coming out of the spacecraft "hat") for one quarter of an orbit, starting at some preselected time (time delay, T_o) from the ascending node, followed by a negative dipole polarity for the duration of a second quarter orbit. This is defined as one QOMAC cycle and is depicted in Figure 4-VIII-6. A sufficient number of these QOMAC cycles are programmed to process the spin axis to within 1 degree of the orbit normal.

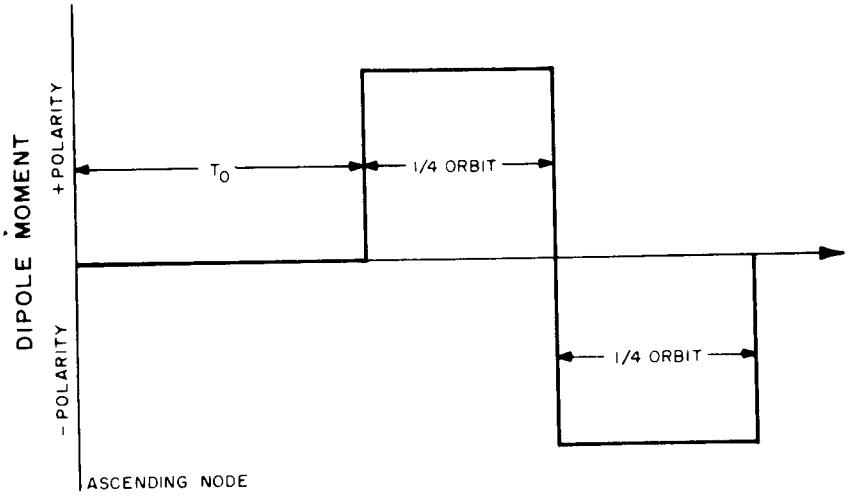

Figure 4-VIII-6. QOMAC Switching

The time delay, T_o, is directly related to the orbit angle and determines the position of the average spin-axis precession vector in the orbit plane. The equation which defines the direction of this vector is:

$$\tan 2\beta_o = \tan\left(\lambda - \tan^{-1}\frac{b}{a}\right), \qquad \text{(VIII-46)}$$

where

$$a = \frac{3}{2}\left(\cos i \sin i_m \cos \Omega - \sin i \cos i_m\right), \text{ and}$$

$$b = \frac{3}{2}\left(\sin i_m \sin \Omega\right).$$

Equation (VIII-46) differs from relationship implied in equations (VIII-16) and (VIII-17) in paragraph B-2-B of this section, that is:

$$\tan 2\beta_o = \tan \lambda ,$$

in that equation (VIII-46) includes the effect of the canted dipole model of the earth's field on an averaged basis. The two equations are plotted in Figure 4-VIII-7 to facilitate comparison. Analyses have shown that, in the worst case, the effect of the canted dipole is to generate an error of 11.4 degrees in the location of the average precession axis when the simpler equation is used. This was also verifed by a computer simulation of the spin-axis motion resulting from magnetic torquing.

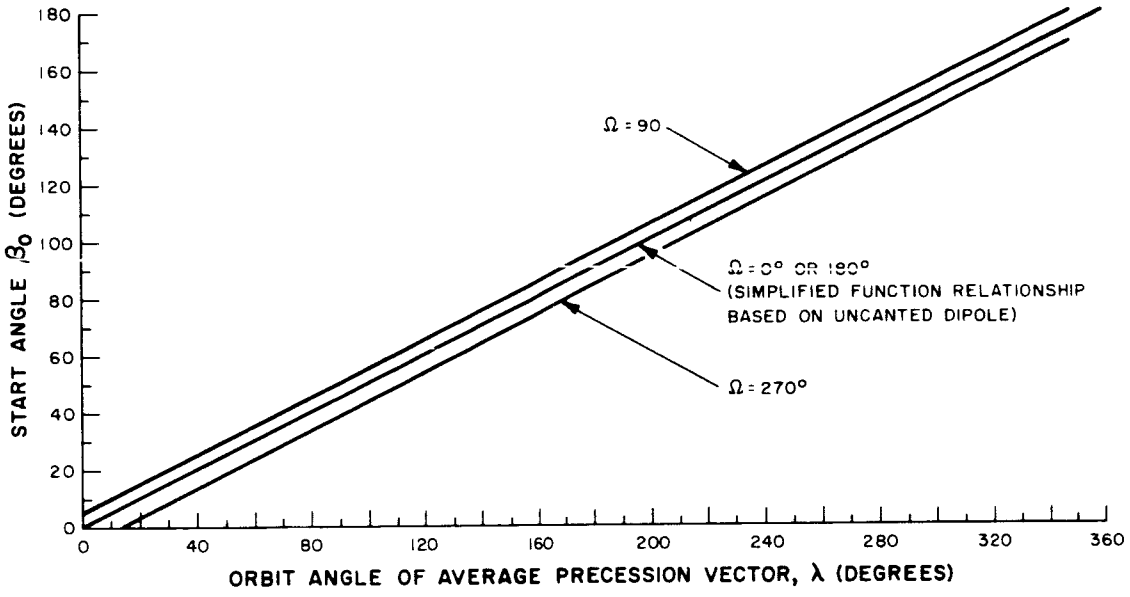

Figure 4-VIII-7. Effect of Canted Dipole on QOMAC Start Time

The approximate magnitude of the precession vector is given in equation (VIII-20) of Paragraph B-2-b as:

$$|\bar{\omega}_p| = \frac{3}{\pi} \eta \sin i,$$

where

$$\eta = \frac{M_E M}{R^3 I_s \omega_s} .$$

Both high-and low-torque modes of QOMAC operation are available. The high-torque mode is used for coarse control such as that required during the initial wheel-orientation maneuver, and determines the basic parameters for the QOMAC coil. Assuming a nominal spin rate of 10 rpm, a spin inertia of 160 inch-pound-seconds, an orbital altitude of 750 nautical miles, and an inclination of 101 degrees, equation (VIII-20) can be used to demonstrate that a precession rate of 10 degrees per orbit, or 5 degrees per QOMAC cycle, requires a dipole moment of 30.7 ampere-turns-meter^2.

The low-torque mode is achieved by the QOMAC coil, which provides a dipole moment of 6.12 ampere-turn-meter^2 (atm^2). The resulting torque causes a precession rate of 2 degrees per orbit, or 1 degree per cycle. This low-torque precession rate has been set to one-half the value proposed for the TIROS "I" spacecraft to permit the maintenance of a closer tolerance on the orbit-normal orientation of the spacecraft.

The high torque mode will be provided by operating the QOMAC coil in parallel with the MBC coil (Paragraph 4-VIII-C), thus resulting in the addition of 6.12 atm^2 to the 26.7 atm^2 maximum MBC dipole (32.8 being somewhat more than the minimum required). Such an addition, occuring at switch position 11 of the MBC switch, generates the high-torque QOMAC mode in a manner somewhat different than in the case of the TIROS "I" spacecraft. Instead of sizing the QOMAC coil for the high-torque mode and obtaining the low-torque level by inserting a series resistor, full use is now made of the availability of the MBC coil. A weight saving of 1.5 pounds is thus attained without increasing the complexity of the control switching circuit. For this mode only, quarter orbit switching of both coils is determined by the QOMAC programmer.

Because the OT-2/AVCS and OT-2/APT configurations are operated at different spin rates (9.23 and 10.9 rpm, respectively) the actual magnitude of the precession vector for a given dipole moment in each will differ, being as defined in equation (VIII-20). Assuming dipole moments of 6.14 and 30.7 ampere-turns meter^2, the precession rate as a function of spin rate is as shown in Figure 4-VIII-8. However, since most of the wheel-orientation maneuver will be performed before the achievement of the nominal spin rate, the precession rate during this maneuver will be a function of the orbit-injection spin rate and the de-spin ratio, and, therefore, can only be nominally predicted. It should be noted, however, that this is not of major significance since minor variations in the spin rate will simply result in a proportional variation in the time required for the maneuver, and will not impair the ability to perform the maneuver.

The effectiveness of the QOMAC technique is indicated in Figure 4-VIII-9, a projected history of the initial wheel-orientation maneuver obtained from a computer simulation. Although the curves shown do not consider the availability of ground-to-spacecraft contacts, they do provide a basis for realistic prediction of performance in orbit.

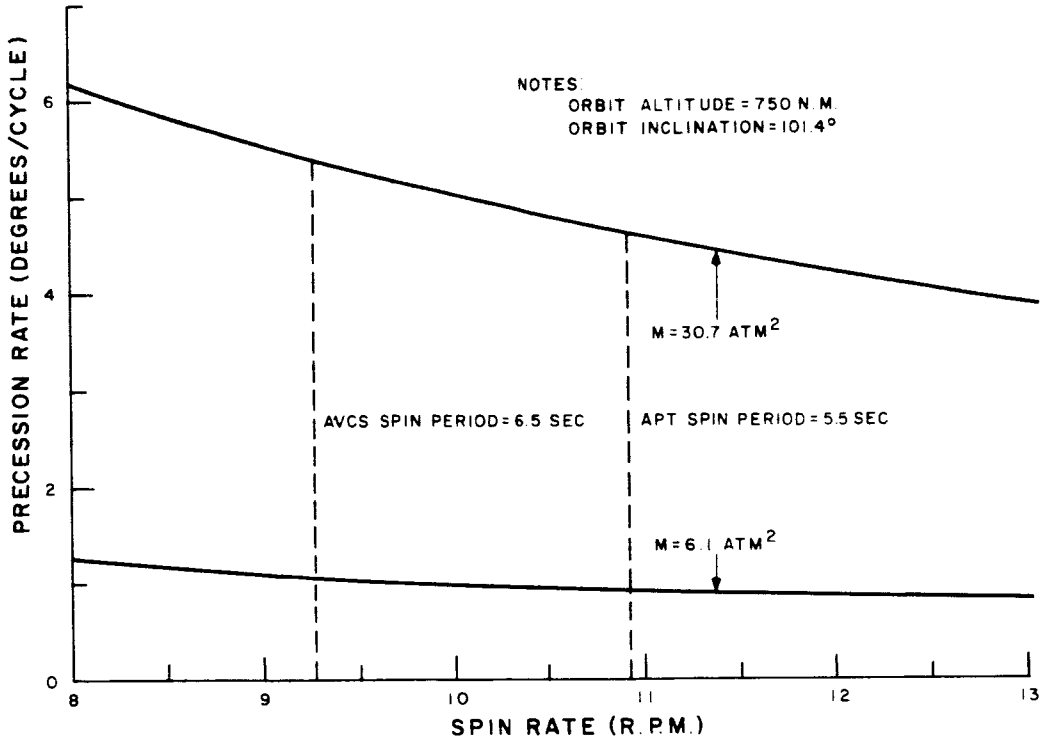

Figure 4-VIII-8. Precession Rate as a Function of Spin Rate

b. QOMAC Coil Design

Since the QOMAC coil is installed on the inside wall of the spacecraft hat, the shape and dimensions of the coil are determined by physical limits of the hat. Major design considerations for the coil are (1) minimum weight and power consumption and, (2) maximum area. To achieve the required 6.12 ampere-turns-meter dipole, a resistance of 200 ohms is inserted in series with the coil. (While the increase resistance could be obtained by using a smaller-diameter wire, problems in manufacturing the coil would result from the extremely thin wire that would be required.)

The parameters of the QOMAC coil are as follows:

type of coil:	center-tapped,
power supply:	-24.0 VDC,
area:	0.746 meter ^{2},
circumference:	3.08 meters,
wire:	30 gauge
total weight of wire:	0.31 pounds,
number of turns:	328,

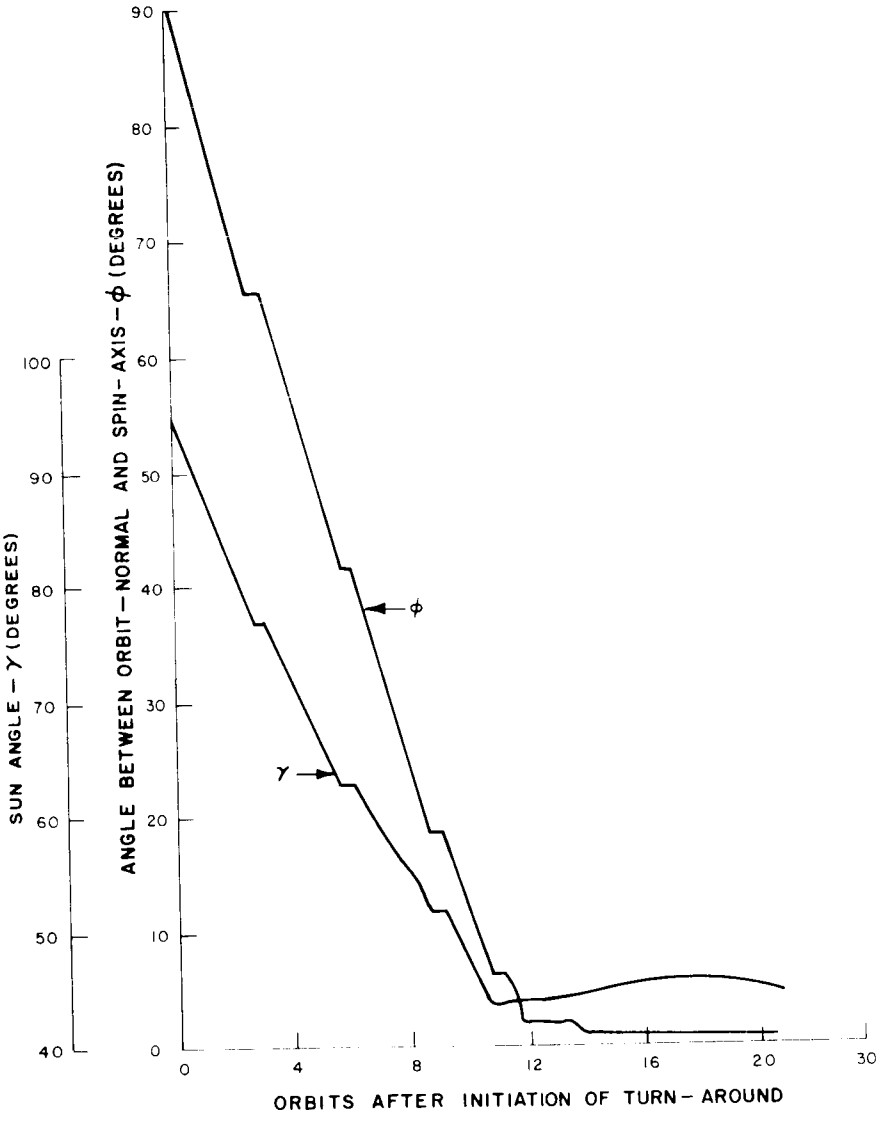

Figure 4-VIII-9. Typical 90-Degree Attitude Maneuver

duty cycle:	one cycle every three to four days in the station-keeping mode; nearly continuous operation in the station-acquisition mode,
resistance in 1/2 coil:	280 ohms at 20°C,
low-torque resistor:	270 ohms,
current:	0.050 amps,

power: 1.2 watts, and

dipole moment*: 6.12 amp-turns-meter^2.

3. Magnetic-Bias Control (MBC)

a. Operational Considerations

The Magnetic-Bias-Control (MBC) technique is essentially the same as employed on the conventional TIROS spacecraft for Magnetic Attitude Control (MAC). However, whereas the MAC technique on TIROS II through VIII was the primary method for controlling attitude, the MBC technique will be used primarily to null the OT-2 spacecraft's residual dipole moment and to compensate for the effects of the regressing orbit, thereby reducing the number of QOMAC cycles required for station keeping. This reduction in QOMAC cycles will be accomplished by introducing a dipole moment into the spacecraft of a magnitude and polarity to reduce the rate of change of the spin vector with respect to the orbit normal to a minimum, once the spin vector has been aligned with the orbit normal.

A mathematical description of the MBC technique is presented in Paragraph 4-VIII-B. Because this theoretical development is based on an uncanted dipole model of the earth's magnetic field, it is only approximately correct. However, a computer simulation has demonstrated that generation of an appropriate dipole moment; M, in accordance with equation VIII-34 of Paragraph 4-VIII-B, that is,

$$M = \frac{2I_s \omega_s \omega_{\rho o}}{\frac{M_E}{R^3}} ,$$

can greatly reduce the rate at which the spin axis drifts from the orbit normal. If a nominal spin rate of 10 rpm, a spin inertia of 160 inch-pound-seconds, orbital altitude of 750 nautical miles, and an orbital inclination of 101 degrees are assumed, the dipole moment required to achieve this reduction becomes +0.45 ampere-turns-meter^2. This value is compared with dipole moments of -0.4 ampere-turns-meter^2 (atm^2) and zero atm^2 in the curves of Figures 4-VIII-10, and 4-VIII-11. Note from Figure 4-VIII-10, that a residual magnetism of -0.4 atm^2 would necessitate QOMAC torquing

---

*The dipole moments differ from the idealized values because of the characteristics of available wire, however, these variations are negligible because of other factors which will have similar effects, the most significant of these being temperature variations and phasing (QOMAC start-time) errors.

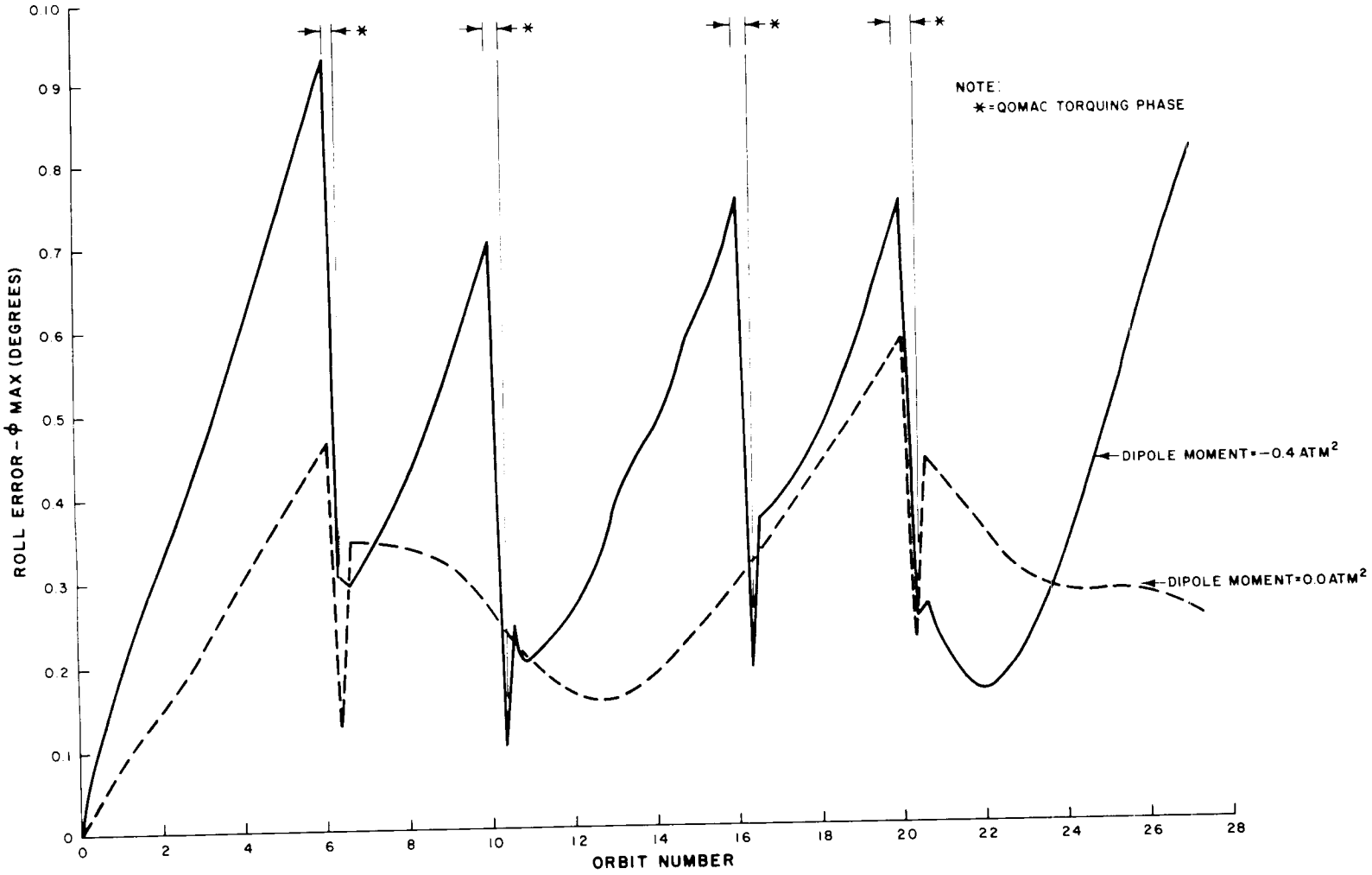

Figure 4-VIII-10. Effects of -0.4-ATM^2 and Zero-ATM^2 Magnetic Dipoles on Attitude Drift

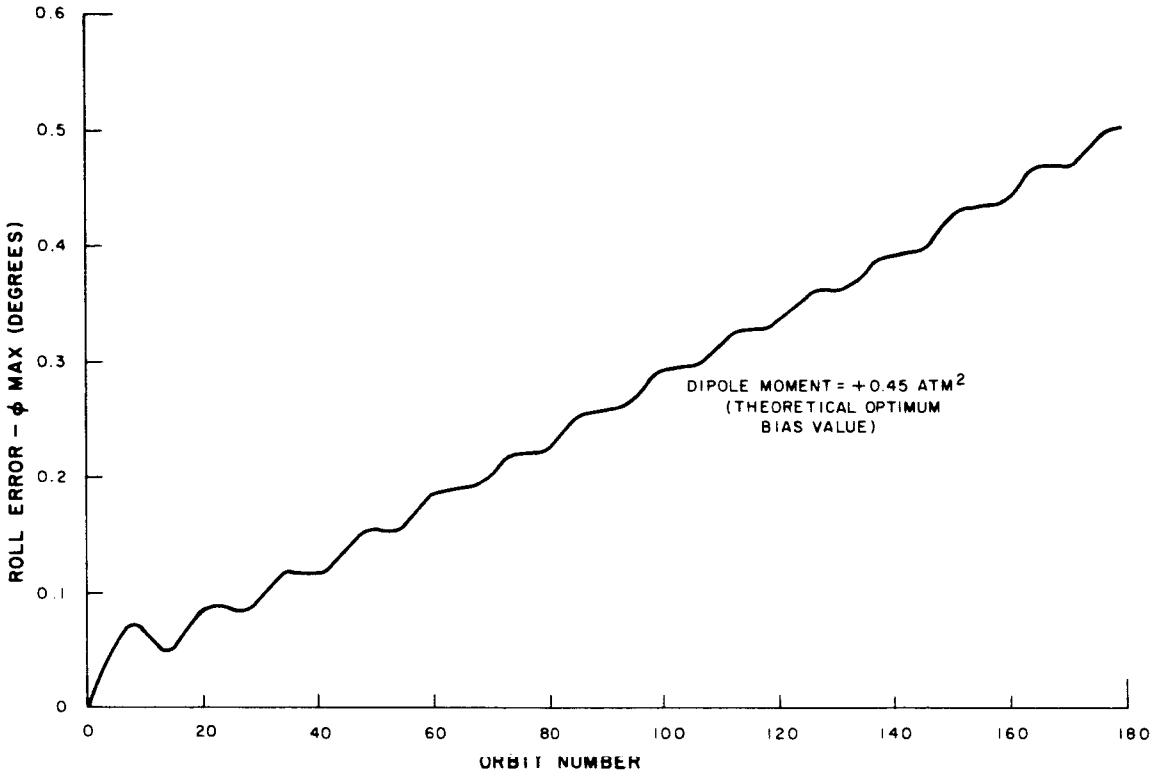

Figure 4-VIII-11. Effects of +0.45 ATM^2 Magnetic Dipole on Attitude Drift

operations at intervals of 4 to 6 orbits. Note also, from the first six orbits on Figure 4-VIII-10, that, undisturbed, a dipole moment of zero atm^2 (i.e., residual magnetism completely nulled) would result in the introduction of an attitude error at a rate that closely follows the 1-degrees-per-day nodal regression rate. However, as indicated in Figure 4-VIII-11, a +0.45 atm^2 dipole moment results in a displacement of the spin axis from the orbit normal of only 0.5 degrees after 14 days.

b. MBC Coil Design

Since the MBC coil, like the QOMAC coil, is installed on the inside wall of the spacecraft hat, the shape and dimensions are determined by the physical dimensions of the hat. The MBC coil parameters are as follows:

type of coil:	center-tapped,
power supply:	-24.0 VDC,
area:	0.746 $meter^2$,
circumference:	3.08 meter,
wire:	26 gauge,

total weight of wire:	1.67 lbs,
number of turns:	714,
resistance in 1/2 coil:	240 ohms (at $20^{o}C$),
current (max):	0.100 amperes (max),
power (max):	2.4 watts, and
dipole moment (max):	26.7 ampere-turns-meter^2.

The MBC switch, a twelve-position stepping switch, will be used in conjunction with a polarity reversing switch to regulate the amount and direction of current in the MBC coil. Position 10 of the MBC switch is used to set the current to the level required to provide the nominal 4-degree-per-orbit precession rate required for QOMAC back-up (See Paragraph C-6). At position 11, the maximum dipole moment, 26.7 ampere-turns-meter^2, is available for use in the high-torque QOMAC mode. As indicated in Table 4-VIII-2, the remaining nine positions are used to provide current levels corresponding to dipole moments of 0 to 1.54 ampere-turns-meter^2, and the polarity of the dipole moments are controlled by the polarity reversing switch.

TABLE 4-VIII-2. MAGNETIC-BIAS-CONTROL SWITCH POSITIONS

Position	Resistance (kilohms)	Current* (milliamperes)	Power* (watts)	Magnetic Dipole (atm^2)
1	39.9	0.61	0.014	0.16
2	19.9	1.18	0.028	0.32
3	13.1	1.81	0.043	0.49
4	10.1	2.35	0.056	0.62
5	8.3	2.84	0.068	0.76
6	6.8	3.42	0.082	0.92
7	5.6	4.05	0.095	1.12
8	4.7	4.86	0.117	1.32
9	3.9	5.63	0.131	1.62
10	0.3	44.5	1.07	12.1**
11	0	100.0	2.4	26.7***
12	-	OFF	-	-

*At positions 1 through 10, the potential is -24.5 volts; at position 11, -24.5 volts.
**QOMAC backup position.
***High-torque QOMAC mode.

4. Nutation Damping

a. General

An effective nutation damping system must provide both rapid elimination of any nutation imparted to the spacecraft and maintenance of a low nutation-threshold angle. To provide such a system for the OT-2 spacecraft, two methods were investigated: method 1, modification of the Tuned Energy-Absorbing Mass (TEAM) nutation-damping devices presently employed on TIROS satellites to meet the more stringent requirements imposed by the 750-mile, OT-2 orbit; and method 2, use of the existing (i.e., unmodified) TEAM system in conjunction with a liquid-type nutation damper* to accomplish the same result.

The TEAM damper has provided excellent nutation damping on all TIROS satellites launched to date. However, the nutation threshold requirement for the OT-2 spacecraft has been set at a half-cone angle of 0.3 degrees or less and the existing TEAM damper will theoretically provide only 0.6 to 0.8-degree half-cone angle threshold indicating a required improvement of at least a factor of two. The threshold limits depend on the friction of the moving parts. The TEAM damper could have been redesigned to meet the theoretical requirement of 0.3-degree threshold; however, it was decided that the implementation of a liquid damper to be used in conjunction with the proven TEAM dampers would be the better approach. This latter approach will utilize the existing TEAM damper for rapid convergence to a nutation angle of approximately 0.7 degrees followed by a somewhat slower damping towards threshold angles below 10^{-2} degrees accomplished by the liquid mechanism. In this fashion, the proven TEAM damper design will not be extended beyond reasonable limits, and the potential threshold angle will be well below the maximum permissible value. A discussion of the basis for this choice is given in the following paragraphs along with a description of the modifications to the TEAM mechanism that would be required if the liquid damper were not used and design details of the liquid damper.

b. Influence of Nutation on Camera Pointing Accuracy

A plot of nutation half-cone angle versus deviation of the principle camera point from the spacecraft subpoint is shown in Figure 4-VIII-12. Notice that no more than a 4-nautical-mile deviation of the principal point from the subpoint can be assured with a 0.6-degree half-cone nutation angle at a nominal altitude of 400 NM (that used for TIROS), whereas a 0.3-degree maximum half-cone angle is required at the OT-2 orbital altitude 750 nautical miles) to achieve a similar tolerance. It should be noted that a tightening of the theoretical nutation cone maintained by the damper mechanisms will facilitate the reduction of attitude-measurement data from the V-head horizon-sensor.

---

*The liquid nutation-damping theory was developed during a recent AR&D effort conducted at the Astro Electronics Division of RCA, near Princeton, N. J.

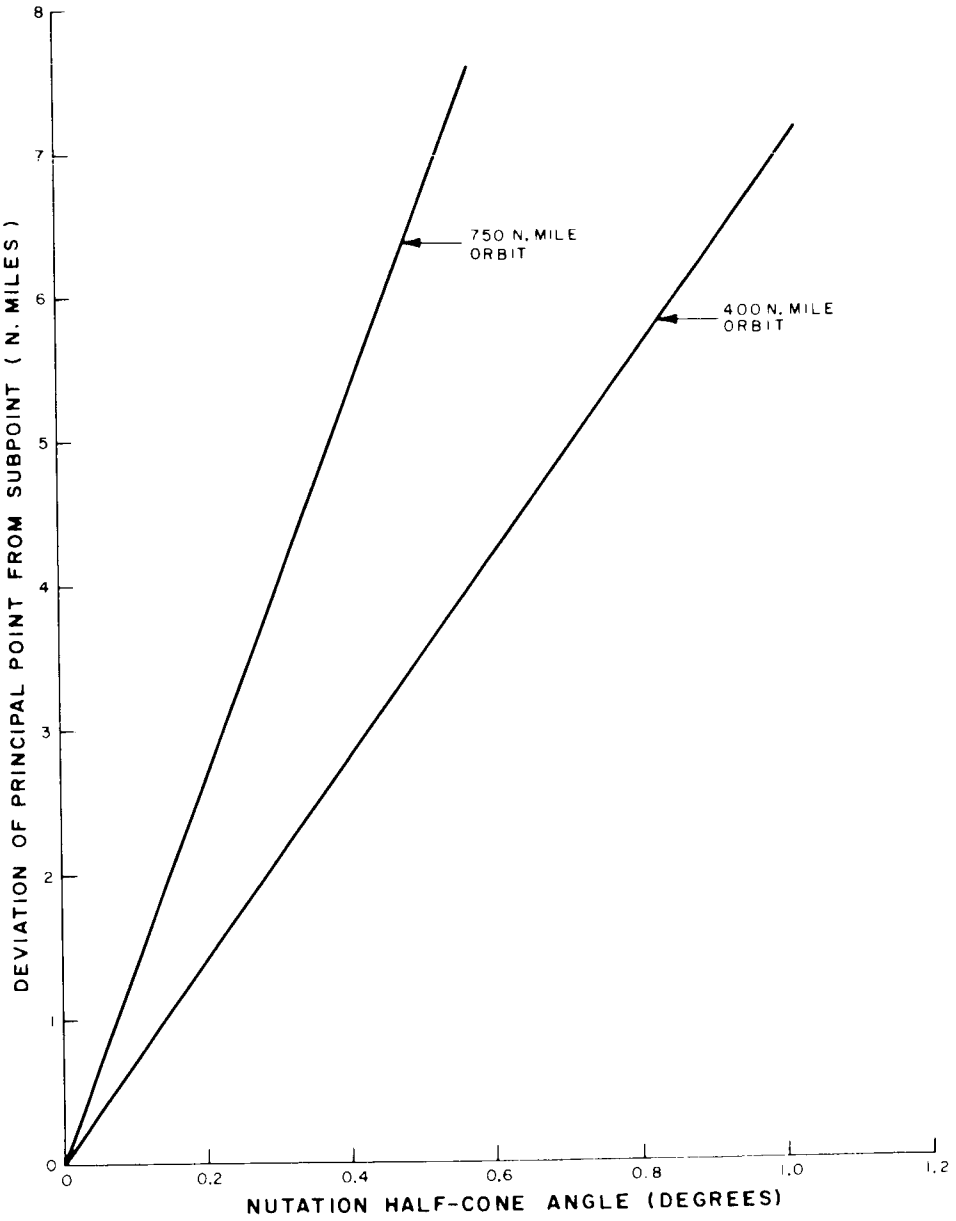

Figure 4-VIII-12. Deviation of Principal Point from Subpoint Versus Nutation Half-Cone Angle for Orbital Altitudes of 750 and 400 Nautical Miles

c. TEAM Damper Modifications (Method 1)

The TEAM mechanism consists of a slightly curved monorail located at the spacecraft periphery and parallel to the spin axis, and a mass in the form of a cart which slides on this monorail. The cart is held in a caged position at one end during launch and ascent and is released at separation of the spacecraft from the third stage. Motion of the mass dissipates energy in the form of heat due to friction, and, since this motion is caused by nutation of the satellite, a one-way energy flow occurs. The energy-conversion process continues until the nutation angle is very small and the spacecraft is very nearly spinning about the maximum moment-of-inertia axis.

In order to satisfy the 0.3-degree maximum threshold requirement imposed by the 750-nautical-mile orbit, the present design would have to be modified. This could be accomplished by increasing the cart weight from 93 grams to 300 grams and by disqualifying all units that display a breakaway friction, K, greater than 0.05 gram. This would bring the nutation-threshold angle just within the tolerance required for the OT-2 spacecraft.

Figure 4-VIII-13 shows the variation of nutation-threshold angle with cart weight for two different K values, based on OT-2 spacecraft parameters. It can be seen that a

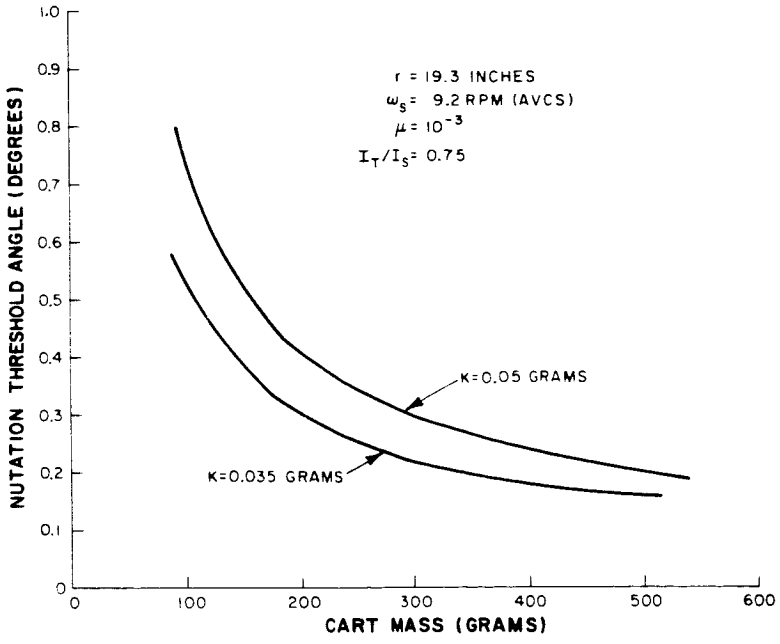

Figure 4-VIII-13. Nutation Threshold Angle Versus Cart Mass

300-gram mass and a breakaway of no more than 0.05 grams would result in a maximum half angle of 0.3 degree. The governing equation is:

$$\theta_o = \frac{\frac{K}{m r \omega_s^2} + \mu_o}{\frac{I_S}{I_T} 2 - \frac{I_S}{I_T}}. \qquad \text{(VII-48)}$$

The cart weight could be increased by using tungsten for the entire cart body and by increasing the cart length by approximately 0.5 inches. Since operation of this configuration before despin would cause the existing rod to deflect 0.71 inches when the cart is at the center position (or 0.49 inches more than with the existing 93-gram cart), it would be necessary to increase the depth of the case by 0.6 inches in order to prevent hangup. Although increasing the diameter of the rod would reduce deflection, it would also require redesign of the wheels, retainers, and spin locations. In addition, the rod would have to withstand a bending stress of 110,000 psi without permanent damage. This would necessitate changing the rod material from RCA Specification No. 2010799 to RCA Specification No. 2010942 (RCA Specification Nos. for precipitation-hardenable-type, stainless-steel rods), thereby increasing the yield point of the rod from 45,000 psi to 185,000 psi.

In order to assure that the maximum permissible breakaway friction will not be exceeded, quality control testing would have to include a careful measurement of this value. In addition to the friction measurement, strict quality control would have to be enforced to guard against flat spots in the bearings.

d. Liquid Nutation Damper (Method 2)

Instead of redesigning the TEAM damper, a better approach with far greater performance potential consists of supplementing the existing TEAM damper with a liquid device. Liquid dampers, which have been proposed and used on space satellites (principally, the Relay Communications Satellites) with good results, fall into two basic types: (1) passages of toroidal geometry completely filled with liquid and (2) passages of toroidal geometry partially filled with liquid. The damper is installed on the spacecraft in a position such that nutational motion excites the liquid in the tube, causing it to move relative to the walls. Energy is absorbed by this mechanism through the viscous drag of the fluid flow.

In the case of a spinning spacecraft having spin inertia greater than the transverse inertia (i.e., a stable configuration) the partly filled toroidal damper is installed with the damper axis co-linear with the spin axis and displaced from the spacecraft's center of gravity. Nutational motion causes the fluid in the damper to form into a

cohesive mass which moves relative to the damper ring. However, at small nutational angles, the liquid loses cohesion, becomes distributed around the damper ring, and damper effectiveness is drastically reduced.

The completely filled liquid damper, on the other hand, is installed with its plane parallel to the spin axis of the vehicle. In this position, it is excited by the transverse spin imparted to the spacecraft during precessional motion. The damper sees an oscillatory spin rate, thus causing the fluid to move relative to the tube wall. At very low nutation angles, small amplitude oscillations continue to excite the damper and the energy loss continues so long as the damper fluid maintains its Newtonian viscosity characteristics. Investigations had shown that the Newtonian characteristics continue down to rates below the order of earth rate. This corresponds to a precession angle of about 4×10^{-3} degrees. This is about two orders of magnitude better than the achievable TEAM damper performance*.

The time constant associated with a completely filled toroidal tube has been computed. The equation relating the damper time constant characteristics and the satellite dynamics is as follows:

$$\bar{T}_n = \frac{I_T^2}{0.189\ H\ I_d}, \qquad \text{(VIII-49)}$$

where 0.189 represents the effectiveness of an optimum ring damper.

The damper for the OT-2 spacecraft, however, is not circular but will consist of two tubes, filled with a liquid and installed on the inside of the hat as shown in Figure 4-VIII-14. Generous curves are provided where bends are required. The damper tubes traverse the top of the hat along parallel chords, turn down along the sides of the hat and follow a partial circumference at the bottom. For a 20-minute time constant, an equivalent toroidal damper requires an inertia, I_d, of 0.35 pound-inch-seconds^2 for I_T = 116 pound-inch-seconds^2, H = 17.2 pound-inch-seconds.

The fluid mass in the damper can be computed by equating its inertia to that of the equivalent toroidal type. A fluid mass of about 0.9 pounds, distributed in a tube of the above (approximate) geometry, will have a theoretical time constant of 1200 seconds. Since the tube geometry is non-circular, the practical fluid mass required could be as much as twice the theoretical value, or 1.8 pounds. Testing on a torsional pendulum fixture at spacecraft frequency levels will permit experimental verification of this time constant.

---

*Whether such a low threshold can be maintained depends upon the amount of disturbing energy to which the spacecraft is subjected. In any case, a liquid damper has the capability of removing energy at far smaller nutation angles than its TEAM counterpart.

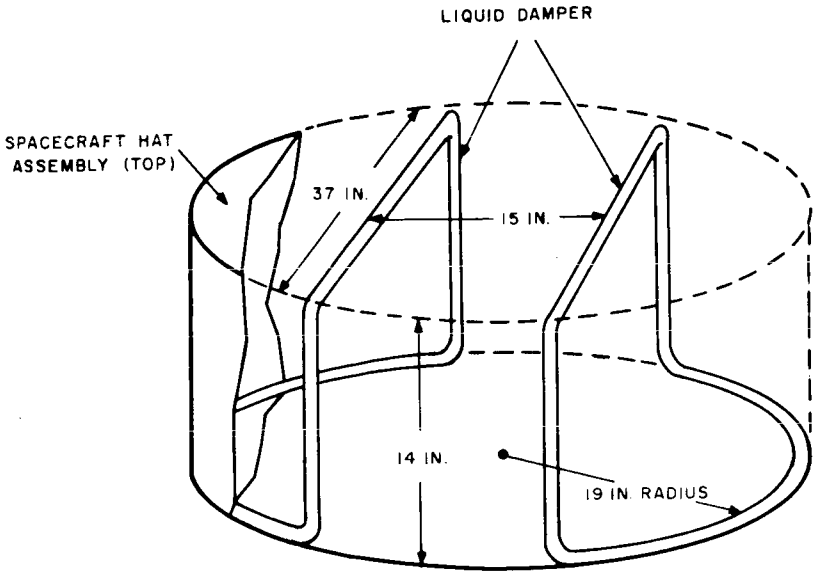

Figure 4-VIII-14. Installation of Liquid Damper in Spacecraft Hat

The theoretical tube diameter, d_o, is a function of the fluids used. For example, in optimally designed toroidal dampers, the following relation applies:

$$d_o = 5.02 \sqrt{\frac{\mu}{\rho \sigma}}, \qquad \text{(VIII-50)}$$

where

$$\sigma = \frac{I_S - I_t}{I_T} \omega_S.$$

Selection of Dow-Corning, Series 200, Silicone Fluid permits the variation of viscosity, μ, for a certain density, ρ, thus permitting the optimization indicated by the above equation. The damper for this fluid consists of hermetically sealed of aluminum tubing of 1/2 inch outer diameter that is bent into the contour of the inside of the hat assembly and fastened thereto. To accommodate fluid volume changes with temperature in the hermetically sealed unit, an expansion bellows (located in the plane of the center of gravity) is included as an integral part of the liquid damper. The effect of radiation on the viscosity of the proposed fluid is minor for the nominal altitude, orbit inclination, and spacecraft life.

The fluid damper does not require caging during the coast phase of the launch sequence, since it has been established that, when the spacecraft is attached to the last stage booster, the time constant for the uncaged damper is 4 to 5 times larger than the design value. For example, if the fluid damper is designed for a 20-minute time

constant in orbital operation, it will develop a time constant of 80 to 100 minutes in the coast phase. This means that a one-degree cone angle in the coast phase will increase to a 2.7^{o} cone angle in 80 minutes. Since the actual coast phase is short, being on the order of a few minutes, caging is not required.

e. Conclusions

The utilization of two TEAM dampers of present design, in combination with two completely-filled liquid dampers, will result in a total damper weight of about 5.6 pounds. This method will achieve rapid convergence to about 0.7 degree half-cone angle, and assure further damping towards a half-cone angle less than 10^{-2} degrees with a time constant of 20 minutes. On the other hand, redesigning the existing TEAM damper would result in the marginal achievement of a threshold angle of 0.3 degree with two TEAM dampers weighing 3.4 pounds. The first of these two methods has been selected in order to avoid marginal performance without a marked increase in spacecraft weight.

5. Spin-Axis Measurement

a. General

Two methods by which the attitude of the spacecraft spin axis can be determined are available in the OT-2 system. The first utilizes both channels of the V-head horizon sensor; the second, the output of either channel of the V-head horizon sensor and the output of the solar-aspect sensor. Two parameters which can be used directly for QOMAC programming are obtained when the first method is used, and after the wheel attitude has been achieved, is more accurate than the second method. However, during periods when V-head horizon-sensor information is sparse and generally insufficient for a complete attitude computation (e.g., during the station-acquisition maneuver or passes with short spacecraft-to-ground contact time) the second method of attitude determination will be employed. When the second method is used, the right ascension and declination of the spin axis are determined and this information, in turn, is used to determine the orientation of the spin axis in terms of orbit coordinates.

b. Attitude Determination Using the V-Head Horizon Sensor

(1) General

The V-head horizon sensor consists of two infrared bolometers arranged with their optical axes in a "Vee" configuration (as shown in Figure 4-VIII-15) and associated electronics circuits. The plane of the "Vee" contains the spin axis, and the

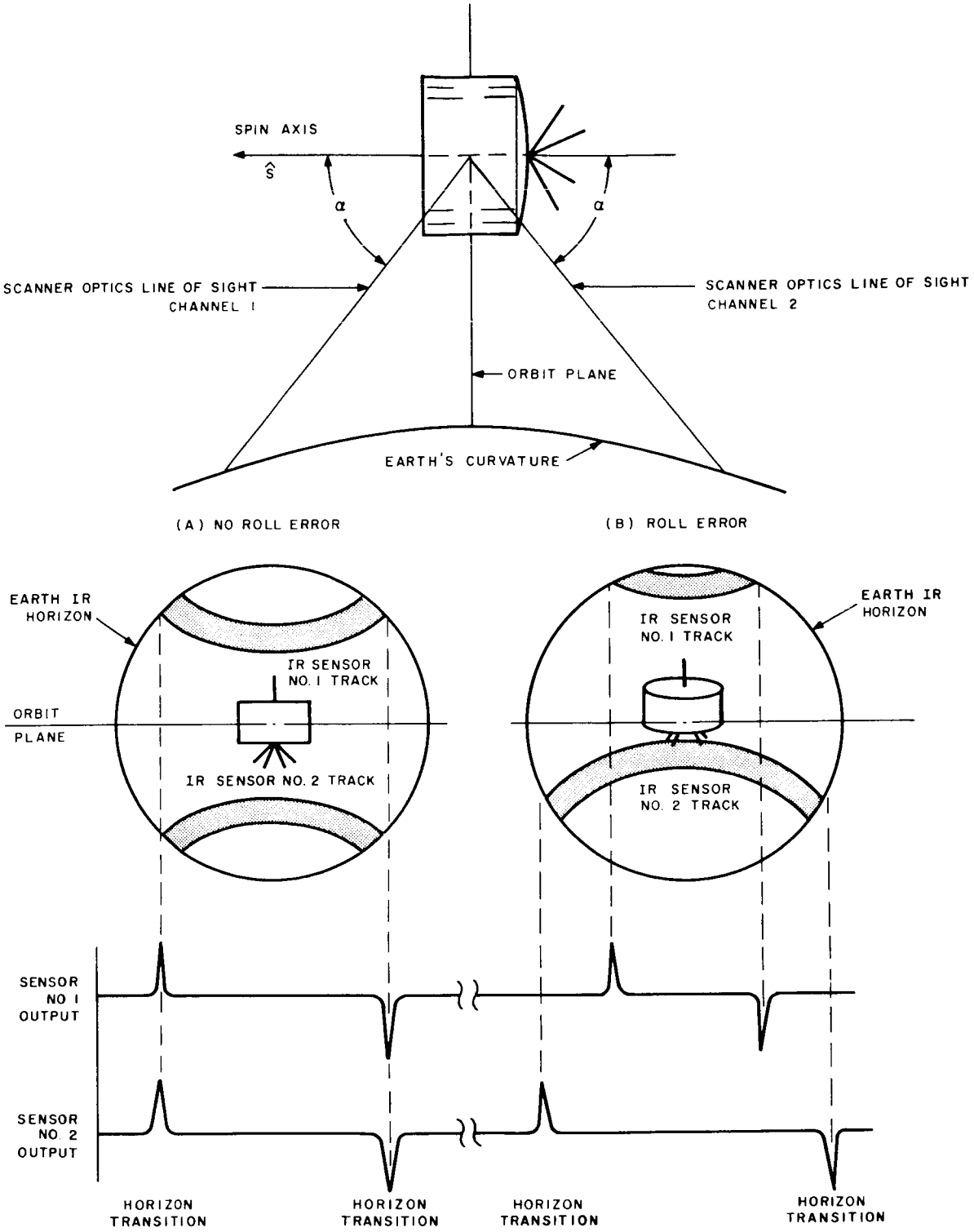

Figure 4-VIII-15. Attitude Sensor Geometry

bisector of the "Vee" angle is normal to the spin vector. As the spacecraft spins, the optical axes trace out two conic sections in space. The intersection of these sensor paths with the earth and the corresponding outputs from the sensors are also shown in Figure 4-VIII-15. When the spin axis of the spacecraft is normal to an earth radius, the outputs of the sensors will be of equal duration as shown in Figure 4-VIII-15A.

Should a roll error (defined as 90 degrees minus the angle between the spin axis and the local vertical) exist, the pulse durations from the two sensors will be unequal, as shown in Figure 4-VIII-15B. Should a pure yaw error (i.e., a displacement from the orbit normal about the local vertical) exist at a given point, it will be evidenced as a roll error 90 degrees later in the orbit and unequal outputs will again be experienced. This shift of the yaw to roll error is due to the inertial rigidity of the spin vector which causes the roll and yaw errors to vary sinusoidally, 90 degrees out of phase with one another. This relationship is apparent from equations (VIII-13) and (VIII-14) given in Paragraph 4-VIII-B, thus:

$$\sin \phi = \sin \phi_{max} \sin (\beta - \lambda), \text{ and}$$

$$\sin \psi = \sin \phi_{max} \cos (\beta - \lambda).$$

The maximum roll angle, ϕ_{max}, must be known in order to determine the maximum number of QOMAC cycles, and the angle λ must be known in order to compute the time delay required between the time of the ascending node and the start of the QOMAC cycle. The time dependence (i.e., β dependence) in the above equations permits complete attitude determination from a sequence of instantaneous roll measurements, the accuracy of which is determined by the resolution and reliability of each of the data points. Approximately 10 minutes of roll-error history for a given pass over a ground station is required to minimize data reduction problems. The actual procedure is outlined in the following paragraphs.

It can be shown that for small roll angles there is a linear relationship between roll error and the difference in earth-scan times of the two sensors. Thus:

$$\phi = S\Delta t_e, \qquad \text{(VIII-51)}$$

where,

$$\Delta t_e = t_{e_1} - t_{e_2}.$$

and S is a roll-angle sensitivity constant and is a function the geometry of the sensors, the orbit altitude, and the spin rate.

Figure 4-VIII-16 is a plot of S versus the included angle of the two optical axes of the V-head horizon sensor for a nominal spin rate of 10 rpm. Also shown is a plot of the physical limits of dynamic range as a function of the included angle. The included angle used in the OT-2 spacecraft is 86 degrees, a compromise for the values determined for the TIROS "I" satellite for the dynamic range and sensitivity of the sensor. The sensitivity for this included angle is 99 milliseconds per degree of roll, and the theoretical dynamic range is ± 12.2 degrees. However, the actual dynamic range will be somewhat less than this value because of the oblique grazing angles that will be experienced by the sensors.

The expression that will be used to facilitate accurate, manual computation of the instantaneous roll angle is:

$$\tan \phi = \frac{\tan \alpha}{2} \left(\cos \frac{t_{e_1}}{t_{s_p}} \pi - \cos \frac{t_{e_2}}{t_{s_p}} \pi \right). \qquad \text{(VIII-52)}$$

As in the case of the TIROS "I" spacecraft, this equation will be reduced to a nomogram from which the roll angle can be graphically determined from the ratio of earth-to-spin time for each sensor. (These ratios can be measured easily and directly using a Gerber scale.) A second nomogram will be provided for graphically determining the roll error from either head of the V-head sensor in the event of a failure in the other head.

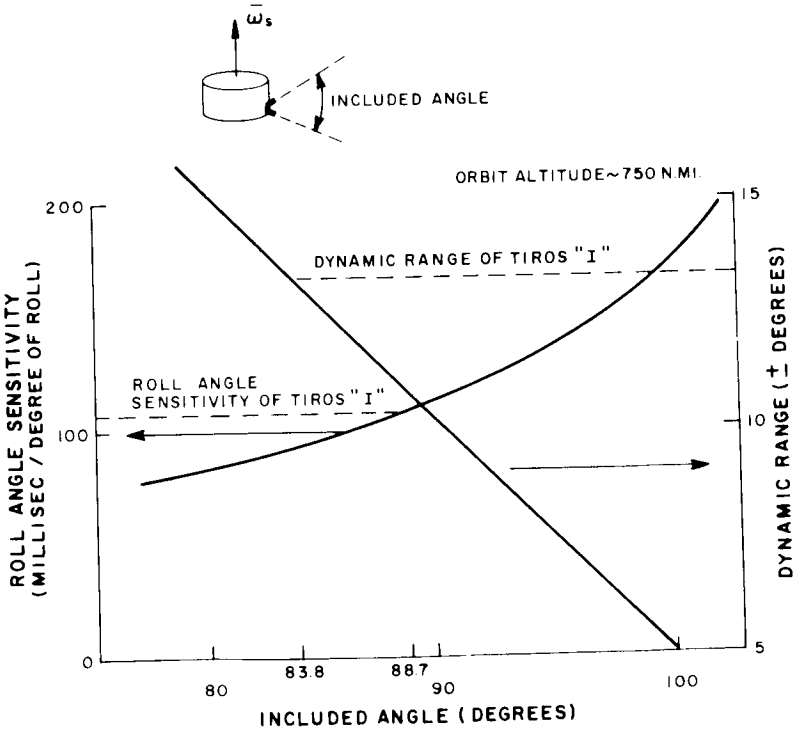

Figure 4-VIII-16. Dynamic Range and Roll-Angle Sensitivity of the Horizon-Sensor

The data obtained from the nomograms will then be plotted on special graph paper for which preprepared overlays are supplied. These overlays, plots of equations (VIII-13) and (VIII-14) for various ϕ_{max} values, can be used for manual reduction of the appropriate ϕ_{max} and λ parameters from the nomogram data.

This method of data reduction is a proven technique for computing the attitude of a wheel-mode spacecraft. It has the advantage of permitting the use of an operator's judgement in determining the location of the horizon crossings, which is particularly useful for locating the earth-to-sky transitions. It will take an operator approximately 30 to 40 minutes to reduce the attitude data from one pass.

Consideration has been given to using a computer for data reduction. Although computer techniques exist for computing attitude from the horizon-scanner data, the problem of automatically converting the horizon-scanner data into a form useable for computer reduction has not been completely solved. Whether or not a computer can provide attitude measurements more accurate than those derived manually depends on the accuracy of the automatic conversion of scanner data into computer format. Manual reduction of attitude data is a simple operation, and the use of a computer can only be justified if it can be shown that greater accuracy than that manually obtainable is operationally significant and that the data conversion problem can be solved.

(2) Error Analysis

Characteristically, there are two types of errors that can be experienced in determining spacecraft attitude from horizon-sensor data: the first is the error inherent in the dynamics of the system due to nutation effects; the second, the error due to ambiguities in using the data. In regard to the first source of possible error, the sinusoidal variation in roll angle (Equation VIII-13) is actually the variation in the average position of the angular-momentum vector with respect to the earth. If nutation exists, a second, periodic variation will be superimposed on the roll-angle variation. The frequency of the oscillation caused by nutation will be equal to $(I_S/I_t - 1)\ \omega_s$, which is approximately 0.4 times the spin rate. Because the frequency of the basic roll-angle variation is the same as the orbital rate, the oscillation resulting from nutation will appear as a high-frequency scattering of points about the mean roll-angle position.

The effects of two different nutation angles of typical roll histories are shown in Figure 4-VIII-17. As represented in the illustration, the amplitude of oscillation is proportional to the nutational amplitude. It is apparent that the problem of reducing roll data to ϕ_{max} and λ is more difficult for a 0.5-degree nutation than for a 0.2-degree nutation. Although averaging techniques are available for eliminating the major part of this error, this task is time consuming and tedious, especially when manual reduction is employed and, therefore, will not be used unless large nutation angles are experienced.

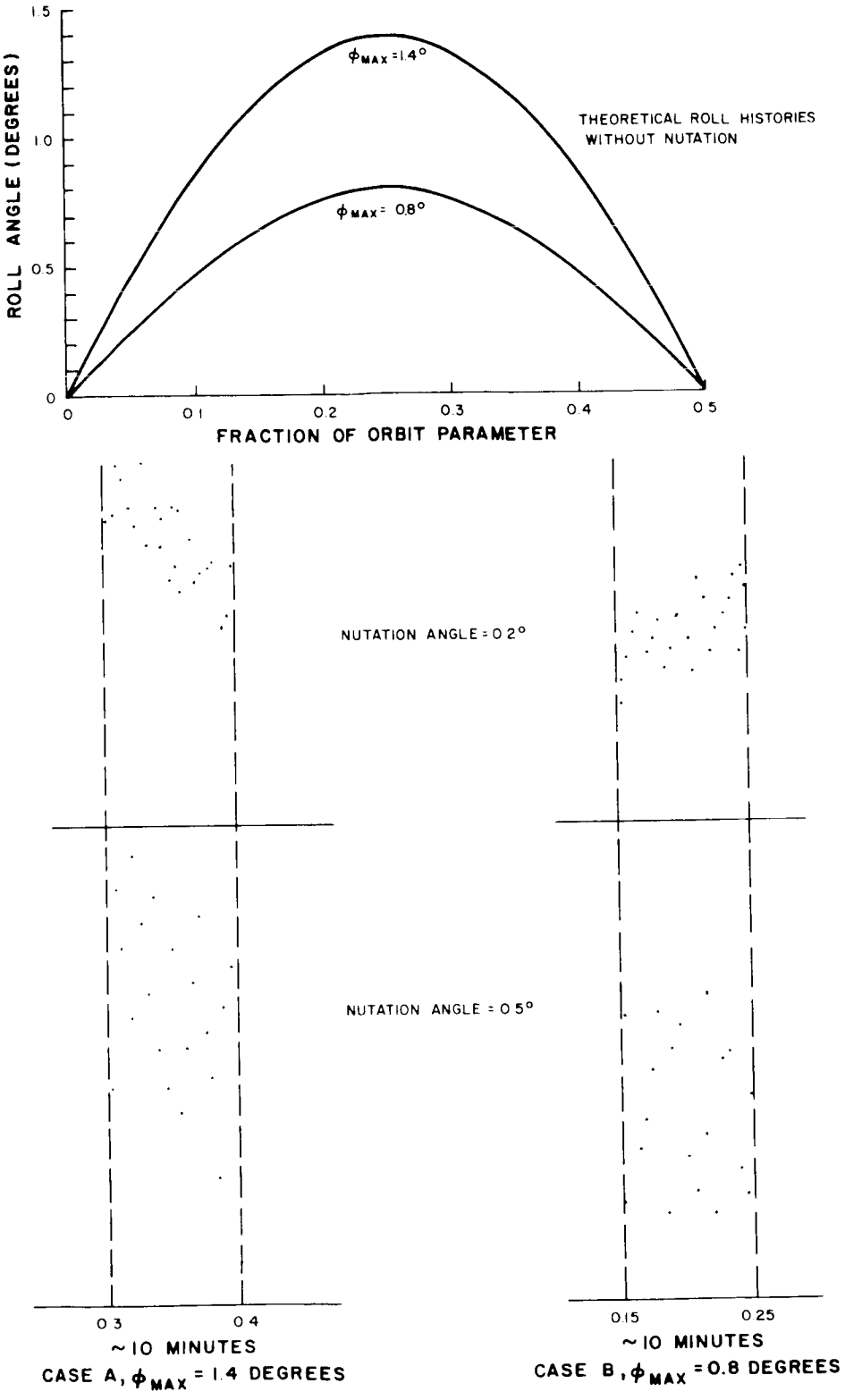

Figure 4-VIII-17. Effect of Nutation Angles on Typical Roll Histories

The second type of error can result from ambiguities in the data due to anomalies of the bolometer electronics, variations in effective earth temperatures, or errors inherent in the method of data reduction. These errors have been computed on the bias of a linearized equation, relating the difference in earth times from each head of the "Vee" to a roll error, i.e.,

$$\Delta\phi = S\Delta t_e, \qquad \text{(VIII-53)}$$

where S is a function of the spin rate, the orbit height and the included angle between the sensors. For the 750-nautical-mile OT-2 altitude and an included angle of 86 degrees, $S \simeq 10$ degrees per second. The nominal spin rate is assumed to be approximately 60 degrees per second and the Sanborn chart speed is 20 millimeters per second.

The equivalent earth temperature variation creates a change in the radiance input to the electronics. This results directly in a change in amplitude of the differentiated horizon-sensor output pulse, while the time required for the signal to peak remains unchanged. Because a threshold technique is used for sensing sky-earth and earth-sky transitions, this will introduce a variation in earth time as indicated in Figure 4-VIII-18.

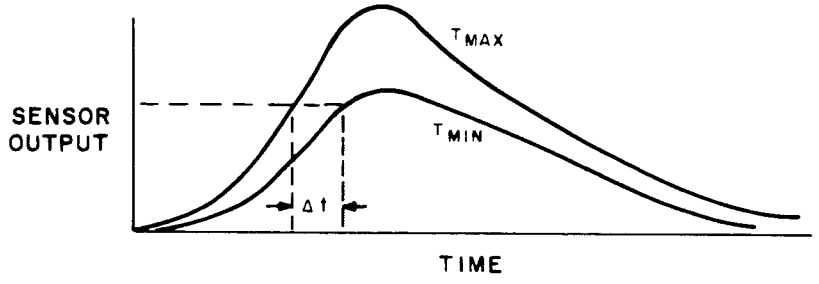

Figure 4-VIII-18. Effects of Earth Temperature Variations on Earth Time

The value of time differential, Δt, between the expected extremes of earth temperature (210°K and 290°K) is 16.5 milliseconds. If a worst-case situation is assumed — where one sensor in the V-head configuration sees maximum earth temperature on the sky-earth transition and minimum earth temperature on the earth-sky transition, while the other sensor sees exactly the reverse — the maximum error in earth time caused by this effect will be 33 milliseconds, and a corresponding worst-case error in attitude determination will be experienced.

The horizon temperature gradient is attributable to the fact that above the limb of the earth there exists an atmosphere approximately 60 kilometers high. As a line of sight is swept from the cold sky to the hotter earth, the transition will be gradual, rather than abrupt, as indicated in Figure 4-VIII-19.

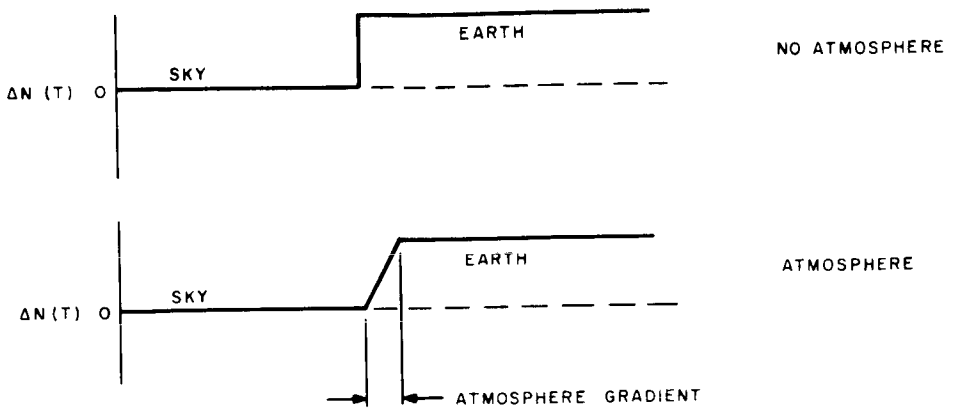

Figure 4-VIII-19. Effect of Atmosphere on Horizon Sensor Output

Using simulated data, the two cases shown in Figure 4-VIII-19 yielded a difference of 8.5 milliseconds in the location of the limb of the earth. The worst case condition introduced by this effect would exist if the gradient phenomena existed on the earth-sky and sky-earth of one sensor in the V-head configuration and not in the other, and would produce an error of 17 milliseconds. This situation is, at best, improbable; other arrangements of gradients will of course, have a lesser effect on earth-time variations.

Because the attitude data is to be reduced manually, the operator performing this reduction must judge, from a Sanborn chart, exactly where a particular point occurs: in particular where the sky-earth and earth-sky crossings for both sensors are located. It is estimated that the operator can locate such data to within 0.25 millimeters on a single point. Again assuming worst case conditions in measuring Δt_e this becomes a maximum error of 0.5 millimeters which, at a paper speed of 20 millimeters per second, is equivalent to a 25-millisecond error in time.

A summation of the worst-case errors introduced by earth-temperature variations, horizon temperature gradients, and manual data reduction, and the corresponding errors in roll-angle determination, is given in Table 4-VIII-3. Since the object of attitude determination is to determine ϕ_{max} and λ from instantaneous error which is random ($3\sigma = 0.44$ degree) can be less than 0.2 degree using a standard least-square-curve-fitting technique.

However, since the phasing of the nutation effect is almost impossible to predict, the uncertainty in roll and yaw at the time the shutter is operated is the sum of nutation (0.3 degrees) plus data ambiguity (0.2 degrees) or 0.5 degrees total.

The above error analysis assumes proper operation of both sides of the V-head horizon sensor, however, since, in the proposed orbit, one side of the sensor will sometimes be nearly colinear with the sun vector, and since past experience indicates that direct exposure of horizon sensors to the sun's energy is detrimental, the possibility of improper operation of one side must be considered.

TABLE 4-VIII-3. SUMMATION OF ATTITUDE DETERMINATION ERRORS

Cause	Maximum Earth-Time Error (milliseconds)	Equivalent Roll Error (degrees)
Earth-temperature variations	33	0.33
Horizon temperature gradient	17	0.17
Manual Data Reduction	25	0.25
Total worst-case Error	75	0.75
RMS of worst-case Errors		0.44

One possibility for abnormal operation is saturation of the system to the degree that the electronic circuits cannot recover before the succeeding pulse is received from the sensor. However, this effect will be reduced by modifying the amplifier design and changing the spectral response to the 13-to-23-micron region. The amplifier redesign and filter addition will restrict the sun's effect so that the saturation condition will be experienced only when the sun is on the horizon. Then, the major problem occurs when the sun is on the leading edge, i.e., sky-earth transition. The geometry of the 3 PM and 9 AM orbits is such that this unfavorable situation exists only the 60- to 80-degree southern latitudes and the 60- to 80-degree northern latitudes during, respectively, the period from September to March. Although the problem is less at the trailing edge, it does exist at the other extreme latitudes. For a 3 PM orbit this does not represent problem because data is not taken in the southern latitudes. Receipt of data at the East Coast station during 9 AM orbits will be unaffected, while at Fairbanks, approximately half the contact time will be clear.

A second possible cause of abnormal operation is an effective increase in the sensor's field of view because of high-energy inputs from the sun. This increase in the field-of-view results in spurious signals even when the sun vector is as much as 10 degrees off the sensor's optical axis. However, the presence of such spurious signals should cause no problem in the manual reduction of data, provided they do not occur near a horizon.

(3) Pitch Errors

The preceding paragraph discusses only those factors which affect the accuracy of attitude data originated by the V-head horizon sensor. However, the orthogonal horizon sensors, which are of a similar design, also experience variations

in earth temperature and horizon-temperature gradient which tend to affect the accuracy of camera alignment with the local vertical. Errors due to mechanical alignment are assumed negligible and those due to altitude variation and shutter actuation delay are assumed known. (The tape recorder is momentum compensated.) Hence the major cause of error is due to random variations in the characteristics of the horizon. These are listed in Table 4-VIII-4 for the nominal altitude of 750 nautical miles.

TABLE 4-VIII-4. FACTORS AFFECTING ORTHOGONAL HORIZON-SENSOR ACCURACY

Cause	Maximum Earth-Time Error (milliseconds)	Pitch Error (degrees)
Earth-temperature variations	$\pm$7.7*	$\pm$0.46
Horizon temperature gradient	$\pm$4	$\pm$0.24
Total worst-case pitch error	$\pm$11.7	$\pm$0.7
RMS pitch errors		$\pm$0.52

The effect of the horizon temperature gradient may be reduced to $\pm$4 milliseconds compensating the alignment of the camera with respect to the theorerical trigger pulse by 4 milliseconds. This, essentially, splits the difference between gradient and no-gradient situation.

c. Attitude Determination Using the Solar-Aspect Sensor

The solar-aspect sensor is normally used to measure the sun angle with respect to the spin axis. However, this data can also be used, in conjunction with data from the V-head horizon sensor, to determine spacecraft attitude. Although use of this method allows attitude determination even when the data is sparse, the accuracy is generally insufficient for the performance specifications of this system. Therefore, it is intended to use this method only during the turn-around maneuver and as a quick check during normal mission operation. A detailed discussion of this method of attitude determination is contained in the design-study report for the TIROS "I" spacecraft.

*The error to the orthogonal sensor introduced by earth-temperature variations is less than that for V-head sensors because of the smaller oblique grazing angles encountered.

6. Redundancy and Failure Modes

In the event of a failure in the QOMAC system (once wheel orientation has been established), it will be possible to use the MBC system for station-keeping purposes. Although the use of this system will limit the accuracy of station keeping because of the coarseness of the control and the loss of flexibility, it will still be possible to limit the maximum roll error to approximately 5 degrees. Tighter limitations on the extent of roll error will require more frequent utilization of the MBC system.

Regarding the use of the MBC system for attitude control, it can be shown that the use of conventional TIROS type torquing on a spacecraft in a polar orbit will generate, approximately, right-ascension changes in the position of the spin vector. It can also be shown that reversing the dipole polarity at the maximum or minimum latitudes of the orbit will generate declination changes over the node-to-node portion of the orbit. Thus, if a particular change in right ascension and declination is necessary to reacquire the orbit normal, this change can be effected by switching the polarity of the dipole moment in accordance with the switching profile (shown in Figure 4-VIII-20), that will effect that change. Either the uncircled or circled profiles are available since the dipole polarity can be controlled from the ground.

It should be noted that the precession rate obtainable in Quadrants I and II is nearly twice that in Quadrants III and IV. The ratio is given by the following relationship:

$$\frac{\omega_{\rho\ \mathrm{I,\ II}}}{\omega_{\rho\ \mathrm{III,\ IV}}} = \frac{\sin i}{\sqrt{(\sin i)^2 + 4(\cos^2 i)^2}} \quad \frac{6}{\pi} \qquad \text{(VIII-54)}$$

and is approximately 1.91 for polar orbits.

More complex switching programs can be derived based on the actual orbital environment and ground-contact studies. However, these programs are generally very inefficient and require frequent operation of the MBC system. It should be noted that the MBC system must be returned to the position corresponding to the minimum drift rate of the spin axis after each switching program.

D. SPIN CONTROL

1. General

After spacecraft separation from the third-stage rocket, the spin rate will be controlled by two devices. First, the de-spin mechanism (Yo-Yo) will provide spin-down from the orbit-injection spin rate to approximately the desired operational spin rate; then the Magnetic Spin Control (MASC) device will be used to acquire and maintain the specified spin rate.

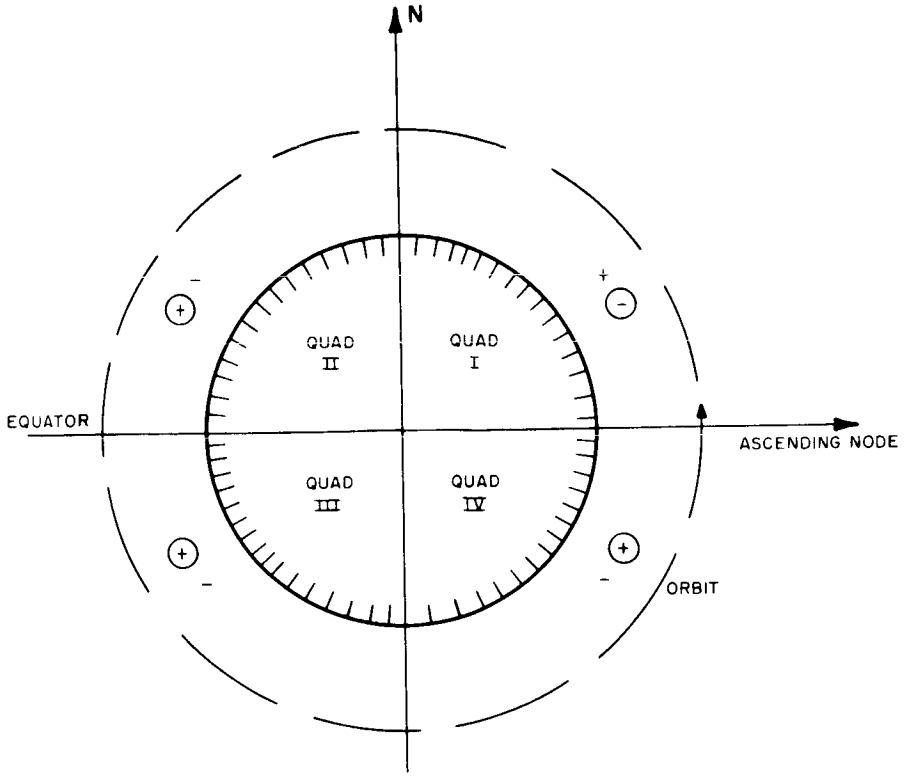

AVERAGE PRECESSION VECTOR DIRECTION

POLARITY	UNCIRCLED		CIRCLED	
QUADRANT DIRECTION	I & II →	III & IV ↓	I & II ←	III & IV ↑

Figure 4-VIII-20. Dipole Polarity Switching Profile

2. Yo-Yo Despin

To achieve stabilization during the boost phase of the launch operation, the carrier rocket and spacecraft are "spun up" to a nominal rate of 125 rpm. After separation from the third stage of the booster rocket, it is necessary to reduce this rate to 10.9 rpm for the OT-2/APT configuration and 9.2 rpm for the OT-2/AVCS configuration. This de-spin is accomplished by releasing two masses that are attached to cables wrapped around and hooked to the solar-cell array structure.

Upon separation of the spacecraft from the third-stage rocket, a control circuit will be activated by the separation switches. After an 8-minute delay (to permit nutation damping), this circuit will cause the firing of squibs, disengaging the retaining pins for the masses, and allowing the masses to swing free. The cables will swing quickly outward until they reach radial orientation with respect to the spacecraft, at which

time loops on the end of the cables will slip from their retaining hooks. The cables and weights will then completely separate and carry away approximately 90 percent of the initial angular momentum into space, slowing the spin-rate of the spacecraft accordingly.

Figure 4-VIII-21 indicates the TIROS despin (Yo-Yo) history for TIROS II through TIROS VIII, all of which were launched with the Thor-Delta vehicle. The scatter displayed is due in part to the fact that the spin moment of inertia was measured to no better than 1 percent in early satellites (points A2, A3, and D); this is equivalent to a final spin-rate error of about 10 percent. Furthermore, the despin analysis utilized for all TIROS vehicles launched to date did not allow for the energy contained in the stretched cable at the moment of separation. Since both the measuring and computing techniques have been refined, future missions should display less deviation from the nominal performance curve. The factors affecting despin accuracy are listed below, in terms of percentage error referenced to the final spin rate:

Moment of Inertia Measurement:	$\pm 5\%$,
Final Stage Speed (before despin)	$\pm 10\%$, and
Reduction Mechanism accuracy:	$\pm 7\%$,

for a worst case of $\pm 22\%$ and an rms value of $\pm 13.2\%$. For a nominal 10 rpm, the worst case despin speed will be 7.8 rpm. This deviation can be corrected by the MASC device within 1.5 days (maximum).

3. Magnetic Spin Control (MASC)

a. General

As applied to a spinning spacecraft, the earth's magnetic field is effectively an oscillating field which penetrates the conductive materials of the spacecraft, thereby inducing electrical currents. In turn, eddy currents are produced, resulting in magnetic fields within the spacecraft that interact with the earth's magnetic field. This interaction not only tends to alter the spacecraft's attitude but, also, tends to de-spin the spacecraft.

In previous TIROS operations, spin decay was cancelled by the occasional firing of spin-up rockets. However, for the TIROS-"I" spacecraft, more precise spin-control is desirable and a MASC capability is being included to provide bi-directional, fine control of the spin rate. In the OT-2 spacecraft, the spin-up rockets are eliminated completely, and the spin rate will be maintained exclusively by the MASC technique.

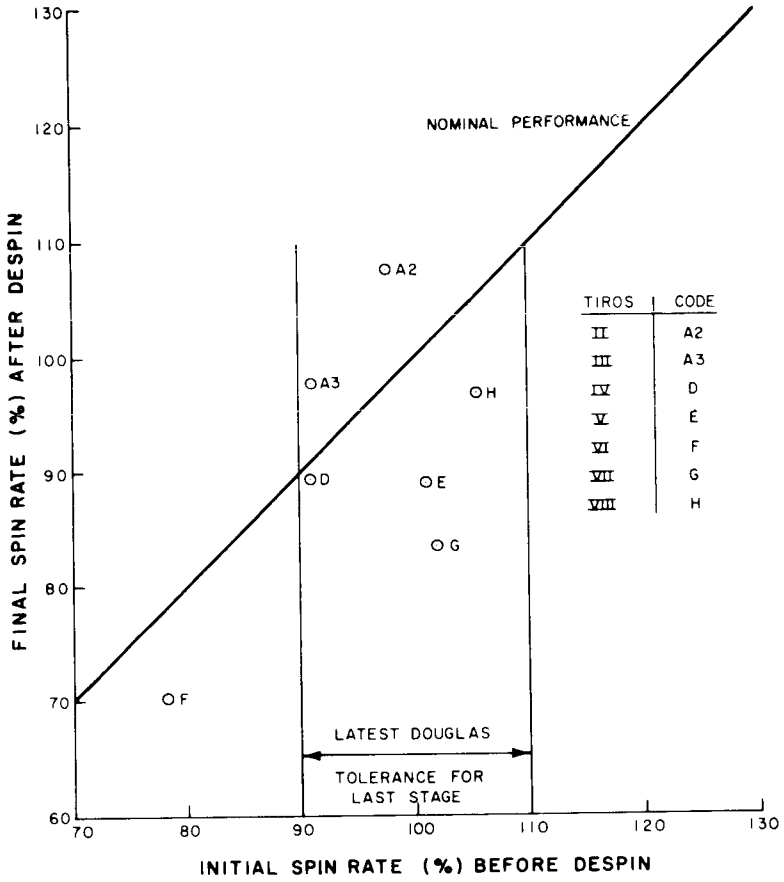

Figure 4-VIII-21. TIROS Despin Performance History

The MASC technique utilizes horizon sensors, a commutation circuit and a MASC coil to effect spin control. Control torques are generated by the coil, which is mounted with its normal perpendicular to the spin axis. The spin rate is controlled by means of magnetic interaction, in a manner similar to that in which QOMAC adjusts the spacecraft's attitude. Since the earth's magnetic field is unidirectional for any one point in the orbit, it will be necessary to reverse the coil current every 180 degrees of spacecraft rotation in order to produce a net torque. The switching of current direction is synchronized by outputs from the orthogonal horizon sensors (which also provide signals for synchronizing the camera shutters). The coil is installed so that the sky-to-earth pulses from the horizon sensors commutate the coil current about the local vertical. This will optimize the commutation efficiency when the spacecraft is in the vicinity of the earth's magnetic poles, where the field is considerably stronger than near the magnetic equator.

The current in the MASC coil generates a magnetic-dipole moment equal to the product of the number of ampere-turns and the circumscribed area. This dipole moment has a vectorial orientation normal to the circumscribed area, i.e., perpendicular to the spin axis. (A detailed mathematical development of the MASC technique is presented in Paragraph 4-VIII-B.)

Commutation of the instantaneous torque produced by the interaction of the earth's magnetic field and the dipole moment of the coil provides an average torque per spin which is expressed as:

$$\frac{T_{AVG}}{SPIN} = \frac{2M}{\pi}\left\{\hat{\ell}\,(B_n \cos\beta) + \hat{b}\,(B_n \sin\beta) + \hat{n}\,(-B_b \sin\beta - B\,\hat{\ell}\cos\beta)\right\}. \quad \text{(VIII-55)}$$

The $\hat{\ell}$ and $\hat{b}$ components of this equation represent, for an approximately polar orbit, the slight amount of precession produced by a given torque, or spin-control, cycle. The $\hat{m}$ component is nominally coincident with the spin axis and represents the desired spin-control torque, T_S. Integrating this spin torque over an angular orbit sector $(B_f - B_i)$ will result in a change in spin rate that can be expressed as:

$$\Delta\omega_S = \int_{B_i}^{B_f} \frac{T_S}{I_S\,\omega_S}\,d\beta. \quad \text{(VIII-56)}$$

Figure 4-VIII-22 is a plot of the nominally achievable spin-rate increment, $\Delta\omega_S$, arbitrarily referenced to the time from the orbital ascending node. The inherent precession per ten minutes of spin-control torquing, due to the $\hat{\ell}$ and $\hat{b}$ component of the torque equation, is small as indicated in Figure 4-VIII-23. For attitude errors as large as 10 degrees, the spin torque will decrease a maximum of 6.8 percent for an ascending pass over the continental United States. For the same conditions, the inherent precession might increase as much as 120 percent; however, the actual increment is still small since the maximum precession for ten minutes of MASC is only 0.1 degrees.

b. Spin-Rate Acquisition

The MASC system requires that an "on" command and a commutation-mode (spin-up or spin-down) command be transmitted to start a spin-correction cycle, and that an "off" command be transmitted to terminate the cycle. In order to maintain programming simplicity, the on/off commands are not stored in the spacecraft, i.e., operation is in "real time." Therefore, the maximum change in spin rate that can be achieved per day is a function of the ground contact time. An example of a typical spin-control sequence, based on a magnetic dipole moment of 14.6 ampere-turns-meter^2, and a 750-nautical-mile, 101.40 degree orbit, is shown in Table 4-VIII-5. As can be seen from this table, within the limits of the contact circle for the two ground stations, a maximum daily correction of about 1.7 rpm can be realized with a coil dipole moment of 12 ampere-turns-meter^2.

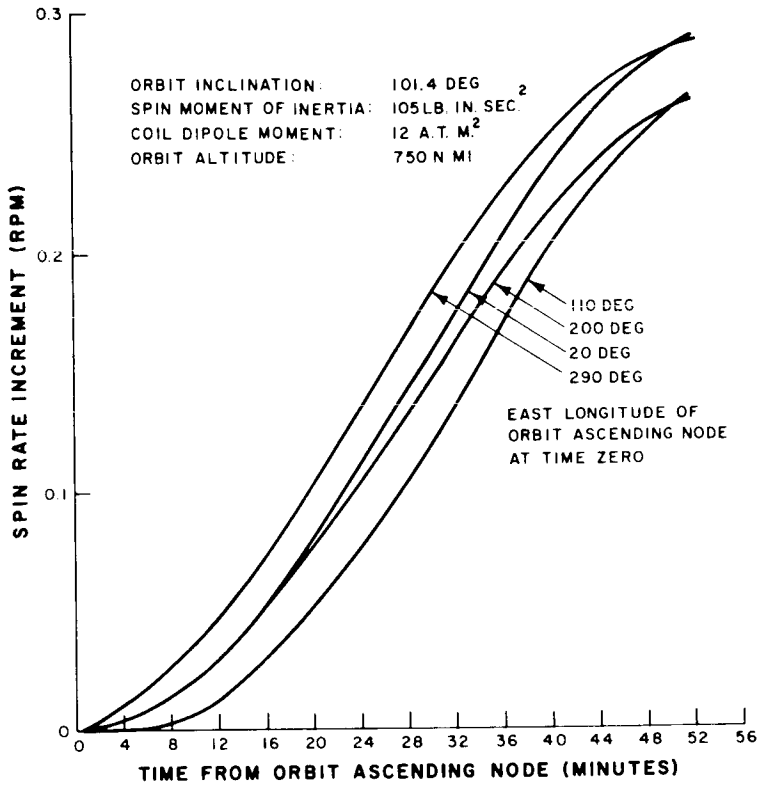

Figure 4-VIII-22. Spin-Rate Increment versus Time

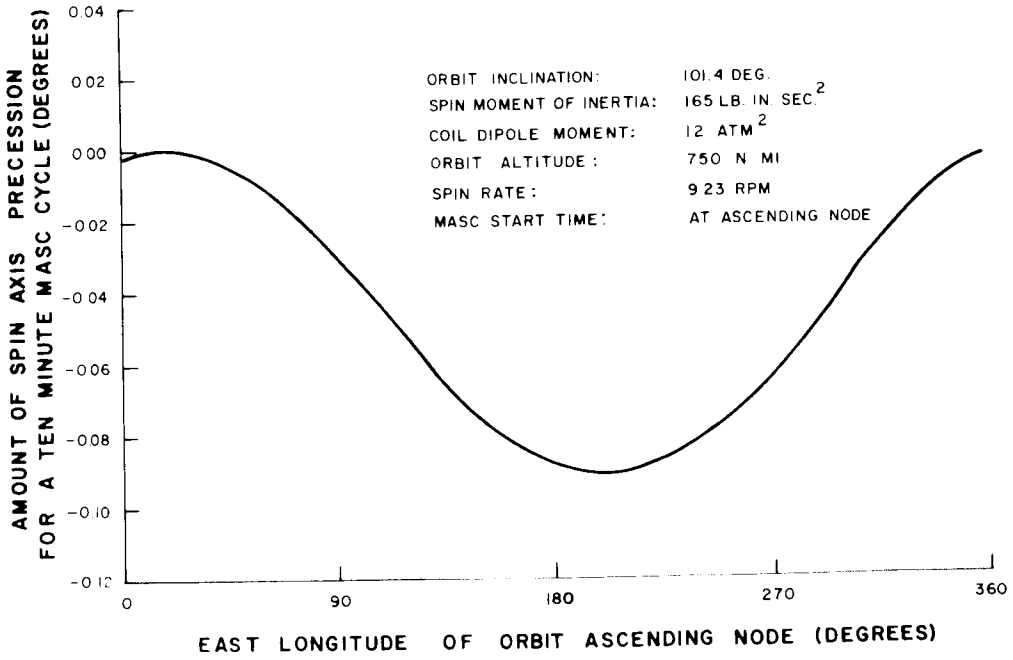

Figure 4-VIII-23. Spin-Axis Precession versus Longitude of Ascending Node

TABLE 4-VIII-5. TYPICAL SPIN-CONTROL SEQUENCE

Interrogating CDA Station	Time from Ascending Node (Minutes)		Position of Ascending Node (Degrees East Longitude)	Spin Rate Increment (rpm)	Inherent Precession (Degrees)	MASC Cycle Duration (Degrees)
	MASC ON	MASC OFF				
East Coast	8	22	320	0.113	0.037	14
Fairbanks	23	37	320	0.128	0.032	14
East Coast	3	19	291.6	0.108	0.085	16
Fairbanks	20	34	291.6	0.121	0.069	14
Fairbanks	15	32	263.2	0.154	0.131	17
Fairbanks	12	30	234.8	0.154	0.181	18
Fairbanks	13	26	206.4	0.104	0.150	13
Fairbanks	18	25	178	0.057	0.080	7
East Coast	39	54	121.2	0.093	0.120	15
East Coast	37	51	92.8	0.105	0.072	14
Fairbanks	30	43	64.4	0.119	0.030	13
Fairbanks	28	45	36.0	0.148	0.009	17
Fairbanks	26	43	7.6	0.148	0.000	17
Fairbanks	24	40	339.2	0.146	0.015	16
Daily Total				1.698	1.011	205

Magnetic Dipole Moment	14.6 atm^2
Orbit Altitude	750 NM
Orbit Inclination	101.4 Degrees

The MASC system includes two separate coils and associated commutation circuits. Both coils will be programmed for operation during spin-rate acquisition to provide a dipole moment of 14.6 ampere-turns-meter^2, thus minimizing the time required for this operation. Once the desired spin rate has been acquired, both MASC coils will be deactivated until such time as a spin-rate correction cycle is required.

c. Maintenance of Spin-Rate

The spin period, as defined by succeeding sky-to-earth horizon pulses from the orthogonal horizon sensor, must be maintained at 5.5 ± 0.025 seconds for the OT-2/APT configuration, and at 6.5 ± 0.025 seconds for the OT-2/AVCS configuration. In order to maintain the spin period within this accuracy, three factors must be taken in into consideration, namely, (1) long-term spin-rate decay because of eddy current effects, (2) short-term fluctuations in the measured period resulting from variations in earth temperature, and (3) the accuracy with which the actual spin period can be measured.

At the stipulated orbital altitude (750 nautical miles) and inclination (101.4 degrees), the first factor, long-term decay, is expected to decrease the spin rate by approximately 0.014 rpm per day. As illustrated in Figure 4-VIII-24, the deviation from the nominal spin period because of this decay rate depends upon the frequency of spin-correction cycles. Assuming three such cycles each week, the maximum error attributable to long-term decay should be no greater than 8.1 milliseconds per spin period.

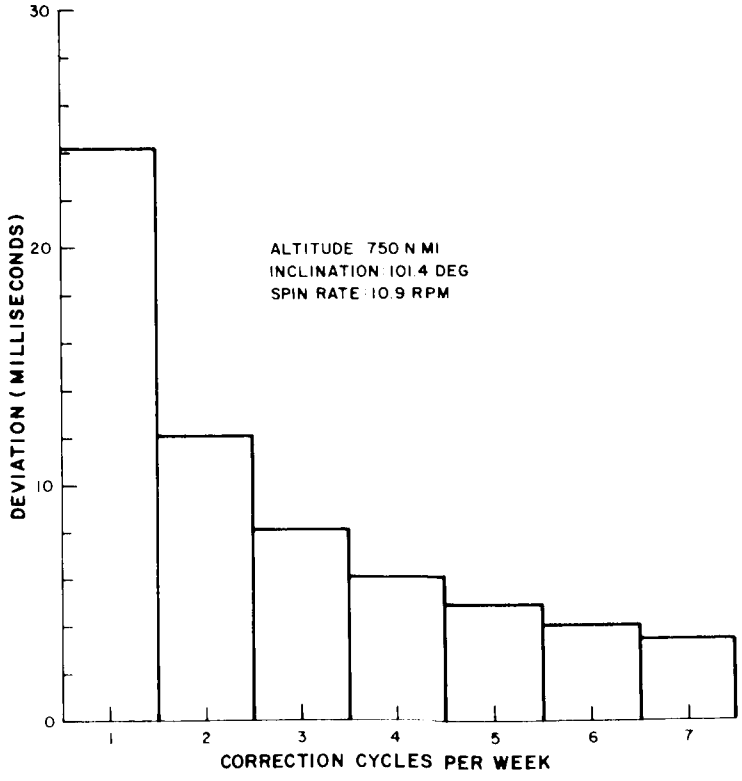

Figure 4-VIII-24. Spin-Period Deviation versus Correction Cycles per Week

Short-term fluctuations in spin period are caused primarily by changes in transient rise time resulting from variations in earth temperature. Although short-term fluctuations do not constitute changes in the actual spin rate, they must be considered because of their effect on the triggering of the TV cameras. These fluctuations could cause errors in the indicated spin period of up to 7.7 milliseconds.

The error introduced by the third factor, the accuracy of spin-rate measurements, should be limited to +0.45 milliseconds by use of the averaging techniques described in paragraph 4 below. Thus, even if all three types of errors were accumulative, the maximum deviation from the nominal spin rate (assuming three MASC cycles per week) would be 17 milliseconds, well within the ±25-millisecond tolerance imposed by the TV-camera subsystems.

4. MASC Coil Design

Two separate MASC coils will be included in spacecraft OT-2. They will be positioned within the hat structure so as to provide the maximum dipole moment for the specified current and weight without interferring with the installation of other components. The parameters of each coil are as follows:

Shape:	fitted to structure (See Figure 4-II-3)
Wire material:	aluminum
Bare-wire diameter:	0.0113 inch
Electrical configuration:	center-tapped
Total no. of turns:	562
Nominal current:	75 milliamperes
Impedance (per half coil):	R = 320 ohms; L = 0.2 henry (at 20°C)
Coil weight:	0.56 pounds
Nominal dipole moment:	7.3 ampere-turns-meter^2

5. Spin-Rate Measurement

Because the delay timing for a remote-picture sequence will be defined in terms of a number of transpired spins, it is essential that the spin rate be measured with a tolerance that will allow accurate determination of the picture center for each remotely taken TV picture. The data for spin-rate determination will be obtained from the dual-channel V-head horizon sensor, since the outputs from this sensor are continuously telemetered for attitude-determination purposes. However, data from only one of the two sensor channels will be used.

Although the use of data from the orthogonal horizon sensors would reduce the maximum error in spin-period measurements by a factor of approximately two, (since the V-head sensor experiences more-oblique grazing angles) the need for a separate readout command and the shorter readout-time availability seems to delegate these sensors for use as a back-up, rather than a primary, source of spin-rate data.

For a maximum roll angle of 1 degree and a nutation half-angle of 0.5 degree, nutation will cause the period defined by successive sky-to-earth outputs from the V-head sensor to vary by ±26.7 milliseconds. The maximum error that can be introduced by variations in the earth's radiance is ±8.25 milliseconds at each horizon crossing based on the threshold technique described previously. However, since this transition actually occurs as a ramp, variations in the slope of the ramp due to atmospheric conditions can cause an additional error of 8.5 milliseconds in horizon location. In addition, an error of ±0.16 millisecond per period is introduced by the sinusoidal variation of the spacecraft roll component.

The spin period could be measured by two standard binary counters, which would record, on an alternate basis, a series of consecutive time increments. Since this measurement would be continuous, errors due to nutation, radiance, and horizon gradient would only affect the occurrence of the last pulse with respect to the first pulse. Therefore, longer recordings would minimize the effect of these errors. If available, Sanborn recorders, provided with 10-pps timing markers, can be used in place of the complimentary digital counters to achieve the required spin-period measurement. Such a change will introduce an additional error of ±12.5 milliseconds in locating the first and last sky-earth pulse recorded on the chart (based on a paper speed of 20 millimeters per seconds, and operator resolving ability of 0.25 millimeters). These errors are summarized in Table 4-VIII-6.

TABLE 4-VIII-6. SPIN-PERIOD MEASUREMENT ERRORS

Errors	Values (ms)
1. Earth radiance	±16.5
2. Horizon gradient	± 8.5
3. Zero-to-peak (due to nutation)	±26.7
4. Data reduction	±12.5
5. Sinusoidal roll component	± 0.16

Since errors 1 through 4 in Table 4-VIII-6 are only significant on the first and last pulse, the spin measurement accuracy is improved by averaging over the measuring periods. The following equation is used to compute the rss error:

$$\left[\text{rss error}\right]^2 = \left[\text{sinusoidal roll component}\right]^2 + \left[\frac{\left[\sum_n (\text{errors})^2\right]^{1/2}}{\frac{\text{measuring period}}{t_{s_p}}}\right]^2 \quad \text{(VIII-57)}$$

Figure 4-VIII-25 shows the root-sum-square value of spin-rate measurement error considering the above factors, while Figure 4-VIII-26 illustrates the spacecraft subpoint accuracy in terms of the rss error. For an 8-minute (480-second) measuring period, the maximum spacecraft subpoint error after 1000 sky-to-earth pulses is 0.51 second, corresponding to a subpoint error of 1.63 nautical miles.

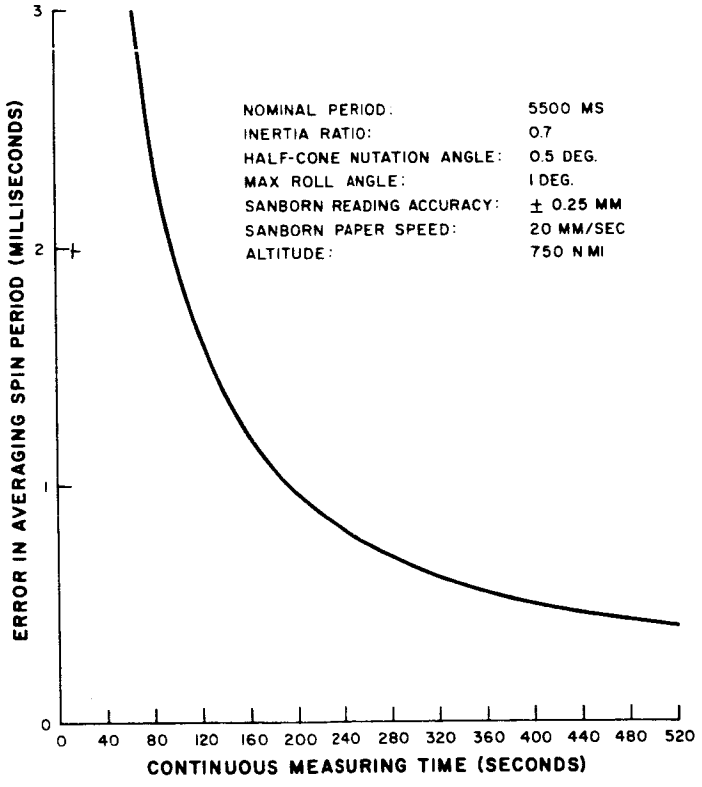

Figure 4-VIII-25. Root-Sum-Square Spin-Period Measurement Error

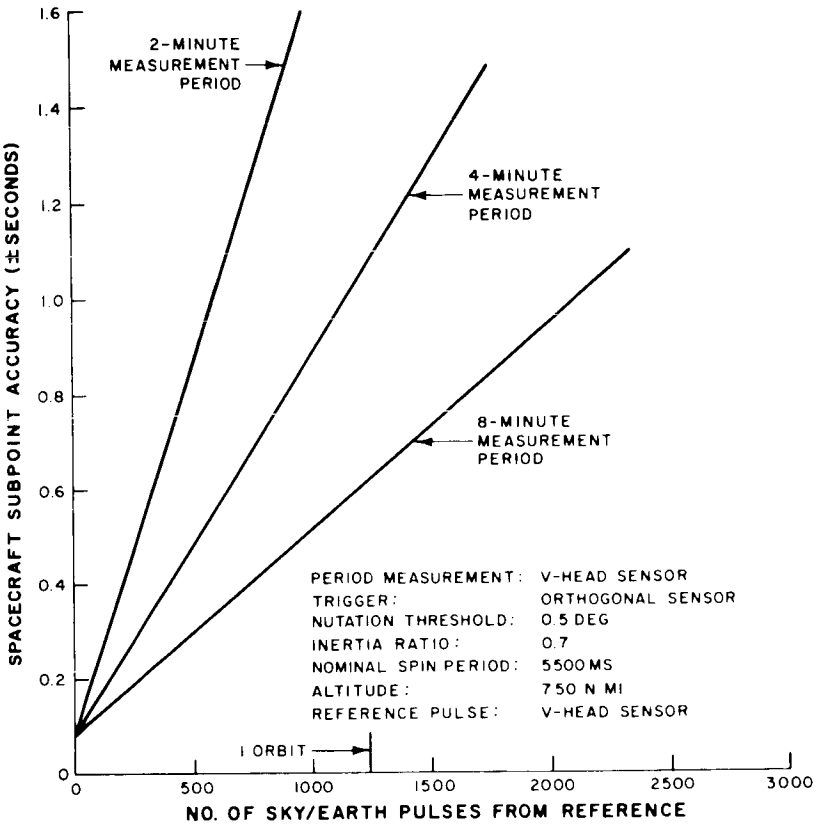

Figure 4-VIII-26. Spacecraft Subpoint Accuracy based on RSS Spin-Period Measurement Error

The above estimate of prediction accuracy assumes an adjustment for the phase shift caused by the long-term decay of approximately 0.014 rpm per day. Furthermore, the angle, θ_s, between the lines of sight of the V-head horizon sensor (used for reference) and the orthogonal sensor (used for triggering) enters the equation which defines the predicted time of a sky-to-earth horizon pulse from the orthogonal sensor. Thus:

$$t_{HP} = t_o + N\left(t_{s_p} + 2.24 \times 10^{-7}\ N\right) - \frac{\theta_s\, t_{s_p}}{2\pi}. \qquad \text{(VIII-58)}$$

For after-the-fact picture rectification, a comparison of anticipated and actual occurrence of the sky-to-earth horizon pulse (subsequent to any number of pulses such as the 1000 mentioned above) will permit an even closer determination of the satellite subpoint for a particular picture. Phase shifts which cannot be justified by short-term disturbances such as temperature and nutation could then be distributed evenly over the transpired number of spin periods. A decision as to whether such a refinement is required can be tempered by the observation that the principal point variation due to half-cone nutation angles as low as 0.3 degree is about 4 nautical miles, whereas a

0.45-second variation in subpoint determination is equivalent to only 1.43-nautical-mile variation. To provide an even greater level of confidence, a comparison between anticipated and actual horizon crossing could be utilized to check the accuracy of the prediction.

6. Redundancy and Failure Modes

The 14.6 ampere-turns-meter^2 dipole moment employed in the MASC technique is generated by two independent electromagnetic coils, each of which provides a 4.3-ampere-turns-meter^2 dipole moment. Should a failure develop in any one of the coils, the MASC capability will still be retained, although the time required for spin-rate adjustments will increase accordingly.

PART 5. GROUND EQUIPMENT

SECTION I. INTRODUCTION

The OT-2 system ground complex includes three major groups of facilities:

(1) Control, Programming, and Analysis (CPA) centers.

(2) Command and Data Acquisition (CDA) stations.

(3) Spacecraft check-out sets.

The CPA centers consist of the following:

(1) National Weather Satellite Center (NWSC), located in Suitland, Maryland.

(2) TOS Control Center (TCC) located at NWSC, Suitland, Maryland.

There are two, nearly identical, CDA ground stations, one located near Fairbanks, Alaska, and the other on the East Coast. Should the government install an 85-foot antenna with its attendant RF equipment, the performance of the East Coast CDA station would be identical to that of the Fairbanks, Alaska, CDA station.

Two spacecraft check-out sets are located in the RCA Space Center, Princeton, N. J. Spacecraft check-out Set No. 1 consists of all the ground equipment needed to check out spacecraft prior to launch and some of the test equipment required during fabrication and assembly of the spacecraft. Spacecraft check-out Set No. 2 has the capability to evaluate the spacecraft while in orbit and also to check out the spacecraft prior to launch. In addition, a go/no-go van is located at the launch site for the purpose of checking out the spacecraft before and during launch operations.

The flow of data among the OT-2 system ground complex is shown in Figure 5-I-1.

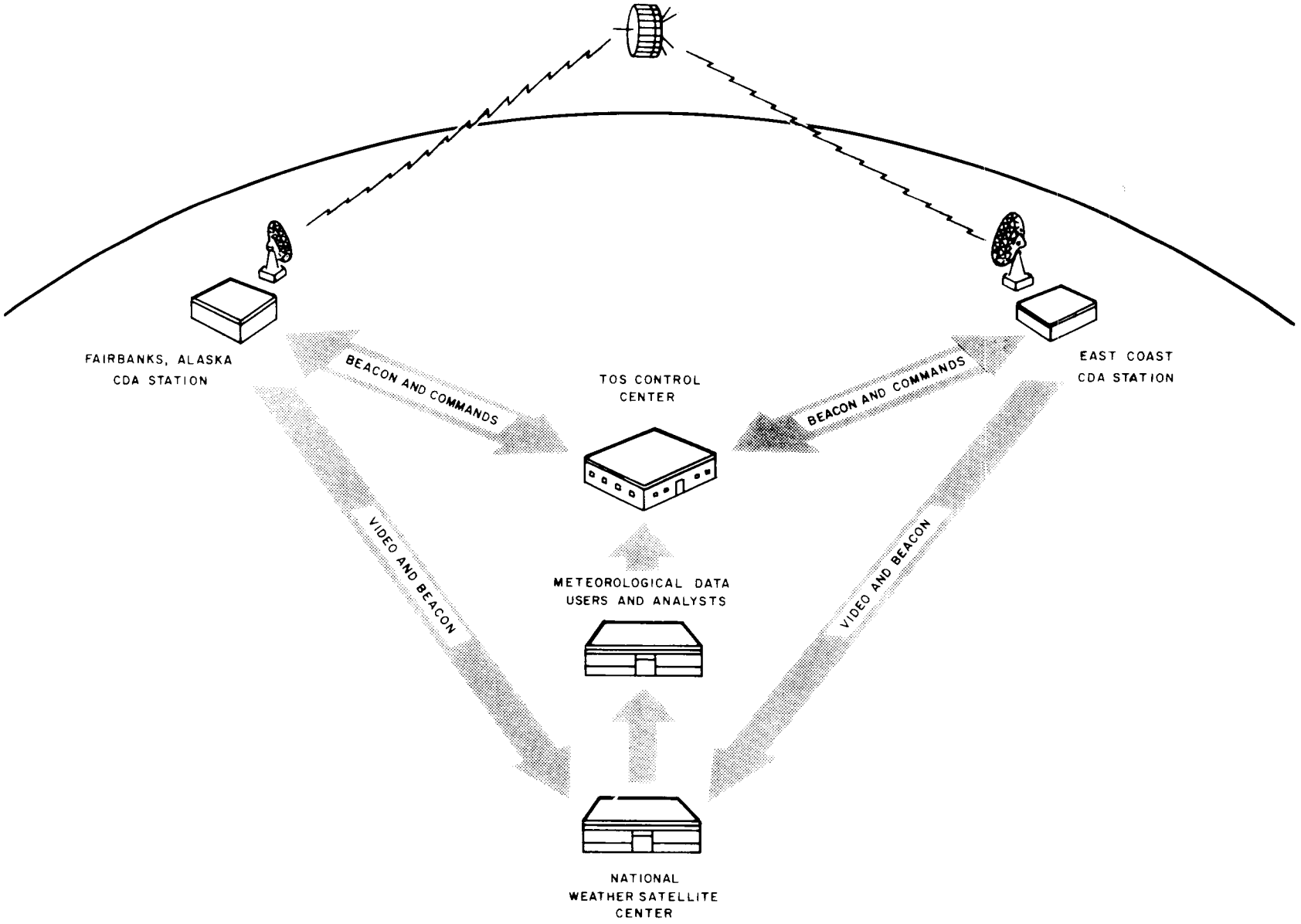

Figure 5-I-1. Data Flow Among the OT-2 System Ground Complex

SECTION II. CONTROL, PROGRAMMING, AND ANALYSIS (CPA) CENTERS

A. TOS CONTROL CENTER (TCC)

The TCC originates all command programs for the normal operation of the satellite. The nature of these commands is based on requests from cognizant agencies for particular cloud coverage in conjunction with ephemeris data.

Satellite performance is analyzed by TCC from telemetered "housekeeping" data received by the CDA stations during each pass. Attitude and spin-correction commands for the satellite are generated based on this information.

To accomplish its mission, TTC is linked to the CDA stations by "long-line" and teletype circuits; both means are used to transmit command programs to the CDA stations and to receive telemetered data, station "real time", and station events. The data is fed to chart recorders for subsequent reduction. The equipment unique to OT-2 which is required at TCC is shown in Figures 5-II-1 and 5-II-2. A tape recorder is required for delayed or repeated display, as well as playback of tapes shipped from CDA stations in the event of long lines failures.

B. NATIONAL WEATHER SATELLITE CENTER (NWSC)

NWSC reduces the video data, received from the CDA stations, to provide meterological usage. The attitude-scanner data (beacon channels 1 and 2) is also required for picture-rectification purposes. The equipment unique to the OT-2 system at NWSC is shown in Figure 5-II-3.

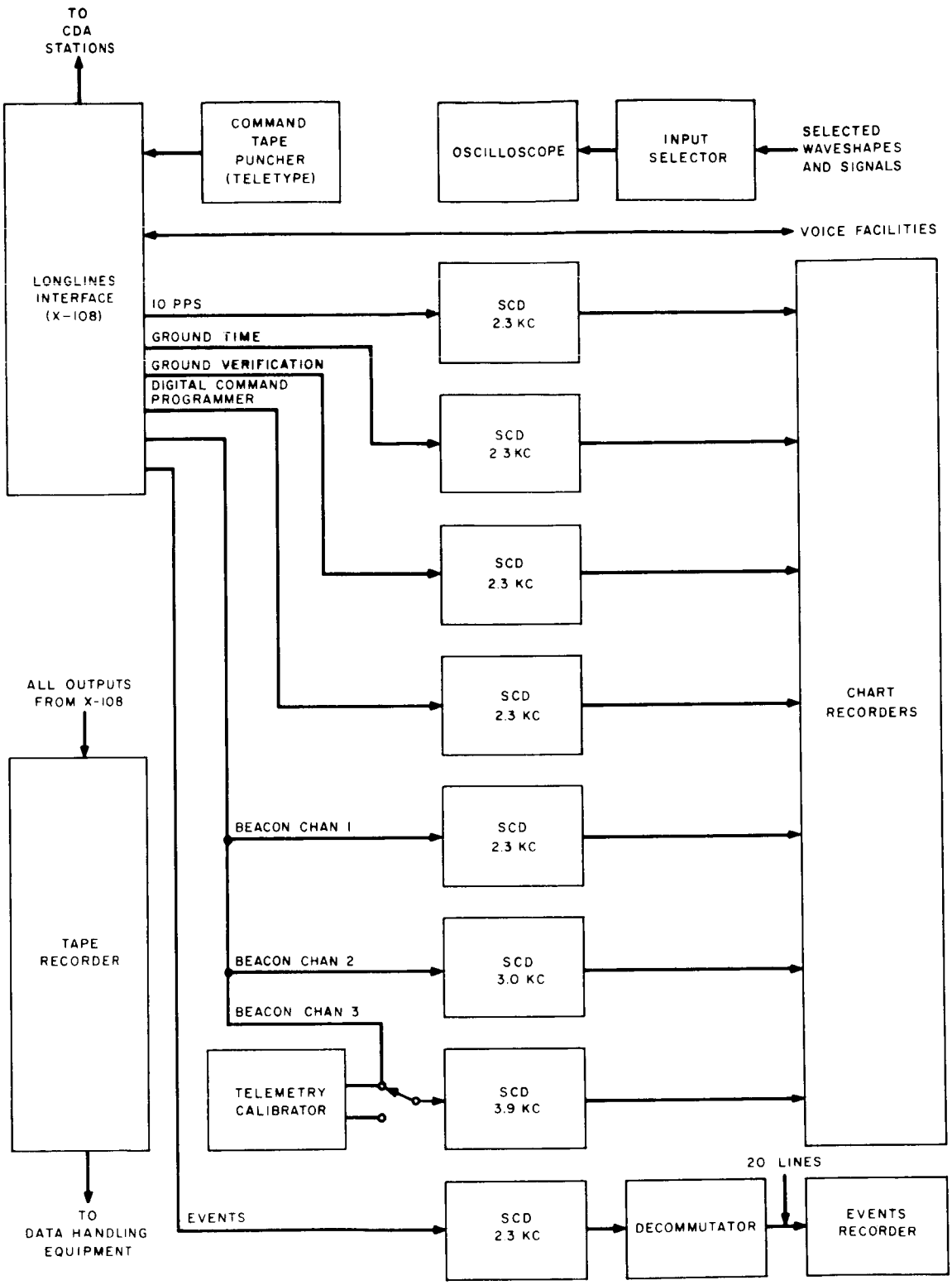

Figure 5-II-1. TOS Control Center Ground Equipment, Block Diagram

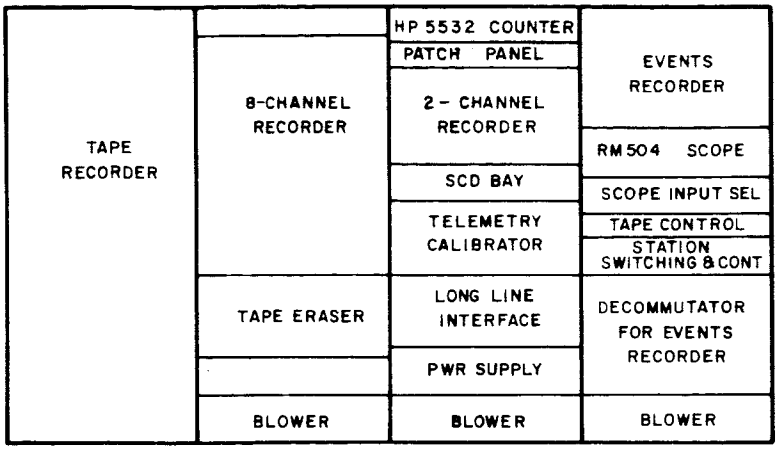

Figure 5-II-2. Physical Layout of TCC Ground Equipment

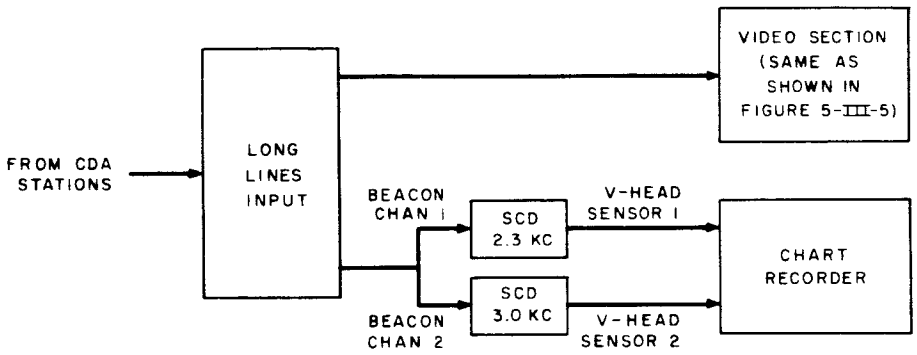

Figure 5-II-3. National Weather Satellite Center Equipment Unique to OT-2 System

SECTION III. COMMAND AND DATA ACQUISITION (CDA)STATIONS

A. INTRODUCTION

The purpose of the CDA stations is to contact the satellite directly and, by appropriate communication, command satellite activities and receive, retransmit, and process (to a limited extent) the video and telemetry information originated by the satellite.

The physical layout of the equipment in the CDA stations is shown in Figures 5-III-1 and 5-III-2. The station can be conveniently separated into the following five sections, as shown in Figure 5-III-3:

(1) the RF section,

(2) the video section,

(3) the command and control section,

(4) the beacon-data processing section, and

(5) the tape recorders, "long-line" circuits, and other peripheral equipments used in performing the station's functions.

B. RF SECTION

1. General

All RF equipment (except the satellite-type receiver) at the CDA stations is government furnished equipment (GFE). These include receiving, combining and demodulating equipment for beacon, AVCS, and APT signals, as well as command-transmitting equipment.

A block diagram of the RF section of the CDA station appears in Figure 5-III-4. Note that the actual receivers and interconnections are not necessarily those now used at the CDA stations. The RF equipment required at the RCA facility and in the go/no-go van will be furnished by the contractor.

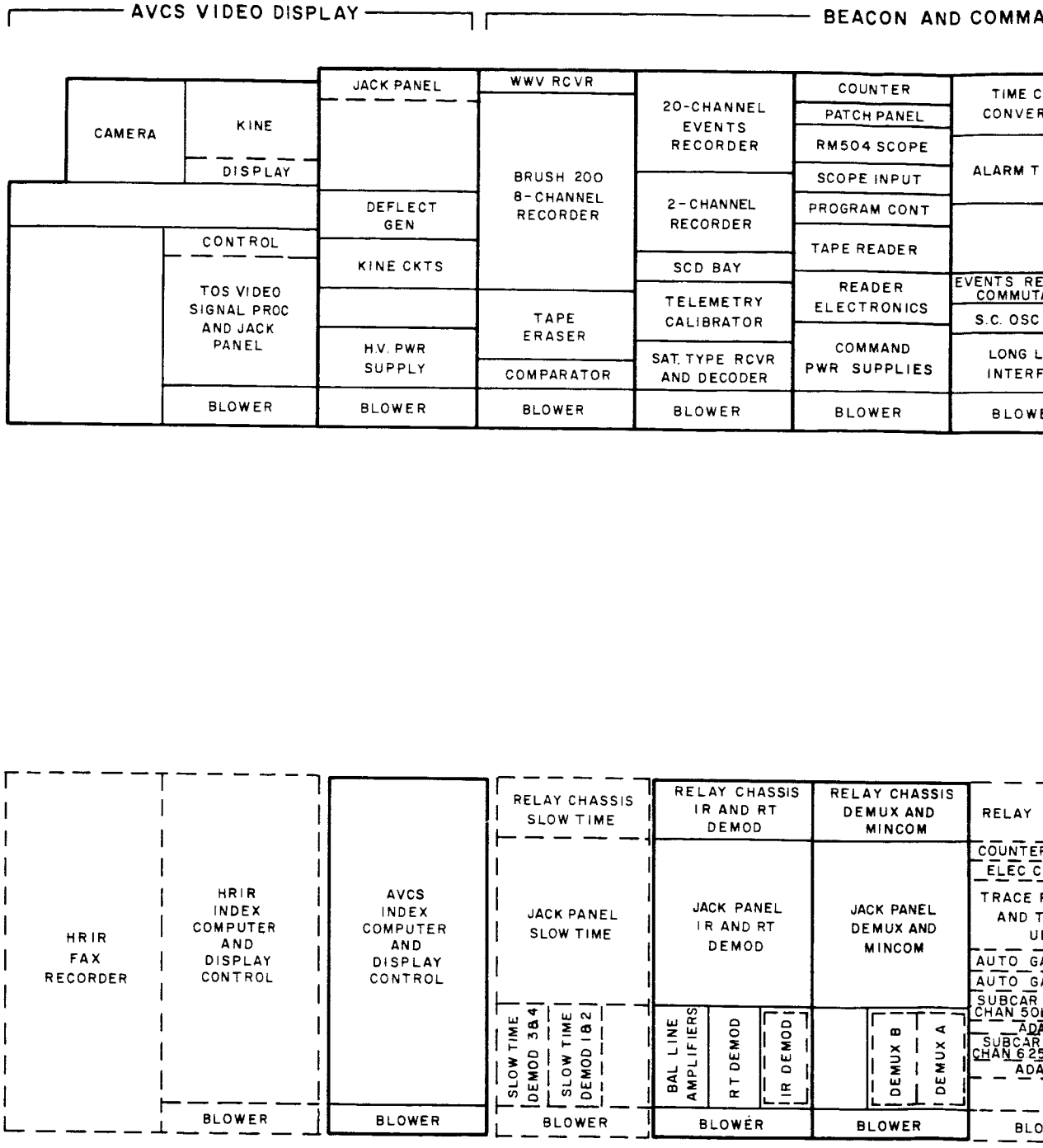

GROUND SUPPORT

NOTE:
— — — INDICATES EQUIPMENT USED ON NIMBUS, NOT ON TOS

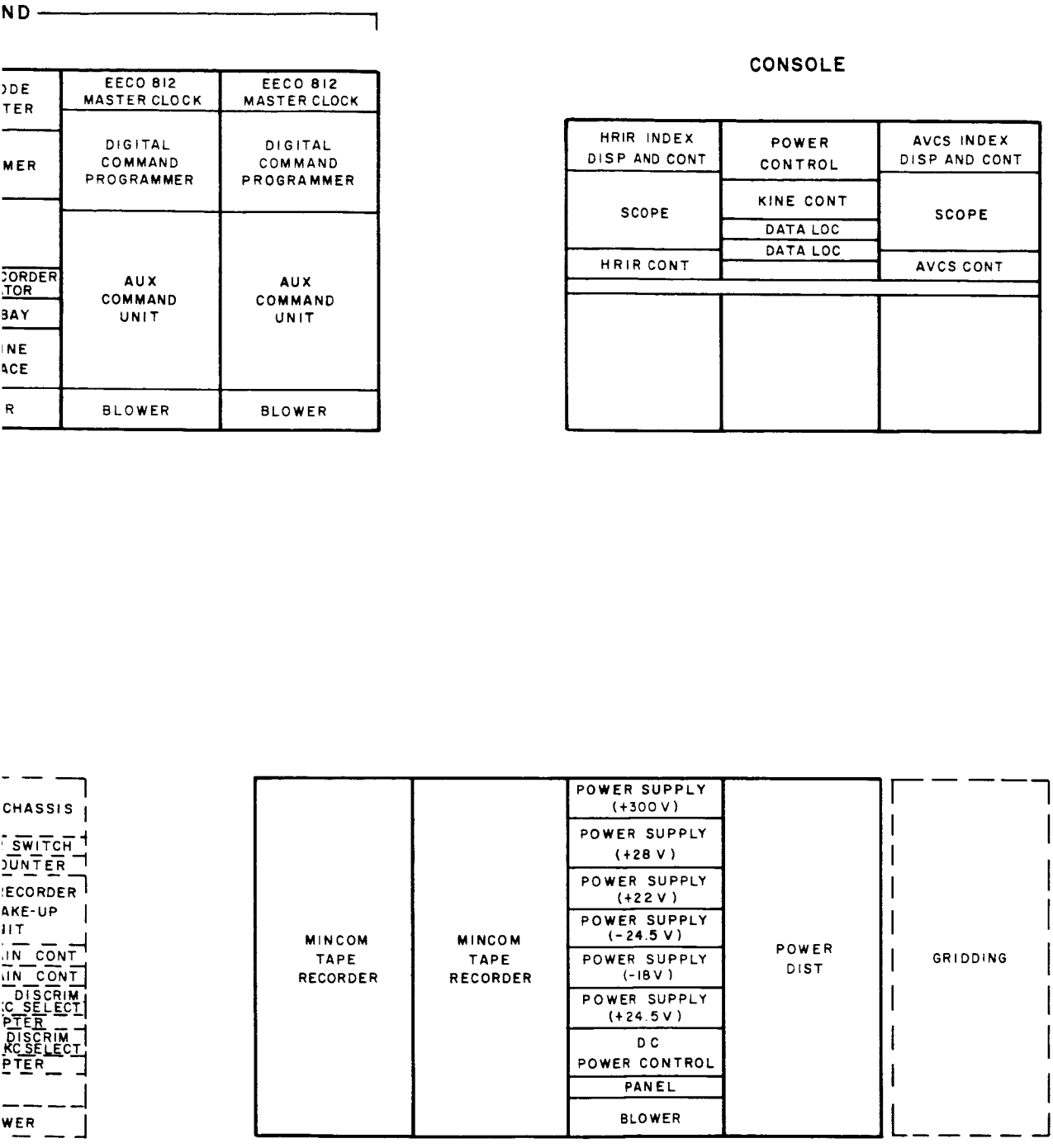

Figure 5-III-1. Alaska CDA Station Equipment

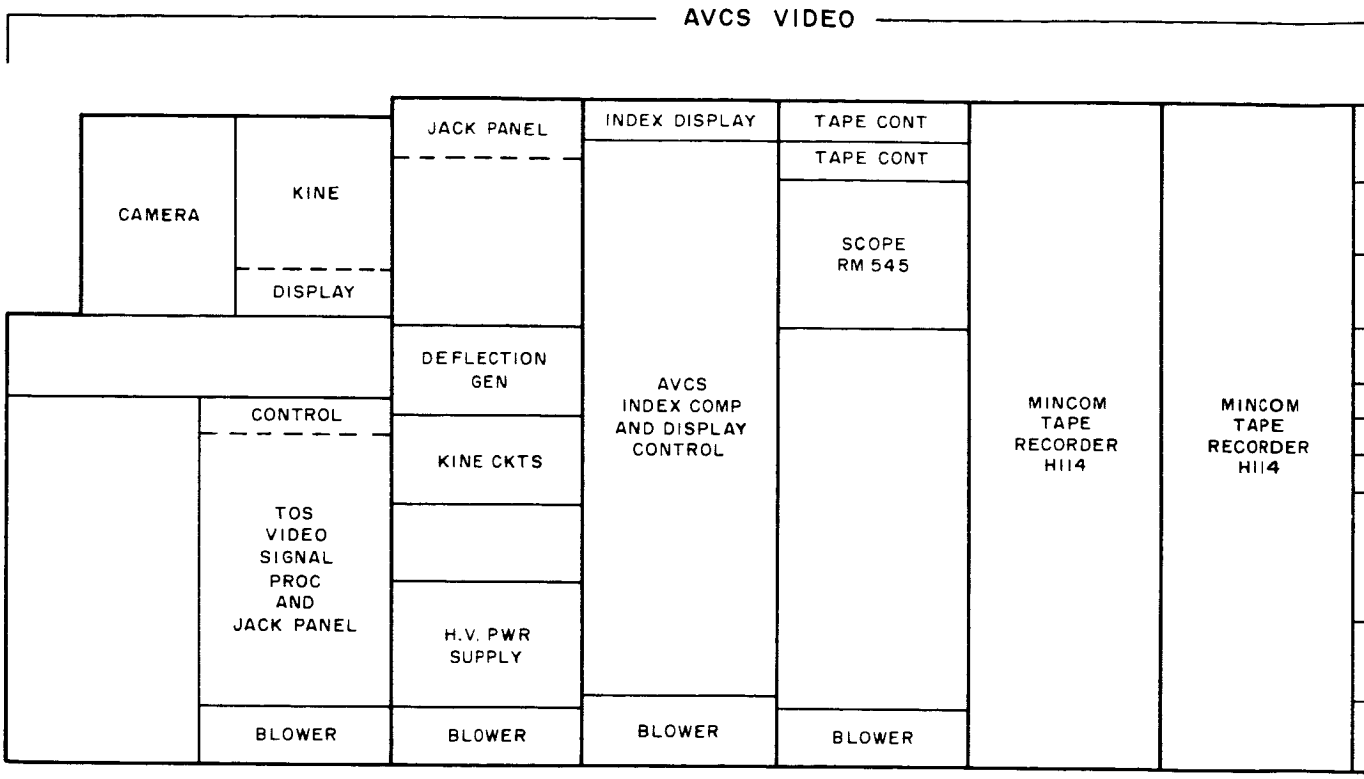

GROUND SUPPORT E

BEACON AND COMMAND

AC POWER CONTROL	WWV RCVR	20-CHANNEL EVENTS RECORDER	COUNTER	TIME CODE CONVERTER	EECO 812 MASTER CLOCK	EECO 812 MASTER CLOCK
D C POWER CONTROL	BRUSH 200 8-CHANNEL RECORDER		PATCH PANEL			
			RM504 SCOPE	ALARM TIMER	DIGITAL COMMAND PROGRAMMER	DIGITAL COMMAND PROGRAMMER
+300V P.S.		2-CHANNEL RECORDER	SCOPE INPUT			
+22V P.S.			PROGRAM CONT			
+24.5V P.S.			TAPE READER			
-24.5V P.S.		SCD BAY				
+28V PWR SUPPLY	TAPE ERASER	TELEMETRY CALIBRATOR	READER ELECTRONICS	EVENTS RECORDER COMMUTATOR	AUX COMMAND UNIT	AUX COMMAND UNIT
				S.C. OSC BAY		
-18V P.S.	COMPARATOR	SAT. TYPE RCVR AND DECODER	COMMAND PWR SUPPLIES	LONG-LINE INTERFACE		
BLOWER	BLOWER	BLOWER	BLOWER	BLOWER	BLOWER	BLOWER

QUIPMENT NO. 2

Figure 5-III-2. East Coast CDA Station Equipment

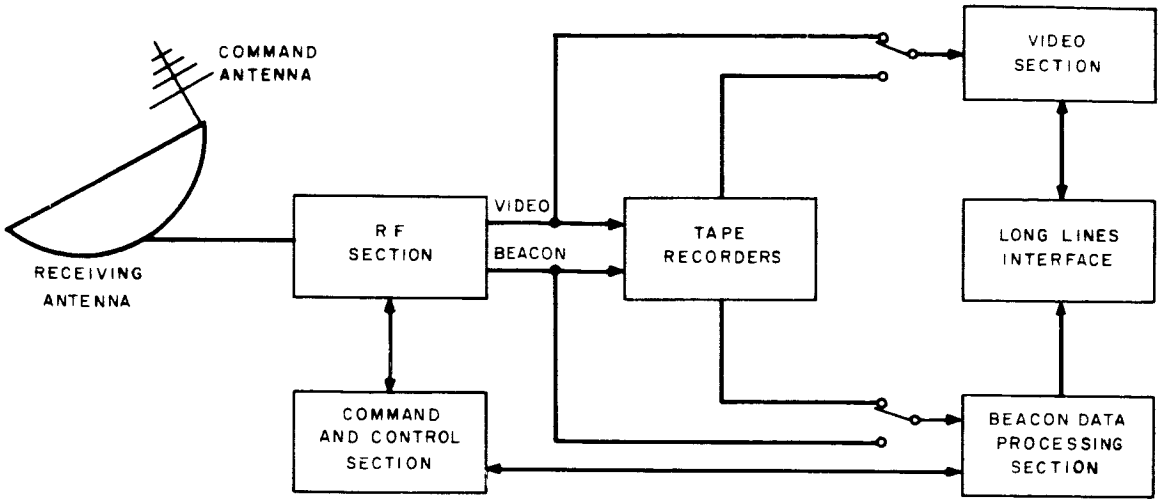

Figure 5-III-3. Sectional Breakdown of CDA Stations

2. **Beacon and Telemetry Requirements**

a. General

The beacon and telemetry information is transmitted from the spacecraft by a 136-Mc, phase-modulated carrier. Three sub-carrier oscillators (SCO's) in the satellite simultaneously modulate the carrier. The RF section of the ground equipment is used to track the beacon carrier and to demodulate the 136-Mc carrier to provide the three SCO signals for subsequent subcarrier demodulation or "long-line" transmission.

b. Antennas

The antennas used to receive the beacon signals will be similar to those presently in use in the TIROS program. The Fairbanks CDA station and the future East Coast CDA station will utilize 85-foot-diameter parabolic reflectors which afford 28-db gain at 136 Mc and are equipped for polarization diversity reception.

c. Preamplifiers

The preamplifiers used presently at the CDA stations will be suitable for OT-2 application. These units have a maximum noise figure of 4.5 db at 136 Mc.

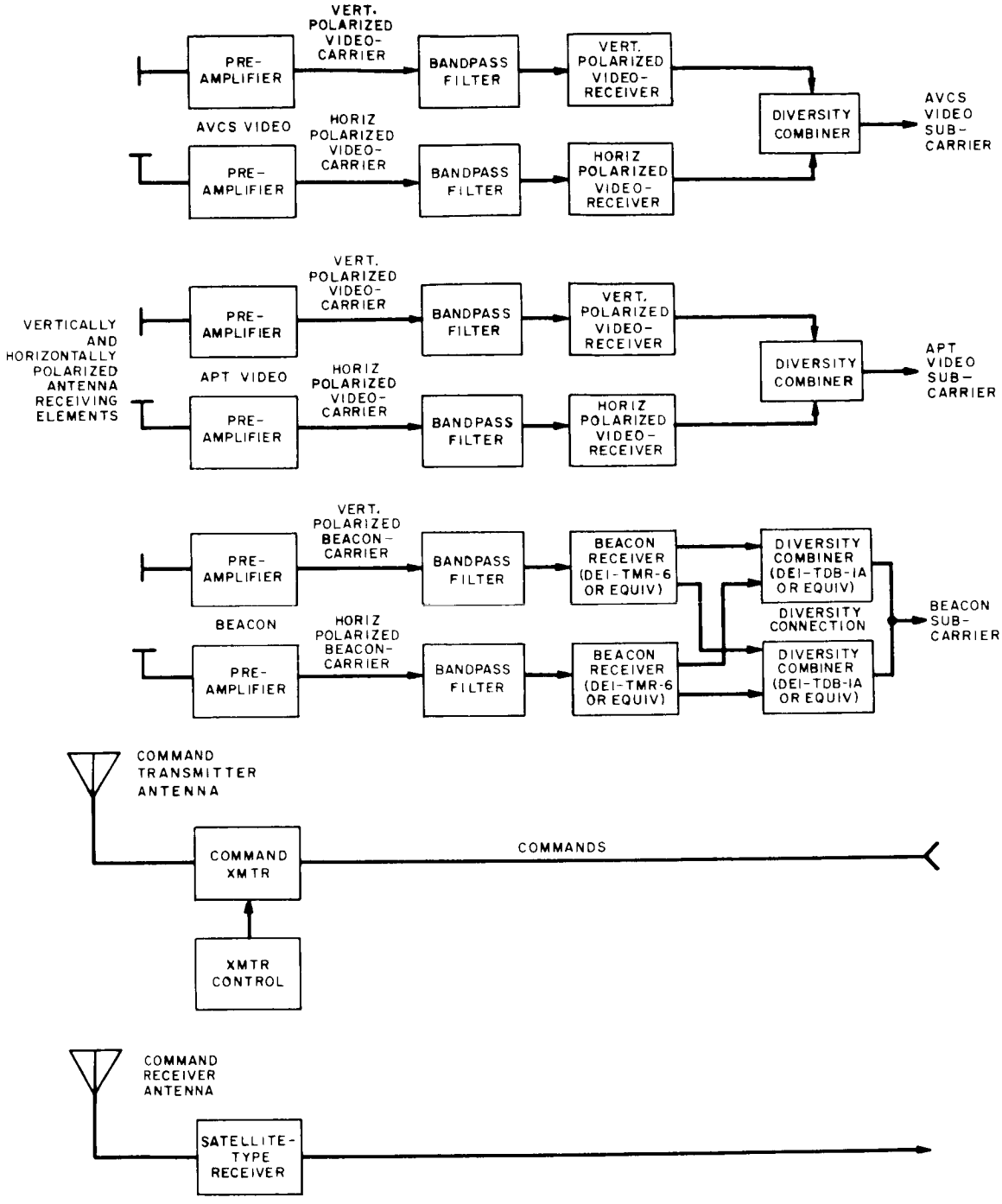

Figure 5-III-4. RF Section of CDA Station, Block Diagram

d. Receivers

The beacon and telemetry receivers used for the OT-2 program will be at least as good as the DEI-TMR-6 telemetry receivers.

The receivers will be equipped with a 30-kc IF bandwidth, and, after acquisition of the beacon signal, will be capable of doppler tracking throughout the pass. The receiver will provide carrier tracking in a narrow-loop bandwidth, resulting in an extremely low receiver threshold.

3. Command Requirements

a. Command Antenna

The command antennas used at the CDA stations can be used for the OT-2 spacecraft. The antennas of both CDA stations utilize circular polarization.

b. Command Transmitter

A transmitter rated at 1000 watts, using 90-percent amplitude-modulation will be used for commanding the spacecraft. The minimum bandwidth will be 12 kc. At the spacecraft check-out stations and in the go/no-go van, a small (milliwatt range) test transmitter will be used.

c. Command Monitoring Equipment

A command receiver and decoder (preferably unqualified spacecraft units) will be used for monitoring the station output signals. In case of a malfunction in the command chain, this system would permit rapid isolation of the trouble to either the satellite or the ground equipment.

4. APT-TV Reception Requirements

a. General

The equipment presently used for reception of APT pictures at the CDA stations will require no modification for OT-2 application. Since the APT signals are received at 136 Mc, i.e., the same band as the beacon signals, the antenna and preamplifier characteristics of the APT receiving equipment can be assumed to be the same as those of the beacon and telemetry equipment.

b. APT Receiver

The receiver recommended for the APT signals at the go/no-go van and at the test stations is the Nems-Clarke 1456A or the DEI-TMR-6 with selectable IF bandwidths of 50 kc and 100 kc and utilizing phase-locked FM demodulation.

APT-video processing equipment will not be supplied for the CDA stations; however, examination of the signal on an oscilloscope is necessary for evaluation of satellite performance and condition.

5. AVCS-TV Reception Requirements

a. General

The AVCS-TV receiving system will be basically similar to the system used to receive TIROS-TV pictures. The Fairbanks station will require a 235-Mc capability.

b. Antennas

The Fairbanks station uses an 85-foot parabolic reflector which provides 31.5-db gain at 235 Mc. The East Coast station will have the same equipment as at the Fairbanks station.

c. Preamplifiers

The preamplifiers presently used for TIROS-TV reception have a 5.0-db maximum noise figure which will be quite adequate for the OT-2 AVCS system.

d. Receiver

The Nems-Clarke 1412 receiver used at present for TIROS-TV signals will be satisfactory for AVCS-TV reception. This receiver employs conventional FM demodulation and has an IF bandwidth of 500 kc. The possibility of using a down-converter to bring the signal to 136 Mc and then using a receiver at 136 Mc has been suggested as a receiving scheme at the CDA stations. Such a technique would be feasible provided that the 500-kc IF bandwidth is present in the new 136-Mc receiver. If a new receiver is considered, it is recommended that a phase-locked demodulator be incorporated to increase the AVCS system margin in the lower receiver threshold inherent in FM receivers with phase-locked demodulators.

C. VIDEO SECTION

The Video Section consists of all equipment associated with the production of AVCS TV pictures. A block diagram of this equipment is shown in Figure 5-III-5.

The output of the diversity combiner is: (1) a frequency-modulated subcarrier which is deviated between 72 kc and 120 kc at a rate up to 60 kc; and (2) a 9.6-kc subcarrier containing the flutter and wow information.

The two bandpass filters separate the video signal from the flutter and wow frequency, and the video subcarrier frequency is then doubled without affecting the video baseband (60 kc). This doubling can be effected by the circuit shown in Figure 5-III-6. The video subcarrier at the output of the doubler is identical to the Nimbus-AVCS video subcarrier and can be used with the appropriate Nimbus equipment, unmodified in either Real Time or Slow Time (tape recorder played-back at one-eighth the recording speed). The Nimbus equipment and its operation are described in detail in the Instruction Manual for the AVCS/HRIR Subsystem CDA Ground Station Equipment, GSE-3, Volumes 1, 2, and 3.

The video is processed at the CDA stations (1) to provide back-up to NWSC for emergency analysis (in case of "long-lines" breakdown), and (2) to permit equipment checks and alignment. The Nimbus equipment includes a Photo Mechanism Rapid Processor which provides both automatic film advance and automatic developing, fixing, and drying of the film, and which supplies a finished frame 90 seconds after exposure.

Experience with this unit has shown that one hour of proper maintenance (consisting mainly of adding chemicals and film) per eight hours of operation, and two hours of thorough cleaning of equipment every two weeks are sufficient to maintain good operation and consistent results. It is therefore recommended that the Nimbus Kinescope Complex with the Rapid Processors be used unmodified for the AVCS application.

As an alternate technique, Polaroid film can be used at the CDA stations. Polaroid Film Type 46 or 46L (transparency) is recommended for use in this application. The specifications for this film are quoted from the manufacturer as follows:

(1)	Speed:	ASA 800
(2)	Latitude:	±1.5 stops
(3)	Maximum density:	2.3 to 2.5
(4)	Minimum density:	0.05
(5)	Gamma:	1.50
(6)	Resolution:	40 line pairs/mm

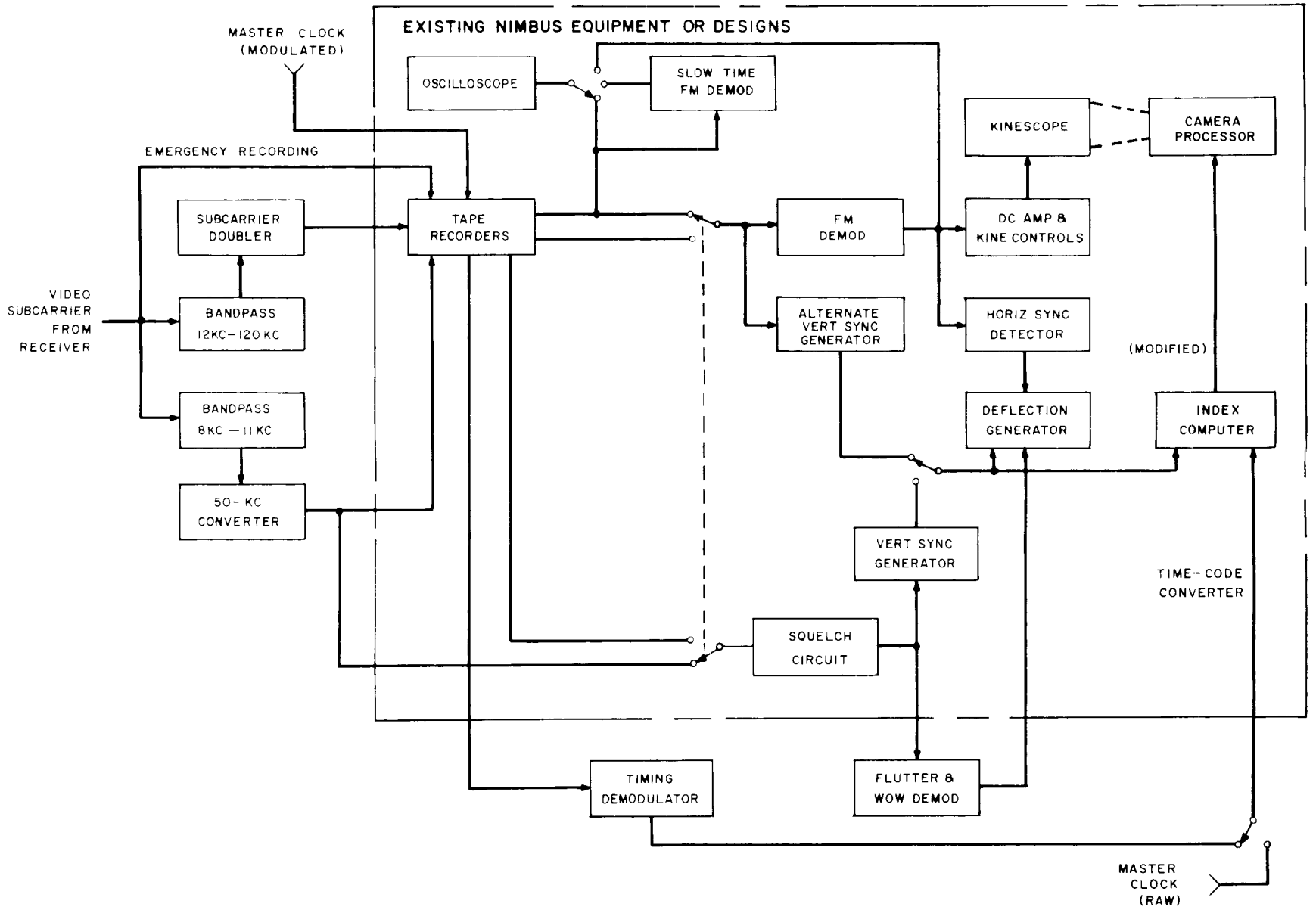

Figure 5-III-5. Video Section of CDA Station, Block Diagram

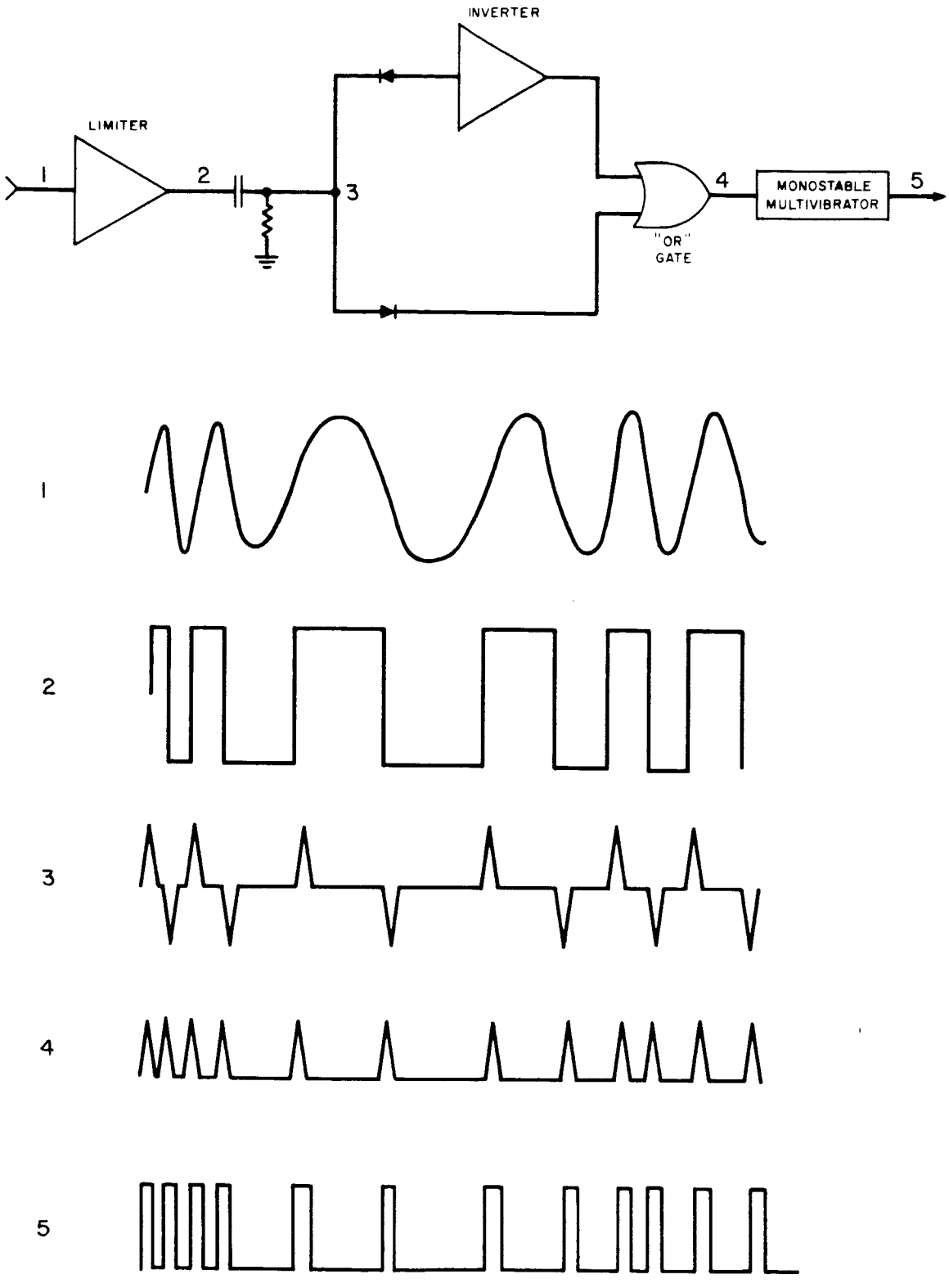

Figure 5-III-6. Subcarrier Doubler Circuit, Block Diagram and Waveforms

If film with these characteristics is used, the resulting pictures would not degrade the system. The disadvantages of using Polaroid film are as follows:

(1) Mechanical modifications to the equipment would be required.

(2) Manual pull-down of the film will not ensure photographing eight consecutive pictures.

(3) The camera would have to be reloaded after eight pictures, and therefore, the entire pass would not be recorded.

(4) Type 46 or 46L film produces a positive transparency, i.e., the opposite of the final product required. It should be noted that Polaroid Film Type 55 produces a negative transparency, but is not suitable for this application due to limited dynamic range, limited grey-level capability, and low gamma (0.66).

(5) Subsequent chemical fixing of the transparency would be required.

The flutter and wow subcarrier can be deviated to a maximum of ±1 percent at rates up to 1 kc by the flutter and wow generated in the satellite recorder. The 9.6-kc subcarrier will be converted to 50 kc for use directly by the Nimbus flutter and wow demodulator. In order to obtain sufficient output from the flutter and wow demodulator, it is necessary to maintain at least a ±0.3 percent deviation. Heterodyning the 9.6 kc directly to 50 kc would reduce the maximum deviation (±96 cps) to less than 0.2 percent. The proposed technique is to double-double to 38.4 kc, then heterodyne to 50 kc.

The flutter and wow subcarrier is keyed-on in the satellite at the start of the vertical pulse. It is, thus, used on the ground to generate vertical sync pulses. A modified Nimbus AVCS vertical sync generator will be used for this application.

Time codes are generated on the ground, but are of such format as to be readily compatible with the Nimbus AVCS timing delay. The time and index annotation will, thus, be very similar to Nimbus. The Nimbus AVCS demodulator will be used to recover tape-recorded code.

It is not necessary to provide back-up or redundancy in the video equipment because a malfunction would simply require a replay of the tape after equipment is rendered operative.

Electronics boards from the Nimbus AVCS station at Valley Forge will be used in some OT-2 stations, as will the kinescope complexes from the Fairbanks Nimbus station. However, the electronics will not be removed from the latter station. Instead, the station will be modified to provide both limited (only one kinescope complex) Nimbus capability and full OT-2 capability.

D. COMMAND SECTION

1. General

A block diagram of the command section is shown in Figure 5-III-7. In the normal mode of operation, punched-tape is fed into the tape reader. The digital command programmer generates the digital codes determined by the tape and by other inputs, as described later. The outputs of the digital command programmer are a FSK'd command tone and a satellite "enable" tone, which is suitable for driving the command transmitter.

A comparison between the transmitted commands and the verification data (decoded commands retransmitted by the satellite on a beacon channel) is performed automatically.

Performance of the command section is checked and verified by a spacecraft-type receiver-decoder combination, which receives the RF signal from the command antenna and provides decoded commands to the comparator. Successful comparison with the output of the digital command programmer ensures proper ground station operation.

A back-up capability for the tape recorder is provided by the auxiliary command unit, which also provides a control panel for the command system.

2. Tape Reader

Commands are received at the CDA station from TCC by means of a teletypewriter which provides a punched tape (each station can also make a command tape with its own teletype equipment). The tape uses a 5-level code which is described fully in Section 4-IV-B, Paragraph 36. The complete command-sequence tape is inserted in the tape recorder. The tape reader begins to advance the tape and "reads" upon receipt of a pulse from the alarm timer (or from a manual pushbutton when the tape reader is in the tape-test mode). Upon reading a command, the tape reader causes the digital command programmer to generate a sync pulse, an address, and the command. After an interval determined by internal electronics, the entire message is transmitted, and the tape advances to read the next command.

In order to obtain a "hard" copy of the commands punched, it is necessary to eliminate all codes controlling teletype-machine functions, such as "line feed", "space", "carriage return", and so forth. All these codes have the common characteristic that the first and fifth levels are both "1" or both "0". The tape reader will ignore any code having this characteristic. (This also allows errors to be obliterated by punching the "letters" key.) Instructions to the tape reader will employ codes with a "1" in the first level and a "0" in the fifth. Actual satellite commands will employ codes with a "0" in the first level and a "1" in the fifth. Only the three center levels contain the

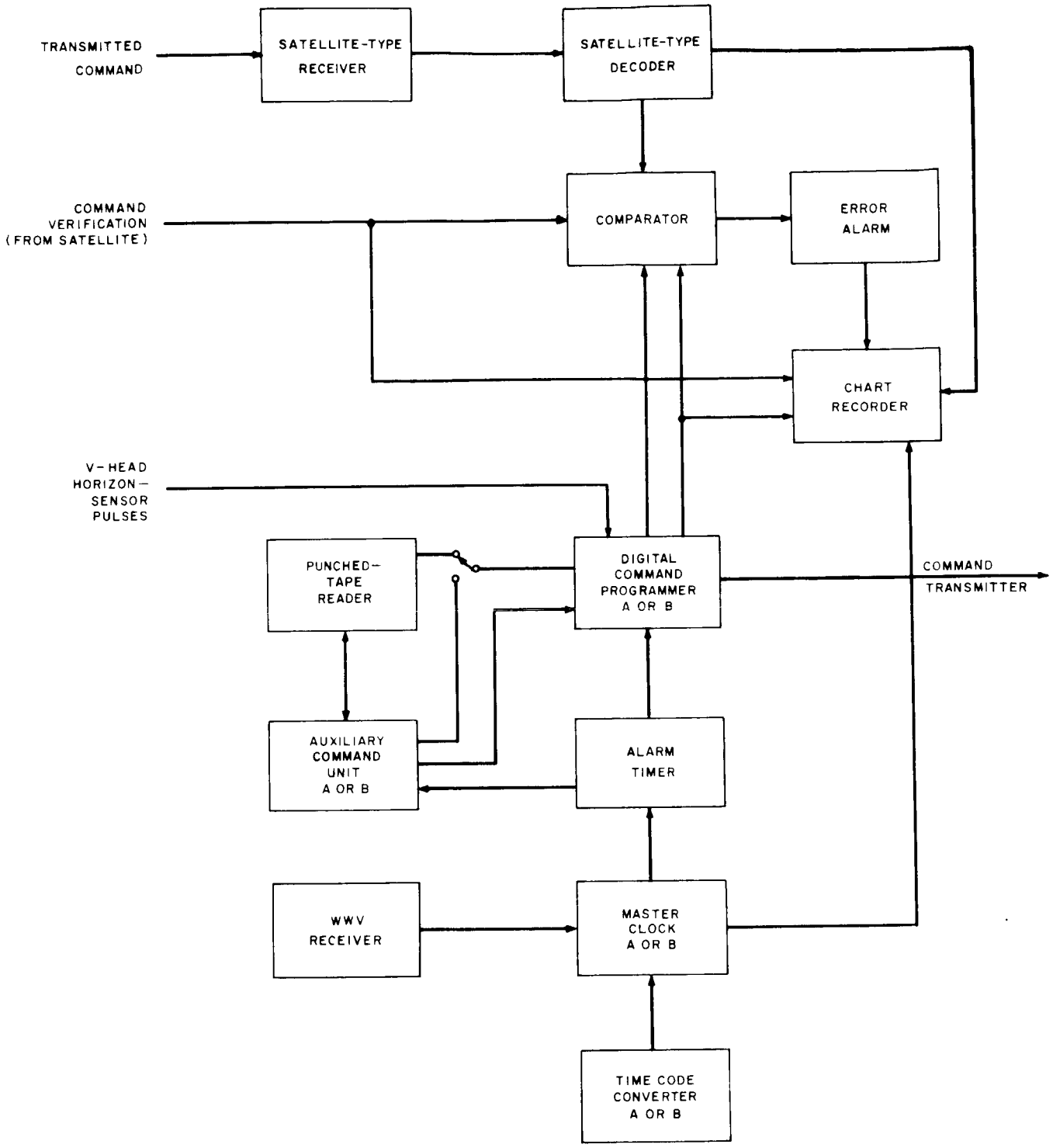

Figure 5-III-7. Command Section, Block Diagram

commands. The satellite address is manually selected at the CDA station. Only the commands are provided by TCC. These consist of two types: (1) Standard commands of 12 bits and (2) loading commands of 12 + 28 bits. The standard commands require 4 levels of tape; the loading commands require 14 levels. Tape reader instructions consist of the following:

(1) Read 4 levels.

(2) Read 14 levels.

(3) Stop. (and wait for next alarm pulse)

This coding of the tape reader instructions is described in Table 5-III-1.

TABLE 5-III-1. TAPE READER INSTRUCTION CODES

Code	Letter	Instruction
10000	E	Read 4 Levels.
11110	K	Read 14 Levels.
10100	S	Stop. (and wait for next alarm pulse)
NOTE: In the tape coding, a hole in the tape represents a "1", and the absence of a hole represents a "0".		

The tape is checked before transmission by placing the command system in the tape-test mode. This connects the digital command programmer output to the decoder input. The decoded commands are then displayed on the paper chart for examination.

Proper reception of the tape from TCC is checked by re-transmitting the tape back to TCC on the teletypewriter and obtaining confirmation.

3. Alarm Timer

The alarm timer receives its input from the master clock and generates the required time pulses for the units within the command section. In particular, it generates alarm pulses at three different times, determined by the front panel settings, to initiate sequences of command transmissions. These pulses are applied to the tape reader and to the auxiliary command unit.

4. Auxiliary Command Unit

The auxiliary command unit acts as a back-up to the tape reader by providing a manual means of setting commands. Most of the controls and indicators used in the command section are located on this unit, and it is closely connected to the digital command programmer and its operation. The proposed front panel of the auxiliary command unit is shown in Figure 5-III-8.

The address of the commanded satellite is set into the "satellite address" bank, and this code is automatically inserted in the command sequence as required.

Selection of the A or B decoder selects two of four possible tones, one for "enable" and the other for FSK. Transmitted spacecraft verification and ground verification indicators are located on the auxiliary command unit. An error-retransmit manual/automatic mode is provided, and an error is recognized only when the spacecraft verification channel does not compare with the digital command programmer output. The ground-verification loop is used only in isolating trouble.

The sequence of events which takes place when an error is detected is as follows:

(1) An alarm indicator (consisting of a bell and a panel light) is energized, and a tick mark is inscribed by a marker pen on the chart recorder.

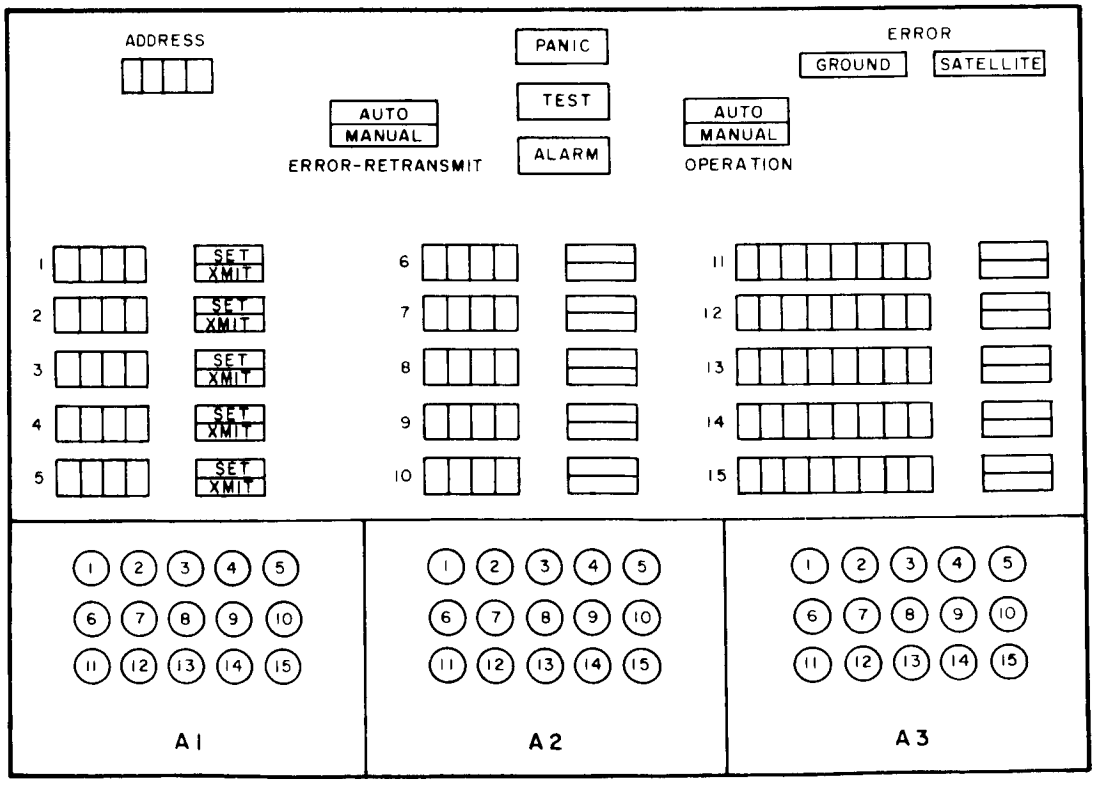

Figure 5-III-8. Auxiliary Command Unit, Front Panel

(2) If the automatic mode of the retransmit switch has been selected, command transmission is immediately stopped, preventing the spacecraft from recognizing the command and the complete command word is immediately retransmitted. If the last bit is in error, the spacecraft will have received a complete command, but since there exist two commands which differ only in the last bit, the command will not be recognized.

A count will be kept of the number of errors detected, and therefore, of the number of retransmissions. This count will then be used to modify the T_0-count contained in any subsequent command in order to compensate for the time that was lost as the result of the retransmissions, and thus cause the T_0 time to occur at the position in orbit at which it would have occurred if no retransmissions had taken place.

(3) If the manual mode of the retransmit switch has been selected, the command transmission continues, and the complete sequence continues. This mode allows examination of the verification channel on the chart recorder to determine if an error actually occurred in the transmission or reception by the command-control decoder in the spacecraft, or whether noise, added on the "down link", caused an error to be made in the comparator. It is safe to delay correction of errors because there are no commands that will damage the spacecraft equipment, and a two-bit error is required for any one command to be recognized as a different command. If an error has been committed, the command can be retransmitted at the end of the sequence, or immediately, by depressing the PANIC switch. Activation of this switch allows the tape reader to complete the "reading" of the command already started, but prevents it from "reading" the next command. Activation of the PANIC switch disconnects the tape reader from the digital command and programmer connects the command banks of the auxiliary command unit. Re-depressing the PANIC switch permits the tape reader to continue the sequence.

The auxiliary command unit contains 10 command banks each consisting of 4 octal switches and a set/transmit switch, and 5 command banks each consisting of 14 octal switches and a set/transmit switch. Commands are set in any of the 15 banks by dialing the first octal switch to a digital equivalent of the first 3 bits of the command, and the second switch to the second 3 bits etc.... (i.e., 100000010000 as 4020). Spacecraft programmer messages are set in the remaining 10 switches of the 14-switch banks. The 15 command banks allow more than a normal full sequence of commands to be programmed prior to the start of the sequence.

With the TRANSMIT switch in the automatic mode, the first command-sequence transmission begins at the first alarm time, determined by time set into the alarm timer. The commands set in banks whose number is selected by the Alarm 1 Timing selector are automatically transmitted in sequence. The program is then stopped until the alarm time indicated by the Alarm 2 Timing selector is reached, and those commands selected by this sequence selector are similarly transmitted. This action is repeated for Alarm 3 Timing. The SET/TRANSMIT switch is used only as an indicator. The set light operates when its bank has been selected in any sequence timing. The transmit light operates when the command is transmitted.

Error detection and re-transmission is identical to that described earlier. The program set in the command banks of the auxiliary command unit is tested as described in the discussion on the action of the tape reader when the PANIC switch is depressed.

When the TRANSMIT switch is in the manual mode, the sequence timers are disconnected and commands are transmitted individually upon activation of the SET/TRANSMIT switch. This mode is used, in particular, for re-transmission of erroneous commands when the unit is in the manual error-retransmit mode.

5. Comparator

This unit compares, bit-by-bit, the command code from the digital command programmer with the verification code which is received on a beacon channel. Any disagreement between two bits causes an alarm, as described earlier. The output of the digital command programmer is also compared to the output of a system consisting of an antenna, receiver, and decoder. This system has an input which, except for transmission path deterioration, is identical to that for the spacecraft. Thus, it provides a complete check of the ground command system. If the beacon verification indicates errors, this system provides a method for rapid isolation of the trouble.

6. Master Clock

The Master Clock is a highly stable crystal-controlled unit which, used in conjunction with a WWV receiver, is calibrated to the time of day. It simultaneously generates the serial 36-bit NASA time code for use with the video information and the NASA 28-bit time code for use in paper-chart recording. The required clock pulses such as 100 pps, 10 pps, and 1 pps used in generating the commands are also provided by this unit.

7. Digital Command Programmer

This unit generates the ditial command code according to the instructions received from either the tape reader or the auxiliary command unit. The address code and the

command sync are also generated. These are timed by circuits referenced to the master clock. The four tones required for signal and FSK are generated from the tuning fork oscillators. One of two of these tones is FSK'd with the digital command and the corresponding tone is transmitted in its proper time sequence as per instructions from the auxiliary command unit and alarm timer.

Attitude-scanner pulses are used within this unit to synchronize command transmission with an unambiguous spacecraft rotation position. Commands are transmitted after a fixed time interval even in the absence of attitude pulses, to ensure that failures in the beacon system do not interfere with command functions.

8. Time-Code Converter

This unit modulates the Minitrack time code for tape recording, and generates timing pulses at rates not obtained directly from the Master clock.

E. BEACON-DATA SECTION

1. General

A block diagram of the beacon-data section is shown in Figure 5-III-9. The beacon subcarrier consists of three multiplexed frequencies. These are separated and demodulated in three subcarrier discriminators (with center frequencies as shown below) and provide the following data:

(1) Channel 1 (2.3 kc): attitude sensor 1, received during 100 percent of the pass.

(2) Channel 2 (3.0 kc): attitude sensor 2, received during 100 percent of the pass.

(3) Channel 3 (3.9 kc), shared between the following functions:

  (a) telemetry (transmitted with each video frame or on command),

  (b) command verification (transmitted automatically during command sequence),

  (c) sun-aspect data (transmitted on command),

  (d) orthogonal horizon-sensor data (present when other data is not requested), and

  (e) satellite picture time (transmitted with each AVCS video frame).

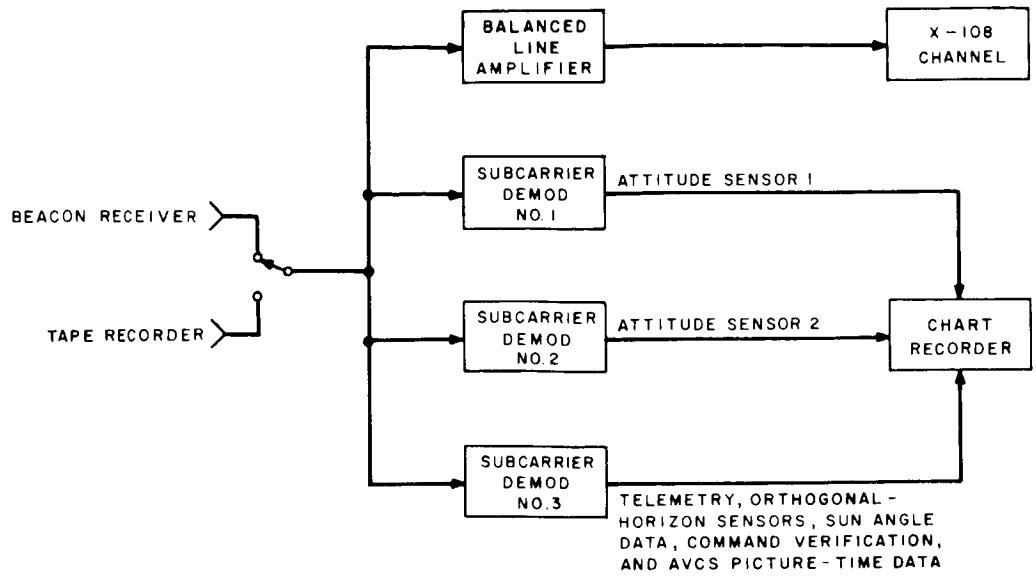

Figure 5-III-9. CDA Station Beacon-Data Handling Section, Block Diagram

Each of these channels is displayed on the chart recorder simultaneously with timing pulses and real time out of the master clock.

2. Chart Recorders

The channel assignments for the chart recorders are as indicated in Table 5-III-2.

Tests indicate that 10 pps signals are readily analysed at a chart speed of 20 mm/sec. (See Figure 5-III-10.) However, the accuracy of the attitude-sensor data reduction is directly related to the resolution accuracy of pulse location reading, which is a direct function of the chart speed. Figure 5-III-11 gives the error of average spin period versus measuring time as a function of the two recording speeds. Figure 5-III-12 gives the satellite subpoint accuracy versus number of sky/earth pulses from a given reference point for the two speeds. At 20 mm/sec, the 100-pps timing code will have marks spaced 0.2 mm apart. This is not resolvable. At 50 mm/sec, 100-pps signals will be 0.5 mm apart. Because of the limited recorder frequency response, such marks could be difficult to resolve. A 10-pps timing code would have marks 5 mm apart, and this could be interpolated to below 1 mm. Hence it is proposed that 10 pps timing code be used.

The receiver AGC is recorded to indicate time of spacecraft transmitter turn-on. Experience on TIROS indicates that the time delay between command and execution of this function is a good indicator of command subsystem performance degradation. The ground camera shutter (or vertical sync) pulses give the time of picture reception and the number of pictures received. Although this information can be retrieved by playing back the video tape, it is considerably more convenient to have it in this form.

TABLE 5-III-2. CHART-RECORDER CHANNEL FUNCTIONS

Channel	Function	Data
1	Beacon Channel 1	Horizon Scanner 1
2	Timing Pulses	10 pps
3	Beacon Channel 2	Horizon Scanner 2
4	Beacon Channel 3	Telemetry Command Verification, Sun Angle Sensor, Orthogonal Horizon Sensors, AVCS Picture Time Data
5	Digital Command Programmer	Transmitted Commands
6	Decoder	Ground System Command Verification
7	Real Time	NASA 28-bit code
8	Ground Receiver AGC	
Marker Pen 1	Ground Video Vertical Sync Pulses	
Marker Pen 2	Comparator	Detected Error

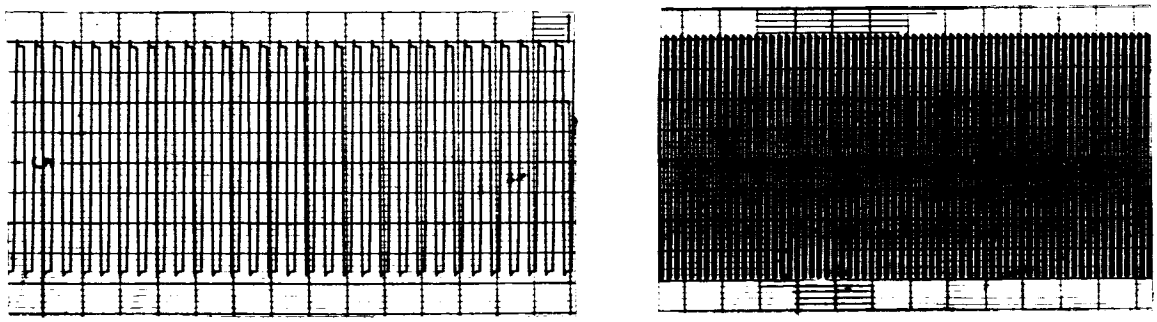

Figure 5-III-10. 10-pps Time Code Recorded At 10 mm/sec and 20 mm/sec

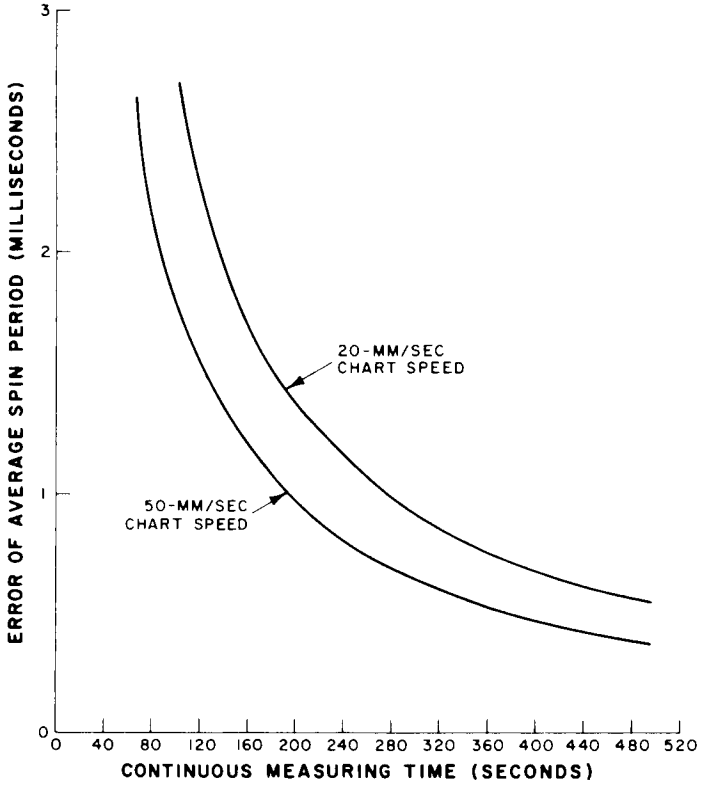

Figure 5-III-11. Spin-Period Measurement Error Using V-Head Horizon Sensor

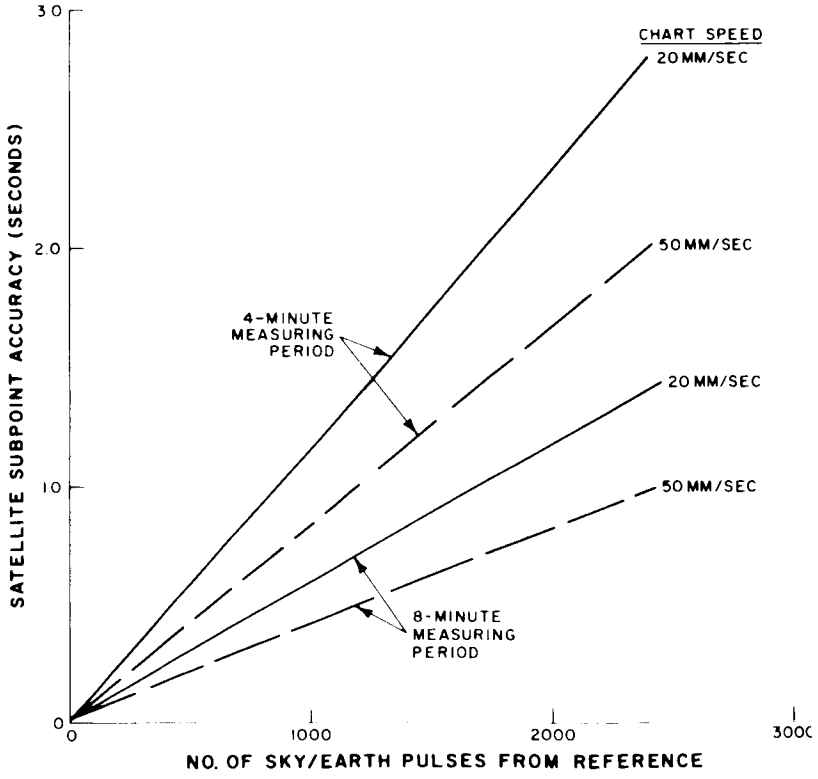

Figure 5-III-12. Satellite Subpoint Accuracy

A single 8-channel Brush recorder satisfies all the chart recording needs at the CDA sites (with the exception of events recording). However, the high speed required by the attitude-data channels makes the operation expensive. It is proposed that the 8-channel Brush recorder be used for all data at a speed of 20 mm/second (see Figure 5-III-10) and that a 2-channel Sanborn recorder be used at 50 mm/sec for the two attitude data channels.

A 20-channel Esterline-Argus recorder is also provided at each station to monitor all station functions as well as certain critical commands.

A partial list of the events recorded by the events recorder is shown in Table 5-III-3.

TABLE 5-III-3. EVENTS RECORDED BY EVENTS RECORDER

Channel	Event
1	Command Tones A or B
2	Alarm Timer Output
3	Horizontal Video Receiver AGC
4	Vertical Video Receiver AGC
5	Horizontal Beacon Receiver AGC
6	Vertical Beacon Receiver AGC
7	Master Clock 0.1 pps
8	Ground Vertical Sync Pulses
9	Transmitter On

3. Tape Recorders

The function of the tape recorders is to record all subcarriers as they are received in "real" time, to playback this information either at real-time speed for processing or slow time for "long-lines" transmission, and to provide a master copy for archival copies. Station-generated "real" time will be recorded on tracks adjacent to the subcarriers.

Two tape recorders are proposed for increased reliability. Since the beacon data will be simultaneously processed and recorded on paper charts, only one tape recorder need be used as back-up during this phase of reception. The video information will not be processed during reception, hence, the second tape recorder will be used at this time.

A time diagram of the operation of the tape recorders is shown in Figure 5-III-13.

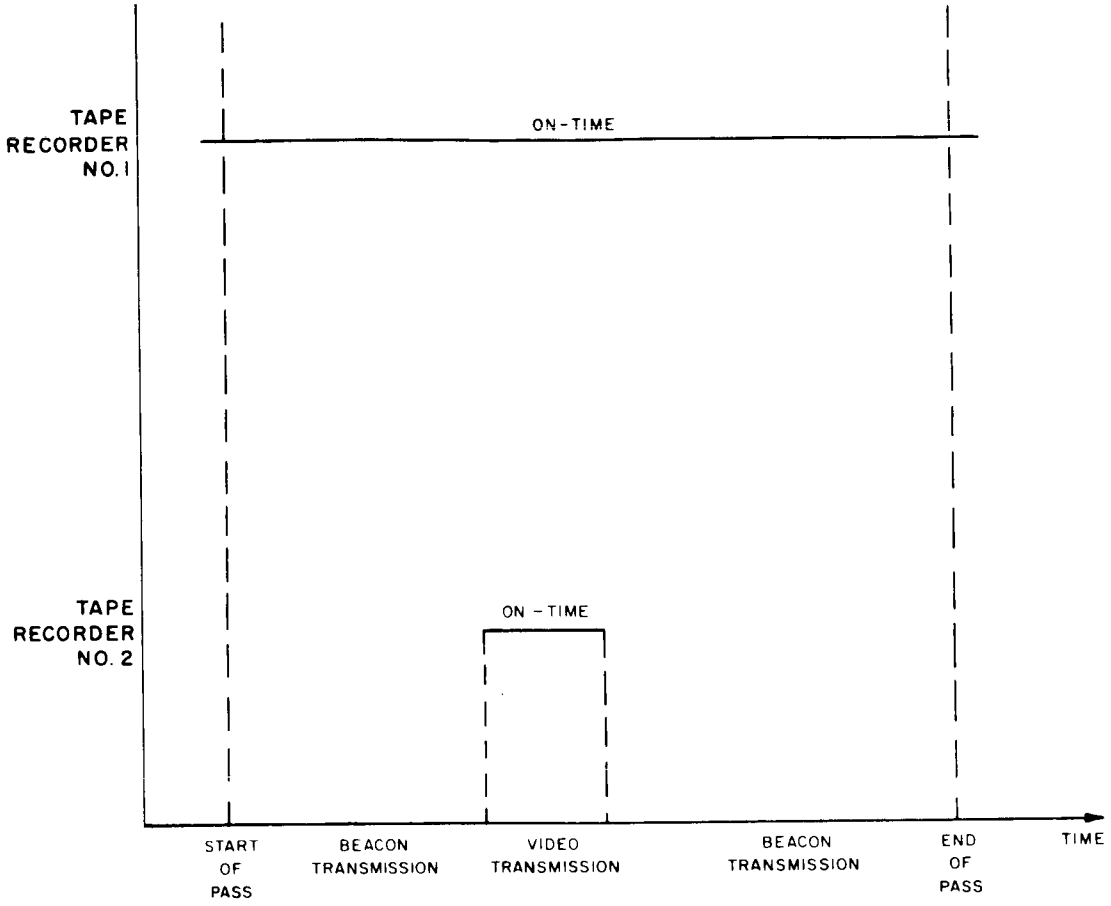

Figure 5-III-13. Timing Diagram of Operation of Tape Recorders

The tape of Tape Recorder No. 1 can be erased and re-used once the successful recording on paper of the beacon data has been verified and the video recording on Tape Recorder No. 2 has been successfully transmitted on the "long-line" circuits. The Tape Recorder No. 2 tape is used until filled, and it is then shipped to NWSC for reproductions.

Track allocations are shown in Table 5-III-4.

An interconnection diagram of the tape recorders is shown in Figure 5-III-14. Note that both tape recorders are connected in parallel even though they do not record identical data. This makes it possible to interchange the functions of the tape recorders and to have immediate recording capability on one if the other should fail.

4. Power Supplies

Power supplies required for this application exist in the Nimbus AVCS equipment. Additional power supplies will be required.

TABLE 5-III-4. TAPE RECORDER TRACK ALLOCATIONS

Track	Channel
1	50-kc Converted Flutter and Wow Frequency
2	Doubled Video Subcarrier
6	NASA 36-Bit Time Code (Minitrack)
4	Undoubled Video Subcarrier with Flutter and Wow Frequency
5	Beacon Subcarriers
3	NASA 28-Bit Time Code

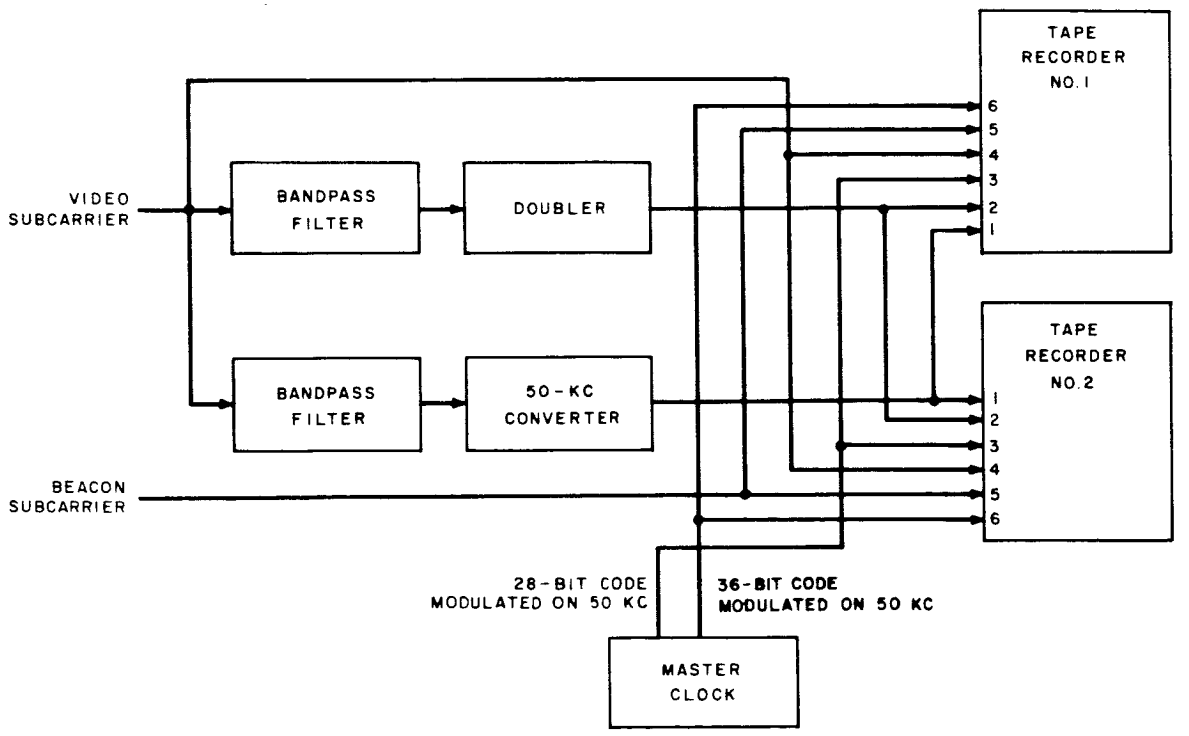

Figure 5-III-14. Tape Recorders, Interconnection Diagram

SECTION IV. TRANSMISSION TO CPA CENTERS

Transmission of beacon and video data to the CPA centers is on the "long-lines" circuits by means of X-108 equipment. A block diagram of this transmission system is shown in Figure 5-IV-1.

All beacon data and timing (10 pps) signals are transmitted at "real" time, simultaneously with reception by the ground station. The video data is transmitted by playing the tape recorder back at 7-1/2 ips (1/8 the recording speed). This reduces the subcarrier instantaneous frequency range to 18 to 30 kc and the baseband to 7-1/2 kc. This is suitable for transmission on the X-108 equipment. The flutter and wow subcarrier is, then, 6.25 kc. A slow-time demodulator (unmodified Nimbus equipment) is used for monitoring purposes at the CDA stations. The video is never processed at slow-time at the CPA centers; it is recorded from the "long-lines" circuits onto a tape recorder running at 7-1/2 ips and played back at 60 ips.

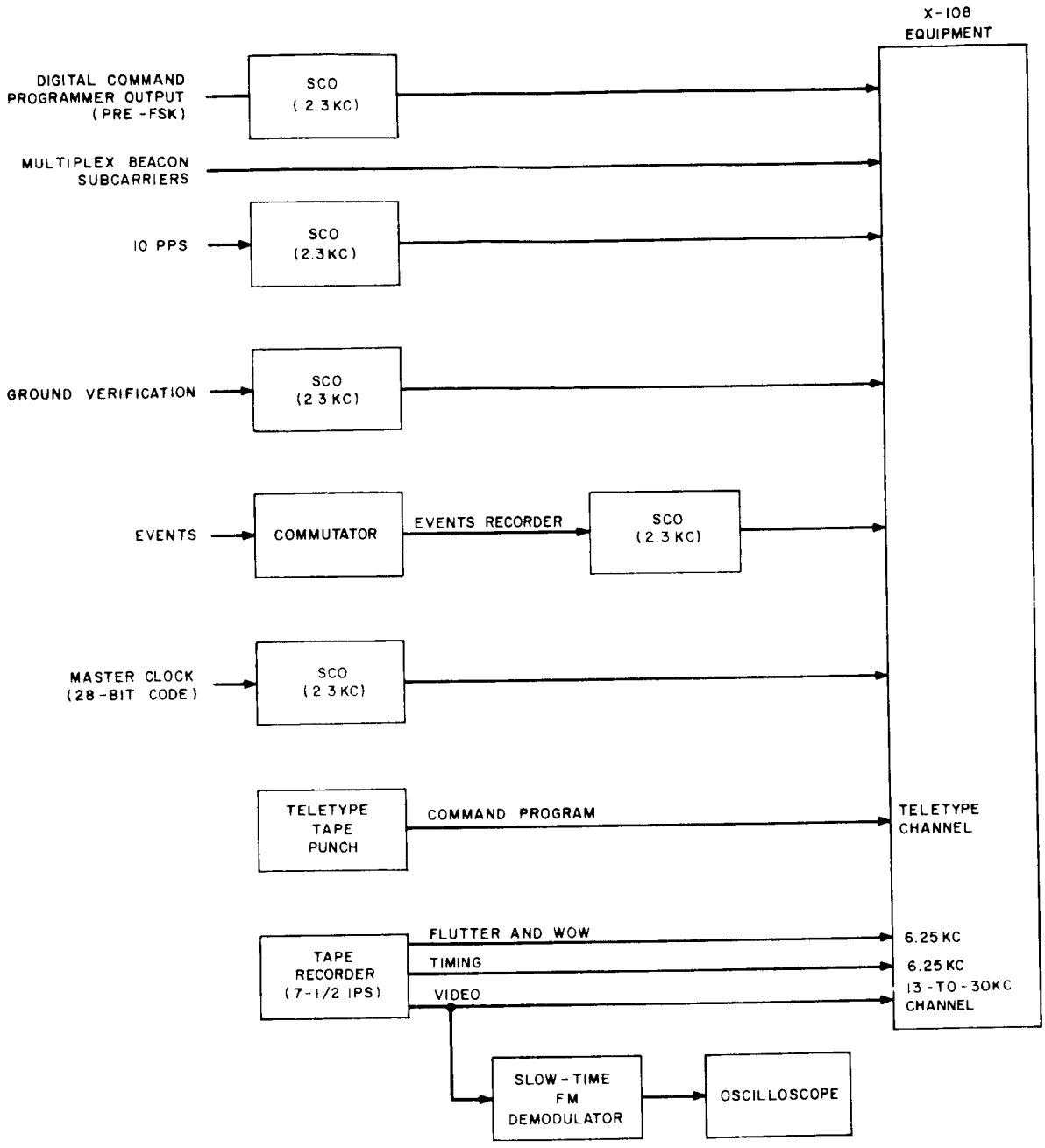

Figure 5-IV-1. Beacon and Video Data Transmission System, Block Diagram

SECTION V. SYSTEM REDUNDANCY

To ensure successful acquisition of data during a pass, system redundancy is built into various sections of the ground equipment at the CDA stations.

System reliability exists in the video section by virtue of the use of two tape recorders and their interconnection. No redundancy is required in the processing system because that equipment can operate from tape recorder playback.

Redundancy has been designed into the command section. It is imperative that commands be successfully transmitted. Command programs are normally transmitted from TCC to the CDA stations by teletypewriter. In the event of failure of this line, command programs can be transmitted either verbally over telephone, or by other means of communication. The CDA stations have the capability of generating a punched tape, using their standard teletype equipment.

Back-up to the tape reader is provided by the auxiliary command units (ACU' s). Failure of the tape reader does not affect the operation of the ACU; however, the ACU controls certain functions of the tape reader, so that the two are not fully interchangeable. As a result of this, two ACU's are proposed. This provides an additional capability in that two alternate programs can be set in advance; one on punched tape, and the second on the first ACU. The second ACU can then be used as a back-up and for error transmission, or for setting up a second program if two satellites will be contacted. The DCP and time-code converter are critical units in the link and also require back-up units.

The alarm timer is not critical because alarms can be simulated manually; however, timing pulses required by the coding equipment are critical, and this requires two units of Master Clocks. The remaining command-section components are not required for emergency operation. Failure of items such as the comparator or ground decoder would disable the verification link, but would not prevent transmission of commands.

Redundant equipment is not required with the beacon-data section, since beacon data is tape-recorded simultaneously with paper chart recording at the CDA station and at the CPA centers. Hence, the use of only one tape recorder at the stations provides sufficient redundancy. Failure of chart recorder would prevent proper monitoring of spacecraft performance; however, this is not deemed to be a critical function of the CDA sites.

SECTION VI. EQUIPMENT REQUIREMENTS

A. APT CONFIGURATION OF SPACECRAFT

The existing Nimbus APT ground stations are capable of receiving and displaying TV-pictures transmitted from the APT-configured spacecraft without equipment modifications. The video signal is received by a circularly polarized antenna, fed into an FM receiver, and processed by facsimile-recording equipment to produce a real-time cloud-cover picture for the locale of the particular ground station. It is anticipated that an APT ground station will be located at each CDA ground station in addition to the APT stations at remote locations throughout the world. Although the CDA station receivers and preamplifiers are identical to APT station components, the data link margin will be higher at the CDA stations than at the remote APT stations because of the higher gain (and other inherent characteristics) of the antenna at the CDA station. A detailed discussion of the relative system margins is presented in the discussion of the spacecraft communications interface in Section 4-VII of this report.

B. AVCS CONFIGURATION OF SPACECRAFT

Modifications of various degrees, and in some places new designs, are required to much of the ground equipment to accommodate the AVCS configuration of the satellite. The required effort for the APT and AVCS configurations are summarized in Tables 5-VI-1 and 5-VI-2. It should be noted that the listing of the number of pieces of each unit required assumes no back-up or spare items.

TABLE 5-VI-1. GROUND STATION EQUIPMENT (GSE) STATUS

GSE Number	Type	Location
1	Full CDA	Alaska
2	Full CDA	East Coast
3	Spacecraft Evaluation and Checkout (Spacecraft Check-out Set No. 2)	RCA Princeton
4	TCC	Maryland
5	Go/No-Go Van	Launch Area
6	Spacecraft Checkout (Spacecraft Check-out Set No. 1)	RCA Princeton

Basic Procurement (AVCS only)

GSE Number	Equipment
1	Modified Nimbus GSE No. 3, dual Nimbus/OT-2
2	Partial Nimbus GSE No. 6 with Nimbus GSE No. 3 Kine Complex
3	Partial Nimbus GSE No. 6 with Nimbus GSE No. 3 Kine Complex
4	New
5	Partial Nimbus GSE No. 6 and Nimbus GSE No. 6 Kine Complex
6	Partial Nimbus GSE No. 6 and Nimbus GSE No. 6 Kine Complex

Station Complements

GSE Number	AVCS	Command	Beacon	RF	APT
1	Full	Full	Full	Full	Receivers
2	Full	Full	Full	Full	Receivers
3	Full	Full	Full	Full	Full
4	None	Partial	Full	None	None
5	Partial	Partial	Full	Partial	Full
6	Partial	Partial	Partial	Partial	Full

TABLE 5-VI-2. COMPONENT STATUS OF GROUND SUPPORT EQUIPMENT (GSE)

Component	Ground Support Equipment (GSE) Number											
	1		2		3		4		5		6	
	Status	No./ Unit	Status	No./ Unit	Status	No./ Unit	Status	No./ Unit	Status	No./ Unit	Status	No./ Unit
	KINE COMPLEX											
Video Amplifier	A	1	A	1	A	1	-	0	A	1	A	1
Deflection Generator	A	1	A	1	A	1	-	0	A	1	A	1
Horizontal Sync Detector	A	1	A	1	A	1	-	0	A	1	A	1
Auxiliary Sync	A	1	A	1	A	1	-	0	A	1	A	1
Focus Regulator	A	1	A	1	A	1	-	0	A	1	A	1
Kine Circuits	A	1	A	1	A	1	-	0	A	1	A	1
Black and White Tester	A	1	A	1	A	1	-	0	A	1	A	1
Blanking Circuits	A	1	A	1	A	1	-	0	A	1	A	1
Kinescope	A	1	A	1	A	1	-	0	A	1	A	1
Processor	A	1	A	1	A	1	-	0	A	1	A	1
High Voltage Power Supply	A	1	A	1	A	1	-	0	A	1	A	1

TABLE 5-VI-2. COMPONENT STATUS OF GROUND SUPPORT EQUIPMENT (GSE) (Continued)

Component	Ground Support Equipment (GSE) Number											
	1		2		3		4		5		6	
	Status	No./ Unit	Status	No./ Unit	Status	No./ Unit	Status	No./ Unit	Status	No./ Unit	Status	No./ Unit
Polaroid Adapter	E	1	E	1	E	1	-	0	E	1	E	1
Racks and Connections (Kine Complex only)	B	1	B	1	B	1	-	0	B	1	C	1
AVCS ELECTRONICS												
Filter 1 (Video Subcarrier)	E	2	E	2	E	1	-	0	E	1	E	1
Filter 2 (Flutter and Wow Subcarrier)	E	2	E	2	E	1	-	0	E	1	E	1
Doubler and Heterodyner	E	2	E	2	E	1	-	0	E	1	E	1
Squelch Circuit	E	1	E	1	E	1	-	0	E	1	E	1
FM Demodulator	A	1	A	1	A	1	-	0	FA	1	FA	1
Vertical Sync Generator	B	1	FB	1	B	1	-	0	FB	1	FB	1
Alternate Vertical Sync Generator	A	1	A	1	FA	1	-	0	FA	1	FA	1

TABLE 5-VI-2. COMPONENT STATUS OF GROUND SUPPORT EQUIPMENT (GSE) (Continued)

Component	Ground Support Equipment (GSE) Number											
	1		2		3		4		5		6	
	Status	No./ Unit	Status	No./ Unit	Status	No./ Unit	Status	No./ Unit	Status	No./ Unit	Status	No./ Unit
Flutter and Wow Demodulator	A	1	FA	1	FA	1	-	0	A	1	FA	1
Slow-time FM Demodulator	A	1	FA	1	FA	1	-	0	-	0	-	0
Control Panel	B	1	E	1	E	1	-	0	E	1	E	1
Jack Panel	B	1	D	1	E	1	-	0	E	1	E	1
Flutter and Wow Doubler and Heterodyner	E	1	E	1	E	1	-	0	E	1	E	1
INDEX												
Master Clock	F	2	F	2	F	1	-	0	F	1	F	1
Time Code Converter	E	1	E	1	E	1	-	0	E	1	E	1
Timing Demod 36 Bit	A	1	A	1	FA	1	-	0	FA	1	FA	1
Timing Demod 28 Bit	E	1	E	1	E	1	-	0	E	1	E	1
Index Display	B	1	B	1	B	1	-	0	B	1	B	1
Index Display Driver	A	1	A	1	E	1	-	0	E	1	E	1

TABLE 5-VI-2. COMPONENT STATUS OF GROUND SUPPORT EQUIPMENT (GSE) (Continued)

Component		Ground Support Equipment (GSE) Number											
		1		2		3		4		5		6	
		Status	No./ Unit	Status	No./ Unit	Status	No./ Unit	Status	No./ Unit	Status	No./ Unit	Status	No./ Unit
AVCS Racks		B	-	E	1	E	-	E	-	E	-	E	-
Power Supplies		A	-	A	-	F	-	F	-	F	-	F	-
BEACON													
Subcarrier Demodulator (3 SCD's per unit)		F	2	F	2	F	1	F	2	F	1	F	1
Chart Recorders	8-Channel	A	1	A	1	A	1	A	1	A	1	A	1
	2-Channel	F	1	F	1	F	1	F	1	F	1	F	1
Switching and Control		E	1	E	1	E	1	E	1	E	1	E	-
Racks		E	-	E	-	E	-	E	-	E	-	E	-
COMMAND SECTION													
Teletype Tape Reader and Printer		-	1	-	1	-	1	-	1	-	0	-	0
Tape Reader and Electronics		E	1	E	1	E	1	-	0	E	1	E	1

TABLE 5-VI-2. COMPONENT STATUS OF GROUND SUPPORT EQUIPMENT (GSE) (Continued)

Component	Ground Support Equipment (GSE) Number											
	1		2		3		4		5		6	
	Status	No./ Unit	Status	No./ Unit	Status	No./ Unit	Status	No./ Unit	Status	No./ Unit	Status	No./ Unit
Auxiliary Command Unit	E	2	E	2	E	1	-	0	E	1	E	1
Digital Command Programmer	E	2	E	2	E	1	-	0	E	1	E	1
Comparator	E	1	E	1	E	1	-	0	E	1	E	1
Alarm Timer	E	1	E	1	E	1	-	0	-	0	-	0
Satellite-Type Receiver	E	1	E	1	E	1	-	0	E	1	E	1
Satellite-Type Decoder	E	1	E	1	E	1	-	0	E	1	E	1
Power Supplies	F	-	F	-	F	-	F	-	F	-	F	-
Racks (Command)	E	-	E	-	E	-	E	-	E	-	E	-
APT												
Receiver	-	2	-	2	F	2	-	0	F	1	F	1
APT Rack	-	0	-	0	A	1	-	0	A	1	A	1

TABLE 5-VI-2. COMPONENT STATUS OF GROUND SUPPORT EQUIPMENT (GSE) (Continued)

Component	Ground Support Equipment (GSE) Number											
	1		2		3		4		5		6	
	Status	No./ Unit	Status	No./ Unit	Status	No./ Unit	Status	No./ Unit	Status	No./ Unit	Status	No./ Unit
RF SECTION												
Antenna	GFE	-	GFE	-	A	1	-	0	E	1	-	0
Video Receivers	GFE	-	GFE	-	F	3	-	0	F	1	F	1
Diversity Combiner	GFE	-	GFE	-	F	2	-	0	-	0	-	0
Check-out Signal Generator	GFE	-	GFE	-	F	1	-	0	F	1	F	1
Beacon Receivers	GFE	-	GFE	-	F	3	-	0	F	1	F	1
Diversity Combiners	GFE	-	GFE	-	F	2	-	0	-	0	-	0
Command Antenna	GFE	-	GFE	-	-	0	-	0	F	1	-	0
Filters, Pre-Amplifiers	GFE	-	GFE	-	F	-	-	0	F	1	-	0
RF Measuring Equipment	-	-	-	-	-	-	-	-	-	-	F	1
MISCELLANEOUS												
Tape Recorders	A	2	FB	2	A	2	FB	1	B	1	B	1
Oscilloscope Tektronix RM 45A	A	2	A	1	F	1	-	0	F	1	F	1
Oscilloscope Tektronix RM 504	F	1	F	1		1	F	1	F	1	F	1

TABLE 5-VI-2. COMPONENT STATUS OF GROUND SUPPORT EQUIPMENT (GSE) (Continued)

Component	Ground Support Equipment (GSE) Number											
	1		2		3		4		5		6	
	Status	No./ Unit	Status	No./ Unit	Status	No./ Unit	Status	No./ Unit	Status	No./ Unit	Status	No./ Unit
Long Lines Interface	B	1	B	1	-	0	B	1	-	0	-	0
Events Recorder	F	1	F	1	F	1	F	1	F	1	F	1
Satellite Support Console	-	-	-	-	E	1	-	-	E	1	E	1

LEGEND FOR TABLE 5-VI-2

A - equipment as is

B - minor modifications

C - moderate modifications

D - extensive modifications

E - new design

F - additional equipment (purchased)

FA - additional equipment, same as previous design

FB - additional equipment with minor modifications over previous design

SECTION VII. PRINCETON CHECK-OUT STATION

Two spacecraft check-out sets will be located in the RCA Space Center, Princeton, N.J. Spacecraft Check-out Set No. 1 will provide for the check-out of spacecraft prior to launch. Spacecraft Check-out Set No. 2 will provide for the check-out of the spacecraft prior to launch and for evaluation of the spacecraft while in orbit.

The equipment in Spacecraft Check-out Set No. 1 will consist of various portions of AVCS, command, beacon, RF, and APT units, to the same extent as the evaluation stations (see Figure 5-VII-1). In addition, a set of RF measuring and attenuating equipment is provided to enable tests on the spacecraft's characteristics in this area. A "portable" console, similar to the spacecraft support console in the go/no-go van, is used for monitoring spacecraft parameters during various stages of testing, such as vacuum-chamber tests.

The equipment in the Spacecraft Check-out Set No. 2 will provide a spacecraft study, evaluation, and analyzing facility, as well as a second spacecraft check-out set. Video information received by Spacecraft Check-out Set No. 2 cannot be transmitted to the CPA Centers unless "long-lines" facilities were to be installed. The operation of each of the subsystems of Spacecraft Check-out Set No. 2 is as described under the corresponding paragraphs of the CDA stations, Section 5-III. Additional equipment such as the RF equipment, which is government-furnished equipment at the CDA stations, and the test equipment required for spacecraft check-out will be procured by RCA. The physical layout of Spacecraft No. 2 is shown in Figure 5-VII-2.

PORTABLE

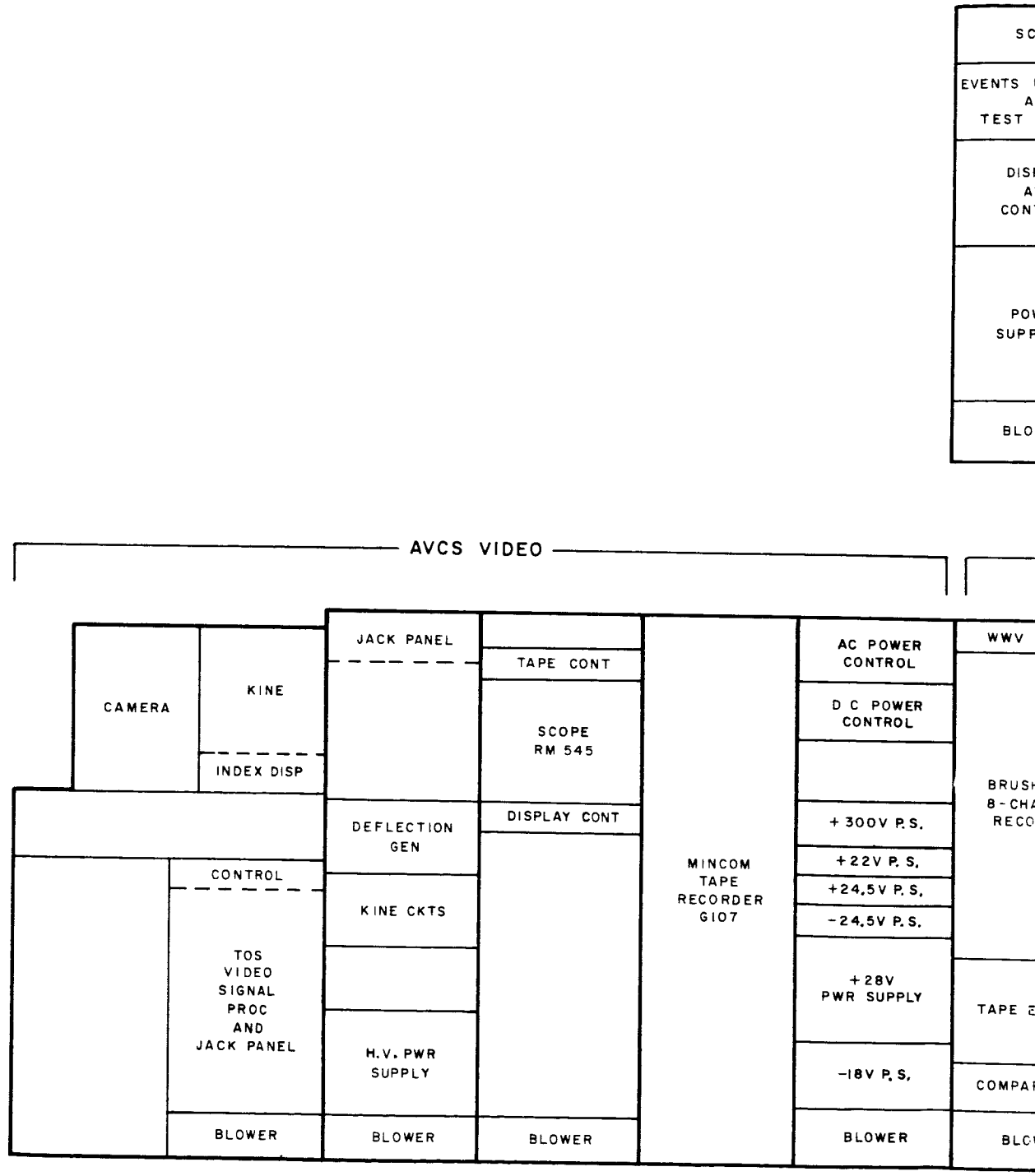

GROUND SUPPORT

CONSOLE

DPE						
RECORDER ND POINTS						
LAY ID ROL						
ER LIES						
WER						

BEACON AND COMMAND				RF		APT
RCVR	20-CHANNEL EVENTS RECORDER	COUNTER	EECO 812 MASTER CLOCK	TIME CODE CONVERTER	DEI CTT-1 TEST GEN	
		PATCH PANEL				NC 1546A RCVR
		RM504 SCOPE	DIGITAL COMMAND PROGRAMMER		HP 608C TEST GEN	FREQ LOCKED OSC
200 NNEL RDER		SCOPE INPUT		RF SIGNAL MEASURING		
	2-CHANNEL RECORDER	PROGRAM CONT			CONTROL	APT FAX RECORDER
		TAPE READER	AUX COMMAND UNIT		TMR-6 BCN RCVR	ELECTRONICS
	SCD BAY					
RASER	TELEMETRY CALIBRATOR	READER ELECTRONICS			NC 1412 AVCS RCVR	PWR SUPPLY
ATOR	SAT. TYPE RCVR AND DECODER	COMMAND PWR SUPPLIES				
WER	BLOWER	BLOWER	BLOWER	BLOWER	BLOWER	BLOWER

EQUIPMENT NO. 6

Figure 5-VII-1. Physical Layout of Spacecraft Check-out Set No. 1

PORTABL

E RE AND T							
DI							
CO							
P SU							
BL							

AVCS VIDEO

CAMERA	KINE	JACK PANEL	TAPE CONT	MINCOM TAPE RECORDER G114	MINCOM TAPE RECORDER G114	AC POWER CONTROL	WWV
	DISPLAY		TAPE CONT			DC POWER CONTROL	
			SCOPE				BR
		DEFLECT GENERATOR	DISPLAY CONT			+300V P. S.	8-
	CONTROL	KINE CIRCUITS				+ 22V P. S.	RE
	TOS VIDEO SIGNAL PROC AND JACK PANEL					+24.5V P. S.	
						-24,5V P. S.	
		H. V. POWER SUPPLY				+28V POWER SUPPLY	TAP
						-18V P. S.	COM
	BLOWER	BLOWER	BLOWER			BLOWER	B

GROUND SUPPOR

.E CONSOLE

;COPE
VENTS CORDER EST POINTS
SPLAY AND NTROL
OWER PPLIES
OWER

BEACON AND COMMAND					RF		APT
RECEIVER	20-CHANNEL EVENTS RECORDER	COUNTER	TIME CODE CONVERTER	EECO 812 MASTER CLOCK	NC 1412 AVCS RECEIVER	DEI TRM6 BCN RECEIVER	DIV COMBINER A
		PATCH PANEL		DIGITAL COMMAND PROGRAMMER			NC1546A RECEIVER
		RM504 SCOPE	ALARM TIMER		NC 1412 AVCS RECEIVER	DEI TRM6 BCN RECEIVER	FREQUENCY LOCKED OSC
SH 200 HANNEL CORDER	2-CHANNEL RECORDER	SCOPE INPUT					
		PROGRAM CONT	HP60BC SIGNAL GENERATOR		NC1412 AVCS RECEIVER	DEI TRM6 BCN RECEIVER	APT RECORDER
		TAPE READER			PATCH PANEL	PATCH PANEL	
	SCD BAY				DIV COMBINER A	DIV COMBINER B	ELECTRONICS
ERASER	TELEMETRY CALIBRATOR	READER ELECTRONICS		AUXILIARY COMMAND UNIT	DIV COMBINER A	DIV COMBINER B	
		COMMAND POWER SUPPLIES				FILTERS AND PREAMPS	POWER SUPPLY
PARATOR	SAT TYPE RCVR AND DECODER						NC 1546A RECEIVER
LOWER	BLOWER	BLOWER	BLOWER	BLOWER	BLOWER	BLOWER	BLOWER

T EQUIPMENT NO. 3

Figure 5-VII-2. Physical Layout of Spacecraft Check-out Set No. 2

SECTION VIII. GO/NO-GO VAN

The purpose of the go/no-go van is to exercise and to check out the spacecraft at the launch area. Except for the spacecraft support console and the blockhouse support equipment, the equipment is mounted in the van and consists of the following units:

(1) Tape recorder and associated electronics,

(2) Partial video section,

(3) Complete beacon-data section,

(4) Partial command section,

(5) Limited RF equipment,

(6) Test equipment not unique to the OT-2 system,

(7) Test-conductor console,

(8) Satellite support console, and

(9) Blockhouse support equipment.

Items (1) through (6) above have been described earlier in Part 5. The spacecraft support console is located on the gantry and monitors various spacecraft parameters not available by telemetry. The blockhouse support equipment consists basically of a power supply used to charge the spacecraft batteries. The test-conductor console provides range communication and a complete ground equipment status display. Figure 5-VIII-1 shows the physical layout of the go/no-go van.

SECTION VIII. GO/NO-GO VAN

The purpose of the go/no-go van is to exercise and to check out the spacecraft at the launch area. Except for the spacecraft support console and the blockhouse support equipment, the equipment is mounted in the van and consists of the following units:

(1) Tape recorder and associated electronics,

(2) Partial video section,

(3) Complete beacon-data section,

(4) Partial command section,

(5) Limited RF equipment,

(6) Test equipment not unique to the OT-2 system,

(7) Test-conductor console,

(8) Satellite support console, and

(9) Blockhouse support equipment.

Items (1) through (6) above have been described earlier in Part 5. The spacecraft support console is located on the gantry and monitors various spacecraft parameters not available by telemetry. The blockhouse support equipment consists basically of a power supply used to charge the spacecraft batteries. The test-conductor console provides range communication and a complete ground equipment status display. Figure 5-VIII-1 shows the physical layout of the go/no-go van.

PORTABLE CONSOLE

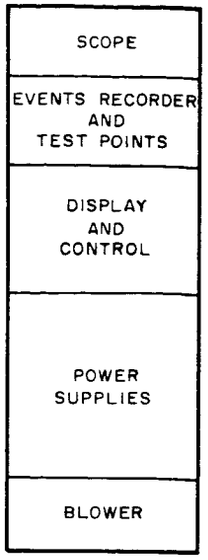

AVCS VIDEO

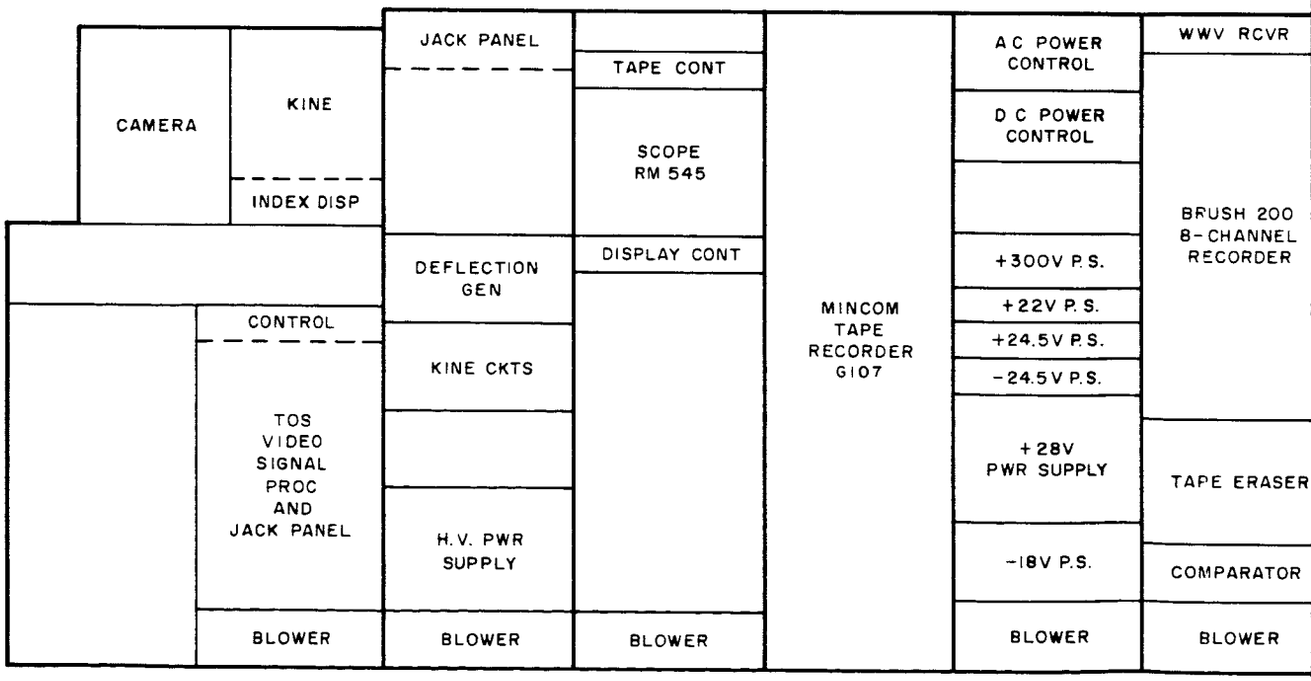

GROUND SUPPORT EQU

TEST CONDUCTOR'S CONSOLE

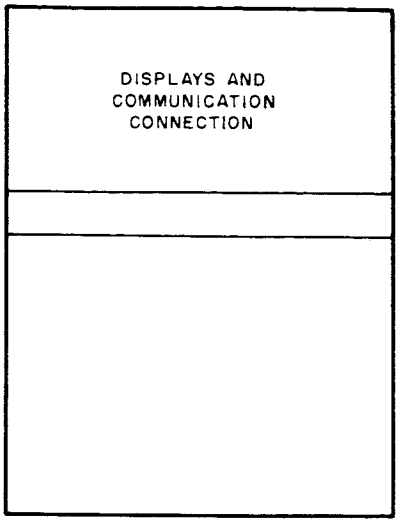

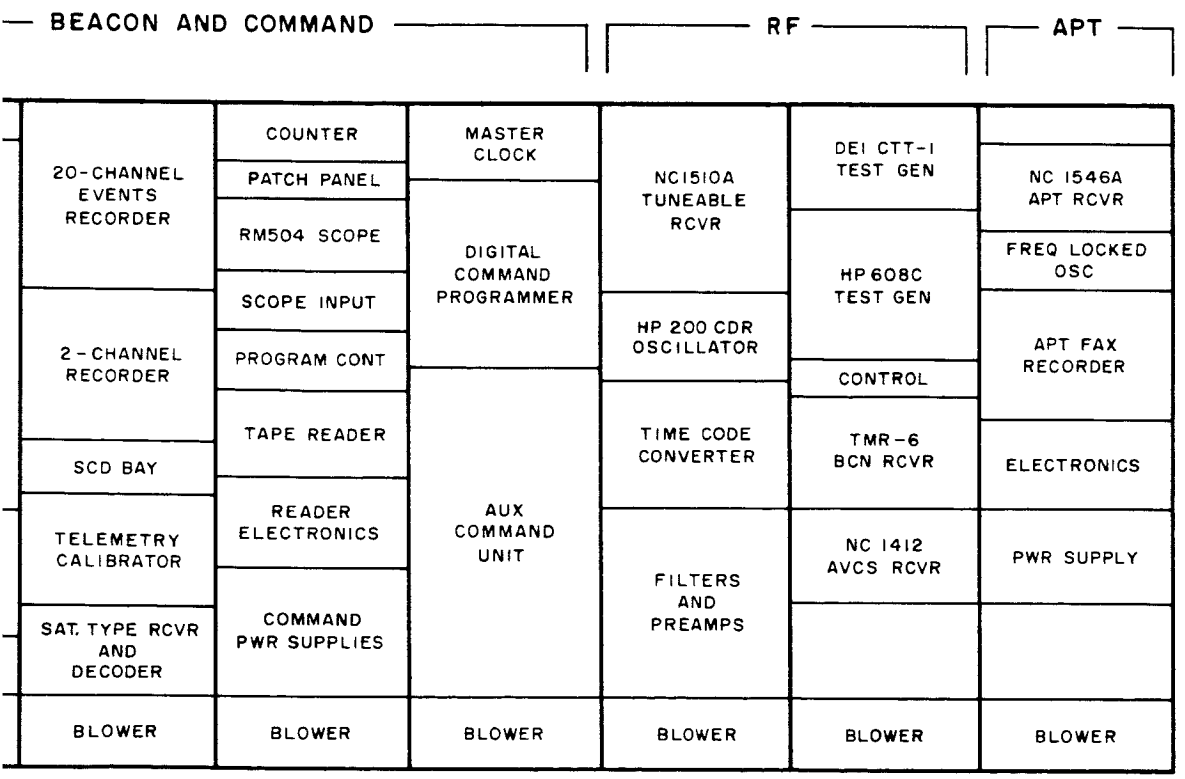

PMENT NO. 5

Figure 5-VIII-1. Physical Layout of Go/No-Go Van

PART 6. APPENDICES

APPENDIX A

ANALYSIS OF DOUBLING VIDEO SUBCARRIER ON SPACECRAFT

In this technique, the video subcarrier is doubled before transmission but the deviation on the 235-Mc carrier is not. This technique doubles the video subcarrier frequency of 96 kc at the tape recorder output and the 235-Mc transmitter is modulated with a peak deviation of 115 kc.

Using the approximation that $B_{IF} = 2$ (fd + fm) a receiver IF bandwidth of 750 kc would be indicated. However, using a 500-kc IF bandwidth, as with the case when the subcarrier is not doubled on the spacecraft, will result in a loss of only a small amount of the energy content and reduce the receiver noise power by 1.8 db.

By the use of the Roth-Baumunk formula, the video signal-to-noise ratio can be determined. In this instance

$F_1 = 115$ kc

$F_2 = 48$ kc

$B_{IF} = 500$ kc

$f_{sc} = 192$ kc

$f_2 = 240$ kc

$f_1 = 132$ kc

$$\text{then; } \frac{S}{N} = \frac{C}{N} \cdot \frac{F\ F\ B_{IF}}{2\frac{f_2^5}{5} - \frac{f_{sc} f_2^4}{2} + \frac{f_{sc}^2 f_2^3}{3} - \frac{f_1^5}{5} + \frac{f_{sc} f_1^4}{2} - \frac{f_{sc}^2 f_1^3}{3}}$$

$$\frac{S}{N} = 20.8 + 1.1 = 21.9 \text{ db.}$$

It can be seen, therefore, that the signal-to-noise ratio will be 8.5-db poorer in this instance than when not doubling on the spacecraft.

Furthermore, the subcarrier power to noise ratio is equal to:

$$\frac{Sc}{N} = \frac{C}{N} \times \frac{3}{2} \left[\frac{B_{IF} \quad F_1^2}{f_2^3 - f_1^3} \right] = \frac{C}{N} \cdot 0.86$$

$$\frac{Sc}{N} = \frac{C}{N} - 0.65 \text{ db}$$

Therefore, the output S/N ratio is 8.5-db poorer than in the undoubled case and the limiting threshold in the system is the second detector rather than the first detector.

APPENDIX B

A COMPARATIVE STUDY ON THE USE OF INTEGRATED CIRCUITRY VERSUS CONVENTIONAL CIRCUITRY FOR THE OT-2 COMMAND AND CONTROL SUBSYSTEM

SECTION I. INTRODUCTION

This appendix attempts to evaluate the relative advantages of integrated circuitry for use in spacecraft digital systems by comparing (1) the implementation of the OT-2 command and control subsystem with conventional "cordwood" modules with (2) its implementation with integrated-circuit modules. The integrated circuits chosen for this comparison were the Texas Instruments Inc. (TI) 51-series modules.* These modules were chosen, instead of other types, because of their inherently low power consumption (2 milliwatts per stage), high reliability (data has been accumulated since 1960), and low weight and volume. The TI 51-series integrated-circuit module used is an RCTL logic-type. This type has been manufactured continuously for a period exceeding three years and is widely used in various space applications. Data supplied by Texas Instruments Inc. indicates that the 51-series circuits have been used (or are planned for use) in the following space vehicles: IMP, GEMINI, OGO, OSO, ADO, MARINER, APOLLO, and NIMBUS.

The data presented has been predominantly abstracted from RCA-sponsored evaluations, vendor-supplied data, and a preliminary design study of the OT-2 command and control subsystem. The comparative study is based upon an evaluation of those areas which would be of major importance in an overall system consideration. Additional information was obtained from an RCA-sponsored program for the design and fabrication of the integrated-circuit TIROS attitude clock. The entirely integrated TIROS attitude clock subsystem was environmentally qualified to specification requirements exceeding those of the standard TIROS subsystems.

---

*The TI 51 series integrated circuits are not suitable for the high-frequency generator because of their low-frequency response. For this application, Fairchild Milli-Watt Micro-Logic will be used.

SECTION II. POWER

Four assemblies of the OT-2 command programmer have been analyzed with respect to their power consumption; circuits built with conventional "cordwood" modules have been compared with circuits built with integrated-circuit modules. A comparison of the power consumed in the case of each of the two packaging methods is shown in Table B-1.

TABLE B-1. POWER CONSUMPTION COMPARISON OF CONVENTIONAL AND INTEGRATED-CIRCUIT MODULES

Assemblies	Duty Cycle (percent)	Conventional "Cordwood" Module: Power Estimate (mw)	Integrated-Circuit Module: Power Estimate (mw)	Average Power Saving for Mission using Integrated Circuits (mw)
High-Freq Time-Base Generator	100	800	100	700
Decoder	6	1,225	143	65
Horizon-Pulse Sync Counter	100	490	60	430
Command Programmer	100	700	175	525

The integrated-circuit modules indicated a 70-percent efficiency in converting 24.5 volts dc to the 3-volt level required for programmer operation. The total power consumption of the conventional "cordwood" modules was 3.06 watts, as compared to 0.34 watts for the integrated-circuit modules. The conventional "cordwood" module total power consumption includes a 1-watt power loss from the 13-volt regulator. Thus, a net power savings of 2.7 watts is gained using integrated circuits.

SECTION III. RELIABILITY

In the design of the logic for a typical unit, 165 modules of the "cordwood" type, or 150 modules of the TI integrated type are required.

Latest information on the TI 51-series modules indicates a failure rate of 0.015 percent per 1000 hours at 45°C. No reliability test data is available for the conventional "cordwood" modules. Therefore, to provide a conservative basis of comparison, a single-gate module has been evaluated (See Table B-2), based on a parts count using standard failure-rate evaluation techniques. The failure rate for a single conventional gate is 0.058 percent per 1000 hours.

TABLE B-2. "CORDWOOD" MODULE FAILURE RATE

Part Description	No Per Module	Failure Rate Per 1000 Hours Per Module (percent)	Failure Rate Per 1000 Hours (percent)
Transistor	1	0.015	0.015
Diode	4	0.010	0.040
Register	3	0.001	0.003

Since the quantities of modules required favor the integrated circuits, and the per module failure rate favors the integrated circuits by four to one, it appears that a substantial reliability improvement can be gained by subsystem implementation with integrated circuits.

The discussion of reliability should also consider the effects of a radiation environment upon the 51-series integrated circuits. Some results of radiation tests on these units by the vendor are quoted in Appendix C and their implications are assessed.

SECTION IV. FUNCTIONAL COMPARISONS

The OT-2 command and control subsystem is basically composed of three assemblies consisting of analog and digital circuits. Restricting this discussion to the digital portion of each assembly, a reasonable comparison of the conventional "cordwood" circuitry with the TI-51-series integrated circuitry can be made.

The present packaging of conventional modules physically separates the flip-flop circuit from its trigger (i.e., the trigger is external to the flip-flop package). This arrangement is ideal for a flip-flop which is used for more than a single function (shift, count forward, count backward) since all that is required to implement such functions are additional trigger networks which do not contain transistors.

The TI flip-flop circuits and their trigger are contained within the same package. This type of configuration is superior for a single-operation mode. Should the requirement for multiple functions (shift and count) arise, additional stages are required. Thus, on a bit basis for shift and count, it takes 2 modules of the conventional type as compared to 2-1/2 modules of the TI integrated type.

A comparison of conventional modules with integrated-circuit modules on a subsystem level yields the following results.

(1) The decoder functional requirements are for a shift register, a binary counter, and control flip-flops. As these are single-operation modes, the integrated-circuit package is more efficient than the Sipican conventional package.

(2) The horizon-pulse synchronized counter functional requirements are for binary counters with feedback and control flip-flops. Here again the integrated circuit package is more efficient.

(3) The command programmer functional requirements are for a register-counter and control logic. Here the conventional logic is more efficient, since only one register is required as compared to the two registers required by the integrated-circuit logic. However, the addition of a second register when employing integrated-circuit logic doubles the storage capacity of the command programmer at a cost of 1/2 module per bit. The small size and low-power consumption of the integrated circuits tend to reduce the burden of the requirement for a second register. This second register can be used as a standby register for storing a second word; or the exact orbit period can be stored providing greater control during remote operations.

(4) The conventional circuitry requires -13-volt and -24.5-volt levels. The -13-volt level is used as a reference voltage and therefore requires good regulation in addition to control of all incoming signals which emanate from other subsystems. The present 13-volt level is derived by regulation from 24.5 volts. Therefore, all power is drawn from the 24.5-volt bus. The integrated circuits require only one voltage level (3 volts) which may be obtained from a DC-to-DC converter with a typical conversion efficiency of 70 percent. Therefore, the present 13-volt regulator may be eliminated with a power savings of at least 1 watt.

(5) Noise susceptibility is a function of numerous test condition and circuit characteristics, i.e., fanout, parameter tolerance, temperature, decoupling, type of noise, etc. The vendor-published data for the 51-series integrated-circuit modules indicates the following noise immunity characteristics:

(a) The clock input noise rejectivity of a typical module (SN 510/511) (at $T = 125^{o}C$, $N = 4$) is in excess of 0.4 volts. Under all other conditions, the clock input noise rejectivity is greater than 0.4 volts.

(b) The minimum gate-noise immunity (at $T = 125^{o}C$, $V_{cc} = 3$ volts, $N = 0$) is 0.25 volts.

SECTION V. MECHANICAL CONSIDERATIONS

A. WEIGHT AND VOLUME

A 65-percent reduction in weight and volume can be achieved in packaging the OT-2 command and control subsystem using present state-of-the-art techniques. This can easily be accomplished through the use of integrated circuits and "cordwood"-type three-dimensional modules. The flat-pack integrated-circuit module manufactured by Texas Instruments Inc. will be used in the digital portion of the subsystem. The dimensions of the flat pack are 1/4 by 1/8 by 1/32 inch. For interface and other circuits, "cordwood"-type three-dimensional modules fabricated from microcomponents will be used. A preliminary estimate of the weight and volume for the integrated circuit and microcircuit "cordwood" packages, as compared to a conventional-component "cordwood" package, is shown in Table B-3.

It can be noted from Table B-3 that a substantial savings in weight and volume can be accomplished with the integrated circuit and microcircuit "cordwood" packages.

B. CONNECTION METHODS

1. General

The flat packs are placed on a printed wiring board in a planar array and connected directly to the printed wiring paths (see Figure B-1). This conventional approach of packaging will be used for the OT-2 command and control subsystem. This method has the advantage of easy accessibility during fabrication and test, since module leads and conductor paths are completely in view for quick access and debugging. In addition, the flat-pack configuration of the module facilitates removal and replacement.

The connection of the flat pack to the printed wiring board will be done by re-flow soldering or parallel-gap welding.

2. Re-flow Soldering

With this technique, the module leads and mounting pads are pre-tinned; then, with heat and pressure applied by a resistance soldering iron or a parallel-gap electrode, the solder is melted and re-flowed to form a joint. This method has been used by RCA in the Apollo space program.

TABLE B-3. WEIGHT AND VOLUME COMPARISON OF CONVENTIONAL AND INTEGRATED-CIRCUIT MODULES

Subsystem Assemblies	Package (A) Conventional-Component "Cordwood" Package		Package (B) Integrated Circuitry and Microcomponent "Cordwood" Package		Savings by Using Package (B)	
	Volume (cubic inches)	Weight (lb)	Volume (cubic inches)	Weight (lb)	Volume (cubic inches)	Weight (lb)
Command	252	7.8	72	2.2	180	5.6
Programmer						
Decoder	306	9.6	125	3.5	181	6.1

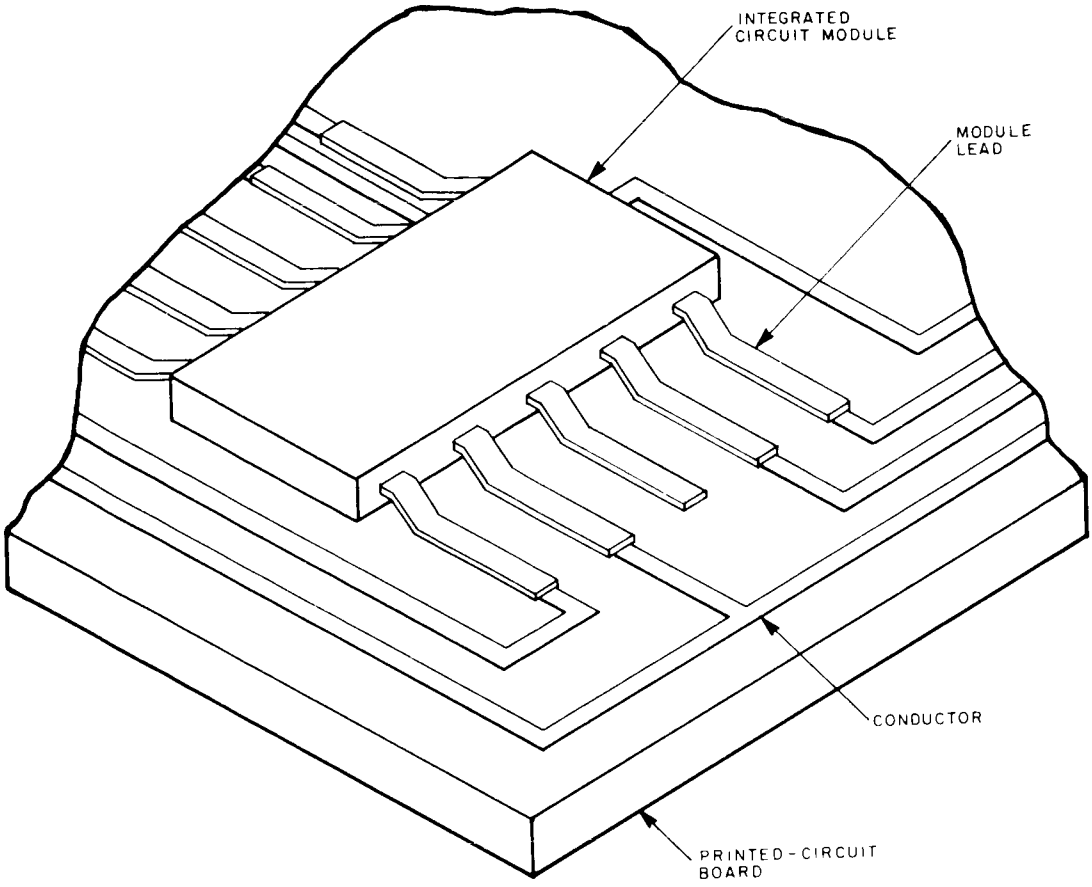

Figure B-1. Typical Module Layout

3. Parallel-Gap Welding

Parallel-gap welding is similar to spot welding except that the bottom electrode is placed next to the top electrode with controlled spacing. Current flows from one electrode to the other, through the materials to be joined and a weld is effected. The advantages of parallel-gap welding are as follows:

(1) Weld joints are more uniform and predictable in their strength

(2) Heat in welded joints is localized and of very short duration; therefore, there is less danger of component damage.

(3) Welding does not require the use of a joint material (solder, flux, etc.).

(4) Because of its permanency, welding is potentially more reliable than solder joints.

Gap welding has been used by RCA for the TIROS attitude clock. The clock has successfully passed environmental specification requirements above those normally invoked on space vehicles.

C. REPLACEMENT OF INTEGRATED MODULES

An integrated-circuit module can be easily replaced when soldered or gap welded. If the module is soldered, the lead of the module can be lifted from the circuit path, as shown in Figure B-2. If the module is welded, the module body is cut away, leaving the leads in place, and a new module is welded directly over the old leads (see Figure B-3).

D. SUBASSEMBLY TECHNIQUES

After assembly of the integrated modules, the boards will be plugged into a harness board with interconnections made at the board edges through a connector. The boards will be in parallel rows and edge-supported. A container will completely enshroud the subassembly to provide radiation shielding.

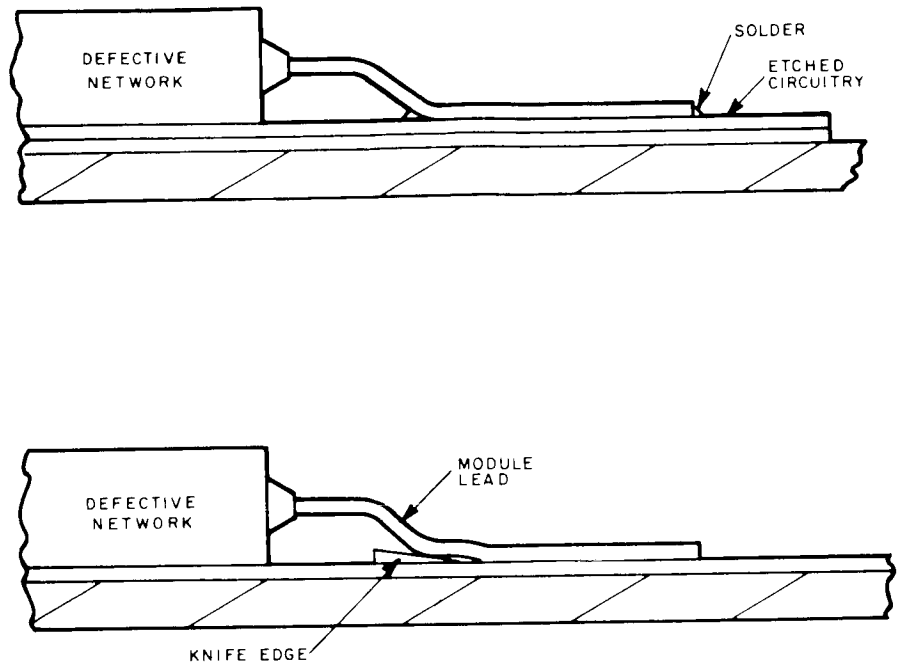

Figure B-2. Replacement of Module When Soldered

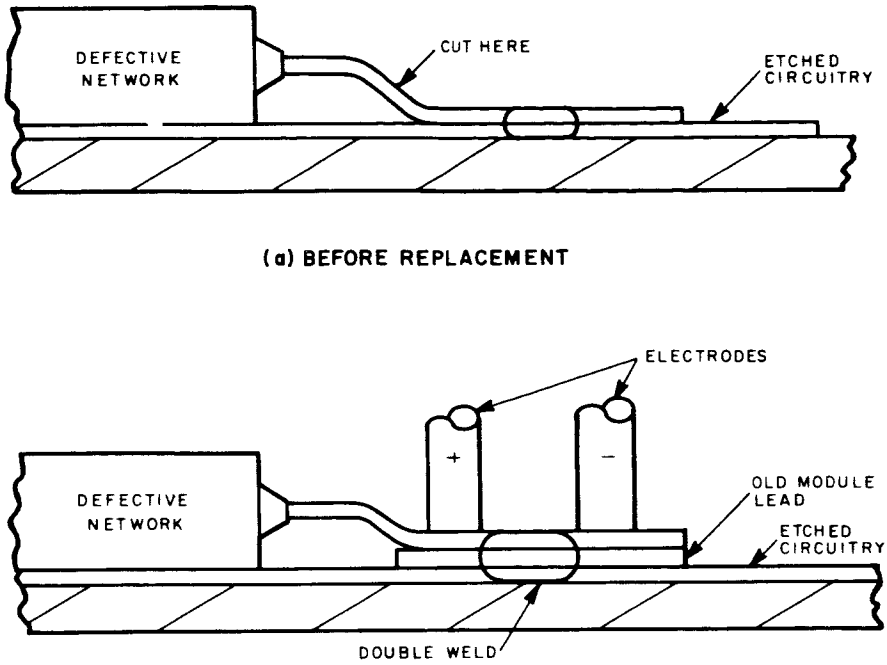

Figure B-3. Replacement of Module When Gap-Welded

SECTION VI. SCHEDULE CONSIDERATIONS

From previous experience in scheduling, it appears that design time when integrated-circuit modules are used is almost identical to the time involved with conventional "cordwood" modules. Vendor data indicates that the units specified are available for immediate delivery. However, this delivery does not include the time required for preconditioning tests. Therefore, it can be concluded that the only element of time to be considered of any consequence in a delivery schedule is the time necessary for preconditioning. This is anticipated to be less than 2 weeks.

APPENDIX C

RADIATION ANALYSIS FOR OT-2 SPACECRAFT

SECTION I. INTRODUCTION

The orbital characteristics for the OT-2 mission have been chosen to permit complete camera coverage of the earth by the spacecraft. The nature of the required orbital parameters, however, involves an associated radiation problem. At the OT-2 orbital altitude, i.e., 750 nautical miles, the radiation effect upon components in the spacecraft is significant and requires a very thorough analysis.

The OT-2 orbit intersects the lower edge of the geomagnetically trapped electron and proton belts. At an orbital altitude of 750 nautical miles, the flux encountered by a spacecraft will be 10 times greater than that which will be encountered by the Nimbus spacecraft (at an altitude of 500 nautical miles) and 50 times more than that encountered by previous TIROS spacecraft (at altitudes of approximately 400 nautical miles).

Six months exposure in the OT-2 orbit could have a very serious effect on the spacecraft's components. However, an effort expended toward producing a "hardened" system would, it is felt, result in a reliable system. It should be noted that the survival of the Relay I satellite appears to substantiate this thought.

The following analysis deals with the determination of fluxes in orbit, radiation doses versus depth within the spacecraft, the consequent radiation effects on components, and the effect of shielding. In addition, the practical experience garnered from the survival of Relay I is presented to add perspective to the theoretical results of radiation-damage predictions.

SECTION II. DETERMINATION OF RADIATION FLUXES IN ORBIT

A. PREDICTIONS FOR 1965

At this time it is only possible to make a conceptual prediction of the environment to be expected on the OT-2 mission with a late-1965 launch date. Consequently, consideration is centered on (1) a model for which actual measurements were made in November 1962, and (2) the factors which should affect the state of the radiation environment between the November 1962 model and late 1965. One such factor is the gradual decay of the fluxes in the Starfish belt, due mainly to atmospheric collisions.

B. "STANDARD" FLUX MODEL FOR NOVEMBER 1962

The intrinsic error in the radiation detectors currently used in space vehicles such as the Explorer satellite and the Relay and Telstar satellites causes considerable error to be present in any mathematical model of the space radiation environment. This error can, in fact, exceed a factor of two. An error in estimated flux causes an equivalent error in predictions of the lifetime (i.e., estimated time to a given condition) of the satellite. Because of this, and because electron readings taken in November 1962 contain some inconsistencies, NASA has produced two radiation map models for electron flux, flux grids E8L and E8U, and two for proton flux, flux grids P1 and P2. E8L and E8U contain optimistic and pessimistic assumptions, respectively, and can be taken as lower and upper working estimates. NASA has stated however, that these estimates do not represent the limits of possible error of the actual measurements in space. The proton environment is better characterized and hence P1 and P2 represent one estimate for proton flux divided into two separate energy ranges. The radiation map models have been programmed by NASA and are available for "flying" an orbital position program through the flux model.

Table C-1 contains (1) upper and lower estimates of the average total flux of electrons to be encountered in the OT-2 mission and (2) estimates, in two separate energy regions, of the average total flux of protons. Table C-2 presents the expected electron energy spectrum. These tables were developed from the NASA-supplied flux grids.

In Table C-1, with respect to the fluxes of protons, the gap in the energy levels covered is caused by a lack of sufficient data at this time on the region from 12 to 30 Mev. It is commonly assumed, however, that fluxes in this region are about double those in the 4- to 12-Mev region. Fluxes of protons below 4 Mev are of limited interest since

TABLE C-1. EXPECTED FLUXES FOR OT-2 MISSION IN LATE - 1965

Average Total Flux of Electrons	
Upper Estimate, From NASA Grid E8U Lower Estimate, From NASA Grid E8L	0.645×10^{13} electrons/cm^2 day 0.347×10^{13} electrons/cm^2 day
Average Total Flux of Protons	
For Energy Levels > 30 Mev, From NASA Grid P1 For Energy Levels > 4 Mev but < 12 Mev, From NASA Grid P2	0.128×10^{9} protons/cm^2 day 0.947×10^{9} protons/cm^2 day

Note: These calculations are based on the assumption of a circular, near-polar orbit at an altitude of 750 nautical miles and an inclination of 100 degrees.

TABLE C-2. EXPECTED ELECTRON ENERGY SPECTRUM FOR OT-2 MISSION IN LATE - 1965

Energy Level: Δ E (Mev)	Percent of Electrons*		6- Mo Flux** (e/cm^2)
	Lower Estimate	Upper Estimate	
0.5-1	25.87	29.92	3.54×10^{14}
1-2	24.21	22.04	2.61×10^{14}
2-3	34.91	33.58	3.97×10^{14}
3-4	12.86	12.40	1.46×10^{14}
4-5	1.45	1.40	0.165×10^{14}
5-6	0.50	0.48	0.057×10^{14}
6-7	0.16	0.16	0.018×10^{14}
7-8	0.03	0.03	- - -
		Total	1.18×10^{15} e/cm^2/6Mo

*As in Table C-1, these calculations are based on the assumption of a circular, near-polar orbit at an altitude of 750 nautical miles and an inclination of 100 degrees.

**Taken from Upper Estimate of Percent of Electrons.

such fluxes are effectively stopped by a 6-mil silica cover glass and, therefore, will only affect components in direct contact with the space environment. However, these fluxes are very high and cannot be completely eliminated from consideration because of their effect on surface skins.

The electron spectrum shown in Table C-2 represents the modified "fission beta spectrum" produced by the "Starfish" explosion in July 1962 and trapped in an extensive belt centered on the geomagnetic equator. The values for fluxes of electrons below 0.5 Mev are not well known, but such fluxes could have strong effects on surface skins. The ranges shown in Table C-2 represent energy levels at which the electrons could penetrate many mils of aluminum and carry sufficient energy to cause lattice displacements in semiconductors and, hence, serious electrical effects.

The likely fluxes of solar protons intersecting the orbit in the polar regions are open to considerable speculation. Such fluxes probably extend as far South as the auroral regions. The fluxes and energies of these particles are very unpredictable, but they can be roughly estimated for a given part of the 11-year solar activity cycle. A "worst case" estimate shows the probable fluxes of these particles over 6 months to be relatively small compared to the fluxes of other particles, and deep penetration of solar protons into the spacecraft is unlikely.

C. FEATURES NOT COVERED BY "STANDARD" FLUX MODEL

1. Degradation of Artificially Produced Fluxes of Electrons

Although fluxes of electrons above 0.5 Mev are generally accepted to be decreasing at all points in the Starfish belt, no firm figures on past and future rates are available for 750- or 450-nautical mile polar orbits. However, data from the Transit satellite series (approximately 650-nautical mile polar orbit) indicates that rates of decay in the lower edge of the belt are of the order of a few months for a halving of the flux, being approximately two months at 650 nautical miles. Thus, when attempting to make predictions for a satellite launched in 1965 into a 750-nautical mile orbit, a strong reduction in flux from that existing in 1962 can be anticipated. This reduction would be of the order of ten times or more. Because fluxes degrade more rapidly at lower altitudes, even more rapid degradation should be assumed in studies of past TIROS performance. Even by mid-1963, actual fluxes could have been reduced by well over ten times compared to the E8U estimates. Also, an increase in the rate of degradation of the lower edges of the electron belt is expected to coincide with an increase in solar activity.

During the first few weeks of the existence of the Starfish belt, "dumping" of electrons from the belt into the atmosphere was rapid. The rate of dumping then decreased, and leveled off. With the anticipated increase in solar activity during the next few years,

(causing a "boiling-up" of the atmosphere and consequent increase of "dumping" into the atmosphere), it is conceivable that this dumping process could cause the Starfish belt to disappear by 1967. The exact significance of this factor in a 1965-6 launch cannot be predicted however, because it is not known when the dissemination will begin again, nor at what rate it will operate.

The order of the decreases in the Starfish belt can be noted in Figure C-1 which contains some estimates of the ionization damage profiles for TOS and TIROS orbits.

2. Fluxes of Low-Energy Electrons

Low-energy electrons are important to this analysis since their flux levels, though oscillating in the short term, are unchanging over the years. Thus, the bremsstralung background which these fluxes will generate even behind thick shielding is likely to persist over the years. At the OT-2 altitude, the bremsstrahlung level resulting from the flux of low-energy electrons could approach the bremsstrahlung level resulting from the flux of high-energy electrons in the Starfish belt (a worst-case estimate would be about 10^4 Rads after 6 months). Such a level could produce appreciable browning in lens glass.

Thus, even if Starfish belt electron fluxes were to degrade by a factor of ten, it cannot be assumed that the bremsstrahlung background resulting from the flux of low-energy electrons would do likewise, and the bremsstrahlung background from low-energy radiation penetrating throughout the spacecraft might be at an irreducible minimum of 10^4 Rads/6 months.

Further study is required before final conclusions can be made on this subject. Such a study should cover, in particular, the distribution of the low-energy electrons in respect to time and altitude.

3. Fluxes of Low-Energy Protons

The camera optics on the spacecraft are in direct contact with the space environment. Therefore, the large, but poorly-characterized fluxes of low-energy protons (energy less than 4 Mev) known to exist in the belts can contribute to lens degradation. These fluxes would cause browning in a very thin surface skin less than 1 mil thick. The fused silica shielding used for higher missions would stop these particles.

4. Fluxes of Medium-Energy Protons

It is expected that an increase in solar activity will mean a concurrent increase in the fluxes of protons at energies from a few Mev to 30 Mev. Such an increase would

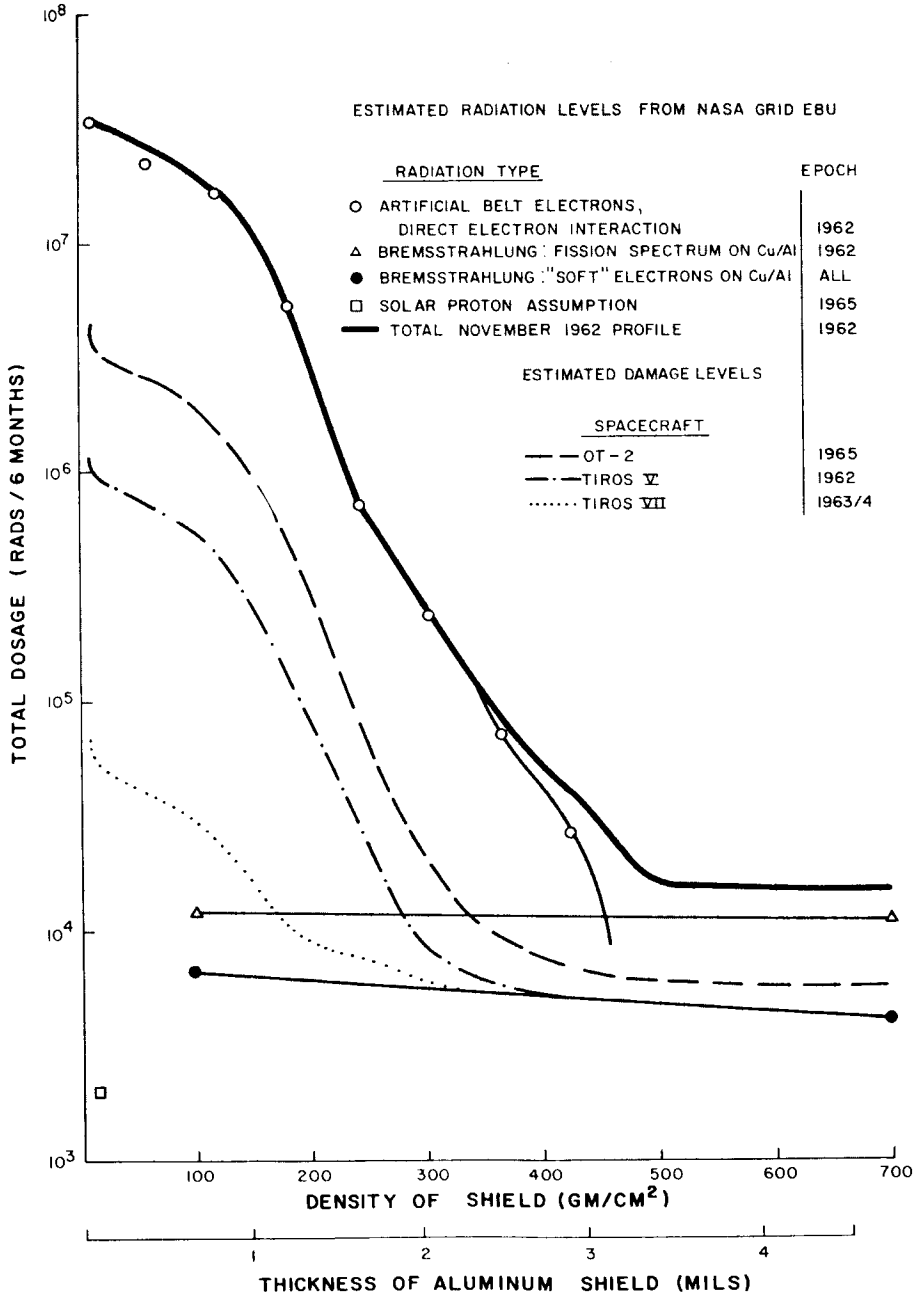

Figure C-1. Estimated Ionization Damage Profiles for OT-2 and TIROS Orbits

be effected by the "pumping" of protons into the trapping regions by an accelerating interaction of the solar wind and the magnetosphere. The increase could be by a factor of 10 or more, and could more than compensate for electron "dumping."

An increase in the flux of medium energy protons is a factor which must be considered in comparisons between previous TIROS environments and that expected in the OT-2 orbit.

SECTION III. RADIATION VERSUS DEPTH WITHIN THE OT-2 SPACECRAFT

A. GENERAL

The study of the radiation effects in the interior of a spacecraft requires a good assessment of the "filtering" or attenuating effect produced by the spacecraft skin, component boxes, and other parts of the spacecraft, upon the radiation dose reaching a component. The model by which this effect can best be considered is the simple concept of a component at the center of a spherical shell of aluminum. All other situations can be related to this situation, for which calculations of electron and proton penetration are not too complicated.

Radiation damage can be of two basic types, as follows:

(1) Crystal lattice damage, often called "bulk damage," in which the displacement of atoms from the crystal lattice by a colliding particle produces semipermanent defects; these defects, in turn, affect the electrical properties of the crystal; and

(2) ionization damage, in which (a) a passing particle causes the ejection of electrons bound to atoms in the material and (b) subsequent rearrangement of the atoms occurs.

In order to calculate the degree of damage caused by a given external spectrum of particles after they have passed through a shield, it is necessary to:

(1) calculate the degradation in energy of particles caused by collisions with atoms of the shield material, and

(2) establish the efficiency of the particles in causing damage after this energy degradation has occurred.

A specimen of these calculations for a particular type of semiconductor crystal behind a particular shield thickness is presented in Table C-3. Further notes on the methods and factors employed in this calculation appear in the following, and the products of calculations of this type appear in Figures C-1 and C-2.

TABLE C-3. SPECIMEN CALCULATIONS OF LATTICE DAMAGE ACCUMULATED AFTER 6-MONTHS in OT-2 ORBIT: FOR P-TYPE SILICON SAMPLE BEHIND 60-MIL THICK SPHERICAL SHIELD

Electrons (From NASA Grid E8U)				
ΔE After Passing Through Shield (Mev)	Assumed Average Energy in ΔE (Mev)	F(E)	ϕ60: Flux After Passing Through Shield (e/cm^2/6 Mo)	F(E) $\cdot$ ϕ60 (d.e.n.i. 1-Mev e/cm^2/6 Mo)*
0.5 - 1	1.0	1.0	2.61×10^{14}	2.61×10^{14}
1 - 2	1.5	2.8	3.97×10^{14}	11.0×10^{14}
2 - 3	2.5	5.0	1.46×10^{14}	7.8×10^{14}
3 - 4	3.5	8.6	0.165×10^{14}	1.42×10^{14}
4 - 5	4.5	10.6	0.057×10^{14}	0.60×10^{14}
5 - 6	5.5	13.0	0.018×10^{14}	0.24×10^{14}
6 - 7	6.5	14.5		
			Total	23.67×10^{14}
Protons (From NASA Grids P1 and P2)				
ΔE at Shield Surface (Mev)	ϕ60: Flux After Passing Through Shield (protons/cm^2/ 6 Mo)		F(E)	F(E) $\cdot$ ϕ60 (d.e.n.i. 1-Mev e/cm^2/6 Mo)
4 - 12	0			
12 - 30	5.5×10^{10}		0.5×10^3	2.75×10^{13}
> 30	2.35×10^{10}		0.5×10^3	1.20×10^{13}
			Total	3.95×10^{13}
Total Accumulated Lattice Damage				
Electrons 2.367×10^{15}				
Protons 0.0395×10^{15}				
2.407×10^{15} d.e.n.i. 1-Mev e/cm /6 Mo				

Note:

*Damage - Equivalent Normal - Incidence 1-Mev e/cm^2/6 Mo

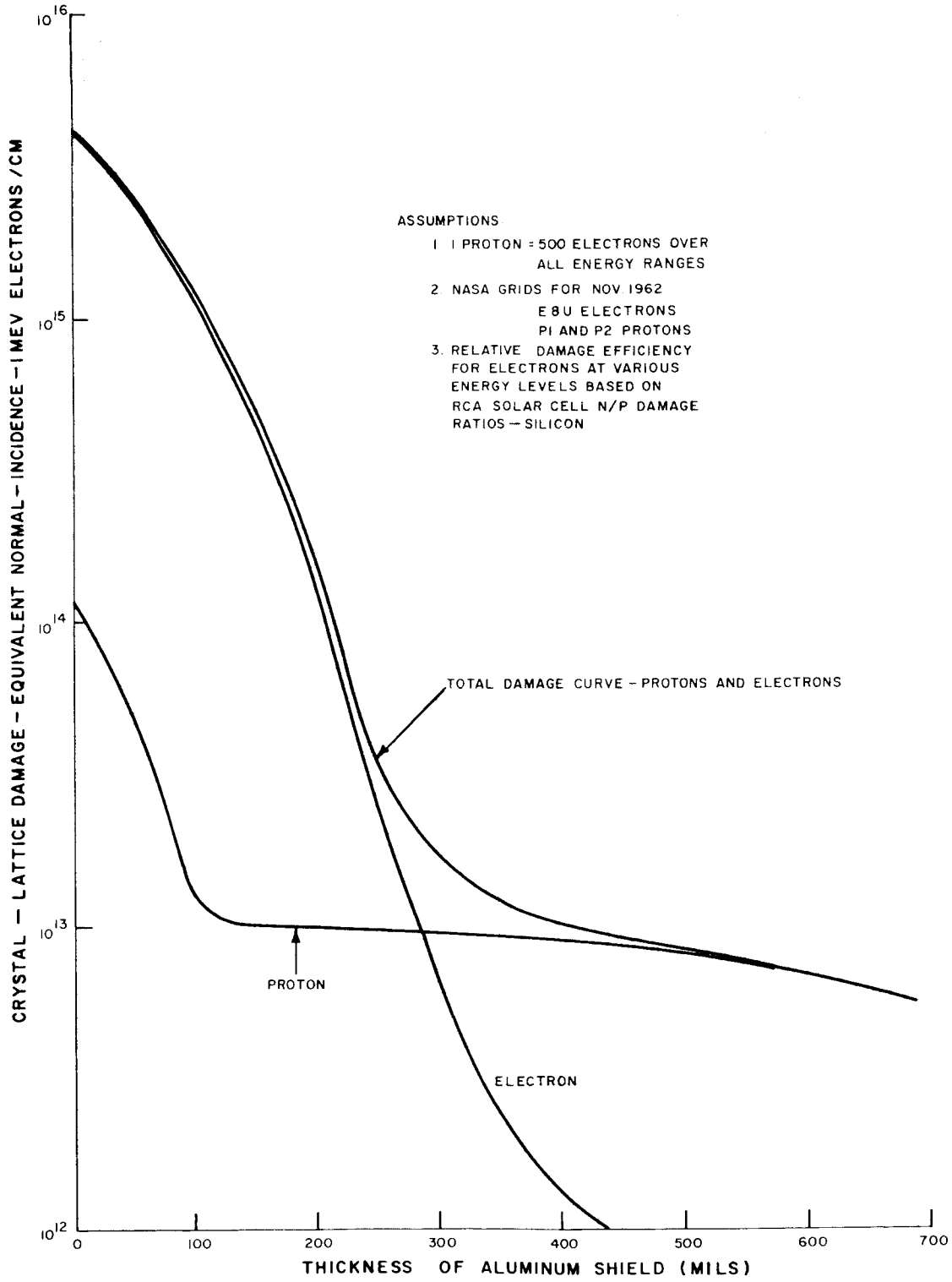

Figure C-2. Crystal Lattice Damage Versus Shielding in OT-2 Orbit After 6 Months

B. LATTICE DAMAGE PROFILE

1. ΔE

ΔE represents an increment of the energy spectrum. In Figures C-1 and C-2 and in Table C-3, a simplifying assumption is made; namely, that an "average" energy with an average damaging efficiency, F(E), can be assigned to the increment. This assumption can be justified for both electrons and protons.

2. ϕ 60

ϕ60, in the case of both electrons and protons, indicates the fluxes calculated to have penetrated 60 mils of shielding. Such radiation is, then, directly available to damage the material, with an efficiency determined by F(E).

An aluminum shield 60-mils thick will stop nearly all of the electrons at and below the 1-Mev level. Therefore, the inexact but justifiable assumption is made than an aluminum shield of this thickness will degrade the energy of any electron by 1 Mev. Consequently, the fluxes listed in Table C-3 reflect a shift which has been made in the fluxes of Table C-2 to account for the absorption of the electrons below 1 Mev and the degradation in energy of the remaining electrons. For successive 60-mil increments in the thickness of the aluminum shield, this upward shift can be repeated.

An aluminum shield 60 mils thick will stop protons at and below the 17-Mev level in the energy spectrum, and the assumption is made that higher energy protons passing through such a shield will degrade in energy by 17 Mev. However, unlike the case with electrons, a loss of energy in protons does not give rise to a large change in F(E) for the energy ranges considered in Table C-3. Therefore, the system of shifts is not used in the tabulation of fluxes and protons.

For thickness of aluminum greater than 60 mils (e.g., 120 mils, which stops protons below the 25-Mev level), it is necessary to calculate for the 12- to 30-Mev range the flux which remains after a portion has been stopped in the shield. For this calculation, it is necessary to know the exact integral spectrum of the fluxes of protons in the TOS orbit, and an assumption of a spectrum has been made which fits known facts as well as possible; however, further work would be required to permit good accuracy for predictions in the OT-2 application.

3. F(E)

F(E), the average damage efficiency in the energy increment ΔE, is a factor for converting a measurement of the omnidirectional flux of particles in space into the

number of 1-Mev electrons which, emerging from a particle accelerator in a parallel beam, will produce the same amount of damage in the laboratory.

The factor F(E) has been derived through laboratory experimentation on the damage efficiency of various monoenergetic particle beams, and it involves the assumption of a certain behavior of the particles which impinge obliquely on the shield (or sample).

The experimental results and, to some extent, the assumed particle behavior, are the subject of controversy as to their absolute values, and different values are being used by different workers.. In this analysis, the values have been derived from published* data. The values given in the data were doubled for this application, because in the referenced article "infinite backshielding" is assumed, whereas it should not be assumed in this analysis. The values used, then, are conservative and based on existing experiments and theory. However, the divergence of the results obtained by several groups which recently performed radiation damage experiments makes it desirable that further theoretical study on the damage factor be performed as a part of the OT-2 program.

C. IONIZATION DAMAGE PROFILE

Calculations of the ionization effects behind given shields were performed. These calculations were similar to those performed for the damage profile; and, as in that case, published** data was used, with similar modifications and approximations in averaging the energies. The resultant ionization profile in profile is presented in Figure C-1.

*Bell System Technical Journal, 42, 1505 (July 1963), Figures 32 and 33. With both Figures, the curve marked "no front shield" was used.

**Bell System Technical Journal, 42, 1505 (July 1963), Figures 34 and 35. With both Figures, the curve marked "no front shield" was used.

SECTION IV. EFFECTS OF RADIATION ON COMPONENTS

A. GENERAL

Most single-crystal semiconductor components, many optical materials and polymers, and miscellaneous other circuit and mechanical components are strongly affected by radiation. The reason for examining two types of radiation profiles, i.e., "Lattice Damage" and "Ionization", is that, while semiconductor properties are changed because of lattice damage caused by "billiard ball" atomic collisions and displacements, most other materials are damaged by the free electrons produced by ionization of orbital electrons in the material. Lattice damage is expressed in terms of change in (1) τ, minority carrier lifetime, or (2) L, diffusion length, or in terms of "Damage-Equivalent Normal-Incident 1-Mev Electrons/cm^2". Ionization is expressed in Rads, which signifies the deposition of 100 ergs of energy (of all kinds, but largely ion energy) from the impinging particles, in each gram of the material. While 10^8 electrons/cm^2 in the 1-Mev range deposit about 100 ergs/gram of low-Z material, the relation is not constant with energy, and conversions from particles/cm^2 to Rads must be treated with caution. Table C-4 shows some typical radiation levels for component damage.

The prediction of component performance under space radiation is an inexact science and is largely a matter of ensuring that a component will stay above a given "failure threshold". The nature of the available published data or the feasible experiments on a component or system often dictate that the prediction be based upon results taken from an irradiation using a radiation type different from that encountered in space. It will certainly never be feasible to synthesize, on the ground, exactly the spectra of electrons, protons, and X-rays encountered by each component in its location on the spacecraft. Thus, some extrapolation and "rough" interpretation of ground and flight data must always be performed using current devices and damage theory, while, at the same time, the circuit designers supply a rough estimate of the "failure threshold" or "end point" below which the component will not serve its function in the circuit.

Thus, "life" and "sensitivity" are not absolute terms for most components, but are determined by what the designer allows for change. Most components do not fail "catastrophically;" rather, they experience gradual degradation. Few components rupture mechanically at space levels of damage, although some types of capacitors might conceivably do so.

In the following sections, component behavior under radiation is discussed in relation to the current NASA model for radiation levels (E8U, P1, P2 flux maps), accepting

TABLE C-4. COMPONENT SENSITIVITY UNDER HIGH-ENERGY RADIATION

6-Months Damage Levels for Given Locations — Integrated Flux Level (d.e.n.i. 1-Mev e/cm²)*	Electrical Effects from Crystal Lattice Damage after 6 Months in TOS Orbit	6-Months Damage Levels for Given Locations — ION Dose Level (RADS)	Electrical Effects from Ionization Damage after 6 Months in TOS Orbit
	Thermistors Affected	10^9	
	Gain of Field-Effect-Transistors Affected	10^8	Leakage of Resistors and Capacitors Affected
		At Surface	Glass Blackened
10^{16}	50% B Loss in UHF (100 Mc) Si Transistors	Under Hat	
At Surface			Insulation Leakage
Under Hat	Forward Resistance of Diodes Affected	10^7	
		Inside Thin Box	
10^{15}	25% Degradation of Solar Cells	10^6	Serious I_{CBO} Effect in Transistors
Inside Thin Box		Inside Thick Box	
Inside Thick Box		400-Mil Cover	
10^{14}	50% B Loss in HF (5 Mc) Si Transistors	10^5	5% Loss of Transmission in Glass
10^{13}	50% B Loss in LF (100 Kc) Si Transistors	10^4	I_{CBO} Affected in Some Transistor Types
Behind 400-Mil Shield			

*Damage-Equivalent Normal-Incidence 1-Mev electrons/cm²

that the order of magnitude of the component degradation problem will be similar whether these levels are used or the somewhat lower levels probable in 1965 are used. Only in the case of lenses, where some numerical predictions of browning behavior are attempted, are figures for the probable 1965 levels employed.

B. TRANSISTORS

1. Degradation in Gain

Figure C-3 shows the variation of gain degradation* with alpha-curoff frequency, original gain value, and lifetime damage in transistors. This curve is constructed using the usual device theory linking these parameters. Since the slope of the degradation curve is very steep (much steeper than for solar cells, i.e., 50 percent per decade versus 20 percent), it is important to know how closely a particular transistor follows this theoretical curve in practice.

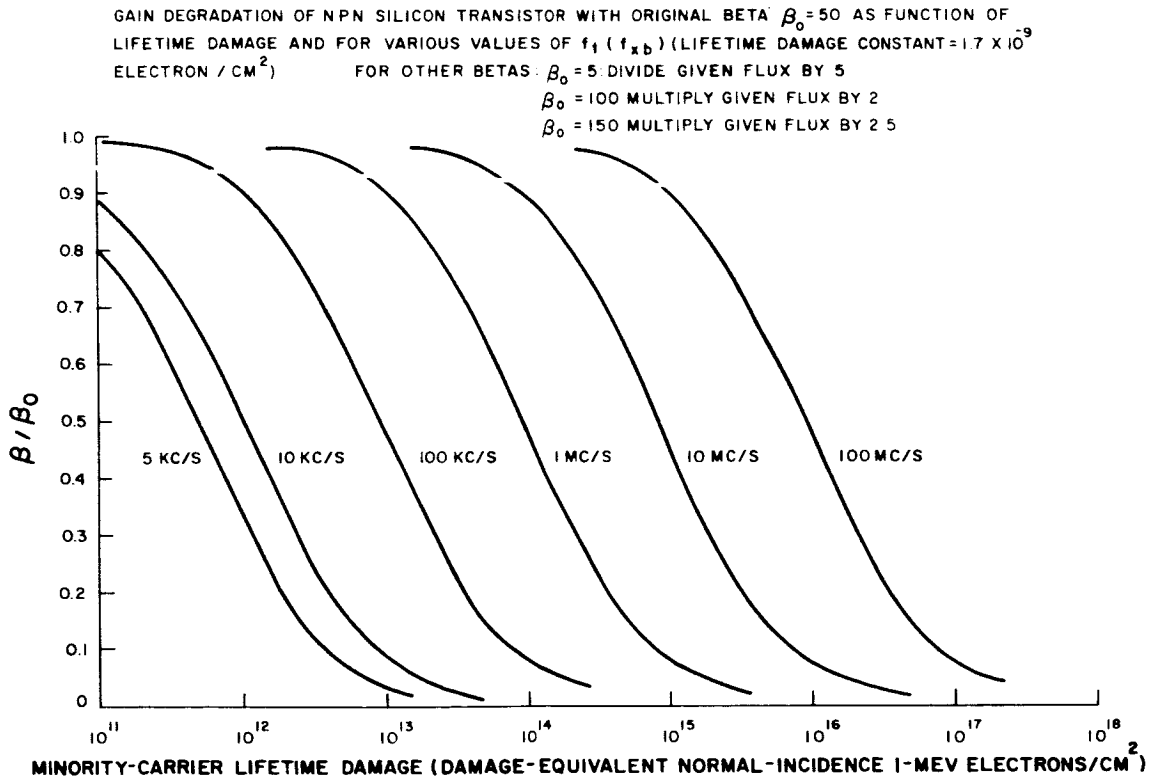

Figure C-3. Lifetime Damage (Damage-Equivalent Normal-Incidence 1 Mev Electrons/Cm^2)

*An arbitrary reference "failure level" often used for transistors is the damage level at which beta falls to 70 percent of original. No such accepted level exists for increases in leakage current in transistors.

Published results on irradiation tests indicate that the correspondence is not always good. Therefore, it would be very desirable to have a test program on the transistor types selected for use on satellites, such as OT-2, which are in high-radiation orbits. It can be seen that it will be difficult to use transistors with alpha-cutoff frequencies less than 10 Mc/s.

2. Increase in I_{CBO}

Most transistors in use at this time experience erratic and large increases of I_{CBO} under any kind of ionizing radiation. For typical planar transistors, the increase in I_{CBO} can be as large a factor as 10^3 (e.g., from 10^{-9} amps to 10^{-16} after 10^5 rads, for transistor type T.I.* 2N727; or 10^{-10} to 10^{-7} after 10^6 rads, for T.I. 2N2412). The curve might rise quickly to high values after a few hundred rads, or it might only turn upwards after 10^5 rads. Apparently identical units might behave very differently. In mesa transistors, the effect has been "cured" by evacuation of gas from the case and, partly, by the occasional removal of bias (this accomplished the "cure" of Telstar I in orbit). Planar devices, however, develop similar conductivity beneath the passivating layer in any set of circumstances.

The leakage effect appears to be caused by the formation of a conductive channel at the semiconductor surface. Annealing the transistor, with the temperature at about 200°C, can completely eliminate the conductivity. About the only predictable feature of the effect is that, if a transistor is irradiated and then annealed, it can be assumed that the transistor will follow the same dose/leakage-current curve as previously when it is re-subjected to radiation. This provides a method by which the effect can be circumvented in flight units, the cycle being performed on a batch of transistors and the "harder" specimens being selected for flight. Such a "screening" program was used for Telstar and might also be used for the "Comsat" project. The order of magnitude of the ionization levels in the OT-2 mission make it mandatory that this "leakage" aspect receive intensive study.

C. DIODES, VARACTORS, AND SCR'S

The minority carriers in diodes, varactors, and SCR's are affected by radiation, to the extent that carrier lifetime and the trapping of carriers will control the operation of such components.

Published data on diodes indicates that forward resistance should change less than 1 percent in a typical location in the OT-2 vehicle; as is the case with transistors (and transistor leakage), however, performance changes from type to type. Continuously energized diodes seem to be more affected than ON-OFF types. Again, individual attention will be required for the selection of component types for the OT-2 vehicle.

*Texas Instruments, Inc.

Switching speed and other high-frequency parameters can also be affected by radiation since radiation-produced lattice defects act as traps for carriers; these traps take a finite time to empty during a transient change of carrier concentration. High-frequency circuits should, therefore, receive special study.

An SCR irradiated under neutrons failed to "fire" at a neutron damage level equivalent to the level after 6 months in the OT-2 orbital environment with an aluminum shield 100 mils thick. This indicates SCR's to be used on the OT-2 spacecraft will require a selection program.

D. INTEGRATED CIRCUITS

Integrated circuits contain all circuit units in close proximity. Therefore, such circuits, in addition to experiencing all the effects described in the preceding sections B and C, will have the added possibilities of crosstalk due to leakage, loss of isolation due to diode breakdown, and change in d-c level (producing spurious turn-on and abnormally fast beta degradation) due to high dopant levels in the multi-diffused transistor base regions. However, sufficient data is not available to determine if, in practice, these damage effects do appear. In addition, because of the smaller volume of integrated circuits, shielding for the integrated circuits can be easier and less costly in weight than for the non-integrated circuits.

An example of integrated circuit performance pertinent to the OT-2 program is contained in a radiation-effects study performed by Texas Instruments Co. on their "51 Series" units. The conclusion was reached in this study that the performance (under radiation) of the integrated circuits tested was not significantly different from that of similar circuits containing discrete components. The tests involved irradiation with 22-Mev protons and 6-Mev electrons. It was concluded from these tests that the "mean flux-to-failure" was about 10^{13} protons/cm^2 or 5×10^{14} electrons/cm^2. Using commonly accepted conversion factors, it can be seen that both of these figures correspond to a damage value of about 10^{16} "damage-equivalent normal-incidence 1-Mev electrons/cm^2." As can be seen in Figure C-1, the damage value reached in ground tests is probably about 10 times greater than that which would be accumulated by a boxed circuit after 6 months in the OT-2 radiation environment.

E. LENS GLASS

1. General

It appears that the OT-2 environment could be the most severe space environment in which lens systems have yet been "flown". Thus, there is no direct flight experience of similar stresses on optics, as there is for electronic systems from the operation of Relay, Telstar, etc.

Despite the lack of information, it does appear from laboratory tests on many glasses (and the Tegea front lens element, in particular) that a serious lens browning problem could exist in the envisaged orbit. Doses equivalent to the 6-month OT-2 radiation dose behind several hundred mils of all-around aluminum shielding, but delivered within a short period of time in the laboratory, could badly discolor unprotected glasses. However, it is not well known what the effect of such doses would be when stretched out over 6 months.

Predictions of the effects on optical glasses after 6 months in the OT-2 environment are hampered by the lack of knowledge on the effects of factors such as the following:

(1) the annealing produced by the temperature and light cycles expected in the mission;

(2) the differences, in particle energy and type, between the actual environment and laboratory tests, which involve relatively fast delivered doses of gamma rays or mono-energetic electrons;

(3) composition changes among the several glasses in the proposed OT-2 lens systems; and

(4) the uncertainties about radiation levels behind shielding.

For what is probably the first time, the possibility arises that shielding cannot completely protect the lens system, because of the irreducible "background" radiation level. Thus, it is considered important that this analysis examine the known facts on the radiation environment to be encountered by the OT-2 vehicle, so that it can be determined what further evidence is required to allow a satisfactory prediction of system performance in space.

2. Theory

It has been proved that in simple ionic crystals the coloration produced by high-energy radiation is due to the expulsion of nevative ions from lattice sites. An unpaired electron remaining at the site is held in the force-field of the surrounding atoms and can, thus, "oscillate" and absorb light at its "resonant frequency." The result is an "F-center" or "color center" which results in a band of absorption. F-centers in simple ionic crystals can be almost completely annealed in time.

Colorations in glass also occur by means of F-center production; but, with the less regular material structire of glass, the absorption bands are broader, the amount of annealing is less predictable, and small amounts of additive can change both the coloration and annealing processes. Because absolutely pure silica and alumina contain no ions, these materials are much more resistant to radiation-induced coloration. However, small traces of impurity in the material (e.g., as in natural quartz or sapphire) can greatly increase the rate of coloration.

At a dose of 10^4 rads of Cobalt^{60} gamma radiation, most glasses develop color in the visible region of the spectrum and show additional absorption bands in the UV region. At a dose of 10^6 rads, most optical glasses become so darkly colored that they are no longer useful. At dosages over 10^{10} rads, the coloration reaches a saturation point. The browning coloration is not stable and after irradiation decreases as a function of time, temperature, and exposure to UV or visible radiation.

Typical browning "figures" for a barium crown glass are shown below. These figures are expressed in terms of the percent of transmission in various parts of the light spectrum before and after the administration of 10^6 roentgens of Co^{60} gamma rays delivered over a few hours. (For the purposes of this analysis, a roentgen and a rad are considered equal.)

Wavelength ($m\mu$)	Percent Transmission	
	Before Exposure	After Exposure
400	30	0
500	91	13
600	91	36
700	91	56

This coloration can be completely eliminated by means of annealing the glass, baking it at 400°C for a few hours. Flint glasses color more readily, but the effect of the annealing is also more rapid. The absorption spectra can invariably be plotted in smooth curves, rising steadily towards the "red" end.

To prevent or decrease the loss of transmission in optical glasses due to particle radiation, the following methods can be used:

(1) The glass can be shielded (e.g., a fused silica plate can be used to shield the optical path).

(2) A few percent of cerium oxide can be added to the composition of the glass.

Several types of optical glass, such as borosilicate crown, barium crown, and flint glasses, have been cerium-protected and have maintained most of their transmission after exposure to 10^6 roentgens. For example, tests of a sample of barium crown

glass, 1 cm thick, which had been doped with a few percent cerium oxide produced the following results:

Wavelength (mμ)	Percent Transmissions	
	Before Exposure	After Exposure
400	77	68
500	91	89
600	91	89
700	91	90

It can be seen from detailed absorption curves that in cerium-doped glasses a large part of the reduction in transmission, both from doping and radiation, is below 450 mμ. Many TV systems do not use this region of the spectrum, since it yields poor contrast in the TV image. Hence, the addition of amall amounts of cerium might not introduce serious losses in TV systems. Certainly, the "browning" losses for cerium-doped glasses will be many times less in the 500 to 700 mμ regions than for undoped glasses. The important question is whether, at doses in the medium range (as in OT-2 type orbits, where doses of 10^4 to 10^5 rads will be present even behind several hundred mils of shielding), the initial loss of transmission due to doping would degrade overall mission performance more than the gradual browning loss of undoped glass over the 6-month period.

3. Experimental Evidence on OT-2 Concept Lenses

a. APT-Tegea Lenses

In NASA experiments for the Nimbus satellite, 0.15-inch lens blanks of dense barium crown glass (supplied by Kinoptik, the manufacturer of the Tegea lens) were irradiated under 2 Mev electrons. One of the blanks was of the same composition as that used in the Tegea front element, while others had 0.5 percent or 1 percent additions of cerium oxide. Figure C-4 shows the result of these tests.

It is not known what changes in transmission took place after more than the recorded 90 minutes of annealing at room temperature, or if light or heat would have any further "bleaching" effect on the glasses. The glass which had been doped with 1 percent CeO_2 showed no loss in transmission during irradiation, but began the test with only 75 percent transmission (in the wavelengths between 400 and 700 mμ). As noted earlier, a glass doped with 0.5 percent CeO_2 would begin with 80 percent transmission over the whole wavelength region.

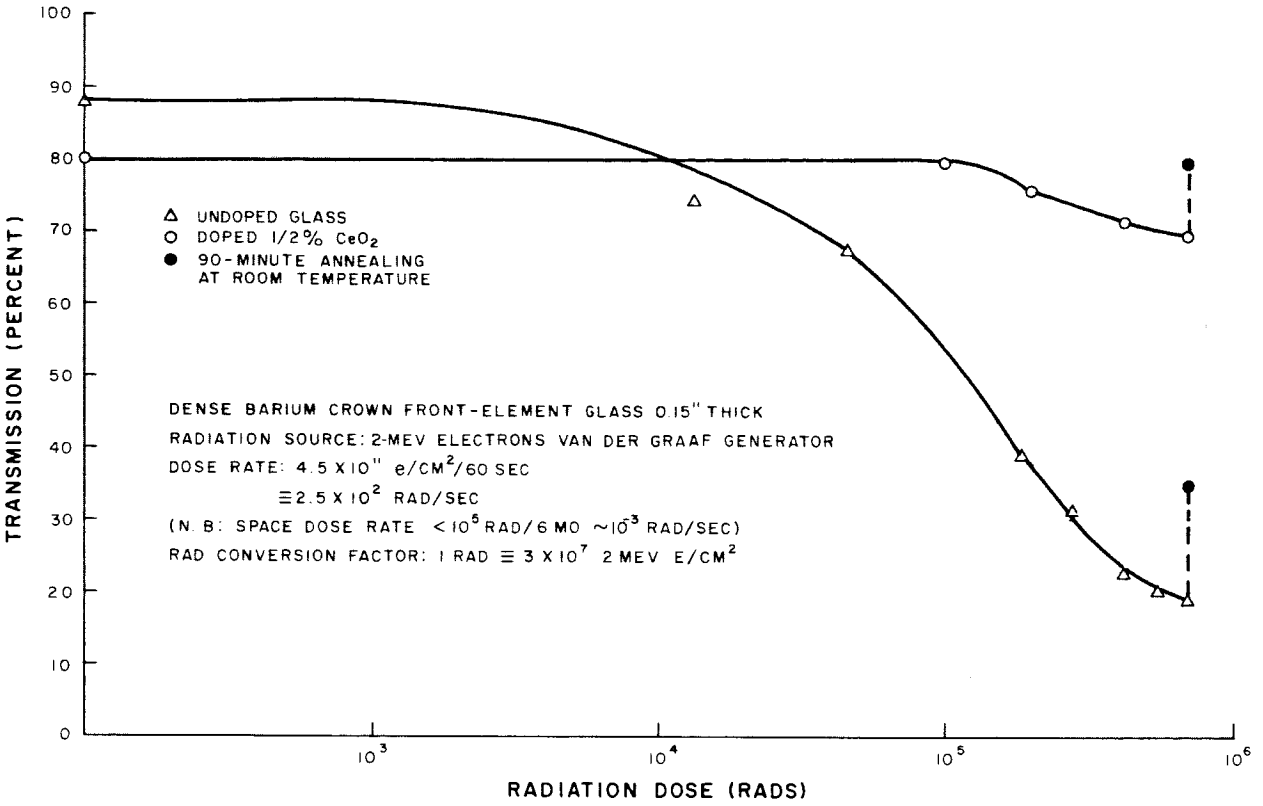

Figure C-4. Electron Irradiations of Tegea Lens Blanks, Doped and Updoped

Spectral transmission measurements taken before and after the irradiation led to the conclusion (noted earlier) that the "yellow" absorption due to the doping with 0.5 percent CeO_2 was mainly in a wavelength region which would not interfere strongly with the operation of a TV system. It was further concluded that this absorption could be offset by modification of the Y-10 filter usually employed with the APT camera (this filter cuts off light below 500 mμ). The undoped Tegea glass, when irradiated, lost transmission almost uniformly throughout the visible spectrum indicating that Tegea glass behaved like most other undoped glasses.

b. AVCS (B and H) Lenses

Several irradiations of an entire Nimbus-AVCS camera lens system have been carried out by NASA. In each case, all lens elements were present and either the usual yellow filters or various thicknesses of silica filter were interposed between the electron beam and the front element of the lens. The majority of the tests employed 2-Mev electrons.

It was necessary to send the lens system to the National Bureau of Standards for absolute transmission tests; the only transmission measurements made on the spot

were relative ones using an optical bench which was not ideal for the purpose. No measurements were made of the absorption spectra. The irradiations of the Nimbus-AVCS camera lens system are very difficult to interpret because of the above features, and particularly because filters were always interposed between the lens and the electron beam. Because of the presence of the filter, the energy of the electron beam reaching the lens elements was degraded, and flux was lost through scattering. In one case, only bremsstrahlung and a few "straggling" electrons would have emerged.

Since the electron beam did not even approach the spectral composition of the electron flux in space, the tests cannot be regarded as satisfactorily simulating the actual flight situation. However, if the necessarily approximate interpretations are made as to the doses reaching the lenses, it appears that many of the results on the B and H front lens element are qualitatively similar to those on the Tegea undoped lens.

c. Coating on Silica Plate

NASA has also tested the effect of 2-Mev electrons on Corning 7940 silica plates coated with a typical anti-reflective coating of magnesium fluoride (as employed on satellite-borne TV cameras). The same maximum dose as specified in Figure C-4 (namely, the equivalent of about 10^6 rads energy deposited) was applied, but no immediate changes in optical density were noted in the sample. The sample did, however, become heated to about 150° F during irradiation, i.e., annealing could have taken place in the course of the irradiation. Some days later, striations were observed in the coatings.

4. Evaluation of Experiments in Relation to the OT-2 Environment

Much semi-quantitative interpretation is necessary in order to relate a laboratory test to the space situation. The latter is a mixture of various types of radiation, each with a broad energy spectrum. The composition can vary with time and with depth in the spacecraft. At this point, it is necessary to interpret the test results for an effect which is possibly dose-rate-sensitive, and which is subject to thermal and light-induced annealing, all of which factors are very sensitive to small variations in trace impurities. It is not known whether, in addition, there is a particle specificity (i.e., whether the same effect is produced by a "rad" of electrons, protons, or bremsstrahlung X-rays). Finally, it must be remembered that extrapolations are involved (1) from a parallel beam in the laboratory to an omnidirectional flux in space and (2) from flat blanks to shaped lenses.

Despite these limitations, it can be said that the inaccuracies of this interpretation are probably not greater than the inaccuracies in the estimation of the environment, except for the effects of annealing. During the whole orbit, the lens will remain at a temperature of about 20°C; once per spin, the camera lens will receive a pulse of

sunlight. Thus, there will be ample opportunity for annealing to take place. Annealing could only be partial, i.e., there could be several color-center types with very long decay times.

Since the browning effect is produced by atom displacements in the glass, it is likely that this browning is dependent on particle type and particle energy. The few known proton irradiations of glass seem to show that protons have an effect which is roughly proportional to the efficiency with which they displace atoms in semiconductors. The effect of gamma rays and X-rays is probably related to the production of high-energy secondary electrons in the material; and thus, qualitatively, such radiation should produce the same type of defect as an electron beam. In any atom displacement, particle energy determines the efficiency of the particle in damaging the material. There is usally a threshold particle energy for the damage and a curve for "efficiency versus energy," which rises with energy. However, F-center formation is known to be unusual, in that X-ray photons with energies much too small to effect an atom displacement can produce colorations. Thus, in any test of radiation effects in glass, the experiment should be designed to give some clue as to the dependence of damage on energy and particle type.

5. Areas of Lens Design Requiring Further Experimentation or Analysis

The foregoing analysis brings to light various areas which require further consideration. These areas can be listed according to the need for either further experimentation or further analysis. It is probable that some of the areas can be covered by consultation with workers experienced with color formation in glasses.

The following is a list of the areas requiring experimentation:

(1) Browning behavior for all Tegea lens elements (or other relevant lens systems).

(2) Particle specificity of browning behavior.

(3) Energy dependence of browning behavior for particles or photons.

(4) Variation of annealing rates versus temperature.

(5) Variation of annealing rates versus illumination.

(6) Amount of CeO_2 doping required for optimization of original loss of transmission (from doping) versus browning loss.

(7) Effects of dopants other than CeO_2.

(8) Accurate analysis or control of glass compositions.

The list of areas requiring further analysis is as follows:

(1) Methods for optimizing doping, annealing, etc.

(2) Geometrical factors involved in lens shielding, etc.

(3) Relevant flight experience with transparencies.

6. Preliminary Outline of Test Program

An idea of the type of preliminary test program required for the OT-2 program has emerged from this analysis, and it is felt that a relatively simple exploratory program could greatly improve current knowledge. Small samples of glasses identical to those of each lens element in the system could be irradiated. The "routine" radiation source coule be Co^{60} or some other isotope yielding gamma rays in the 1-Mev region; a few irradiations employing protons and electrons at more than one energy level should also be performed.

The main advantages in the choice of gamma irradiation are as follows. Gamma-emitting isotopes give isotropic radiation. Hence, by varying the distance of samples from the isotope source, dose rates can be varied over several orders of magnitude, and various temperatures or ambient light levels can be conveniently introduced. The fact that the isotope source radiates in all directions means many samples could be irradiated at once. The fact that the radiation is highly penetrating means that, possibly, some samples could be enclosed in light-tight boxes for environmental control.

Dosimetery for gamma rays is much better developed than for particle beams at the beam currents which are normal for particle accelerators. Since gamma-ray damage effects are caused mainly by photoelectrons of about 1-Mev electron energy, the damage caused by gamma rays will be qualitatively the same as that caused by electron beams.

It is possible that, after a few exploratory tests, the optical transmission of routine samples could be checked at a few wavelengths, rather than over the whole spectrum.

The main problem in this experiment is the time element, i.e., both the time required for procurement of the doped samples and the time involved in tests at very low dose rates.

7. Tentative Predictions of Performance of the Lens-System in Space

a. General

It has been noted that insufficient data exists for a good engineering estimate of lens-system degradation in the OT-2 orbit. However, for the purposes of orientation it is possible to postulate some model semi-qualitative calculations. In all the following cases, we envisage a silica plate in front of the lens, while the lens barrel and other supporting structure provides the same degree of shielding in other directions.

b. Undoped Glass With 0.350-Inch Silica Shield (2 gm/cm^2)

This model is chosen as an example of a shield which greatly cuts down, but does not eliminate, the artificial-belt electrons. Figure C-2 shows that the E8U ionization dose for a spherical shield of that thickness is about 2 x 10^5 rads in 6 months. Figure C-4 shows that, for undoped glass, even a thin plate is reduced by this dose to 40 percent transmission (given no annealing). However, as shown in the "conceptual" curve in Figure C-2 for the OT-2 orbit and a 1965 launch, the E8U estimate could be high by a factor of 10. A dose of 2 x 10^4 rads (given no annealing) will result in only about 15 percent degradation. Assuming that annealing over 6 months can return over half of the lost transmission, the overall loss over optical paths of several inches (as in the complete lens system) could be about 30 percent, assuming that the other lens elements suffer damage of the same order or slightly less than the front element. It must be remembered, however, that, with the Tegea wide-angle lens, optical paths for rays near the edge of the field are greater than for those near the center. Thus, image degradation will not be homogeneous over the field.

c. Undoped Glass With 0.550-Inch Silica Shield (3 gm/cm^2)

This amount of shielding will eliminate all direct electron impacts on the lens glass and leave only the X-ray and proton "background". Such a shield would be considerably better than the 0.350-inch shield for the E8U situation, but little better than that shield for the "OT-2 at launch" curve of Figure C-1. Both situations, within the error of the calculations, give doses in the "background" region of 10^4 rads over 6 months. Thus, again, transmission degradation can be of the order of 30 percent.

d. Lightly Doped Lens Elements With 0.350-Inch Spherical Shield

From Figure C-4, it can be seen that, provided the 6-month dose for the lenses can be kept down to about 10^5 rads, there is negligible darkening from radiation when the glass has been doped with 0.5 percent CeO_2. While the E8U environment yeilds a dose slightly more than this (See Figure C-1), the 1965 environment will almost certainly provide less than 10^5 rads in 6 months. In the NASA experiments it was found that, even for higher doses, annealing was complete in 90 minutes for 0.5-percent CeO_2 doped glass. Thus, this glass would probably not degrade in orbit. The initial image would be poorer, since even a thin slab of 0.5-percent doped glass yields a few percent more degradation over the spectrum from 500 to 700 mμ than undoped glass. It is thought that the effective degradation for the 0.5-percent CeO_2 doped glass would be significantly smaller than that from the browning of the undoped lens elements and, as an additional advantage, unchanging over the mission. It is quite possible that experimentation could establish that doping with smaller amounts of CeO_2 would give adequate radiation protection and degrade the initial image less than would 0.5 percent CeO_2 doping.

8. Conclusions on Lens Study

A first analysis of the complex situation represented in the OT-2 mission indicates that the design of a reliable lens system for this mission is feasible, although radiation could be the overriding design parameter. Consideration of the one available test series indicates that light doping with CeO_2 is desirable for all lens elements, although heavy all-round shielding might make a lens system with undoped lenses feasible.

Before a decision on lens unit design is made, more information should be gained, particularly in the following areas: (1) radiation tests; (2) bremsstrahlung backgrounds in orbit; and (3) past performance of TIROS satellites, in respect to their radiation environments.

F. TRANSPARENT MATERIALS OTHER THAN LENSES

1. Fused Silica

The highest-purity fused silica has been shown to withstand a very high level of radiation, including that experienced in the Relay orbit, without coloration. It thus seems certain that even the extremely high rad doses incurred in the outer skin of the cover-glasses and other component shields should not affect carefully selected fused silica.

2. Optical Cements

Since fused silica is transparent to ultraviolet radiation, adhesives used on the underside of silica covers which do not carry a blue interference filter will probably darken, whatever their type. Lens cements, if any, should be carefully examined and, if possible, air-spacing construction should be used in the lens systems.

3. Germanium

There is no known evidence of significant radiation-induced changes in transmission for the germanium lenses used on typical IR radiometers in space applications. However, because of the high fluxes involved, tests would be advisable.

G. OTHER SENSORS

1. APT Vidicon

A form of APT vidicon camera was irradiated by RCA in a neutron pile reactor to neutron-gamma levels well above 10^6 rads/hr. In this test, slow image degradation took place on a particular stored picture while in the radiation field; however, a new image could always be stored and was retained if taken out of the radiation field. Thus, there appeared to be no permanent damage to the APT vidicon camera and the faceplate glass apparently did not lose transmission under the ionizing dose expected in the camera. Faceplate glass performance under radiation should be checked for the OT-2 flight units.

2. Thermistor Bolometer in IR Sensors

The thermistor flake used in the OT-2 horizon scanner is a mixture of amorphous oxides, and no damage of the order experienced in single-crystal devices is expected for this unit. However, since the device is necessarily under thin shielding, irradiation testing would be desirable.

3. Digital Solar Aspect Sensor

This device consists of a lightly shielded silicon p/n solar cell on the exterior of the vehicle. It is possible that considerable redesign will be necessary, replacing the p/n cell with a solar cell which is highly resistant to radiation.

SECTION V. SHIELDING ANALYSIS

A. GENERAL

As an attempt to place the previous calculations in perspective, a rough geometrical analysis of a highly simplified box layout within the baseplate and solar cell "hat" proposed for the OT-2 vehicle was made. A more refined and accurate form of this type of analysis should proceed on a continuing basis throughout the engineering design of the vehicle. Almost any change in configuration or containers could change the radiation susceptibility of a satellite in the OT-2 mission, just as it would change the thermal profile of the satellite.

B. METHOD

Figure C-5 represents the methodology used in the shielding analysis. As shown in the figure, it has been postulated for this analysis that a component in a box "sees" radiation penetrating from three characteristic zones, each of which involves one third of the total 4π steradians "seen".

(1) Zone I: Through the top of the solar-cell hat, with minor interruption by other component boxes.

(2) Zone II: Through the side of the solar-cell hat, but strongly interrupted by other component boxes.

(3) Zone III: Through the baseplate, with minor interruption by other component boxes.

Each zone is divided into two sectors; the half of the field most thinly protected is called the "A" sector, and the opposite half, the "B" sector. In Zone II, for the model layout assumed, Sector B can be divided into three subsectors (other layouts would require different subdivisions of Zone II).

C. ASSUMED THICKNESSES

Table C-5 presents the dimensions for a cross-sectional breakdown of the spacecraft hat. The values listed are the assumed values used in the shielding analysis.

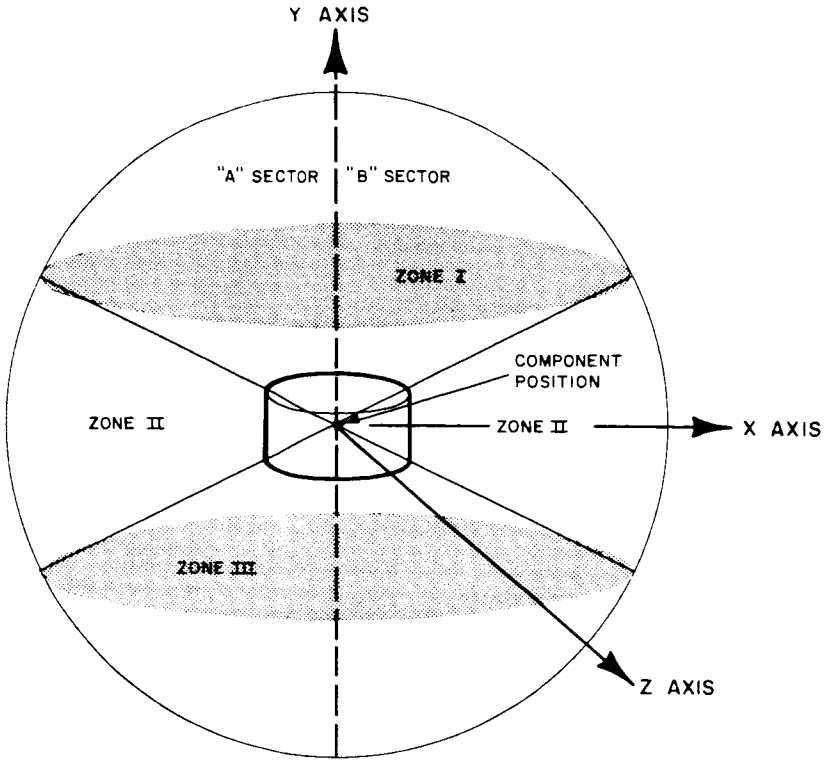

GEOMETRICAL RELATIONSHIPS
USED IN SHIELDING ANALYSIS

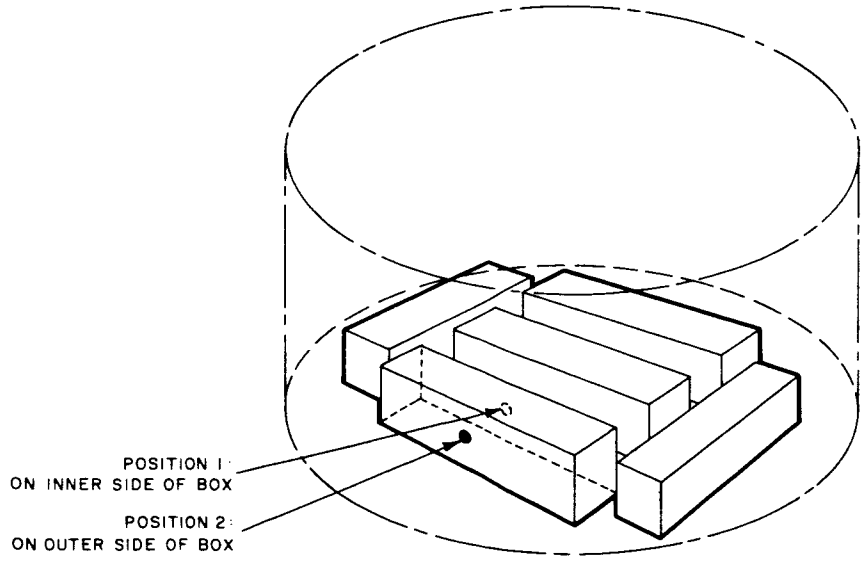

BOX LAYOUT ASSUMED
FOR SHIELDING ANALYSIS

AVERAGE SCANNING FROM COMPONENT LOCATION 1

	A SECTOR	B SECTOR
SCAN IN ZONE I		
THICKNESSES TRAVERSED BY RAY SCANNING IN XZ PLANE	120 MIL *BB* 120 MIL *SH*	30 MIL *BC* 120 MIL *SH*
SCAN IN ZONE II		(SUBSECTOR 1)
THICKNESSES TRAVERSED BY RAY SCANNING IN XZ PLANE	120 MIL *BB* 120 MIL *SH*	30 MIL *BC* 120 MIL *BB* 120 MIL *SH*
		(SUBSECTOR 2)
		30 MIL *BC* 120 MIL *BB* 120 MIL *BB* 120 MIL *SH*
		(SUBSECTOR 3)
		30 MIL *BC* 120 MIL *BB* 120 MIL *SH*
SCAN IN ZONE III		
THICKNESSES TRAVERSED BY RAY SCANNING IN XZ PLANE	120 MIL *BB* 60 MIL *SB*	30 MIL *BC* 60 MIL *SB*

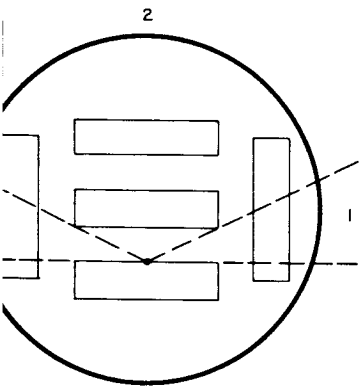

COMPONENT LAYOUT

ZONE II, B SECTOR;
SUBSECTORS 1, 2 AND 3

ASSUMED THICKNESSES

BC (BOX COVER): 30 MIL
SB (SPACECRAFT BASEPLATE): 60 MIL
BB (COMPONENT BOX BULK): 120 MIL
SH (SPACECRAFT HAT): 120 MIL

Figure C-5. Average Scanning from Component Location 1

The following values are fairly realistic dimensions for the thicknesses of various parts of a TIROS-type satellite:

(1) Solar-cell Hat: This dimension is taken as equivalent to 120 mils (aluminum: 0.82 gm/cm^2).

(2) Baseplate: This dimension is taken as equivalent to 60 mile (aluminum: 0.42 gm/cm^2).

(3) Component Box Covers: This dimension is taken as equivalent to 30 mils (aluminum: 0.21 gm/cm^2).

(4) Average Component Box: This is the dimension viewed normal to circuit boards, and is taken as equivalent to 120 mils (aluminum).

TABLE C-5. CROSS-SECTIONAL BREAKDOWN OF SOLAR-CELL HAT

Material	Thickness (inches)	Thickness (cm)	Average Density (gm/cm)	Superficial Density (gm/cm)
Solar-Cell Assembly	0.022	0.056	2.54	0.14
Solder	0.002	0.005	11.4	0.06
Epoxy-Bonded Fiber Board	0.040	0.102	1.7	0.17
Aluminum	0.064	0.163	2.70	0.44
Miscellaneous Adhesives	-	-	-	0.02
			Total Superficial Density	0.83 gm/sm^2

D. TABULATION

A box layout can be analyzed according to the following. As shown in Figure C-5, the parts of each zone of view filled by surrounding boxes and the vehicle skin parts are laid out graphically and then tabulated. The result is a sum of the thicknesses of aluminum "seen" and a weighting factor for the solid angle over which seen. The flux admitted by a given thickness of aluminum can be read from Figure C-2. The

thicknesses "seen" by the component in both sectors of each zone are presented in Table C-6 for one position of the component, and in Table C-7 for a different position. The equivalent flux for each the thickness (as if "seen" from a sphere of equivalent thickness) is presented and weighted according to the magnitude of the solid angle over which the flux is received.

The result of the calculation in each table is a value for the total lattice damage predictable for that component in the given location, expressed in terms of "Damage-Equivalent Normal-Incidence I-Mev Electrons". The effects of this damage on the electrical performance of semiconductor devices can be noted from Figure C-3 and Table C-4.

E. CONCLUSIONS

The following are some tentative conclusions resulting from the layout analysis.

First, as can be noted in the "Sum, Each Zone" row of Tables C-6 and C-7, a large proportion of the radiation reaching the components comes from the baseplate direction. In rather loose-packed configurations, such as shown in Figure C-5, the addition of 60 mils to the thickness of the baseplate would increase the life to a given component degradation point by a factor of 1.5. Another calculation (not presented here) in which a 150-mil spherical aluminum shield was added to one component showed a reduction in the damage incurred in that component by a factor of six, which is a better value of reduction than that for a comparable weight utilized as an addition to the thickness of the baseplate.

After a more detailed survey of sensitive components, it should become clear whether it would be better to add to the baseplate or specially shield particular component boxes, groups of transistors, etc.

Secondly, for the component layouts studied it appears that the satellite, as a whole, provides the same shielding as a continuous aluminum sphere 160 mils in thickness. Greater massing of boxes would increase this value in many locations.

TABLE C-6. DAMAGE ANALYSIS: EXAMPLE 1*

	Zone I		Zone II			Zone III	
Fraction of Zone Occupied (f)	1/2	1/2	1/2	1/4	1/4	1/2	1/2
Sector	A	B	A	B	B	A	B
Subsector	---	---	---	1 and 3	2	---	---
Thicknesses "Seen" (mils) (from Figure 5)							
Box Cover	---	30	---	30	30	---	30
Spacecraft Hat	120	120	120	120	120	---	---
Box Bulk	120	---	120	120	120	120	---
Box Bulk	---	---	---	---	120	---	---
Spacecraft Baseplate	---	---	---	---	---	60	60
Total Shileding (or Thickness "Seen")	240	150	240	270	390	180	90
Equivalent Flux: ϕ ($e/cm^2/6Mo$)	1.5×10^{14}	6×10^{14}	1.5×10^{14}	1×10^{14}	0.7×10^{14}	3×10^{14}	15×10^{14}
$f\varphi \times 10^{-14}$	0.75	3.0	0.75	0.3	0.2	1.5	7.5
Sum, Each Zone	3.75		1.25			9.0	
Sum, All Zones	14.0×10^{14}						
Damage in Given Satellite Loaction: (Sum, All Zones) ÷ 3:	4.7×10^{14} Damage Equivalent Normal-Incidence 1-Mev $e/cm^2/6Mo$						

*For this example, the component is at Location 1 in Figure C-5, i.e., the component is located on the inner side of the box.

TABLE C-7. DAMAGE ANALYSIS: EXAMPLE 2*

	Zone I		Zone II			Zone III	
Fraction of Zone Occupied (f)	1/2	1/2	1/2	1/4	1/4	1/2	1/2
Sector	A	B	A	B	B	A	B
Subsector	---	---	---	1 and 3	2	---	---
Thicknesses "Seen" (mils) (from Figure 5)							
Box Cover	30	---	30	---	---	---	30
Spacecraft Hat	120	120	120	120	120	---	---
Box Bulk	---	120	---	120	120	120	---
Box Bulk	---	---	---	---	240	---	---
Spacecraft Baseplate	---	---	---	---	---	60	60
Total Shielding (or Thickness "Seen")	150	240	150	240	480	180	90
Equivalent Flux: ϕ							
($e/cm^2/6Mo$)	$6x10^{14}$	$1.5x10^{14}$	$6x10^{14}$	$1.5x10^{14}$	$0.7x10^{14}$	$3x10^{14}$	$15x10^{14}$
$f\phi \times 10^{-14}$	3	0.75	3	0.25	0.2	1.5	7.5
Sum, Each Sector	3.75		3.45			9.0	
Sum, All Sectors	$16.2x10^{14}$						
Damage in the Given Location: (Sum, All Zones) ÷ 3:	5.4×10^{14} Damage Equivalent Normal-Incidence 1-Mev $e/cm^2/6Mo$						

*For this example, the component is at Location 2 in Figure C-5, i.e., the component is located on the outer side of the box.

SECTION VI. FLIGHT EXPERIENCE

Because of the great many unknowns entering into the foregoing theoretical analysis, it is important that the results of actual flight experience be considered.

A tentative profile for damage to p-type silicon semiconductor after 1 year in the Relay I orbit is included in Figure C-2. This profile was calculated from NASA computer runs of the electron and proton spectra in the Relay orbit, by the same methods as indicated previously. Although the profile of radiation effects for the Relay orbit is slightly different from that for the OT-2 orbit (since Relay traversed different regions of the radiation belts)[3] the radiation levels are quite similar; and it should be noted that the Relay circuits have worked.

In Figure C-1, in the parts of the graph representing thin shielding, the curves have good agreement with published results on the radiation-caused degradation of variously shielded solar cells on the Relay damage panels.

The circuits on the Relay satellite were designed, for the most part, before data on the Starfish belt was available. Thus, several wide-base transistors were included in the design and p/n solar cells were used for the power supply. The only design changes to accomodate the new radiation hazard were small additions of radiation shielding intended to give the satellite a few months life before damage levels, i.e., transistor beta decreases and I_{CBO} increases, exceeded the expected tolerances of the circuits. Yet, it must be noted that Relay I has worked for a longer period than could have been anticipated by theoretical predictions. It appears, then, that the methods of making theoretical predictions yield pessimistic results.

The pessimistic nature of the theoretical predictions might be due to the following possibilities:

(1) That the actual fluxes are lower than has been estimated.

(2) That the actual damage in space is lower than that resulting from laboratory tests (because of annealing).

(3) That, in addition to total dosage, the dose rate, in itself, is important.

The answer to these possibilities is presently beyond the "state of the art". However, flight experience would tend to indicate that a vehicle can be designed to operate successfully in the OT-2 environment.

Such a design must consider radiation effects, but not to an extent that will jeopardize the mission objectives because of excessive weight or cost. For this reason, a section of this appendix discusses a program which attempts to fill some of the divergences between flight experience and theoretical prediction by further study of past satellite operation and closer laboratory simulations of flight conditions.

SECTION VII. CONCLUSIONS

A. GENERAL

The preliminary conclusion from a study of the radiation problem to be encountered in the OT-2 mission is that radiation damage must be a major consideration in the design of the spacecraft.

Accumulated radiation levels in the component boxes after 6 months of exposure in orbit will be in the megarad range. It seems clear that components can be selected which will tolerate the levels of radiation expected after 6 months. This tolerance might require the addition of further shielding; however, as the selection of components becomes more effective, the amount of shielding required will be reduced.

One factor which, by itself, can have a strong bearing on mission feasibility is the camera-lens behavior in the radiation environment. Present data indicates shielding and doping can achieve the required environment. A question remains, though, as to the feasibility of shielding or doping the camera lens to an amount which will reduce radiation effects to the minimum while retaining suitable lens transmission.

The Relay I satellite operated for a surprisingly long period of time in radiation levels similar to those expected for the OT-2 mission; and, as noted earlier, only small additions of radiation shielding had been made to equip Relay I to withstand the hazards of the Starfish belt. Thus, it would appear that similar performance can be achieved with the OT-2 vehicle. The behavior of the radiation levels over the next 3 years is difficult to predict, but it is felt that conditions will probably improve over the current assumptions, which are based on measurements made in 1962. The OT-2 mission should, then, gain considerable advantage in this improvement in the radiation levels.

B. REQUIRED STUDY PROGRAM

As a result of the foregoing analysis, it appears that in the continuing study of the radiation aspects in the OT-2 concept particular consideration should be given to the following:

(1) The results of glass irradiations, especially those performed for the Nimbus satellite.

(2) The damage factors for electron and proton radiation in semiconductors, especially in transistors.

(3) The effects of radiation on IR sensors.

(4) A possible redesign of the solar-aspect sensor.

(5) Improved estimates of radiation background behind thick shielding.

(6) Possible radiation experiments to be included in the OT-2 vehicle.

The further study required on the solar-cell program has been noted in another section of this report.

In addition to the areas already noted, consideration should be given to the following general areas:

(1) The radiation-caused decrease in the beta value for transistors and increase in I_{CBO} for all types of semiconductors anticipated for use in the OT-2 vehicle.

(2) The radiation-caused changes in other components to be used in OT-2.

(3) The relevancy, in respect to the OT-2 mission, of the performance of Relay I and the circuit tolerances in that spacecraft.

(4) The effect upon standard TIROS circuits of component degradation such as could result in the envisaged OT-2 environment.

C. REQUIRED TEST PROGRAMS

Careful consideration as to the selection of types of components to be used on the OT-2 vehicle will aid in achieving a system capable of withstanding the expected radiation environment. Three types of test programs which should constitute one phase of this selection process are detailed in Table C-8. These test programs comprise a necessary part of the engineering design of the OT-2 system and should occupy an early phase of the effort, since type selection could depend on irradiation results. RCA has accumulated experience in conducting particle-and gamma-irradiation tests, and the necessary facilities are already available.

D. ON-BOARD EXPERIMENTS

As mentioned earlier in this appendix, the difficulty of simulating the space radiation environment realistically on the ground makes the testing of certain critical components in flight clearly worthwhile. The philosophy of on-board experimentation is meeting with growing acceptance, and such experimentation has already been performed with solar cells on several vehicles, with transistors on Telstar and on Navy

satellite 1963 38C, and with diodes on Relay I and II. The necessary on-board experimentation for this application could be performed in early OT-2 vehicles or on other NASA satellites launched before OT-2. The object of the experimentation would be to provide basic data for the improvement of the OT-2 design and for the analysis of any system degradation observed in flight.

The components to be tested would be types selected for wide use in OT-2 and would include (several lens glasses, transistors, diodes, solar cells, coverglass adhesives, and thermal-control surfaces. These components would be mounted on test panels behind typical amounts of shielding, possible inside the baseplate, where they would not interfere with solar-panel continuity. The measurements obtained would result in simple voltage outputs to be telemetered to the ground.

TABLE C-8. TEST PROGRAMS TO AID IN SELECTION OF COMPONENTS FOR OT-2 VEHICLE

Test Program	Components Covered	Parameters Measured	Radiation Type
Component Type Selection	Transistors	β, I_{CBO}	Co^{60} γ-Radiation
	Diodes	Reverse and Forward Resistance	
	Capacitors	Leakage Current	3 to 6 Mev Electrons
	Organic Materials	Mechanical Factors	
	Transistors	β	
	Diodes	Reverse and Forward Resistance	
	Lenses	Transmission	
	IR Sensor	Sensitivity	
Component Screening	All Transistors for Flight Use	β, I_{CBO}	Co^{60} γ-Radiation
Boxes	Selected Boxes, to be Exposed to Destruction		Electron or γ-Radiation

APPENDIX D
THERMAL ANALYSIS

SECTION I. GENERAL

Since one of the main functions of this design study is to evaluate the APT/AVCS system concept and obtain an optimized design, the thermal analysis has proceeded so as to compute temperature predictions from a parametric viewpoint. Solar-cell temperatures and average component temperatures have been determined for various sun angles and internal power-dissipation levels. A 25- to 75-watt orbit-average power-dissipation range and a 0- to 90-degree sun-angle range have been covered. Both of these parameters should cover the anticipated values for the OT-2 mission. The sun angle of the spacecraft is defined as the angle between the spin axis and the sun vector. This should not be confused with the angle between the orbit normal and the sun vector. Although these angles are the same once the spacecraft has been torqued into the wheel mode, at the initial injection they are not necessarily equal since at this point, the spin axis is in the direction of the velocity vector and thus perpendicular to the final spin axis.

The placement of the OT-2 spacecraft in a "Wheel" mode at a 750-nautical mile retrograde orbit is similar to conditions in the TIROS "I" Wheel system. At this altitude, heat inputs from earth radiation and albedo are reduced; however, the average internally generated power and percent suntime are higher than in TIROS "I".

The three-body mathematical model developed in earlier TIROS thermal designs has been used for the initial phase of the thermal study. Upon finalization of a component arrangement and power profile per component, a more accurate N-body mathematical model will be made.

As in the case of TIROS "I", the worst-case condition, insofar as spacecraft temperatures are concerned, will occur during the period from orbit injection to station acquisition, while the spacecraft is experiencing a 90-degree sun angle.

Thus, it becomes essential to mission success that the station acquisition maneuver be initiated within a designated number of orbits after launch. Because the 90-degree sun-angle period represents the worst-case condition insofar as thermal performance is concerned, the initial thermal analysis was based on this value of sun angle. A more detailed analysis will be made when final launch and orbit parameters are established.

SECTION II. ANALYSIS

The three-body mathematical model combines all the component weights and power dissipations, and considers only radiative coupling between the top and sides of the spacecraft (conduction coupling between components is assumed to be infinite). This method of analysis provides a quick, relatively accurate indication of overall spacecraft temperatures and points out gross problem areas. An inherent advantage is obtained by the ease of changing surface properties, power levels, component weights, etc. After the major perturbations are removed (i.e., power, and component arrangement changes), a refinement and extension of the analysis to include conduction coupling and radiation coupling between the major components will be made.

The thermal equations for a spacecraft structure (three-body mathematical model) were derived for the spacecraft top, sides, and baseplate (including components) by considering each section as isothermal. The temperature of the orbiting spacecraft at any time is a function of the time in the sun, and the spacecraft orientation angle between the vehicle-sun vector and the normal to the orbital plane.

Equations were derived as a function of the angle between the spin axis and the sun vector (γ), the external energy inputs, and the internal radiation coupling. Conduction coupling between the top, sides, and baseplate was not considered. Each section has two equations, one for the orbital day and one for the orbital night.

In the mathematical model under consideration, the daytime condition for the spacecraft top is given by the expression:

$$M_T C_T \frac{dT_T}{d\theta} = A_T \epsilon_T \mu_T + A_T \alpha_T P_T + A_T (\alpha_T - \eta) S \cos\gamma$$

$$+ K_{TC} \sigma T_C^4 + K_{TS} \sigma T_S^4 - (A_T \epsilon_T + K_{TC} + K_{TS}) \sigma T_T^4 . \quad \text{(D-1)}$$

The nighttime condition for the spacecraft top is

$$M_T C_T \frac{dT_T}{d\theta} = A_T \epsilon_T \mu_T + K_{TC} \sigma T_C^4 + K_{TC} \sigma T_S^4$$

$$- (A_T \epsilon_T + K_{TC} + K_{TS}) \sigma T_T^4 . \quad \text{(D-2)}$$

The daytime condition for the spacecraft components is

$$M_C C_C \frac{dT_C}{d\theta} = A_B \epsilon_B \mu_B + A_B \alpha_B P_B + K_{TC} \sigma T_T^4 + K_{SC} \sigma T_S^4 - (A_B \epsilon_B + K_{CS} + K_{CT}) \sigma T_C^4 + Q_C \quad \text{(D-3)}$$

The nighttime condition for the spacecraft components is

$$M_C C_C \frac{dT_C}{d\theta} = A_B \epsilon_B \mu_B + K_{TC} \sigma T_T^4 + K_{SC} \sigma T_S^4 - (A_B \epsilon_B + K_{CS} + K_{CT}) \sigma T_C^4 + Q_C \quad \text{(D-4)}$$

The daytime condition for the spacecraft sides is

$$M_S C_S \frac{dT_S}{d\theta} = \pi A_S \epsilon_S \mu_S + \pi A_S \alpha_S P_S + A_S (\alpha_S - \eta) S \sin \gamma - K_{ST} \sigma T_T^4 + K_{CS} \sigma T_C^4 - (\pi A_S \epsilon_S + K_{CS} + K_{TS}) \sigma T_S^4. \quad \text{(D-5)}$$

The nighttime condition for the spacecraft sides is

$$M_S C_S \frac{dT_S}{d\theta} = \pi A_S \epsilon_S \mu_S + K_{ST} T_T^4 + K_{CS} T_C^4 - (\pi A_S \epsilon_S + K_{CS} + K_{TS}) \sigma T_S^4. \quad \text{(D-6)}$$

In these equations, the following definitions are involved:

M_T, M_S, M_C* : the mass of the top, sides, and components, respectively.

C_T, C_S, C_C : the specific heat of the top, sides, and components, respectively.

A_T, A_B : area of the top and base, respectively.

A_S : projected area of the sides.

α_T, α_S, α_B : solar absorptivity of the top, sides, and base, respectively.

σ_T, σ_S, σ_B : Stefan-Boltzmann constant for top, sides, and base, respectively.

ϵ_T, ϵ_S, ϵ_B : emissivity of the top, sides, and base, respectively.

μ_T, μ_S, μ_B : earthshine to top, sides, and base respectively, in watt/in.^{2}

P_T, P_S, P_B : albedo to top, sides, and base, respectively, in watt/in.^{2}

K_{TS} : radiative coupling factor, top to sides.

K_{TC} : radiative coupling factor, top to components.

K_{SC} : radiative coupling factor, sides to components.

S : direct solar energy, in watt/in.^{2}

θ : time.

Q_C : average component power dissipation, in watts.

γ : angle between spin axis and sun vector.

η : solar-cell efficiency.

*Note that T, S, B, and C used as subscripts represent the satellite top, sides, base, and components, respectively. However, the classic symbols for absolute temperature and specific heat (T and C, respectively) are also used in these equations, but not as subscripts.

The term "radiative coupling factor", as used in TIROS "I", can be defined as follows:

$$Q_{1-2} = A_1 \epsilon_{1-2} \theta_{1-2} \sigma(T_1^4 - T_2^4) \qquad \text{(D-7)}$$

where,

A_1 : area of the first body in $in.^2$,

ϵ_{1-2} : some function of the emissivities of both bodies,

θ_{1-2} : angle factor from first body to second body in radians,

T_1 : absolute temperature of first body in ^{o}K, and

T_2 : absolute temperature of second body in ^{o}K.

The coupling factor from the first body to the second body is therefore,

$$K_{1-2} = A_1 \theta_{1-2} \epsilon_{1-2} \qquad \text{(D-8)}$$

where,

K_{1-2} = coupling factor in $in.^2$

The coupling factors form a symmetrical matrix in which $K_{1-2} = K_{2-1}$.

Therefore, $K_{TS} = K_{ST}$, $K_{SC} = K_{CS}$, and $K_{TC} = K_{CT}$.

The values of the direct solar flux and albedo energy inputs were calculated for each surface and averaged for the illuminated portion. The earthshine was averaged over the complete orbit.

SECTION III. CONCLUSION

Figures D-1 through D-5 present the temperature-time history of the three-body mathematical model for several representative sun angles and internal power dissipation levels. These curves represent dynamic-equilibrium conditions, i.e., the spacecraft has been in that particular orbit for a sufficient period of time to damp out all transient temperature effects due to injection conditions or torquing periods. The temperature-time history will then repeat itself every orbit.

An examination of these curves shows the OT-2 spacecraft thermal characteristics. The top and side structures have relatively low weight-to-area ratios (approximately 1.8 lb/ft^2). This causes rapid response whenever the solar input to these areas changes when going from day into night or night into day. The temperature extremes during any one day can then be widely separated, as can be observed from the temperature-time curves. However, the components and baseplate structure comprise a high-density unit. The thermal inertia of this section is much greater than the hat sections. This results in a small orbital variation in average component temperature during conditions of dynamic equilibrium. This, in part, enhances the long-term reliability of the OT-2 components.

Once the average power dissipation and sun angles which the actual flight conditions will create for the vehicle are established, the resulting temperatures for the components, top hat, and side hat can then be obtained with good accuracy from the temperature-time graphs. All of these graphs are summarized in Figure 3-III-1 of Part 3; this graph shows the maximum temperatures each section will reach in orbit versus sun angle. In predicting these temperatures the average power dissipation data presented in Figure D-6 was used.

For the normal 45-degree sun-angle condition as shown in Figure D-3, the APT system has a maximum component temperature of 16°C while dissipating 62 watts of internal power; this is well within the desired temperature range of 0 to 30°C.

Figure D-7 presents the injection transients for the situation of an initial 90-degree sun angle at injection. If the spacecraft remains in this parking orbit for "n" orbits before station acquisition, the component temperature will be that which is shown. The system dissipates 28 watts during this condition. Thus, after 5 orbits (9.45 hours) the average component temperature will be -6°C; after 9 orbits (17) hours) the temperature will have dropped further to an average of -10°C. To ensure a lower temperature limit of -6°C, the station acquisition should, therefore, take place before the end of the 5 orbits.

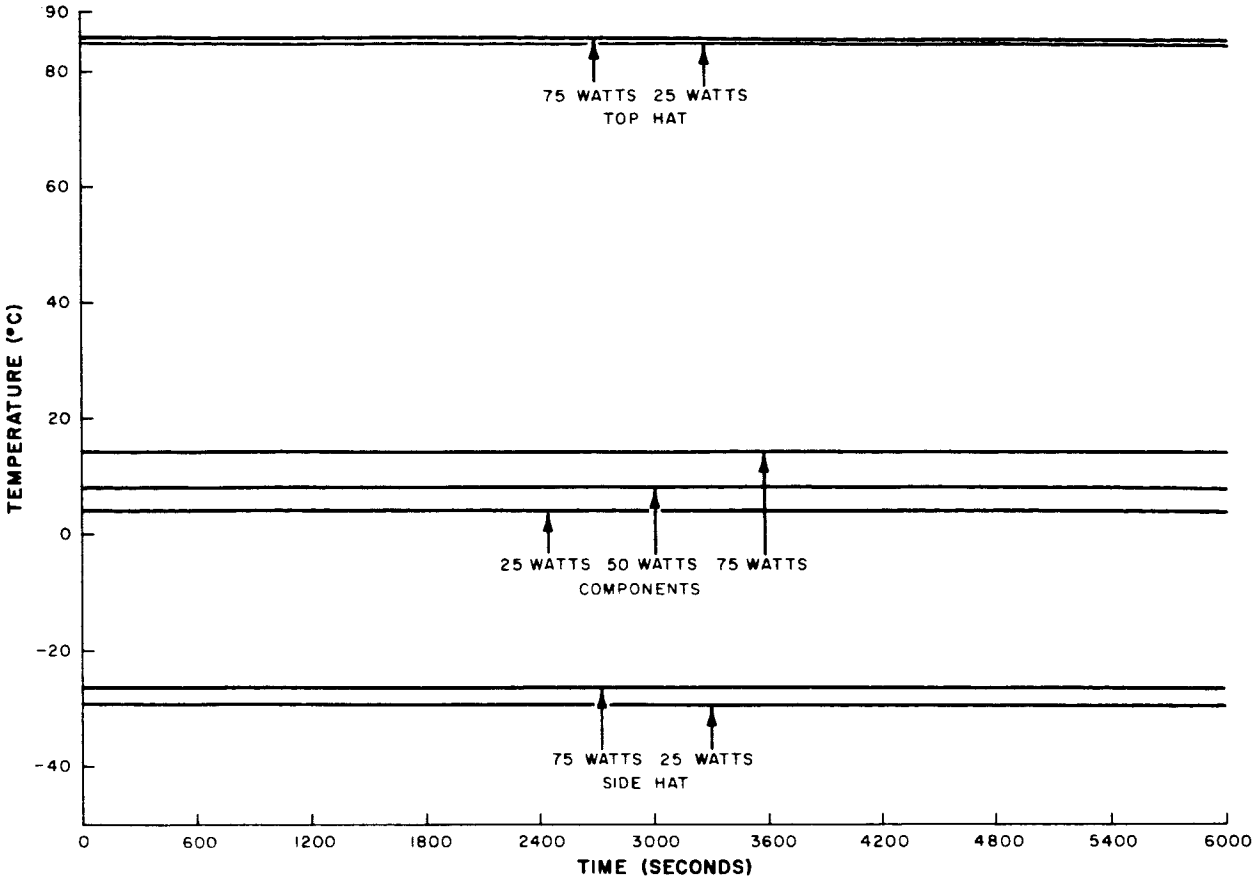

Figure D-1. Spacecraft Temperature vs Time at Zero-Degree Sun Angle, 100-Percent Sun Time (Baseplate Emissivity of 0.29)

Once torquing commences, the predicted response of the spacecraft will be as shown in Figure 4-II-8. In this graph, torquing is assumed to begin at 3 orbits, or at 6 orbits. In the former case the minimum temperature would be 0°C, while in the latter case it would be -8°C; the importance of torquing early is therefore evident. Thus, the 90-degree worst case sun-angle condition can be substantially eliminated by using QOMAC before the 5 orbit.

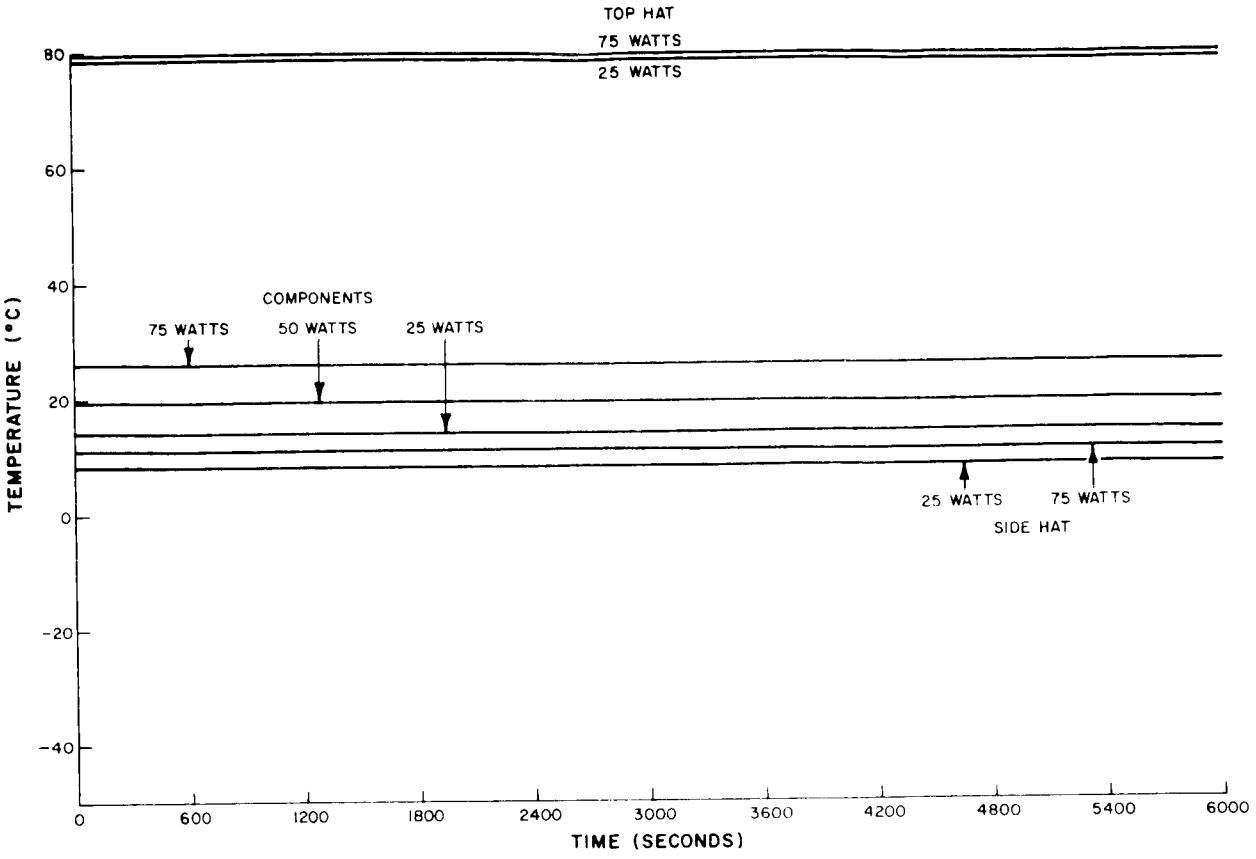

Figure D-2. Spacecraft Temperature vs Time at 30-Degree Sun Angle, 100-Percent Sun Time (Baseplate Emissivity of 0.29)

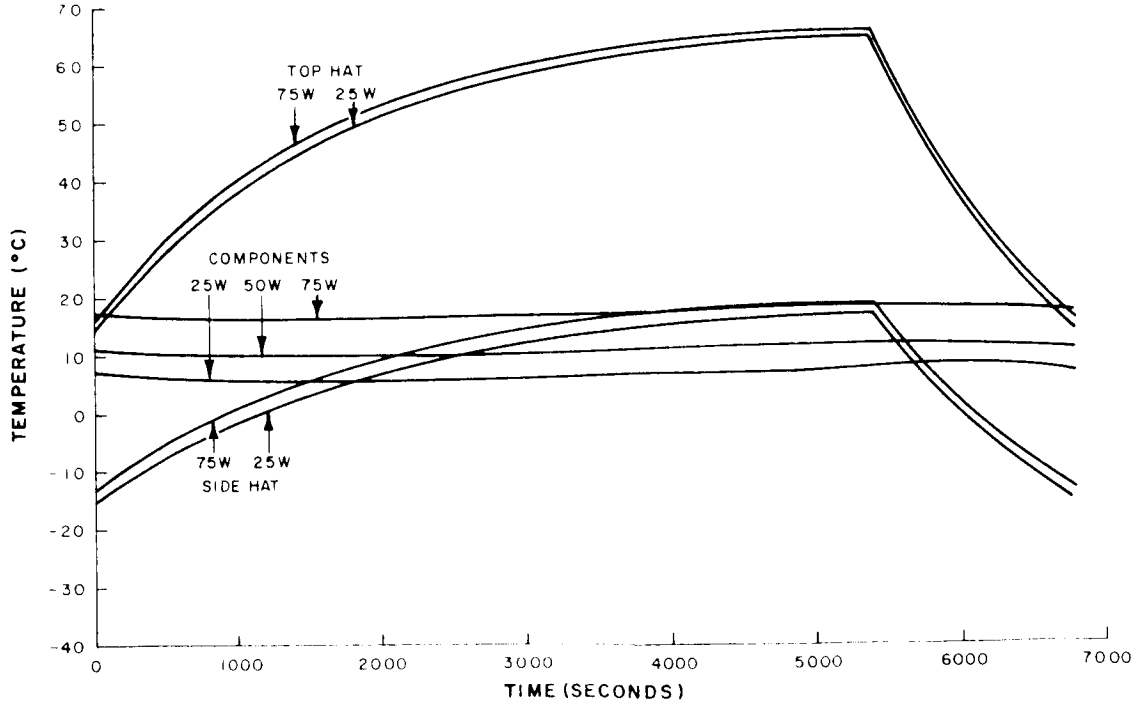

Figure D-3. Spacecraft Temperature vs Time at 45-Degree Sun Angle, 79.5-Percent Sun Time (Baseplate Emissivity of 0.29)

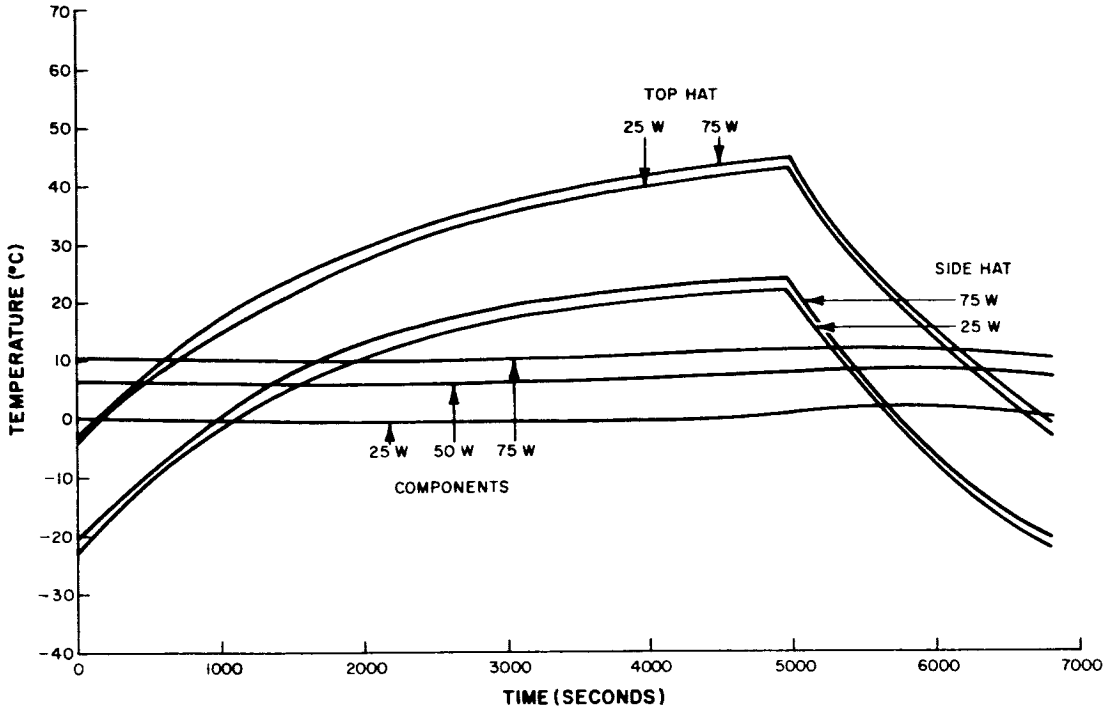

Figure D-4. Spacecraft Temperature vs Time at 60-Degree Sun Angle, 72.6-Percent Sun time (Baseplate Emissivity of 0.29)

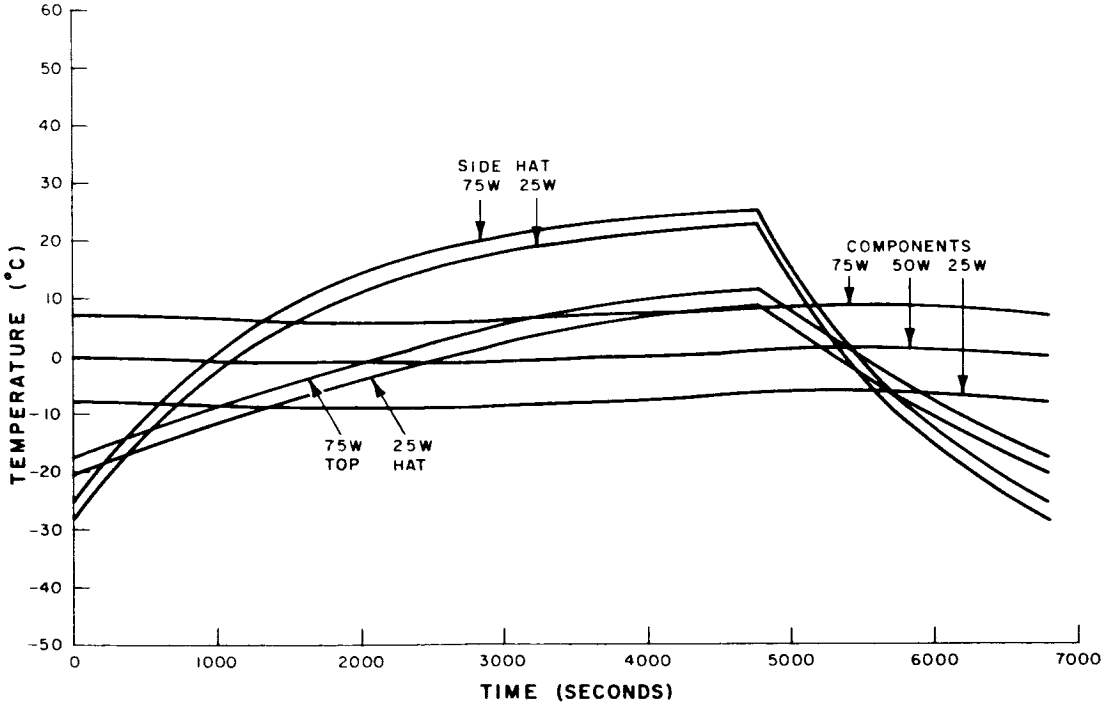

Figure D-5. Spacecraft Temperature vs Time at 75-Degree Sun Angle, 70-Percent Sun Time (Baseplate Emissivity of 0.29)

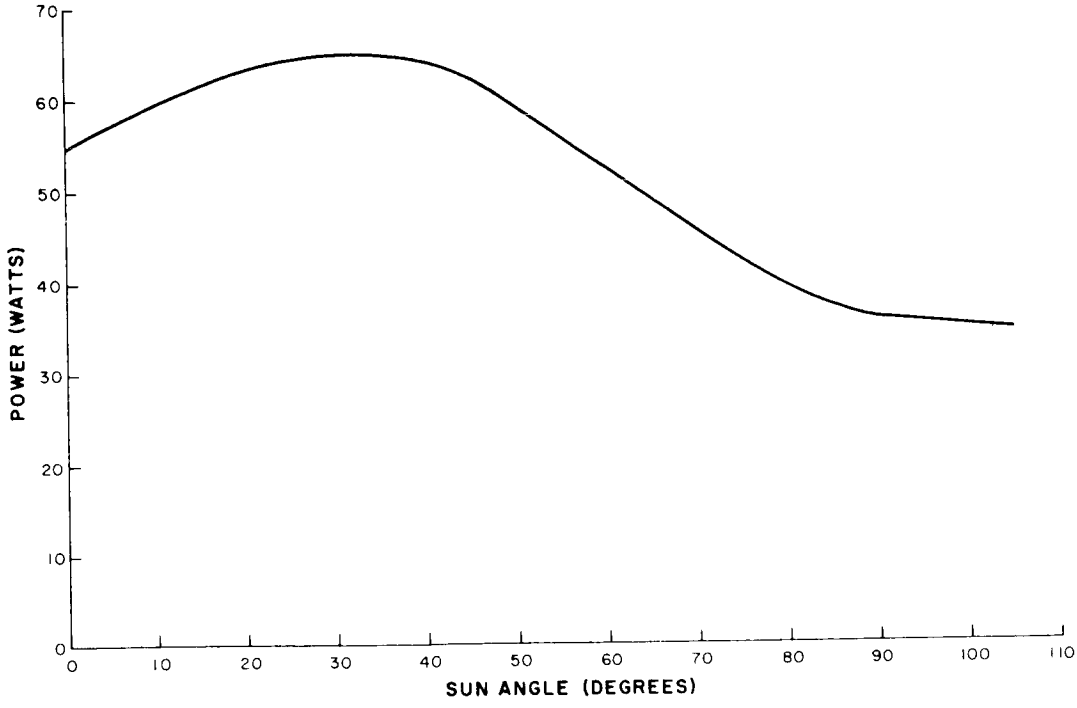

Figure D-6. Spacecraft Average Power Dissipation

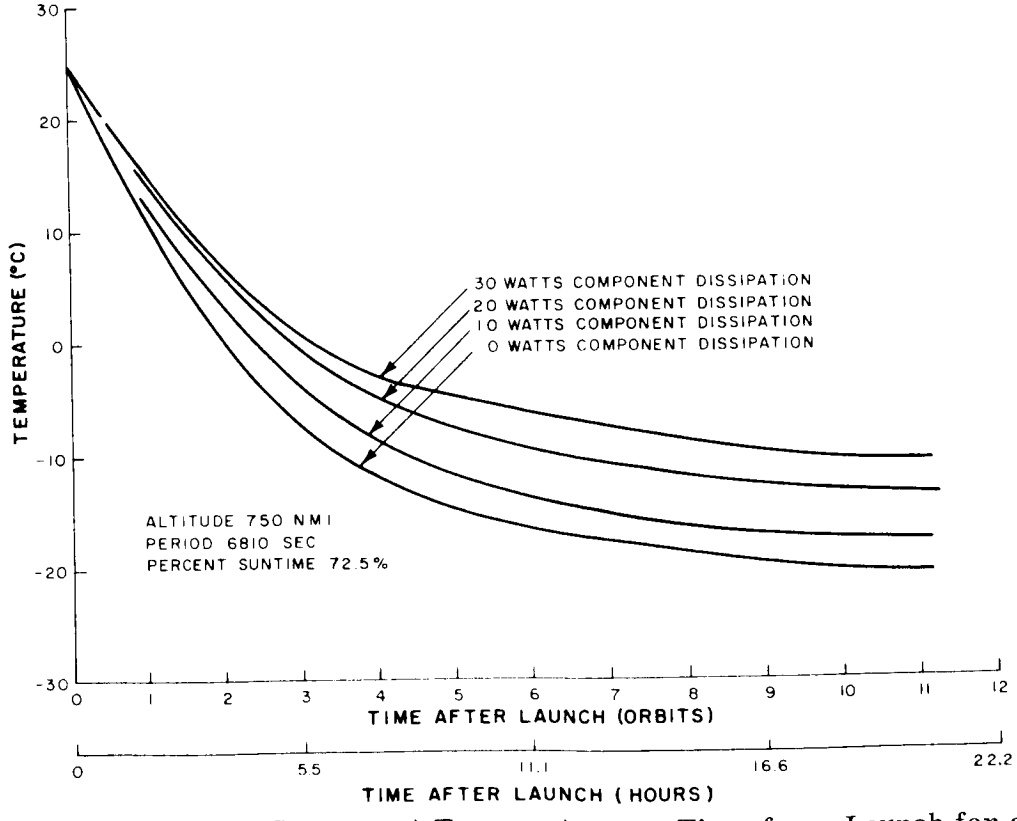

Figure D-7. Average Component Temperature vs Time from Launch for a 90-Degree Sun Angle Parking Orbit (Angle between Orbit Normal and Sun Vector equal to 60 Degrees)